Table 10.6 UE-Specific SRS Periodicity and Subframe Offset for SRS Trigger Types 0 and 1 [5]

SRS Trigger Type	SRS Configuration Index I_{SRS}	SRS Periodicity T_{SRS} (ms)	SRS Subframe Offset $T_{SRS\text{-}offset}$
	FDD		
0	0–1	2	I_{SRS}
	2–6	5	$I_{SRS} - 2$
	7–16	10	$I_{SRS} - 7$
	17–36	20	$I_{SRS} - 17$
	37–76	40	$I_{SRS} - 37$
	77–156	80	$I_{SRS} - 77$
	157–316	160	$I_{SRS} - 157$
	317–636	320	$I_{SRS} - 317$
	637–1023	Reserved	Reserved
	TDD		
	0	2	0, 1
	1	2	0, 2
	2	2	1, 2
	3	2	0, 3
	4	2	1, 3
	5	2	0, 4
	6	2	1, 4
	7	2	2, 3
	8	2	2, 4
	9	2	3, 4
	10–14	5	$I_{SRS} - 10$
	15–24	10	$I_{SRS} - 15$
	25–44	20	$I_{SRS} - 25$
	45–84	40	$I_{SRS} - 45$
	85–164	80	$I_{SRS} - 85$
	165–324	160	$I_{SRS} - 165$
	325–644	320	$I_{SRS} - 325$
	645–1023	Reserved	Reserved
1	FDD		
	0–1	2	I_{SRS}
	2–6	5	$I_{SRS} - 2$
	7–16	10	$I_{SRS} - 7$
	17–31	Reserved	Reserved
	TDD		
	0	2	0, 1
	1	2	0, 2
	2	2	1, 2

(*Continued*)

Table 10.6 (Continued)

SRS Trigger Type	SRS Configuration Index I_{SRS}	SRS Periodicity T_{SRS} (ms)	SRS Subframe Offset $T_{SRS\text{-}offset}$
		FDD	
	3	2	0, 3
	4	2	1, 3
	5	2	0, 4
	6	2	1, 4
	7	2	2, 3
	8	2	2, 4
	9	2	3, 4
	10–14	5	$I_{SRS} - 10$
	15–24	10	$I_{SRS} - 15$
	25–31	Reserved	Reserved

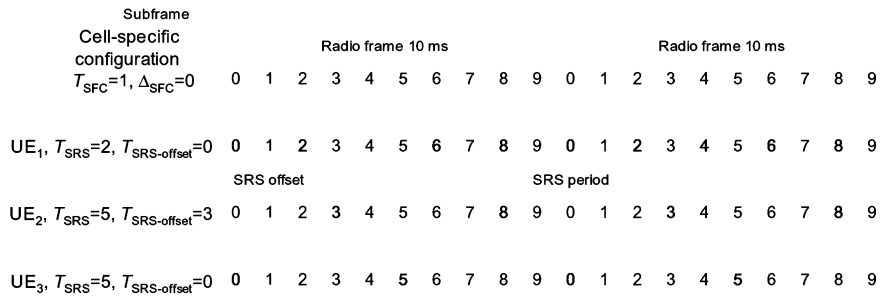


FIGURE 10.25

SRS parameter configuration example (frame structure type 1) [14].

of the SRS, and $N_{SRS}(B_{SRS}) = 6m_{SRS}(B_{SRS})$ is the bandwidth-dependent length of the SRS sequence (see Table 10.8 for the permissible values). The cell-specific SRS bandwidth configuration $C_{SRS} \in \{0, 1, 2, 3, 4, 5, 6, 7\}$ and the UE-specific SRS bandwidth $B_{SRS} \in \{0, 1, 2, 3\}$ are signaled to the UE via higher layers.

10.7 Uplink physical channel processing

The uplink multiple access scheme (SC-FDMA) in LTE employs separate physical channels for transmission of data and control signaling. The structure of the uplink physical channels is designed to make efficient use of the available time–frequency resources, and to effectively support multiplexing between data and control signaling. LTE Rel-8/9 utilizes few uplink multiple antenna techniques,

Table 10.7 Cell-Specific SRS Parameters for Frame Structure Type 1 and Type 2 [3]

SRS Subframe Configuration	Frame Structure Type 1		Frame Structure Type 2	
	Configuration Period T_{SFC}(ms)	Transmission Offset Δ_{SFC}(ms)	Configuration Period T_{SFC}(Subframes)	Transmission Offset Δ_{SFC}(ms)
0	1	{0}	5	{1}
1	2	{0}	5	{1,2}
2	2	{1}	5	{1,3}
3	5	{0}	5	{1,4}
4	5	{1}	5	{1,2,3}
5	5	{2}	5	{1,2,4}
6	5	{3}	5	{1,3,4}
7	5	{0,1}	5	{1,2,3,4}
8	5	{2,3}	10	{1,2,6}
9	10	{0}	10	{1,3,6}
10	10	{1}	10	{1,6,7}
11	10	{2}	10	{1,2,6,8}
12	10	{3}	10	{1,3,6,9}
13	10	{0,1,2,3,4,6,8}	10	{1,4,6,7}
14	10	{0,1,2,3,4,5,6,8}	Reserved	Reserved
15	Reserved	Reserved	Reserved	Reserved

Table 10.8 SRS Bandwidth Configuration Parameters [3]

SRS Bandwidth Configuration C_{SRS}	Uplink Bandwidth N_{RB}^{UL}	SRS-Bandwidth $B_{SRS} = 0$		SRS-Bandwidth $B_{SRS} = 1$		SRS-Bandwidth $B_{SRS} = 2$		SRS-Bandwidth $B_{SRS} = 3$	
		m_0	N_0	m_1	N_1	m_2	N_2	m_3	N_3
0	$6 \le N_{RB}^{UL} \le 40$	36	1	12	3	4	3	4	1
1		32	1	16	2	8	2	4	2
2		24	1	4	6	4	1	4	1
3		20	1	4	5	4	1	4	1
4		16	1	4	4	4	1	4	1
5		12	1	4	3	4	1	4	1
6		8	1	4	2	4	1	4	1
7		4	1	4	1	4	1	4	1
0	$40 < N_{RB}^{UL} \le 60$	48	1	24	2	12	2	4	3
1		48	1	16	3	8	2	4	2
2		40	1	20	2	4	5	4	1
3		36	1	12	3	4	3	4	1
4		32	1	16	2	8	2	4	2
5		24	1	4	6	4	1	4	1
6		20	1	4	5	4	1	4	1
7		16	1	4	4	4	1	4	1
0	$60 < N_{RB}^{UL} \le 80$	72	1	24	3	12	2	4	3
1		64	1	32	2	16	2	4	4
2		60	1	20	3	4	5	4	1
3		48	1	24	2	12	2	4	3
4		48	1	16	3	8	2	4	2
5		40	1	20	2	4	5	4	1
6		36	1	12	3	4	3	4	1
7		32	1	16	2	8	2	4	2
0	$80 < N_{RB}^{UL} \le 110$	96	1	48	2	24	2	4	6
1		96	1	32	3	16	2	4	4
2		80	1	40	2	20	2	4	5
3		72	1	24	3	12	2	4	3
4		64	1	32	2	16	2	4	4
5		60	1	20	3	4	5	4	1
6		48	1	24	2	12	2	4	3
7		48	1	16	3	8	2	4	2

including closed-loop antenna selection and a simple form of MU-MIMO. More advanced multi-antenna techniques including closed-loop spatial multiplexing for SU-MIMO and transmit diversity for control signaling were introduced in LTE Rel-10. This section describes the theoretical and implementation aspects of the procedures that are used for processing the uplink physical channels.

Figure 10.26 illustrates different phases of the physical channel processing. For uplink carrier aggregation, different component carriers are associated with separate transport channels with separate physical layer processing. Most of the uplink physical processing steps outlined in Figure 10.26 are similar to the corresponding steps in the downlink physical channel processing. The physical processing of the transport channels can be summarized as follows:

- CRC calculation and insertion per transport block: The CRC is calculated for and appended to each uplink transport block.
- Code block segmentation and code block CRC insertion: Similar to downlink, code block segmentation, including code block CRC insertion, is applied to transport blocks larger than 6144 bits.
- Channel coding: A rate 1/3 turbo code with quadratic permutation polynomial (QPP)-based interleaving is used for the uplink.
- Rate matching and HARQ functions: The physical layer part of the uplink rate-matching and HARQ functionality are essentially the same as downlink, with sub-block interleaving and insertion into a circular buffer, followed by bit selection with four redundancy versions (RVs). Note that there are some important differences between downlink and uplink HARQ protocols, such as asynchronous versus synchronous and adaptive versus non-adaptive HARQ schemes.
- Bit-level scrambling: The goal of the scrambling function in the uplink is to randomize the interference and to ensure that the processing gain provided by the channel coding can be fully utilized.
- Data modulation: QPSK, 16QAM, and 64QAM modulation schemes can be used for the uplink transport channel.
- DFT precoding: The modulation symbols form blocks of N_{DFT} symbols and are fed through a DFT module, where N_{DFT} corresponds to the number of sub-carriers assigned to transmission. The DFT precoding is done to reduce the CM of the transmitted signal. From an implementation point of view, the DFT size should be a power of 2. However, such a constraint would limit the scheduler flexibility in terms of the amount of resources that could be assigned to an uplink transmission. On the other hand, all possible DFT sizes should ideally be allowed for more flexibility. The LTE/LTE-Advanced have chosen to limit the DFT size and the size of the resource allocation to products of the integers 2, 3, and 5.
- Resource element mapping: Mapping of precoded complex-valued symbols to resource elements.
- Antenna mapping and generation of a complex-valued time-domain SC-FDMA signal for each antenna port: In the first release of LTE, only

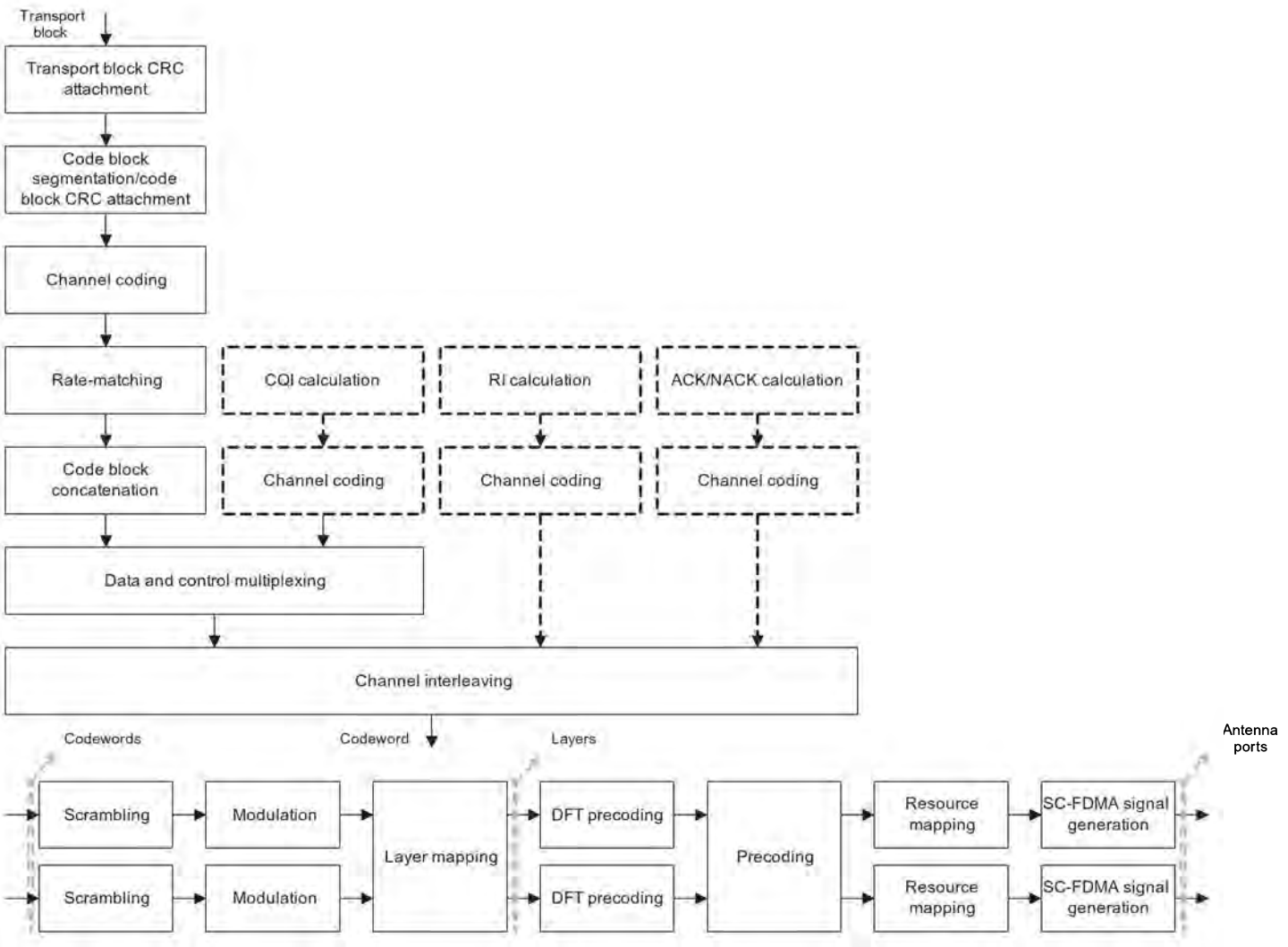


FIGURE 10.26

Uplink physical layer procedures for transport block processing [3].

single-antenna transmission was supported in the uplink. However, as part of LTE Rel-10 improvement of multi-antenna transmission, antenna precoding with up to four antennas ports is now supported in the uplink.

10.7.1 Physical uplink control channel

Uplink control signaling is typically used for the following purposes:

- Control signaling associated with user data, which is always transmitted together with uplink data and is used in the processing of that data. Examples include transport format indications, new data indicators (NDI), and MIMO parameters.
- Control signaling not associated with data is transmitted independent of any uplink data packets. Examples include HARQ ACK/NACK for downlink data packets, CQIs to support link adaptation, and MIMO feedback such as rank indicators and precoding matrix indicators for downlink transmissions, as well as scheduling requests (SRs) for uplink transmissions.

In LTE, the use of an orthogonal uplink multiple access scheme implies that the eNB controls resource allocation and determination of the uplink transmission parameters for the UEs. When simultaneous uplink PUSCH data and control signaling are scheduled, the control signaling is normally multiplexed with data prior to the DFT spreading, in order to preserve the single-carrier low CM property of the uplink transmission (see Figure 10.26). The PUCCH is used by a UE to transmit any necessary control signaling only in subframes in which the UE does not have any allocated resources for PUSCH transmission. In the design of PUCCH, the low PAPR and low CM property has been taken into consideration. The control signaling information on PUCCH is transmitted in a frequency region that is configured at the edges of the uplink system bandwidth. In order to minimize the resources needed for transmission of control signaling, PUCCH in LTE is designed to exploit frequency diversity, i.e., each PUCCH transmission in one subframe comprises a single resource block at or near one edge of the system bandwidth, followed by a second resource block in the second slot of the subframe at or near the opposite edge of the system bandwidth, where the two resource blocks are referred to as a PUCCH region. This design can achieve frequency diversity gain of approximately 2 dB compared to transmission in the same resource block throughout the subframe [16] (Figure 10.27). A snapshot of an uplink slot carrying a single PUCCH is shown in Figure 10.28 [153].

One important aspect of LTE transmitter design is the necessity to minimize unwanted emissions. Because LTE is deployed in the same frequency bands as UMTS and other legacy 3G cellular technologies, the 3GPP specifications [1] regulate the UE emissions to minimize interference and to ensure compatibility between different radio systems. The primary concern is the control of spurious emissions, which can occur at any frequency band. However, new challenges arise at the band edges, where the transmitted signal must comply with rigorous

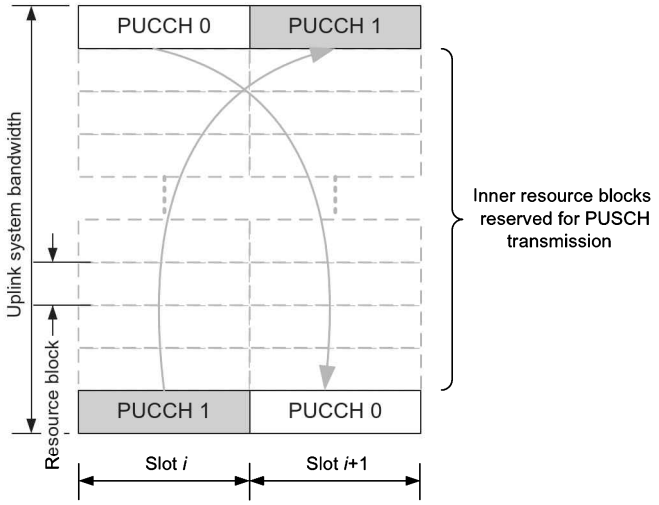


FIGURE 10.27

Example of PUCCH resource-block allocation [3,16].

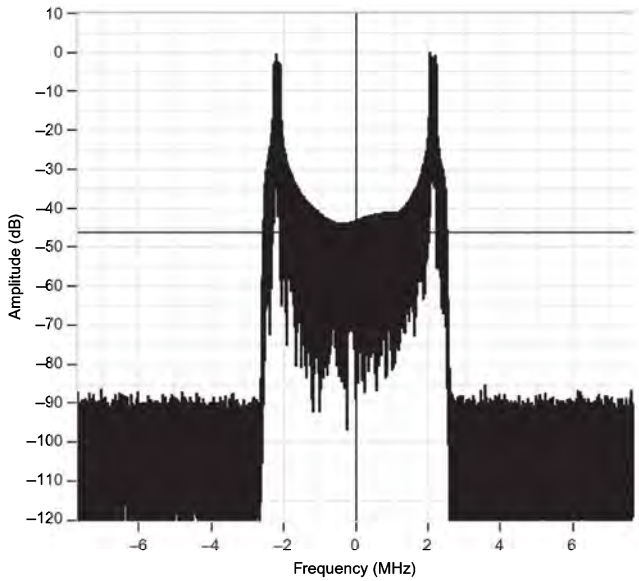


FIGURE 10.28

Snapshot of an uplink slot carrying a single PUCCH [153].

power leakage requirements. With LTE supporting channel bandwidths up to 20 MHz, and with many bands too narrow to support more than a few channels, a large proportion of the LTE channels will be at the edge of the band. Controlling transmitter performance at the edge of the band requires a design with filtering to attenuate OOB emissions without affecting in-channel performance. Factors such as cost, power efficiencies, physical size, and location in the transmitter block diagram are also important considerations. Ultimately the LTE transmitter must meet all specified limits for unwanted emissions, including limits on the amount of power that leaks into adjacent channels, as defined by the adjacent-channel leakage power ratio (ACLR).

The uplink control signaling must be transmitted regardless of whether the UE has data to send or whether any uplink resources are allocated for the terminal. As a result, there are two methods for transmission of the uplink control signaling as follows:

- Non-simultaneous transmission of PUCCH and PUSCH: When the terminal does not have any scheduling grant for PUSCH transmission in the current subframe, the uplink control signaling is transmitted on PUCCH. In uplink carrier aggregation scenarios, PUCCH is only transmitted on the primary component carrier. Consequently, data transmissions on multiple component carriers in the downlink can be acknowledged on a single uplink component carrier.
- Simultaneous transmission of PUCCH and PUSCH: When the terminal has a scheduling grant for PUSCH transmission in the current subframe, the uplink control signaling is time-multiplexed with the coded data on the PUSCH prior to DFT precoding and SC-FDMA signal generation (see Figure 10.26). Since the terminal has already been assigned radio resources, there is no need to support transmission of the SR in this case. Instead, scheduling information can be included in the MAC headers. In carrier aggregation scenarios, all control signaling is transmitted on the primary component carrier, i.e., uplink control signaling cannot be distributed across multiple component carriers.

One must differentiate between the above cases in consideration of efficient operation of the uplink PA and maximization of the uplink coverage. However, when there is sufficient power available in the terminal, simultaneous transmission of PUSCH and PUCCH can be used with minimal impact on the uplink coverage. The possibility of simultaneous PUSCH and PUCCH transmission was introduced in LTE Rel-10 which added more flexibility at the expense of slight increase in the CM value. Simultaneous transmission of PUSCH and PUCCH can always be avoided by using the basic mechanism introduced in LTE Rel-8. It should be noted that while PUCCH is only transmitted on the primary component carrier, as the primary component carrier is specified on a per-terminal basis, from a network perspective, PUCCH resources are used on multiple component carriers [16].

Since the size of a resource block in any subframe might be too large for control signaling payload transmitted by a single terminal, and in order to efficiently utilize the resources designated for control signaling transmission, multiple terminals can share the same resource block. This can be done by assigning different orthogonal phase rotations (cyclic shifts) of a cell-specific length-12 frequency-domain sequence to the UEs simultaneously using the resource block. Note that a linear phase rotation in the frequency-domain is equivalent to applying a cyclic shift in the time-domain. The resource used by PUCCH is not only specified in the time–frequency-domain by the resource-block pair, but also by the phase rotation applied. There are up to 12 different phase rotations specified, providing up to 12 different orthogonal sequences from each cell-specific sequence. However, in the frequency-selective channels, only some of the 12 phase rotations can be used in order to maintain orthogonality. Typically, up to six rotations are considered usable in a cell from a radio propagation perspective, although inter-cell interference may result in a smaller number of useful phase rotations from an overall system perspective. Higher-layer signaling is used to configure the number of phase rotations used in a cell [16]. There are three formats defined for PUCCH, formats 1, 2, and 3, each capable of carrying a different payload size.

In summary, placing the control regions at the edges of the system bandwidth has a number of advantages, including the following [15]:

- The frequency diversity achieved through frequency hopping is maximized by allowing hopping from one edge of the band to the other.
- OOB emissions[4] are smaller, if a UE only transmits on a single resource block per slot compared to multiple resource blocks. The PUCCH regions can serve as a virtual guard band between the wider-bandwidth PUSCH transmissions of adjacent carriers, and can therefore improve coexistence.
- Using control regions on the band edges maximizes the achievable PUSCH data rate, as the entire central portion of the band can be allocated to a single UE. If the control regions were in the central portion of a carrier, a UE bandwidth allocation would be limited to one side of the control region in order to maintain the single-carrier characteristic of the signal, thus limiting the maximum achievable data rate.
- Control regions on the band edges impose fewer constraints on the uplink data scheduling, both with and without inter-subframe and/or intra-subframe frequency hopping.

[4]Unwanted emissions consist of out-of-band emissions and spurious emissions. Spurious emissions are emissions caused by unwanted transmitter effects such as harmonics emissions, parasitic emissions, intermodulation products, and frequency conversion products. Out-of-band emissions are unwanted emissions outside the channel bandwidth resulting from the modulation process and non-linearity in the transmitter. If unwanted emissions are not sufficiently suppressed, they can considerably impair other intra-band radio services.

10.7.2 PUCCH formats

The physical uplink control channel carries uplink control information. The UCI can also be transmitted via PUSCH. The UCI typically consists of (1) SR; (2) HARQ ACK/NACK in response to downlink data packets received on PDSCH (one ACK/NACK bit transmitted in the case of single-codeword downlink transmission, while two ACK/NACK bits are used in the case of two codeword downlink transmission); and (3) CSI, which includes CQI as well as the MIMO-related feedback consisting of RI and PMI (20 bits per subframe are used for the CSI). The amount of UCI that a UE can transmit in a subframe depends on the number of SC-FDMA symbols available for transmission of control signaling excluding the SC-FDMA symbols used for reference signal transmission for coherent detection of PUCCH. For frame structure type 2, PUCCH is not transmitted in the UpPTS field. It must be noted that concurrent transmission of PUCCH and PUSCH in the same subframe by a UE is not allowed in LTE Rel-8/9. Support for simultaneous transmission of PUCCH and PUSCH in the same subframe from the same UE was added in LTE Rel-10, provided that it is configured by the higher layers. The PUCCH supports the multiple formats given in Table 10.9. Formats 2a and 2b are only supported for a normal cyclic prefix. Using the PUCCH formats, the following combinations of UCI on PUCCH are supported [5]:

- Format 1 is used for carrying positive SR.
- Format 1a is used for transmitting 1-bit HARQ ACK/NACK, or in case of FDD for sending 1-bit HARQ ACK/NACK with positive SR.
- Format 1b is used for carrying 2-bit HARQ ACK/NACK, or for transmitting 2-bit HARQ ACK/NACK with positive SR. PUCCH format 1b is further used for sending up to 4-bit HARQ ACK/NACK with channel selection, when the UE is configured with more than one serving cell, or in the case of TDD when the UE is configured with a single serving cell.
- Format 2 is used for sending a CSI report when it is not multiplexed with HARQ ACK/NACK. PUCCH format 2 is also used for transmission of a CSI report multiplexed with HARQ feedback for an extended cyclic prefix.
- Format 2a is used for carrying a CSI report multiplexed with 1-bit HARQ ACK/NACK for a normal cyclic prefix.
- Format 2b is used for sending a CSI report multiplexed with 2-bit HARQ ACK/NACK for a normal cyclic prefix.
- Format 3 is used for transmitting up to 10-bit HARQ ACK/NACK for FDD, and for up to 20-bit HARQ ACK/NACK for TDD. PUCCH format 3 is also used for sending up to 11-bit corresponding to 10-bit HARQ ACK/NACK and 1-bit positive/negative SR for FDD, and for up to 21-bit corresponding to 20-bit HARQ ACK/NACK and 1-bit positive/negative SR for TDD.

All PUCCH formats use a cyclic shift $N_{CS}(n_s, l)$, which used to be cell-specific until LTE Rel-11, which is a function of the SC-FDMA symbol number l and the slot number n_s according to $N_{CS}(n_s, l) = \sum_{i=0}^{7} c(8N_s^{UL}n_s + 8l + i)2^i$, where

Table 10.9 PUCCH Formats and Their Usage [3]

PUCCH Format	Modulation Scheme	Number of Bits per Subframe	Usage	Multiplexing Capacity[a] (UE/ Resource Block)
1	N/A	N/A	SR	36, 18[b], 12
1a	BPSK	1	ACK/NACK	36, 18[b], 12
1b	QPSK	2	ACK/NACK	36, 18[b], 12
2	QPSK	20	CQI (20 coded bits)	12, 6[b], 4
2a	QPSK + BPSK	21	CQI (20 coded bits) + ACK/NACK (1 bit)	12, 6[b], 4
2b	QPSK + QPSK	22	CQI (20 coded bits) + ACK/NACK (2 bits)	12, 6[b], 4
3	QPSK	48	Multiple ACK/NACK bits for carrier aggregation (up to 10 ACK/NACK bits in FDD systems with carrier aggregation or up to 20 bits ACK/NACK bits + 1 SR bit in TDD systems with carrier aggregation)	5

[a]The combination of time-domain cyclic shifts and time-domain orthogonal codes determines the number of UEs which can be multiplexed within a single pair of PUCCH resource blocks. The total number of multiplexing possibilities is defined by the product of the number cyclic shifts and the number of the orthogonal codes.
[b]Typical value with six different rotations (choosing every other cyclic shift).

the pseudo-random sequence $c(i)$ is initialized with $c_{\text{init}} = N_{\text{ID}}^{\text{RS}}$, where $N_{\text{ID}}^{\text{RS}}$ denotes the virtual cell identifier,[5] at the beginning of each radio frame. The definition of the virtual cell identifier $N_{\text{ID}}^{\text{RS}}$ depends on the type of transmission. For transmissions associated with PUSCH $N_{\text{ID}}^{\text{RS}} = N_{\text{ID}}^{\text{cell}}$, if no value for $N_{\text{ID}}^{\text{PUSCH}}$ is configured by higher layers if PUSCH transmission corresponds to a *Random Access Response* or a retransmission of the same transport block as part of the contention-based random access procedure; otherwise $N_{\text{ID}}^{\text{RS}} = N_{\text{ID}}^{\text{PUSCH}}$. For transmissions associated with PUCCH $N_{\text{ID}}^{\text{RS}} = N_{\text{ID}}^{\text{cell}}$, if no value for $N_{\text{ID}}^{\text{PUCCH}}$ is configured by higher layers; otherwise $N_{\text{ID}}^{\text{RS}} = N_{\text{ID}}^{\text{PUCCH}}$. The virtual cell identifier for SRS is defined as $N_{\text{ID}}^{\text{RS}} = N_{\text{ID}}^{\text{cell}}$ [3].

The physical resource allocation for PUCCH depends on two parameters, $N_{\text{RB}}^{(2)}$ and $N_{\text{CS}}^{(1)}$, that are signaled by the higher layers. The variable $N_{\text{RB}}^{(2)} \geq 0$ denotes the

[5]A simple approach is to use the PUCCH resource offset parameter to facilitate frequency-domain separation between inter-cell orthogonal and non-orthogonal resources. A virtual cell identifier may be used in the newly reserved PUCCH resource pool.

bandwidth in terms of the number of resource blocks that are available to be used for the PUCCH format 2/2a/2b transmission in each slot. The variable $N_{CS}^{(1)}$ denotes the number of cyclic shifts used for PUCCH format 1/1a/1b in a resource block which is used for a combination of PUCCH formats 1/1a/1b and 2/2a/2b. The value of $N_{CS}^{(1)}$ is an integer multiple of Δ_{shift}^{PUCCH} within the range of $\{0, 1, \ldots, 7\}$, where Δ_{shift}^{PUCCH} is signaled via the higher layers. There is no mixed resource block if $N_{CS}^{(1)} = 0$. There is only one resource block in each slot that can support a mix of PUCCH formats 1/1a/1b and 2/2a/2b. The resources used for transmission of PUCCH formats 1/1a/1b, 2/2a/2b, and 3 are represented by non-negative indices $n_{PUCCH}^{(1,\overline{p})}, n_{PUCCH}^{(2,\overline{p})} < 12N_{RB}^{(2)} + \left\lceil \frac{N_{CS}^{(1)}}{8} \right\rceil (10 - N_{CS}^{(1)})$ and $n_{PUCCH}^{(3,\overline{p})}$, respectively.

The mapping of various PUCCH formats to PUCCH regions is shown in Figure 10.29. The mapping of PUCCH to PRBs follows the steps below:

1. Start from resource blocks in the outer edge of the band toward middle of the band.
2. Allocate PUCCH format 2/2a/2b resources.
3. Allocate PUCCH formats containing mixed ACK/NACK and CQI.
4. Allocate PUCCH format 1/1a/1b resources.

It can be seen in the figure that PUCCH format 2/2a/2b is mapped and transmitted on the outermost band-edge resource blocks followed by a mixed PUCCH resource block of CSI format 2/2a/2b and SR/HARQ ACK/NACK format 1/1a/1b, and then by a PUCCH SR/HARQ ACK/NACK format 1/1a/1b allocation toward the center of the band. The number of PUCCH resource blocks available for use by CSI format 2/2a/2b is signaled to the UEs in the cell through broadcast signaling.

10.7.2.1 PUCCH formats 1, 1a, 1b

The structure of PUCCH format 1 is illustrated in Figure 10.31. PUCCH format 1 is used for transmission of HARQ ACK/NACK (i.e., a single-bit HARQ feedback corresponding to one downlink component carrier is used to generate one BPSK-modulated symbol, and in the case of downlink spatial multiplexing, 2 bits of HARQ feedback are used to generate one QPSK-modulated symbol) and for sending a positive SR, where the same constellation point as for a HARQ NACK is used. The BPSK/QPSK-modulated symbol is then used to generate the signal for transmission in each of the two PUCCH slots. In each of the seven SC-FDMA symbols of a slot assuming a normal cyclic prefix, a length-12 sequence obtained via phase rotation of the cell-specific base sequence is transmitted. Three SC-FDMA symbols are used for reference signals to enable channel estimation and coherent detection by the eNB, and the remaining four SC-FDMA symbols are modulated to generate the BPSK/QPSK-modulated symbols (as shown in Figure 10.31). In principle, the BPSK/QPSK-modulated symbol could directly

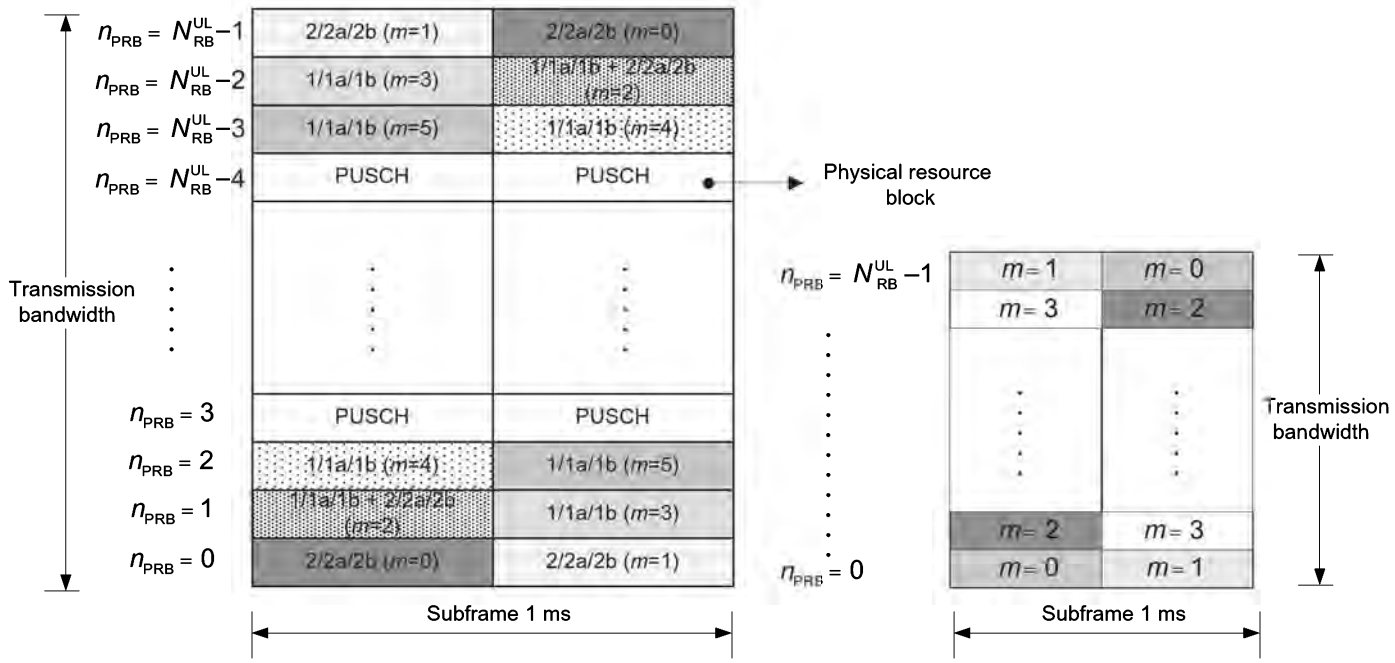


FIGURE 10.29

Example mappings of PUCCH to PRBs in a subframe [3].

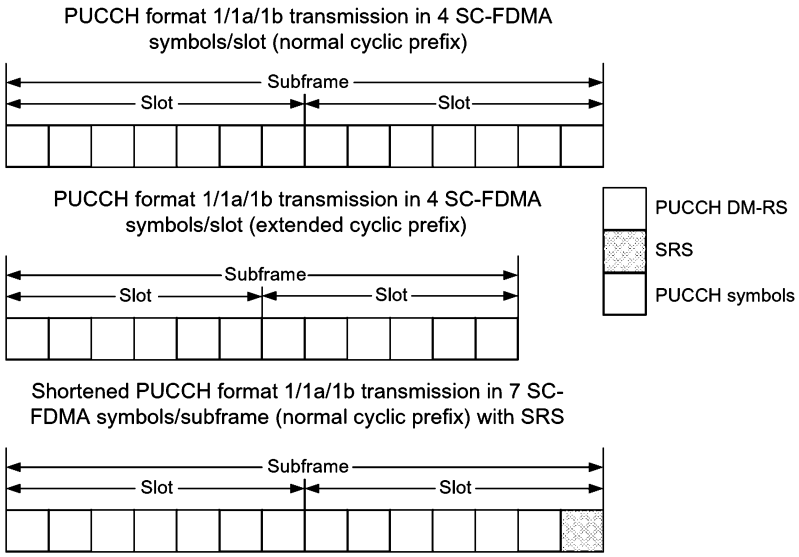


FIGURE 10.30

Relative position of PUCCH, DM-RS, and SRS symbols.

modulate the rotated length-12 sequence used to differentiate terminals transmitting on the same time–frequency resource. However, this would result in unnecessarily lower PUCCH capacity. Therefore, the BPSK/QPSK-modulated symbol is multiplied by a length-4 orthogonal cover code. Multiple terminals may transmit on the same time–frequency resource using the same phase-rotated sequence and can still be separated through different OCCs. In order to estimate the channels for the respective terminals, the reference signals are also scrambled by appropriate orthogonal cover sequences with different length, i.e., three for the case of a normal cyclic prefix and two for an extended cyclic prefix. Each cell-specific sequence can be used for up to 36 different terminals (assuming all 12 phase rotations or cyclic shifts are available, whereas typically 6 of the cyclic shifts are utilized), there is a threefold improvement in the PUCCH capacity compared to the case when no cover sequence is used. The cover sequences are three Walsh sequences of length 4 for the data part and three DFT sequences of length 3 for the reference signals [3,14,16].

A PUCCH format 1 resource, used for either a HARQ feedback or an SR, is represented by a single scalar resource index. From the index, the phase rotation and the orthogonal cover sequence are derived. The use of a phase rotation of a cell-specific sequence, together with orthogonal sequences as described earlier, provides orthogonality between different terminals in the same cell when transmitting PUCCH on the same set of resource blocks. Therefore, there is ideally no intra-cell interference, which helps improve the overall performance. However,

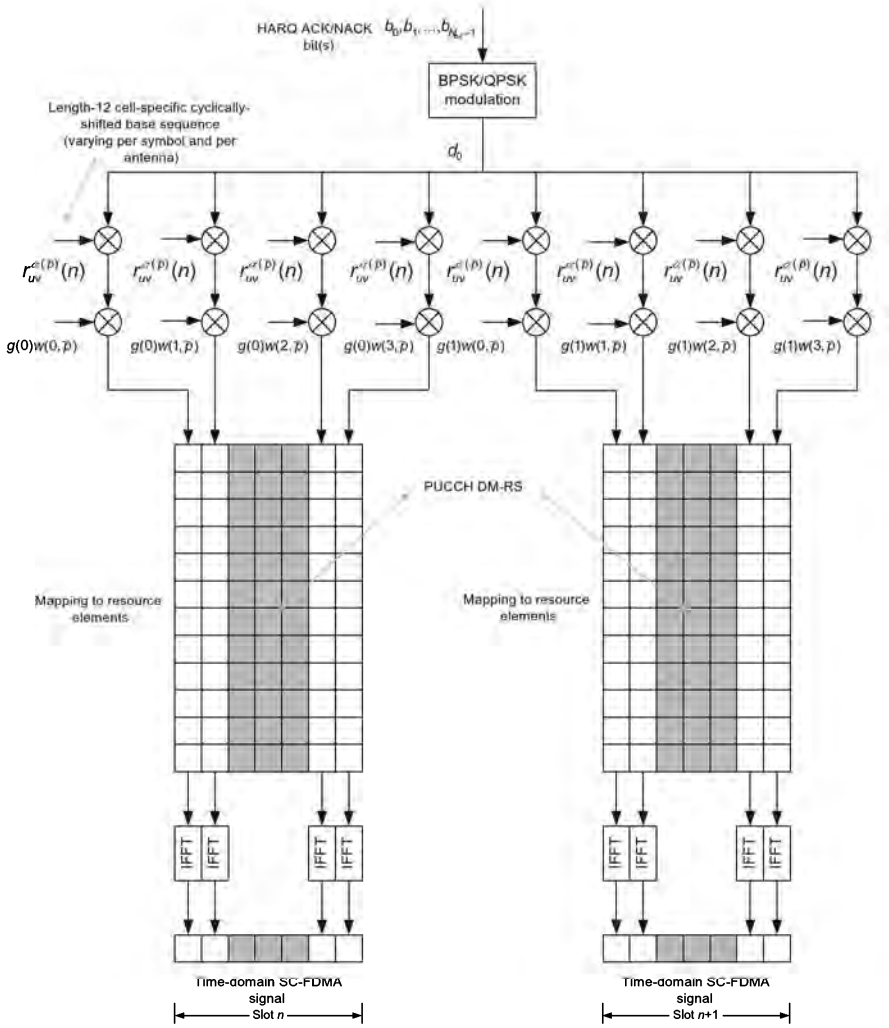


FIGURE 10.31

Physical layer processing for PUCCH format 1/1a/1b (HARQ ACK/NACK and normal cyclic prefix).

PUCCH typically suffers from inter-cell interference since different sequences used in neighboring cells are non-orthogonal. In order to randomize the inter-cell interference, the phase rotation of the sequence used in a cell is changed on a symbol-by-symbol basis in a slot according to a hopping pattern derived from the physical layer cell identity. In addition, slot-level hopping is applied to the orthogonal cover and phase rotation to further randomize the interference.

The UE scheduling request is carried by PUCCH format 1 and is signaled by the presence or absence of PUCCH format 1 transmission. For PUCCH formats 1a and 1b, 1 or 2 bits are transmitted depending on the HARQ feedback. The block of bits $b_0, b_1, \ldots, b_{N_{\text{bit}}-1}$ are modulated using BPSK (format 1a) or QPSK (format 1b) modulation, resulting in a complex-valued symbol d_0. Note that the number of bits is $N_{\text{bit}} = 1$ for format 1a and $N_{\text{bit}} = 2$ for format 1b carrying HARQ ACK/NACK. The complex-valued symbol d_0 is multiplied by a cyclically shifted sequence of length $N_s^{\text{PUCCH}} = 12$, $r_{\text{uv}}^{\alpha(\bar{p})}(n)$ for each of the N_p antenna ports used for PUCCH transmission according to the following equation [3]:

$$y^{\bar{p}}(n) = \frac{1}{\sqrt{N_p}} d_0 r_{\text{uv}}^{\alpha(\bar{p})}(n)|_{n=0,1,\ldots,N_s^{\text{PUCCH}}-1} \tag{10.5}$$

where $r_{\text{uv}}^{\alpha(\bar{p})}(n)$ is the cyclically shifted Zadoff–Chu base sequence. The antenna-port-specific cyclic-shift $\alpha(\bar{p})$ varies across symbols and slots. The block of complex-valued symbols $y^{\bar{p}}(0), y^{\bar{p}}(1), \ldots, y^{\bar{p}}(N_s^{\text{PUCCH}} - 1)$ are scrambled by scrambling sequence $g(n_s)$ and are block-wise spread with the antenna-port-specific orthogonal sequence $w(i, \bar{p})$ according to the following equation [3]:

$$z^{\bar{p}}(m' N_{\text{SF}}^{\text{PUCCH}} N_s^{\text{PUCCH}} + m N_s^{\text{PUCCH}} + n) = g(n_s) w(m, \bar{p}) y^{\bar{p}}(n) \tag{10.6}$$

where $m = 0, 1, \ldots, N_{\text{SF}}^{\text{PUCCH}} - 1; n = 0, 1, \ldots, N_s^{\text{PUCCH}} - 1; m' = 0, 1$ and $g(n_s) = 1$ if $n'_{\bar{p}}(n_s) \bmod 2 = 0$; otherwise $g(n_s) = e^{j\pi/2}$, $N_{\text{SF}}^{\text{PUCCH}} = 4$ for both slots of normal PUCCH format 1/1a/1b and $N_{\text{SF}}^{\text{PUCCH}} = 4$ for the first slot and $N_{\text{SF}}^{\text{PUCCH}} = 3$ for the second slot of shortened PUCCH format 1/1a/1b (see Figure 10.30).

In addition to dynamic scheduling using PDCCH, a UE can be semi-persistently scheduled according to a specific pattern. In that case, there will be no PDCCH to assign the PUCCH resources in the uplink. The configuration of the semi-persistent scheduling includes information on the PUCCH index to be used for uplink HARQ feedback. Note that a UE can use PUCCH resources only when it has been scheduled in the downlink. The amount of PUCCH resources required for HARQ feedback does not necessarily increase if the number of terminals in the cell increases; rather it is a function of the number of control channel elements (CCEs) in the downlink control signaling.

For downlink carrier aggregation, when there are multiple simultaneous downlink allocations for a single terminal, multiple feedback bits are transmitted in the uplink (i.e., 1 or 2 bits in the case of spatial multiplexing per downlink component carrier). PUCCH format 1b can be used to support more than 2 bits in the uplink by using resource selection. Let us assume that 4 bits are going to be transmitted in the uplink. With resource selection, 2 bits would indicate which PUCCH resource should be used and the remaining 2 bits are transmitted using the normal PUCCH structure, but on the resource addressed by the first 2 bits. One resource is derived from the first CCE using the same rule used in the absence of carrier aggregation, assuming that the scheduling assignment is

transmitted on the primary cell. The remaining resources are semi-statically configured by RRC signaling. For more than 4 bits, resource selection is less efficient and PUCCH format 3, which was introduced in LTE Rel-10 for carrier aggregation, is utilized.

Unlike HARQ feedback, whose occurrence is expected and predicable by the eNB, a specific terminal's need for uplink resources is unpredictable, which is why a contention-based mechanism has been provisioned in LTE to allow uplink resource scheduling request. The random-access mechanism is used for SRs. A contention-based mechanism may work well for a small number of UEs; however, by increasing the number of UEs simultaneously requesting resources, the probability of collision increases. Therefore, LTE further provides a contention-free scheduling-request mechanism on PUCCH, where each terminal in the cell is assigned a reserved resource on which it can transmit a request for uplink resources. The contention-free resource is represented by a PUCCH resource index every *n*th subframe. In other words, a request for uplink resources can be made by means of the random-access channel; however, due to the probability of collisions during congestion periods, an alternative method is provided using PUCCH format 1. Each UE in the cell is assigned a specific resource index mapping, a resource which can be used every *n*th subframe in order to transmit a scheduling request. Therefore, if PUCCH energy is detected, the eNB will consider it as an SR from the corresponding UE. Since each UE will have a specific resource allocated, there is no probability of collision. However, as a drawback, the number of available PUCCH resources is reduced.

A single SR is deemed sufficient for the case of carrier aggregation. The discussion earlier has considered transmission of either a HARQ feedback or an SR. However, there are cases where the UE needs to concurrently transmit HARQ feedback and an SR. In such cases, the HARQ ACK/NACK is transmitted on the scheduling-request resource. As we discussed earlier, this is possible because the scheduling request carries no explicit information. By comparing the amount of energy detected on the ACK resource and the scheduling-request resource for a specific terminal, the eNB can determine whether the terminal is requesting resources, as well.

10.7.2.2 PUCCH formats 2, 2a, 2b

The CSI reports are used to provide the eNB with an estimate of the downlink communication channel observed by the UE in order to assist channel-dependent scheduling (Figure 10.32). The CSI report consists of multiple bits transmitted in one subframe and is transmitted using PUCCH format 2. Channel status reports include CQI, RI, and PMI. The HARQ ACK/NACK can also be transmitted with channel status information. There are two forms of channel coding for this purpose, one for the channel quality information (i.e., CQI) only and another one for the combination of CQI and HARQ feedback. The channel quality indicator represents the recommended modulation scheme and coding rate that should be

used for the downlink transmission. The RI provides information about the rank of the channel, which is used to determine the optimal number of layers that should be used for the downlink transmission which is only used for spatial multiplexing modes. The PMI provides information about which precoding matrix to use, which is only used in closed-loop spatial multiplexing modes. PUCCH format 2, as shown in Figure 10.32, is generated by phase rotation of a cell-specific base sequence (same as PUCCH format 1), followed by a block coding function using a punctured Reed–Muller code[6] and QPSK modulation of the CSI. There are ten QPSK symbols to be transmitted in a subframe where the first five complex-valued modulation symbols are transmitted in the first slot and the remaining in the next slot. In PUCCH format 2/2a/2b, two SC-FDMA symbols are used as reference signals to allow coherent detection and demodulation at the eNB. In the remaining modulation symbols, each QPSK-modulated symbol is multiplied by a phase-rotated length-12 cell-specific base sequence, inverse Fourier-transformed, and the resulting signal is transmitted over the corresponding SC-FDMA symbol. For an extended cyclic prefix, there are six SC-FDMA symbols per slot; therefore, only one reference symbol per slot is allocated. The transmission of PUCCH format 2 relies on phase rotation of a cell-specific sequence similar to that for PUCCH format 1, which allows the two formats to be transmitted in the same resource block. Note that orthogonal cover sequences are not used for PUCCH format 2. The rotation angles for different symbols carrying PUCCH format 2 are the hopping across symbol and slot boundaries for interference randomization [16].

Resources for transmission of PUCCH format 2 can be represented by an index, which can be interpreted as a channel number that is configurable via higher-layer signaling for each terminal to transmit its CSI report. The CSI reports on PUCCH are periodic. There are also aperiodic reports that are only transmitted on PUSCH. In case of carrier aggregation, multiple periodic reports, one per component carrier, are transmitted that are offset in time such that reports for two different component carriers do not collide (Table 10.10).

---

[6]Reed–Muller codes are a family of linearerror-correcting codes used in communication systems. The special cases of Reed–Muller codes include Hadamard codes, Walsh–Hadamard codes, and Reed–Solomon codes. Reed–Muller codes are denoted by an $RM(d,r)$ notation, where d is the order of the code and r determines the length of code $n = 2^r$. Reed–Muller codes are related to binary functions on field $GF(2^r)$ over the elements $\{0, 1\}$. It can be shown that $RM(0,r)$ codes are repetition codes of length, rate $R = 1/n$ and minimum distance $d_{\min} = n$, $RM(1,r)$ codes are parity check codes of length $n = 2^r$, rate $R = (r+1)/n$ and minimum distance $d_{\min} = n/2$. Reed–Muller codes have the following properties [ref]:

1. The set of all possible exterior products of up to d of v_i form a basis for $\mathbf{F}_2^n$.
2. The rank of $RM(d,r)$ code is defined as $\sum_{s=0}^{r} \binom{d}{s}$
3. $RM(d,r) = RM(d, r-1)|RM(d-1, r-1)$, where '|'. denotes the bar product of two codes.
4. $RM(d,r)$ has minimum Hamming weight2^{d-r}.

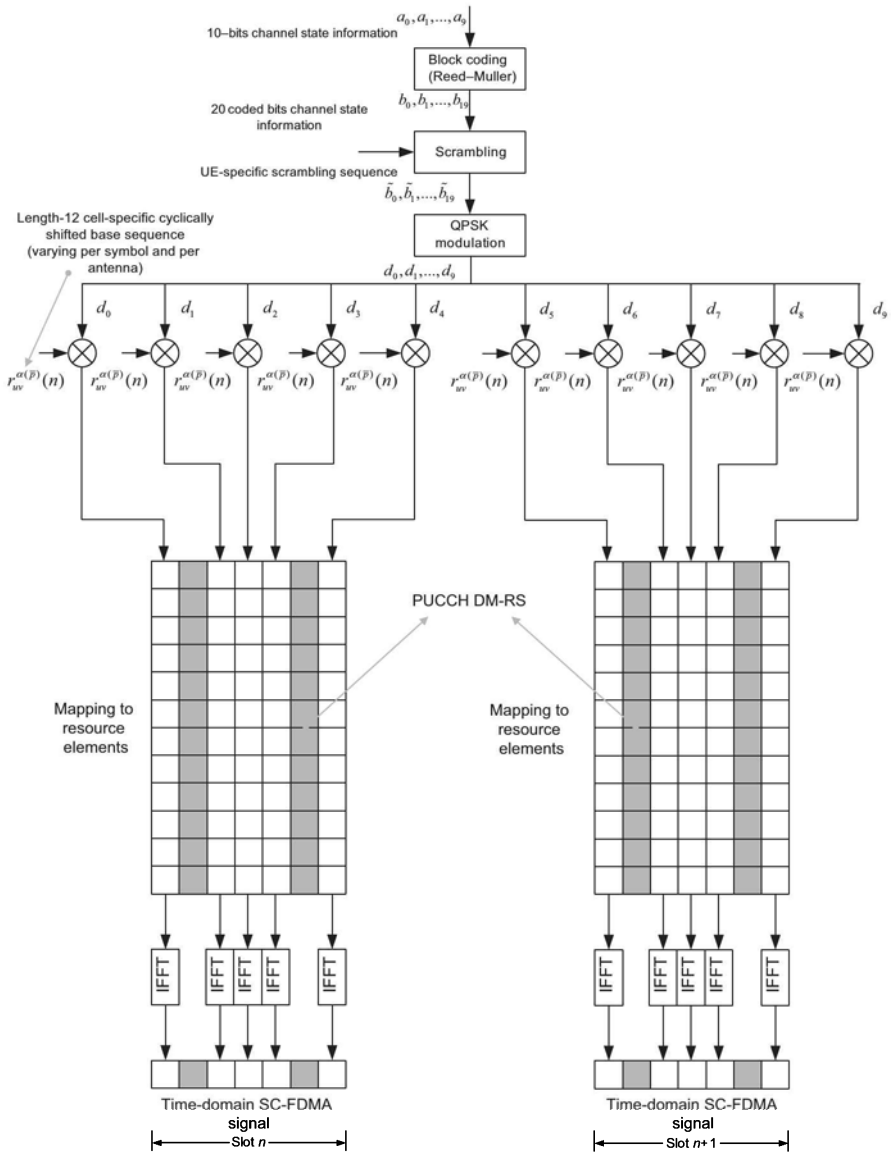


FIGURE 10.32

Physical layer processing for PUCCH format 2/2a/2b (normal cyclic prefix, CQI only) [16].

The structure of PUCCH format 2 in one subframe with normal cyclic prefix is shown in Figure 10.32. The first and the fifth SC-FDMA symbols are used for PUCCH DM-RS transmission with a normal cyclic prefix, whereas in the case of an extended cyclic prefix only one reference symbol is transmitted on the third

Table 10.10 Size of the PUCCH Region [15]

System Bandwidth (MHz)	Number of Resource Blocks per Subframe	Number of PUCCH Regions
1.4	2	1
3	4	2
5	8	4
10	16	8
20	32	16

SC-FDMA symbol. The number of reference symbols per slot results from a trade-off between channel estimation accuracy and the sustainable code rate for the UCI bits. For a small number of UCI bits at a low SINR operating point (for a typical 1% target error rate), improving the channel estimation accuracy by using more reference symbols is more desirable than using a lower channel code rate. However, with larger numbers of UCI bits, the required SINR increases and the higher code rate resulting from a larger overhead of reference symbols becomes more critical, thus fewer reference symbols are utilized. In consideration of the above facts, two reference symbols per slot were found to provide the best trade-off in terms of performance and overhead, given the payload sizes required. Therefore, ten CSI bits are channel coded with a rate 1/2 punctured $(20, k)$ Reed–Muller code to generate 20 coded bits, which are then scrambled, similar to PUSCH data, with a length-31 Gold sequence[7] prior to QPSK modulation. One QPSK-modulated symbol (according to Table 10.11) is transmitted on each of the ten SC-FDMA symbols in the subframe by multiplying with a cyclically shifted base sequence of length-12 prior to OFDM modulation. The 12 cyclic shifts allow 12 different UEs to be orthogonally multiplexed on the same PUCCH format 2 resource blocks. The processing of a PUCCH DM-RS reference sequence, i.e., transmitted on the second and sixth SC-FDMA symbols for the normal cyclic prefix and the fourth symbol for the extended cyclic prefix, is similar to the frequency-domain CSI signal sequence without the CSI data modulation. In order to provide inter-cell interference randomization, cell-specific

[7]A Gold sequence is a type of binary sequence that is often used in telecommunication and satellite navigation signal processing. Gold sequences have bounded small cross-correlations within a set. A set of Gold sequences consists of $2^n - 1$ sequences each with a period of $2^n - 1$. A set of Gold sequences can be generated by taking two maximum-length sequences of the same length $2^n - 1$ such that their absolute cross-correlation is less than or equal to $2^{(n+2)/2}$, where n is the size of the linear feedback shift register used to generate the maximum length sequence [165]. The set of $2^n - 1$ logical XOR or of the two sequences in their various phases is a set of Gold codes. The highest absolute cross-correlation in this set of codes is $2^{(n+2)/2} + 1$ for even n and $2^{(n+1)/2} + 1$ for odd n. The logical XOR of two Gold codes from the same set is another Gold code.

Table 10.11 Modulation Symbols for PUCCH Format 1a/1b and PUCCH Format 2a/2b [3]

PUCCH Format	$b_0, b_1, \ldots, b_{N_{bit}-1}$	d_0
1a	0	1
	1	−1
1b	00	1
	01	−j
	10	j
	11	−1
PUCCH Format	$b_{20}, b_{21}, \ldots, b_{N_{bit}-1}$	d_{10}
2a	0	1
	1	−1
2b	00	1
	01	−j
	10	j
	11	−1

symbol-level cyclic-shift hopping is used. Intra-cell interference randomization is achieved by cyclic-shift re-mapping in the second slot [15].

In mathematical terms, a block of coded bits $b_0, b_1, \ldots, b_{19}$ is scrambled with a UE-specific scrambling sequence, resulting in a block of scrambled coded bits $\tilde{b}_0, \tilde{b}_1, \ldots, \tilde{b}_{19}$ according to $\tilde{b}(i) = [b(i) + c(i)] \bmod 2$, where the scrambling sequence $c(i)$ was defined in Chapter 9 and is initialized with $c_{\text{init}} = \left(\lfloor n_s/2 \rfloor + 1\right)\left(2N_{\text{ID}}^{\text{cell}} + 1\right)2^{16} + n_{\text{RNTI}}$ at the start of each subframe, where n_{RNTI} denotes the 16-bit temporary UE identity in the connected mode.[8] The block of scrambled bits $\tilde{b}_0, \tilde{b}_1, \ldots, \tilde{b}_{19}$ are QPSK modulated, resulting in a block of complex-valued modulation symbols $d_0, d_1, \ldots, d_9$. Each complex-valued symbol $d_0, d_1, \ldots, d_9$ is multiplied by a cyclically shifted length $N_{\text{s}}^{\text{PUCCH}} = 12$ sequence $r_{\text{uv}}^{\alpha(\overline{p})}(n)$ for each of the N_p antenna ports used for PUCCH transmission according to the following equation [3]:

$$z^{(\overline{p})}(N_{\text{s}}^{\text{PUCCH}} n + i) = \frac{1}{\sqrt{N_p}} d(n) r_{\text{uv}}^{\alpha(\overline{p})}(i)|_{n=0,1,\ldots,9; i=0,1,\ldots,11} \tag{10.7}$$

[8]Pseudo-random sequences are defined by a length-31 Gold sequence. The output sequence $c(n), \forall n = 0, 1, \ldots, M-1$ of length M is defined by $c(n) = (x_1(n + N_C) + x_2(n + N_C)) \bmod 2$ in which:
$x_1(n + 31) = (x_1(n + 3) + x_1(n)) \bmod 2$;
$x_2(n + 31) = (x_2(n + 3) + x_2(n + 2) + x_2(n + 1) + x_2(n)) \bmod 2$, and $N_C = 1600$. The first m-sequence is initialized with $x_1(0) = 1, x_1(n) = 0, n = 1, 2, \ldots, 30$. The second m-sequence is initialized by $c_{\text{init}} = \sum_{i=0}^{30} x_2(i)2^i$ with the value depending on the application of the sequence.

where $r_{uv}^{\alpha(\overline{p})}(n)$ is an antenna-port-dependent cyclically shifted Zadoff–Chu sequence of length 12. The resources used for transmission of PUCCH format 2/2a/2b are identified by resource index $n_{\text{PUCCH}}^{(2,\overline{p})}$ in which the cyclic shift $\alpha_{\overline{p}}(n_s, l)$ is determined according to $\alpha_{\overline{p}}(n_s, l) = \frac{\pi n_{cs}^{\overline{p}}(n_s,l)}{6}$, where $n_{cs}^{\overline{p}}(n_s, l) = [n_{cs}^{\text{cell}}(n_s, l) + n'_{\overline{p}}(n_s)]$ mod 12 [3]. A UE is semi-statically configured via higher-layer signaling to periodically report different CQI, PMI, and RI types in PUCCH format 2 using a resource index $n_{\text{PUCCH}}^{(2)}$, which indicates both the PUCCH region and the cyclic shift to be used. The allocation index for PUCCH format 2/2a/2b transmission regions is given by $m = \left\lfloor n_{\text{PUCCH}}^{(2)}/12 \right\rfloor$ and the assigned cyclic shift is given by $n_{\text{RS}}^{\text{PUCCH}} = n_{\text{PUCCH}}^{(2)} \bmod 12$. The simultaneous transmission of uplink HARQ feedback and CSI on PUCCH can be enabled by UE-specific higher-layer signaling. However, if simultaneous transmission is not enabled or supported and the UE needs to transmit HARQ feedback on PUCCH in the same subframe in which a CSI report has been configured, the CSI is dropped and only HARQ feedback is transmitted. In subframes where the eNB scheduler allows for simultaneous transmission of CSI and HARQ feedback on PUCCH from a UE, the CSI and the 1- or 2-bit HARQ feedback are multiplexed in the same PUCCH resource block without compromising the low cubic-metric property of single-carrier signal.

The time and frequency resources that can be used by the UE to report CSI which consists of CQI, PMI, precoding type indicator (PTI),[9] and/or RI are controlled by the eNB. For spatial multiplexing, the UE determines an RI corresponding to the number of useful transmission layers. A UE is semi-statically configured via higher-layer signaling to periodically send feedback on different CSI metrics (CQI, PMI, PTI, and/or RI) on the PUCCH using the reporting modes given in Table 10.12 [5].

Two periodic CSI reporting modes are supported in LTE/LTE-Advanced as follows:

1. *Wideband reports*, where the average channel quality across the entire cell bandwidth is calculated and represented with a single CQI value. In this case, a single PMI value for the entire bandwidth is further reported, if PMI reporting is enabled.

[9]PTI was introduced in LTE Rel-10 and allows a UE to dynamically switch between different types of PMI reports to the serving eNB. It is applicable to transmission mode 9 which uses a two-stage approach to PMI reporting. The first stage corresponds to reporting wideband and long-term channel characteristics (PMI_1), and the second stage concerns frequency-selective short-term channel properties (PMI_2). A PTI value of "0" indicates that the UE has detected PMI_1 is changing, thus it needs to send an update to the eNB. A PTI value of "1," on the other hand, indicates that PMI_1 is not changing and the report should be on PMI_2, which means that a number of sub-band PMI_2 values as opposed to a single wideband value should be sent to the eNB [14].

Table 10.12 CQI and PMI Feedback Types and Corresponding Transmission Modes for PUCCH CSI Reporting [5]

		PMI Feedback Type	
		No PMI	**Single PMI**
PUCCH CQI Feedback Type	Wideband (Wideband CQI)	Mode 1-0	Mode 1-1
		TM1	TM4
		TM2	TM5
		TM3	TM6
		TM7	TM8[a]
		TM8[a]	TM9[b]
		TM9[b]	TM10[c]
		TM10[c]	
	UE selected (sub-band CQI)	Mode 2-0	Mode 2-1
		TM1	TM4
		TM2	TM5
		TM3	TM6
		TM7	TM8[a]
		TM8[a]	TM9[b]
		TM9[b]	TM10[c]
		TM10[c]	

[a] *TM 8: Mode 1-1 or 2-1, if the UE is configured with PMI/RI reporting; otherwise, modes 1-0 or 2-0, if the UE is configured without PMI/RI reporting.*
[b] *TM 9: Mode 1-1 or 2-1, if the UE is configured with PMI/RI reporting and the number of CSI-RS ports is greater than one; otherwise, mode 1-0 or 2-0, if the UE is configured without PMI/RI reporting or the number of CSI-RS ports is equal to one.*
[c] *TM10: Mode 1-1 or 2-1, if the UE is configured with PMI/RI reporting and the number of CSI-RS ports is greater than one; otherwise modes 1-0 or 2-0, if the UE is configured without PMI/RI reporting or the number of CSI-RS ports is equal to one.*

2. *UE-selected reports*, where the total bandwidth of a cell is divided into one to four bandwidth parts, with the number of bandwidth parts derived from the cell bandwidth as given in Table 10.13. For each bandwidth part, the terminal selects the best sub-band within that part. The sub-band size ranges from four to eight resource blocks. Since the supported PUCCH payload size is limited, the reporting cycles through the bandwidth parts and in one subframe reports the wideband CQI and PMI (if enabled) for that bandwidth part, as well as the best sub-band and the CQI for that sub-band. The RI (if enabled) is reported in a separate subframe.

The periodic CSI reporting mode for each serving cell is configured via higher-layer signaling. For wideband periodic CQI reporting, the reporting period can be configured as $\{2, 5, 10, 16, 20, 32, 40, 64, 80, 128, 160\}$ subframes, or it can

Table 10.13 PUCCH Reporting Type Payload Size per PUCCH Reporting Mode and Mode State [5]

PUCCH Reporting Type	Report Contents	Mode State	PUCCH Reporting Modes			
			Mode 1-1 (Bits/ Bandwidth Part)	Mode 2-1 (Bits/ Bandwidth Part)	Mode 1-0 (Bits/ Bandwidth Part)	Mode 2-0 (Bits/ Bandwidth Part)
	Sub-band CQI	RI = 1	N/A	4 + L	N/A	4 + L
		RI > 1	N/A	7 + L	N/A	4 + L
a	Sub-band CQI/ PMI_2	$N_p = 8$ RI = 1	N/A	8 + L	N/A	N/A
		$N_p = 8$ 1 < RI < 5	N/A	9 + L	N/A	N/A
		$N_p = 8$ RI > 4	N/A	7 + L	N/A	N/A
	Wideband CQI/ PMI	$N_p = 2$ RI = 1	6	6	N/A	N/A
		$N_p = 4$ RI = 1	8	8	N/A	N/A
		$N_p = 2$ RI > 1	8	8	N/A	N/A
		$N_p = 4$ RI > 1	11	11	N/A	N/A
a	Wideband PMI_1	$N_p = 8$ RI < 3	N/A	4	N/A	N/A
		$N_p = 8$ 2 < RI < 8	N/A	2	N/A	N/A
		$N_p = 8$ RI = 8	N/A	0	N/A	N/A
b	Wideband CQI/ PMI_2	$N_p = 8$ RI = 1	8	8	N/A	N/A
		$N_p = 8$ 1 < RI < 4	11	11	N/A	N/A

		$N_p = 8$ RI = 4	10	10	N/A	N/A
		$N_p = 8$ RI > 4	7	7	N/A	N/A
c	Wideband CQI/ PMI_1/PMI_2	$N_p = 8$ $RI = 1$	8	N/A	N/A	N/A
		$N_p = 8$ $1 < RI \leq 4$	11	N/A	N/A	N/A
		$N_p = 8$ $4 < RI \leq 7$	9	N/A	N/A	N/A
		$N_p = 8$ RI = 8	7	N/A	N/A	N/A
	RI	$N_p = 2, 4$ two-layer spatial multiplexing	1	1	1	1
		$N_p = 8$ two-layer spatial multiplexing	1	N/A	N/A	N/A
		$N_p = 4$ four-layer spatial multiplexing	2	2	2	2
		$N_p = 8$ four-layer spatial multiplexing	2	N/A	N/A	N/A
		Eight-layer spatial multiplexing	3	N/A	N/A	N/A
	Wideband CQI	$RI = 1, RI > 1$	N/A	N/A	4	4
	RI/PMI_1	$N_p = 8$ two-layer spatial multiplexing	4	N/A	N/A	N/A
		$N_p = 4$ and eight-layer spatial multiplexing	5			
	RI/PTI	$N_p = 8$ two-layer spatial multiplexing	N/A	2	N/A	N/A
		$N_p = 8$ four-layer spatial multiplexing	N/A	3	N/A	N/A
		$N_p = 8$ eight-layer spatial multiplexing	N/A	4	N/A	N/A

Table 10.14 Relationship of Sub-band Size and Bandwidth Parts with System Bandwidth [5]

System Bandwidth N_{RB}^{DL} (Resource Blocks)	Sub-band Size L_{SB} (Resource Blocks)	Bandwidth Parts N_{BP}
6–7	N/A	N/A
8–10	4	1
11–26	4	2
27–63	6	3
64–110	8	4

be set to off. For the UE-selected sub-band CQI, a CQI report in a certain subframe of the serving cell describes the channel quality in a particular part or parts of the bandwidth of that serving cell. The bandwidth parts are indexed in order of increasing frequency and decreasing sizes starting at the lowest frequency. The CQI and PMI payload sizes of each PUCCH CSI reporting mode are given in Table 10.14. While the wideband feedback mode is similar to that sent via PUSCH, the UE-selected sub-band CQI transmitted via PUCCH is different. In this case, the total number of sub-bands N_{SB} is divided into fractions called bandwidth parts. The value of the parameters (N_{SB}, L_{SB}, N_{BP}) depends on the system bandwidth as summarized in Table 10.14. In this case, one CQI value is computed and reported for a single selected sub-band from each bandwidth part, along with the corresponding sub-band index. The concept of periodic CQI reporting modes (wideband and sub-band) in time- and frequency-domains is illustrated in Figure 10.33.

For each serving cell, there are a total of N_{SB} equally sized sub-bands corresponding to system bandwidth N_{RB}^{DL} where $N_{SB} = \lfloor N_{RB}^{DL}/L_{SB} \rfloor$ sub-bands of size L_{SB}. A bandwidth part *bp* is frequency-consecutive and consists of N_{bp} sub-bands where N_{BP} bandwidth parts cover the system bandwidth. If the total number of bandwidth parts $N_{BP} = 1$, i.e., the wideband measurement, then $N_{bp} = \lceil N_{RB}^{DL}/L_{SB} \rceil$; otherwise, if $N_{BP} > 1$, then $N_{bp} = \lceil N_{RB}^{DL}/L_{SB}/N_{BP} \rceil$ depending on the values of these parameters, each bandwidth part is scanned in sequential order according to increasing frequency. For UE-selected sub-band feedback, a single sub-band out of N_{bp} sub-bands of a bandwidth part is selected along with the corresponding L bit label indexed in order of increasing frequency, where $L = \lceil \log_2 \lceil N_{RB}^{DL}/L_{SB}/N_{BP} \rceil \rceil$.

For each serving cell, the CQI/PMI reporting period P_{CQI} in number of subframes and relative reporting offset N_{offset}^{CQI} in number of subframes are configured by higher layers. The RI reporting period P_{RI} and relative reporting offset N_{offset}^{RI} are determined based on a parameter provided by higher layers. The relative RI

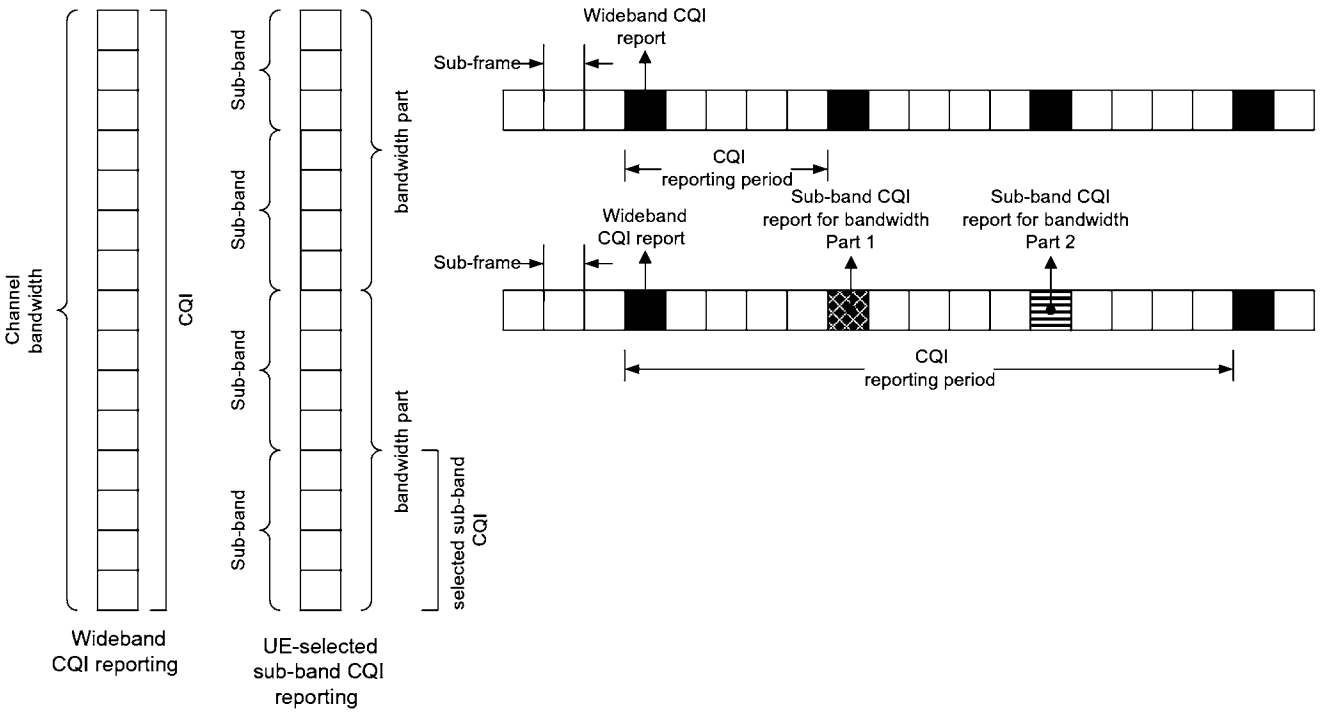


FIGURE 10.33

Illustration of the concept of periodic CQI reporting modes in time and frequency [14].

Table 10.15 Reporting Period, Reporting Offset, and Configuration Index of CQI/PMI and RI [5]

CQI/PMI Configuration Index	CQI/PMI Reporting Period P_{CQI}	CQI/PMI Reporting Offset N_{offset}^{CQI}
$0 \le \alpha \le 1$	2	α
$2 \le \alpha \le 6$	5	$\alpha-2$
$7 \le \alpha \le 16$	10	$\alpha-7$
$17 \le \alpha \le 36$	20	$\alpha-17$
$37 \le \alpha \le 76$	40	$\alpha-37$
$77 \le \alpha \le 156$	80	$\alpha-77$
$157 \le \alpha \le 316$	160	$\alpha-157$
$\alpha = 317$	Reserved	
$318 \le \alpha \le 349$	32	$\alpha-318$
$350 \le \alpha \le 413$	64	$\alpha-350$
$414 \le \alpha \le 541$	128	$\alpha-414$
$542 \le \alpha \le 1023$	Reserved	
RI configuration index	RI reporting period P_{RI}	RI reporting offset N_{offset}^{RI}
$0 \le \beta \le 160$	1	$-\beta$
$161 \le \beta \le 321$	2	$-(\beta-161)$
$322 \le \beta \le 482$	4	$-(\beta-322)$
$483 \le \beta \le 643$	8	$-(\beta-483)$
$644 \le \beta \le 804$	16	$-(\beta-644)$
$805 \le \beta \le 965$	32	$-(\beta-805)$
$966 \le \beta \le 1023$	Reserved	

reporting offset values are chosen in the range of $N_{offset}^{RI} \in \{0, -1, \ldots, -(P_{CQI}-1)\}$. If a UE is configured to report more than one CSI subframe set, then different sets of parameters corresponding to different subframe sets will be provided to the UE. When wideband CQI/PMI reporting is configured, the reporting instances satisfy the expression $(10n_f + \lfloor n_s/2 \rfloor - N_{offset}^{CQI}) \bmod P_{CQI} = 0$. When RI reporting is configured, the reporting interval is an integer multiple P_{RI} of period P_{CQI} subframes. The reporting instances for RI are subframes that satisfy the equation $(10n_f + \lfloor n_s/2 \rfloor - N_{offset}^{CQI} - N_{offset}^{RI}) \bmod (P_{CQI}P_{RI}) = 0$. When both wideband CQI/PMI and sub-band CQI reporting are configured, the reporting instances satisfy the equation $(10n_f + \lfloor n_s/2 \rfloor - N_{offset}^{CQI}) \bmod P_{CQI} = 0$. Figure 10.33 illustrates an example of wideband and sub-band CQI reporting. Reporting period, reporting offset, and configuration index of CQI/PMI and RI reports are listed in Table 10.15 [5].

In the case of collision of a CSI report with PUCCH reporting type 3, 5, or 6 of one serving cell with a CSI report with PUCCH reporting type 1, 1a, 2, 2a, 2b, 2c, or 4 of the same serving cell, the CSI report with PUCCH reporting type

(1, 1a, 2, 2a, 2b, 2c, or 4) has lower priority and will be dropped. If the UE is configured with more than one serving cell, it transmits a CSI report corresponding to only one serving cell in any given subframe.

10.7.2.3 PUCCH format 3

For downlink carrier aggregation and when there are simultaneous transmissions on multiple downlink component carriers, multiple HARQ feedback bits are generated and sent by the UE. As discussed earlier, PUCCH format 1b in conjunction with resource selection can be used in this case; however, if the number of HARQ feedback bits is greater than four, this method is not going to be an efficient solution from a performance perspective. In order to support efficient transmission of a larger number of HARQ feedback bits, PUCCH format 3, which was introduced in LTE Rel-10, can be used. The main distinction of PUCCH format 3, as illustrated in Figure 10.34, is DFT-precoded OFDM, i.e., the same transmission scheme used for the uplink transmission. The HARQ feedback bits, one or two per downlink component carrier, depending on the transmission mode configured for that particular component carrier, are concatenated with an SR bit into a sequence of bits where the bits corresponding to unscheduled transport blocks are set to zero. The concatenated bits are block coded and scrambled using a cell-specific scrambling sequence to randomize inter-cell interference.

The resulting 48 bits are QPSK-modulated and divided into two groups, one per slot, i.e., 12 QPSK symbols per slot. PUCCH format 3 employs two SC-FDMA symbols in each slot (with normal cyclic prefix) for reference signal transmission. In each slot, the block of 12 DFT-precoded QPSK symbols is transmitted in the remaining SC-FDMA symbols. To further randomize the inter-cell interference, a cyclic shift is applied to the block of 12 QPSK symbols prior to DFT precoding. The cyclic shifts vary from one symbol to another. To increase the multiplexing capacity, an orthogonal sequence of length 5 is multiplied by each of the five SC-FDMA symbols carrying data in a slot. As a result, up to five terminals may share the same resource-block pair for PUCCH format 3. Different orthogonal cover sequences are used in the two slots to improve the performance in high-Doppler scenarios. To enable channel estimation for different transmissions sharing the same resource block, different reference signal sequences are used.

The orthogonal cover sequences are obtained as five DFT sequences. A Walsh sequence of length 4 may be used in the second slot of a subframe in order to make the last SC-FDMA symbol available when SRS is configured in that subframe. Similar to other PUCCH formats, a PUCCH format 3 resource can be represented by a single index from which the orthogonal sequence and the resource-block number can be derived. A terminal can be configured with four different resources for PUCCH format 3. In the scheduling grant for a secondary component carrier, 2 bits are used to inform the terminal of the four resources. In that case, the scheduler can avoid PUCCH collisions between different terminals by assigning different resources to different UEs. Due to significant differences in

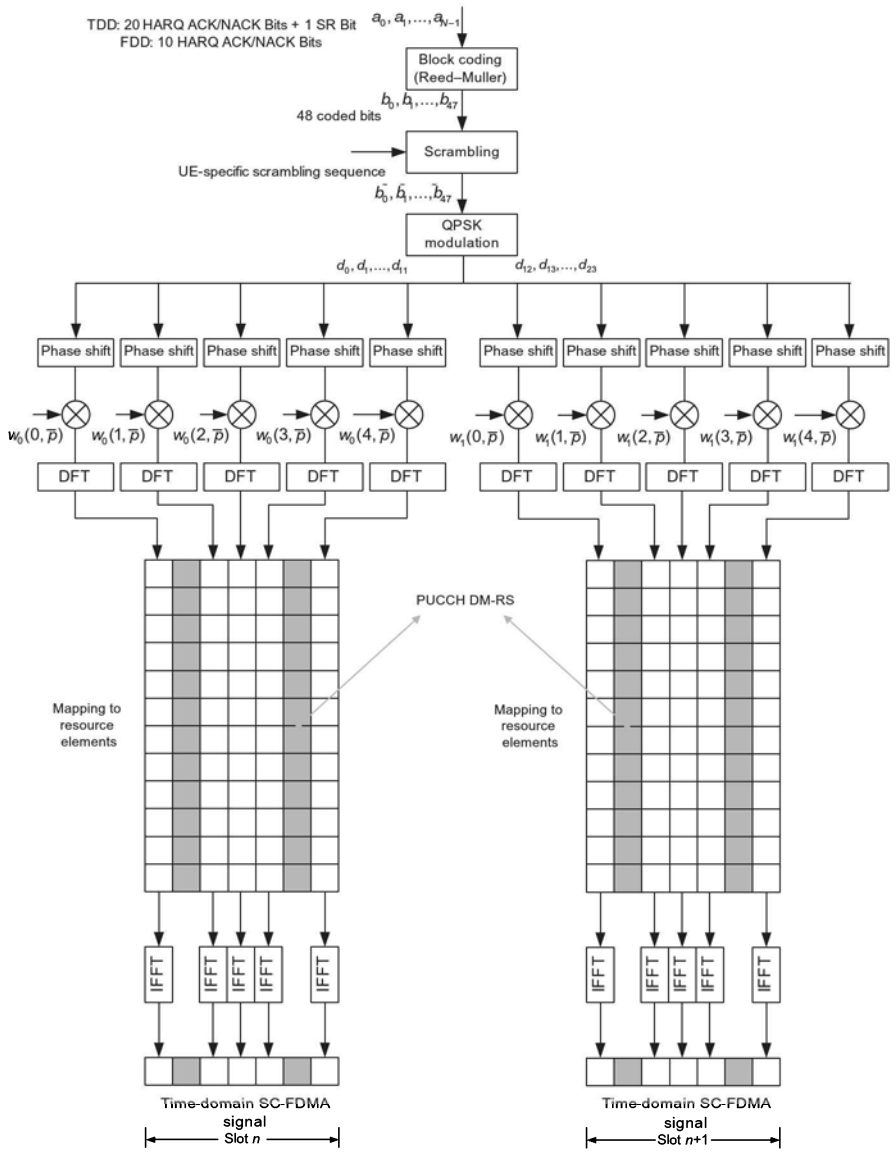


FIGURE 10.34

Illustration of PUCCH format 3 processing [14–16].

the structure of PUCCH format 3 compared to other PUCCH formats, resource blocks cannot be shared between them.

The physical layer processing of PUCCH format 3 can be described as follows. The block of coded bits $b_0, b_1, \ldots, b_{N_{\text{bit}}-1}$ are scrambled with a UE-specific

Table 10.16 Values of PUCCH Format 3 Orthogonal-Spreading Sequences [3]

Sequence Index n	Orthogonal Sequence $[w_0(0), w_1(0), \ldots, w_n(N_{SF}^{PUCCH}-1)]$	
	$N_{SF}^{PUCCH}=5$	$N_{SF}^{PUCCH}=4$
0	$[1 \quad 1 \quad 1 \quad 1 \quad 1]$	$[+1 \quad +1 \quad +1 \quad +1]$
1	$[1 \quad e^{j2\pi/5} \quad e^{j4\pi/5} \quad e^{j6\pi/5} \quad e^{j8\pi/5}]$	$[+1 \quad -1 \quad +1 \quad -1]$
2	$[1 \quad e^{j4\pi/5} \quad e^{j8\pi/5} \quad e^{j2\pi/5} \quad e^{j6\pi/5}]$	$[+1 \quad +1 \quad -1 \quad -1]$
3	$[1 \quad e^{j6\pi/5} \quad e^{j2\pi/5} \quad e^{j8\pi/5} \quad e^{j4\pi/5}]$	$[+1 \quad -1 \quad -1 \quad +1]$
4	$[1 \quad e^{j8\pi/5} \quad e^{j6\pi/5} \quad e^{j4\pi/5} \quad e^{j2\pi/5}]$	–

scrambling sequence, resulting in a block of scrambled coded bits $\bar{b}_0, \bar{b}_1, \ldots, \bar{b}_{N_{bit}-1}$ such that $\bar{b}_i = (b_i + c(i)) \bmod 2$, where the scrambling sequence $c(i)$ was defined in Chapter 9 and is initialized with $c_{init} = (\lfloor n_s/2 \rfloor + 1)(2N_{ID}^{cell} + 1)2^{16} + n_{RNTI}$ at the start of each subframe where n_{RNTI} denotes the UE temporary identifier C-RNTI. The block of scrambled bits is then QPSK-modulated, resulting in a block of complex-valued modulation symbols $d_0, d_1, \ldots, d_{N_s-1}$ in which $N_s = N_{bit}/2 = 12$. The complex-valued symbols $d_0, d_1, \ldots, d_{N_s-1}$ is block-wise spread with the orthogonal sequences $w_0(i, \bar{p})$ and $w_1(i, \bar{p})$, yielding $N_{SF_0}^{PUCCH} + N_{SF_1}^{PUCCH}$ sets containing 12 values where:

$$y_n^{\bar{p}}(i) = \begin{cases} w_0(\bar{n}, \bar{p}) \exp\left(j\pi \lfloor n_{cs}^{cell}(n_s, l)/64 \rfloor / 2\right) d_i & n < N_{SF_0}^{PUCCH} \\ w_1(\bar{n}, \bar{p}) \exp\left(j\pi \lfloor n_{cs}^{cell}(n_s, l)/64 \rfloor / 2\right) d_{i+12} & n \geq N_{SF_0}^{PUCCH} \end{cases} \tag{10.8}$$

where $\bar{n} = n \bmod N_{SF_0}^{PUCCH}; n = 0, 1, \ldots, N_{SF_0}^{PUCCH} + N_{SF_1}^{PUCCH} - 1; N_{SF_0}^{PUCCH} = N_{SF_1}^{PUCCH} = 5$; and $i = 0, 1, \ldots, 11$ in both slots in a subframe using normal PUCCH format 3 and $N_{SF_0}^{PUCCH} = 5; N_{SF_1}^{PUCCH} = 4$ in a subframe using shortened PUCCH format 3 to accommodate the SRS placement. The orthogonal sequences $w_0(i, \bar{p})$ and $w_1(i, \bar{p})$ are Walsh sequences whose values are given in Table 10.16.

Each set of the generated complex-valued symbols following the spreading function are cyclically shifted according to $\bar{y}_n^{\bar{p}}(i) = y_n^{\bar{p}}([i + n_{cs}^{cell}(n_s, l)] \bmod 12)$, where $n_{cs}^{cell}(n_s, l)$ is a cell-specific cyclic shift, n_s is the slot number within a radio frame, and l is the SC-FDMA symbol number within a slot. The cyclically shifted sets of complex-valued symbols are DFT-precoded according to:

$$z^{\bar{p}}(12n+k) = \frac{1}{\sqrt{12N_p}} \sum_{i=0}^{11} \bar{y}_n^{\bar{p}}(i) e^{-j\frac{\pi ik}{6}}; k = 0, 1, \ldots, 11; n = 0, 1, \ldots, N_{SF_0}^{PUCCH} + N_{SF_1}^{PUCCH} - 1 \tag{10.9}$$

where N_p is the number of antenna ports used for PUCCH format 3 transmission, resulting in a block of complex-valued symbols $z_0^{\bar{p}}, z_1^{\bar{p}}, \ldots, z_{11 \times (N_{SF_0}^{PUCCH} + N_{SF_1}^{PUCCH})}^{\bar{p}}$. The

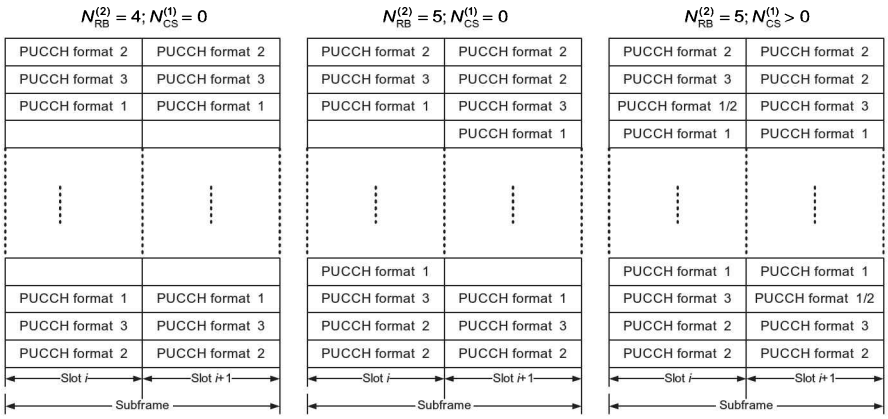


FIGURE 10.35

Example of resource-block allocation for various PUCCH formats [14].

amplitudes of the resulting complex-valued symbols are scaled in order to conform to the PUCCH transmit power, and are mapped in sequence starting with $z_0^{\bar{p}}$ to resource elements. PUCCH uses one resource block in each of the two slots in a subframe. Within the PRB used for PUCCH format 3 transmission, the mapping of complex symbols $z_i^{\bar{p}}|_{0,1,\ldots,11\times(N_{SF_0}^{PUCCH}+N_{SF_1}^{PUCCH})}$ to resource elements (k,l) on antenna port $\bar{p}$ that are not reserved for transmission of reference signals is in increasing order of the first index and then the second index, i.e., frequency first, starting with the first slot in the subframe. The relation between the antenna index $\bar{p}$ and the antenna port number p is given in 3GPP TS 36.211 [3]. In case of simultaneous transmission of SRS and PUCCH format 1, 1a, 1b, or 3 when there is one configured serving cell, a shortened PUCCH format is used where the last SC-FDMA symbol in the second slot of a subframe is skipped. Figure 10.35 shows an example of resource mapping for various PUCCH formats [14].

Precoder-based multi-layer transmission is only applied to uplink data transmission on PUSCH. LTE Rel-10 allows a terminal with multiple transmit antennas to use multi-antenna transmission for uplink control signaling on PUCCH, in order to achieve diversity gain. In that case, two-antenna transmit diversity is used for PUCCH transmission. The scheme is referred to as spatial orthogonal resource transmit diversity (SORTD). The main concept of SORTD is to transmit the uplink control signaling using different resources (time, frequency, and/or code) on different antennas. In principle, the PUCCH transmissions from the two antennas will be identical to PUCCH transmissions from two different terminals using different resources. Thus, SORTD provides additional diversity at the expense of using twice as many PUCCH resources compared to non-SORTD transmission. For four physical antennas at the terminal, implementation-specific antenna virtualization is used, where a transparent scheme is used to map the two-antenna-port signal to four physical antennas [16]. Figure 10.36 illustrates

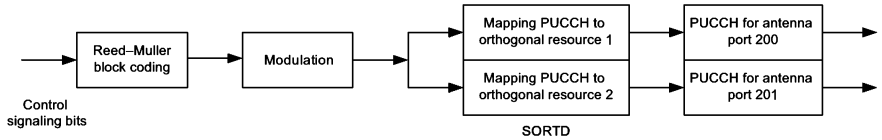


FIGURE 10.36

Illustration of SORTD concept [14,166].

PUCCH transmission using the SORTD concept [14]. SORTD is applicable to PUCCH formats 2/2a/2b and 3. The transmit diversity is not supported in LTE Rel-10 for PUCCH format 1b with channel selection. If the transmit antennas are uncorrelated, the SORTD scheme provides the optimal diversity performance at the expense of consuming extra resources which may reduce the PUCCH multiplexing capacity [15].

As mentioned earlier, PUCCH format 3 supports transmission of 48 coded bits. The actual number of HARQ feedback bits depends on the number of configured cells (active component carriers), the configured transmission modes of each carrier, and the HARQ ACK/NACK bundling window size (i.e., the number of downlink subframes associated with a single uplink subframe applicable to TDD systems). In FDD mode, the maximum payload size of ten HARQ ACK/NACK bits is supported corresponding to five component carriers each configured for MIMO transmission. In TDD mode, PUCCH format 3 supports HARQ feedback payload size of up to 20 bits. If the number of HARQ ACK/NACK bits is greater than 20, spatial bundling (i.e., a logical AND) of the ACK/NACK bits corresponding to the two codewords within a downlink subframe is performed for each of the serving cells. The maximum payload size carried by PUCCH format 3 in LTE Rel-10 is 21 bits, in which 20 bits are associated with HARQ ACK/NACK and 1 bit corresponds to SR. The HARQ feedback bits are concatenated in ascending order of the downlink component-carrier index. For payload sizes less than or equal to 11 bits, Reed–Muller channel codes from LTE Rel-8 are used in conjunction with circular-buffer rate-matching. When the payload size is larger than 11 bits, alternate ACK/NACK bits are input to two separate Reed–Muller encoders [15].

In order to alleviate inter-cell interference effects, cell-specific scrambling per SC-FDMA symbol was introduced. The PUCCH resource to be used for format 3 is signaled explicitly to the UE. A set of four resources is configured by RRC signaling, of which one resource is assigned dynamically for each ACK/NACK occurrence using an indicator transmitted in the transmit power control (TPC) field of the PDCCH corresponding to PDSCH on the secondary component carrier(s) [15]. The PDCCH assignments on the secondary component carriers in a given subframe indicate the same value. If transmit diversity is used for PUCCH format 3, higher-layer signaling is used to configure four pairs of PUCCH resources. The PDCCH assigning resources for the secondary cell PDSCH indicates one of these pairs to be used by the two antenna ports. If no PDCCH

corresponding to PDSCH on a secondary cell is received in a given subframe and a single PDSCH is received on the primary cell, a UE that is configured for PUCCH format 3 would instead use the LTE Rel-8 PUCCH format 1a or 1b.

10.7.3 Physical uplink shared channel

The PUSCH is used to transmit the uplink shared channel (UL-SCH) and L1/L2 control information. The UL-SCH is the transport channel used for transmitting uplink data (a transport block). The L1/L2 control signaling carries HARQ acknowledgments for received downlink shared channel (DL-SCH) transport blocks, channel quality reports, and SRs. The physical layer processing stages are shown in Figure 10.37. The information bits are channel coded by a turbo coder with a basic code rate of 1/3, which is adapted to a suitable code rate through a rate-matching process. This is followed by symbol-level channel interleaving which follows a simple time-first mapping where adjacent data symbols are mapped first to the adjacent SC-FDMA symbols in the time-domain and then across the sub-carriers. The coded and interleaved bits are then scrambled by a length-31 Gold code prior to modulation mapping, DFT-spreading, sub-carrier mapping, and OFDM modulation. The signal is frequency-shifted by half a sub-carrier prior to transmission, to avoid the distortion caused by the DC sub-carrier being concentrated in one resource block. The modulation schemes supported in the uplink are QPSK, 16QAM, and 64QAM (optional for lower UE categories). To generate the PUSCH payload, each transport block undergoes transport block coding. The encoding process includes 24-bit CRC calculation, code block segmentation and 24-bit CRC attachment to code segments (if any), turbo encoding, and rate-matching with redundancy and code block concatenation. Furthermore, coding of control signaling information is carried out with the resulting codewords time-multiplexed and interleaved with the UL-SCH data. The control information includes CQI, PMI, RI, and HARQ feedback.

The transport block size for PUSCH data transmission is signaled in the corresponding resource grant in PDCCH, i.e., DCI format 0 or LTE Rel-10 DCI format 4 for SU-MIMO. Combined with the MCS, the transport block size reflects the effective code rate. The permissible transport-block-size indices, MCSs, and RVs for PUSCH are given in Table 10.17. In most cases, a generally linear range of code rates are available for each resource allocation size. However, one exception is an index which allows a transport block size of 328 bits in a single resource-block allocation with QPSK modulation, which corresponds to a code rate greater than unity. This is primarily designed to support cell-edge VoIP transmissions using only one resource block per subframe, allowing the UE's power spectral density to be maximized for improved coverage, as well as using the TTI bundling where the transmission is repeated in four consecutive subframes, together with typically three retransmissions at 16 ms intervals [16].

Following the above summary, let us discuss the physical layer processing of the UL-SCH in more detail. When a transport block $a_0, a_1, \ldots, a_{N_A-1}$ of length N_A

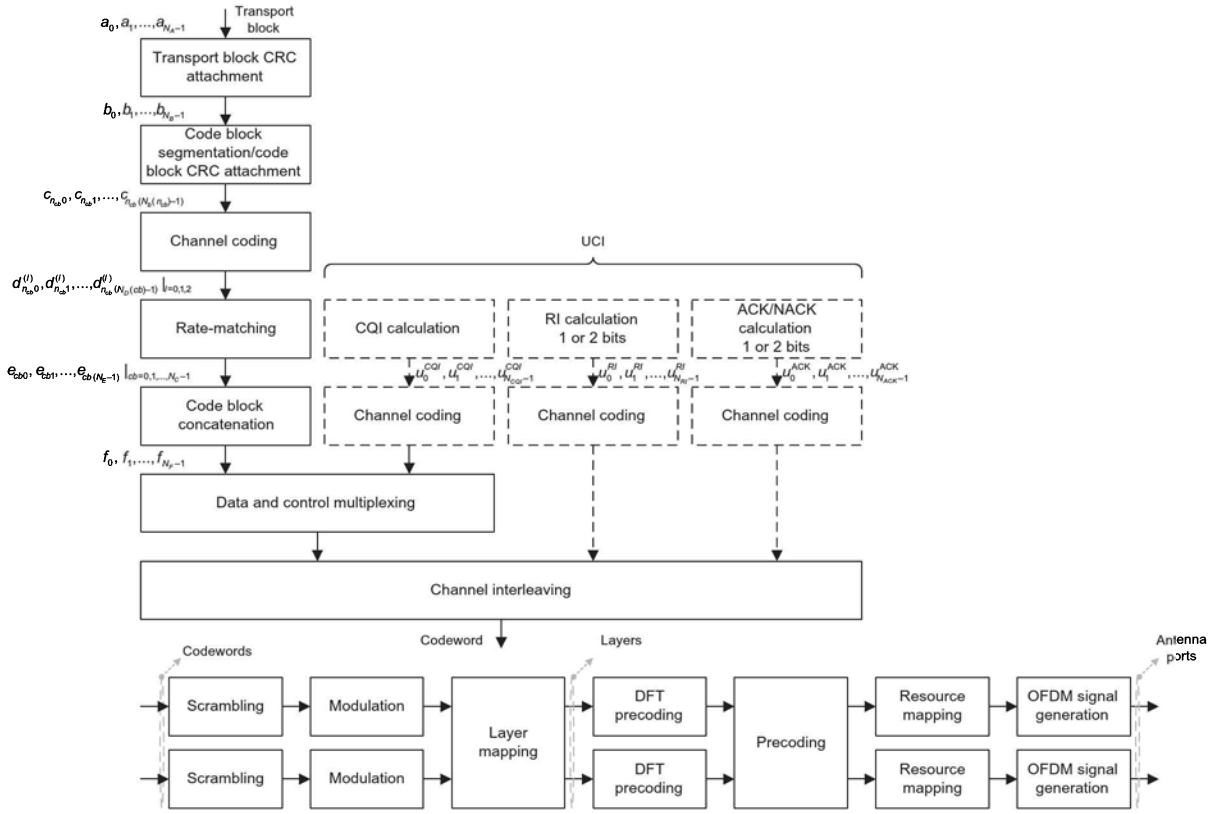


FIGURE 10.37

Physical layer processing for uplink shared channel [15,153].

Table 10.17 Modulation, Transport Block Size Index, and Redundancy Version for PUSCH [5]

MCS Index	Modulation Order	Transport Block Size Index	Redundancy Version
0	2	0	0
1	2	1	0
2	2	2	0
3	2	3	0
4	2	4	0
5	2	5	0
6	2	6	0
7	2	7	0
8	2	8	0
9	2	9	0
10	2	10	0
11	4	10	0
12	4	11	0
13	4	12	0
14	4	13	0
15	4	14	0
16	4	15	0
17	4	16	0
18	4	17	0
19	4	18	0
20	4	19	0
21	6	19	0
22	6	20	0
23	6	21	0
24	6	22	0
25	6	23	0
26	6	24	0
27	6	25	0
28	6	26	0
29	Reserved		1
30			2
31			3

is delivered to the physical layer, it is appended by 24 parity bits $p_0, p_1, \ldots, p_{23}$ where the entire transport block is used to calculate the CRC parity bits. The lowest order information bit a_0 is mapped to the most significant bit of the transport block. The 24 parity bits are calculated using the generator polynomial

$G_{\text{CRC-24A}}(D)$.[10] The CRC-attached bits $b_0, b_1, \ldots, b_{N_B-1}$ are fed to the code block segmentation unit, where $N_B = N_A + 24$ is the number of bits in the transport block including CRC (see Figure 10.37).

In LTE/LTE-Advanced, a minimum and maximum code block size is specified so that the block sizes are compatible with the block sizes supported by the turbo interleaver, where the minimum code block size is 40 bits and the maximum code block size is 6144 bits. If the length of the CRC-added input block is greater than the maximum code block size, the input block is segmented. When the input block is segmented, it is segmented into $N_C = \left\lceil N_B / (\underbrace{6144}_{\text{Maximum TB Size}} - \underbrace{24}_{\text{CRC Length}}) \right\rceil$ code blocks. Each code block is appended with 24-bit CRC. Padding bits are appended to the beginning of the segment (if required) so that the code block sizes match a set of valid turbo interleaver block sizes. If no segmentation is needed, then only one code block is produced. If N_B is less than the allowed minimum code block size, then zeros are added to the beginning of the code block in order to attain a total of 40 bits. Figure 10.38 illustrates the code segmentation and second CRC attachment process.

The code block segments, following the code block segmentation function, are denoted by $c_{n_{\text{cb}}0}, c_{n_{\text{cb}}1}, \ldots, c_{n_{\text{cb}}(N_b(n_{\text{cb}})-1)}$, where n_{cb} denotes the code block number and $N_b(n_{\text{cb}})$ is the number of bits in the code block number n_{cb}. The code blocks are appended with 24-bit CRC and are fed to the channel coding block. The total number of code blocks is denoted by N_C and each code block is individually turbo-coded.

The code block segments then go through turbo coding. Turbo coding is a form of forward error correction which improves the transmission reliability and robustness by adding redundancy to the code. The turbo encoder scheme used is a parallel concatenated convolutional code (PCCC)[11] with two recursive convolutional coders and a contention-free QPP interleaver, as shown in Figure 10.39. The encoder generates three output streams $d_k^{(0)}, d_k^{(1)}, d_k^{(2)}$, achieving a code rate of 1/3. Turbo-coded blocks are delivered to the rate-matching block. As shown in Figure 10.39, the input to the first constituent encoder is the input bit stream to the turbo coding block. The input to the second constituent encoder is the output of the QPP interleaver, i.e., a permutated version of the input sequence. The role of the interleaver is to spread the information bits such that in the event of a burst error, the two code streams are affected differently allowing data to be recoverable. There are two output sequences from each encoder: a systematic (x_k, x_k') output and a parity (z_k, z_k') output. Only one of the systematic sequences, x_k is used

[10] $G_{\text{CRC-24A}}(D) = D^{24} + D^{23} + D^{18} + D^{17} + D^{14} + D^{11} + D^{10} + D^7 + D^6 + D^5 + D^4 + D^3 + D + 1$.

[11] The first class of turbo code was the PCCC. Since the introduction of the original parallel turbo codes in 1993, many other classes of turbo code have been discovered, including serial versions and repeat-accumulate codes. Iterative turbo decoding methods have also been applied to more conventional FEC systems, including Reed-Solomon corrected convolutional codes [28,54].

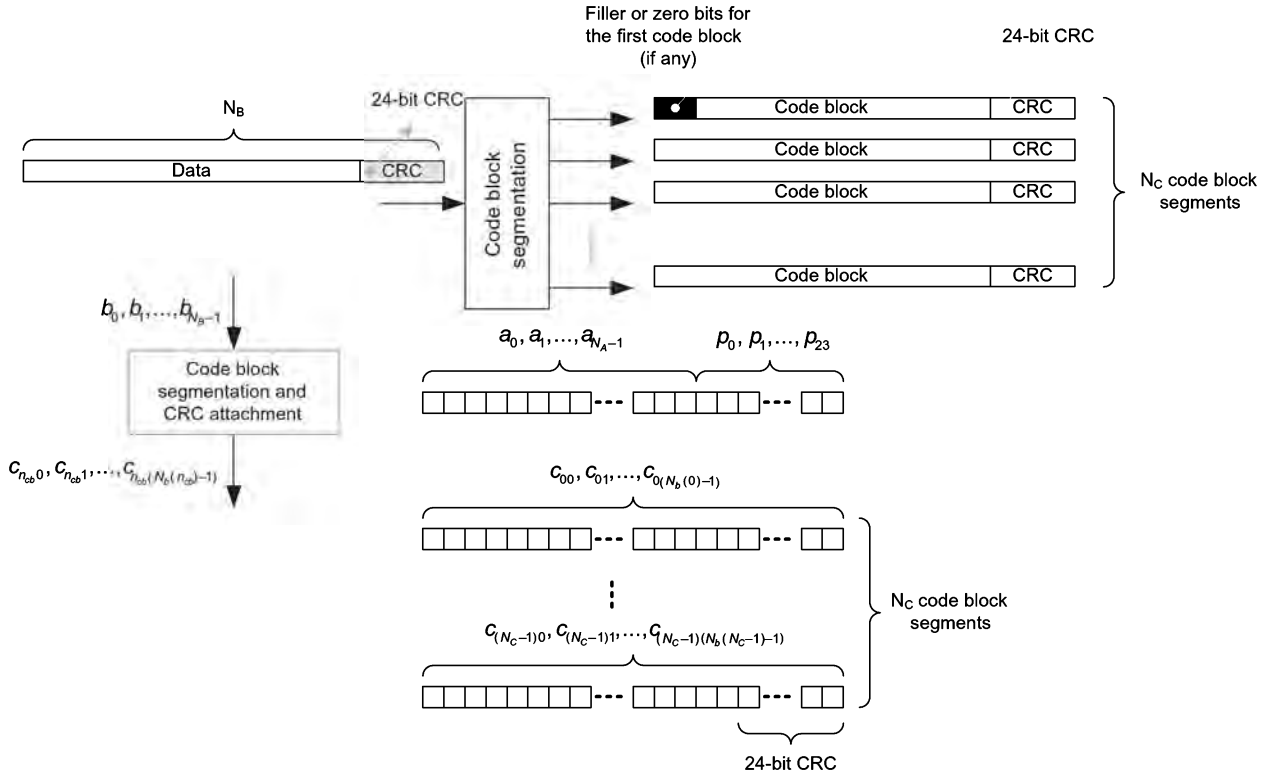


FIGURE 10.38

Code block segmentation and CRC attachment [4,153,155].

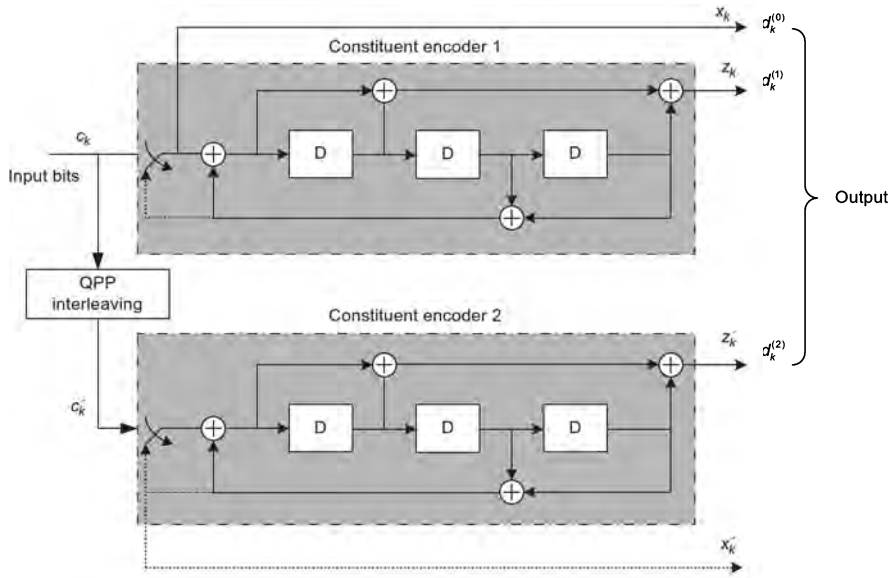


FIGURE 10.39

LTE/LTE-Advanced turbo encoder structure [4].

as an output, as the other x'_k is simply a permutated version of the chosen systematic sequence. After the turbo coding procedure, the output bits are denoted by $d^{(i)}_{n_{cb}0}, d^{(i)}_{n_{cb}1}, \ldots, d^{(i)}_{n_{cb}(N_D-1)}|_{i=0,1,2}$, where $N_D = N_{cb} + 4$ denotes the number of bits in the ith coded stream for code block number n_{cb}.

Note that a standard convolutional coder initializes its internal registers to an all-zeros state and ensures that the coder finishes in an all-zeros state by padding the end of the input sequence with $L_{\text{constraint-length}}$ zeros. Since the decoder has prior knowledge of the start and end state of the encoder, it can decode the data. Driving a recursive coder to an all-zeros state using this method is not possible. To overcome this problem trellis termination is used. A tail-biting convolutional coder initializes its internal shift registers to the last $L_{\text{constraint-length}}$ bits of the current input block, rather than an all-zeros state. This means that the start and end states are the same without the need to append zeros to the input block, eliminating the unnecessary overhead to terminate the coder by padding the input with zeros. The drawback to this method is that the decoder becomes more complicated since the initial state is unknown. However, it is known that the start and end sequences are the same [28]. Note that the number of output bits N_D following tail-biting convolutional coding with rate 1/3 is $N_D = N_{cb}$. The tail-biting convolutional coding with different rates is used for coding of control information in the downlink and uplink [4] (Figure 10.40).

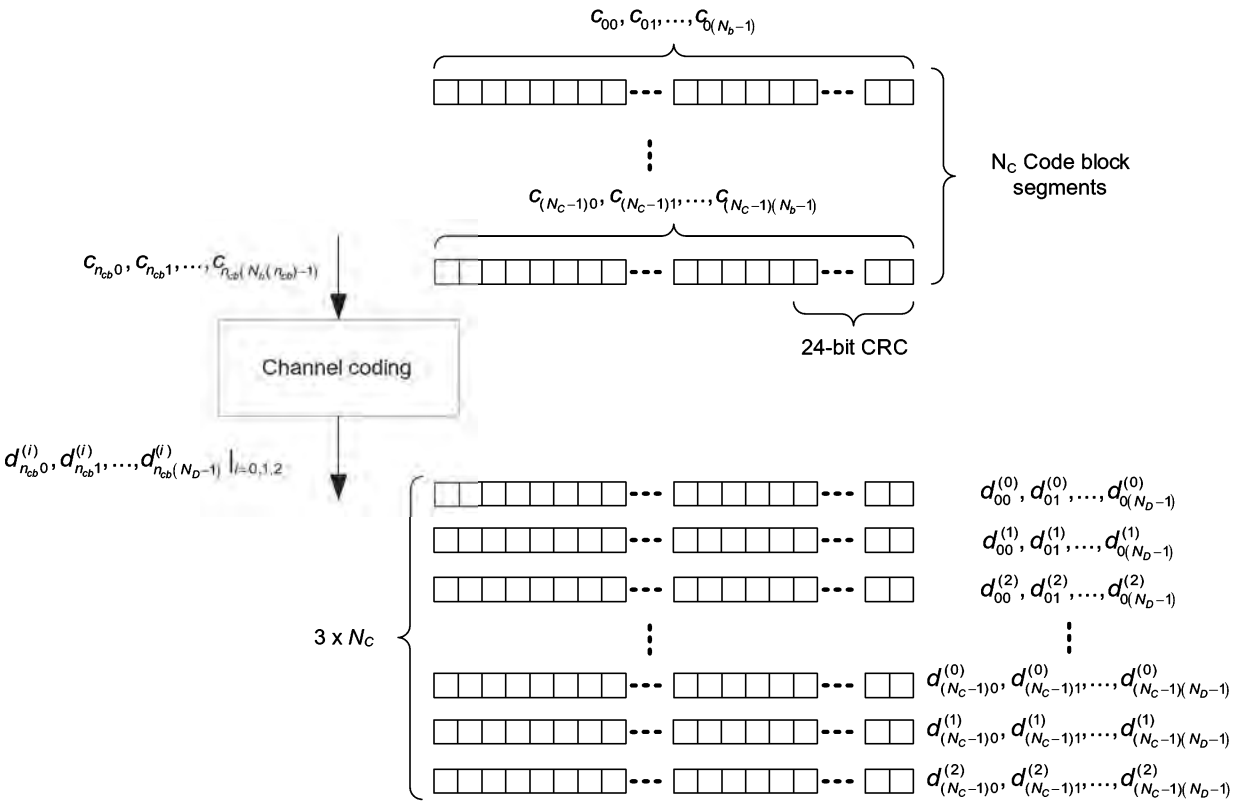


FIGURE 10.40

Demonstration of the channel coding process in LTE/LTE-Advanced [153].

The rate-matching block creates an output bit stream with a desired code rate. As the number of bits available for transmission depends on the available resources, the rate-matching algorithm is capable of producing any arbitrary rate. The 3-bit streams from the turbo encoder are interleaved, followed by bit collection to create a circular buffer. Bits are selected and pruned from the buffer to create an output bit stream with the desired code rate. The process is illustrated in Figure 10.41. The three sub-block interleavers used in the rate-matching block are identical. Interleaving is a technique to reduce the impact of burst errors on a signal, as consecutive bits of data will not be corrupted. The sub-block interleaver reshapes the encoded bit sequence in a row-by-row fashion to form a matrix. The bit collection stage creates a virtual circular buffer by combining the three interleaved encoded bit streams. Bits are then selected and pruned from the circular buffer to create an output sequence length which meets the desired code rate.

The HARQ error correction scheme is incorporated into the rate-matching algorithm of LTE/LTE-Advanced. For any desired code rate, the coded bits are output serially from the circular buffer from a starting location, given by the RV, wrapping around to the beginning of the buffer, if the end of the buffer is reached and null bits are discarded. Different redundancy versions and hence starting points allow retransmission of selected data. Being able to select different starting points enables the two main methods of reassembling data at the receiver in the HARQ process. In chase combining, retransmissions contain the same data and parity bits, whereas in incremental redundancy, the retransmissions contain different redundancy information so that the receiver gains knowledge upon each retransmission. The rate-matched code blocks are now concatenated back together. This is done by sequentially concatenating the rate-matched blocks together to create the output of the channel coding.

The output of the rate-matching function $e_{\text{cb0}}, e_{\text{cb1}}, \ldots, e_{\text{cb}(N_E(cb)-1)}$, where cb denotes the code block index and $N_E(\text{cb})$ is the number of rate-matched bits for code block number cb, serves as input to the code block concatenation module, which sequentially concatenates the rate-matched blocks together to create the output of the channel coding $f_0, f_1, \ldots, f_{N_F-1}$, where N_F represents the total number of coded bits for transmission of the given transport block over N_l transmission layers. The latter excludes the bits used for control information when it is multiplexed with UL-SCH data. The control information comprises CQI (and/or PMI), HARQ ACK/NACK, and RI. Different coding rates for the control information are achieved by allocating a different number of coded symbols for its transmission (Figure 10.42).

As shown in Figure 10.37, when control data is transmitted in PUSCH, the channel coding procedures for HARQ feedback $u_0^{\text{ACK}}, u_1^{\text{ACK}}, \ldots, u_{N_{\text{ACK}}-1}^{\text{ACK}}$, RI information $u_0^{\text{RI}}, u_1^{\text{RI}}, \ldots, u_{N_{\text{RI}}-1}^{\text{RI}}$, and CQI information $u_0^{\text{CQI}}, u_1^{\text{CQI}}, \ldots, u_{N_{\text{CQI}}-1}$ are performed independently.

An important issue related to transmission of control signaling on PUSCH is how to maintain the performance/reliability of control signaling at the desired level. It is noted that power control will set the SINR target of PUSCH according

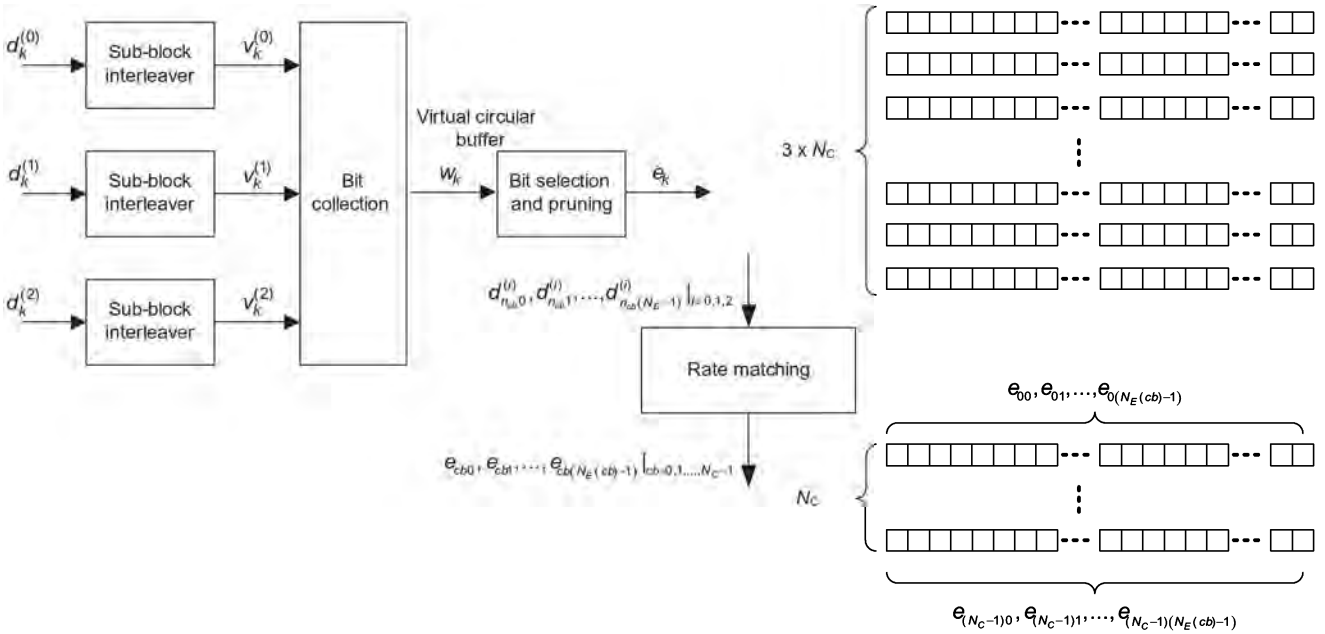


FIGURE 10.41

LTE/LTE-Advanced rate-matching procedures [4].

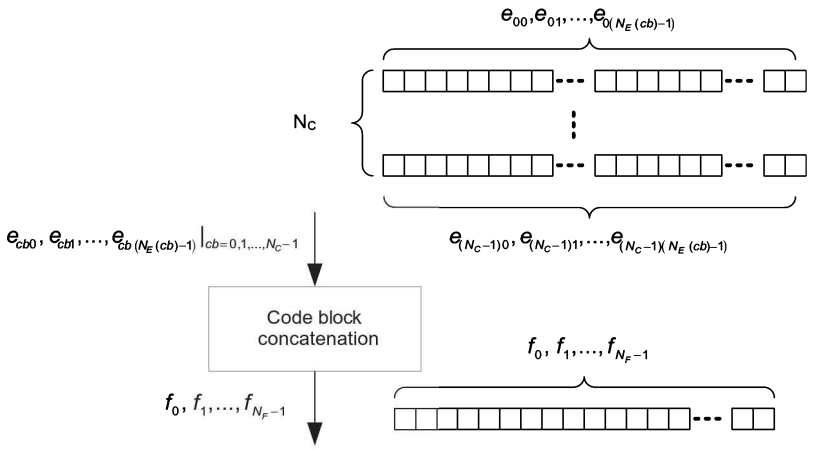


FIGURE 10.42

Illustration of code block concatenation.

to the data channel. Therefore, the control channel has to adapt to the SINR operating point set for data. One way to adjust the available resources would be to apply different power offset values for data and control parts. The problem with the latter power adjustment scheme is that the single-carrier property of the uplink signal is compromised. Therefore, this scheme is not used in the LTE uplink control and data multiplexing. Instead, a scheme based on a variable coding rate for the control information is used. This is achieved by varying the number of coded symbols for control channel transmission. To minimize the overall overhead related to inclusion of the control signaling information, the size of physical resources allocated to control transmission is scaled according to PUSCH quality. Note that the coding rate of control signaling, in this case, is given implicitly by the MCS of PUSCH data.

When the UE transmits HARQ feedback or RI bits, it is required to determine the number of coded modulation symbols per layer N_Q for HARQ ACK/NACK or RI. When only a single transport block is transmitted in PUSCH containing HARQ feedback or RI bits, the number of modulation symbols per layer is determined using the following equation [4]:

$$N_Q = \min\left(\left\lceil \frac{N_x N_{\text{sc}}^{\text{PUSCH-initial}} N_s^{\text{PUSCH-initial}} \beta_{\text{offset}}^{\text{PUSCH}}}{\sum_{\text{cb}=0}^{N_C-1} N_{\text{cb}}} \right\rceil, \; 4\, N_{\text{sc}}^{\text{PUSCH}}\right) \tag{10.10}$$

where $N_x = N_{\text{ACK}}$ or N_{RI} is the number of HARQ ACK/NACK bits or RI bits, $N_{\text{sc}}^{\text{PUSCH}}$ is the number of sub-carriers associated with scheduled PUSCH transmission over one SC-FDMA symbol, and $N_s^{\text{PUSCH-initial}}$ is the number of SC-FDMA symbols per subframe for initial PUSCH transmission for the same transport

block, given by $N_s^{\text{PUSCH-initial}} = \left[2(N_s^{\text{UL}} - 1) - N_{\text{SRS}}\right]$, in which $N_{\text{SRS}} = 1$, if the UE transmits PUSCH and SRS in the same subframe for initial transmission, or if the PUSCH resource allocation for initial transmission even partially overlaps with the cell-specific SRS subframe and bandwidth configuration, or if the subframe for initial transmission is a UE-specific type-1 SRS subframe; otherwise $N_{\text{SRS}} = 0$. The parameters $N_{\text{sc}}^{\text{PUSCH-initial}}$, N_C, and N_{cb} are obtained from the initial PDCCH/ePDCCH for the same transport block. For the case where two transport blocks are transmitted in PUSCH containing HARQ feedback or RI bits, the number of modulation symbols per layer is determined by $N_Q = \max[\min(N'_Q, 4N_{\text{sc}}^{\text{PUSCH}}), \min(N_Q)]$ [5].

The offset parameter $\beta_{\text{offset}}^{\text{PUSCH}}$ is used to adjust the quality of control signals for the PUSCH data channel. It is a UE-specific parameter configured by higher layer signaling. Different control channels need their own offset-parameter setting. There are some issues that need to be taken into consideration when configuring the offset parameter as follows [17]:

- BLER operation point for the PUSCH data.
- BLER operation point for the L1/L2 control signaling.
- Difference in coding gain between control and data parts, due to different coding schemes and different coding block sizes (no coding gain with 1-bit ACK/NACK).

Different BLER operating points for data and control parts are due to the fact that HARQ is used for the data channels, whereas the control channels do not benefit from HARQ. The higher the difference in the BLER operating point between data and control channels, the larger is the offset parameter (and vice versa). Similar behavior also relates to the packet size. The highest offset values are needed with ACK/NACK signals due to the lack of coding gain.

The number of coded symbols N_Q used by the UE to transmit the HARQ feedback is determined using the number of HARQ bits (1 or 2 depending on the number of codewords in use), the scheduled PUSCH bandwidth expressed as a number of sub-carriers, the number of SC-FDMA symbols per subframe for the initial PUSCH transmission, and information obtained from the initial PDCCH/ePDCCH for the same transport block. Each positive ACK is encoded as "1", and NACK is encoded as "0." If HARQ feedback consists of a single bit of information u_0^{ACK}, corresponding to a single codeword, then it is encoded depending on the modulation order used for the transport block, e.g., if the transport block is modulated using 16QAM, then encoded HARQ feedback is represented as $\begin{bmatrix} u_0^{\text{ACK}} & * & * & * \end{bmatrix}$. If the HARQ feedback consists of 2 bits of information $\begin{bmatrix} u_0^{\text{ACK}} & u_1^{\text{ACK}} \end{bmatrix}$, where u_0^{ACK} and u_1^{ACK} correspond to the first and second codewords, respectively, and $u_2^{\text{ACK}} = (u_0^{\text{ACK}} + u_1^{\text{ACK}}) \bmod 2$, then they are encoded depending on the number of coded symbols, e.g., if $N_Q = 2$ then the encoded HARQ feedback is represented as $\begin{bmatrix} u_0^{\text{ACK}} & u_1^{\text{ACK}} & u_2^{\text{ACK}} & u_0^{\text{ACK}} & u_1^{\text{ACK}} & u_2^{\text{ACK}} \end{bmatrix}$. For some values of N_Q, placeholders "*" are used to scramble the HARQ ACK/NACK

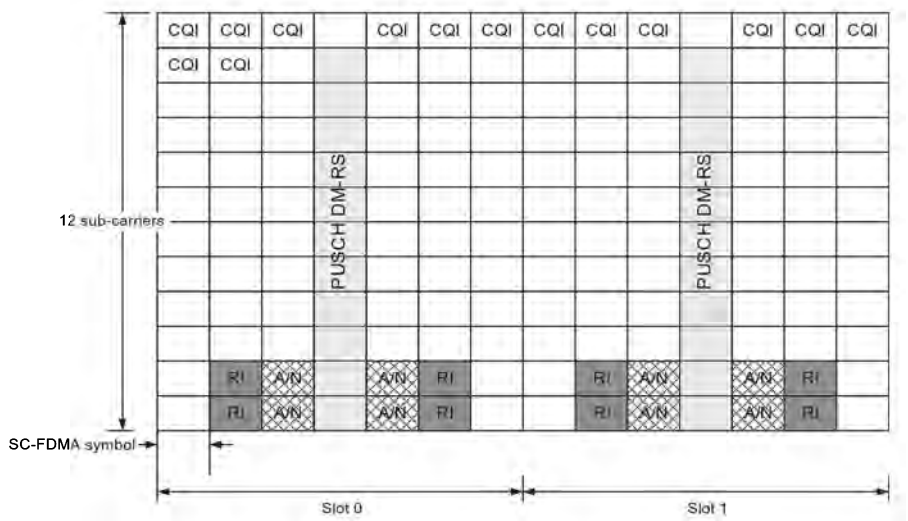


FIGURE 10.43

Multiplexing of control and data bits in PUSCH [15,16].

bits in such a way as to maximize the Euclidean distance of the modulation symbols carrying the HARQ information [4].

Let us further elaborate on the control and data multiplexing scheme on PUSCH. When a UCI is transmitted in a subframe in which the UE has been allocated resources on PUSCH, the UCI is multiplexed with the UL-SCH data prior to DFT operation in order to limit the uplink transmit power. In LTE Rel-8/9, UE is never allocated PUCCH and PUSCH in the same subframe. The number of resource elements reserved for transmission of the control bits in PUSCH is based on the MCS assigned for PUSCH and offset parameters $\beta_{\text{CQI-offset}}$, $\beta_{\text{HARQ-ACK-offset}}$, or $\beta_{\text{RI-offset}}$, which are semi-statically configured by higher layers. This would allow the use of different code rates for different types of UCI. The PUSCH data and UCI are never mapped to the same resource element. The UCI is mapped in such a way that it is present in both slots of the subframe. Since the eNB has prior knowledge of a UCI transmission, it can easily demultiplex the UCI and data. An example of multiplexing of CQI/PMI, HARQ ACK/NACK, and RI with the PUSCH data symbols to uplink resource elements is shown in Figure 10.43. As shown in the figure, the CQI/PMI symbols are mapped first followed by the data symbols. In this example, the RI bits occupy four symbols around DM-RS. The RI symbols are multiplexed with data symbols. The HARQ indicator (HI) ACK/NACK symbols are punctured into data symbols around DM-RS.

A modulation order similar to that used for UL-SCH data is applied to CQI/PMI. For small CQI and/or PMI report sizes up to 11 bits, a $(32, k)$ simplex code,[12] similar to the one used for PUCCH, is used, with optional circular repetition of encoded data and no CRC attached. For large CSI reports with greater than 11 bits, an 8-bit CRC is calculated and attached, and channel coding and rate-matching is performed using the tail-biting convolutional code.

The modulated HARQ ACK/NACK symbols are mapped immediately around the DM-RS position and modulated CQI/PMI symbols are time-first mapped across the subframe. The HARQ feedback resources are punctured into data starting from the lowest sub-carrier in the resource block. The maximum number of resources for HARQ ACK/NACK is four SC-FDMA symbols. In the case of 2-bit HARQ ACK/NACK, a $(3, 2)$ simplex coding is performed (see Table 10.18 for the mapping). The CQI resources are placed at the beginning of the data resources. For a CQI payload less than or equal to 11 bits, $(32, k)$ simplex code is used. For a CQI payload larger than 11 bits, tail-biting convolutional code is utilized. The RI bits are positioned next to the HARQ feedback bits in the resource block, irrespective of the presence or absence of HARQ ACK/NACK bits. In case of a 2-bit RI, a $(3, 2)$ simplex coding is employed.

The HARQ ACK/NACK resources are mapped to SC-FDMA symbols by puncturing the UL-SCH data. The positions next to the DM-RS are used in order to improve channel estimation. The maximum amount of resource for HARQ ACK/NACK is four SC-FDMA symbols. The coded RI symbols are placed next to the HARQ ACK/NACK symbol positions regardless of HARQ ACK/NACK presence in a given subframe. The modulation of 1- or 2-bit

Table 10.18 (3,2) Simplex Code for 2-Bit HARQ ACK/NACK and RI [15]

Input Bits	Output Bits
00	000
01	011
10	101
11	110

[12]Simplex codes belong to the family of linear error-correcting or error-detecting block codes that are simply implemented as polynomial codes by means of shift registers. Considered as (n, k) codes, they have a codeword length of $2^k - 1$. The minimum Hamming distance of binary simplex codes is equal to 2^{k-1}. They can be regarded as Reed–Muller codes shortened by one digit and are identical to the m-sequences of length 2^{k-1}, together with the zero word. They are called simplex because their codewords form a simplex, i.e., a finite graph of k points (the vertices) or a geometric figure, in which every vertex is connected to every other vertex, e.g., a triangle, in Hamming space (a Hamming space is the set of all 2^n binary strings of length n) [28].

HARQ ACK/NACK or RI is such that the Euclidean distance of the modulation symbols carrying HARQ ACK/NACK and RI is maximized; therefore, the outermost constellation points of the higher-order modulations are used, resulting in increased transmit power for ACK/NACK/ and RI transmission relative to the average PUSCH data power. The coding of the RI and CQI/PMI are performed separately, with the UL-SCH data being rate-matched around the RI resource elements similar to the case of CQI/PMI. The reference CQI/PMI MCS is computed from the CSI payload size and resource allocation. The channel coding and rate-matching of the control signaling without UL-SCH data is the same as that of multiplexing control with UL-SCH data. It is possible for the network to configure a UE to repeat each HARQ ACK/NACK transmission in multiple consecutive subframes in order to improve the reliability of the ACK/NACK transmission from power-limited UEs at the cell-edge, particularly in large cell deployments. The number of subframes over which each ACK/NACK transmission is repeated is signaled to the UE by a UE-specific parameter. Therefore, four different channel coding methods may be applied to control signals that are transmitted on PUSCH as follows:

- Repetition coding when 1-bit ACK/NACK is transmitted.
- $(3, 2)$ simplex coding when 2-bit ACK/NACK or RI are transmitted.
- $(32, k)$ Reed–Muller block codes are used when CQI/PMI information is less than 11 bits.
- Tail-biting convolutional coding with basic code rate of 1/3 is used when CQI/PMI information is greater than 11 bits.

As shown in Figure 10.37, the block of bits $b_0^{cw}, b_1^{cw}, \ldots, b_{N_{bit}(cw)}^{cw}$, in which $N_{bit}(cw)$ denotes the number of bits transmitted in codeword cw on PUSCH in one subframe, are scrambled with a UE-specific scrambling sequence prior to modulation, resulting in a block of scrambled bits $\overline{b}_0^{cw}, \overline{b}_1^{cw}, \ldots, \overline{b}_{N_{bit}(cw)}^{cw}$. Note that each codeword is bit-wise multiplied with an orthogonal sequence and a UE-specific scrambling sequence to create a sequence of symbols for each codeword. The parameter $N_{bit}(cw)$ is the number of bits transmitted using codeword cw. The scrambling sequence is a pseudo-random sequence based on length-31 Gold sequence which is initialized using the radio network temporary identifier associated with PUSCH transmission n_{RNTI}, the cell identifier N_{ID}^{cell}, the slot number within the radio frame n_s, and the codeword index at the start of each subframe as $c_{init} = n_{RNTI}2^{14} + cw2^{13} + \lfloor n_s/2 \rfloor 2^9 + N_{ID}^{cell}|_{cw=0,1}$. Scrambling with a cell-specific sequence serves the purpose of inter-cell interference mitigation. When a base station descrambles a received bit stream with a known cell-specific scrambling sequence, interference from other cells will be descrambled incorrectly and therefore only appear as uncorrelated noise. The scrambled codeword undergoes QPSK, 16QAM, or 64QAM modulation to generate complex-valued symbols, which provides the flexibility to optimize the data transmission depending on the channel conditions.

For each codeword *cw*, the block of scrambled bits $\overline{b}_0^{cw}, \overline{b}_1^{cw}, \ldots, \overline{b}_{N_{bit}(cw)}^{cw}$ is modulated as described in 3GPP TS 36.211 [3], resulting in a block of complex-valued symbols $d_0^{cw}, d_1^{cw}, \ldots, d_{N_s(cw)}^{cw}$. The complex-valued modulation symbols for each of the codewords to be transmitted are mapped to one or two layers. Complex-valued modulation symbols $d_0^{cw}, d_1^{cw}, \ldots, d_{N_s(cw)}^{cw}$ associated with codeword *cw* are mapped to spatial layers $\mathbf{x}(i) = [x_0(i), x_1(i), \ldots, x_{N_l-1}(i)]^T|_{i=0,1,\ldots,N_s^l-1}$, where N_l is the number of layers and N_s^l is the number of modulation symbols per layer.

The precoding function in the uplink is not the same as that in the downlink (multi-antenna) precoding in LTE Rel-8/9. The block of complex-valued symbols $d_0^{cw}, d_1^{cw}, \ldots, d_{N_s(cw)}^{cw}$ is divided into $N_s(cw)/N_{sc}^{PUSCH}$ sets. Each set of size $N_{sc}^{PUSCH} = N_{DFT}$ corresponds to one SC-FDMA symbol. A DFT is then applied to each set, which is essentially the precoding part of the SC-FDMA modulation. The size of the DFT, i.e., the value of $N_{sc}^{PUSCH} = N_{DFT}$, must be a prime number that is a product of 2, 3, and/or 5 and satisfies the following equation $N_{RB}^{PUSCH} = 2^{\alpha_2}3^{\alpha_3}5^{\alpha_5} \leq N_{RB}^{UL}$, where α_2, α_3, and α_5 are a set of non-negative integers. The final stage in PUSCH physical layer processing is to map the symbols to the allocated physical resource elements. The allocation sizes are limited to values which are multiples of 2, 3, and 5 as described earlier. The latter limitation is imposed by the precoding stage. The symbols are mapped in increasing order beginning with sub-carriers, then SC-FDMA symbols. The SC-FDMA symbols carrying DM-RS or SRS are avoided during the mapping process. Figure 10.44 illustrates the order of mapping of the output of the precoder to the allocated resource blocks.

The codeword processing structure shown in Figure 10.37 includes enhancements that were added as part of LTE Rel-10, where the complex-valued symbols are mapped to one or more spatial layers following the baseband modulation. The layer mapping function maps the codeword(s) to spatial layer (s). For transmission on a single antenna port, a single layer is used and the antenna mapping is defined by $x_0(i) = d_0(i)|_{i=0,1,\ldots,N_s^l-1}$. For uplink spatial multiplexing, the number of layers N_l is less than or equal to the number of antenna ports N_p used for transmission of the PUSCH. The case of a single codeword mapped to multiple layers is only applicable when there are four antenna ports for PUSCH transmission [3].

As illustrated in Figure 10.37, the modulation symbols in units of $N_{sc}^{PUSCH} = 12N_{RB}^{PUSCH}$ symbols are fed to N_{sc}^{PUSCH} – point DFT, where N_{sc}^{PUSCH} denotes the number of sub-carriers assigned to the transmission of PUSCH. The reason for the precoding is to reduce the cubic metric of the transmitted signal. For LTE, the DFT size and thus the size of resource allocation is limited to products of integer powers of 2, 3, and 5 ($N_{RB}^{PUSCH} = 2^{\alpha_2}3^{\alpha_3}5^{\alpha_5} \leq N_{RB}^{UL}$, where α_2, α_3, and α_5 are non-negative integers). For each layer, the block of complex-valued symbols $x^{(l')}(0), x^{(l')}(1), \ldots, x^{(l')}(N_s^l - 1)|_{l'=0,1,\ldots,N_l-1}$ is divided into N_s^l/N_{sc}^{PUSCH} sets, each corresponding to one SC-FDMA symbol. The transform

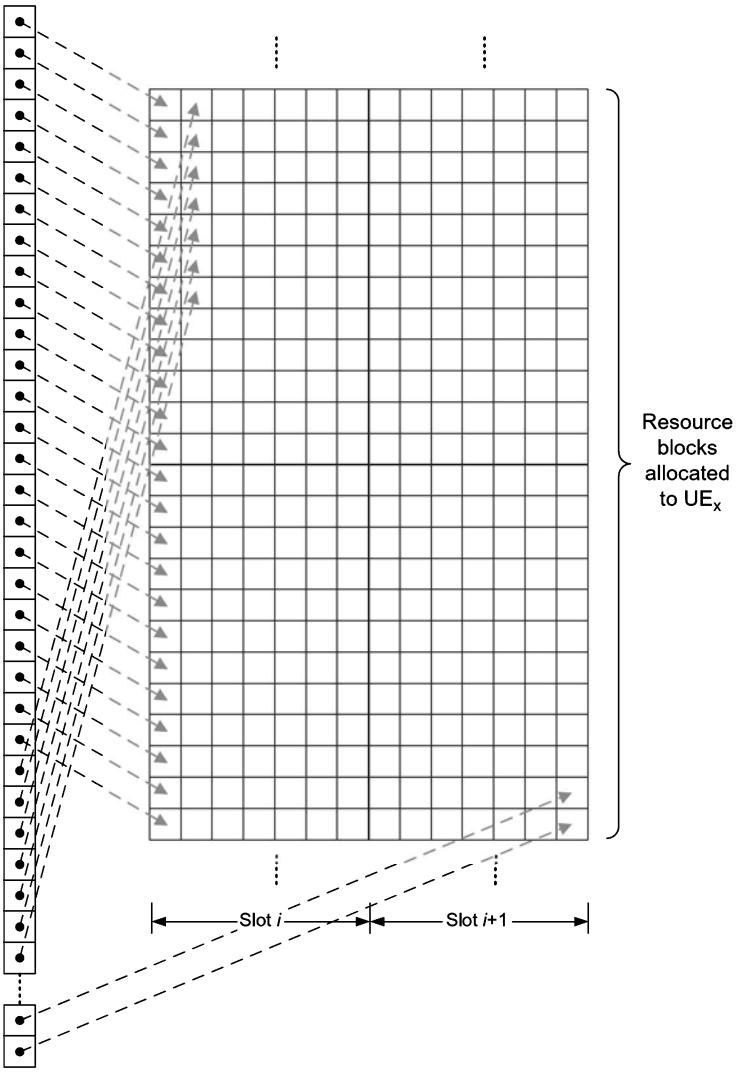


FIGURE 10.44

Example of mapping of the output of the precoder to resource elements in a subframe [155].

precoding is applied to each set, resulting in a block of complex-valued symbols $y^{(l')}(0), y^{(l')}(1), \ldots, y^{(l')}(N_s^l - 1)$ as follows (Table 10.19):

$$y^{(l')}(lN_{\text{sc}}^{\text{PUSCH}} + k) = \frac{1}{\sqrt{N_{\text{sc}}^{\text{PUSCH}}}} \sum_{i=0}^{M_{\text{sc}}^{\text{PUSCH}}-1} x^{(l')}(lN_{\text{sc}}^{\text{PUSCH}} + i)$$
$$\exp\left(-\text{j}\frac{2\pi ik}{N_{\text{sc}}^{\text{PUSCH}}}\right)\Big|_{k=0,1,\ldots,N_{\text{sc}}^{\text{PUSCH}}-1;l=0,1,\ldots,N_s^l/N_{\text{sc}}^{\text{PUSCH}}-1}$$

Table 10.19 Codeword-to-Layer Mapping for Uplink Spatial Multiplexing [3]

Number of Layers N_l	Number of Codewords N_{cw}	Layer Mapping $i = 0, 1, \ldots, M_s^l - 1$
1	1	$x_0(i) = d_0(i)$
2	1	$x_0(i) = d_0(2i)$ $x_1(i) = d_0(2i+1)$
2	2	$x_0(i) = d_0(i)$ $x_1(i) = d_1(i)$
3	2	$x_0(i) = d_0(i)$ $x_1(i) = d_1(2i)$ $x_2(i) = d_1(2i+1)$
4	2	$x_0(i) = d_0(2i)$ $x_1(i) = d_0(2i+1)$ $x_2(i) = d_1(2i)$ $x_3(i) = d_1(2i+1)$

The precoder module takes as input a block of vectors $\mathbf{y}(i) = (y^{(0)}(i), y^{(1)}(i), \ldots, y^{(N_l-1)}(i))^{\mathrm{T}}|_{i=0,1,\ldots,M_s^l-1}$ from the transform precoder, and generates a block of vectors $\mathbf{z}(i) = \mathbf{W}\mathbf{y}(i) = (z^{(0)}(i), z^{(1)}(i), \ldots, z^{(N_p-1)}(i))^{\mathrm{T}}|_{i=0,1,\ldots,M_s^p-1}$ that are mapped to resource elements. The precoding matrix $\mathbf{W}$ (codebook) is an $N_p \times N_l$ matrix and is given for $N_p = 2$ in Table 10.20 [3].

For each antenna port $\bar{p}$ that is used for transmission of PUSCH in a subframe, the block of complex-valued symbols $z^{(\bar{p})}(0), z^{(\bar{p})}(1), \ldots, z^{(\bar{p})}(M_s^p - 1)$ are multiplied with an amplitude scaling factor β_{PUSCH} in order to adjust the transmit power P_{PUSCH} and are then mapped sequentially, starting with $z^{(\bar{p})}(0)$, to PRBs on antenna port $\bar{p}$ assigned for transmission of PUSCH. The relation between the index $\bar{p}$ and the antenna port number p is given in 3GPP TS 36.211 [3]. The resource element (k, l) that is assigned to PUSCH information is required to meet certain criteria including the following:

- It is not used for transmission of reference signals.
- It is not part of the last SC-FDMA symbol in a subframe, if the UE transmits SRS in the same subframe.
- It is not part of the last SC-FDMA symbol in a subframe configured with cell-specific SRS, if the PUSCH transmission partly or fully overlaps with the cell-specific SRS bandwidth.
- It is not part of an SC-FDMA symbol reserved for possible SRS transmission in a UE-specific aperiodic SRS subframe.

The mapping to physical resource elements, as shown in Figure 10.44, is in increasing order of first, the sub-carrier (frequency) index k, and then the symbol

Table 10.20 Precoding Codebook for Transmission with Two Antenna Ports [3]

	Number of Layers	
Codebook Index	**Single Layer**	**Dual Layer**
0	$\frac{1}{\sqrt{2}}\begin{bmatrix}1\\1\end{bmatrix}$	$\frac{1}{\sqrt{2}}\begin{bmatrix}1 & 0\\0 & 1\end{bmatrix}$
1	$\frac{1}{\sqrt{2}}\begin{bmatrix}1\\-1\end{bmatrix}$	–
2	$\frac{1}{\sqrt{2}}\begin{bmatrix}1\\j\end{bmatrix}$	–
3	$\frac{1}{\sqrt{2}}\begin{bmatrix}1\\-j\end{bmatrix}$	–
4	$\frac{1}{\sqrt{2}}\begin{bmatrix}1\\0\end{bmatrix}$	–
5	$\frac{1}{\sqrt{2}}\begin{bmatrix}0\\1\end{bmatrix}$	–

(time) index l, starting with the first slot in the subframe. If uplink frequency hopping is disabled or the resource blocks allocated to PUSCH transmission are not contiguous in frequency, the set of PRBs to be used for transmission are identified by $n_{\text{PRB}} = n_{\text{VRB}}$, where n_{VRB} is obtained from the uplink scheduling grant. If uplink frequency hopping with a predefined hopping pattern is enabled, the set of PRBs used for PUSCH transmission in slot n_s is identified by the scheduling grant along with a predefined pattern according to the following equation [3]:

$$\underbrace{n'_{\text{PRB}}(n_s)}_{\substack{\text{Allocated PRB with adjusted indexing starting at 0 following PUCCH allocation}}} = \left(\underbrace{n'_{\text{VRB}}}_{\substack{\text{Allocated VRB with adjusted indexing starting at 0 following PUCCH allocation}}} + \underbrace{f_{\text{hopping}}(i)L_{\text{sub-band}}}_{\text{Hopping function}} + \underbrace{\left((L_{\text{sub-band}}-1)-2(n'_{\text{VRB}} \bmod L_{\text{sub-band}})\right)f_{\text{mirror}}(i)}_{\text{Mirroring function}} \right) \bmod (L_{\text{sub-band}}N_{\text{sub-band}}) \tag{10.11}$$

In the above equation $i = \lfloor n_s/2 \rfloor$ for the case of inter-subframe hopping and $i = n_s$ for the case of intra- and inter-subframe hopping, $n_{\text{PRB}}(n_s) = n'_{\text{PRB}}(n_s) + \lceil N_{\text{RB}}^{\text{offset}}/2 \rceil | N_{\text{sub-band}} > 1$, and $n'_{\text{VRB}} = n_{\text{VRB}} - \lceil N_{\text{RB}}^{\text{offset}}/2 \rceil | N_{\text{sub-band}} > 1$. The parameter n_{VRB} is obtained from the scheduling grant and PUSCH hopping offset $N_{\text{RB}}^{\text{offset}}$ is provided by the higher layers. The size of each sub-band is given as $L_{\text{sub-band}} = \lfloor (N_{\text{RB}}^{\text{UL}} - N_{\text{RB}}^{\text{offset}} - N_{\text{RB}}^{\text{offset}} \bmod 2)/N_{\text{sub-band}} \rfloor | N_{\text{sub-band}} > 1$. The number

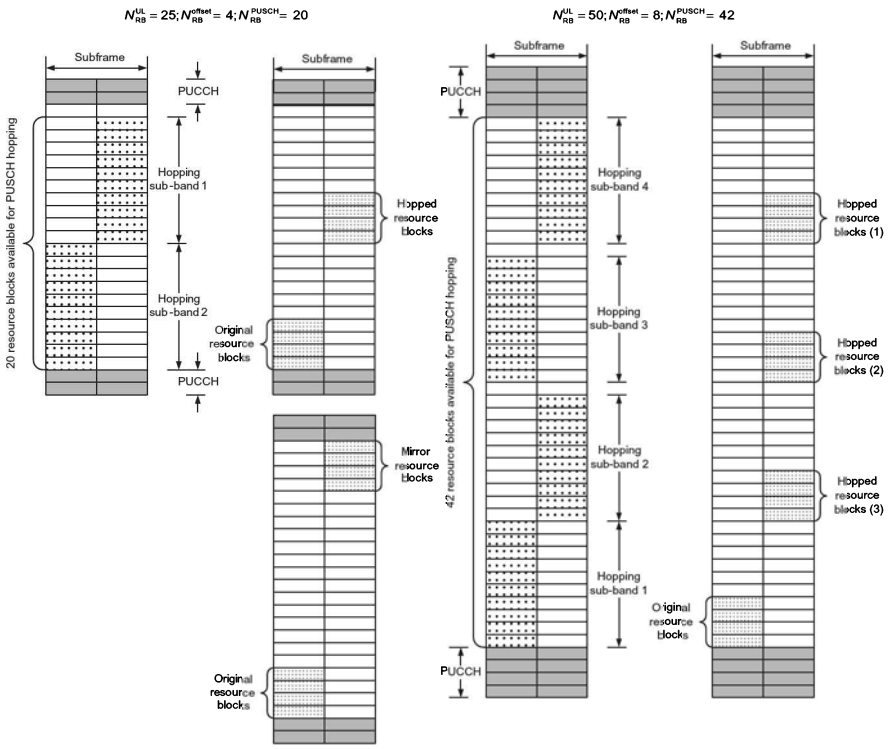


FIGURE 10.45

Example of PUSCH resource hopping/mirroring in 5 and 10 MHz channels [14].

of sub-bands $N_{\text{sub-band}}$ is signaled by the higher layers. The binary function $f_{\text{mirror}}(i) \in \{0, 1\}$ determines if the mirroring function is used.

In the above equation, the component identified as hopping function shifts the VRB allocation by an integer number of sub-bands. The shift is defined using a pseudo-random sequence which can be calculated by the UE and the eNB. In type 1 frame structure, the pseudo-random sequence is initialized using the physical layer cell identity $N_{\text{ID}}^{\text{cell}}$, whereas in type 2 frame structure, the pseudo-random sequence is initialized using a combination of the physical layer cell identity and the radio frame number $(2^9(n_f \bmod 4) + N_{\text{ID}}^{\text{cell}})$. The mirroring component in the above equation mirrors the VRB allocation within the sub-band. Mirroring is applied when the binary pseudo-random function $f_{\text{mirror}}(i) = 1$, which results in reflecting a VRB allocation starting "x" resource blocks from the bottom of the sub-band around the center of the sub-band such that the mirrored VRB allocation starts "x" resource blocks from the top of the sub-band (Figure 10.45). The pseudo-random mirroring component is initialized similar to the hopping component. Modular arithmetic is applied to the result of the hopping pattern function to provide wrap around, which ensures that the resource blocks after hopping remain within the boundaries of the subframe.

Note that in addition to the hopping pattern, there is also a cell-specific mirroring pattern defined in a cell. The mirroring pattern controls, on a slot-by-slot basis, whether mirroring within each sub-band should be applied to the assigned resource blocks. In principle, mirroring implies that the resource blocks within each sub-band are numbered in reversed order. Figure 10.45 illustrates an example of PUSCH resource allocations assuming 5 and 10 MHz channel bandwidth. In this example, PUCCH occupies four or eight resource blocks (depending on the bandwidth) in each slot, and the UE is informed through higher-layer signaling that those resource blocks are not available for hopping. The PUSCH hopping offset N_{RB}^{offset} is used for this purpose. The value of the hopping offset is rounded up to an even number, if the received value is not even.

As shown in Figure 10.45, there are two hopping modes specified in LTE/LTE-Advanced: (1) inter-subframe hopping where the resource blocks allocated by DCI format 0 are used for even-numbered transmission of uplink transport blocks, while hopped resource blocks are used for odd-numbered transmission of uplink resource blocks; and (2) intra- and inter-subframe hopping where the resource blocks allocated by DCI format 0 are used in the first time slot within the subframe while the hopped resource blocks are used in the second time slot [14].

10.7.4 Physical random-access channel

The physical random access channel is used by non-synchronized UEs during initial system access, handover, and prior to downlink data transmission. The UE transmits a preamble sequence over PRACH, which may be randomly selected from a group of sequences assigned by the eNB. The structure of the sequence is shown in Figure 10.46. The sequences are Zadoff–Chu sequences of length 839 for the FDD mode (139 for TDD mode). There are 64 different cyclic shifts that are generated from each root Zadoff–Chu sequence with zero cross-correlation. Therefore, different cyclic shifts of the base sequence are mutually orthogonal. The PRACH resource consists of six consecutive resource blocks. The location of PRACH is indicated by an offset parameter signaled by higher layers. There is one PRACH region per subframe in the FDD mode. Multiple UEs can access the PRACH region using different preambles. The UEs may select preambles randomly, which may result in a collision. Therefore, contention resolution mechanisms are necessary. The PRACH may not always present in every subframe and every radio frame. The PRACH configuration parameter indicates frame number and subframe numbers in which the PRACH resource is available.

The sub-carrier spacing for PRACH transmission is different from that of other channels in the uplink. The number of sub-carriers is equal to the length of preamble (839 for the FDD mode and 139 for TDD). The sub-carrier spacing is 1.25 kHz, resulting in longer symbol duration of 800 μs for the FDD mode (133 μs for TDD mode). The sub-carrier spacing also results in an effective guard band because the entire 1.08 MHz (six resource blocks) is not used for PRACH transmission.

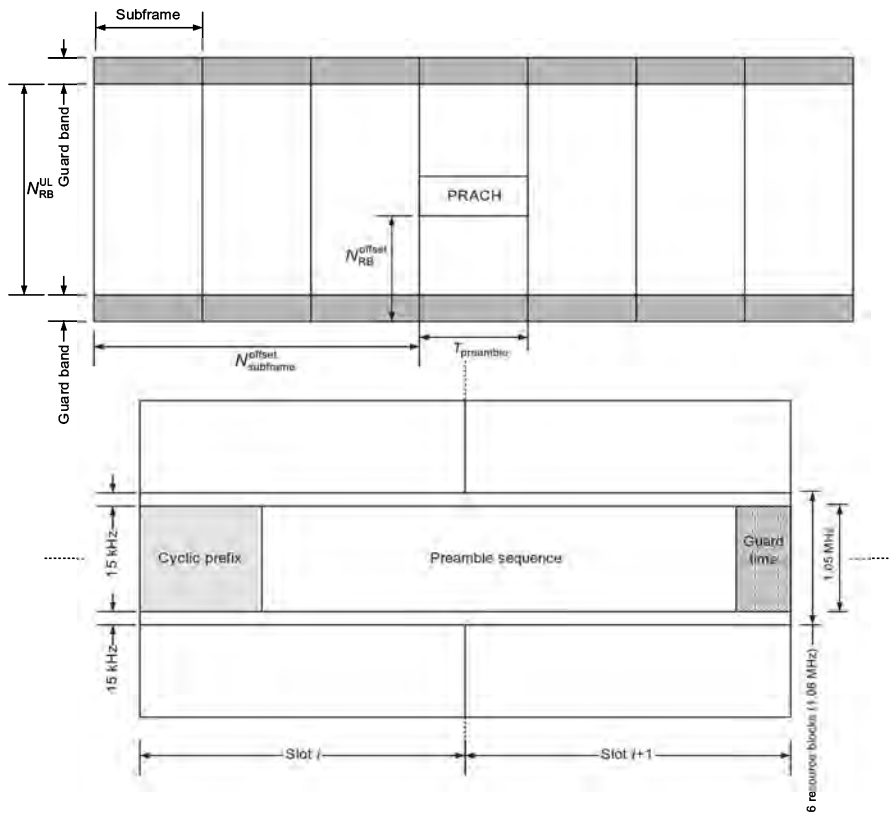


FIGURE 10.46

Structure of PRACH in time- and frequency-domain [14,153].

The PRACH preamble is an OFDM-based signal, but it is generated using a different structure from other uplink transmissions; most notably it uses narrower sub-carrier spacing which is not orthogonal to the PUSCH, PUCCH, and SRS; therefore, those channels will suffer from some interference from the PRACH. However, the sub-carrier spacing used by PRACH is an integer sub-multiple of the sub-carrier spacing used for the other channels, thereby PUSCH, PUCCH, and SRS do not interfere on the PRACH. Prior to initiation of the non-synchronized physical random-access procedure, the physical layer receives random-access channel parameters (i.e., PRACH configuration and time/frequency position), and parameters for determining the root sequences and their cyclic shifts in the preamble sequence set for the primary cell (i.e., index to logical root sequence table, cyclic shift N_{CS}, and whether set type is unrestricted or restricted) from the higher layers.

The PRACH preamble consists of a cyclic prefix, useful part of the sequence, and then a guard period which is simply an unused portion of time up to the end of the last subframe occupied by PRACH. This guard period allows for timing

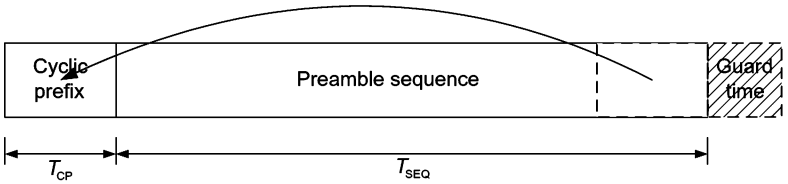


FIGURE 10.47

PRACH preamble structure in time.

uncertainty due to variability of the UE to eNB distance. Therefore, the size of the guard period determines the cell radius, as any propagation delay exceeding the guard time (GT) would cause the random-access preamble to overlap with the following subframe at the eNB receiver. The use of OFDM transmission with a cyclic prefix allows for implementation of an efficient frequency-domain-based receiver in the eNB to perform PRACH detection.

The UE aligns the start of the random-access preamble with the start of the corresponding uplink subframe at the UE, assuming a timing advance of zero. The preamble length is shorter than the PRACH slot in order to accommodate a gap for GT in order to absorb the variable propagation delay. Figure 10.48 shows two preambles received at the eNB with different timings depending on the propagation delay. The PRACH preamble sequence is optimized relative to its periodic autocorrelation property [15]. The random-access preamble, illustrated in Figure 10.47, consists of a cyclic prefix of length T_{CP} and a sequence of length T_{SEQ}. The parameter values are given in Table 10.21 and are configured by higher layers.

The transmission of the random-access preamble is triggered by the MAC sublayer and is restricted to certain time and frequency resources. These resources are identified in increasing order of the subframe number within the radio frame and the PRBs in the frequency-domain such that index 0 corresponds to the lowest numbered PRB and subframe within the radio frame. The PRACH resources within the radio frame are identified by a PRACH resource index. For frame structure type 1 with preamble formats 0–3, there is a maximum of one random-access resource per subframe. The start of the random-access preamble is aligned with the start of the corresponding uplink subframe at the UE assuming $N_{TA} = 0$, where N_{TA} is the length of the timing advance. The first PRB N_{RA} allocated to the PRACH transmission corresponding to preamble formats 0, 1, 2, and 3 is defined as $N_{RA} = N_{RA}^{offset}$, where the PRACH frequency offset parameter $0 \leq N_{RA}^{offset} \leq N_{RB}^{UL} - 6$ is defined as a PRB number configured by the higher layers (see Figure 10.46). For frame structure type 2 supporting PRACH preamble formats 0–4, there is a possibility for multiple random-access resources in an uplink subframe (or UpPTS for preamble format 4) depending on the uplink/downlink ratio. The PRACH sequence duration T_{SEQ} is chosen taking the following considerations into account (Table 10.22):

- There is a trade-off between sequence length and overhead, where on the one hand, the sequence length must be as long as possible to maximize the number

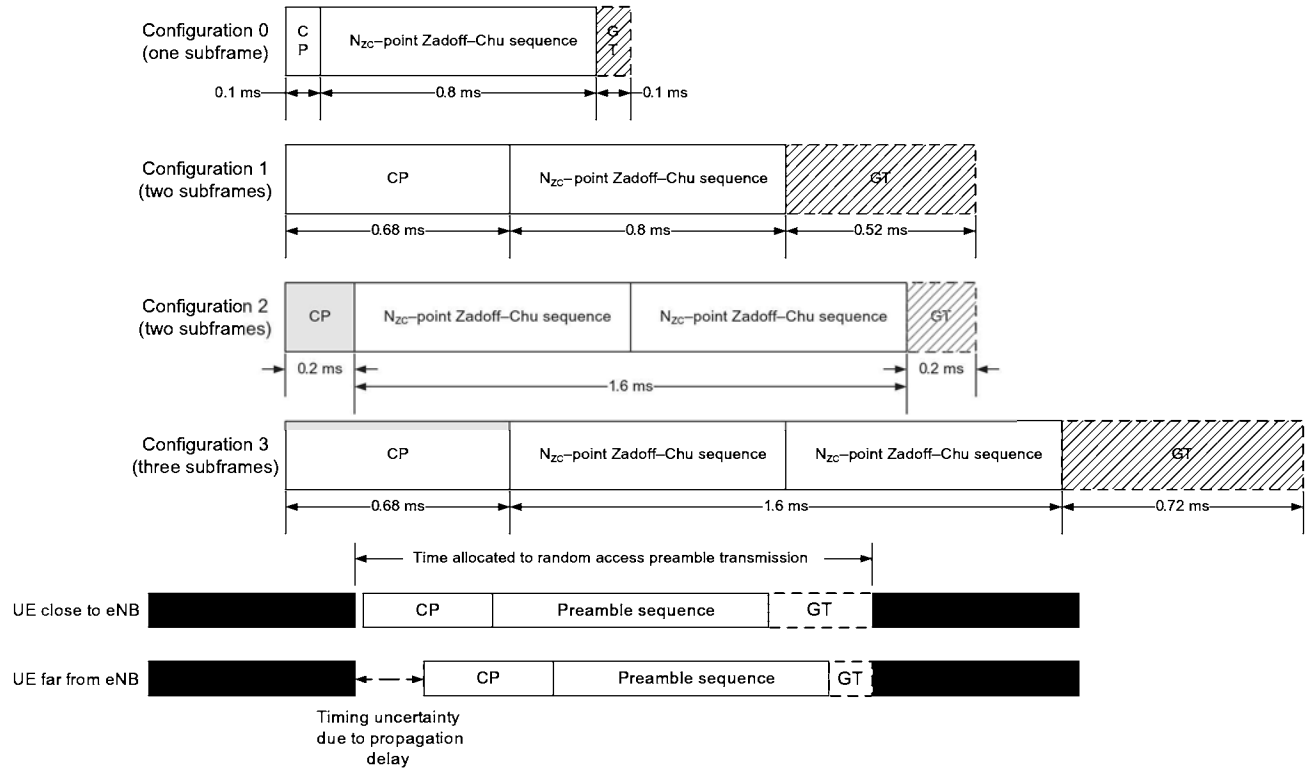


FIGURE 10.48

Illustration of PRACH preamble formats and mitigation of the impact of variable propagation delay on PRACH preamble [16].

Table 10.21 PRACH Preamble Parameters [3,14]

PRACH Preamble Format	Cyclic Prefix T_{CP}(μs)	Sequence Duration T_{SEQ}(μs)	Guard Time (μs)	Preamble Length (ms)	Maximum Supported Cell Range (km)
0	103.13	800	96.88	1	14.5
1	684.38	800	515.53	2	77.3
2	203.13	1600	196.88	2	29.5
3	684.38	1600	715.63	3	100.2
4[†]	14.58	133	9.38	0.16	1.4

[†]*Applicable to frame structure type 2 and special subframe configurations with UpPTS lengths of 142.71 μs (2 symbols with normal cyclic prefix) and 166.67 μs (2 symbols with extended cyclic prefix).*

of available orthogonal preambles, while on the other hand, the sequence must fit within a subframe in order to minimize the PRACH overhead. The lower bound for T_{SEQ} should support unambiguous round-trip time estimation for a UE located at the edge of the largest expected cell size including the maximum delay spread expected in such large cells.

- The length of the cyclic prefix must encompass the maximum round-trip delay and the maximum delay spread of the channel. Furthermore, for a cell-edge UE, the delay-spread energy at the end of the preamble is replicated at the end of the cyclic prefix, and is therefore within the preamble interval. Consequently, there is no need to include the maximum delay spread in the GT. Therefore, instead of locating the sequence in the center of the PRACH slot, it is shifted later by half of the maximum delay spread, allowing the maximum round-trip delay to be increased by the same amount. Note that, similar to a regular OFDM symbol, the residual delay spread at the end of the preamble from a cell-edge UE leaks into the next subframe, but this is taken care of by the cyclic prefix at the start of the next subframe to avoid any ISI.
- The sub-carrier spacing of PRACH and PUSCH must be numerically proportional. An additional benefit of this property is the possibility to reuse the FFT module from the SC-FDMA signal processing for PUSCH to implement the large DFT block involved in the PRACH transmitter and receiver. It is further desirable to minimize the orthogonality loss in the frequency-domain between the preamble sub-carriers and the sub-carriers of the adjacent uplink data transmissions. This is achieved if the PUSCH data symbol sub-carrier spacing Δf_{PUSCH} is an integer multiple of the PRACH sub-carrier spacing Δf_{RA}.
- Under a noise-limited scenario, which is typical in low density and medium to large suburban or rural cells, coverage performance can be estimated from a link budget calculation. Assuming an Okumura–Hata empirical model of

Table 10.22 Frame Structure Type 1 Random-Access Configuration [3]

Configuration Index	Preamble Format	System Frame Number (SFN)	Subframe Number	Configuration Index	Preamble Format	System Frame Number (SFN)	Subframe Number
0	0	Even	1	32	2	Even	1
1	0	Even	4	33	2	Even	4
2	0	Even	7	34	2	Even	7
3	0	Any	1	35	2	Any	1
4	0	Any	4	36	2	Any	4
5	0	Any	7	37	2	Any	7
6	0	Any	1, 6	38	2	Any	1, 6
7	0	Any	2,7	39	2	Any	2,7
8	0	Any	3, 8	40	2	Any	3, 8
9	0	Any	1, 4, 7	41	2	Any	1, 4, 7
10	0	Any	2, 5, 8	42	2	Any	2, 5, 8
11	0	Any	3, 6, 9	43	2	Any	3, 6, 9
12	0	Any	0, 2, 4, 6, 8	44	2	Any	0, 2, 4, 6, 8
13	0	Any	1, 3, 5, 7, 9	45	2	Any	1, 3, 5, 7, 9
14	0	Any	0, 1, 2, 3, 4, 5, 6, 7, 8, 9	46	N/A	N/A	N/A

15	0	Even	9	47	2	Even	9
16	1	Even	1	48	3	Even	1
17	1	Even	4	49	3	Even	4
18	1	Even	7	50	3	Even	7
19	1	Any	1	51	3	Any	1
20	1	Any	4	52	3	Any	4
21	1	Any	7	53	3	Any	7
22	1	Any	1, 6	54	3	Any	1, 6
23	1	Any	2,7	55	3	Any	2,7
24	1	Any	3, 8	56	3	Any	3, 8
25	1	Any	1, 4, 7	57	3	Any	1, 4, 7
26	1	Any	2, 5, 8	58	3	Any	2, 5, 8
27	1	Any	3, 6, 9	59	3	Any	3, 6, 9
28	1	Any	0, 2, 4, 6, 8	60	N/A	N/A	N/A
29	1	Any	1, 3, 5, 7, 9	61	N/A	N/A	N/A
30	N/A	N/A	N/A	62	N/A	N/A	N/A
31	1	Even	9	63	3	Even	9

distance-dependent path loss, the PRACH signal power received at the eNB can be written as follows [15]:[13]

$$\underbrace{P_{RA}(R)}_{\text{PRACH signal power at the eNB}} = \underbrace{P_{max}}_{\text{UE transmitter EIRP}} + \underbrace{G_{RX}}_{\text{eNB receiver antenna gain (including cable loss)}} - \underbrace{P_{L}(R)}_{\text{Distance-dependent path loss}} - \underbrace{P_{PL}}_{\text{Penetration loss}} - \underbrace{P_{FM}}_{\text{Log-normal fade margin}} \tag{10.12}$$

In the above equation, variable R is the cell radius in kilometers. From the above path-loss estimate, the initial PRACH transmission power is obtained by adding a configurable offset. The random-access mechanism allows power ramping where the actual PRACH transmission power is increased following each unsuccessful random-access attempt. For the first attempt, the PRACH transmission power is set to the initial PRACH power. In most cases, this is sufficient for the random-access attempt to be successful. However, if the random-access attempt fails, the PRACH transmission power for the next attempt is increased by a configurable step size to increase the likelihood of the next attempt being successful. Since the random-access preamble is orthogonal to the user data, the need for power ramping to control intra-cell interference is more relaxed than in other systems with non-orthogonal random-access, and in many cases the transmission power is set such that the first random-access attempt with a high likelihood is successful, which results in lower access latencies.

As mentioned earlier, PRACH uses a narrower sub-carrier spacing than normal uplink transmission, specifically 1250 Hz for random-access preamble formats 0–3, and 7500 Hz for random-access preamble format 4. The ratio of the normal uplink sub-carrier spacing to PRACH sub-carrier spacing is 12 for random-access preamble formats 0–3 and 2 for random-access preamble format 4. The PRACH is designed to fit in the same bandwidth as six resource blocks of normal uplink transmission, i.e., 72 sub-carriers at 15,000 Hz sub-carrier spacing (1.08 MHz). This simplifies scheduling gaps in normal uplink transmission to allow for PRACH transmission opportunities. Therefore, there are 864 sub-carriers for random-access preamble formats 0–3, and 144 sub-carriers for random-access preamble format 4. However, in practice, random-access preamble formats 0–3 use 839 active sub-carriers, and random-access preamble format 4 uses 139 active sub-carriers.

[13]Effective isotropic radiated power (EIRP), also known as equivalent isotropic radiated power, is the measured radiated power in a single direction (i.e., for fixed azimuth and elevation angles). Typically, for antenna radiation pattern measurement, if a single value of EIRP is given, this will be the maximum value of the EIRP over all measured angles. EIRP can also be interpreted as the amount of power that a perfectly isotropic antenna would need to radiate to achieve the same measured value.

Similar to normal uplink SC-FDMA transmission, there is a shift equal to half sub-carrier spacing (7500 Hz), which for PRACH is equivalent to six sub-carrier shift. A further sub-carrier offset (seven sub-carriers for random-access preamble formats 0–3 and two sub-carriers for random-access preamble format 4) centers the PRACH transmission within the 1.08 MHz transmission bandwidth. In practice, PRACH sequence is an OFDM-based reconstruction of a Zadoff–Chu sequence in the time-domain. The OFDM modulator is used to position the Zadoff–Chu sequence in the frequency-domain, i.e., to place six resource blocks of PRACH in six consecutive resource blocks starting from a particular PRB denoted as N_{RA}. The output of the OFDM modulator in the time-domain is a Zadoff–Chu sequence, if the input to the OFDM modulator is a Zadoff–Chu sequence in the frequency-domain. Therefore, N_{ZC} active sub-carriers are set to the values of an N_{ZC}-point DFT of an N_{ZC}-sample Zadoff–Chu sequence.

The cyclically shifted Zadoff–Chu sequences have several properties including the following: the amplitude of the sequences is constant, which ensures efficient PA utilization and maintains the low PAPR properties of the single-carrier transmitter; the sequences further have ideal cyclic autocorrelation, which is important for obtaining an accurate timing estimation at the eNB. Finally, the cross-correlation of different preambles based on cyclic shifts of the same Zadoff–Chu root sequence is zero at the receiver as long as the cyclic shift N_{CS} used when generating the preambles is larger than the maximum round-trip propagation time in the cell plus the maximum delay spread of the channel. Therefore, due to the ideal cross-correlation property, there is no intra-cell interference from multiple random-access attempts using preambles derived from the same Zadoff–Chu root sequence. To support different cell sizes, the cyclic shift N_{CS} is broadcast as part of the system information. Therefore, in smaller cells, a small cyclic shift can be configured, resulting in a larger number of cyclically shifted sequences from each root sequence. For cell sizes under 1.5km, all 64 preambles can be generated from a single root sequence. In larger cells, a larger cyclic shift is configured in order to generate 64 preamble sequences, since a greater number of root Zadoff–Chu sequences are in use in the cell. Although the larger number of root sequences is not an issue, the zero cross-correlation property only holds between shifts of the same root sequence and from an interference perspective, it is advantageous to use as few root sequences as possible.

The detection of the random-access preamble, in principle, is based on the cross-correlation of the received signal with the root Zadoff–Chu sequences. One disadvantage of Zadoff–Chu sequences is the difficulty in separating a frequency offset from the distance-dependent delay. A frequency offset results in an additional correlation peak in the time-domain, a correlation peak that corresponds to a spurious terminal-to-base-station distance. In addition, the actual correlation peak is attenuated. At low-frequency offsets, this effect is negligible and the detection performance is hardly affected. However, at high Doppler frequencies,

the spurious correlation peak can be larger than the true peak. This results in erroneous detection, i.e., the correct preamble may not be detected or the delay estimate may be incorrect. To avoid the ambiguities resulting from spurious correlation peaks, the set of preamble sequences generated from each root sequence can be restricted. Restrictions imply that only some of the sequences that can be generated from a root sequence are used to define random-access preambles. The location of the spurious correlation peak relative to the actual peak depends on the root sequence; thus different restrictions should be applied for different root sequences. The restrictions are broadcast by the eNB as part of the system information [16].

The transmission opportunities for PRACH are allocated in time first and then in frequency, if time multiplexing is not sufficient to hold all opportunities of a PRACH configuration needed for a certain density value D_{RA} without overlapping in time, for random-access preamble formats 0–3, frequency multiplexing is performed according to the following equation: $N_{RA} = N_{RA}^{offset} + 6\left\lfloor \frac{f_{RA}}{2} \right\rfloor$ if $f_{RA} \bmod 2 = 0$; otherwise $N_{RB}^{UL} - 6 - N_{RA}^{offset} - 6\left\lfloor \frac{f_{RA}}{2} \right\rfloor$, where N_{RB}^{UL} is the total number of uplink resource blocks (uplink bandwidth), f_{RA} is a frequency resource index within the considered time instance, N_{RA} is the first PRB allocated to the PRACH transmission, and PRACH frequency offset parameter $0 \le N_{RA}^{offset} \le N_{RB}^{UL} - 6$ is the first PRB available for PRACH expressed as a PRB number configured by higher layers (see Figure 10.46). Each random-access preamble occupies a bandwidth corresponding to six consecutive resource blocks for both frame structure types.

The random-access preambles are generated from Zadoff–Chu sequences with a zero-correlation zone. This means that the PRACH sequences are generated from one or several root Zadoff–Chu sequences. The network configures the set of preamble sequences which the UE is allowed to use. There are 64 preambles available in each cell. The set of 64 preamble sequences in a cell is obtained by including, in the order of increasing cyclic shift, all the available cyclic shifts of a root Zadoff–Chu sequence with the logical index *RACH_ROOT_SEQUENCE*, where the parameter *RACH_ROOT_SEQUENCE* is broadcast as part of the system information. Additional preamble sequences, in case 64 preambles cannot be generated from a single root Zadoff–Chu sequence, are obtained from the root sequences with the consecutive logical indices until all 64 sequences are found. The logical root sequence order is cyclic, i.e., the logical index 0 is consecutive to 837. The uth root Zadoff–Chu sequence is defined by:

$$x_u(n) = \exp\left(-\mathrm{j}\frac{\pi u n(n+1)}{N_{ZC}}\right); 0 \le n \le N_{ZC} - 1 \tag{10.13}$$

where the length N_{ZC} of the Zadoff–Chu sequence is either 839 for random-access preamble formats 0–3, or 139 for random-access preamble format 4. From the uth root Zadoff–Chu sequence, random-access preambles with zero

correlation zones (ZCZs)[14] of length $N_{CS} - 1$ are defined by cyclic shifts according to $x_{uv}(n) = x_u[(n + C_v) \bmod N_{ZC}]$, in which the value of the cyclic shift depends of the type of the sequence set. The unrestricted set or restricted sets are distinguished based on higher layer signaling.

The parameter N_{CS} is given in 3GPP TS 36.211 [3] for preamble formats 0–3 and 4. The parameter *ZCZ configuration* is provided by the higher layers (Table 10.23). The parameter *high-speed flag* is also provided by higher layers and determines whether unrestricted set or restricted set is used (Table 10.24).

The PRACH preamble sequence duration $T_{SEQ} = 1/\Delta f_{RA}$ is derived from the required PRACH preamble sequence energy to thermal noise power ratio E_s/N_0 in order to meet the target miss detection and false alarm probabilities, as follows: $T_{SEQ} = \frac{N_0 N_F}{P_{RA}(R)} \left(\frac{E_s}{N_0}\right)$, where N_0 is the thermal noise power density (in mW/Hz) and N_F is the noise figure of the eNB receiver. Typical target values for miss detection and false alarm probabilities are 10^{-2} and 10^{-3}, respectively. The 1600 μs preamble sequence of formats 2 and 3 is implemented by repeating the baseline 800 μs preamble sequence. These formats can provide up to 3dB link budget improvement, which is useful in large cells and/or to balance PUSCH/PUCCH and PRACH coverage at low data rates (Figure 10.49).

The PRACH slots shown in Figure 10.50 can be configured to occur in up to 16 different patterns or resource configurations. Depending on the number of UEs attempting to access the system in the same time interval, one or more PRACH resources may be allocated per PRACH slot period. The eNB is required to process the PRACH signal as soon as it is detected so that Msg2 of the RACH procedure can be sent within the required time window. If there is more than one PRACH resource per PRACH period, it is desirable to multiplex the PRACH resources in time rather than in frequency. This helps to avoid excessive processing at the eNB [15]. The available slot configurations are designed to simplify

[14]Definition of ZCZ sequences: let S denote a sequence set with M sequences of period L. Generally, the set of ZCZ sequences are characterized by the period of sequences L, the number of sequences in the set M, the length of the ZCZ L_{ZCZ}, and the number of phases P. It can be shown that the following mathematical upper bound concerning L_{ZCZ} exist $L_{ZCZ} \le L/M - 1$. The set S can be represented as $S = \{S_0, S_1, \ldots, S_p, \ldots, S_{M-1}\}$ and $S_p = \{s_0^p, s_1^p, \ldots, s_q^p, \ldots, s_{L-1}^p\}$, where $0 \le p \le M - 1$ and $0 \le q \le L - 1$, S_p and s_q^p denote a sequence and a sequence element, respectively. If all of the sequences in the set S satisfy the following autocorrelation and cross-correlation properties, then S is referred to as a set of ZCZ sequences or a ZCZ sequence set $\rho_{S_p}(l) = \sum_{q=0}^{L-1} s_q^p s_{(q+l) \bmod L}^{p*} = \begin{cases} 0 & -L_{ZCZ} \le l \le -1; 1 \le l \le L_{ZCZ} \\ \varepsilon_p & l = 0 \end{cases}$ and $\rho_{S_p S_{p'}}(l) = \sum_{q=0}^{L-1} s_q^p s_{(q+l) \bmod L}^{p'*} = 0$. In the above equation, symbol "*" denotes complex conjugate, $\rho_{S_p}(l)$ represents the periodic autocorrelation function of the sequence S_p, and $\rho_{S_p S_{p'}}(l)$ denotes the periodic cross-correlation function between the sequences S_p and $S_{p'}$, ε_p is the energy of the sequence S_p. If all of the elements of the sequence S_p are normalized complex-valued numbers, then the sequence energy ε_p is equal to L. In general, M, L, and L_{ZCZ} are referred to as the family size of the ZCZ sequence set, the period of the sequences, and the length of the ZCZ, respectively [167].

Table 10.23 PRACH Parameters [3,10]

Parameter	Size (bits)	Signaling Method	Description
PRACH time-domain configuration index	6	Broadcast (SIB2)	Provides information about the PRACH time-domain (subframe) configuration
PRACH frequency offset	7	Broadcast (SIB2)	Provides information about the PRACH frequency-domain configuration. Only applicable to TDD mode
Preamble format	2	Broadcast (SIB2)	For TDD there is also a short preamble, i.e., a total of five preamble formats
Root-sequence index	10	Broadcast (SIB2)	Used to generate cyclically shifted Zadoff–Chu sequences
Zero-correlation-zone length	4	Broadcast (SIB2)	Different interpretation depending on high-speed flag
High-speed flag	1	Broadcast (SIB2)	Selects between restricted and unrestricted preamble sets
PRACH transmit power setting	power Ramping Step 2 preamble Initial Received Target Power 4	Broadcast (SIB2)	*powerRampingStep* (0, 2, 4, or 6 dB), *preambleInitialReceivedTargetPower* (−120, −118, −116, −114, −112, −110, −108, −106, −104, −102, −100, −98, −96, −94, −92, or −90 dBm)

Table 10.24 Classification of PRACH Preambles to Restricted and Unrestricted Sets [3]

ZCZ Configuration Parameter	Format 4	Formats 0–3	
		N_{CS}	
	N_{CS}	Unrestricted Set	Restricted Set
0	2	0	15
1	4	13	18
2	6	15	22
3	8	18	26
4	10	22	32
5	12	26	38
6	15	32	46
7	N/A	38	55
8	N/A	46	68
9	N/A	59	82
10	N/A	76	100
11	N/A	93	128
12	N/A	119	158
13	N/A	167	202
14	N/A	279	237
15	N/A	419	–

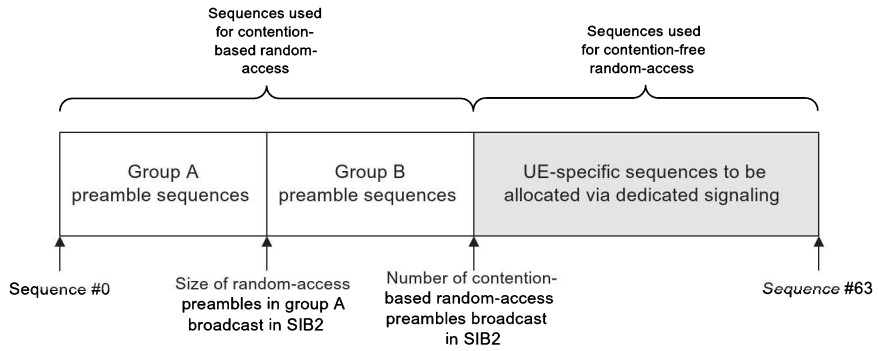


FIGURE 10.49

Classification of random-access preamble sequences [14].

PRACH receiver which may be used for multiple cells of an eNB, assuming a periodic pattern with period 10 or 20 ms.

The random-access preamble sequence can be generated at the system sampling rate by means of a large IDFT unit. The DFT block in Figure 10.51 is optional because the sequence can be directly mapped to the IDFT input in the frequency-domain. The cyclic shift can be implemented either in the time-domain after the IDFT or in the frequency-domain before the IDFT through a phase shift. For all possible system sampling rates, both cyclic prefix and sequence duration correspond to an integer number of samples. The method of Figure 10.51 does not require any time-domain filtering in the baseband, but requires large IDFT sizes (up to 24,576 for a 20 MHz spectrum allocation), which are practically cumbersome. Therefore, another option for generating the preamble consists of using small-size IDFT and shifting the preamble to the required frequency location through time-domain up-sampling and filtering (hybrid frequency/time-domain sequence generation method). Given that the preamble sequence length is 839, the smallest IFFT size that can be used is 1024. The size of the random-access cyclic prefix and preamble sequence duration has been chosen to provide an integer number of samples at the system sampling rate. The cyclic prefix can be inserted before the up-sampling and time-domain frequency shift, in order to minimize the intermediate storage requirements.

Given that the sampling rate for a 20 MHz LTE system is 30.72 MHz, and considering that the random-access preamble spans 0.8 ms, it can be concluded that the number of samples in time is equal to 24,576. Furthermore, it was mentioned that the PRACH sub-carrier spacing is 1.25 kHz, while the sub-carrier spacing for PUSCH and PUCCH is 15 kHz. As shown in Figure 10.51, in order to maintain the same sampling rate, a 12×2048 point DFT operation is needed for the PRACH signal generation at the transmitter side, if the entire processing is done in the frequency-domain. An alternative approach is to use time-domain signal generation and extraction which involves up-sampling and filtering operations at the transmitter. The drawback of

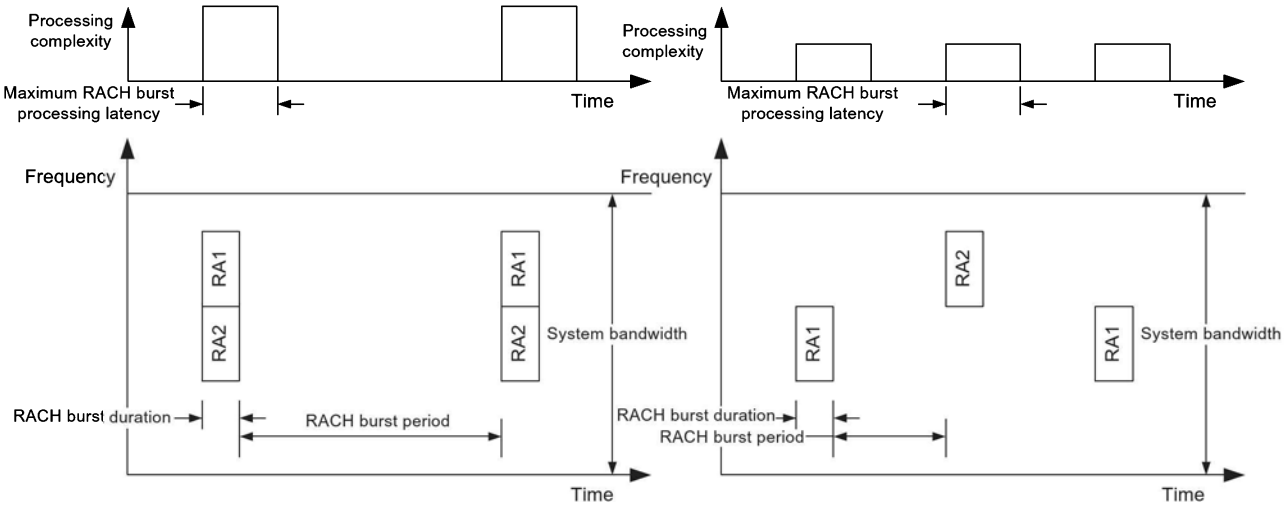


FIGURE 10.50

Example of PRACH resource configuration and processing [15].

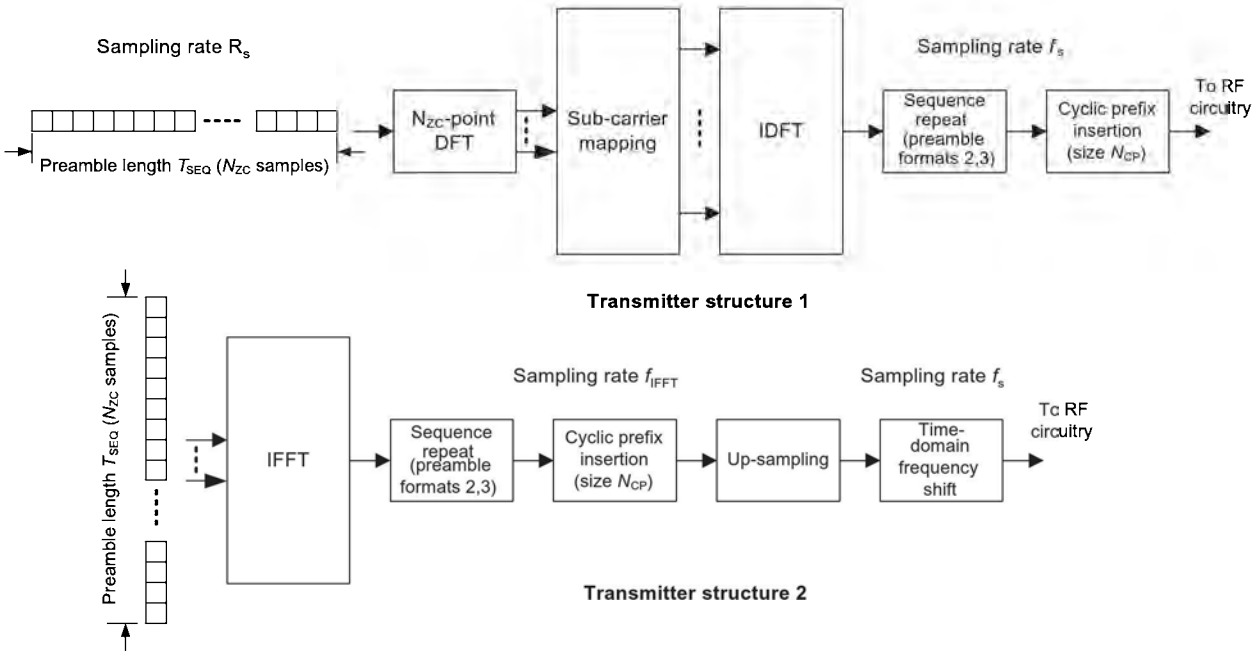


FIGURE 10.51

PRACH transmitter structure options [15,168].

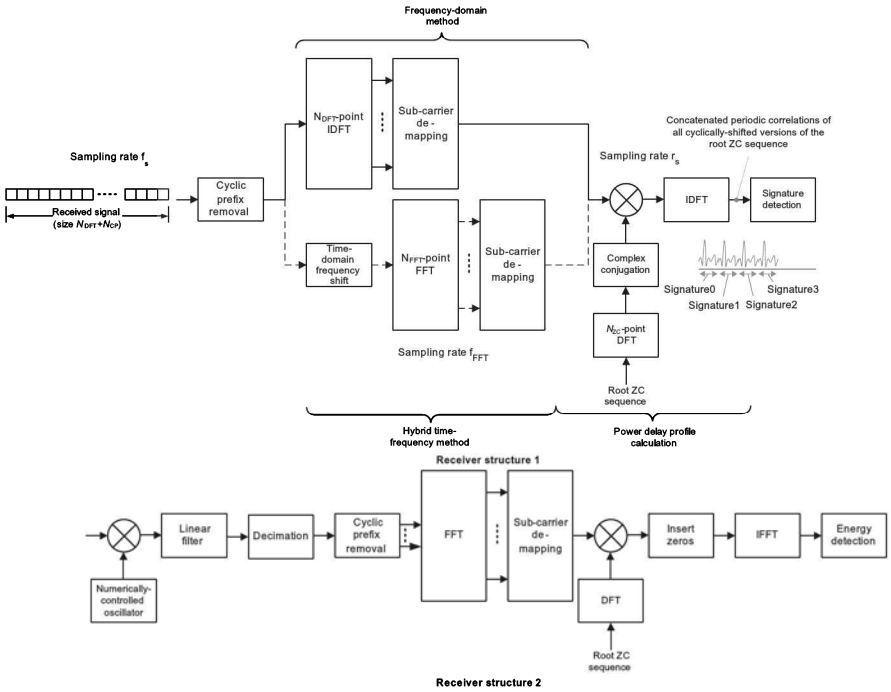


FIGURE 10.52

PRACH receiver structure options [15,168].

time-domain implementation is that the up-sampling from 1.08 MHz to the system sampling rate of 30.72 MHz is difficult to implement.

The implementation of the PRACH signal at the eNB receiver can take a frequency-domain or a hybrid time/frequency-domain approach. As illustrated in Figure 10.52 as an example, the common parts to both approaches are the cyclic prefix removal, which always occurs at the front end at the system sampling rate, the power delay profile calculation, and signature detection. The two approaches differ only in the computation of the sub-carriers carrying the PRACH signal(s). The frequency-domain method computes the full range of sub-carriers used for uplink transmission over the system bandwidth from 800-μs-long received input samples. As a result, the PRACH sub-carriers are directly extracted from the set of uplink sub-carriers, which does not require any frequency shift or time-domain filtering but involves an extremely large DFT computation. Note that even though DFT size $N_{\text{DFT}} = n2^m$, thus allowing fast and efficient DFT computation algorithms, the DFT computation cannot start until the complete sequence is stored in memory, which increases the processing delay.

In order to reduce the implementation complexity, particularly for the number of multiplications in the PRACH detector at the eNB, frequency-domain processing

may be adopted for PRACH preamble detection. As shown in Figure 10.52, the received signal is first processed in the time-domain, is then transformed to the frequency-domain by FFT, and is multiplied by the DFT-transformed RACH sequences (i.e., cross-correlation calculation). The cross-correlation is obtained by transforming back to the time-domain by IFFT, followed by zero insertion. Figure 10.52 further illustrates the main components of another RACH preamble receiver structure using the DFT-based (frequency-domain) method. In the receiver, the down-conversion block uses a numerically controlled oscillator, which shifts the frequency band of PRACH to the lowest frequency band. The down-converted signal is filtered with a linear filter to prevent aliasing effect after decimation.

The hybrid time/frequency-domain method extracts the desired PRACH signal using a time-domain frequency shift along with down-sampling and anti-aliasing filtering. The down-sampling ratio and the corresponding anti-aliasing filter characteristics are chosen to provide a number of PRACH time samples suitable for an FFT or simple DFT computation at a sampling rate which is an integer fraction of the system sampling rate. Unlike the frequency-domain approach, the hybrid time/frequency-domain computation can start as soon as the first samples have been received, reducing the processing latency.

The analog random-access signal $s(t)$ is defined as follows:

$$s(t) = \beta_{\text{PRACH}} \sum_{k=0}^{N_{\text{ZC}}-1} \sum_{n=0}^{N_{\text{ZC}}-1} x_{\text{uv}}(n) \text{e}^{-\text{j}(2\pi nk/N_{\text{ZC}})} \exp[\text{j}2\pi(k+\varphi+\gamma(k_0+1/2))\Delta f_{\text{RA}}(t-T_{\text{CP}})] \tag{10.14}$$

where $0 \le t < T_{\text{SEQ}} + T_{\text{CP}}$, β_{PRACH} is an amplitude scaling factor in order to ensure conformance to the transmit power P_{PRACH}, and $k_0 = 12N_{\text{RA}} - 6N_{\text{RB}}^{\text{UL}}$. The location of PRACH in the frequency-domain is controlled by the parameter N_{RA}. The factor $\gamma = \Delta f / \Delta f_{\text{RA}}$ accounts for the difference in sub-carrier spacing between the random-access preamble and uplink data transmission. The sub-carrier spacing for the random-access preamble $\Delta f_{\text{RA}} = 1250$ Hz for random-access preamble formats 0–3, and $\Delta f_{\text{RA}} = 7500$ Hz for random-access preamble format 4. The fixed offset determining the frequency-domain location of the random-access preamble within the PRBs $\phi = 7$ for random-access preamble formats 0–3, and $\phi = 2$ for random-access preamble format 4 [3].

10.8 SC-FDMA signal generation

The time-domain analog signal $s_l^p(t)$ for antenna port p over SC-FDMA symbol l in an uplink slot is defined as follows (applicable to all uplink physical signals and physical channels except PRACH):

$$s_l^p(t) = \sum_{k=-\lfloor 6N_{\text{RB}}^{\text{UL}} \rfloor}^{\lceil 6N_{\text{RB}}^{\text{UL}} \rceil - 1} \alpha_{k'}^p(l) \exp\{\text{j}\pi(2k+1)\Delta f[t - N_{\text{CP}}(l)T_{\text{s}}]\}, 0 \le t < (N_{\text{CP}}(l) + N_{\text{FFT}})T_{\text{s}} \tag{10.15}$$

where $k' = k + \lfloor 6N_{RB}^{UL} \rfloor$, $N_{FFT} = 2048$, $\Delta f = 15$ kHz, and a_{kl}^{p} is the complex-valued content of resource element (k, l) on antenna port p. The SC-FDMA symbols in a slot are transmitted in increasing order of symbol index l, starting with $l = 0$, where SC-FDMA symbol $l > 0$ starts at time $\sum_{l'=0}^{l-1}[N_{CP}(l') + N]T_s$ within the slot [3].

10.9 LTE/LTE-Advanced uplink multi-antenna transmission schemes

Simultaneous transmission from multiple transmit antennas from a single UE was not supported in LTE Rel-8/9. In order to simplify the UE implementation and to reduce power consumption, a single-power amplifier was assumed to be available at the UE. However, LTE Rel-8/9 provided support for open/closed-loop antenna-selection transmit diversity in the uplink from UEs which are equipped with multiple transmit antennas. LTE Rel-8/9 also supported virtual MIMO in the uplink. More advanced multi-antenna techniques, including closed-loop spatial multiplexing for SU-MIMO and transmit diversity for control signaling, were introduced in LTE Rel-10. Uplink closed-loop antenna selection for up to two transmit antennas is supported as an optional UE capability in LTE and is configurable by higher layers. If a UE indicates support for uplink antenna selection, the eNB may configure and schedule the UE based on that capability.

LTE/LTE-Advanced use the concept of antenna ports to differentiate between logical and physical antennas. Logical antennas or antenna ports are mapped to physical antennas based on certain deployment considerations. Prior to LTE Rel-10, there was only one transmit antenna on the UE, thus the notion of antenna ports did not apply. However, LTE Rel-10 extended the multi-antenna capabilities of the uplink and provided support for spatial multiplexing up to four transmit antennas for PUSCH and dual-antenna transmit diversity for PUCCH. Therefore, a new set of logical antennas or antenna ports have been defined that are listed in Table 10.25. As an example, PUSCH transmission, including its DM-RS as well as SRS transmission, is associated with antenna ports $\{10\}, \{20, 21\}$, and $\{40, 41, 42, 43\}$, for one, two, and four transmit antennas, respectively. The virtual antenna port $\bar{p} \in \{0, 1, 2, 3\}$ is used in this book and in 3GPP specifications to refer to the actual uplink antenna ports. Note that each antenna port has its own reference signals, enabling the eNB to estimate the channel from each UE transmit antenna.

Before proceeding to the next sections, recall that a spatial layer is the term used in LTE for one of the different streams generated by spatial multiplexing. A layer can be described as a mapping of complex-valued symbols onto the transmit antenna ports. Each layer is identified by a precoding vector/matrix of size equal to the number of transmit antenna ports, and can be associated with a radiation pattern. The rank of the transmission is the number of layers transmitted. A codeword is an independently encoded data block, corresponding to a single transport block delivered from the MAC sub-layer in the transmitter to the physical layer and protected with a CRC.

Table 10.25 Virtual and Physical Antennas in the Uplink [3]

Physical Channel/Signal	Virtual Antenna Port $\bar{p}$	Uplink Antenna Port p Number of Physical Antennas		
		1	2	4
PUSCH and DM-RS for PUSCH	0	10	20	40
	1	–	21	41
	2	–	–	42
	3	–	–	43
SRS	0	10	20	40
	1	–	21	41
	2	–	–	42
	3	–	–	43
PUCCH and DM-RS for PUCCH	0	100	200	–
	1	–	201	–

10.9.1 Transmit antenna selection

When closed-loop antenna selection is enabled, the eNB indicates which antenna should be used for PUSCH transmission, by implicitly coding this information in the uplink scheduling grant (i.e., DCI format 0 or 4). The 16-bit CRC is scrambled (modulo-2 addition) by one of two antenna selection masks $\langle 0,0,0,0,0,0,0,0,0,0,0,0,0,0,0,0 \rangle$ for the UE's first transmit antenna, and/or $\langle 0,0,0,0,0,0,0,0,0,0,0,0,0,0,0,1 \rangle$ for the second antenna [4]. The antenna selection mask is applied in addition to the UE identity (RNTI) masking, identifying the UE for which the scheduling grant is intended. This implicit encoding avoids the use of explicit antenna selection bits which would result in an increased overhead for UEs not supporting (or not configured for) transmit antenna selection. The UE identity can be detected directly from the 15 least-significant bits of the decoded mask with no need to use the transmitted antenna selection mask (the 16th bit).

When using the adaptive HARQ, the antenna indicator, using CRC masking, is always sent in the uplink grant to indicate which antenna to use. For example, for a high-Doppler UE with adaptive HARQ, the eNB might instruct the UE to alternate between the transmit antennas or, alternatively, to select the primary antenna. In typical UE implementations, a transmit antenna gain imbalance of 3–6 dB between the secondary and primary antennas is not uncommon. Alternatively, when using non-adaptive HARQ, the UE may choose either antenna; therefore, in low-Doppler scenarios, the UE may use the same antenna

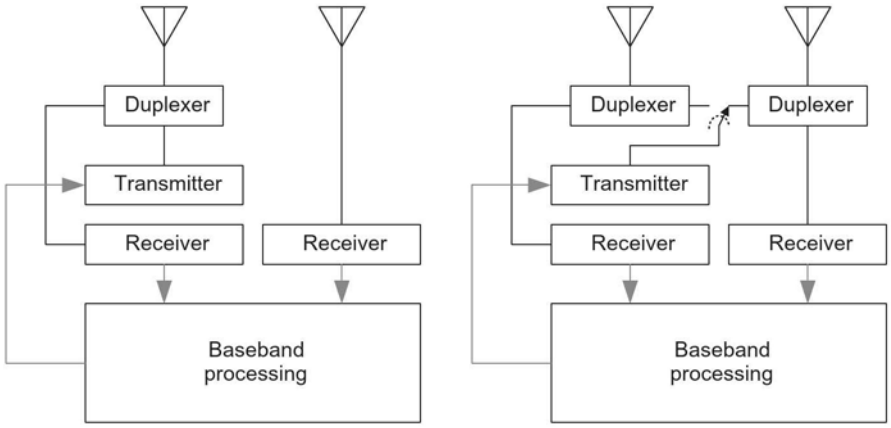


FIGURE 10.53

Illustration of a UE front end with/without transmit antenna selection [14].

signaled in the uplink grant, while in high-Doppler conditions the UE may switch between antennas or select the primary antenna. For a large number of retransmissions with non-adaptive HARQ, the antenna indicated in the uplink grant may not be the best and it is better to let the UE select the antenna. If the eNB instructs the UE to use a specific antenna for the retransmissions, it can use adaptive HARQ. If the eNB enables a UE's closed-loop antenna selection capability, the SRS transmissions alternate between the transmit antennas in successive SRS transmission subframes, irrespective of enablement of the frequency hopping feature [15].

It must be noted that receive diversity is mandatory for all UE categories in LTE, and as such there is more than one antenna on the UE that may be used for transmit antenna selection, as shown in Figure 10.53, with minimal changes to implementation. The transmit antenna selection scheme can be useful, if the UE is held in such a way that one transmit antenna is covered by hand and the other antenna is not covered. Although the inclusion of an RF switch may introduce some insertion loss, this drawback may be overcome by the benefits of the diversity scheme in some practical scenarios. It is not mandatory for the UEs to support transmit antenna selection. The UE capability information message can be used to inform the network of whether the UE supports this feature. The eNB can instruct the UEs supporting this feature to use either open-loop or closed-loop transmit antenna selection.

10.9.2 Virtual MU-MIMO (cooperative MIMO)

Another uplink MIMO mode that was introduced in LTE Rel-8/9 was MU-MIMO. The legacy uplink MU-MIMO is based on transmission from multiple UEs on the same set of resource blocks, each using a single transmit antenna. From the point of view of an individual UE, this is a single-antenna transmission

scheme; however, from an eNB perspective, this is a MU-MIMO scheme that requires more sophisticated scheduling and uplink reception. In order to support uplink MU-MIMO, LTE Rel-8/9 provides orthogonal DM-RS using different cyclic shifts to allow the eNB to obtain independent channel estimations for the uplink from each UE. A cell can assign up to eight different cyclic shifts using a 3-bit PUSCH cyclic shift offset in the uplink scheduling grant; therefore, uplink MU-MIMO of up to eight UEs can be theoretically supported in a cell. The inter-cell or cooperative MU-MIMO is supported in LTE by assigning the same base sequence groups and/or reference signal hopping patterns to the different cells.

The main objective of MU-MIMO is to increase the overall system throughput. The uplink MU-MIMO is transparent to the UE and has no effect on the UE implementation. The cooperative or virtual MIMO in the uplink requires the eNB to select and group the spatially uncorrelated UEs that are going to share the same resource blocks, to schedule the UEs within the group for uplink transmission over PDCCH, and to separate and decode uplink transmissions from each UE within the group. Each UE within the group will be assigned a different cyclic shift for the corresponding DM-RS to allow the eNB to estimate the channel from each UE and to decode the corresponding payload. The use of different cyclic shifts provides orthogonality among the UEs within the group, and enables the eNB to separate them as long as the same number of resource blocks is used for the UEs within group. The orthogonality will be lost if each UE is allocated a different number of resource blocks. While LTE Rel-8/9 defined only cyclic shifts to differentiate the UEs in the uplink, LTE Rel-10 introduced an additional level of differentiation using OCCs, as discussed earlier. Therefore, OCC will allow the UEs within the same MU-MIMO group to be allocated a different number of resource blocks.

10.9.3 Closed-loop spatial multiplexing

Closed-loop spatial multiplexing with up to four antennas was introduced as part of the LTE Rel-10 improvements in the uplink. The physical antenna elements required for uplink spatial multiplexing might be already available on the UEs that support spatial multiplexing in the downlink, which can be shared in both directions via an RF switch, e.g., a UE that supports 2×2 spatial multiplexing in the downlink already has two antenna elements. Nevertheless, the uplink spatial multiplexing further requires additional transmission chains and PAs in the uplink that operate simultaneously. The eNB provides the UE with instructions on the number of spatial layers and the codebooks or precoding matrices that must be used. The criterion for selecting the precoding matrix is to maximize the SNR at the eNB receiver [14].

The design principles of spatial multiplexing with precoding for the uplink data transmission are similar to those for the downlink. The precoding operation can mathematically be expressed as multiplication of an $N_{RX} \times 1$ DFT-spread signal vector by an $N_{TX} \times N_{RX}$ precoding matrix, which is chosen from a predefined

set of matrices, also known as a codebook. Note that the *i*th column vector of the precoding matrix represents the antenna-spreading weight of the *i*th layer. The main purpose of precoding is to match the precoding matrix with the channel characteristics in order to increase the received signal power and reduce inter-layer interference, thereby improving the SINR of each layer.

Let us assume that the eNB has N_{RX} receive antennas and the eigen-beamforming module precodes each layer with one of $\min(N_{TX}, N_{RX})$ eigenvectors of the channel correlation matrix in order to improve the capacity. In practice, the choice of the precoder must be signaled from the eNB to the UE; therefore, the number of precoding matrices (i.e., codebook size) is limited by the size of the downlink control signaling. The use of a finite codebook results in a reduced precoding gain. If the alphabet for the non-zero elements of the precoding matrix is confined to $(\pm 1, \pm j)$, the matrix calculations involved in the selection of the codebook are significantly simplified. Furthermore, the constant-modulus property of the QPSK alphabet enables all PAs to transmit with equal power level. This balanced power distribution would result in maximization of the PA efficiency, regardless of which precoding matrix is used. A drawback of this alphabet constraint is further reduction of the precoding gain.

The design of a precoding codebook used for downlink MIMO is different from that in the uplink in the sense that the uplink codebook structure should not increase the CM of the transmitted signal relative to single-antenna transmission (measured at each individual antenna port). The Householder codebook of downlink MIMO linearly combines multiple layers and inevitably increases the CM. A design constraint on uplink codebooks is that each row should have at most one non-zero element. In other words, each transmit antenna is not allowed to convey more than one layer; therefore, no linear combination is allowed. This constraint, while it preserves the CM, gives rise to further reduction of the precoding gain. One of the objectives of the uplink precoder design is to optimize the precoding gain under the CM preserving constraint [122].

It is recognized from an information theory perspective that the codebooks with maximum chordal distance are optimal. However, the UE antennas are likely to be practically correlated due to proximity; therefore, the UE antenna configuration and indexing, antenna spacing, and polarization should be carefully considered in selecting the codebook vectors. Since each layer is assigned to a separate group of UE antennas, antenna grouping with lower inter-layer correlation is preferred, leading to lower inter-layer interference. This is also consistent with the eigen-beamforming principle in that eigenvectors of channel correlation tend to have elements with larger amplitude in one antenna group than in the other antenna groups. Under the above constraints, it can be concluded that the full-rank codebooks consist of the identity matrices. For non-full-rank codebooks, it is desirable to maximize the precoding gain while preserving the low CM property.

Since PUSCH DM-RS is precoded with uplink data at the same time, it is impossible to select the precoder (i.e., the rank and precoding matrix) based on DM-RS, since only a subset of the spatial channel dimensions is observed.

Table 10.26 Codebook for Uplink Transmission on Two Antenna Ports [20, 21][3]

	Number of Layers	
Codebook Index	$N_l = 1$	$N_l = 2$
0	$\frac{1}{\sqrt{2}}\begin{bmatrix}1\\1\end{bmatrix}$	$\frac{1}{\sqrt{2}}\begin{bmatrix}1 & 0\\0 & 1\end{bmatrix}$
1	$\frac{1}{\sqrt{2}}\begin{bmatrix}1\\-1\end{bmatrix}$	–
2	$\frac{1}{\sqrt{2}}\begin{bmatrix}1\\j\end{bmatrix}$	–
3	$\frac{1}{\sqrt{2}}\begin{bmatrix}1\\-j\end{bmatrix}$	–
4	$\frac{1}{\sqrt{2}}\begin{bmatrix}1\\0\end{bmatrix}$	–
5	$\frac{1}{\sqrt{2}}\begin{bmatrix}0\\1\end{bmatrix}$	–

Instead, non-precoded SRS transmission is the conventional method for the eNB to efficiently select an appropriate precoder for the uplink data. The SRS is antenna-specific, as opposed to layer-specific in the case of DM-RS; therefore, the required number of orthogonal resources is the same as the number of transmit antennas. There exists a great amount of similarity between DM-RS and SRS. The SRS is derived from the same cell-specific base sequence as DM-RS, and the SRS orthogonality is further provided through different cyclic shifts [122].

In the case of two transmit antennas and rank 1 transmission, the codebook consists of four constant-modulus vectors and two antenna selection vectors (Table 10.26). The inclusion of constant-modulus vectors enables the signals from multiple UE antennas to be combined constructively at the receiving eNB by introducing a relative phase shift of 0°, 90°, 180°, or 270° between UE antennas. In the example shown in Figure 10.54, a phase shift of 270° maximizes the SNR of received signal due to constructive combining, whereas a phase shift of 90° minimizes the SNR due to destructive combining. On the other hand, the inclusion of antenna selection vectors reduces transmit power and is intended for UE power saving. For example, if UE antennas experience significant gain imbalance, one of the antenna selection vectors can be used to switch off the low-gain antenna [122].

The case of four transmit antennas and rank-1 codebook involves 16 constant-modulus vectors for constructive combining and eight antenna-selection vectors for UE power saving. For constant-modulus vectors, four relative phase shifts are considered between the first two antennas. Additional relative phase shifts are applied between the first and third antennas, and between the second and fourth antennas, accounting for imperfect antenna polarization. The rank-2 codebook (given in Table 10.27) covers every possible antenna grouping. For the rank-3

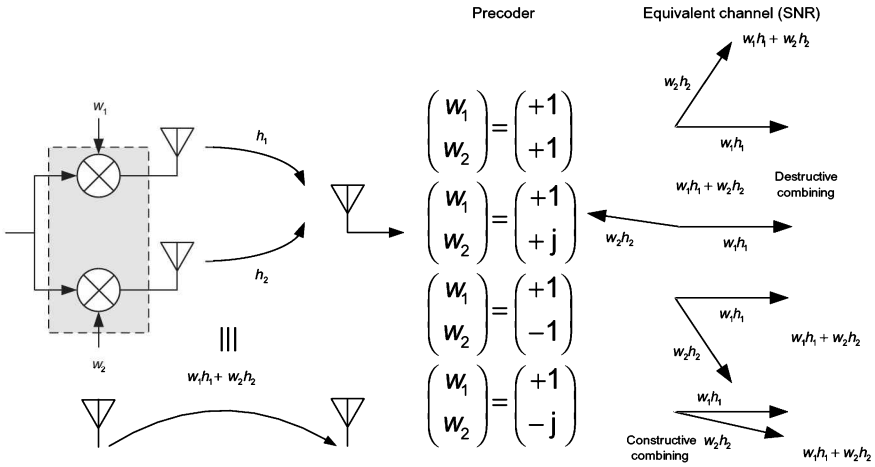


FIGURE 10.54

Illustration of the effect of precoding on SNR (rank 1 transmission) [122].

codebook, the first layer is assigned to two transmit antennas, whereas layers 2 and 3 are each assigned one antenna. Every antenna grouping (six groupings in total) for the first layer is covered, along with an intra-group phase shift of 0° or 180°. It should be noted that no inter-group phase shift is considered in the rank-2 and rank-3 codebooks, since it does not contribute to layer separation. The performance of the system with these codebooks is similar to the Householder codebook used in the downlink MIMO, unless the UE antennas are highly correlated. Note that the Householder codebook has a similar codebook size, while its alphabet is 8PSK and the CM is not concerned. Therefore, it can be concluded that the loss of precoding gain (compared to eigen-beamforming) largely originates from the codebook size constraint, rather than the alphabet restriction and the limitation concerning the CM of the transmitted signal. The precoder is defined by rank and PMI, which are selected by the eNB based on uplink channel measurements and signaled to the UE through the rank indicator and PMI fields in an uplink grant. The rank and PMI may be selected to maximize the throughput.

10.9.4 Transmit diversity

Multi-antenna transmit-diversity techniques are used to provide reliability and to improve coverage for uplink control channels. The transmit diversity scheme introduced for PUCCH in LTE Rel-10 was designed to ensure backward compatibility with the LTE Rel-8 PUCCH design. A dual-antenna transmit diversity scheme for HARQ and SR (PUCCH format 1/1a/1b) is utilized by transmitting the same control information from different UE antennas by using different orthogonal resources, thus providing no multiplexing gain. This is referred to as

e 10.27 Codebook for Transmission on Four Antenna Ports {40, 41, 42, 43} [3]

book	Number of Layers $N_l = 2$				Codebook Index	Number of Layers $N_l = 2$			
	$\frac{1}{2}\begin{bmatrix}1 & 0\\1 & 0\\0 & 1\\0 & -j\end{bmatrix}$	$\frac{1}{2}\begin{bmatrix}1 & 0\\1 & 0\\0 & 1\\0 & j\end{bmatrix}$	$\frac{1}{2}\begin{bmatrix}1 & 0\\-j & 0\\0 & 1\\0 & 1\end{bmatrix}$	$\frac{1}{2}\begin{bmatrix}1 & 0\\-j & 0\\0 & 1\\0 & -1\end{bmatrix}$	8–11	$\frac{1}{2}\begin{bmatrix}1 & 0\\0 & 1\\1 & 0\\0 & 1\end{bmatrix}$	$\frac{1}{2}\begin{bmatrix}1 & 0\\0 & 1\\1 & 0\\0 & -1\end{bmatrix}$	$\frac{1}{2}\begin{bmatrix}1 & 0\\0 & 1\\-1 & 0\\0 & 1\end{bmatrix}$	$\frac{1}{2}\begin{bmatrix}1\\0\\-1\\0\end{bmatrix}$
	$\frac{1}{2}\begin{bmatrix}1 & 0\\-1 & 0\\0 & 1\\0 & -j\end{bmatrix}$	$\frac{1}{2}\begin{bmatrix}1 & 0\\-1 & 0\\0 & 1\\0 & j\end{bmatrix}$	$\frac{1}{2}\begin{bmatrix}1 & 0\\j & 0\\0 & 1\\0 & 1\end{bmatrix}$	$\frac{1}{2}\begin{bmatrix}1 & 0\\j & 0\\0 & 1\\0 & -1\end{bmatrix}$	12–15	$\frac{1}{2}\begin{bmatrix}1 & 0\\0 & 1\\0 & 1\\1 & 0\end{bmatrix}$	$\frac{1}{2}\begin{bmatrix}1 & 0\\0 & 1\\0 & -1\\1 & 0\end{bmatrix}$	$\frac{1}{2}\begin{bmatrix}1 & 0\\0 & 1\\0 & 1\\-1 & 0\end{bmatrix}$	$\frac{1}{2}\begin{bmatrix}1\\0\\0\\-1\end{bmatrix}$

spatial orthogonal resource transmit diversity and is illustrated in Figure 10.36. In LTE Rel-8/9, the orthogonal resources are available through either various cyclic shifts of length-12 base sequences or OCCs of length-4 for transmission of control information of uplink control channels. The DM-RS for the uplink control channel also uses the orthogonal resources through the cyclic shifts of length-12 base sequences or OCCs of length-3.

In general, there are theoretically 36 orthogonal resources available for the uplink control channel in each subframe. Assuming perfect orthogonality, the signals from multiple transmit antennas are received separately and combined constructively. In the case of four transmit antennas and from the eNB perspective, the UE transmissions use two orthogonal resources, i.e., the cyclic shift and the OCCs, and it is up to the UE implementation if and how the transmission is distributed over the four transmit antennas. One possibility is to allow the third and fourth antennas to use the same orthogonal resources allocated to the first and second antennas, respectively, and transmit the same information. Another possibility is to transmit only on two of the four UE antennas. The same transmit diversity scheme is also applied for the channel quality information report (PUCCH format 2/2a/2b) [122]. If the UE transmit antennas are uncorrelated, SORTD provides the best diversity performance at the expense of consuming multiple orthogonal resources, reducing PUCCH multiplexing capability in general.

10.9.5 Uplink MIMO receivers

The practical constraints against implementing spatial multiplexing particularly in the uplink are the cost of multiple transmit and receive radio chains and the form-factor limitation of multi-antennas for handheld devices. By making use of advanced signal-processing techniques in the baseband processing stage, high-performance MIMO transmission can be achieved. A number of MIMO receiver algorithms can be used, depending on the requirements pertaining to receiver complexity.

In principle, the downlink MIMO channel is a broadcast channel. In this case, the individual data streams transmitted from each antenna are mixed with other transmit data streams at each receive antenna. To separate the mixed data streams at the receiver, designers can multiply the (mixed-stream) received signals with a matrix that is the inverse of the MIMO channel matrix. This is called a zero-forcing receiver. It is a simple MIMO receiver that often suffers performance loss at higher noise and interference levels. To minimize performance loss, the inversion of the MIMO channel matrix operation is adjusted according to the interference or noise level. This is called an MMSE receiver. But both the ZF and MMSE receivers typically have up to 2 dB performance loss compared with maximum likelihood detection (MLD) receivers.

Improved reception of spatial multiplexing MIMO transmission requires an exhaustive search of MIMO signal constellation combinations. The MIMO transmission process is modeled at the receiver in such a way that a specific complex

modulation constellation is generated for each transmit antenna stream. The constellations are then applied to the MIMO channel input. At the MIMO channel output, the corresponding received signal is generated for each receive antenna. At this point, the Euclidean distance is computed for the modeled MIMO channel output signal relative to the received signal. In this way, the different modulation constellations at the MIMO channel input constitute different hypothesis tests. If all possible combinations of constellations at the MIMO channel input can be emulated, their associated MIMO channel outputs can be generated, and the Euclidean distance can be computed against the received signal. The minimum Euclidian distance associated with the constellation combination hypothesis provides the most likely decoding. Such an exhaustive constellation search at the MIMO channel input is the optimal MIMO receiver.

Optimal receiver performance, however, comes at the cost of receiver complexity. Performing all the hypothesis tests requires $2^{M \times N_{TX}}$ complex operations, where M is the modulation order and N_{TX} is the number of transmit antennas. As an example, for 64QAM with two transmit antennas, the MLD decoding complexity is $2^{12} = 4096$ complex operations. For 64QAM with four transmit antennas, the MLD decoding complexity is $2^{24} = 16,777,216$ complex operations. On the other hand, the exhaustive constellation-search-based MLD receiver provides a good modular structure. The MLD receiver is suitable for application-specific integrated-circuit implementation. Several fast constellation search algorithms are available such as the sphere decoding algorithm [169]. The MLD-based MIMO receivers have many advantages compared with ZF and MMSE receivers. The MLD receiver performance advantages are significant when the MIMO channels are correlated, i.e., small-form-factor user devices require a compact packaging of multiple antennas, resulting in a high level of antenna correlation as well as a correlated MIMO channel. The ZF and MMSE receivers, conversely, can both suffer sharp performance losses when MIMO channels are correlated.

In addition, because of the limitations of small-form-factor user devices, it is difficult to achieve the same antenna gain for the two receive antennas embedded in the device. In the case of 4 dB antenna gain imbalance, the performance loss for the MLD receiver is negligible. Another advantage is diversity gain. The MLD receiver can not only separate the transmit data streams, but also can achieve the receive diversity gain for multiple receive antennas. Furthermore, the receiver can support a very high-mobility environment including reception at speeds exceeding 120km/h. Reception of the spatial multiplexing MIMO transmissions can be optimized by selecting the best receiver operation, based on the MIMO channel condition and the modulation constellation, to reduce the average processing power required. This reduces the power consumption of the user device and extends its battery life.

Since an MMSE receiver requires fewer computations than the MLD receiver, under certain transmission conditions, the performance difference between the MMSE receiver and the MLD is negligible. We can measure and test the correlation condition of the MIMO channel before we decide which receiver should be

used. If the MIMO channel correlation is very low or is orthogonal, the MMSE receiver can be used with no performance loss, while reducing the computational complexity by avoiding the use of the MLD receiver. Similarly, we can use the MMSE receiver when the SNR is high.

The advanced receiver can be further extended by successive interference cancellation (SIC) receiver architecture. The rationale behind the SIC receiver is that the signal quality of the multiple transmit data streams are not the same, because of the fading variations of the MIMO channel. We can successfully demodulate the first data stream, re-modulate it, and then subtract the first data stream from the received input combination in the absence of interference from the first data stream. We can then demodulate the second data stream successfully with a simple maximum ratio combining receiver.

Due to the nature of the MIMO channel, the eigenvalue of the MIMO channel matrix represents the signal strength for the data stream. For the two-transmit and two-receive MIMO configuration, different modulations for the different data streams can be scheduled for transmission at the base station. The user device measures the signal quality (typically one strong data stream and one weak data stream) and uses the feedback channel to request the coding and modulation for each data stream transmitted from the base station. If the user device implements an SIC receiver, the signal-quality measurement can be based on the receiver operation. In this case, the weak data stream's signal quality is measured in the absence of interference from the strong data stream. Therefore, the user device can request the increased coding and modulation transmission level for the second data stream. This can improve the throughput of the second data stream, increasing the overall throughput of the user device.

In the LTE/LTE-Advanced uplink, the use of SC-FDMA for multiple-access introduces ISI in dispersive channels. As a result, the ideal MIMO receiver should address both ISI and spatial multiplexing interference. There are a number of receiver implementation options including linear minimum mean-square error (LMMSE) equalization and SIC that can be used for MIMO detection in the LTE uplink.

In general, the downlink $N_{RX} \times 1$ received-signal vector $\mathbf{y}(k,l)$ at the kth subcarrier and the lth OFDM symbol can be expressed as the sum of the desired signal $\mathbf{H}_1(k,l)\mathbf{s}_1(k,l)$ from the serving eNB and the interference signals $\mathbf{H}_j(k,l)\mathbf{s}_j(k,l)|_{\forall j \neq 1}$ from other base stations and the noise vector $\mathbf{n}(k,l)$ as follows:

$$\mathbf{y}(k,l) = \mathbf{H}_1(k,l)\mathbf{s}_1(k,l) + \sum_{j=2}^{N_{eNB}} \mathbf{H}_j(k,l)\mathbf{s}_j(k,l) + \mathbf{n}(k,l) \tag{10.16}$$

where $\mathbf{s}_j(k,l)|_{j=1,2,\ldots,N_{eNB}}$ and $\mathbf{H}_j(k,l)|_{j=1,2,\ldots,N_{eNB}}$ represent the $N_{TX} \times 1$ transmitted signal vector and the $N_{RX} \times N_{TX}$ channel matrix between the jth cell and the UE including the contribution from both receiver branches. In the above equation $\mathbf{H}_j(k,l) = \begin{pmatrix} \mathbf{H}_j^1(k,l) & \mathbf{H}_j^2(k,l) \end{pmatrix}^T$ in which $\mathbf{H}_j^i(k,l)$ denotes the $N_{TX} \times 1$ channel matrix as seen at the ith receive antenna. The $N_l \times 1$ recovered signal vector at

the UE denoted by $\hat{\mathbf{s}}_1(k,l)$ is detected using the $N_l \times N_{RX}$ receiver weighting matrix $\mathbf{W}_1(k,l)$ as follows:

$$\hat{\mathbf{s}}_1(k,l) = \mathbf{W}_1(k,l)\mathbf{y}_1(k,l) \tag{10.17}$$

The above generic model will be exploited in the receiver algorithms described in the following sections.

10.9.5.1 LMMSE receiver

An LMMSE receiver is a widely used solution which generates an MMSE estimate for each time-domain symbol. The MMSE has been used as a baseline receiver in LTE/LTE-Advanced evaluations due to its simplicity. The detection problem in an LMMSE receiver reduces to finding a weighting matrix such that $\hat{\mathbf{s}}_1(k,l) = \mathbf{W}_1(k,l)\mathbf{y}_1(k,l)$, where the weighting matrix is given as follows [25–27,43,44]:

$$\mathbf{W}_1(k,l) = \hat{\mathbf{H}}_1^H(k,l)\mathbf{R}^{-1}; \quad \mathbf{R} = P_1\hat{\mathbf{H}}_1(k,l)\mathbf{H}_1^H(k,l) + \sigma^2\mathbf{I} \tag{10.18}$$

where $\hat{\mathbf{H}}_j(k,l)$ and σ^2 denote the estimated channel matrix and noise power, respectively, P_1 is the transmission power of the serving cell and is given by $P_1 = E[|\mathbf{s}_1(k,l)|^2]$.

Due to the linearity and unitary properties of DFT, an equivalent equalization method would be to obtain a frequency-domain MMSE estimate for each symbol in the frequency-domain, and then take the IDFT to obtain the time-domain MMSE symbol estimation. The MMSE estimation for each frequency-domain symbol is obtained by linearly combining received signals collected from multiple receive antennas in the frequency-domain, using MMSE combining weights $\mathbf{W}(k) = [\mathbf{H}(k)\mathbf{H}^H(k) + \mathbf{R}(k)]^{-1}\mathbf{H}(k)$, where k is the sub-carrier index, $\mathbf{H}(k)$ is a vector representing the frequency response for the layer signal of interest (one element per receive antenna), and $\mathbf{R}(k)$ is the impairment covariance matrix encompassing the spatial correlation between the impairment components. The performance of this simple MMSE equalizer asymptotically approaches the theoretical capacity in a SIMO channel. However, in a MIMO channel, LMMSE equalizer performance is far from the SIMO capacity due to the presence of spatial multiplexing interference [127].

10.9.5.2 MRC receiver

The weighting matrix in an MRC receiver for rank-1 transmission can be represented as follows [25–27,43,44]:

$$\mathbf{W}_1(k,l) = \hat{\mathbf{H}}_1^H(k,l) \tag{10.19}$$

where $\hat{\mathbf{H}}_1(k,l)$ is the estimated channel matrix.

10.9.5.3 MMSE-IRC receiver

As an enhanced receiver, the MMSE-IRC receiver can suppress not only the inter-stream interference, but also the inter-cell interference when the degrees of

freedom at the receiver are sufficient, i.e., the number of receiver antennas is greater than the number of desired data streams. The MMSE-IRC receiver weighting matrix can be expressed as follows:

$$\mathbf{W}_1(k,l) = \hat{\mathbf{H}}_1^H(k,l)\mathbf{R}^{-1} \tag{10.20}$$

where $\hat{\mathbf{H}}_1(k,l)$ and $\mathbf{R}$ denote the estimated channel matrix and channel covariance matrix, respectively. To obtain the MMSE-IRC receiver weighting matrix, the covariance matrix including the sources of inter-cell interference must be estimated. Various schemes can be considered for this purpose, as described below.

In a covariance matrix estimation scheme based on cell-specific reference signals, the covariance matrix is estimated at the location of the CRSs using the following equations:

$$\begin{aligned}\mathbf{R} &= P_1\hat{\mathbf{H}}_1(k,l)\hat{\mathbf{H}}_1^H(k,l) + \frac{1}{N_{\text{sp}}}\sum_{(k,l)\in\{(k_{\text{CRS}},l_{\text{CRS}})\}}\tilde{\mathbf{r}}(k,l)\tilde{\mathbf{r}}^H(k,l)\\ \tilde{\mathbf{r}}(k,l) &= \mathbf{r}(k,l) - \hat{\mathbf{H}}_1(k,l)\mathbf{s}_1(k,l)\end{aligned} \tag{10.21}$$

where P_1 is the transmission power of the serving cell which is given by $P_1 = E[|\mathbf{s}_1(k,l)|^2]$ and N_{sp} is the number of sampling resource elements.

In a DM-RS-based covariance matrix estimation scheme, which is applicable when DM-RS are configured, the covariance matrix is estimated at DM-RS resource elements using the following equations:

$$\begin{aligned}\mathbf{R} &= P_1\hat{\mathbf{H}}_1(k,l)\hat{\mathbf{H}}_1^H(k,l) + \frac{1}{N_{\text{sp}}}\sum_{(k,l)\in\{(k_{\text{DM-RS}},l_{\text{DM-RS}})\}}\tilde{\mathbf{r}}(k,l)\tilde{\mathbf{r}}^H(k,l)\\ \tilde{\mathbf{r}}(k,l) &= \mathbf{r}(k,l) - \hat{\mathbf{H}}_1(k,l)\mathbf{s}_1(k,l)\end{aligned} \tag{10.22}$$

In a data-based covariance matrix estimation scheme, the covariance matrix is estimated at PDSCH resource elements using the following equations:

$$\mathbf{R} = \frac{1}{N_{\text{sp}}}\sum_{(k,l)\in\{(k_{\text{PDSCH/DM-RS}},l_{\text{PDSCH/DM-RS}})\}}\mathbf{r}(k,l)\,\mathbf{r}^H(k,l) \tag{10.23}$$

where $\{(k_{\text{PDSCH/DM-RS}}, l_{\text{PDSCH/DM-RS}})\}$ denotes the set of resource elements assigned to DM-RS or PDSCH data sub-carriers.

10.9.5.4 SIC receiver

An SIC receiver is a good candidate for MIMO reception. It can be shown that SIC receivers with per-layer rate control can achieve MIMO capacity in non-dispersive channels [127]. The operation of an SIC receiver can be described as follows. The receiver first detects the signal sent by the first layer and after successful detection, it cancels the interference contributed by the detected signal before it detects the other layers. The process is repeated until all the layers are detected. Typically, each layer is canceled only when the CRC check is successful. With perfect per-layer rate control, the transmission rate for each layer is

chosen to satisfy sufficiently low BLER; consequently, the SIC receiver can cancel interference contributed by previously detected layers. An SIC receiver typically consists of a number of LMMSE equalizers. The role of these MMSE equalizers is to suppress the residual interference. The cancelation of other layers is reflected in the impairment correlation, and thus in the MMSE combining weights. The cancelation of the detected layers allows the MMSE equalizer to use its available degree of freedom to better suppress other dominant interfering signals, resulting in a reduced interference level and a higher SINR.

In practice, there are some limitations pertaining to an SIC receiver operation e.g., an SIC receiver does not address the ISI problem. Although frequency-domain MMSE equalization is effective in suppressing ISI, there is an opportunity to achieve small performance improvement by properly canceling ISI. Moreover, turbo encoding and CRC checking is not necessarily performed on a per-layer basis, rather per-codeword rate control and CRC checking is used for uplink MIMO. For example, for the rank-4 transmission, the first and second layers are mapped to the same codeword and share the same CRC bits. Hence, these two layers need to be decoded jointly rather than individually. As a result, prior to the decoding stage, the second layer receiver cannot cancel the interference contributed by the first layer, resulting in high intra-codeword interference [127].

10.10 Uplink transmission modes

In order to support uplink SU-MIMO, the concept of transmission mode for PUSCH was introduced in the LTE Rel-10 to differentiate between single-antenna and spatial multiplexing transmission. The uplink transmission modes are as follows:

- PUSCH transmission mode 1, in which uplink transmission is from a single antenna port.
- PUSCH transmission mode 2, where uplink transmission is from multiple antenna ports. In this mode, the UE can be configured to transmit from either two or four antenna ports. If a UE is configured in PUSCH transmission mode 2, it can transmit up to two transport blocks per subframe.

The eNB signals the uplink transmission mode to the UE via an RRC connection setup, RRC connection reconfiguration, or RRC connection reestablishment message. Transmission mode 2 allows dynamic switching between single-antenna and spatial multiplexing transmission [14]. The transport blocks are mapped to one or more layers according to the same rules discussed for the downlink in LTE Rel-8. Each transport block is independently acknowledged through PHICH. The PHICH index for the first codeword is the same as that used in LTE Rel-8 for single-codeword PUSCH transmission, i.e., associated with the lowest PRB index of the PUSCH resource allocation. The PHICH index for the second

codeword is related to the first by an offset. The PDCCH resource grant for uplink MIMO transmissions includes two independent NDIs to indicate whether a retransmission is anticipated. The closed-loop codebook-based precoding is used for PUSCH in a similar way to the LTE Rel-8 PDSCH in transmission mode 4. The UE is instructed by the eNB to use a specific rank and precoding matrix signaled within the uplink grant [15]. The uplink transmission modes are applicable when UE is addressed by its C-RNTI. The closed-loop spatial multiplexing is not supported when the UE is addressed by an SPS-RNTI [14]. Transmission mode 1 is the default uplink transmission mode for a UE unless the UE is configured for another uplink transmission mode via higher-layer signaling. When a UE configured in transmission mode 2 receives a DCI format 0 (uplink scheduling grant), it assumes that PUSCH transmission is associated with transport block 1 and that transport block 2 is disabled.

10.11 Uplink feedback in LTE/LTE-Advanced

In wireless communications, CSI refers to channel properties of a wireless communication link. This information describes how a signal propagates from the transmitter to the receiver and represents the combined effect of scattering, multipath fading, signal power attenuation with distance, etc. The knowledge of CSI at the transmitter and/or the receiver makes it possible to adapt data transmission to current channel conditions, which is crucial for achieving reliable and robust communication with high data rates in multi-antenna systems. The CSI is often required to be estimated at the receiver, and usually quantized and fed back to the transmitter. The downlink channel can be estimated from uplink reference signals in TDD systems under certain conditions due to reciprocity. In general, the transmitter and receiver can observe different CSI.

There are two types of CSI, i.e., instantaneous CSI and statistical CSI. In instantaneous CSI or short-term CSI, the current channel conditions are known, which can be interpreted as knowing the impulse response of a digital filter. This provides an opportunity to adapt the transmitted signal to the impulse response and thereby to optimize the received signal for spatial multiplexing or to achieve low bit error rates. In statistical CSI or long-term CSI, the statistical characteristics or statistics of the channel are known. The latter information may include the type of fading distribution, the average channel gain, the line-of-sight component, and the spatial correlation. Similar to the instantaneous CSI, this information can be used for optimization of transmission parameters.

The CSI estimation accuracy is practically limited by how fast the channel conditions are varying. In fast-fading channels where the channel conditions may vary rapidly during transmission of a single information symbol, only statistical CSI is reasonable. On the other hand, in slow-fading scenarios, the instantaneous CSI can be estimated with reasonable precision and used for transmission

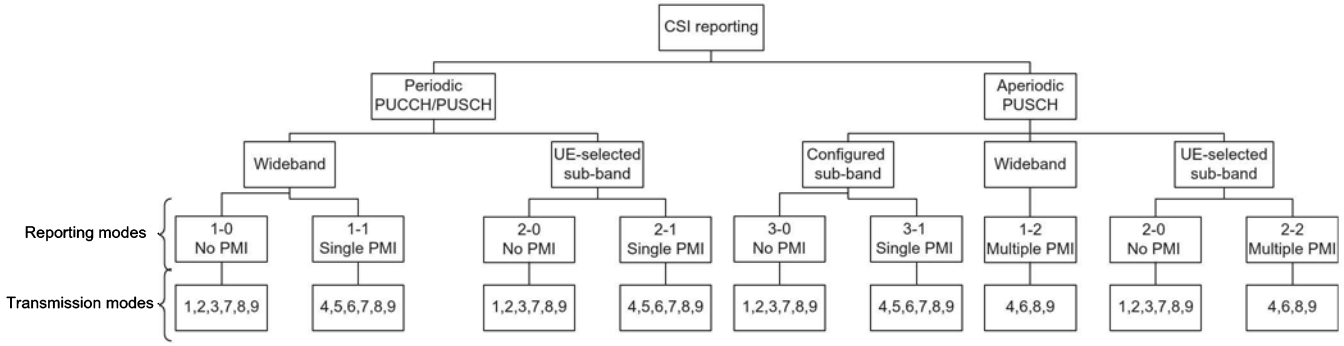
adaptation for a period of time before becoming obsolete. In practical scenarios, the available CSI is often manifested as instantaneous CSI with some estimation/quantization error combined with some statistical information. Recall that in a narrowband flat-fading channel with multiple transmit and receive antennas, the system is modeled as $\mathbf{y} = \mathbf{Hx} + \mathbf{n}$, where $\mathbf{y}$ and $\mathbf{x}$ are the received and transmitted signal vectors, respectively, $\mathbf{H}$ and $\mathbf{n}$ are the channel matrix and the receiver noise vector, respectively. The noise is often modeled as circular symmetric complex normal random variable with statistical distribution $\mathbf{n} \sim Z(\mathbf{0}, \mathbf{R_n})$ where the mean value is zero and the noise covariance matrix $\mathbf{R_n}$ can be estimated. In the case of instantaneous CSI, the channel matrix $\mathbf{H}$ is known; however, due to channel estimation errors, the channel information can be represented as $\hat{\mathbf{H}} = \mathbf{H} + \mathbf{e}$ in which $\text{vec}(\hat{\mathbf{H}}) \sim Z(\text{vec}(\mathbf{H}), \mathbf{R_e})$, where $\hat{\mathbf{H}}$ denotes the estimated channel matrix and $\mathbf{R_e}$ is the estimation error covariance matrix. The vectorization operator[15] $\text{vec}(\cdot)$ is used to obtain the column representation of matrix $\mathbf{H}$. In the case of statistical CSI, the statistics of $\mathbf{H}$ are known. For instance, in a Rayleigh fading channel, this corresponds to $\text{vec}(\mathbf{H}) \sim Z(\mathbf{0}, \mathbf{R_H})$ for a known channel covariance matrix $\mathbf{R_H}$ [170].

The uplink feedback in LTE/LTE-Advanced for support of downlink data transmission consists of RI, PMI, PTI, and CQI. The UE uses the UCI to provide the eNB with feedback that includes CQI, PMI, PTI, RI, scheduling requests, and HARQ acknowledgments. The UE sends the uplink feedback to the eNB using PUCCH or PUSCH. As mentioned earlier, LTE Rel-8/9 does not support simultaneous transmission of PUCCH and PUSCH in the uplink.

Figure 10.55 illustrates the various forms of CSI reporting. The CSI reporting is divided into periodic and aperiodic categories. The periodic CSI reporting uses PUCCH unless data transmission is already scheduled on PUSCH. The aperiodic CSI reporting is always transmitted via PUSCH. The aperiodic reporting can be triggered using a flag within the DCI that is used to allocate PUSCH resources. Since the capacity of PUSCH is greater than that of PUCCH, larger control information payload can be included in aperiodic CSI feedback.

The scheduling request is not explicitly sent on PUSCH, rather the UE includes a buffer status report (BSR) MAC control element in the uplink MAC PDUs. The BSR MAC control element provides the eNB with information regarding the amount of data in the UE's local buffer awaiting transmission. The LTE Rel-10 allows simultaneous transmission of PUCCH and PUSCH in the same uplink subframe. In this case, the UCI and feedback can be sent on PUCCH, whereas aperiodic CSI reports and user data can be transmitted on PUSCH.

[15]In linear algebra and matrix theory, the vectorization of a matrix is a linear transformation which converts the matrix into a column vector. More specifically, the vectorization of an $M \times N$ matrix $\mathbf{H}$, denoted by $\text{vec}(\mathbf{H})$, in which $\text{vec}(\mathbf{H})$ is an $MN \times 1$ column vector is obtained by stacking the columns of the matrix $\mathbf{H}$ on top of each other, as follows: $\text{vec}(\mathbf{H}) = (h_{11}, h_{21}, \ldots, h_{M1}; h_{12}, h_{22}, \ldots, h_{M2}; \ldots; h_{1N}, h_{2N}, \ldots, h_{\text{MN}})^{\text{T}}$ where h_{ij} represents the (i,j) element of matrix $\mathbf{H}$ and the superscript T denotes the transpose operation. The vectorization operation can be interpreted as the isomorphism $\mathbf{H}^{M \times N} := \mathbf{H}^{M} \otimes \mathbf{H}^{N} \cong \mathbf{H}^{\text{MN}}$ between these vector spaces (of matrices and vectors) in coordinates [30–33].



IGURE 10.55

Classification of CSI reporting modes [14].

The RI indicates the number of spatial layers which can be supported by the UE under current channel conditions. It has been observed in the course of LTE evaluation that the frequency-selective RI reporting does not provide significant performance benefit; therefore, only one wideband RI is reported for the entire bandwidth [122]. However, the reporting of PMI and CQI can be in the form of wideband or sub-band (frequency-selective). For RI values equal to one, only one CQI is reported for each reporting unit in frequency, which is either wideband or sub-band in the case of frequency-selective reporting. For RI values greater than one, the CQI for each codeword is reported for the closed-loop spatial multiplexing, as different codewords may be assigned to different layers, while only one CQI is reported for the open-loop spatial multiplexing, as one codeword interacts with all layers. The PMI indicates the preferred precoding candidate for the corresponding frequency unit, e.g., a particular sub-band or the entire system bandwidth, and is selected from the possible precoding candidates depending on the number of transmit antennas and according to the RI value.

The CQI metric indicates a combination of the maximum data rate and the modulation scheme, which can achieve BLER less than 10% at the UE after detection, assuming that the reported rank and PMI are applied to the time–frequency resource (see Figure 10.57). Given this definition of CQI, PMI, and RI, the UE can report the maximum data rate that it can receive and demodulate, taking into account its receiver capability and channel conditions. In the case of the frequency-selective PMI/CQI reporting, the UE reports a PMI/CQI for each sub-band (Figure 10.56). For the non-frequency-selective wideband PMI/CQI reporting, the UE reports a single wideband PMI/CQI corresponding to the entire bandwidth. In the frequency-selective reporting mode, the sub-band CQI is reported as a differential value with respect to the wideband CQI in order to reduce the signaling overhead. The sub-band CQI reports are encoded differentially with respect to the wideband CQI using 2 bits as follows: $\Delta\text{CQI}_{\text{sub-band}} = \text{CQI}_{\text{sub-band(index)}} - \text{CQI}_{\text{wideband}}(\text{index})$, where the permissible sub-band differential CQI offset values are $\{\leq -1, 0, 1, \geq 2\}$. In best-$M$ average reporting, the UE first estimates the channel quality for each sub-band. Then it selects the M best values and reports to the eNB a single average CQI corresponding to the MCS/TBS that the UE can receive correctly, assuming that the eNB schedules the UE on those M sub-bands. The parameter M depends on the system bandwidth and corresponds to approximately 20% of the system bandwidth. Figure 10.56 shows the principle of the best-M average CQI measurement and reporting scheme. The CQI value for the M selected sub-bands for each codeword is encoded differentially using 2 bits relative to the corresponding wideband CQI as follows: $\Delta\text{CQI} = \text{CQI}_{\text{average-bestM-sub-band}}(\text{index}) - \text{CQI}_{\text{wideband}}(\text{index})$, where the possible differential CQI values are $\{\leq 1, 2, 3, \geq 4\}$. It must be noted that the subtraction of the wideband CQI value prior to quantization of sub-band CQI values reduces the dynamic range and thus the quantization error.

When the frequency-selective CQI reporting is configured, sub-band CQIs as well as wideband CQI are reported, and the wideband CQI serves as the baseline

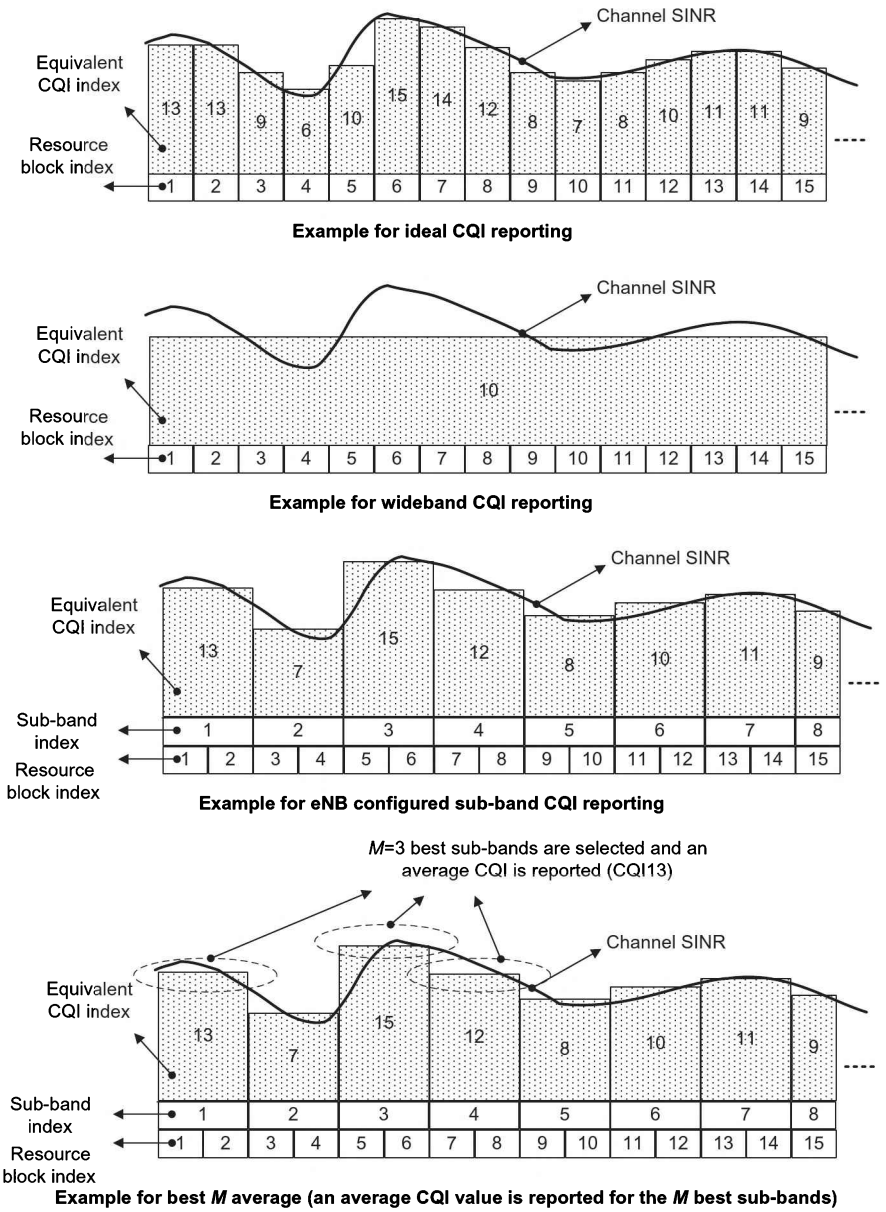


FIGURE 10.56

Graphic comparison of various CQI reporting methods [170].

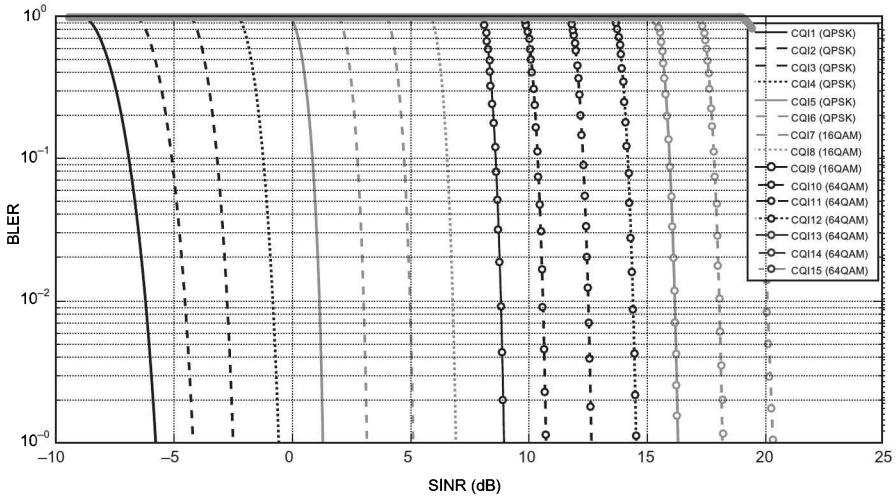


FIGURE 10.57

Link-level variation of BLER versus SINR with CQI as a parameter [137].

for recovering the downlink channel condition over the entire frequency band. The frequency-selective reporting results in a large signaling overhead. In the cases where the uplink overhead is the limiting factor, the eNB can also configure non-frequency-selective CQI/PMI reports, to mitigate various channel conditions and different antenna configurations, while keeping the signaling overhead at an appropriate level. Thus, various feedback modes are specified depending on the frequency selectivity of the CQI and the PMI reports.

The physical channels that can be used for uplink feedback signaling are PUCCH and PUSCH. The uplink feedback via PUSCH is used to accommodate a large amount of feedback information in a single reporting instance. For example, the reporting on PUSCH can include RI, wideband CQI per codeword, and the PMI for each sub-band. Note that the rank indicator is separately encoded from the other fields using 1 bit for the case of two transmit antennas and 2 bits for the case of four transmit antennas. The number of bits for the other information fields is determined according to the rank indicator. Another example is the reporting of the RI, wideband PMI, wideband CQI per codeword, and the sub-band differential CQI for each sub-band per codeword. It is noted that simultaneous reporting of sub-band differential CQI and sub-band PMI is not supported due to excessive signaling overhead.

The physical uplink control channel, on the other hand, is designed for transmission of small amounts of control signaling information. Therefore, for PUCCH reporting modes, separate time instances are used for reporting RI, wideband CQI/PMI, and sub-band CQI of the sub-band selected by the UE. The spatial differential CQI represents the difference between the CQIs of two codewords

and is defined for wideband CQI and sub-band CQI. In the case of sub-band CQI feedback, each reporting instance corresponds to a group of sub-bands, from which the UE selects the sub-band with the best CQI. Due to these characteristics, the eNB may configure periodic reporting of a limited amount of feedback information on PUCCH, while triggering the UE to report a large amount of detailed feedback information on PUSCH, if accurate channel information is necessary for transmission of large amounts of data in the downlink.

The set of sub-bands S that the UE is required to conduct measurements for CQI reporting spans the entire downlink system bandwidth. A sub-band is a set of L_{sb} contiguous PRBs, where L_{sb} is dependent on the system bandwidth. Note that the last sub-band in set S may have fewer than k contiguous PRBs depending on N_{RB}^{DL}. The number of sub-bands for system bandwidth N_{RB}^{DL} is defined by $N_{sb} = \lceil N_{RB}^{DL}/L_{sb} \rceil$. The sub-bands are indexed in the order of increasing frequency and non-increasing size starting at the lowest frequency while taking the following rules into consideration [5]:

- For transmission modes 1, 2, 3, and 5 as well as transmission modes 8, 9, and 10 without PMI/RI reporting, transmission mode 4 with RI equal to one, and transmission modes 8, 9, and 10 with PMI/RI reporting and RI equal to one, a single 4-bit wideband CQI is reported.
- For transmission modes 3 and 4 as well as transmission modes 8, 9, and 10 with PMI/RI reporting, CQI is calculated assuming transmission of one codeword for RI equal to one and two codewords for RI greater than one.
- For transmission mode 4 with RI greater than one as well as transmission modes 8, 9, and 10 with PMI/RI reporting, PUSCH-based triggered reporting includes reporting of a wideband CQI which comprises a 4-bit wideband CQI for codeword 0 and a 4-bit wideband CQI for codeword 1.
- For transmission mode 4 with RI greater than one 1 as well as transmission modes 8, 9, and 10 with PMI/RI reporting, PUCCH-based reporting includes reporting a 4-bit wideband CQI for codeword 0 and a wideband spatial differential CQI. The wideband spatial differential CQI value includes a 3-bit wideband spatial differential CQI value for codeword 1 offset level where codeword 1 offset level is the difference between the wideband CQI index for codeword 0 and wideband CQI index for codeword 1.

A UE is semi-statically configured by higher layers to feed back CQI, PMI, and corresponding RI on the same PUSCH using one of the CSI reporting modes provided in Table 10.28. Note that CQI/PMI feedback modes via PUSCH are not supported for a serving cell with bandwidth $N_{RB}^{DL} \leq 7$ [5].

As given in Table 10.28 and shown Figure 10.55, the aperiodic CQI/PMI feedback types reported via PUSCH can be categorized and described as follows [5]:

- *Wideband feedback*
  - Mode 1-2: For each sub-band, a preferred precoding matrix is selected from the codebook subset assuming transmission is scheduled only in that

Table 10.28 CQI and PMI Feedback Types for PUSCH/PUCCH CSI Reporting Modes [5]

	PMI Feedback Types via PUSCH			PMI Feedback Types via PUCCH	
	No PMI	Single PMI	Multiple PMI	No PMI	Single PMI
Wideband (wideband CQI)	–	–	Mode 1-2	Mode 1-0	Mode 1-1
UE Selected (sub-band CQI)	Mode 2-0	–	Mode 2-2	Mode 2-0	Mode 2-1
Higher-layer configured sub-band CQI)	Mode 3-0	Mode 3-1	–	–	–

sub-band. The UE reports one wideband CQI value per codeword, which is calculated assuming the use of the corresponding selected precoding matrix in each sub-band and transmission on a set of sub-bands. The UE further reports the selected PMI for a set of sub-bands, except for transmission modes 9 and 10 configured with eight CSI-RS ports where the first PMI is reported for the set of sub-bands, and the second PMI is reported for each sub-band in the set.

- *Higher-layer configured sub-band feedback*
  - Mode 3-0: The UE reports a wideband CQI value which is calculated assuming transmission on a set of sub-bands. The UE also reports one sub-band CQI value for each set of sub-bands. The sub-band CQI value is calculated assuming transmission is scheduled only in that sub-band. Both wideband and sub-band CQI represent channel quality for the first codeword, even if the rank indicator is greater than one.
  - Mode 3-1: A single precoding matrix is selected from the codebook subset assuming transmission on a set of sub-bands. The UE reports one sub-band CQI value per codeword for each set of sub-bands, which are calculated assuming the use of a single precoding matrix in all sub-bands and assuming transmission is scheduled in the corresponding sub-band. The UE reports a wideband CQI value per codeword, which is calculated assuming the use of a single precoding matrix in all sub-bands, and transmission is scheduled on a set of sub-bands. The UE reports the selected single precoding matrix indicator, except for transmission modes 9 and 10 configured with eight CSI-RS ports where two precoding matrix indicators are reported.
- *UE-selected sub-band feedback*
  - Mode 2-0: The UE selects a set of M preferred sub-bands of size L_{sb} (where L_{sb} and M are given in Table 10.29 for each system bandwidth) within the set of sub-bands S. The UE also reports one CQI value

Table 10.29 Sub-band Size L_{sb} and Number of Sub-bands M in S as a Function of System Bandwidth [5]

Number of Downlink Resource Blocks N_{RB}^{DL}	Sub-band Size L_{sb} (Resource Blocks)	Number of Sub-bands M
6–7	N/A	N/A
8–10	2	1
11–26	2	3
27–63	3	5
64–110	4	6

reflecting transmission only over the M selected sub-bands determined in the previous step. The CQI represents channel quality for the first codeword, even when RI > 1. Additionally, the UE reports one wideband CQI value which is calculated assuming transmission on a set of sub-bands S. The wideband CQI represents channel quality for the first codeword, even when RI > 1. For transmission mode 3, the reported CQI values are calculated conditioned on the reported RI. For other transmission modes, they are reported conditioned on rank 1.

- Mode 2-2: The UE performs joint selection of the set of M preferred sub-bands of size L_{sb} within the set of sub-bands S and a preferred single precoding matrix selected from the codebook subset that is preferred to be used for transmission over the M selected sub-bands. The UE reports one CQI value per codeword reflecting transmission only over the selected M preferred sub-bands and using the same selected single precoding matrix in each of the M sub-bands. Except for transmission modes 9 and 10 with eight CSI-RS ports configured, the UE also reports the selected single precoding matrix indicator preferred for the M selected sub-bands. A UE further reports the selected single precoding matrix indicator for all sub-bands in the set S. For transmission modes 9 and 10 with eight CSI-RS ports configured, the UE reports the first precoding matrix indicator for all sub-bands in the set S. A UE further reports a second precoding matrix indicator for all sub-bands in the set S and a second precoding matrix indicator for the M selected sub-bands A single precoding matrix is selected from the codebook subset assuming transmission on a set of sub-bands S. A UE provides the wideband CQI value per codeword which is calculated assuming the use of a single precoding matrix in all sub-bands and transmission on a set of S sub-bands S. For transmission modes 4, 8, 9, and 10, the reported PMI and CQI values are calculated conditioned on the reported RI. For other transmission modes, they are reported conditioned on rank 1. For all UE-selected sub-band feedback modes, the UE further provides the positions of the M selected sub-bands using a combinatorial index [5].

A UE can be semi-statically configured by higher layers to periodically send different CSI (CQI, PMI, PTI, and/or RI) on PUCCH using the reporting modes given in Table 10.28. The periodic CSI reporting mode for each serving cell is configured by higher-layer signaling. For the UE-selected sub-band CQI, a CQI report in a certain subframe of a certain serving cell describes the channel quality in a particular part or in particular parts of the bandwidth of that serving cell, described subsequently as bandwidth part or parts. The bandwidth parts are indexed in the order of increasing frequency and decreasing sizes starting at the lowest frequency. The following CQI/PMI and RI reporting types with distinct periods and offsets are supported for the PUCCH CSI reporting modes given in Table 10.28 [5]:

- Type 1 report supports CQI feedback for the UE selected sub-bands.
- Type 1a report supports sub-band CQI and second PMI feedback.
- Type 2, 2b, and 2c report supports wideband CQI and PMI feedback.
- Type 2a report supports wideband PMI feedback.
- Type 3 report supports RI feedback.
- Type 4 report supports wideband CQI.
- Type 5 report supports RI and wideband PMI feedback.
- Type 6 report supports RI and PTI feedback.

10.12 Uplink transmitter and receiver chain

An example of a transmitter/receiver chain of an LTE modem is depicted in Figures 10.58 and 10.59 [171–173]. Note that the modem implementation presented in this section only includes the physical layer processing functions assuming higher layer protocols are processed by another processor. The digital front-end unit is the interface between the analog front-end and digital baseband modules in the wireless systems. The function of the digital front end (block of digital filters) is typically to perform gain control, sampling rate conversion, pulse shaping, matched filtering, and phase correction. The digital front end is functionally simple relative to other baseband blocks; however, it consumes a significant portion of the chip area and power. As an OFDM system, LTE is sensitive to carrier frequency offset (CFO) which causes inter-carrier interference. The timing synchronization and fractional CFO estimation/correction can mitigate the effects of CFO and the oscillator phase noise. Integer frequency offset estimation is then applied to remove misalignment, which is an integer multiple of the sub-carrier spacing. Although a large portion of CFO can be compensated, there is still a residual frequency offset due to estimation errors. The residual frequency offset is estimated based on the frequency-domain symbols after the FFT operation in the receiver.

Similar to other OFDM systems, reference signals are inserted during sub-carrier mapping in both time and frequency dimensions. The reference signals

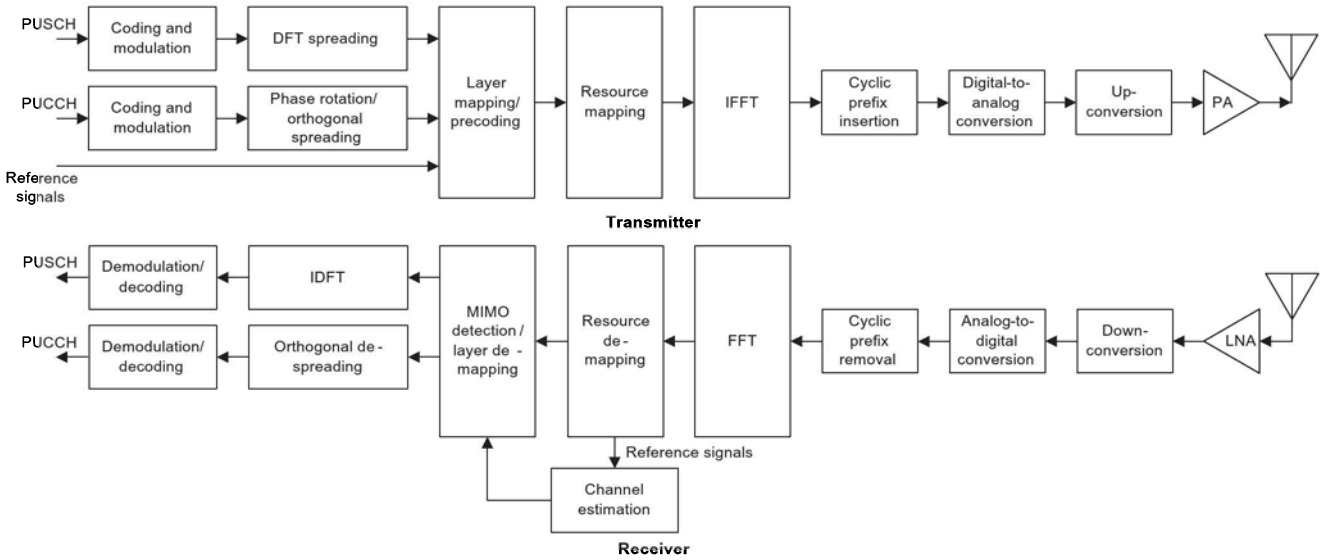


FIGURE 10.58

Example of uplink transmission and reception chains [14].

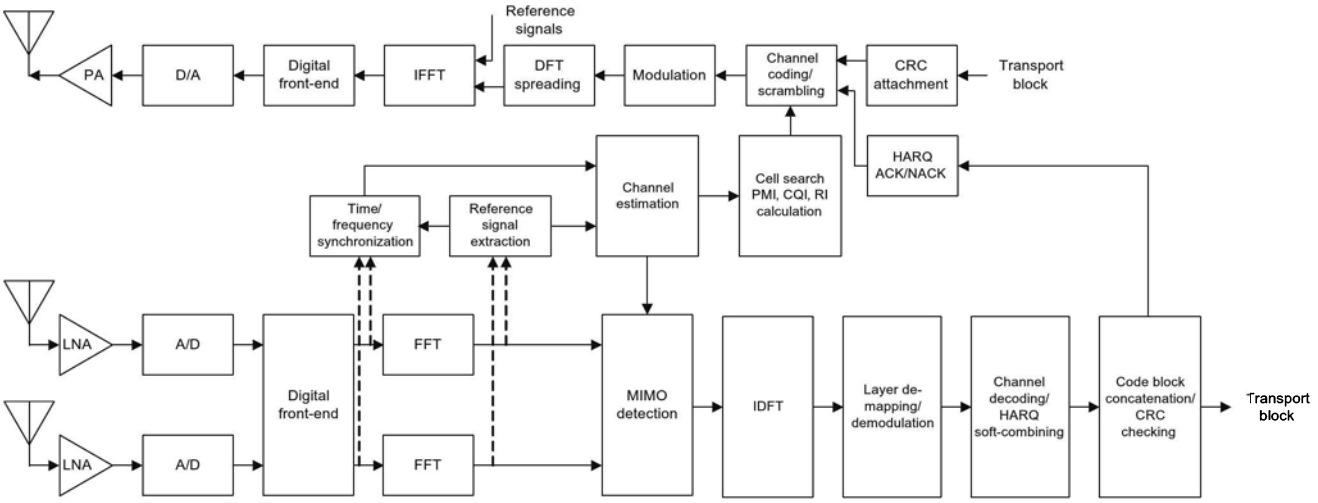


FIGURE 10.59

Block diagram of an example LTE UE modem (physical layer) [173].

transmitted from multiple antennas are mutually orthogonal (provided that the antennas are uncorrelated), which means the channel impulse response between different transmit-receive antenna pairs can be separately estimated. This assumption would reduce high complexity of MIMO channel estimation at the cost of lower spectral efficiency. For MIMO systems, a major challenge is the separation and detection of the transmitted symbols at the receiver given the amount of operations involved (e.g., matrix inversion and multiplication/division). Among different detection algorithms, maximum likelihood detection is an optimum detector that computes the following likelihood function:

$$L(b_i|\mathbf{r}) = \log\left(\frac{\sum_{\mathbf{s}:b_i(\mathbf{s})=1}\exp(-\sigma_0^{-2}||\mathbf{r}-\hat{\mathbf{H}}\mathbf{s}||^2)}{\sum_{\mathbf{s}:b_i(\mathbf{s})=0}\exp(-\sigma_0^{-2}||\mathbf{r}-\hat{\mathbf{H}}\mathbf{s}||^2)}\right) \tag{10.24}$$

In the above equation, $b_i(\mathbf{s})$ denotes the ith bit of the input sequence $\mathbf{s}$, σ_0^2 is the noise variance, and $\mathbf{r} = \mathbf{H}\mathbf{s} + \mathbf{n}$ is the received signal. The functional block diagram in Figure 10.59 shows an example of the internal data flows through an LTE UE with two receive antennas and one transmit antenna. The RF signal is received by the receiver antennas, down-converted, scaled by an automatic gain control, and digitized by an analog-to-digital converter (A/D) within the analog and digital front-end module including a sample rate converter and a numerically controlled oscillator.

The baseband processor receives the digitized signal in the form of complex-valued samples from the A/D and delivers the decoded bit stream to a higher layer protocol and application processor. It first removes the cyclic prefix, transforms the signal into frequency-domain by an FFT operation, performs channel estimation, equalization, log-likelihood ratio (LLR) calculation, HARQ combining, channel decoding, and CRC check for different physical channels. In addition, control information for closed-loop MIMO operation is generated, i.e., CQI, PMI, and RI. In the uplink direction, PUSCH data is channel coded, DFT spread, and mapped to resource elements together with modulated PUCCH and modulated reference signals. Following IFFT and cyclic prefix insertion procedures, the data is sent to transmitter front end and RF circuitry. For random access, the corresponding PRACH is processed. In a typical receiver, synchronization is usually initially conducted to acquire information such as the beginning of frame and the CFO calculation and correction [173].

The solution to Eq. (10.24) requires calculation of the likelihood function over the entire set of possible transmitted vectors, resulting in a significant amount of complexity in practice. However, since maximum likelihood provides the best theoretical performance, it is commonly used as a benchmark when comparing other algorithms. Linear detection algorithms such as MMSE have very low complexity. The MMSE equalizer is defined as follows: $\hat{s}_{\text{MMSE}} = \mathbf{W}_{\text{MMSE}}\mathbf{r} = (\hat{\mathbf{H}}^H\hat{\mathbf{H}} + \sigma_0^2\mathbf{I})^{-1}\hat{\mathbf{H}}^H\mathbf{r}$. The MMSE detection is the most commonly used detection scheme and involves matrix inversion which can be efficiently performed through direct inversion with sufficient numerical stability. Despite the low complexity,

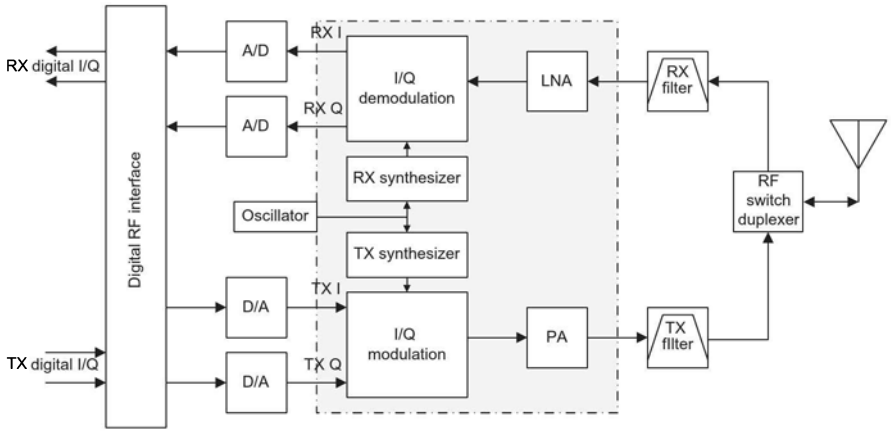


FIGURE 10.60

Simplified block diagram of RF transmitter and receiver in an LTE device [159].

MMSE detection has relatively poor performance, especially in slow fading channels. As a trade-off between detection performance and implementation complexity, soft-output MIMO detectors and sphere decoders can be used [169].

As shown in Figures 10.59 and 10.60, the radio signals received by the RF front end are down-converted to analog baseband signals (using a zero-IF converter), then they are converted to digital baseband signals using A/D converters. The digital front end applies filtering to the baseband signals and FFT is applied to transform the time-domain signal into frequency-domain where channel estimation and symbol detection are performed. In LTE, the channel estimator uses the reference signals to estimate the channel matrix $\mathbf{H}$ for all data sub-carriers. The estimated channel matrix $\hat{\mathbf{H}}$ and the received symbol vector $\mathbf{r}$ belonging to the current user will be extracted for MIMO detection. The above functions are performed by the baseband processor. The estimated channel matrix is conveyed to the MIMO detector together with the received symbols extracted from data sub-carriers. The coefficients are fed to the detector to compute the LLR soft-output $L(b_i^k)$ (i.e., ith bit of the input vector on the kth sub-carrier). For example, in case of MMSE detection, the detector fetches the MMSE weighting matrix $\mathbf{W}_{\text{MMSE}}$ from the local memory and multiplies the MMSE weighting matrix $\mathbf{W}_{\text{MMSE}}$ with the received symbol vectors $\mathbf{r}$ in order to compute $\hat{s}$ and to map $\hat{s}$ to LLR values. The LLR values are then passed to the FEC decoder where it will be de-interleaved and processed by the channel decoder to generate the output bits. The FEC module contains the soft buffer for chase combining in HARQ and a parallel turbo decoder. Although many baseband processing functions can be assigned to a programmable processor, there are still some tasks which need to be implemented in dedicated hardware to meet the performance and power constraints. In that case, hardware accelerators are added to the on-chip system. They are typically

controlled by a number of control registers which can be set by the baseband processor.

The RFICs in the UE may include different portions of the schematic block diagram shown in Figure 10.60, with some containing the transmitter or receiver only, and others combining transmitter and receiver in one component. Traditionally RFICs have used analog baseband I/Q inputs and outputs. However, digital I/Q interfaces are becoming more common. The mobile industry processor interface (MIPI) alliance has developed the DigRF standard [174], which describes the high-speed digital baseband to RFIC interface for new generation of cellular radios, which includes embedded control protocols for the RFIC.

References

3GPP Specifications[16]

[1] 3GPP TS 36.101, Evolved Universal Terrestrial Radio Access (E-UTRA); User Equipment (UE) radio transmission and reception (Release 11), December 2012.

[2] 3GPP TS 36.104, Evolved Universal Terrestrial Radio Access (E-UTRA); Base Station (BS) radio transmission and reception (Release 11), December 2012.

[3] 3GPP TS 36.211, Evolved Universal Terrestrial Radio Access (E-UTRA), Physical Channels and Modulation (Release 11), December 2012.

[4] 3GPP TS 36.212, Evolved Universal Terrestrial Radio Access (E-UTRA) Multiplexing and Channel Coding (Release 11), December 2012.

[5] 3GPP TS 36.213, Evolved Universal Terrestrial Radio Access (E-UTRA); Physical layer procedures (Release 11), December 2012.

[6] 3GPP TS 36.214, Evolved Universal Terrestrial Radio Access (E-UTRA); Physical layer – Measurements (Release 11), December 2012.

[7] 3GPP TS 36.300, Evolved Universal Terrestrial Radio Access (E-UTRA) and Evolved Universal Terrestrial Radio Access Network (E-UTRAN) Overall description, Stage 2 (Release 11), December 2012.

[8] 3GPP TS 36.306, Evolved Universal Terrestrial Radio Access (E-UTRA); User Equipment (UE) Radio Access Capabilities (Release 11), December 2012.

[9] 3GPP TS 36.321, Evolved Universal Terrestrial Radio Access (E-UTRA); Medium Access Control (MAC) Protocol specification (Release 11), December 2012.

[10] 3GPP TS 36.331 Evolved Universal Terrestrial Radio Access (E-UTRA); Radio Resource Control (RRC); Protocol specification (Release 11), December 2012.

[11] 3GPP TR 36.912 Feasibility Study for Further Advancements for E-UTRA (LTE-Advanced) (Release 11), September 2012.

[12] 3GPP TR 36.814 Feasibility Study for Further Advancements for E-UTRA (LTE-Advanced) (Release 9), March 2010.

[13] 3GPP TR 36.819 Coordinated Multi-Point Operation for LTE Physical Layer Aspects (Release 11), December 2011.

[16] 3GPP specifications can be found at the following URL: http://www.3gpp.org/ftp/Specs/archive/36_series/.

Books

[14] C. Johnson, Long Term Evolution in Bullets, second ed., Create Space Independent Publishing Platform, 2012.
[15] S. Sesia, I. Toufik, M. Baker, LTE, the UMTS Long Term Evolution, From Theory to Practice, second ed., John Wiley & Sons, 2011.
[16] E. Dahlman, S. Parkvall, J. Skold, 4G, LTE/LTE-Advanced for Mobile Broadband, Academic Press, 2011.
[17] H. Holma, A. Toskala, LTE Advanced, 3GPP Solution for IMT-Advanced, John Wiley & Sons, 2012.
[18] H. Holma, A. Toskala, LTE for UMTS, Evolution to LTE-Advanced, John Wiley & Sons, 2011.
[19] S. Ahmadi, Mobile WiMAX, A Systems Approach to Understanding IEEE 802.16m Radio Access Technology, Academic Press, 2010.
[20] B. Sklar, Digital Communications, Fundamentals and Applications, second ed., Prentice Hall, 2001.
[21] A. Paulraj, et al., Introduction to Space-Time Wireless Communications, Cambridge University Press, 2008.
[22] W.C. Jakes, Microwave Mobile Communications, second ed., Wiley-IEEE Press, 1994.
[23] S.G. Glisic, Advanced Wireless Communications, 4G Cognitive and Cooperative Broadband Technology, second ed., Wiley Inter-science, 2007.
[24] D.E. Dudgeon, R.M. Mersereau, Multidimensional Digital Signal Processing, Prentice Hall, 1984.
[25] D. Tse, P. Viswanath, Fundamentals of Wireless Communication, Cambridge University Press, 2005.
[26] E. Biglieri, et al., MIMO Wireless Communications, Cambridge University Press, 2010.
[27] A. Goldsmith, Wireless Communications, Cambridge University Press, 2005.
[28] S. Lin, D.J. Costello, Error Control Coding, second ed., Prentice Hall, 2004.
[29] S.L. Marple, Digital Spectral Analysis with Applications, Prentice Hall, 1987.
[30] G.H. Golub, C.F. Van Loan, Matrix Computations, third ed., Johns Hopkins University Press, 1996.
[31] A. Papoulis, Probability, Random Variables and Stochastic Processes, fourth ed., McGraw Hill Higher Education, 2002.
[32] L. Rade, Mathematics Handbook for Science and Engineering, Springer, 2010.
[33] G.A. Korn, T.M. Korn, Mathematical Handbook for Scientists and Engineers, Definitions, Theorems, and Formulas for Reference and Review (Revised Edition), Dover Publications, 2000.
[34] C.E. Shannon, W. Weaver, The Mathematical Theory of Communication, University of Illinois Press, 1998.
[35] F. Dowla, Handbook of RF and Wireless Technologies, Newnes, 2003.
[36] G. Arfken, *Bessel Functions*, Mathematical Methods for Physicists, third ed., Academic Press, 1985.
[37] W.G. Bickley, Bessel Functions and Formulae, Cambridge University Press, Cambridge, England, 1957.
[38] F. Bowman, Introduction to Bessel Functions, Dover, 2010.

[39] H.G. Myung, D. Goodman, Single Carrier FDMA, A New Air Interface for Long Term Evolution, John Wiley & Sons, 2008.
[40] T.M. Cover, J.A. Thomas, Elements of Information Theory, John Wiley & Sons, 1991.
[41] J.G. Proakis, Digital Communications, fifth ed., McGraw-Hill, 2007.
[42] N. Costa, S. Haykin, Multiple-Input Multiple-Output Channel Models, Theory and Practice, John Wiley & Sons, 2010.
[43] C. Oestges, B. Clerckx, MIMO Wireless Communications, from Real-World Propagation to Space-Time Code Design, Academic Press, 2007.
[44] A. Sibille, C. Oestges, A. Zanella, MIMO, from Theory to Implementation, Academic Press, 2010.
[45] I. Stakgold, M.J. Holst, Green's Functions and Boundary Value Problems, third ed., John Wiley & Sons, 2011.
[46] R.G. Gallager, Principles of Digital Communication, Cambridge University Press, 2008.
[47] K. Fazel, G.P. Fettweis, Multi-Carrier Spread-Spectrum, Kluwer Academic Publishers, 1997.

Articles

[48] G. Bauch, G. Dietl, MIMO for 3GPP LTE-Advanced and beyond, Global Telecommunications Conference (GLOBECOM), 2010.
[49] C. Mehlfuhrer, et al., The Vienna LTE simulators—enabling reproducibility in wireless communication research, EURASIP J. Adv. Signal Process, (1) (2011).
[50] H.G. Myung, J. Lim, D.J. Goodman, Single carrier FDMA for uplink wireless transmission, IEEE Veh. Technol. Mag. I (3) (2006).
[51] H. Ekström, et al., Technical solutions for the 3G long-term evolution, IEEE Commun. Mag. 44 (3) (2006).
[52] D. Falconer, et al., Frequency domain equalization for single-carrier broadband wireless systems, IEEE Commun. Mag. 40 (4) (2002).
[53] H. Sari, et al., Transmission techniques for digital terrestrial TV broadcasting, IEEE Commun. Mag. 33 (2) (1995).
[54] C. Berrou, A. Glavieux, P. Thitimajshima, Near Shannon limit error correcting coding and decoding, "turbo codes", in: Proceedings of the IEEE International Conference on Communications, Geneva, Switzerland, May 1993.
[55] 3GPP R1-050397, E-UTRA uplink numerology and frame structure 3GPP TSG RAN WG1, meeting 41, Athens, Greece, 2005.
[56] 3GPP R1-050584, E-UTRA uplink numerology and design, 3GPP TSG RAN WG1, meeting 41bis, Sophia Antipolis, France, 2005.
[57] 3GPP R1-050971, Single carrier uplink options for E-UTRA, 3GPP TSG RAN WG1, meeting 42, London, UK, 2005.
[58] U. Sorger, I. De Broeck M. Schnell, Interleaved FDMA—a new spread-spectrum multiple-access scheme, In: Proceedings of the IEEE International Conference on Communications (ICC), 1998.
[59] K. Bruninghaus, H. Rohling, Multi-carrier Spread Spectrum and its Relationship to Single-Carrier Transmission, In: Proceedings of the IEEE Vehicular Technology Conference (VTC), May 1998.

[60] D. Galda, H. Rohling, A Low Complexity Transmitter Structure for OFDM-FDMA Uplink Systems, in: Proceedings of the IEEE Vehicular Technology Conference (VTC), May 2002.
[61] R. Dinis, D. Falconer, C.T. Lam, M. Sabbaghian, A Multiple Access Scheme for the Uplink of Broadband Wireless Systems, in: Proceedings of the IEEE Global Telecommunications Conference, November 2004.
[62] H. Sari, G. Karam I. Jeanclaude, Frequency-Domain Equalization of Mobile Radio and Terrestrial Broadcast Channels, in: Proceedings of the IEEE Global Telecommunications Conference, November 1994.
[63] D. Falconer, S.L. Ariyavisitakul, A. Benyamin-Seeyar, B. Eidson, Frequency domain equalization for single-carrier broadband wireless systems, IEEE Commun. Mag. 40 (2002).
[64] V. Nangia, K.L. Baum, Experimental broadband OFDM system—field results for OFDM and OFDM with frequency domain spreading, in: Proceedings of the IEEE International Conference on Vehicular Technology, Vancouver, BC, Canada, 2002.
[65] 3GPP R1-062061, Uplink DC subcarrier distortion considerations in LTE, 3GPP TSG RAN WG1, meeting 46, Tallinn, Estonia, 2006.
[66] 3GPP R1-050702, DFT-spread OFDM with pulse shaping filter in frequency domain in evolved UTRA uplink, 3GPP TSG RAN WG1, meeting 42, London, UK, 2005.
[67] 3GPP R1-051434, Optimum family of spectrum-shaping functions for PAPR reduction in SC-FDMA, 3GPP TSG RAN WG1, meeting 43, Seoul, Korea, 2005.
[68] D.C. Chu, Poly-phase codes with good periodic correlation properties, IEEE Trans. Inform. Theory (1972).
[69] B.M Popovic, Generalized chirp-like poly-phase sequences with optimal correlation properties, IEEE Trans. Inform. Theory 38 (1992) 1406–1409.
[70] 3GPP R1-060878, E-UTRA SC-FDMA uplink pilot/reference signal design & TP, 3GPP TSG RAN WG1, meeting 44bis, Athens, Greece, 2006.
[71] 3GPP R1-080576, Way forward on the sequence grouping for UL DM-RS, 3GPP TSG RAN WG1, meeting 51bis, Sevilla, Spain, 2008.
[72] 3GPP R1-072584, Way Forward for PUSCH RS, 3GPP TSG RAN WG1, meeting 49, Kobe, Japan, 2007.
[73] 3GPP R1-072585, Way forward for PUCCH RS, 3GPP TSG RAN WG1, meeting 49, Kobe, Japan, 2007.
[74] 3GPP R1-074278, Hopping and planning of sequence groups for uplink RS, 3GPP TSG RAN WG1, meeting 50bis, Shanghai, China, 2007.
[75] 3GPP R1-080719, Hopping patterns for UL RS, 3GPP TSG RAN WG1, meeting 52, Sorrento, Italy, 2008.
[76] 3GPP R1-081133, WF on UL DM-RS hopping pattern generation, 3GPP TSG RAN WG1, meeting52, Sorrento, Italy, 2008.
[77] 3GPP R1-071341, Uplink reference signal planning aspects, 3GPP TSG RAN WG1, meeting 48bis, St. Julian's, Malta, 2007.
[78] 3GPP R1-080983, Way forward on the cyclic shift hopping for PUCCH, 3GPP TSG RAN WG1, meeting 52, Sorrento, Italy, 2008.
[79] 3GPP R1-073756, Benefit of non-persistent UL sounding for frequency hopping PUSCH, 3GPP TSG RAN WG1, meeting 50, Athens, Greece, 2007.
[80] 3GPP R1-082199, Physical-layer parameters to be configured by RRC, 3GPP TSG RAN WG1, meeting 53, Kansas City, MI, 2008.

[81] 3GPP R1-072671, Uplink channel interleaving, 3GPP TSG RAN WG1, meeting 49bis, Orlando, FL, 2007.
[82] B. Classon et al., Multi-dimensional adaptation and multi-user scheduling techniques for wireless OFDM systems, in: Proceedings of the IEEE International Conference on Communications, Anchorage, Alaska, 2003.
[83] 3GPP R1-071340, Considerations and recommendations for UL sounding RS, 3GPP TSG RAN WG1, meeting 48bis, St Julian's, Malta, March 2007.
[84] 3GPP R1-073756, Benefit of non-persistent UL sounding for frequency hopping PUSCH, 3GPP TSG RAN WG1, meeting 50, Athens, Greece, 2007.
[85] A. Ghosh et al., Uplink control channel design for 3GPP LTE, in: Proceedings of the IEEE International Symposium on Personal, Indoor and Mobile Radio Communications, Athens, Greece, 2007.
[86] 3GPP R1-070084, Coexistance simulation results for 5 MHz E-UTRA/UTRA FDD uplink with revised simulation assumptions, 3GPP TSG RAN WG4, meeting 42, St. Louis,MI, 2007.
[87] S. Zhou, G.B. Giannakis, C.L. Martret, Chip-interleaved block-spread code division multiple access, IEEE Trans. Commun. 50 (2002).
[88] 3GPP R1-080190, Embedding ACK/NACK in CQI reference signals and receiver structures, 3GPP TSG RAN WG1, meeting 51bis, Sevilla, Spain, 2008.
[89] 3GPP R1-073564, Selection of orthogonal cover and cyclic shift for high speed UL ACK channels, 3GPP TSG RAN WG1, meeting 50, Athens, Greece, 2007.
[90] 3GPP R1-080035, Joint proposal on uplink ACK/NACK channelization, 3GPP TSG RAN WG1, meeting 51bis, Sevilla, Spain, 2008.
[91] 3GPP R1-062072, Uplink reference signal multiplexing structures for E-UTRA, 3GPP TSG RAN WG1, meeting 46, Tallinn, Estonia, 2006.
[92] 3GPP R1-080983, Way forward on the cyclic shift hopping for PUCCH, 3GPP TSG RAN WG1, meeting 52, Sorrento, Italy, 2008.
[93] 3GPP R1-080931, ACK/NACK channelization for PRBs containing both ACK/NACK and CQI, 3GPP TSG RAN WG1, meeting 52, Sorrento, Italy, 2008.
[94] 3GPP R1-104135, Confirmation of UE behavior in case of simultaneously-triggered SR, SRS and CQI, 3GPP TSG RAN WG1, meeting 61bis, Dresden, Germany, 2010.
[95] 3GPP R1-081928, Way forward on indication of UE antenna selection for PUSCH, 3GPP TSG RAN WG1, meeting 53, Kansas City, MI, May 2008.
[96] 3GPP R1-082109, UE transmit antenna selection, 3GPP TSG RAN WG1, meeting 53, Kansas City, MI, May 2008.
[97] 3GPP R1-062175, Random access burst design for E-UTRA, 3GPP TSG RAN WG1, meeting 46, Tallinn, Estonia, 2006.
[98] R.L. Frank, S.A. Zadoff, R. Heimiller, Phase shift pulse codes with good periodic correlation properties, IEEE Trans. Inform. Theory 7 (October 1961).
[99] D.C. Chu, Poly-phase codes with good periodic correlation properties, IEEE Trans. Inform. Theory 18 (1972).
[100] 3GPP R1-072325, Multiple values of cyclic shift increment NCS, 3GPP TSG RAN WG1, meeting 49, Kobe, Japan, 2007.
[101] 3GPP R1-073624, Limitation of RACH sequence allocation for high mobility cell, 3GPP TSG RAN WG1, meeting 50, Athens, Greece, 2007.

[102] 3GPP R1-040642, Comparison of PAR and cubic metric for power de-rating, 3GPP TSG RAN WG1, meeting 37, Montreal, Canada, 2004.
[103] 3GPP R1-060023, Cubic metric in 3GPP-LTE, 3GPP TSG RAN WG1, LTE ad-hoc meeting, Helsinki, Finland, 2006.
[104] 3GPP R1-071517, RACH sequence allocation for efficient matched filter implementation, 3GPP TSG RAN WG1, meeting 48bis, St Julian's, Malta, 2007.
[105] 3GPP R1-071409, Efficient matched filters for paired root Zadoff–Chu sequences, 3GPP TSG RAN WG1, meeting 48bis, St Julian's, Malta, 2007.
[106] 3GPP R1-063377, UL timing control accuracy and update rate, 3GPP TSG RAN WG1, meeting 47, Riga, Latvia, 2006.
[107] 3GPP R1-072841, Simulation of uplink timing error impact on PUSCH, 3GPP TSG RAN WGI, meeting 49bis, Orlando, FL, 2007.
[108] M.P.J. Baker, T.J. Moulsley, Power control in UMTS release 99, in: Proceedings of the First IEE International Conference on 3G Communications, 2000.
[109] 3GPP R1-080881, Range and representation of Delta_MCS, 3GPP TSG RAN WG1, meeting 52, Sorrento, Italy, 2008.
[110] J. Lee, J.-K. Han, J. Zhang, MIMO technologies in 3GPP LTE and LTE-advanced, EURASIP J. Wireless Commun. Netw. (2009).
[111] S. Catreux, P.F. Driessen, L.J Greenstein, Attainable throughput of an interference-limited multiple-input multiple-output (MIMO) cellular system, IEEE Trans Commun. 49 (8) (2001).
[112] I. Telatar, Capacity of multi-antenna Gaussian channels, AT&T Tech. Memo. (1995).
[113] G.J. Foschini, M.J. Gans, On limits of wireless communications in a fading environment when using multiple antennas, Wireless Personal Commun. (1998).
[114] M.-S. Alouini, A. Goldsmith, Capacity of Nakagami multipath fading channels, in: Proceedings of the Vehicular Technology Conference, 1997.
[115] D. Chizhik, G.J. Foschini, R.A. Valenzuela, Capacities of multi-element transmit and receive antennas: correlations and keyholes, Electron. Lett. 36 (2000).
[116] D. Gesbert, H. Bölcskei, D. Gore, A. Paulraj, MIMO wireless channels: capacity and performance prediction, Global Telecommunications Conference (GLOBECOM), 2000.
[117] D.A. Gore, R.U. Nabar, A. Paulraj, Selecting an optimal set of transmit antennas for a low rank matrix channel, Proc. ICASSP 2000 49 (8) (2000).
[118] S. Sandhu, R.U. Nabar, D.A. Gore, A. Paulraj, Near-optimal selection of transmit antennas for a MIMO channel based on Shannon capacity, in: Proceedings of the 34th Asilomar Conference on Signals, Systems and Computers, 2000.
[119] A.F. Molisch, M.Z. Win, J.H. Winters, A. Paulraj, Capacity of MIMO systems with antenna selection, in: Proceedings of the IEEE International Conference on Communications (ICC), 2001.
[120] Z. Shen, et al., Overview of 3GPP LTE-advanced carrier aggregation for 4G wireless communications, IEEE Commun. Mag. 50 (2) (2012).
[121] Y.-H. Nam, et al., Evolution of reference signals for LTE-advanced systems, IEEE Commun. Mag. 50 (2) (2012).
[122] L. Liu, et al., Downlink MIMO in LTE-advanced: SU-MIMO vs. MU-MIMO, IEEE Commun. Mag. 50 (2) (2012).

[123] D. Lee, et al., Coordinated multipoint transmission and reception in LTE-advanced: deployment scenarios and operational challenges, IEEE Commun. Mag. 50 (2) (2012).
[124] D. Bai, et al., LTE-advanced modem design: challenges and perspectives, IEEE Commun. Mag. 50 (2) (2012).
[125] J. Lee, Kim, et al., Coordinated multipoint transmission and reception in LTE-advanced systems, IEEE Commun. Mag. 50 (2) (2012).
[126] Z. Shen, et al., Dynamic uplink−downlink configuration and interference management in TD-LTE, IEEE Commun. Mag. 50 (2) (2012).
[127] C.S. Park, et al., Evolution of uplink MIMO for LTE-Advanced, IEEE Commun. Mag. 49 (2) (2011).

Miscellaneous

[128] 3G Americas, MIMO and smart antennas for 3G and 4G wireless systems. <http://www.3gamericas.org>, May 2010.
[129] Rohde & Schwarz Application Notes, LTE-Advanced Technology Introduction, March 2010.
[130] 3G Americas, 3GPP Mobile Broadband Innovation Path to 4G: Release 9, Release 10 and Beyond: HSPA + , SAE/LTE and LTE-Advanced, February 2010.
[131] 3G Americas, HSPA to LTE-Advanced: 3GPP Broadband Evolution to IMT-Advanced (4G), September 2009.
[132] 3G Americas, The Mobile Broadband Evolution: 3GPP Release 8 and Beyond HSPA + , SAE/LTE and LTE-Advanced, February 2009.
[133] IEEE 802.16m-07/244r1, Yang Song, Liyu Cai, Keying Wu, and Hongwei Yang, Collaborative MIMO, November 2007.
[134] Agilent Technologies, 3GPP long term evolution: system overview, product development, and test challenges. <http://www.agilent.com>, 2009.
[135] IEEE C802.16m-08/153, Bin-Chul Ihm, Jinsoo Choi and Wookbong Lee, "Pilot Related to DL-MIMO", March 2008.
[136] MATLAB CENTRAL, An open exchange for the MATLAB and SIMULINK user community. <http://www.mathworks.com/matlabcentral>.
[137] Vienna University of Technology, Institute of Telecommunications, LTE link-level and system-level simulators. <http://www.nt.tuwien.ac.at/about-us/staff/josep-colom-ikuno/lte-simulators>, 2012.
[138] 3GPP R1-060385 Motorola, Cubic Metric in 3GPP-LTE, February 2006.
[139] The Coded Modulation Library (The Iterative Solutions Coded Modulation Library (ISCML) is an open source toolbox for simulating capacity approaching codes in Matlab). <http://www.iterativesolutions.com>.
[140] 4G Americas, 4G Mobile Broadband Evolution: Release 10, Release 11 and Beyond - HSPA, SAE/LTE and LTE-Advanced, October 2012.
[141] 4G Americas, MIMO and Smart Antennas for Mobile Broadband Networks, October 2012.
[142] 4G Americas, Developing & Integrating a High Performance HET-NET, October 2012.
[143] 4G Americas, 4G Mobile Broadband Evolution: 3GPP Release 10 and Beyond - HSPA + , SAE/LTE and LTE-Advanced, February 2011.

[144] 3GPP R1-113297, NTT DOCOMO, Enhanced PDCCH for DL MIMO in Rel-11, October 2011.
[145] 3GPP R1-112928, Ericsson, ST-Ericsson, On enhanced PDCCH design, October 2011.
[146] 3GPP R1-113175, Renesas Mobile, Link-level evaluation of E-PDCCH design aspects, October 2011.
[147] 3GPP R1-113194, LG Electronics, Consideration on transmit diversity scheme for enhanced PDCCH transmission, October 2011.
[148] 3GPP R1-113202, Intel Corporation, Performance analysis of enhanced downlink control signaling, October 2011.
[149] 3GPP R1-113238, Research in Motion, E-PDCCH transmission with transmit diversity, October 2011.
[150] 3GPP R1-114302, NTT DOCOMO, DM-RS design for E-PDCCH in Rel-11, November 2011.
[151] Anritsu, Future technologies and testing for fixed mobile convergence, SAE and LTE in Cellular mobile communications. <http://www.anritsu.com/search/en-US/downloadssearch.aspx>, 2008.
[152] Wireless World Initiative New Radio—WINNER + , Enabling techniques for LTE-A and beyond, deliverable D2.2. <http://projects.celtic-initiative.org/winner + /deliverables_winnerplus.html>, 2010.
[153] LTE system description. <http://www.sharetechnote.com>.
[154] DSPLOG signal processing for communication. <http://www.dsplog.com>.
[155] 4G Evolution Lab—LTE and LTE-Advanced Toolbox and Block-set: a simulation library for the 3GPP LTE and LTE Advanced specification for the Mathworks MATLAB and Simulink. <http://www.steepestascent.com>.
[156] Samsung electronics, LTE PHY specification. <http://www.slideshare.net/allabout4g/lte-rel-8-physical-layer>, 2008.
[157] MOTOROLA WHITE PAPER, TD-LTE, exciting alternative global momentum. <www.motorola.com>, 2010.
[158] B. Schulz, LTE Transmission modes and beamforming, Rohde & Schwarz White Paper, 2011.
[159] M. Lew, Real-world stimulus-response testing for LTE transmitter RF components, agilent technologies. <http://www.microwavejournal.com/articles/print/9158-real-world-stimulus-response-testing-for-lte-transmitter-rf-components>, 2010.
[160] Adaptive Multi-Rate (AMR) Feature Descriptions, Agilent Technologies <http://wireless.agilent.com/rfcomms/refdocs/gsm/gprsla_amr_bse_config.html>
[161] Jinbiao Xu, LTE-Advanced Signal Generation and Measurement Using SystemVue, Agilent Technologies, Inc., December 2010.
[162] 3GPP R1-080182, Labelling of UE-selected subbands on PUSCH, Huawei, January 2008.
[163] 3GPP R1-080555, Labelling complexity of UE selected subbands on PUSCH, Huawei, January 2008.
[164] Ben Cooke, Reed-Muller Error Correcting Codes, MIT Undergraduate Journal of Mathematics, Number 1, June 1999 <http://www-math.mit.edu/phase2/UJM/vol1/>.
[165] R. Gold, "Optimal binary sequences for spread spectrum multiplexing", IEEE Transactions on Information Theory, Vol. 13 , Issue 4, February 1967.

[166] Hidekazu Taoka et al., "MIMO and CoMP in LTE-Advanced", NTT DoCoMo Tech Journal, September 2010.

[167] Hideyuki Torii et al., "A New Class of Zero-Correlation Zone Sequences", IEEE Transactions on Information Theory, Vol. 50, No. 3, March 2004.

[168] Technical Note, "An Overview of LTE PRACH Detection for the PC20x", picoChip felexible wireless, January 2008.

[169] Ernesto Zimmermann et al., "On the Complexity of Sphere Decoding", in Proceedings International Symposium on Wireless Personal Multimedia Communication, 2004.

[170] Mathew William Churchman Barata, LTE Performance Evaluation with Realistic Channel Quality Indicator Feedback, Universitat Politècnica de Catalunya, April 2011.

[171] J.P.T. Dobbelsteen, Mapping an LTE Baseband Receiver on a Multi-Core Architecture, Eindhoven University of Technology, november 2009.

[172] Di Wu et al., "System Architecture for 3GPP LTE Modem using a Programmable Baseband Processor", International Symposium on System-on-Chip, 2009.

[173] Jens Berkmann et al., "On 3G LTE Terminal Implementation - Standard, Algorithms, Complexities and Challenges", International Wireless Communications and Mobile Computing Conference (IWCMC '08), 2008.

[174] DigRF(SM) Specifications, MIPI Alliance, <http://www.mipi.org/specifications/digrfsm-specifications>.

CHAPTER

11 Link-Level and System-Level Performance of LTE-Advanced

CHAPTER CONTENTS

11.1 Definition of the performance metrics 882
11.1.1 Link budget 882
11.1.2 User and sector throughput 883
11.1.3 Outage throughput 885
11.1.4 Packet delay 885
11.1.5 Spectral efficiency 886
11.1.6 Jain fairness index 886
11.1.7 Geometry (wideband SINR distribution) 887
11.1.8 Effective interference over thermal 887
11.1.9 Cell spectral efficiency and cell-edge user spectral efficiency 888
11.2 Calculation of static and dynamic overhead 889
11.3 Traffic models 891
11.3.1 Statistical model for conversational speech 891
11.3.2 Full-buffer traffic model 893
11.4 Link-to-system mapping (PHY abstraction) 893
11.5 IMT-Advanced test environments 902
11.6 Network layout for system-level simulations 902
11.7 IMT-Advanced evaluation methodology and baseline configurations 904
11.8 Link-level and system-level channel models 904
11.9 LTE-Advanced link-level and system-level performance 916
11.9.1 Cell spectral efficiency and cell-edge spectral efficiency 916
11.9.2 VoIP capacity 922
11.9.3 Mobility 923
11.9.4 Peak spectral efficiency 925
11.9.5 User-plane/control-plane latency and handover interruption time 925
11.9.6 Estimation of the L1/L2 overhead 932
11.9.7 Link budget 936
11.9.8 Evaluation of LTE-Advanced against LTE Rel-10 requirements 936
11.10 Miscellaneous evaluations 936
References 947

LTE-Advanced.

© 2014 Elsevier Inc. All rights reserved.

Ex.1005.00906

International telecommunication union-radio telecommunications (ITU-R) was responsible for defining of a global standard for the fourth generation of mobile communication systems known as international mobile telecommunications (IMT)-Advanced. One of the technologies included in this global standard was the LTE-Advanced proposed by 3GPP. The IMT-Advanced systems were required to fulfill a set of requirements specified by ITU-R working party 5D [12–16]. The first set of requirements was verified through inspection of the proposed technologies. Those requirements included the support of scalable bandwidths in the IMT spectrum, a wide range of services and inter-system handover capability with at least with one of systems in the IMT-2000 family. The satisfaction of the second set of requirements was confirmed analytically by conducting numerical calculations of peak spectral efficiency, user-plane and control-plane latency, and handover interruption times. The third set of requirements was required to be evaluated via link-level and system-level simulations initially by the proponent and later by designated external evaluation groups. These requirements were cell spectral efficiency, cell-edge user spectral efficiency, mobility, and VoIP capacity.

In order to reduce the complexity of the process, simulations are often divided into two stages or levels of abstraction known as link-level and system-level. The link-level simulations are used to assess the performance of the physical layer and those higher layer aspects directly related to the radio interface. In link-level simulation, a single-cell radio link is modeled, including some specific features such as synchronization, modulation, channel coding, channel fading, channel estimation, demodulation, multi-antenna processing, etc. On the other hand, a system-level simulator allows evaluation of the performance of a network comprising multiple cells and moving mobile stations. At this level, system modeling encompasses a set of base stations and all their associated mobile terminals. Both the signal level received by each user and other users' interferences are modeled, taking into account the propagation losses and channel fading effects. Signal to interference plus noise ratio (SINR) is calculated for each active user considering the current network configuration and relative random placement of the base stations and mobile stations. These SINR values can be then translated to block error rate (BLER) or effective throughput values using models whose development is based on the results obtained in the link-level simulations. This interaction between link- and system-level simulators is usually referred to as link-to-system mapping or link-level abstraction models.

After developing the simulation platform, a calibration process is performed. The calibration is of paramount importance to ensure the validity of the results obtained with the simulation platform. Calibration is performed through comparison of the outcomes of the developed simulator with the outcomes of the simulation platforms of other sources. The calibration process involves comparison and adjustment of downlink wideband SINR, also known as geometry, and coupling loss distributions under common assumptions. Following the first step, the calibration further includes evaluation and comparison of downlink and uplink

spectral efficiencies, user throughput distributions, and SINR distributions for a basic LTE system configuration.

The link-level and system-level simulations are used to evaluate the performance of mobile radio access technologies under various operating conditions and deployment scenarios. While the simulations do not model the entire deployment parameters and propagation conditions that may be involved in a practical scenario due to increased computational complexity of the model, the statistical modeling of the parameters and estimation/measurement errors should be sufficiently accurate such that the simulation results are a faithful representation of the performance in an actual deployment [51]. More specifically:

- *Link-level simulations* would facilitate the study of channel estimation, tracking, and prediction algorithms, as well as synchronization algorithms, MIMO performance, adaptive modulation and coding, and feedback techniques. Furthermore, receiver structures (e.g., MMSE, ZF, MLD, SIC), modeling of channel encoding and decoding, and physical-layer modeling which is crucial for system-level simulations are typically analyzed at the link-level. Although MIMO broadcast channels have been investigated quite extensively over the past decade, there are still many open theoretical and practical questions that need to be resolved. For example, LTE offers the flexibility to adjust many transmission parameters, but it is not clear how to exploit the available degrees of freedom to achieve the optimum performance under different deployment scenarios.
- *System-level simulations* focus more on network-related issues, such as resource allocation and scheduling, multi-user handling, mobility management, admission control, interference management, and network planning optimization. Furthermore, in a multi-user system, such as LTE, it is not directly clear which figure of merits (metrics) should be used to evaluate the performance of the system. The classical measures of (un)coded bit error rate, (un)coded BLER, and throughput may not accurately reflect multi-user properties. More comprehensive measures of the LTE performance include fairness, multi-user diversity, or degree of freedom. However, these theoretical concepts have to be mapped to performance values that can be verified by means of simulations.

As shown in Figure 11.1, an example of an LTE link-level simulation platform comprises three basic building blocks; namely, transmitter, channel model, and receiver. Depending on the type of simulation, one or several instances of these basic building blocks are utilized. The transmitter and receiver blocks are linked by the channel model, which is used to transmit the downlink data, while signaling and uplink feedback are ideally assumed to be error free. Since signaling is more strongly protected than data, by means of lower coding rates and/or lower-order modulations, the assumption of error-free signaling is in fact fairly realistic. Equivalently, errors on the signaling channels will only occur when the data channels are already facing severe performance degradation. In the downlink,

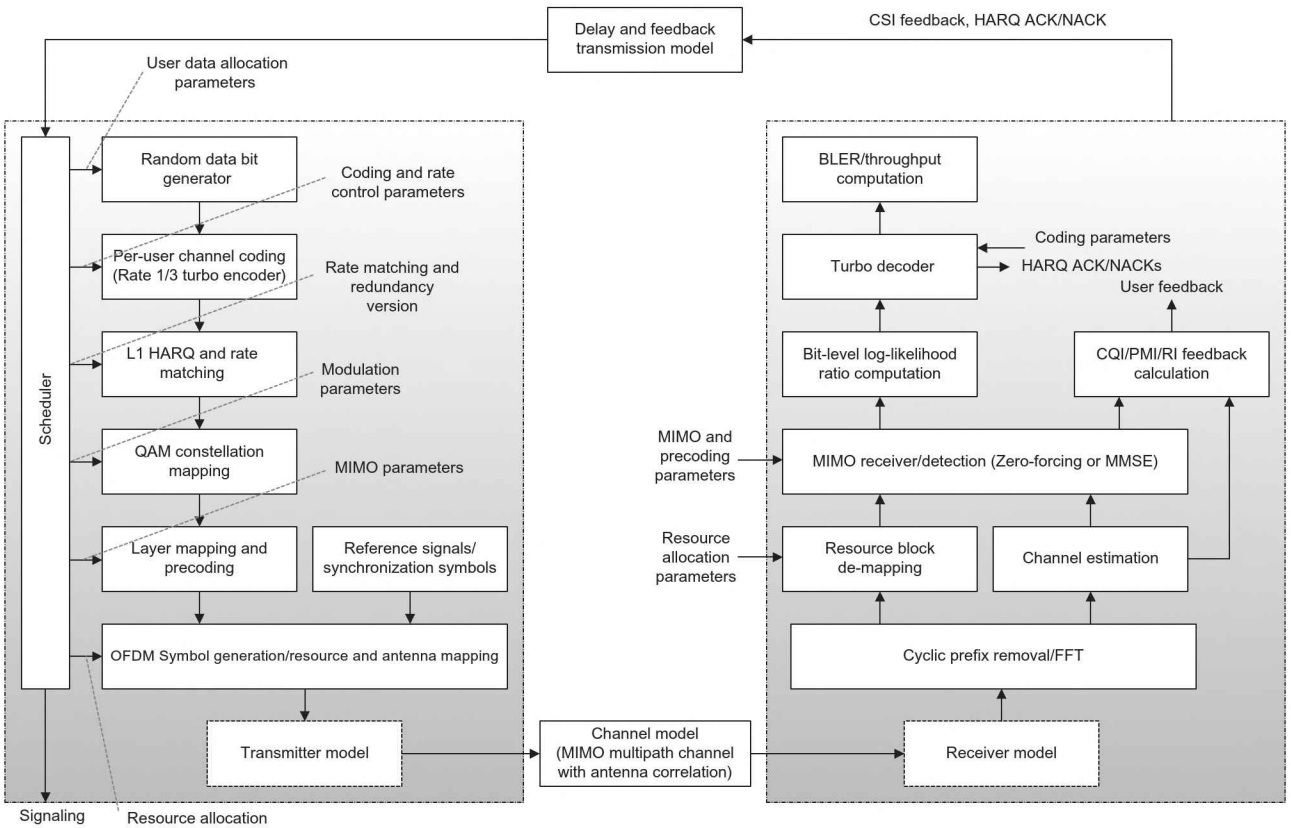


FIGURE 11.1

General structure of an LTE downlink link-level simulation platform [8,9,45].

the signaling information generated by the transmitter to the receiver contains coding, HARQ, scheduling, and precoding parameters. In the uplink, channel quality indicator (CQI), precoding matrix index (PMI), and rank indicator (RI) are signaled, which together form the channel state information (CSI) feedback [45].

In system-level simulations as illustrated in Figure 11.2, the performance of the entire network is evaluated. In an LTE system, such network consists of a number of eNBs that cover a specific geographical area in which several mobile stations are randomly dropped. The system-level simulation platform (shown in Figure 11.2) consists of a link measurement model and a link performance model. The link measurement model measures the link quality, obtained via the UE CSI measurement reports, which is required to perform link adaptation, resource allocation, and MIMO mode selection. An appropriate link quality measure is evaluated per sub-carrier. Based on the SINR metric, the UE calculates the uplink feedback (PMI, RI, and CQI), which is used as input for link adaptation at the eNB. The scheduling algorithm assigns resources to users in order to optimize the performance of the system based on CSI feedback. The scheduling is a key

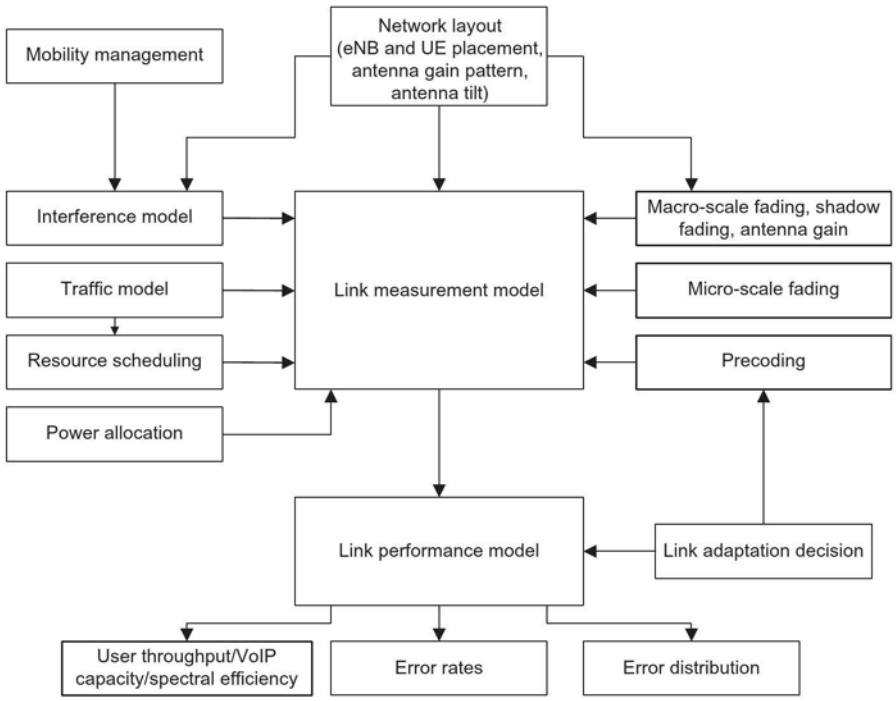


FIGURE 11.2

General structure of an LTE system-level simulation platform [45].

component in the proper functioning of the radio interface. Two types of schedulers can be identified: the opportunistic, where the scheduler considers the state of the radio channel to make the best allocation possible; and the non-opportunistic, where the allocation has no knowledge of the radio channel's state.

Based on the link measurement model outputs, the link performance model predicts the BLER of the link according to the receiver SINR and the transmission parameters (e.g., modulation and coding). In order to generate the network topology, transmission sites are generated. The scheduler assigns physical resources, precoding matrices, and selects a suitable modulation and coding scheme for each active UE attached to an eNB. The actual assignment depends on the scheduling algorithm and the UE feedback. At the UE side, the received post-processing SINR is calculated in the link measurement model. The SINR is determined by the signal, interference, and noise power levels, which are dependent on the cell layout that is defined by the eNB relative positions, large-scale (macroscopic, macro-scale) path loss, shadow fading, and the time-variant small-scale (microscopic, micro-scale) fading parameters. The CQI feedback is calculated based on the sub-carrier SINRs and the target transport BLER. The CQI reports are generated by SINR-to-CQI mapping and made available to the eNB via a feedback channel with adjustable delay where the feedback imperfections are modeled. At the transmitter, the appropriate MCS is selected by the CQI value to achieve the targeted BLER during the transmission. In particular, in high mobility scenarios, the feedback delay caused by computation and signaling timings can lead to performance degradation, if the channel state changes rapidly during the delay period. In the link performance model, an additive white Gaussian noise (AWGN)-equivalent SINR γ_{AWGN} is obtained via mutual information effective signal to interference and noise ratio mapping (MIESM). In a second step, γ_{AWGN} is mapped to the BLER via AWGN link performance curves. The BLER value acts as a probability for computing HARQ ACK/NACKs, which are combined with the transport-block size to compute the link throughput. The simulation output consists of traces, containing link throughput and error rates for each user, as well as cell aggregate throughput, from which statistical distributions of throughputs and errors can be extracted [45].

The large-scale path loss and the shadow fading are modeled as position-dependent maps. The large-scale path loss is calculated according to the available models and combined with the antenna gain pattern of the corresponding eNB. An inter-site map correlation for shadow fading is similarly obtained. While the large-scale path loss and the shadow fading are modeled as a position-dependent trace, the small-scale fading is modeled as a time-dependent trace. The calculation of the latter trace is based on the transmitter precoding, the small-scale fading MIMO channel matrix, and the receive filter. The small-scale fading trace consists of the signal power and the interference power after the receive filter.

The link-level and system-level evaluation of the IMT-Advanced candidates was comprehensively performed in strict compliance with the technical

parameters and the methodology specified by ITU-R [12–16]. Each requirement was independently evaluated, except for the cell and cell-edge user spectral efficiencies criteria that were jointly assessed using the same system-level simulation; consequently, the candidates were required to simultaneously satisfy the corresponding minimum requirements. Furthermore, the system-level simulation setup used in the assessment of the mobility requirement was the same as that used for the evaluation of cell spectral efficiency and cell-edge user spectral efficiency. In general, the evaluation of the IMT-Advanced candidate technologies followed the following principles [14]:

1. Use of reproducible methods including computer simulation, analytical/theoretical approach, and inspection.
2. Technical evaluation against performance targets that were set for each test environment.
3. Consistency between self-evaluations and technical descriptions provided in technology description templates.
4. Use of unified methodology, software, and common parameter sets by the evaluation groups including channel models, link-level parameters, and link-to-system mapping.
5. Evaluation of multiple proposals using one simulation platform by each evaluation group to ensure comparability of the results.
6. Inclusion of an L1/L2 overhead in the evaluation of cell spectral efficiency, cell-edge user spectral efficiency, and VoIP capacity.
7. Independent drop of the users with uniform distribution over the coverage area where each mobile user corresponds to an active session that runs for the duration of the drop.
8. Random assignment of line-of-sight (LoS) *and* non-line-of-sight (NLoS) path loss models to the users.
9. Cell assignment to a user is based on the air-interface cell selection schemes.
10. Fading signal and fading interference are computed from each mobile station to each cell, and from each cell to each mobile station (in both directions on an aggregated basis).
11. Consideration of the interference over thermal (IoT) constraint in the uplink design such that the average IoT value remains less than or equal to 10 dB.
12. In a full-buffer traffic model, packets are not blocked upon their arrival; that is, buffer sizes are assumed to be infinite.
13. Data and VoIP packets are scheduled with appropriate packet schedulers for full-buffer and VoIP traffic models separately.
14. Modeling of channel quality feedback delay, feedback channel errors, packet errors, and real channel estimation (as opposed to ideal channel estimation) effects and retransmission of erroneous packets.
15. Realistic modeling of the overhead channels, that is, the overhead due to feedback and control channels.

For each drop, the system-level simulations were conducted and the process was repeated with the users dropped at new random geographical locations within the network. A large number of drops were simulated to ensure convergence in the system performance metrics, and the width of confidence intervals of the user and system performance metrics was calculated and reported. The confidence interval[1] and the associated confidence level indicate the reliability of the estimated parameter value [23,53]. The confidence level is the probability that the true parameter value is within the confidence interval such that the higher the confidence level, the larger the confidence interval. All cells in the network were simulated assuming dynamic channel models and use of a 19-cell wrap-around scheme to model the inter-cell interference except for the indoor environment.

This chapter describes the link-level and system-level evaluation of 3GPP LTE-Advanced against ITU-R requirements for IMT-Advanced systems using the methodology specified by ITU-R [14]. The theoretical background, including definition of performance metrics, channel models, physical-layer abstraction schemes, and the traffic models are provided to ensure in-depth understanding of the evaluation process and the results.

11.1 Definition of the performance metrics

11.1.1 Link budget

Link budget is a commonly used metric to evaluate the coverage of a cellular system in the downlink or uplink. In order to calculate the link budget, one must account for all gains and losses from the transmitter to the receiver over the air-interface. It accounts for the attenuation of the transmitted signal due to propagation as well as the antenna gains, cable and implementation loss, and other miscellaneous losses. The time-varying channel gains such as fading are taken into account by adding some margin depending on the anticipated severity of its effects. The amount of

[1]A confidence interval provides an estimated range of values which is likely to include an unknown population parameter, the estimated range being calculated from a given set of sample data. If independent samples are taken repeatedly from the same population and a confidence interval is calculated for each sample, then a certain percentage (confidence level) of the intervals will include the unknown population parameter. Confidence intervals are more informative than the simple results of hypothesis tests since they provide a range of plausible values for the unknown parameter.
In mathematical terms, let X denote a random sample from a probability distribution with statistical parameters α, which is a quantity to be estimated, and β, representing quantities that are not of immediate interest. A *confidence interval* for the parameter α, with confidence level or confidence coefficient γ, is an interval with random endpoints $(f_1(X), f_2(X))$, determined by the pair of random variables $f_1(X)$ and $f_2(X)$, with the property $\Pr_{\alpha,\beta}(f_1(X) < \alpha < f_2(X)) = \gamma \forall \alpha, \beta$. The number γ, with typical values close to but not greater than one, is sometimes given in the form $1 - \gamma'$, where γ' is a small non-negative number close to zero. In the latter expression, $\Pr_{\alpha,\beta}(x)$ indicates the probability distribution of X characterized by (α, β). An important part of this definition is that the random interval $(f_1(X), f_2(X))$ covers the unknown value α with a high probability no matter what the true value of α actually is [23,53].

margin required can be reduced by the use of mitigating techniques, such as antenna diversity or frequency hopping. An abstract description of the link budget in any direction (downlink/uplink) has the following form [14,26]:

$$\text{Received power (dBm)} = \text{Transmitted power (dBm)} + \text{Gains (dB)} - \text{Losses (dB)} \tag{11.1}$$

Link budget evaluation is a well-known method for initial cell planning that needs to be carried out separately for the downlink and uplink. Although the link budget can be calculated separately for each link, it is the combination of the links that determines the performance of the system. Using the margins in the link budget, the expected signal-to-noise ratio can be evaluated at given distances. Using these results, the noise-limited range can be evaluated for the system. The typical link budget parameters are summarized in Table 11.1.

11.1.2 User and sector throughput

Although a user may be sufficiently covered within certain areas of a cell for a given service, when multiple users are in a cell, the radio resources (time, frequency, space, and power) must be shared among the active users. It can be expected that a user's average data rate may be reduced by a factor of N_{user} when

Table 11.1 Typical Link Budget Parameters [14,26]

Link Budget Parameters	Link Budget Parameters
Carrier frequency/channel bandwidth	Number of receive antennas
BS/MS antenna heights (m)	Receive antenna gain (dBi)
Area coverage (km)	Receiver cable, connector, or body losses (dB)
Type of service (VoIP, full-buffer data, etc.)	Receiver noise figure (dB)
MCS	Thermal noise density (dBm/Hz)
Multipath channel model	Receiver interference density (dBm/Hz)
Mobile speed (km/h)	Required SNR (dB)
Number of transmit antennas	Receiver implementation margin (dB)
Maximum transmitter power per antenna (dBm)	Fast fading margin including scheduler gain (dB)
Transmitter power amplifier back-off (dB)	HARQ combining gain (dB)
Transmit antenna gain (dBi)	Handover gain (dB)
Transmit array gain (dB)	BS/MS diversity gain (dB)
Control channel power boosting gain (dB)	Lognormal shadow fading standard deviation (dB)
Data carrier power loss due to pilot/control boosting (dB)	Shadow fading margin (dB)
Transmitter cable, connector, combiner, body losses (dB)	Penetration loss (dB)

there are N_{user} active users, assuming resources are equally shared among active users and there is no multi-user diversity gain, relative to that of a single user. Therefore, any coverage assessment for any particular service must be coupled with the number of active users in the cell and their associated quality of service requirements. If the users with poor channel conditions are provided with more radio resources, it would adversely impact the total cell throughput. Thus, there is a trade-off between coverage and capacity. The performance metric that is typically used is the number of admissible users, parameterized by the service minimum bit rate, maximum tolerable latency, permissible outage probability, etc. It is assumed that simulation statistics are collected from sectors belonging to the test cells of a 19-cell deployment scenario in order to model the effects of inter-cell interference. In the following, downlink and uplink throughputs are separately evaluated and the corresponding metrics are differentiated by superscripts "DL" and "UL," respectively.

The user throughput is defined as the ratio of the number of information bits that the user successfully received divided by the total simulation time. If user k has $p_k^{\text{DL(UL)}}$ downlink (uplink) packet transmissions during the simulation period T_{sim}, if there are $q_{ik}^{\text{DL(UL)}}$ packets in the ith transmission, and if b_k^{ij} denotes the number of the correctly received bits in the jth packet; then the average user throughput for user k is given as follows:

$$R_k^{\text{DL(UL)}} = \frac{\sum_{i=1}^{p_k^{\text{DL(UL)}}} \sum_{j=1}^{q_{ik}^{\text{DL(UL)}}} b_k^{ij}}{T_{\text{sim}}} \tag{11.2}$$

The average user throughput is defined as the sum of the user throughput of each user in the cell divided by the total number of users in the cell. Let N_{user} denote the number of users in the sector/cell and user $k = 1, 2, \ldots, N_{\text{user}}$ has throughput $R_k^{\text{DL(UL)}}$, then DL (or UL) sector throughput is defined as:

$$R^{\text{DL(UL)}} = \sum_{k=1}^{N_{\text{user}}} R_k^{\text{DL(UL)}} \tag{11.3}$$

The user throughput per transmission is the number of correctly received bits per packet divided by the duration of the transmission. If user k has $p_k^{\text{DL(UL)}}$ downlink (uplink) transmissions, if there are $q_{ik}^{\text{DL(UL)}}$ packets in the ith transmission, and if there are b_k^{ij} correctly received bits in the jth packet, then the average transmission throughput can be defined as follows:

$$R_k^{\text{DL(UL)}} = \frac{1}{p_k^{\text{DL(UL)}}} \left(\sum_{i=1}^{p_k^{\text{DL(UL)}}} \frac{\sum_{j=1}^{q_{ki}^{\text{DL(UL)}}} b_k^{ij}}{\Delta T_{ki}^{\text{DL(UL)}}} \right) \tag{11.4}$$

where $\Delta T_{ki}^{\text{DL(UL)}}$ denotes the duration of the ith transmission to user k. The average user throughput per transmission is defined as the sum of the user throughputs per transmission divided by the number of users in the cell.

11.1.3 Outage throughput

The outage throughput $\eta_{\text{outage}}(R_{\min})$ is defined as the percentage of users with data rate R_k^{DL} less than a predefined minimum data rate $R_{\min}$. The cell-edge user throughput is defined as the fifth percentile point of the cumulative distribution function (CDF) of users' average throughput per transmission assuming that 95% of the users are expected to achieve a certain throughput per transmission regardless of their geographical location in the cell.

11.1.4 Packet delay

If the jth packet of the ith transmission belongs to user k, if the packet arrives at the BS (or MS) MAC at time instant T_{arrival}^{kij} and is delivered to the MS (or BS) MAC sublayer at time instant $T_{\text{departure}}^{kij}$, then the packet delay can be calculated as follows:

$$D_{kij}^{\text{DL(UL)}} = T_{\text{arrival}}^{kij} - T_{\text{departure}}^{kij} \tag{11.5}$$

The downlink and uplink delays are denoted by superscript "DL" or "UL," respectively. The packets that are dropped or erased may not be included in the analysis of packet delays depending on the traffic model. For example, in the modeling of traffic for delay sensitive applications, packets may be dropped, if packet transmissions are not completed within a specified delay bound. The impact of the dropped packets is included in the packet loss rate. The CDF of the packet delay per user provides a basis in which maximum latency, second percentile, and average latency as well as jitter can be derived. The second percentile point of the CDF of packet delay denotes the packet delay value for which 98% of packets have a delay less than that value. As an example, the VoIP capacity is defined such that the percentage of users in outage is less than 2% where a user is assumed to have experienced a service outage, if less than 98% of the VoIP packets have been delivered successfully to the user within a one-way radio access delay bound of 50 ms.

The average packet delay is defined as the average interval between packets originated at the source (either MS or BS) and received at the destination (either BS or MS) in a system for a given duration of transmission. The average packet delay for user k, $\overline{D}_k^{\text{DL(UL)}}$ is given by:

$$\overline{D}_k^{\text{DL(UL)}} = \frac{\sum_{i=1}^{p_k} \sum_{j=1}^{q_{ki}} (T_{\text{departure}}^{kij} - T_{\text{arrival}}^{kij})}{\sum_{i=1}^{p_k} q_{ki}} \tag{11.6}$$

The CDF of users' average packet delay is the cumulative distribution of the average packet delay observed by all users in the cell. The packet loss ratio per user is defined as:

$$\text{Packet loss ratio} = 1 - \frac{\text{Total number of successfully delivered packets}}{\text{Total number of packets}} \tag{11.7}$$

where the total number of packets includes packets that were transmitted over the air-interface and packets that were dropped prior to transmission. The data throughput of a BS is defined as the number of information bits per second that a cell can successfully deliver or receive via the air-interface using appropriate scheduling algorithms.

11.1.5 Spectral efficiency

We consider both physical-layer spectral efficiency and MAC sublayer spectral efficiency as important performance indicators for a cellular system. The physical-layer spectral efficiency is the system throughput measured at the interface of the physical layer and the MAC sublayer, thus including physical-layer overhead but excluding MAC and upper layer protocol overheads. The MAC sublayer spectral efficiency represents the system throughput measured at the interface of the MAC sublayer and the upper layers, thus including both the physical layer and MAC protocol overheads. The MAC efficiency of the system is evaluated by dividing the MAC sublayer spectral efficiency by the physical-layer spectral efficiency. The average cell spectral efficiency is defined as:

$$\mathrm{SE}_{\mathrm{cell}} = \frac{R_{\mathrm{aggregate}}}{\mathrm{BW}_{\mathrm{effective}}} \tag{11.8}$$

where $R_{\mathrm{aggregate}}$ denotes the aggregate cell throughput and $\mathrm{BW}_{\mathrm{effective}}$ is the effective channel bandwidth. The effective channel bandwidth is defined as $\mathrm{BW}_{\mathrm{effective}} = \alpha_{\mathrm{DL-UL}}\mathrm{BW}_{\mathrm{transmission}}$ where $\mathrm{BW}_{\mathrm{transmission}}$ denotes the channel bandwidth, and $\alpha_{\mathrm{DL-UL}}$ is the downlink/uplink ratio in the TDD systems. Note that for FDD systems $\alpha_{\mathrm{DL-UL}} = 1$ and for TDD systems with DL:UL ratio of 2:1; $\alpha_{\mathrm{DL-UL}} = 2/3$ for the downlink and 1/3 for the uplink, respectively.

The CDF of SINR is defined as the CDF for the signal to interference plus noise ratio measured at the BS for each MS on the uplink, or at the MS for the BS in the downlink. This metric would allow comparison between different reuse scenarios, network loading conditions, multi-antenna algorithms, resource allocation, power control schemes, etc.

11.1.6 Jain fairness index

Fairness measures or metrics are used in network engineering to determine whether users or applications are receiving a fair share of system resources. There are several mathematical and conceptual definitions of fairness among which the Jain index is a commonly used metric defined as follows [44]:

$$J(x_1, x_2, \ldots, x_n) = \frac{\left(\sum_{i=1}^{n} x_i\right)^2}{n\sum_{i=0}^{n} x_i^2} \tag{11.9}$$

The Jain index rates the fairness of a set of values where there are n users and x_i is the throughput for the ith connection. The result ranges from $J = 1/n$ (worst case) to $J = 1$ (best case), and it is maximum when all users receive the same allocation. This index is $J = k/n$ when k users equally share the resources, and the other $n - k$ users receive zero allocation. This metric identifies under-utilized channels and is not excessively sensitive to atypical network flow patterns. Alternatively, the Jain index can be defined as:

$$J = \frac{\overline{R}^2_{\text{throughput}}}{\overline{R}^2_{\text{throughput}} + \sigma_{R_{\text{throughput}}}} \tag{11.10}$$

where $\overline{R}_{\text{throughput}}$ and $R_{\text{throughput}}$ denote the average throughput and throughput values, respectively.

11.1.7 Geometry (wideband SINR distribution)

In the calibration of the large-scale parameters of the channel model, all the multipath effects are not considered. Simulations are conducted to obtain for each user a path gain and a wideband SINR value. The path gain is defined as the average signal gain between an MS and its serving BS. It includes distance attenuation, shadowing, and antenna gains. The wideband SINR is the ratio of the average power received from the serving cell and the average interference power received from other cells plus noise. Sometimes this measure is called the geometry factor, since it presents a great dependency with the position of the user in relation to the position of the base stations. Then, the calibration of this measure ensures not only the calibration of the channel model, but also the calibration of the network layout. In addition, it involves the calibration of the physical layer considered in the simulation platform functional description, since the SINR is calculated in this layer.

11.1.8 Effective interference over thermal

In code division multiple access (CDMA) systems, the rise over thermal (RoT) indicates the ratio between the total power received from wireless sources at a base station and the thermal noise. In order to decode the data at the base station, a minimum SINR at the receiver must be guaranteed. The RoT metric is a measure of the uplink loading. By increasing the number of transmitting UEs and their transmit power, the level of interference in the uplink increases. This interference is perceived by the base station as noise adversely affecting the SINR. The base station controls the interference level by adjusting the UE uplink assignments and transmit power [25]. Similarly, IoT reflects the effective interference received by the base station. The definition of effective IoT measure takes the interference suppression capabilities of the base station receiver into consideration.

In order to formulate a mathematical expression for effective IoT, we consider a single-input multiple-output (SIMO) system and further assume that the base station has a linear receiver, such as maximal ratio combining (MRC) or MMSE with N_{RX} antennas. The received signal at the mth receive antenna can be expressed as $r_m = h_m x + e_m + n_m$ where h_m is the channel between the single transmit antenna and the mth receive antenna, x is the transmitted symbol, e_m is the sum of the interfering signals, and n_m is the thermal noise at the mth receive antenna. The receiver processing consists of estimating the transmitted symbol x by appropriately weighting the received signal at each antenna with a complex-valued weight w_m^H, and then summing the weighted signals. The sum-weighted output signal is given by $y = \sum_{m=1}^{N_{RX}} w_m^H r_m = \sum_{m=1}^{N_{RX}} w_m^H (h_m x + e_m + n_m)$. Alternatively, using vector notations, one can write the latter equation as $\mathbf{y} = \mathbf{w}^H(\mathbf{h}x + \mathbf{e} + \mathbf{n})$.

The effective SINR at the receiver output is given by the ratio of the power of the desired part of the filtered received signal $\mathbf{w}^H\mathbf{h}x$ to the power of the undesired part of the weighted received signal $\mathbf{w}^H(\mathbf{e} + \mathbf{n})$ which under the assumption that noise and interference are independent can be written as:

$$\text{SINR}_{\text{effective}} = \frac{\mathbf{w}^H\mathbf{h}\mathbf{h}^H\mathbf{w}}{\mathbf{w}^H(\mathbf{Q} + \mathbf{N})\mathbf{w}} \tag{11.11}$$

where $\mathbf{Q} = \varepsilon\{\mathbf{e}\mathbf{e}^H\}$ is the covariance matrix of the interference, and $\mathbf{N} = \varepsilon\{\mathbf{n}\mathbf{n}^H\}$ is the covariance matrix of the thermal noise. Note that typically $\mathbf{N} = \sigma^2\mathbf{I}$ where σ^2 is the noise variance per antenna and $\mathbf{I}$ is the $N_{RX} \times N_{RX}$ identity matrix. The denominator in Eq. (11.11) is defined as the power of the interference and thermal noise. $P_{I+N_{\text{effective}}} = \mathbf{w}^H(\mathbf{Q} + \mathbf{N})\mathbf{w}$. The effective IoT can now be defined as the ratio between the total effective noise and interference power to the effective thermal noise power:

$$IoT_{\text{effective}} = \frac{P_{I+N_{\text{effective}}}}{P_{N_{\text{effective}}}} = \frac{\mathbf{w}^H(\mathbf{Q} + \mathbf{N})\mathbf{w}}{\mathbf{w}^H\mathbf{N}\mathbf{w}} \tag{11.12}$$

Since receiver weights typically vary over frequency and time, the effective IoT should be calculated per frequency and time instant, and then averaged. The average is taken over allocated resources and unused resources are excluded.

11.1.9 Cell spectral efficiency and cell-edge user spectral efficiency

Cell spectral efficiency SE_{cell} is defined as the aggregate throughput of all users, that is, the number of correctly received bits delivered to the upper layers at the MAC service access point over a certain period of time, divided by the channel bandwidth divided by the number of cells. The channel bandwidth is defined as the effective bandwidth multiplied by the frequency reuse factor, where the effective bandwidth is the operating bandwidth that is appropriately scaled by the uplink/downlink ratio. The cell spectral efficiency is measured in bits/s/Hz/cell.

If d_i denotes the number of correctly received bits by user i (in the downlink) or from user i (in the uplink) in a system comprising N_{user} active users and N_{cell} cells, and if B denotes the channel bandwidth and T the time over which the data bits are received. The cell spectral efficiency can be expressed as follows:

$$\text{SE}_{\text{cell}} = \frac{\sum_{i=1}^{N_{\text{user}}} d_i}{TBN_{\text{cell}}} \tag{11.13}$$

The (normalized) user throughput is defined as the average user throughput, that is, the number of correctly received bits by users delivered to upper layers at the MAC service access point over a certain period of time, divided by the channel bandwidth, and is measured in bits/s/Hz. The cell-edge user spectral efficiency is defined as the 5% point of the CDF of the normalized user throughput. Let d_i, T_i, and B denote the number of correctly received bits by user i, the active session duration for user i, and the channel bandwidth, respectively. The (normalized) user throughput of user i is defined as:

$$R^{(i)}_{\text{user-throughput}} = \frac{d_i}{T_i B} \tag{11.14}$$

11.2 Calculation of static and dynamic overhead

The calculation and analysis of the signaling and control channels' overhead, as well as the physical-layer overhead associated with synchronization and broadcast channels, guard times and guard bands, reference signals, and that of the cyclic prefix are important in determining the actual performance of a cellular system. In general, the overhead channels are essential for proper operation of a cellular system and statically (independent of the number of the users in the cell) or dynamically (depending on the number of the users in the cell) consume some radio resources and make them permanently or temporarily unavailable for data transmission. There are two types of overhead channels: static and dynamic. A static overhead channel requires fixed base station power, time slot, and/or bandwidth. On the other hand, a dynamic overhead channel requires base station power, time, and/or bandwidth which dynamically change over time as a function of the number of active users.

The layer 1 (L1) and layer 2 (L2) overhead are accounted for in time, frequency, or space for calculation of system performance metrics, such as spectral efficiency, user throughput, VoIP capacity, etc. Examples of L1 overhead include synchronization signals, guard sub-carriers and DC sub-carrier, guard time (in TDD systems), reference signals, and cyclic prefix. Examples of L2 overheads include common and dedicated control channels, HARQ ACK/NACK feedback, channel quality feedback, random access channel, packet headers and sub-headers, as well as cyclic redundancy check (CRC). The power allocation/boosting should

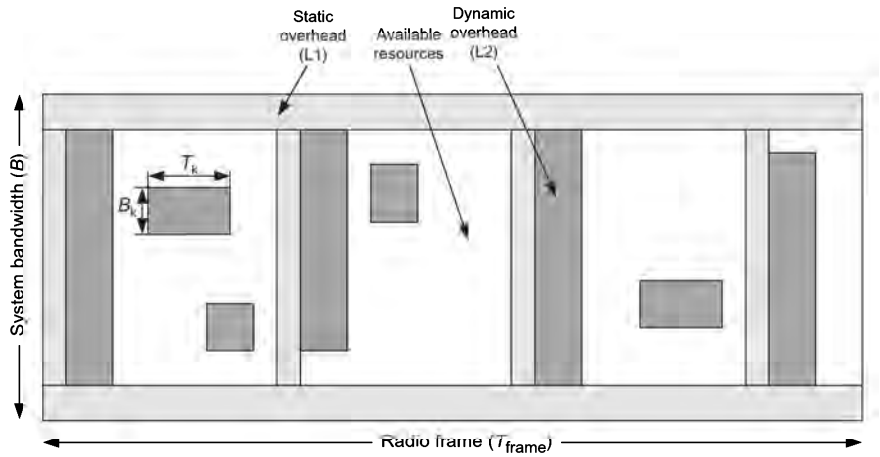


FIGURE 11.3

Illustration of the static and dynamic overhead.

also be accounted for in modeling resource allocation for control channels. Based on the example two-dimensional time-frequency model shown in Figure 11.3, the L1 and L2 overhead can be calculated as:

$$O_{\mathrm{L1+L2}} = \lim_{T_{\mathrm{frame}} \to \infty} \frac{\sum_{k \in S(\mathrm{L1}) \cup S(\mathrm{L2})} B_k T_k}{B T_{\mathrm{frame}}}, \quad 0 \le O_{\mathrm{L1+L2}} < 1 \tag{11.15}$$

where B denotes the system bandwidth and T_{frame} is the radio frame size, B_k is the resource occupied by the kth L1 (or L2) overhead channel across frequency dimension, and T_k denotes the required time resource for transmission of the kth L1 (or L2) overhead channel in time.

Using this model, the total resources consumed by the L1 overhead over a relatively long period of time is given as:

$$O_{\mathrm{L1}} = \lim_{T_{\mathrm{frame}} \to \infty} \frac{1}{B T_{\mathrm{frame}}} \sum_{k \in S(\mathrm{L1})} B_k T_k, \quad 0 \le O_{\mathrm{L1}} < 1 \tag{11.16}$$

where S(L1) denotes the set of resources used for static L1 overhead channels. The total resources consumed by the L2 overhead over a relatively long period of time is given as:

$$O_{\mathrm{L2}} = \lim_{T_{\mathrm{frame}} \to \infty} \frac{1}{B T_{\mathrm{frame}}(1 - O_{\mathrm{L1}})} \sum_{k \in S(L2)} B_k T_k, \quad 0 \le O_{\mathrm{L2}} < 1 \tag{11.17}$$

Note that the amount of resources that have already been used by the L1 overhead must not be recounted in calculation of O_{L2} and that $O_{\mathrm{L1+L2}} \neq O_{\mathrm{L1}} + O_{\mathrm{L2}}$. Furthermore, S(L2) denotes the set of resources used for L2 overhead channels

The average spectral efficiency inclusive of the effect of the L1/L2 overhead can be obtained as $SE_{average}(1 - O_{L1+L2})$ where $SE_{average}$ denotes the average spectral efficiency that has been obtained via system-level simulation excluding the L1/L2 overhead.

11.3 Traffic models

11.3.1 Statistical model for conversational speech

VoIP refers to real-time delivery of coded voice packets across a network using the Internet protocols. Several robust voice codecs for encoding conversational speech have been developed and discussed in the literature, including ITU-T G.729 (8 kbps) [17] and adaptive multi-rate (AMR) codec (4.75–12.2 kbps) [5,27]. In the following discussion, a VoIP session is defined as the entire user call time, and a typical conversation is characterized by periods of active speech or talk spurts followed by silence periods. Figure 11.4 illustrates a two-state Markov model[2] for conversational speech [23,24,54].

The steady-state condition of the model requires that $P_0 = a/(a + c)$ and $P_1 = c/(a + c)$ where P_0 and P_1 are the probabilities of being in state 0 and state 1, respectively. As shown in Figure 11.4, the probability of a transition from state 1 (the active speech state) to state 0 (the inactive state) while in state 1 is equal to a, whereas the probability of a transition from state 0 to state 1 while in state 0 is c. The model is updated at the speech encoder frame rate $R = 1/T$, where T is the

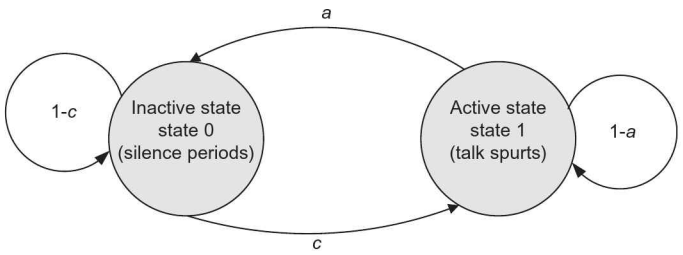


FIGURE 11.4

Two-state Markov model for speech [23,24].

[2]A sequence $X_1, X_2, \ldots, X_{n-1}, X_n$ of random variables is called a Markov sequence, if for any n, the conditional probability of X_n satisfies the following condition $F(X_n|X_{n-1}, X_{n-2}, \ldots, X_1) = F(X_n|X_{n-1})$, that is, the conditional distribution of X_n given $X_{n-1}, X_{n-2}, \ldots, X_1$ have been observed is equal to the conditional distribution X_n assuming only X_{n-1} has been observed. The transitional densities of a Markov sequence satisfy the Chapman–Kolmogorov equation. A random process whose future probabilities are determined by its most recent values is called a Markov process. A stochastic process $x(t)$ is called Markov, if for any n and $t_1 < t_2 < \ldots < t_n$ we have $P(x(t_n) \leq x_n|x(t_{n-1}), x(t_{n-2}), \ldots, x(t_1)) = P(x(t_n) \leq x_n|x(t_{n-1}))$[23,24,54].

encoder frame duration which is typically 20 ms for most speech encoders. Packets are generated at time intervals $iT + \tau$ where τ is the packet arrival delay, and i denotes the encoder frame index. During the active state, packets of fixed sizes are generated at these time intervals, while the model is updated at regular frame intervals. The size of the packets and the rate at which the packets are sent depend on the corresponding voice codecs and compression schemes. The voice activity factor (VAF) λ is defined as $\lambda = P_1 = c/(a+c)$. A talk-spurt is defined as the time period τ_{TS} between entering the active state and leaving the active state. The probability that a talk spurt has duration nT is given by $P(\tau_{TS} = nT) = a(1-a)^{n-1}, n = 1, 2, \ldots$ whereas the probability that a silence period has duration mT is given as $P(\tau_{SP} = mT) = c(1-c)^{m-1}, m = 1, 2, \ldots$. The average talk spurt duration μ_{TS} (in number of speech frames) is defined as $\mu_{TS} = \varepsilon[\tau_{TS}] = 1/a$. The mean silence period duration μ_{SP} (in number of speech frames) is given by $\mu_{SP} = \varepsilon[\tau_{SP}] = 1/c$. The distribution of the time period τ_{AE} (in number of speech frames) between successive active state entries is defined as the convolution of the distributions of τ_{SP} and τ_{TS}:

$$P(\tau_{AE} = nT) = \frac{c}{c-a}a(1-a)^{n-1} + \frac{a}{a-c}c(1-c)^{n-1}, \quad n = 1, 2, \ldots \tag{11.18}$$

It must be noted that τ_{AE} can be further considered as the time between MAC layer resource reservations, provided that a single reservation is made per user per talk-spurt. Note that in practice, very small values of τ_{AE} may not result in separate reservation requests. Since the transitions from state 1 to state 0 and vice versa are independent, the mean time μ_{AE} between active state entries is the sum of the mean time in each state, that is, $\mu_{AE} = \mu_{TS} + \mu_{SP}$. Therefore, the mean rate of arrival $\overline{R}_{AE}$ of transitions into the active state can be expressed as $\overline{R}_{AE} = 1/\mu_{AE}$.

The voice capacity calculation assumes the use of 12.2 kbps mode of 3GPP AMR codec with a 50% VAF provided that the percentage of users in outage is less than 2%, where a user is defined to have experienced outage if more than 2% of the VoIP packets are dropped, erased, or otherwise not delivered successfully to the user within the delay bound of 50 ms. The packet delay is defined based on the 98th percentile of the CDF of all individual users' 98th percentiles of packet delay (i.e., the 98th percentile of the packet delay CDF is first determined for each user and then the 98th percentile of the CDF that describes the 98th percentiles of the individual user delay is obtained). The VoIP capacity is measured in terms of the number of active users/MHz/cell. It is the minimum of the capacity calculated for either downlink or uplink divided by the effective bandwidth in the respective direction. In other words, the effective bandwidth is the operating bandwidth normalized appropriately considering the uplink/downlink ratio (in TDD systems).

During each VoIP session, a user will be in the active or inactive state. The duration of time that the user stays in each state is exponentially distributed. In the active or inactive state, voice packets of fixed sizes will be generated at

Table 11.2 VoIP Traffic Model Parameters [4,26]

VoIP Model Attribute	Statistical Distribution	Parameters	Probabilistic Distribution
Active/inactive state duration	Exponential	$\mu = 1.25$ s	$f_x = \lambda e^{-\lambda x}, x \geq 0$ $\lambda = 1/\mu$
Probability of state transition	N/A	$c = 0.01$, $d = 0.99$	N/A
Packet arrival delay jitter (downlink only)	Laplacian	$\beta = 5.11$ ms	$f_x = \frac{1}{2\beta} e^{\frac{-\lvert x \rvert}{\beta}}$ $-80 \text{ ms} \leq \tau \leq 80 \text{ ms}$

intervals of $iT + \tau$ seconds, where T is the voice-codec frame size which is typically 20 ms, τ is the network delay jitter (delay variations) in the downlink, and i is the VoIP frame number. In the uplink direction, τ is equal to zero. Given that the range of the delay jitter is limited to 120 ms, the model may be implemented by generating packets at times $iT + \tau'$ seconds where $\tau' = \tau + 80$ (ms) denotes a positive delay value (Table 11.2). The air-interface delay is measured as the time interval between the packet arrival time $iT + \tau'$ to successful reception and decoding of the packet at the receiver. Statistical distribution and parameters associated with the VoIP traffic model are summarized in Table 11.2. The assumptions that were used for VoIP capacity calculation are shown in Table 11.3.

11.3.2 Full-buffer traffic model

In the full-buffer user traffic model, all users in the system are assumed to have data to send or receive at any given time. In other words, there is always a constant amount of data that needs to be transferred, as opposed to bursts of data with probabilistic arrival time distribution. This model allows the assessment of the spectral efficiency of the system independent of the actual user traffic distribution model. A user is in outage if the residual packet error rate after HARQ retransmissions exceeds 1%.

11.4 Link-to-system mapping (PHY abstraction)

The objective of physical-layer abstraction is to model link-level performance and to reduce the amount of computations and complexity in system-level simulations. The motivation for abstraction of the physical layer is that simulating the physical layer across multiple base stations and mobile stations in a cellular network simulation platform can be computationally cumbersome and practically impossible [46,50]. The abstraction must be reasonably accurate, computationally simple,

Table 11.3 EESM/MIESM Parameters and MSE for all CQIs in a Bandwidth of Four PRBs [50]

CQI	Code Block Size	Approximate Code Rate	EESM					MIESM		
			β	MSE	α_1	α_2	MSE	α_1	α_2	MSE
1	72	0.072	0.372	0.003	0.363	0.360	0.003	0.278	0.276	0.002
2	112	0.113	0.531	0.004	0.519	0.515	0.004	0.389	0.385	0.003
3	192	0.185	0.865	0.004	0.858	0.855	0.003	0.633	0.629	0.002
4	312	0.297	1.403	0.014	1.439	1.460	0.012	1.056	1.067	0.008
5	456	0.435	1.636	0.076	1.647	1.675	0.073	1.111	1.112	0.045
6	608	0.585	1.646	0.023	1.636	1.621	0.022	1.035	1.019	0.013
7	768	0.368	3.418	0.159	3.748	4.123	0.057	1.065	1.121	0.002
8	1008	0.477	5.042	0.182	5.160	5.491	0.121	1.034	1.065	0.008
9	1248	0.600	6.122	0.106	6.307	6.649	0.066	0.937	0.980	0.013
10	1440	0.455	1.010	0.553	9.790	12.262	0.064	0.942	1.150	0.008
11	1728	0.553	0.399	0.713	11.489	14.827	0.024	0.556	0.727	0.010
12	2048	0.650	0.621	0.658	17.669	23.625	0.051	0.700	0.935	0.017
13	2368	0.753	0.962	0.825	24.081	32.971	0.069	0.760	1.017	0.038
14	2688	0.852	7.933	0.382	22.622	28.049	0.007	0.657	0.821	0.006
15	2880	0.925	15.859	0.077	25.245	28.103	0.034	0.840	0.985	0.024

ble 11.4 Baseline Configuration Parameters for IMT-Advanced Evaluations [14]

nulation rameters	Indoor Hotspot (InH)	Urban Micro-Cellular (UMi)	Urban Macro-Cellular (UMa)	Rural Macro-Cellular (RMa)
		Baseline Parameters		
se station antenna ght (m)	6 (on the ceiling)	10 (below rooftop)	25 (above rooftop)	35 (above rooftop)
mber of BS antennas ceive/transmit)	Up to 8/up to 8	Up to 8/up to 8	Up to 8/up to 8	Up to 8/up to 8
se station transmit wer (dBm)	24 (40 MHz) 21 (20 MHz)	41 (10 MHz) 44 (20 MHz)	46 (10 MHz) 49 (20 MHz)	46 (10 MHz) 49 (20 MHz)
bile station transmit wer (dBm)	21	24	24	24
mber of MS antennas ceive/transmit)	Up to 2/up to 2	Up to 2/up to 2	Up to 2/up to 2	Up to 2/up to 2
nimum distance ween MS and BS (m)	≥ 3	≥ 10	≥ 25	≥ 35
carrier quency (GHz)	3.4	2.5	2	0.8
tdoor-to-indoor netration loss	N/A	See Annex 1, Table A1-2 of [14]	N/A	N/A
tdoor to in-car netration loss	N/A	N/A	9 dB (lognormal, $\sigma = 5$ dB)	9 dB (lognormal, $\sigma = 5$ dB)
		Parameters for Analytical Assessment of Peak Spectral Efficiency		
mber of BS antennas ceive/transmit)	Up to 4/up to 4	Up to 4/up to 4	Up to 4/up to 4	Up to 4/up to 4
mber of MS antennas ceive/transmit)	Up to 4/up to 2	Up to 4/up to 2	Up to 4/up to 2	Up to 4/up to 2

(Continued)

ble 11.4 (Continued)

nulation rameters	Indoor Hotspot (InH)	Urban Micro-Cellular (UMi)	Urban Macro-Cellular (UMa)	Rural Macro-Cellular (RMa)
		Parameters for System-Level Simulations		
twork layout	Indoor floor	Hexagonal grid	Hexagonal grid	Hexagonal grid
r-site distance (m)	60	200	500	1732
annel model	Indoor hotspot channel model	Urban micro-cellular channel model	Urban macro-cellular channel model	Rural macro-cellular channel model
r distribution	Randomly and uniformly distributed over area	Randomly and uniformly distributed over area	Randomly and uniformly distributed over area	Randomly and uniformly distributed over area
		50% pedestrian users and 50% users indoor	100% vehicular users	100% high-speed vehicular users
r mobility	All mobile stations have fixed and identical speed with randomly and uniformly distributed direction	All mobile stations have fixed and identical speed with randomly and uniformly distributed direction	All mobile stations have fixed and identical speed with randomly and uniformly distributed direction	All mobile stations have fixed and identical speed with randomly and uniformly distributed direction
speed (km/h)	3	3	30	120
r-site interference	Explicitly modeled	Explicitly modeled	Explicitly modeled	Explicitly modeled
noise figure (dB)	5	5	5	5
noise figure (dB)	7	7	7	7
antenna gain (bore-ht) (dBi)	0	17	17	17
antenna gain (dBi)	0	0	0	0
rmal noise level m/Hz)	−174	−174	−174	−174

Parameters for Assessment of Cell Spectral Efficiency and Cell-Edge User Spectral Efficiency				
ffic model	Full buffer	Full buffer	Full buffer	Full buffer
stem bandwidth	2 × 20 MHz (FDD) 40 MHz (TDD)	2 × 10 MHz (FDD) 20 MHz (TDD)	2 × 10 MHz (FDD) 20 MHz (TDD)	2 × 10 MHz (FDD) 20 MHz (TDD)
mber of users/cell	10	10	10	10
Parameters for Evaluation of VoIP Capacity				
ffic model	VoIP	VoIP	VoIP	VoIP
stem bandwidth	2 × 5 MHz (FDD) 10 MHz (TDD)	2 × 5 MHz (FDD) 10 MHz (TDD)	2 × 5 MHz (FDD) 10 MHz (TDD)	2 × 5 MHz (FDD) 10 MHz (TDD)
nulation duration for a gle drop(s)	20	20	20	20
Parameters for Link-Level Simulation (Mobility Requirement)				
ffic model	Full buffer	Full buffer	Full buffer	Full buffer
annel model	Indoor hotspot channel model	Urban micro-cellular channel model	Urban macro-cellular channel model	Rural macro-cellular channel model
stem bandwidth (MHz)	10	10	10	10
mber of users/cell	1	1	1	1

relatively independent of channel models, and extensible to interference models and multi-antenna processing methods. The system-level simulations are used to characterize the average user/system performance, which may be useful in providing insights for deployment of the system in terms of cell and frequency planning. For such simulations, the average performance of a system is quantified using the topology and macro channel characteristics to calculate a wideband SINR distribution across the cell (alternatively known as geometry). Each subscriber's SINR distribution is then mapped to the highest MCS that could be supported, based on link-level SINR tables which include fast fading characteristics of the channel. The link-level SINR-BLER look-up tables serve as the PHY abstraction for predicting average link-level performance. The instantaneous channel conditions are used to improve the performance of the cellular systems. Channel-dependent scheduling and adaptive coding and modulation are examples of channel-adaptive schemes employed to improve system performance. Therefore, properly designed system-level simulation methodologies do explicitly model the dynamic behavior of the system [28,37,50,51].

In system-level simulations, an encoded data/control packet may be transmitted over a time-frequency selective channel. In OFDM-based systems, the encoded block is transmitted over several sub-carriers, the post-processing SINR values of the pre-decoded streams are thus non-uniform, and the channel gains of sub-carriers can be time-varying. As a result, in the transmission of a large encoded packet, the encoded symbols with unequal SINR ratios at the input of the decoder are considered due to the time or frequency selectivity of the channel impulse or frequency response over the duration of packet transmission.

The goal of a PHY abstraction or a link-to-system mapping is to predict the encoded BLER for a given received channel realization across the OFDM sub-carriers that are used to transmit the channel-coded blocks. In order to predict the performance, the post-processing SINR values at the input to the forward error correction (FEC) decoder are considered as input to the PHY abstraction. As the link-level curves are generated assuming a frequency flat channel response at a given SINR, an effective SINR is defined to accurately map the system-level SINR to the link-level curves in order to determine the resulting BLER. The latter mapping is known as effective SINR mapping (ESM) in the literature. The ESM PHY abstraction compresses the vector of received SINR values to a single effective SINR value, which can then be further mapped to a BLER value. Several ESM approaches to predict the instantaneous link-level performance have been studied in the literature. Examples include mean instantaneous capacity, exponential effective SINR mapping (EESM), and mutual information (MI) ESM. Each of these PHY abstractions uses a different function to map the vector of SINR values to a single number. Given the instantaneous EESM SINR, mean capacity or mutual information effective SINR, the BLER for each MCS is calculated using a suitable mapping function. The general process of link-to-system mapping is illustrated in Figure 11.5.

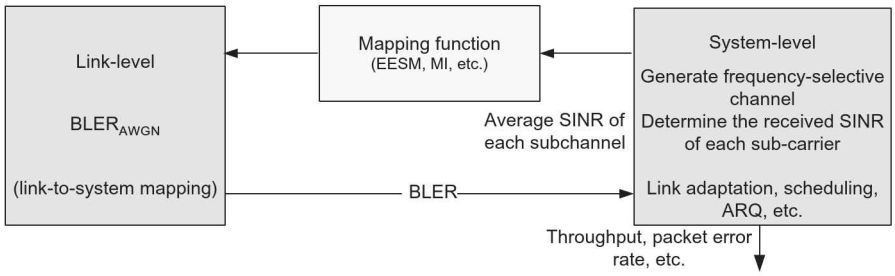


FIGURE 11.5

Link-to-system mapping process [26].

Given an experimental BLER measured in a multi-state channel with a specific MCS, the effective SINR of that channel is defined as the SINR that would produce the same BLER, with the same MCS, in AWGN conditions. In general, for a given multi-state channel with N_{FFT} different SINR measurements $\{\text{SINR}_1, \text{SINR}_2, \text{SINR}_3, \ldots, \text{SINR}_{NFFT}\}$, the effective SINR can be described as follows:

$$\text{SINR}_{\text{effective}} = \alpha_1 \Phi^{-1}\left(\frac{1}{N_{\text{FFT}}}\sum_{n=1}^{N_{\text{FFT}}} \Phi\left(\frac{\text{SINR}_n}{\alpha_2}\right)\right) \tag{11.19}$$

where $\text{SINR}_{\text{effective}}$ denotes the effective SINR, SINR_n is the SINR measured at the nth sub-carrier, N_{FFT} is the number of symbols in a coded block, or the number of sub-carriers used in an OFDM system, and $\Phi(.)$ is an invertible function. In the case of the mutual information-based ESM the function $\Phi(.)$ is derived from the constrained capacity, whereas in the case of EESM, the function $\Phi(.)$ is derived from the Chernoff bound[3] on the probability of error [55]. The EESM model uses the mapping function $\Phi(x) = 1 - \exp(-x)$ for all modulation schemes and in many cases, the constants α_1 and α_2 are assumed to be equal $\alpha_1 = \alpha_2 = \beta$. The parameter β can be interpreted as a shift in $\Phi(.)$ function to adapt the model to different MCSs. If a MIMO scheme is utilized assuming use of linear processing (ZF or MMSE) in the receiver, one still can use the effective SINR concept

[3]In the theory of probability and stochastic processes, the Chernoff bound provides exponentially decreasing bounds (asymptotic) on tail distributions of sums of independent random variables compared to the first or second moment based tail bounds such as Markov's inequality or Chebyshev inequality, which only yield power-law bounds on tail decay. Let $\mathbf{x}_1, \mathbf{x}_2, \ldots, \mathbf{x}_n$ denote discrete and independent random variables with probability $p > 1/2$. Then, the probability of simultaneous occurrence of more than $n/2$ of the events x_k has an exact value P, where $P = \sum_{i=\lfloor n/2 \rfloor}^{n} \binom{n}{i} p^i (1-p)^{n-i}$. The Chernoff bound provides a lower bound for P given by $P \geq 1 - \exp[-2n(p-1/2)^2]$. The Chernoff bound applies to a class of random variables and provides exponential falloff of probability with distance from the mean. The critical condition that is needed for a Chernoff bound is that the random variable must be a sum of independent indicator random variables [55].

by taking the MIMO post-processing SINR as the set of measurements $\{SINR_1, SINR_2, SINR_3, \ldots, SINR_{NFFT}\}$ of the multi-state channel. Assuming that the receiver has a good estimation of the MIMO channel matrix, it can calculate the post-processing SINR based on well-known expressions. In spatial multiplexing mode, the antenna correlation is translated into degradation of the post-processing SINR, thus assuming that the channel is known, the effective SINR model may also capture the effect of antenna correlation. The parameters α_1 and α_2 depend on the modulation scheme, the code block size, and the code rate, but should be valid for SISO and MIMO with linear equalization regardless of the MIMO antenna correlation. Based on the above discussion, in the case of EESM, the effective SINR in snapshot i can be written as follows:

$$\mathrm{SINR}^{i}_{\mathrm{effective}}(\beta) = \beta \ln\left(\frac{1}{N_{\mathrm{FFT}}}\sum_{n=1}^{N_{\mathrm{FFT}}}\exp\left(\frac{\mathrm{SINR}^{i}_{n}}{\beta}\right)\right) \tag{11.20}$$

If M denotes the number of simulated snapshots, the value of β can be obtained as follows:

$$\hat{\beta} = \arg\min_{\beta}\left\{\sum_{i=1}^{N_{\mathrm{snapshots}}}\left[\log(\mathrm{BLER}_i) - \log(\mathrm{BLER}_R(\mathrm{SINR}^{i}_{\mathrm{effective}}(\beta)))\right]^2\right\} \tag{11.21}$$

where $\mathrm{BLER}_R(.)$ is the reference BLER curve in the AWGN channel for the current MCS and code block size. That is, to obtain β, we minimize the mean squared error between the estimated BLER and the simulated BLER for the set of simulated snapshots using numerical methods. By using the logarithmic BLER error in Eq. (11.21), the minimization algorithm tries to obtain minimal error at low BLER, which is the region of interest. For MIESM Eq. (11.19) is rewritten as follows:

$$\mathrm{SINR}^{i}_{\mathrm{effective}}(\alpha_1, \alpha_2) = \alpha_1 \ln\left(\frac{1}{N_{\mathrm{FFT}}}\sum_{n=1}^{N_{\mathrm{FFT}}}\exp\left(\frac{\mathrm{SINR}^{i}_{n}}{\alpha_2}\right)\right) \tag{11.22}$$

In which, the calculation of α_1 and α_2 involves a two-dimensional minimization of the mean square error (MSE) as follows:

$$(\hat{\alpha}_1, \hat{\alpha}_2) = \arg\min_{\alpha_1,\alpha_2}\left\{\sum_{i=1}^{N_{\mathrm{snapshots}}}\left[\log(\mathrm{BLER}_i) - \log(\mathrm{BLER}_R(\mathrm{SINR}^{i}_{\mathrm{effective}}(\alpha_1, \alpha_2)))\right]^2\right\} \tag{11.23}$$

In the case of MIESM, there is an additional challenge that the mutual-information function $\Phi(.)$ must be inverted numerically. Table 11.3 lists the obtained EESM/MIESM parameters as well as the MSE for each CQI. The values of the parameters in each case are in good agreement with those previously

published in the literature [50,51]. The main advantage of EESM over MIESM is that the nonlinear weighting function $\Phi(.)$ and its inverse function used to calculate the effective SINR are closed-form and easy to compute. The performance of EESM to predict the BLER in the MIMO high-correlation scenarios can be tested in two ways, that is, using a single parameter (one-dimension minimization) or using two different parameters. The advantage of using a single parameter is that minimization effort is simple and there is a single minimum. This is the reason that there are two sets of parameters for EESM shown in Table 11.3. The values of the EESM parameters in Table 11.3 are in good agreement with those published in the literature for QPSK and 16QAM and deviate for 64QAM [28,34,50,51]. Comparing the MSEs corresponding to MIESM and EESM in the table suggests that MIESM outperforms EESM and provides more accurate link-abstraction relative to reference link-level curves at the expense of more complexity.

The accuracy of a mutual information-based metric depends on the equivalent channel over which this metric is defined. The capacity is defined as the mutual information based on a Gaussian channel with Gaussian distributed inputs. The modulation constrained capacity is the mutual information of a symbol channel, that is, constrained by the input symbols drawn from a complex set. The computation of the mutual information per coded bit can be derived from the received symbol-level mutual information which is regarded as received bit mutual information rate (RBIR) link-to-system mapping. An alternative approach directly arrives at the bit-level mutual information and is known as the mean mutual information per bit (MMIB) PHY abstraction method. The procedure of the MIESM approach is illustrated in Figure 11.6. Given a set of N received encoder symbol SINRs from the system-level simulation, denoted as $\{\text{SINR}_1, \text{SINR}_2, \text{SINR}_3, \ldots, \text{SINR}_N\}$; a mutual-information metric is calculated. Based on the computed MI metric, an equivalent SINR is obtained and used to look-up the BLER value [34,50,51].

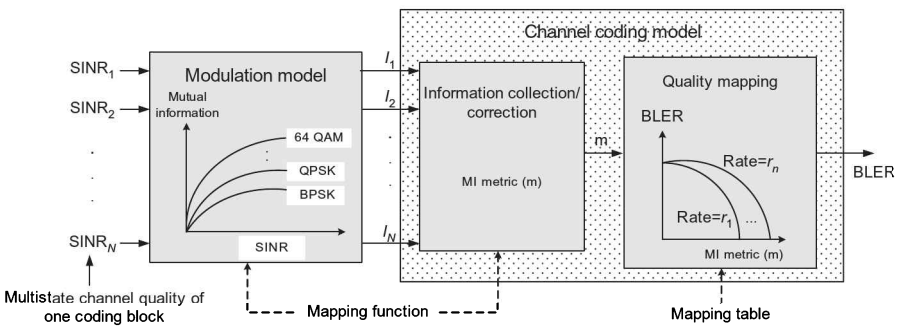


FIGURE 11.6

Procedure for MIESM link-to-system mapping method [26].

11.5 IMT-Advanced test environments

For evaluation of the IMT-Advanced candidates, the ITU-R WP 5D defined several test environments where each test environment is characterized with certain user mobility, path loss and channel models, and system configuration parameters. The evaluation of candidate radio access technologies was performed in selected scenarios of the following test environments [12–14]:

- Indoor test environment models isolated cells at offices and/or in hotspots comprising stationary and pedestrian users. In this model, the emphasis is on very small cells, very high user throughputs, and high user density inside buildings.
- Urban micro-cellular test environment with higher user density was defined to model pedestrian and slow vehicular users. The micro-cellular test environment's focus is on small cells and high user densities which demonstrates typical traffic load in city centers and dense urban areas. The key characteristic of this test environment is high traffic loads as well as outdoor and outdoor-to-indoor coverage. This scenario is interference-limited. A continuous cellular layout and the associated interference are assumed and radio access points are located below rooftop level.
- Urban macro-cellular environment (base coverage urban) was defined to model coverage for pedestrian users up to fast-moving vehicular users. The base coverage urban test environment focuses on large cells and continuous coverage. The main characteristics of this test environment are continuous and ubiquitous coverage in urban areas. This scenario is interference-limited, using macro-cells with radio access points above rooftop level. In an urban macro-cell test environment, mobile stations are located outdoor at street level and fixed base station antennas are located clearly above surrounding building heights. Therefore, NLoS or obstructed sight can be considered in this scenario.
- High-speed or rural test environment models high-speed vehicular and trains. The high-speed test environment focuses on larger cells and continuous coverage. The key characteristics of this test environment are continuous wide area coverage supporting high-speed vehicles. This scenario will therefore be noise-limited and/or interference-limited and uses macro-sized cells.

11.6 Network layout for system-level simulations

In the rural or high-speed, macro- and micro-cellular environments, no specific topographical details are taken into consideration. Base stations are placed in regular grids conforming to a hexagonal layout. A basic hexagonal layout with three cells/sectors per site is shown in Figure 11.7 where antenna bore-sight, cell range, and inter-site distance are also illustrated. The system-level simulations use a wrap-around model with 19 sites each comprising 3 cells. The users are dropped

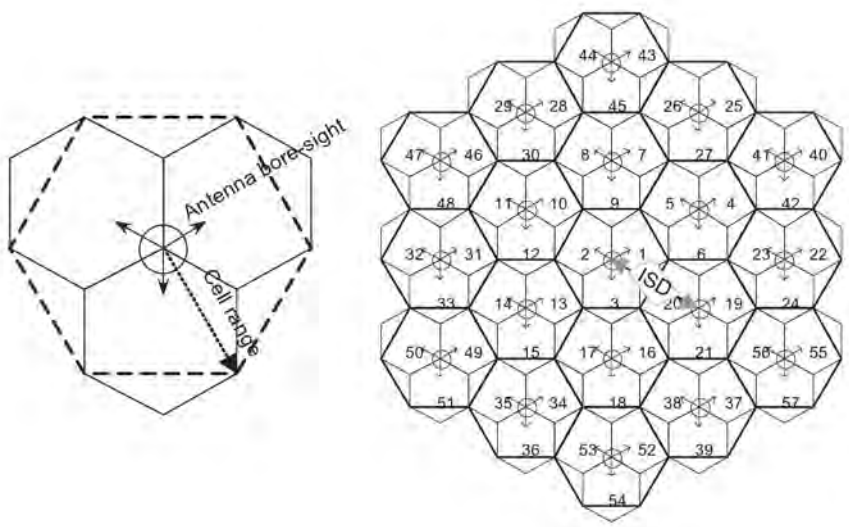


FIGURE 11.7

Illustration of a hexagonal cellular network layout [14].

uniformly over the entire coverage area (Monte Carlo method[4]) in order to model the inter-cell interference. Depending on the configuration being simulated and required output, the effect of the surrounding outer cells may be disregarded. In such cases, only 19 cells of the center cluster may be modeled. For the cases where modeling of the interfering outer cells is necessary for accuracy of the results, the wrap-around structure with the seven cluster network can be used. A cluster is defined as six displacements of the center hexagon. In the wrap-around inter-cell interference model, the network is extended to a cluster of networks consisting of seven replicas of the original hexagonal network, with the original hexagonal network in the middle while the other six copies are attached to it symmetrically on six sides. The number of mobile stations is predetermined for each sector/cell, where each MS location is randomly distributed with uniform distribution (see Figure 11.7).

The serving cell of each MS is determined in two steps due to the wrap-around nature of the cell layout. The first step is to determine the 19 shortest-distanced cells for each MS from all seven logical cell clusters, and the second step is to determine the serving cell/sector among the nearest 19 cells for each MS based on the strongest link according to the path loss and shadowing. To determine the shortest-distanced cell for each MS, the distances between the MS

[4]Monte Carlo methods are a class of computational algorithms that rely on repeated random sampling to compute their results. Monte Carlo methods are often used in simulating physical and mathematical systems. Because of their reliance on repeated computation of random or pseudorandom quantities, these methods are most suited to calculation by a computer and tend to be used when it is unfeasible or impossible to find a closed-form result with a deterministic algorithm [56].

and all logical cell clusters are calculated and the 19 cells with a shortest distance in all seven cell clusters are selected. The serving cell for each MS provides the strongest link with a strongest received long-term signal power. It should be noted that the shadowing experienced on the link between MS and cells located in different clusters is the same.

11.7 IMT-Advanced evaluation methodology and baseline configurations

The IMT-Advanced candidate technologies were required to be evaluated under at least three test environments. ITU-R WP 5D specified a common evaluation methodology based on which the candidates were required to be configured and assessed against the IMT-Advanced minimum system requirements. Table 11.4 provides the common parameters for evaluation of radio access technologies as specified by ITU-R recommendations [6,12–14].

The BS antennas in each sector are assumed to have antenna patterns in azimuth and elevation directions that are given by:

$$\begin{aligned} A_e(\phi) &= -\min\left[12\left(\frac{\phi-\phi_{\text{tilt}}}{\phi_{3\text{dB}}}\right)^2, A_m\right] \text{ Elevation direction} \\ A(\theta) &= -\min\left[12\left(\frac{\theta}{\theta_{3\text{dB}}}\right)^2, A_m\right] \text{ Azimuth direction} \end{aligned} \tag{11.24}$$

where $A(\theta)$ is the relative antenna gain (in dB) in the direction of $-180° \le \theta \le 180°$, $\theta_{3\ \text{dB}}$ is the 3 dB beam-width ($\theta_{3\text{dB}} = 70°$),$A_m = 20$ dB is the maximum attenuation, $A_e(\phi)$ is the relative antenna gain (in dB) in the elevation direction $-90° \le \phi \le 90°$, $\phi_{3\text{dB}}$ is the elevation 3 dB beam-width ($\phi_{3\text{dB}} = 15°$), and ϕ_{tilt} is the tilt angle. The value of the antenna tilt angle is assumed to be $\phi_{\text{tilt}} = 0°$ for InH, $\phi_{\text{tilt}} = 12°$ for UMi, $\phi_{\text{tilt}} = 12°$ for UMa, and $\phi_{\text{tilt}} = 6°$ for RMa test environments.

The combined antenna pattern at angles off the cardinal axes is computed as $-\min[-(A(\theta) + A_e(\phi)), A_m]$. The antenna bearing is defined as the angle between the main antenna lobe center and a line directed due east given in degrees. The bearing angle increases in a clockwise direction. The center directions of the main antenna lobe in each sector point to the corresponding side of the hexagon. For an indoor test environment, the BS is assumed to have an omni-directional antenna pattern. The mobile station is assumed to have omni-directional antennas.

11.8 Link-level and system-level channel models

The channel behavior is described by its long- and short-term fading characteristics where the former often depends on the geometrical location of a user in a wireless network and the latter defines the time-variant spatial channels.

In general, there are two ways of modeling a channel, deterministic and stochastic. The deterministic category encompasses all models that describe the propagation channel for a specific transmitter location, receiver location, and environment. Deterministic channel models are site-specific, as they clearly depend on the location of transmitter, receiver, and the properties of the environment. They are therefore most suitable for network planning and deployment. In many cases, it is not possible or desirable to model the propagation channel in a specific environment. Especially for system testing and evaluation, it is more appropriate to consider channels that reflect "typical," "best case," and "worst case" propagation scenarios. A stochastic channel model thus reflects the statistics of the channel impulse responses and during the actual simulation; impulse responses are generated as realizations according to those statistics[18–22,29–33,35–43].

Essential to the evaluation of multiple-antenna techniques, which are the key enabling technology for IMT-Advanced systems, is the modeling of MIMO channels that can be represented as double-directional channels or as vector (or matrix) channels. The former representation is more related to the physical propagation effects, while the latter is more focused on the mathematical effect of the channel on the system. The double-directional model is a physical model in which the channel is constructed from summing over multiple waves or rays. Thus, it can also be referred to as a "ray-based model." The vector or matrix channel is a mathematical or analytical model in which the space-time channel as seen by the receiver is constructed mathematically, assuming certain system and antenna parameters. In this approach, the channel coefficients are correlated random processes in both space and time, where the correlation is defined mathematically.

The ITU-R WP 5D specified channel models for the evaluation of IMT-Advanced candidate technologies which consisted of primary and extension modules. The framework of the primary module is based on the WINNER II channel model,[5] which applies the same approach as the 3GPP/3GPP2 spatial channel model (SCM).[6] The extension module extends the capabilities of the IMT-Advanced channel model to cover additional deployment scenarios beyond that of IMT-Advanced candidate technology evaluations, allowing the use of modified parameters to generate large-scale parameters. The ITU-R WP 5D specified channel model is a geometric stochastic model. It does not explicitly specify the locations of the scatterers, rather the directions of the rays generated as a result of scattering objects. The geometric modeling of the radio channel enables separation of propagation parameters and antennas. The channel parameters for individual snapshots are determined stochastically based on statistical distributions extracted from channel measurements. Antenna geometries and radiation patterns

[5]Information on WINNER II channel models can be found at http://www.ist-winner.org/deliverables.html.

[6]Information on the 3GPP/3GPP2 spatial channel model can be found in 3GPP TR 25.996 *spatial channel model for multiple input multiple output* (MIMO), September 2003.

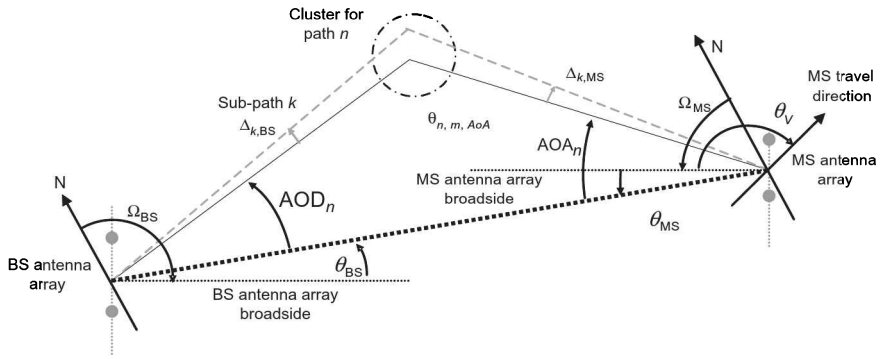


FIGURE 11.8

Illustration of angular parameters in the MIMO channels [1,14].

can be defined properly by the user of the model. As shown in Figure 11.8, channel realizations are generated through the application of the geometrical principle by summing the rays (plane waves) with specific small-scale parameters, such as delay, power, angle-of-arrival (AoA), and angle-of-departure (AoD). The superposition results in correlation between antenna elements and temporal fading with geometry-dependent Doppler spectrum. A number of rays constitute a cluster. A cluster and a propagation path diffused in space are equivalent in delay and angle domains. A generic MIMO channel model is applied to all test scenarios. The time-variant impulse response matrix of the MIMO channel can be written as (assuming N_{TX} transmit antennas at the BS and N_{RX} receive antennas at the MS) $\mathbf{H}(t;\tau) = \sum_{n=1}^{N} \mathbf{H}_n(t;\tau)$ where τ denotes the delay and $N = N_{RX} \times N_{TX}$ is the number of multipaths. The channel impulse response is composed of the antenna array response matrices $\mathbf{F}_{TX}$ and $\mathbf{F}_{RX}$ for the transmitter and the receiver, respectively, as well as the dual-polarized propagation channel response matrix $\mathbf{h}_n$ for the nth cluster, hence:

$$\mathbf{H}_n(t;\tau) = \iint \mathbf{F}_{RX}(\phi)\, \mathbf{h}_n(t;\tau,\varphi,\phi)\, \mathbf{F}_{TX}^{T}(\varphi)\, d\varphi\, d\phi \tag{11.25}$$

The channel from transmit antenna element s to receive antenna element u for cluster n can be expressed as follows:

$$H_{u,s,n}(t;\tau) = \sum_{m=1}^{M} \begin{bmatrix} \mathbf{F}_{RX,u,V}(\phi_{n,m}) \\ \mathbf{F}_{RX,u,H}(\phi_{n,m}) \end{bmatrix}^{T} \begin{bmatrix} \alpha_{n,m,VV} & \alpha_{n,m,VH} \\ \alpha_{n,m,HV} & \alpha_{n,m,HH} \end{bmatrix} \begin{bmatrix} \mathbf{F}_{TX,s,V}(\varphi_{n,m}) \\ \mathbf{F}_{TX,s,H}(\varphi_{n,m}) \end{bmatrix} \times \exp(j2\pi\upsilon_{n,m}t)\delta(\tau - \tau_{n,m}) \times \exp(j2\pi\lambda_0^{-1}(\overline{\phi}_{n,m} \cdot \overline{r}_{RX,u}))\exp(j2\pi\lambda_0^{-1}(\overline{\varphi}_{n,m} \cdot \overline{r}_{TX,s})) \tag{11.26}$$

where $\mathbf{F}_{RX,u,V}$ and $\mathbf{F}_{RX,u,H}$ denote the antenna element u field patterns for vertical and horizontal polarizations, respectively, $\alpha_{n,m,VV}$ and $\alpha_{n,m,VH}$ are the

complex-valued gains of vertical-to-vertical and horizontal-to-vertical polarizations of ray n,m, respectively, λ_0 represents the wave length of the RF carrier, $\overline{\varphi}_{n.m}$ AoD unit vector, $\overline{\phi}_{n.m}$ is the AoA unit vector, $\overline{r}_{\mathrm{TX},s}$ and $\overline{r}_{rx,u}$ are the location vectors of element s and u, respectively, and $\upsilon_{n,m}$ denotes the Doppler frequency component of ray n,m [1,14,26]. If the radio channel is dynamically modeled, the above-mentioned small-scale parameters are going to be time-variant.

In Figure 11.8, the placement of the MS with respect to each BS is to be determined according to the cell layout. From this placement, the distance between the MS and the BS d and the LoS directions with respect to the BS and MS, θ_{BS} and θ_{MS} can be determined. Note that θ_{BS} and θ_{MS} are defined relative to the broadside directions. The MS antenna array orientations Ω_{MS} are independent and identically distributed and are obtained from a uniform $0-360^\circ$ distribution.

The generic MIMO channel model is a stochastic model with two levels of unpredictability: large-scale parameters, such as shadow fading, delay, and angular spreads that are drawn randomly from tabulated distribution functions; and small-scale parameters, such as delay, power, and direction of arrival and departure that are selected randomly according to tabulated distribution functions and large-scale parameters. An infinite number of different realizations of the channel model can be generated randomly selecting different initial phases for the scattering objects.

The general approach in the SCM is based on the geometry of a network layout. The large-scale parameters, such as path loss and shadowing factor, are generated according to the geometric positions of the BS and MS. Then the statistical channel behavior is defined using distribution functions of delay and angle, and also by the power delay and angular profiles. Typically, an exponential power delay profile and Laplacian power angular profile are assumed with the function completely defined once the root mean-square (RMS) delay spread and angular spread are specified. The RMS delay and angular spread parameters can be random variables with a mean and standard deviation. The RMS delay and angular spread can be mutually correlated, together with other large-scale parameters, such as shadowing factors. According to the exact profile and distribution functions defined by the particular RMS delay and angular spread values, a finite number of channel taps are randomly generated with a per-tap delay, mean power, mean AoA and AoD, and RMS angular spread. They are defined in a way such that the overall power profile and distribution function are satisfied. Each tap is the contribution of a number of rays (plane waves) arriving at the same time, with each ray having its own amplitude, AoA, and AoD. The number of taps and their delay and angles may be randomly defined, but a reduced-complexity model can specify the delays, mean powers, and angles of the channel taps in a predetermined manner when typical values are often chosen. Similar to the well-known tapped-delay-line version of the wide-sense stationary uncorrelated scattering model, where the power delay profile is fixed, a spatial tapped-delay-line reduced-complexity model additionally defines the spatial information, such as per-tap mean AoA, AoD, and per-tap angular spread, and the power angular

profile. Spatial tapped-delay-line models are also referred to as cluster-delay-line models as each tap is modeled as the effect of a cluster of rays arriving at the same time. Each tap suffers from fading in space and over time. The spatial fading process will satisfy a predetermined power angular profile.

The realization of a time-varying spatial channel can be performed in two ways:

- Ray-based: The channel coefficient between each transmit and receive antenna pair is the summation of all rays at each tap and at each time instant, according to the antenna configuration, gain pattern, AoA, AoD of each ray. The temporal channel variation depends on the traveling speed and direction relative to the AoA/AoD of each ray.
- Correlation-based: The antenna correlation for each tap is computed first according the per-tap mean AoA/AoD, per-tap power angular profile, and antenna configuration parameters (e.g., spacing and polarization). The per-tap Doppler spectrum depends on the traveling speed and direction relative to the mean per-tap AoA/AoD, as well as the per-tap power angular profile. The MIMO channel coefficients at each tap can then be generated mathematically by transforming typically the independent and identically distributed Gaussian random variables according to the antenna correlation and the temporal correlation (correspondingly the particular Doppler spectrum).

The generic channel model is based on the drop concept. The system-level simulation is performed in a sequence of "drops," where a "drop" is defined as one simulation run over a certain time period when using the generic model. A drop (or snapshot of a channel segment) is a simulation instance where the random properties of the channel remain constant except for the fast fading caused by the changing phases of the rays. The constant properties during a single drop are the power, delay, and direction of the rays. In a simulation, the number and the length of drops are selected based on the evaluation requirements and the deployment scenario. The generic channel model allows simulation of several statistically independent drops in order to obtain a statistical representation of system performance. The channel model parameters for evaluation of IMT-Advanced technologies in various test environments are shown in Table 11.5. In Table 11.5, DS is the RMS delay spread, ASD is the RMS azimuth spread of departure angles, ASA denotes the RMS azimuth spread of arrival angles, SF represents the shadow fading, and parameter K denotes the Rician K-factor. IMT-Advanced primary module path loss model parameters for a hexagonal cell layout are summarized in Table 11.6.

The break point distance in the above table is defined as $d'_{BP} = 4h'_{BS}h'_{MS}f_c/c$ where f_c is the center frequency (Hz), $c = 3.0 \times 10^8$ m/s is the propagation velocity in free space, h'_{BS} and h'_{MS} are the effective antenna heights at the BS and the MS, respectively. The effective antenna heights h'_{BS} and h'_{MS} are computed as follows: $h'_{BS} = h_{BS} - 1$ and $h'_{MS} = h_{MS} - 1$ where h_{BS} and h_{MS} are the actual antenna heights. The effective height in urban environments is assumed to be equal to 1.0m. In the above table, PL_b denotes basic path loss, PL_{B1} is loss of UMi

able 11.5 Channel Model Parameters for IMT-Advanced Test Environments [4,14]

Channel Model Parameters		InH		UMi			UMa		RMa	
		LoS	NLoS	LoS	NLoS	Outdoor-to-Indoor	LoS	NLoS	LoS	NLoS
elay spread	μ	−7.70	−7.41	−7.19	−6.89	−6.62	−7.03	−6.44	−7.49	−7.43
S) $\log_{10}$(s)	σ	0.18	0.14	0.40	0.54	0.32	0.66	0.39	0.55	0.48
oD spread	μ	1.60	1.62	1.20	1.41	1.25	1.15	1.41	0.90	0.95
SD) g_{10}(degrees)	σ	0.18	0.25	0.43	0.17	0.42	0.28	0.28	0.38	0.45
oA spread	μ	1.62	1.77	1.75	1.84	1.76	1.81	1.87	1.52	1.52
SA) g_{10}(degrees)	σ	0.22	0.16	0.19	0.15	0.16	0.20	0.11	0.24	0.13
hadow fading F) (dB)	σ	3	4	3	4	7	4	6	4	8
-factor (K) (dB)	μ	7	N/A	9	N/A	N/A	9	N/A	7	N/A
	σ	4	N/A	5	N/A	N/A	3.5	N/A	4	N/A
ross-rrelations	ASD vs. DS	0.6	0.4	0.5	0	0.4	0.4	0.4	0	−0.4
	ASA vs. DS	0.8	0	0.8	0.4	0.4	0.8	0.6	0	0
	ASA vs. SF	−0.5	−0.4	−0.4	−0.4	0	−0.5	0	0	0
	ASD vs. SF	−0.4	0	−0.5	0	0.2	−0.5	−0.6	0	0.6
	DS vs. SF	−0.8	−0.5	−0.4	−0.7	−0.5	−0.4	−0.4	−0.5	−0.5
	ASD vs. ASA	0.4	0	0.4	0	0	0	0.4	0	0
	ASD vs. K	0	N/A	−0.2	N/A	N/A	0	N/A	0	N/A
	ASA vs. K	0	N/A	−0.3	N/A	N/A	−0.2	N/A	0	N/A
	DS vs. K	−0.5	N/A	−0.7	N/A	N/A	−0.4	N/A	0	N/A
	SF vs. K	0.5	N/A	0.5	N/A	N/A	0	N/A	0	N/A

(*Continued*)

Table 11.5 (Continued)

Channel Model Parameters		InH		UMi			UMa		RMa	
		LoS	NLoS	LoS	NLoS	Outdoor-to-Indoor	LoS	NLoS	LoS	NLoS
Delay distribution		Exponential	Exponential	Exponential	Exponential	Exponential	Exponential	Exponential	Exponential	Exponential
AoD and AoA distribution		Laplacian		Wrapped Gaussian			Wrapped Gaussian		Wrapped Gaussian	
Delay scaling parameter r_τ		3.6	3	3.2	3	2.2	2.5	2.3	3.8	1.7
Cross-polarization ratio (dB)	μ	11	10	9	8.0	9	8	7	12	7
Number of clusters		15	19	12	19	12	12	20	11	10
Number of rays per cluster		20	20	20	20	20	20	20	20	20
Cluster ASD		5	5	3	10	5	5	2	2	2
Cluster ASA		8	11	17	22	8	11	15	3	3
Per cluster shadowing standard deviation ζ (dB)		6	3	3	3	4	3	3	3	3
Correlation distance (m)	DS	8	5	7	10	10	30	40	50	36
	ASD	7	3	8	10	11	18	50	25	30
	ASA	5	3	8	9	17	15	50	35	40
	SF	10	6	10	13	7	37	50	37	120
	K	4	N/A	15	N/A	N/A	12	N/A	40	N/A

e 11.6 IMT-Advanced Primary Module Path Loss Models (f_c Is in GHz, All Distances Are in Meters, and a Hexagonal Cell Layout ssumed) [14]

nario	Path Loss PL (dB)	Shadow Fading Standard Deviation (dB)	Applicability Range (m)/Antenna Height (m)
LoS	$16.9 \log_{10}(d) + 32.8 + 20 \log_{10}(f_c)$	$\sigma = 3$	$3 < d < 100$ $h_{BS} = 3 - 6$ $h_{MS} = 1 - 2.5$
NLoS	$43.3 \log_{10}(d) + 11.5 + 20 \log_{10}(f_c)$	$\sigma = 4$	$10 < d < 150$ $h_{BS} = 3 - 6$ $h_{MS} = 1 - 2.5$
LoS	$22.0 \log_{10}(d) + 28.0 + 20 \log_{10}(f_c)$ $40 \log_{10}(d_1) + 7.8 - 18 \log_{10}(h'_{BS}) -$ $18 \log_{10}(h'_{MS}) + 2 \log_{10}(f_c)$	$\sigma = 3$	$10 < d_1 < d'_{BP}$ $d'_{BP} < d_1 < 5000$ $h_{BS} = 10; h_{MS} = 1.5$
NLoS	$36.7 \log_{10}(d) + 22.7 + 26 \log_{10}(f_c)$	$\sigma = 4$	$10 < d < 2000$ $h_{BS} = 3$ $h_{MS} = 1 - 2.5$
Outdoor-to-indoor	$PL_b + PL_{tw} + PL_{in}$ $PL_b = PL_{B1}(d_{out} + d_{in})$; $PL_{tw} = 20$; $PL_{in} = 0.5 d_{in}$	$\sigma = 7$	$10 < d_{out} + d_{in} < 1000$ $0 < d_{in} < 25$
LoS	$22.0 \log_{10}(d) + 28.0 + 20 \log_{10}(f_c)$ $40.0 \log_{10}(d_1) + 7.8 - 18.0 \log_{10}(h'_{BS})$ $- 18.0 \log_{10}(h'_{MS}) + 2.0 \log_{10}(f_c)$	$\sigma = 4$	$10 < d_1 < d'_{BP}$ $d'_{BP} < d_1 < 5000$ $h_{BS} = 25; h_{MS} = 1.5$
NLoS	$161.04 - 7.1 \log_{10}(W) + 7.5 \log_{10}(h)$ $- (24.37 - 3.7(h/h_{BS})^2) \log_{10}(h_{BS})$ $+ (43.42 - 3.1 \log_{10}(h_{BS})) (\log_{10}(d) - 3)$ $+ 20 \log_{10}(f_c) - (3.2 (\log_{10}(11.75 h_{MS}))^2 - 4.97$	$\sigma = 6$	$10 < d < 5000$ $h_{BS} = 25$; $h_{MS} = 1.5$; $W = 20; h = 205 < h < 50;$ $5 < W < 50$ $10 < h_{BS} < 150;$ $1 < h_{MS} < 10$

(Continued)

ble 11.6 (Continued)

enario		Path Loss PL (dB)	Shadow Fading Standard Deviation (dB)	Applicability Range (m)/Antenna Height (m)
a	LoS	$PL_1 = 20\ \log_{10}(40\pi d f_c/3) + \min(0.03h^{1.72}, 10)$ $\log_{10}(d) - \min(0.044h^{1.72}, 14.77) + 0.002\log_{10}(h)d$ $PL_2 = PL_1(d_{BP}) + 40\ \log_{10}(d/d_{BP})$	$\sigma = 4$ $\sigma = 6$	$10 < d < d_{BP}$ $d_{BP} < d < 10000$ $h_{BS} = 35; h_{MS} = 1.5$ $W = 20; h = 5$
	NLoS	$161.04 - 7.1\ \log_{10}(W) + 7.5\ \log_{10}(h)$ $-(24.37 - 3.7(h/h_{BS})^2)\log_{10}(h_{BS})$ $+ (43.42 - 3.1\ \log_{10}(h_{BS}))(\log_{10}(d) - 3)$ $+ 20\ \log_{10}(f_c) - (3.2\ (\log_{10}(11.75\ h_{MS}))^2 - 4.97)$	$\sigma = 8$	$10 < d < 5000$ $h_{BS} = 35;$ $h_{MS} = 1.5W = 20; h = 5$

outdoor scenario, PL_{tw} is penetration loss through the wall, PL_{in} denotes the loss inside, d_{out} is the distance from the BS to the wall next to the MS location, d_{in} denotes the perpendicular distance from the wall to the MS which is evenly distributed between 0 and 25 m, and the break point distance is defined as $d_{BP} = 2\pi h_{BS} h_{MS} f_c / c$.

Spatial correlation is often said to degrade the performance of multi-antenna systems and impose a limit on the number of antennas that can effectively fit in a small mobile device. This seems intuitive as the spatial correlation decreases the number of independent channels that can be created by precoding. When modeling spatial correlation, it is useful to employ the Kronecker model, where the correlation between transmit and receive antennas are assumed independent and separable. This model is reasonable when the main scattering appears close to the antenna arrays and has been validated by outdoor and indoor measurements. Assuming Rayleigh fading, the Kronecker model means that the channel matrix can be represented as $\mathbf{H} = \mathbf{R}_{RX}^{1/2} \mathbf{H}_{channel} (\mathbf{R}_{TX}^{1/2})^T$ where the elements of $\mathbf{H}_{channel}$ are independent and identically distributed as circular symmetric complex Gaussian with zero-mean and unit variance. The important part of the model is that $\mathbf{H}_{channel}$ is pre-multiplied by the receive-side spatial correlation matrix $\mathbf{R}_{RX}$ and post-multiplied by the transmit-side spatial correlation matrix $\mathbf{R}_{TX}$. Equivalently, the channel matrix can be expressed as $\mathbf{H} \sim Z(0, \mathbf{R}_{TX} \otimes \mathbf{R}_{RX})$ where $\otimes$ denotes the Kronecker product.

Using the Kronecker model, the spatial correlation depends directly on the eigenvalue distributions of the correlation matrices $\mathbf{R}_{RX}$ and $\mathbf{R}_{TX}$. Each eigenvector represents a spatial direction of the channel and its corresponding eigenvalue describes the average channel/signal gain in this direction. For the transmit-side, the correlation matrix $\mathbf{R}_{TX}$ describes the average gain in a spatial transmit direction, while the receive-side correlation matrix $\mathbf{R}_{RX}$ describes a spatial receive direction. High spatial correlation is represented by a large eigenvalue spread in $\mathbf{R}_{TX}$ or $\mathbf{R}_{RX}$, implying that some spatial directions are statistically stronger than the others. On the other hand, low spatial correlation is represented by a small eigenvalue spread in $\mathbf{R}_{TX}$ or $\mathbf{R}_{RX}$, which implies that almost the same signal gain can be expected from all spatial directions [57].

Let us now focus on a specific case of downlink transmission from a base station to a mobile station. Denoting the nth snapshot of the spatial correlation matrices at the BS and the MS by $\mathbf{R}_{BS,n}$ and $\mathbf{R}_{MS,n}$, the per-tap spatial correlation is determined as the Kronecker product[7] of the BS and MS's antenna correlation matrices:

[7]Given an $m \times n$ matrix $\mathbf{A}$ and a $p \times q$ matrix $\mathbf{B}$, the Kronecker product $\mathbf{C} = \mathbf{A} \otimes \mathbf{B}$, also called the matrix direct product, is an $mp \times nq$ matrix with elements defined by $c_{\alpha\beta} = a_{ij} b_{kl}$, where $\alpha \equiv p(i-1) + k$ and $\beta \equiv q(j-1) + l$. The matrix direct product provides the matrix of the linear transformation induced by the vector space tensor product of the original vector spaces. More precisely, suppose that operators $S: V_1 \to W_1$ and $T: V_2 \to W_2$ are given by $S(x) = Ax$ and $T(y) = By$. Then $S \otimes T: V_1 \otimes V_2 \to W_1 \otimes W_2$ is determined by $S \otimes T(x \otimes y) = (Ax) \otimes (By) = (A \otimes B)(x \otimes y)$[57].

$$\mathbf{R}_n = \mathbf{R}_{\mathrm{BS},n} \otimes \mathbf{R}_{\mathrm{MS},n} \tag{11.27}$$

We denote the number of receive antennas by N_{RX} and the number of transmit antennas by the N_{TX}. If cross-polarized antennas are present at the receiver, it is assumed that $N_{\mathrm{RX}}/2$ receive antennas have the same polarization, while the remaining $N_{\mathrm{RX}}/2$ receive antennas have orthogonal polarization. Likewise, if cross-polarized antennas are present at the transmitter, it is assumed that the $N_{\mathrm{TX}}/2$ transmit antennas have the same polarization; while the remaining $N_{\mathrm{TX}}/2$ transmit antennas have orthogonal polarization. It is further assumed that the antenna arrays are composed of pairs of collocated antennas with orthogonal polarization. With these assumptions, the per-tap channel correlation is determined as follows:

$$\mathbf{R}_n = \mathbf{R}_{\mathrm{BS},n} \otimes \boldsymbol{\Gamma} \otimes \mathbf{R}_{\mathrm{MS},n} \tag{11.28}$$

Where $\mathbf{R}_{\mathrm{MS},n}$ is an $N_{\mathrm{RX}} \times N_{\mathrm{RX}}$ matrix if all receive antennas have the same polarization, or an $N_{\mathrm{RX}}/2 \times N_{\mathrm{RX}}/2$ matrix if the receive antennas are cross-polarized. Likewise, $\mathbf{R}_{\mathrm{BS},n}$ is an $N_{\mathrm{TX}} \times N_{\mathrm{TX}}$ matrix if all the transmit antennas have the same polarization, or an $N_{\mathrm{TX}}/2 \times N_{\mathrm{TX}}/2$ matrix if the transmit antennas are cross-polarized. Matrix $\boldsymbol{\Gamma}$ is a cross-polarization matrix based on the cross-polarization defined in the cluster-delay-line models. Matrix $\boldsymbol{\Gamma}$ is a 2×2 matrix if cross-polarized antennas are used at the transmitter or at the receiver. It is a 4×4 matrix if cross-polarized antennas are used at both the transmitter and the receiver.

Table 11.7 defines the correlation matrices for the eNB and UE in E-UTRA with a different number of transmit/receive antennas at each entity [4].

For the scenarios with more antennas at either eNB, UE, or both, the channel spatial correlation matrix can be expressed as the Kronecker product of $\mathbf{R}_{\mathrm{eNB}}$ and $\mathbf{R}_{\mathrm{UE}}$ according to $\mathbf{R}_{\mathrm{spatial}} = \mathbf{R}_{\mathrm{eNB}} \otimes \mathbf{R}_{\mathrm{UE}}$. The parameters α and β for different antenna correlation types are given in Table 11.8.

Table 11.7 eNB/UE Correlation Matrix [4,58]

	Number of Antennas		
Entity	**1**	**2**	**4**
eNB	$\mathbf{R}_{\mathrm{eNB}} = 1$	$\mathbf{R}_{\mathrm{eNB}} = \begin{pmatrix} 1 & \alpha \\ \alpha^* & 1 \end{pmatrix}$	$\mathbf{R}_{\mathrm{eNB}} = \begin{pmatrix} 1 & \alpha^{1/9} & \alpha^{4/9} & \alpha \\ \alpha^{1/9*} & 1 & \alpha^{1/9} & \alpha^{4/9} \\ \alpha^{4/9*} & \alpha^{1/9*} & 1 & \alpha^{1/9} \\ \alpha^* & \alpha^{4/9*} & \alpha^{1/9*} & 1 \end{pmatrix}$
UE	$\mathbf{R}_{\mathrm{UE}} = 1$	$\mathbf{R}_{\mathrm{UE}} = \begin{pmatrix} 1 & \beta \\ \beta^* & 1 \end{pmatrix}$	$\mathbf{R}_{\mathrm{UE}} = \begin{pmatrix} 1 & \beta^{1/9} & \beta^{4/9} & \beta \\ \beta^{1/9*} & 1 & \beta^{1/9} & \beta^{4/9} \\ \beta^{4/9*} & \beta^{1/9*} & 1 & \beta^{1/9} \\ \beta^* & \beta^{4/9*} & \beta^{1/9*} & 1 \end{pmatrix}$

Table 11.8 Values of α and β for Different Antenna Correlations [4]

Low Correlation		Medium Correlation		High Correlation	
α	β	α	β	α	β
0	0	0.3	0.9	0.9	0.9

Table 11.9 EPA/EVA/ETA Multipath Power Delay Profiles [4,58]

Tap Excess Delay (ns)	Relative Power (dB)	Tap Excess Delay (ns)	Relative Power (dB)	Tap Excess Delay (ns)	Relative Power (dB)
EPA		EVA		ETU	
0	0.0	0	0.0	0	−1.0
30	−1.0	30	−1.5	50	−1.0
70	−2.0	150	−1.4	120	−1.0
90	−3.0	310	−3.6	200	0.0
110	−8.0	370	−0.6	230	0.0
190	−17.2	710	−9.1	500	0.0
410	−20.8	1090	−7.0	1600	−3.0
–	–	1730	−12.0	2300	−5.0
–	–	2510	−16.9	5000	−7.0

Table 11.10 Delay Profiles of LTE Channel Models [4,58]

Model	Number of Channel Taps	RMS Delay Spread (ns)	Maximum Tap Excess Delay (ns)
EPA	7	45	410
EVA	9	357	2510
ETU	9	991	5000

The multipath fading channel model specifies three different delay profiles which are representative of low, medium, and high delay spread environments, that is, extended pedestrian A (EPA) model, extended vehicular A (EVA) model, and extended typical urban (ETU) model [52]. The multipath delay profiles for these channels are shown in Table 11.9 and the associated number of channel taps, RMS delay spread, and maximum tap excess delays are provided in Table 11.10. In addition to a multipath delay profile, a maximum Doppler frequency is specified for each multipath fading propagation condition as follows: EPA 5 Hz ($\nu_{\max} = 5$ Hz), EVA 70 Hz ($\nu_{\max} = 70$ Hz), and ETU 300 Hz ($\nu_{\max} = 300$ Hz).

11.9 LTE-Advanced link-level and system-level performance

The 3GPP LTE-Advanced was a candidate for IMT-Advanced whose performance was fully characterized based on the ITU-R defined evaluation methodology. The following sections summarize the performance characterization of the 3GPP LTE-Advanced as part of the IMT-Advanced submission.

11.9.1 Cell spectral efficiency and cell-edge spectral efficiency

Cell spectral and cell-edge spectral efficiencies were evaluated through extensive simulations conducted by a number of 3GPP member companies. The simulation results were reported based on specific 3GPP LTE-Advanced configurations, that is, downlink and uplink MU-MIMO, downlink and uplink CoMP, and uplink SU-MIMO, for both FDD and TDD duplex schemes in various test scenarios. It must be noted that during LTE Rel-10 development and prior to IMT-Advanced submission, CoMP was an incomplete study item in 3GPP and no standard technique was specified for CoMP at that time; therefore, CoMP simulation results presented in this chapter, which were provided by a number of 3GPP member companies, did not use standard techniques and may not agree with each other in various conditions. Nevertheless, the CoMP study item was later completed and CoMP was specified as a feature in LTE Rel-11 specifications that will be discussed in the next chapter [11].

The performance differences among contributing sources can be explained by implementation-specific functionalities at the transmitter and the receiver that are not explicitly specified by the standard, such as receiver type, scheduling algorithms, and error modeling. In the results reported for the downlink, the size of the control channel (L OFDM symbols) and the number of the MBSFN subframes are the factors that affect the overhead. Note that in 3GPP submission, the control channel overhead is statically modeled, that is, the downlink control channels occupy a fixed number of OFDM symbols irrespective of the number of users, although it is expected that the size of the physical downlink control channel dynamically varies with the number of active users in the cell. In the MBSFN subframes and in the MBSFN region, there are no cell-specific reference signals (CRS), which effectively reduces the overhead.

Channel estimation and receiver types are the factors that affect the demodulation performance. Availability of CSI at the eNB is the assumption that impacts the transmit signal processing at the eNB for MU-MIMO and CoMP schemes. In the tables for the uplink, physical uplink control channel bandwidth is the factor that affects the overhead. Each value in Tables 11.11 and 11.12 is obtained as an average of all samples provided by different companies. The results suggest that the requirements are fulfilled with $L = 3$ corresponding to the largest overhead except for the system bandwidth of 1.4 MHz where the requirements cannot be met. If the control overhead

Table 11.11 LTE-Advanced Downlink Cell Spectral and Cell-Edge Spectral Efficiencies [2,6]

Scheme and Antenna Configuration	Test Environment	Duplex Scheme	ITU-R Requirement Cell Spectral Efficiency/Cell-Edge Spectral Efficiency	Cell Spectral Efficiency (bits/s/Hz/cell)			Cell-Edge Spectral Efficiency (bits/s/Hz)		
				$L=1$	$L=2$	$L=3$	$L=1$	$L=2$	$L=3$
Rel-8 SU-MIMO 4 × 2(A)	InH	FDD	3/0.1	4.8	4.5	4.1	0.23	0.21	0.19
MU-MIMO 4 × 2 (C)			3/0.1	6.6	6.1	5.5	0.26	0.24	0.22
Rel-8 SU-MIMO 4 × 2 (A)		TDD	3/0.1	4.7	4.4	4.1	0.22	0.20	0.19
MU-MIMO 4 × 2 (C)			3/0.1	6.7	6.1	5.6	0.24	0.22	0.20
MU-MIMO 4 × 2 (C)	UMi	FDD	2.6/0.075	3.5	3.2	2.9	0.10	0.096	0.087
MU-MIMO 4 × 2 (A)			2.6/0.075	3.4	3.1	2.8	0.12	0.11	0.099
CS/CB-CoMP 4 × 2 (C)			2.6/0.075	3.6	3.3	3.0	0.11	0.099	0.089
JP-CoMP 4 × 2 (C)			2.6/0.075	4.5	4.1	3.7	0.14	0.13	0.12
MU-MIMO 8 × 2 (C/E)			2.6/0.075	4.2	3.8	3.5	0.15	0.14	0.13
MU-MIMO 4 × 2 (C)		TDD	2.6/0.075	3.5	3.2	3.0	0.11	0.096	0.089
MU-MIMO 4 × 2 (A)			2.6/0.075	3.2	2.9	2.7	0.11	0.10	0.095

(Continued)

Table 11.11 (Continued)

Scheme and Antenna Configuration	Test Environment	Duplex Scheme	ITU-R Requirement Cell Spectral Efficiency/Cell-Edge Spectral Efficiency	Cell Spectral Efficiency (bits/s/Hz/cell)			Cell-Edge Spectral Efficiency (bits/s/Hz)		
				$L=1$	$L=2$	$L=3$	$L=1$	$L=2$	$L=3$
CS/CB-CoMP 4 × 2 (C)			2.6/0.075	3.6	3.3	3.1	0.10	0.092	0.086
JP-CoMP 4 × 2 (C)			2.6/0.075	4.6	4.2	3.9	0.10	0.092	0.085
MU-MIMO 8 × 2 (C/E)			2.6/0.075	4.2	3.9	3.6	0.12	0.11	0.099
MU-MIMO 4 × 2 (C)	UMa	FDD	2.2/0.06	2.8	2.6	2.4	0.079	0.073	0.066
CS/CB-CoMP 4 × 2 (C)			2.2/0.06	2.9	2.6	2.4	0.081	0.074	0.067
JP-CoMP 4 × 2 (A)			2.2/0.06	3.0	2.7	2.5	0.080	0.073	0.066
CS/CB-CoMP 8 × 2 (C)			2.2/0.06	3.8	3.5	3.2	0.10	0.093	0.084
MU-MIMO 4 × 2 (C)		TDD	2.2/0.06	2.9	2.6	2.4	0.079	0.071	0.067
CS/CB-CoMP 4 × 2 (C)			2.2/0.06	2.9	2.6	2.4	0.083	0.075	0.070
JP-CoMP 4 × 2 (C)			2.2/0.06	3.6	3.3	3.1	0.090	0.082	0.076
CS/CB-CoMP 8 × 2 (C/E)			2.2/0.06	3.7	3.3	3.1	0.10	0.093	0.087

Rel-8 SU-MIMO 4 × 2 (C)	RMa	FDD	1.1/0.04	2.3	2.1	1.9	0.081	0.076	0.069
Rel-8 SU-MIMO 4 × 2 (A)			1.1/0.04	2.1	2.0	1.8	0.067	0.063	0.057
MU-MIMO 4 × 2 (C)			1.1/0.04	3.9	3.5	3.2	0.11	0.099	0.090
MU-MIMO 8 × 2 (C)			1.1/0.04	4.1	3.7	3.4	0.13	0.12	0.11
Rel-8 SU-MIMO 4 × 2 (C)		TDD	1.1/0.04	2.0	1.9	1.8	0.072	0.067	0.063
Rel-8 SU-MIMO 4 × 2 (A)			1.1/0.04	1.9	1.7	1.6	0.057	0.053	0.049
MU-MIMO 4 × 2 (C)			1.1/0.04	3.5	3.2	3.0	0.098	0.089	0.083
MU-MIMO 8 × 2 (C/E)			1.1/0.04	4.0	3.6	3.4	0.12	0.11	0.10
Rel-8 Single-Layer BF 8 × 2 (E)			1.1/0.04	2.5	2.3	2.1	0.11	0.10	0.093

Table 11.12 3GPP LTE-Advanced Uplink Cell Spectral and Cell-Edge Spectral Efficiencies [2,6]

Scheme and Antenna Configuration	Test Environment	Duplex Scheme	ITU-R Requirement Cell Spectral Efficiency/Cell-Edge Spectral Efficiency	Cell Spectral Efficiency (bits/s/Hz/cell)	Cell-edge Spectral Efficiency (bits/s/Hz)
Rel-8 SIMO 1 × 4 (A)	InH	FDD	2.25/0.07	3.3	0.23
Rel-8 SIMO 1 × 4 (C)			2.25/0.07	3.3	0.24
Rel-8 MU-MIMO 1 × 4 (A)			2.25/0.07	5.8	0.42
SU-MIMO 2 × 4 (A)			2.25/0.07	4.3	0.25
Rel-8 SIMO 1 × 4 (A)		TDD	2.25/0.07	3.1	0.22
Rel-8 SIMO 1 × 4 (C)			2.25/0.07	3.1	0.23
Rel-8 MU-MIMO 1 × 4 (A)			2.25/0.07	5.5	0.39
SU-MIMO 2 × 4 (A)			2.25/0.07	3.9	0.25
Rel-8 SIMO 1 × 4 (C)	UMi	FDD	1.8/0.05	1.9	0.073
Rel-8 MU-MIMO 1 × 4 (A)			1.8/0.05	2.5	0.077
MU-MIMO 2 × 4 (A)			1.8/0.05	2.5	0.086
Rel-8 SIMO 1 × 4 (C)		TDD	1.8/0.05	1.9	0.070
Rel-8 MU-MIMO 1 × 4 (A)			1.8/0.05	2.3	0.071
MU-MIMO 2 × 4 (A)			1.8/0.05	2.8	0.068
MU-MIMO 1 × 8 (E)			1.8/0.05	3.0	0.079

Rel-8 SIMO 1 × 4 (C)	UMa	FDD	1.4/0.03	1.5	0.062
CoMP 1 × 4 (A)			1.4/0.03	1.7	0.086
CoMP 2 × 4 (C)			1.4/0.03	2.1	0.099
Rel-8 SIMO 1 × 4 (C)		TDD	1.4/0.03	1.5	0.062
CoMP 1 × 4 (C)			1.4/0.03	1.9	0.090
CoMP 2 × 4 (C)			1.4/0.03	2.0	0.097
MU-MIMO 1 × 8 (E)			1.4/0.03	2.7	0.076
Rel-8 SIMO 1 × 4 (C)	RMa	FDD	0.7/0.015	1.8	0.082
Rel-8 MU-MIMO 1 × 4 (A)			0.7/0.015	2.2	0.097
CoMP 2 × 4 (A)			0.7/0.015	2.3	0.13
Rel-8 SIMO 1 × 4 (C)		TDD	0.7/0.015	1.8	0.080
Rel-8 MU-MIMO 1 × 4 (A)			0.7/0.015	2.1	0.093
CoMP 2 × 4 (A)			0.7/0.015	2.5	0.15
MU-MIMO 1 × 8 (E)			0.7/0.015	2.6	0.10

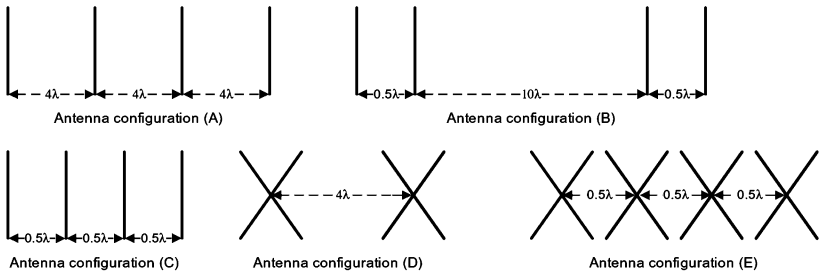


FIGURE 11.9

Illustration of antenna configurations used in LTE evaluations.

assumption is relaxed, that is the number of active users decreases, $L = 1, 2$ can be considered and thereby the performance can be further improved. The tables show that LTE Rel-8 with SU-MIMO 4×2 configuration can already fulfill the ITU-R requirements. The tables also show that further performance improvements can be achieved using additional technical features.

In the following tables, various antenna configurations have been utilized. There are four or eight transmit antennas with the following configurations: (A) uncorrelated co-polarized, that is, co-polarized antennas are four-wavelength apart; (B) grouped co-polarized, that is, two groups of co-polarized antennas where there is a 10-wavelength distance between the center of each group and 0.5-wavelength separation between antennas within each group; (C) correlated and co-polarized, that is, 0.5-wavelength between antennas; (D) uncorrelated and cross-polarized, that is, columns with $\pm 45^\circ$ linearly polarized antennas and separated by four wavelengths; and (E) correlated and cross-polarized, that is, columns with $\pm 45^\circ$ linearly polarized antennas and separated by 0.5-wavelengths. These configurations are illustrated in Figure 11.9.

The downlink and uplink cell spectral and cell-edge spectral efficiencies in various test environments for the TDD and FDD duplex schemes are shown in Tables 11.11 and 11.12, respectively. In these tables, the acronyms "JP-CoMP," "CS-CoMP," and "CB-CoMP" refer to joint processing, coordinated scheduling, and coordinated beamforming multi-point transmission schemes, respectively. The joint processing refers to a CoMP scheme where data is available at each of the geographically separated transmission points and physical downlink shared channel (PDSCH) transmission occurs from multiple points, whereas coordinated scheduling/beamforming is an alternative CoMP technique where data is only available at serving cell and data transmission is from that point, but user scheduling/beamforming decisions are made with coordination among different cells.

11.9.2 VoIP capacity

While most of the modern packet-switched air-interfaces do not specify voice codecs, calculation of the VoIP capacity requires explicit assumptions about a particular voice codec and its parameters, such as the frame rate, real-time

transport protocol (RTP) payload size, and discontinuous transmission (DTX) capability. The VoIP capacity of LTE-Advanced was calculated assuming use of AMR 12.2 kbps codec with a 50% speech activity factor. It was further assumed that the percentage of users in outage is less than 2% where a user is defined to have experienced outage if less than 98% of the VoIP packets have been delivered successfully to the user within a one-way radio access delay bound of 50 ms. The assumptions and the configuration parameters used in the system-level simulations for VoIP are as described in Table 11.13. The number of active VoIP users was calculated through extensive system-level simulations that were conducted by a number of 3GPP member companies. Table 11.14 shows the VoIP capacity results in the indoor, micro-cellular, macro-cellular, and high-speed test environments for FDD and TDD duplex schemes. The results suggest that LTE-Advanced satisfies the ITU-R requirements in various deployment scenarios. The antenna configurations are illustrated in Figure 11.9.

11.9.3 Mobility

IMT-Advanced specified four mobility classes based on UE speeds as follows: Stationary (0 km/h); Pedestrian (0 to 10 km/h); Vehicular (10 to 120 km/h); and High-speed vehicular (120 to 350 km/h). In order to evaluate LTE-Advanced against mobility requirement, the methodology that is set forth in Report ITU-R M.2135-1 [14] is followed, where in the first step the system-level simulation is performed for each test environment in the uplink to obtain the uplink SINR distribution (see Figure 11.10). From the uplink SINR distribution the 50% point of CDF is obtained for each test environment. In the second step, link-level simulation is conducted to generate the spectral efficiency versus SINR curves for each test environment. The spectral efficiency values include the effect of control channel overhead from the uplink system-level simulations for each test scenario. The mobility requirement in each mobility class is satisfied, if the uplink traffic channel

Table 11.13 Assumptions for VoIP Capacity Calculation [14,26]

Parameter	Value
Codec	AMR12.2 kbps mode
Encoder frame length	20 ms
VAF	50%
Payload	Active: 33 bytes (octet-aligned mode) Inactive: 7 bytes SID packet is sent every 160 ms during silence intervals
Protocol overhead with compressed header	10 bits + padding (RTP-pre-header) 4 bytes (RTP/UDP/IP) 2 bytes (radio link control (RLC)/ security) 16 bits (CRC)

Table 11.14 LTE-Advanced VoIP Capacity [6]

Antenna Configuration	Duplex Scheme	Test Environment	ITU-R Requirement	VoIP Capacity (Active Users/MHz/Cell)
Antenna configuration (A)	FDD	InH	50	140
		UMi	40	80
		UMa	40	68
		RMa	30	91
Antenna configuration (C)		InH	50	131
		UMi	40	75
		UMa	40	69
		RMa	30	94
Antenna configuration (A)	TDD	InH	50	137
		UMi	40	74
		UMa	40	65
		RMa	30	86
Antenna configuration (C)		InH	50	130
		UMi	40	74
		UMa	40	67
		RMa	30	92

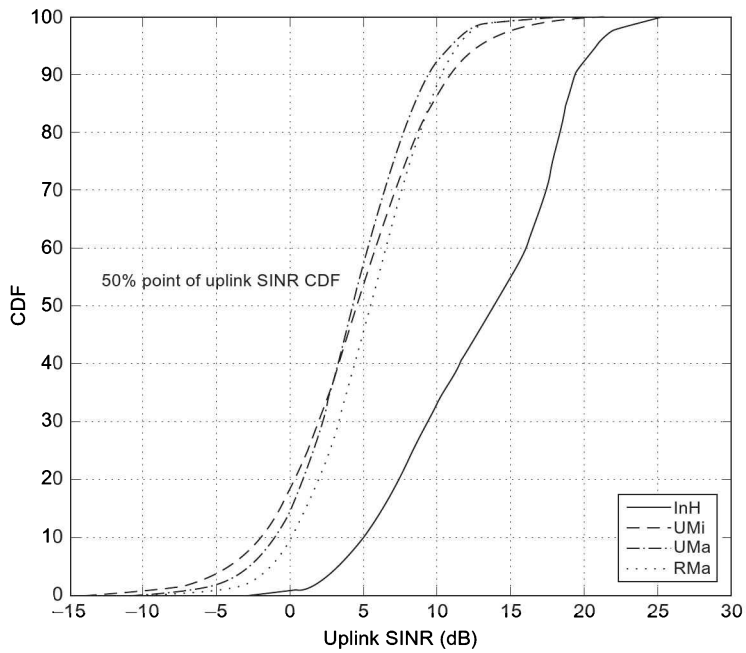


FIGURE 11.10

Statistical distribution of the uplink SINR in various test environments [6].

link-level data rate, normalized by bandwidth, is greater than the minimum requirements shown in Table 11.15, when the user is moving at the maximum speed in that mobility class in each of the test environments [14].

It can be concluded from Table 11.15 that the evaluated LTE-Advanced configurations can fulfill the ITU-R requirements concerning the mobility in all test environments.

11.9.4 Peak spectral efficiency

The peak spectral efficiency of LTE-Advanced is calculated based on the following assumptions: 20 MHz bandwidth; one OFDM symbol for downlink control signaling; CRS corresponding to one and four antenna ports; UE-specific reference signals corresponding to 24 and zero resource elements per resource-block pair. It was further assumed that physical broadcast channel and synchronization sequences occupy a total of 564 (Rel-10 MU-MIMO/CoMP with six MBSFN subframes per 10 ms) and 528 (Rel-8 downlink SU-MIMO) resource elements per radio frame for downlink eight- and four-layer spatial multiplexing, respectively. In addition, DL/UL configuration 1 (2 DL subframes, 1 special subframe, 2 uplink subframes) and special-subframe configuration 4 (12 DwPTS, 1 GP, 1 UpPTS, UpPTS is used for sounding reference signal transmission) are assumed for the TDD mode. The results shown in Table 11.16 suggest that LTE Rel-8 already fulfills the ITU-R requirements for downlink peak spectral efficiency. The table also shows the additional performance improvement that can be achieved using advanced features, for example, downlink eight-layer spatial multiplexing.

The uplink peak spectral efficiency is calculated assuming 20 MHz bandwidth, PUCCH occupying two pairs of resource blocks per subframe, and physical random access channel consuming six resource-block pairs per radio frame. The same TDDDL/UL and special-subframe configurations are assumed as for the downlink peak spectral efficiency calculation. Table 11.16 shows that the extension of LTE Rel-8 with two-layer spatial multiplexing can fulfill the ITU-R requirement in the uplink.

11.9.5 User-plane/control-plane latency and handover interruption time

The LTE user-plane one-way access latency for a scheduled UE consists of fixed node-processing delays, which include radio frame alignment and 1 ms transmission time interval (TTI) duration. Using the latency calculation model shown in Figure 11.11, and assuming that the number of HARQ processes is 8 for the FDD mode, the one-way latency is given as $T_{\text{USER-PLANE}} = 4 + 8p$ where p is the probability of HARQ retransmissions or the error probability of the first HARQ retransmission. While the minimum latency of $T_{\text{USER-PLANE}} = 4$ ms is achieved for $p = 0$, a more realistic value of $T_{\text{USER-PLANE}} = 4.8$ ms is obtained for $p = 0.1$.

Table 11.15 3GPP LTE Uplink Link-Level Simulation Results for the Mobility Requirements [2,6,14]

Path Loss Model (LoS/NLoS)	Duplex Scheme	Test Environment	ITU-R Requirements	Median SINR (dB)	Uplink Spectral Efficiency (bits/s/Hz)
Antenna configuration 1 × 4 (NLoS)	FDD	InH	1.0	13.89	2.56
		UMi	0.75	4.54	1.21
		UMa	0.55	4.30	1.08
		RMa	0.25	5.42	1.22
Antenna configuration 1 × 4 (LoS)		InH	1.0	13.89	3.15
		UMi	0.75	4.54	1.42
		UMa	0.55	4.30	1.36
		RMa	0.25	5.42	1.45
Antenna configuration 1 × 4 (NLoS)	TDD	InH	1.0	13.89	2.63
		UMi	0.75	4.54	1.14
		UMa	0.55	4.30	0.95
		RMa	0.25	5.42	1.03
Antenna configuration 1 × 4 (LoS)		InH	1.0	13.89	3.11
		UMi	0.75	4.54	1.48
		UMa	0.55	4.30	1.36
		RMa	0.25	5.42	1.38

Table 11.16 3GPP LTE-Advanced Peak Spectral Efficiency [2]

Scheme	Duplex Scheme	Direction	Spectral Efficiency (bits/s/Hz)
ITU-R requirement	FDD	Downlink	15
Rel-8 four-layer spatial multiplexing			16.3
Eight-layer spatial multiplexing			30.6
ITU-R requirement		Uplink	6.75
Two-Layer spatial multiplexing			8.4
Four-Layer spatial multiplexing			16.8
ITU-R requirement	TDD	Downlink	15
Rel-8 four-layer spatial multiplexing			16.0
Eight-Layer spatial multiplexing			30.0
ITU-R requirement		Uplink	6.75
Two-Layer spatial multiplexing			8.1
Four-Layer spatial multiplexing			16.1

The user-plane one-way latency for a scheduled UE in the TDD mode consists of fixed node-processing delays, radio frame alignment, and TTI duration. The latency component can be seen in Figure 11.11 for the downlink and uplink. Using the latency model shown in Figure 11.11, the total one-way processing time is 2.5 ms, T_{FA} is the radio frame alignment which depends on various configurations of the TDD frame structure, and the TTI duration is 1 ms, hence, the user-plane latency of the TDD mode can be written as $T_{USER\text{-}PLANE} = 3.5 + T_{FA} + pT_{RTT}$ where T_{RTT} is the average HARQ round-trip time and p is the error probability of the first HARQ transmission.

Table 11.17 shows the user-plane latency component breakdown in downlink and uplink for different TDD DL/UL configurations when $p = 0.1$ is assumed. It is shown that in all cases, LTE can meet the ITU-R requirements for user-plane latency.

The above analysis further shows that the 5 ms user-plane latency requirement can be satisfied in the TDD mode in uplink and downlink using the DL/UL configuration 6 only when $p = 0$ is assumed.

In order to calculate the control-plane latency, the model shown in Figure 11.12 is used. The transition from the RRC_IDLE to the RRC_CONNECTED state in LTE comprises several steps that are shown in sequential order in Table 11.18.

While the results of the analysis suggest that LTE Rel-8 satisfies the ITU-R requirements, using the improved features and protocols introduced in later releases would allow reduction of the control-plane latency to 50 ms. Note that since the non-access stratum (NAS) setup process can be executed in parallel with the RRC connection setup, it does not appear in the total latency calculation.

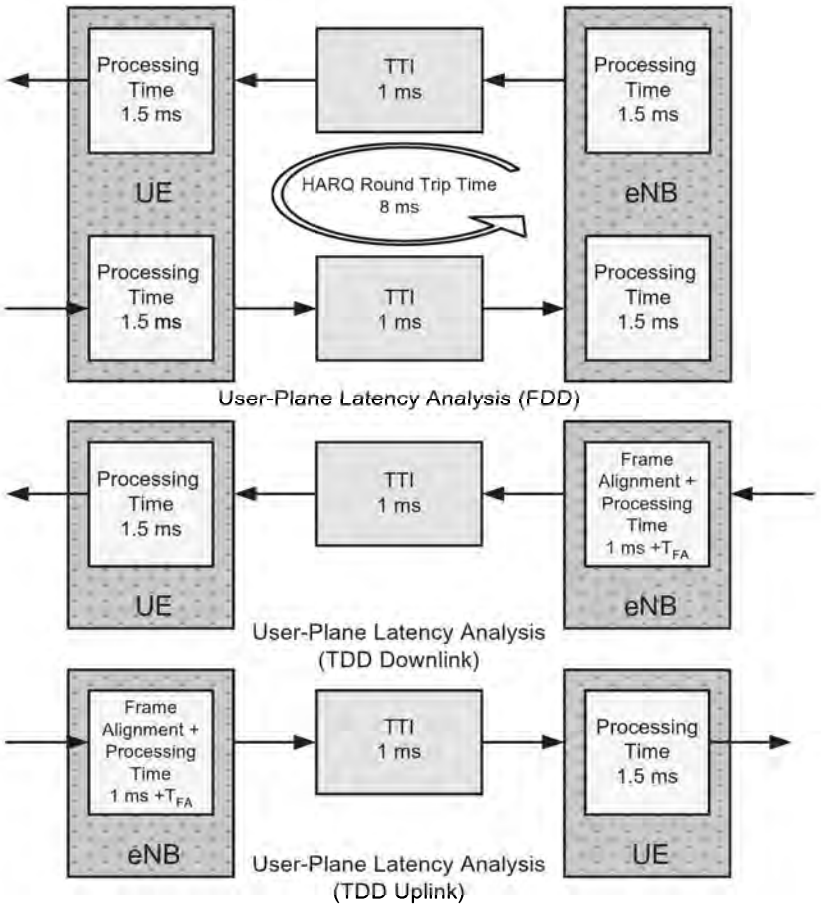


FIGURE 11.11

LTE user-plane latency calculation model [2].

The analysis shown in Table 11.18 shows that any of the LTE configurations can fulfill the ITU-R requirements related to control-plane latency.

The calculation of the user-plane latency was carried out for synchronized (or prescheduled) UEs. In the case where the UE is not prescheduled or when the UE is required to synchronize in order to be allocated uplink resources, reduced RACH scheduling period, shorter PUCCH cycle, and reduced processing delays can be applied to satisfy the control-plane latency requirements.

The LTE-Advanced general handover procedure is based on that of LTE Rel-8, which was described in Chapter 4, and is illustrated in Figure 11.13. The model shown in the figure has been used for calculation of the handover interruption time. As shown in the figure, once the handover command has been processed by

Table 11.17 TDD Mode User-Plane Latency Analysis with 10% HARQ Retransmission Probability [2]

			DL/UL Configuration						
Step	**Procedure**	**Direction**	**0**	**1**	**2**	**3**	**4**	**5**	**6**
1	eNB processing delay (ms)	Downlink	1	1	1	1	1	1	1
2	Frame alignment (ms)		1.7	1.1	0.7	1.1	0.8	0.6	1.4
3	TTI duration (ms)		1	1	1	1	1	1	1
4	UE processing delay (ms)		1.5	1.5	1.5	1.5	1.5	1.5	1.5
5	HARQ retransmission (ms)		0.1×10	0.1×10.2	0.1×9.8	0.1×10.5	0.1×11.6	0.1×12.4	0.1×11.2
	Total one-way delay (ms)		6.2	5.62	5.18	5.65	5.46	5.34	6.02
1	UE processing delay (ms)	Uplink	1	1	1	1	1	1	1
2	Frame alignment (ms)		1.1	1.7	2.5	3.3	4.1	5	1.4
3	TTI duration (ms)		1	1	1	1	1	1	1
4	eNB processing delay (ms)		1.5	1.5	1.5	1.5	1.5	1.5	1.5
5	HARQ retransmission (ms)		0.1×11.6	0.1×10	0.1×10	0.1×10	0.1×10	0.1×10	0.1×11.5
	Total one-way delay (ms)		5.76	6.2	7	7.8	8.6	9.5	6.05

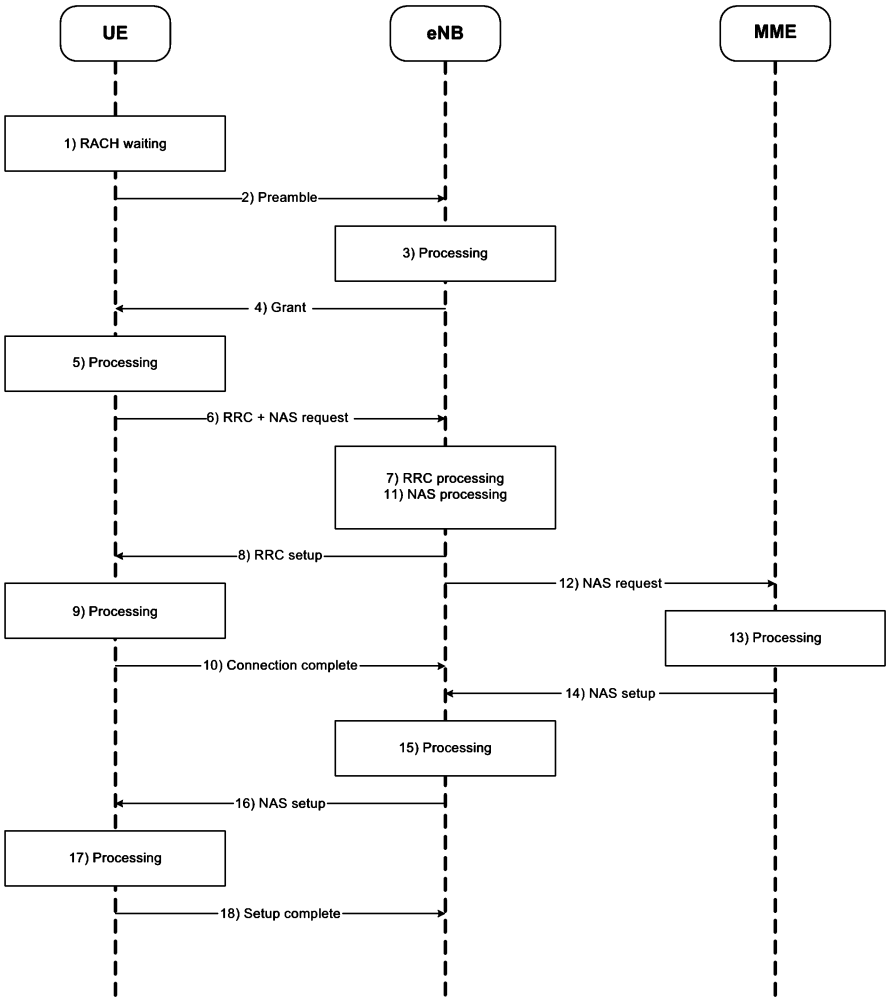


FIGURE 11.12

Analysis of RRC_IDLE to RRC_CONNECTED state transition in 3GPP LTE [2].

the UE, the UE detaches from the source eNB and stops receiving data. This marks a point in time where the user-plane connectivity is interrupted. The UE then performs frequency synchronization with the target eNB depending on whether the target cell is operating on the same carrier frequency as the current serving cell. Since the UE has already identified and measured the target cell, the corresponding delay will be negligible. The UE then performs downlink synchronization. Although baseband and RF timing alignments are part of the delay budget, since the UE has already acquired downlink synchronization with the target

Table 11.18 Analysis of Control-Plane Latency Components [2]

Step	Procedure	Processing Time (ms)
1	Average delay due to RACH scheduling period (1 ms RACH cycle)	0.5
2	RACH preamble	1
3–4	Preamble detection and transmission of random access response (time between the end RACH transmission and UE's reception of scheduling grant and timing adjustment)	3
5	UE processing delay (decoding of scheduling grant, timing alignment, and C-RNTI assignment + L1 encoding of RRC connection request)	5
6	Transmission of RRC and NAS request	1
7	Processing delay in eNB (L2 and RRC)	4
8	Transmission of RRC connection setup and UL grant	1
9	Processing delay in the UE (L2 and RRC)	12
10	Transmission of RRC connection setup complete	1
11	Processing delay in eNB (Uu → S1-C)	–
12	S1-C transfer delay	–
13	MME Processing Delay (including UE context retrieval of 10 ms)	–
14	S1-C transfer delay	–
15	Processing delay in eNB (S1-C → Uu)	4
16	Transmission of RRC security mode command and connection reconfiguration + TTI alignment	1.5
17	Processing delay in UE (L2 and RRC)	16
	Control-plane delay	50

cell in conjunction with previous measurements and can relate the target cell downlink timing to the source cell downlink timing with a time offset, the corresponding delay is going to be less than 1 ms. The data forwarding between the two eNBs is initiated before the UE moves and establishes connection to the target cell, and because the backhaul is faster than the radio interface, forwarded data is already awaiting transmission in the target cell when the user-plane with the target cell is reestablished. The latter delay component thereby does not affect the overall delay.

Based on the analysis shown in Table 11.19, the minimum handover interruption time is 10.5 ms for the FDD mode and 12.5 ms for the TDD mode. Note that this delay does not depend on the frequency of the target cell as long as the cell frequency has already been measured by the UE during the measurement gap.

As explained earlier, the minimum handover interruption time is 10.5 ms for FDD and 12.5 ms for TDD regardless of the frequency of the target cell and

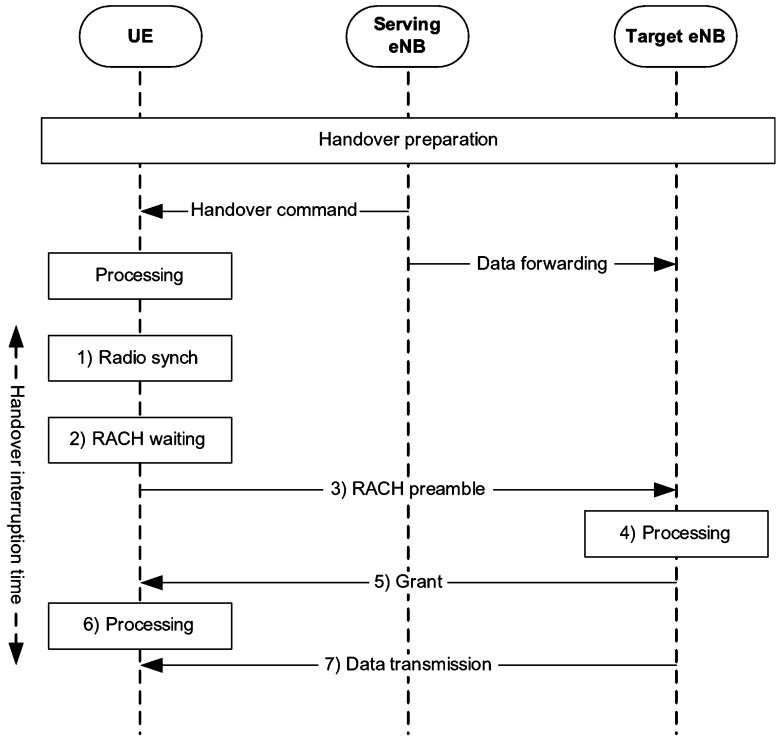


FIGURE 11.13

Model for calculation of handover interruption time [2,10].

measurements. Note that in the FDD mode, the average delay due to RACH scheduling is 0.5 ms assuming 1 ms RACH periodicity, whereas in the TDD mode, the minimum delay is obtained with configuration 0 (i.e., six normal uplink subframes); however, when taking into account the average waiting time for a downlink subframe to receive the random access response and to initiate transmission of downlink data, TDD configuration 1 (with random access preambles in special subframes) offers the shortest handover interruption time.

11.9.6 Estimation of the L1/L2 overhead

The downlink L1/L2 overhead of the LTE-Advanced includes different types of reference signals, that is, CRS transmitted within each resource block, UE-specific demodulation reference signals (DM-RS), and the reference signals that are specifically utilized in the estimation of CSI (CSI-RS). The overhead channels further include control signaling channels that are transmitted in the first L OFDM symbols ($L = 1$, 2, or 3) of each subframe ($L = 4$ in the case of 1.4 MHz bandwidth system bandwidth) and the synchronization signals, as

Table 11.19 Breakdown of Handover Interruption Time [2]

Step	Procedure	FDD Mode Processing Time (ms)	TDD Mode Processing Time (ms)
1	Radio synchronization to the target cell	1	1
2	Average delay due to RACH scheduling period assuming 1 ms periodicity	0.5	2.5
3	RACH preamble	1	1
4–5	Preamble detection and transmission of random access response (time between the end RACH transmission and UE's reception of scheduling grant and timing adjustment)	5	5
6	Decoding of scheduling grant and timing alignment	2	2
7	Transmission of downlink data	1	1
	Handover interruption time	10.5	12.5

well as physical broadcast control channel. The protocol headers corresponding to layer-2 sub-layers (MAC/RLC/PDCP) were also included in the self-evaluation results. The overhead due to CRS and L1/L2 control signaling depend on the number of antenna ports and the number of OFDM symbols used for the control region. The number of overhead resource elements per resource-block pair (168 resource elements in total) and the corresponding relative overhead is shown in Table 11.20 for non-MBSFN and MBSFN subframes. The overhead (due to L1/L2 control signaling and CRS) in Table 11.20 is shown in terms of the number of resource elements per resource-block pair and in percentages.

In the case of MBSFN subframes, the overhead is reduced. All subframes in a radio frame are assumed to be either regular or MBSFN type in overhead estimation. The total overhead depends on the fraction of MBSFN subframes. In the self-evaluation results, a fraction of 0% and 60% was assumed. The overhead due to UE-specific reference signals depends on the number of UE-specific antenna-ports and is 12 resource elements (7.1%) for one and two antenna ports, and 24 resource elements (14.3%) for three to eight antenna ports. Note that the overhead due to UE-specific reference signals is only present in resource blocks in which UE-specific reference signals are transmitted.

The relative overhead due to synchronization signals and physical broadcast channel depends on the operation bandwidth. A total of 528 resource elements per 10 ms radio frame are used for the synchronization signals and physical broadcast channel for four CRS antenna ports, corresponding to approximately 0.6% and 0.3% overhead for 10 and 20 MHz operating bandwidth, respectively.

Table 11.20 LTE-Advanced L1/L2 Overhead [2,6]

		FDD Duplex Scheme			TDD Duplex Scheme		
		Number of Cell-Specific Antenna Ports			Number of Cell-Specific Antenna Ports		
Control-Region Size	**Subframe Type**	**1**	**2**	**4**	**1**	**2**	**4**
$L = 1$	Regular subframes	18 (10.7%)	24 (14.3%)	32 (19.0%)	18 (10.7%)	24 (14.3%)	32 (19.0%)
$L = 2$		30 (17.9%)	36 (21.4%)	40 (23.9%)	30 (17.9%)	36 (21.4%)	40 (23.9%)
$L = 3$		42 (25%)	48 (28.6%)	52 (31.0%)	42 (25%)	48 (28.6%)	52 (31.0%)
$L = 1$	MBSFN subframes	12 (7.1%)	12 (7.1%)	12 (7.1%)	12 (7.1%)	12 (7.1%)	12 (7.1%)
$L = 2$		24 (14.2%)	24 (14.2%)	24 (14.2%)	24 (14.2%)	24 (14.2%)	24 (14.2%)
$L = 3$		36 (21.4%)	36 (21.4%)	36 (21.4%)	36 (21.4%)	36 (21.4%)	36 (21.4%)

The overhead due to protocol headers is proportional to data packet size and is approximately 2.7%, 0.51%, and 0.32% for physical-layer data rates of 1, 10, and 100 Mbps, respectively. This overhead was not included in the self-evaluation results. The relative overhead due to CSI-RS depends on the number of antennas and periodicity. In a typical case, it is about 0.12% per antenna port (0.48% for four antenna ports and 0.96% for eight antenna ports). The relative overhead due to UE-specific reference signals is estimated at approximately 7% in case of rank 1 and rank 2 transmission, and 14% for rank 3 to rank 8 transmission.

In the uplink, the L1/L2 overhead includes the demodulation reference symbols that are used in uplink channel estimation for coherent demodulation and are transmitted once every 0.5 ms. It further includes the sounding reference signal used for uplink channel state estimation at the eNB and the L1/L2 control signaling transmitted on configurable amount of resource blocks, as well as L2 control overhead due to random access, uplink time-alignment control, power headroom reports, and buffer-status reports. The L2 overhead associated with the PDU headers (MAC/RLC/PDCP) is further taken into consideration in the total overhead calculation. The amount of overhead due to DM-RS is approximately 14%, corresponding to one SC-FDMA symbol in each slot. The relative overhead is estimated independent of the rank of the transmission. The amount of SRS overhead depends on the sounding reference signal transmission interval and the bandwidth. Using a 10 ms SRS transmission interval and full-band SRS, the relative overhead is approximately 0.7%. The amount of uplink resources reserved for random access depends on the PRACH configuration, for example, a typical case with PRACH preamble format 0 is six resource blocks per radio frame, resulting in a relative overhead of 0.6%, 1.2%, and 2.4% for a channel bandwidth of 20, 10, and 5 MHz, respectively.

The relative overhead due to uplink timing-alignment control depends on the configuration and the number of active UEs within a cell. The absolute overhead is typically less than 32 bits/s per UE. The amount of overhead for buffer-status reports depends on the configuration; assuming a continuous data and reporting interval of 10–20 ms, the absolute overhead is 0.8–3.2 kbps. The amount of overhead due to protocol headers depends on the data packet size and is approximately 2.7%, 0.51%, and 0.32% for L1 data rates of 1, 10, and 100 Mbps, respectively. The above overhead calculations are based on a normal cyclic prefix length. In the case of MBSFN subframes in the TDD mode, all the subframes are assumed to be of MBSFN type in the overhead estimation. The total overhead depends on the fraction of MBSFN subframes. In self-evaluation results, a fraction of 0% and 33% has been assumed for a TDDDL:UL ratio of 3:2 (i.e., TDDDL/UL configuration 1).

In the TDD mode, the relative overhead due to synchronization signals and physical broadcast channel depends on the operation bandwidth and DL/UL configuration. A total of 528 resource elements per 10 ms radio frame are used for the synchronization signals and the broadcast channel when using four CRS antenna ports. For a DL:UL ratio of 3:2, the latter overhead translates into

approximately 1.0% and 0.5%, for 10 and 20 MHz operation bandwidth, respectively. The amount of SRS overhead depends on the SRS transmission interval and bandwidth as well as the usage of UpPTS in the special subframe. For a DL:UL ratio of 3:2 with four DL/UL switching points per 10 ms radio frame, the SRS transmission interval of 5 ms and full-band SRS within UpPTS, the relative overhead is approximately 3.45%. The amount of uplink resources reserved for random access depends on the configuration of the random access channel. In a typical case with a DL:UL ratio of 3:2 and PRACH preamble format 0, i.e., six resource blocks per radio frame are used for the PRACH, resulting in a relative overhead of 1.4%, 2.8%, and 5.6% for channel bandwidth of 20, 10, and 5 MHz, respectively.

11.9.7 Link budget

The LTE-Advanced link budget under various deployment scenarios specified by ITU-R was evaluated as part of the IMT-Advanced submission (Table 11.21). Table 11.21 summarizes the link budget of the TDD mode. It is shown that LTE-Advanced control and data channel coverage meets the IMT-Advanced link budget requirements.

11.9.8 Evaluation of LTE-Advanced against LTE Rel-10 requirements

This section provides the self-evaluation results of LTE-Advanced against LTE Rel-10 requirements [3], where the target values for cell spectral efficiency and cell-edge spectral efficiency are specified for 3GPP case 1 channel model [4] with 2×2, 4×2, and 4×4 antenna configurations in the downlink, and 1×2 and 2×4 antenna configurations in the uplink. Table 11.22 shows the downlink/uplink cell and cell-edge spectral efficiency results under 3GPP Case 1 configuration for the FDD and TDD modes. The results suggest that, if LTE Rel-8 is extended with MU-MIMO 4×2 in the downlink, the LTE Rel-10 performance targets can be fulfilled. The table also includes the advanced features by which the performance can be further improved. The uplink performance results indicate that LTE Rel-8 SIMO and LTE-Advanced CoMP, SU-MIMO, and MU-MIMO schemes can fulfill the LTE Rel-10 requirements. In 3GPP case 1 scenario, the center frequency is 2.0 GHz, the transmission bandwidth is 2×10 MHz for the FDD mode and 20 MHz for the TDD mode, inter-site distance is 500 m, the penetration loss is 20 dB, and all users are assumed moving at 3 km/h.

11.10 Miscellaneous evaluations

In order to investigate the usage and advantages of various LTE downlink MIMO schemes in realistic deployment scenarios, link-level and system-level simulations were performed under certain assumptions [47–49]. In order to

Table 11.21 LTE-Advanced Link Budget in Various Deployment Scenarios for the TDD Mode [2,6,15]

	InH		UMi		UMa		RMa	
Parameter	**Downlink**	**Uplink**	**Downlink**	**Uplink**	**Downlink**	**Uplink**	**Downlink**	**Uplink**
System Configuration								
Carrier frequency (GHz)	3.4	3.4	2.5	2.5	2.0	2.0	0.8	0.8
BS antenna heights (m)	6	6	10	10	25	25	35	35
MS antenna heights (m)	1.5	1.5	1.5	1.5	1.5	1.5	1.5	1.5
Cell area reliability for control channels	95%	95%	95%	95%	95%	95%	95%	95%
Cell area reliability for control channels	90%	90%	90%	90%	90%	90%	90%	90%
Transmission bit rate for control channel (kbps)	46.93	1.60	44.80	1.60	44.80	1.60	44.80	1.60
Transmission bit rate for data channel (Mbps)	4.65	0.37	2.25	0.074	2.25	0.074	2.25	0.074
Target packet error rate for control channels	1%	1%	1%	1%	1%	1%	1%	1%
Target packet error rate for data channels	10%	10%	10%	10%	10%	10%	10%	10%
Spectral efficiency (bits/s/Hz) for data	0.23	0.52	0.22	0.21	0.22	0.21	0.22	0.21
Path loss model	NLoS	NLoS	NLoS	NLoS	NLoS	NLoS	NLoS	NLoS
Mobile speed (km/h)	3	3	3	3	30	30	120	120
Feeder loss (dB)	2	2	2	2	2	2	2	2
Transmitter								
Number of transmit antennas	2	1	2	1	2	1	2	1
Maximum transmit power per antenna (dBm)	21	21	41	24	46	24	46	24
Total transmit power (dBm)	24	21	44	24	49	24	49	24
Transmitter antenna gain (dBi)	0	0	17	0	17	0	17	0

(*Continued*)

Table 11.21 (Continued)

Parameter	InH		UMi		UMa		RMa	
	Downlink	Uplink	Downlink	Uplink	Downlink	Uplink	Downlink	Uplink
Transmitter array gain (dB)	0	0	0	0	0	0	0	0
Control channel power boosting gain (dB)	0	0	0	0	0	0	0	0
Data channel power loss due to pilot/control boosting (dB)	0	0	0	0	0	0	0	0
Cable, connector, combiner, body losses, etc. (dB)	3	1	3	1	3	1	3	1
Control channel EIRP (dBm)	21	20	58	23	63	23	63	23
Data channel EIRP (dBm)	21	20	58	23	63	23	63	23
Receiver								
Number of receive antennas	2	4	2	4	2	4	2	4
Receiver antenna gain (dBi)	0	0	0	17	0	17	0	17
Cable, connector, combiner, body losses, etc. (dB)	1	3	1	3	1	3	1	3
Receiver noise figure (dB)	7	5	7	5	7	5	7	5
Thermal noise density (dBm/Hz)	− 174	− 174	− 174	− 174	− 174	− 174	− 174	− 174
Receiver interference density for control channels (dBm/Hz)	− 174	− 174.9	− 169.3	− 161.7	− 169.3	− 161.7	− 169.3	− 161.7
Receiver interference density for data channels (dBm/Hz)	− 174	− 174.9	− 169.3	− 165.7	− 169.3	− 165.7	− 169.3	− 165.7
Total noise plus interference density for control channels (dBm/Hz)	− 167	− 168	− 165	− 161	− 165	− 161	− 165	− 161
Total noise plus interference density for data channels (dBm/Hz)	− 167	− 168	− 165	− 164	− 165	− 164	− 165	− 164

Occupied channel bandwidth for control channels (MHz)	36	0.18	18	0.18	18	0.18	18	0.18
Occupied channel bandwidth for data channels (MHz)	36	1.8	18	0.90	18	0.9	18	0.90
Effective noise power for control channels (dBm)	−91	−115	−92	−108	−92	−108	−92	−108
Effective noise power for control channels (dBm)	−91	−105	−92	−104	−92	−104	−92	−104
Required SNR for the control channel (dB)	−4.2	−10.6	−4.2	−10.5	−4.2	−10.1	−4.2	−9.9
Required SNR for the data channel (dB)	−1.6	−2.3	−1.7	−5.5	−1.7	−5.1	−1.7	−4.8
Receiver implementation margin (dB)	2	2	2	2	2	2	2	2
HARQ gain for control channel (dB)	0	0	0	0	0	0	0	0
HARQ gain for data channel (dB)	0.5	0.5	0.5	0.5	0.5	0.5	0.5	0.5
Receiver sensitivity for control channel (dBm)	−94	−124	−95	−117	−95	−117	−95	−116
Receiver sensitivity for data channel (dBm)	−91	−106	−93	−108	−93	−108	−93	−108
Hardware link budget for control channel (dB)	115	144	153	157	158	157	158	156
Hardware link budget for data channel (dB)	113	126	151	148	156	148	156	148
Calculation of Available Path Loss								
Lognormal shadow fading standard deviation (dB)	4	4	4	4	6	6	8	8
Shadow fading margin for control channels (dB)	2.8	2.8	3.1	3.1	5	5	5	5
Shadow fading margin for data channels (dB)	0.9	0.9	1.3	1.3	8.1	8.1	10.5	10.5
BS selection/macro-diversity gain (dB)	0	0	0	0	4.9	4.9	6.7	6.7

(Continued)

Table 11.21 (Continued)

Parameter	InH		UMi		UMa		RMa	
	Downlink	Uplink	Downlink	Uplink	Downlink	Uplink	Downlink	Uplink
Penetration loss (dB)	0	0	0	0	0	0	0	0
Other gains (dB)	0	0	0	0	9	9	9	9
Available path loss for control channel (dB)	111	138	149	151	0	0	0	0
Available path loss for data channel (dB)	111	122	148	144	140	136	137	134
Range/Coverage Efficiency Calculation								
Maximum range for control channel (m)	100.0	100.0	1405.2	1621.2	1175.6	978.0	3210.9	2634.3
Maximum range for data channel (m)	100.0	100.0	1383.9	1062.7	1258.4	714.4	3565.5	1975.1
Coverage area for control channel (km^2/site)	0.031	0.031	6.20	8.26	4.34	3.01	32.4	21.8
Coverage area for data channel (km^2/site)	0.031	0.031	6.02	3.55	4.97	1.60	39.9	12.3

Table 11.22 Self-Evaluation of LTE-Advanced Against LTE Rel-10 Requirements [4]

Scheme and Antenna Configuration	Direction	Duplex Scheme	Rel-10 Requirements (Cell Spectral Efficiency/Cell-Edge Spectral Efficiency)	Cell Spectral Efficiency (bits/s/Hz/cell) $L = 3$	Cell-Edge Spectral Efficiency (bits/s/Hz) $L = 3$
MU-MIMO 2 × 2 (C)	Downlink	FDD	2.4/0.07	2.69	0.090
JP-CoMP 2 × 2 (C)			2.4/0.07	2.70	0.104
MU-MIMO 4 × 2 (C)			2.6/0.09	3.43	0.118
CS/CB-CoMP 4 × 2 (C)			2.6/0.09	3.34	0.129
JP-CoMP 4 × 2 (C)			2.6/0.09	3.87	0.162
MU-MIMO 4 × 4 (C)			3.7/0.12	4.69	0.203
CS/CB-CoMP 4 × 4 (C)			3.7/0.12	4.66	0.205
JP-CoMP 4 × 4 (C)			3.7/0.12	5.19	0.269
MU-MIMO 2 × 2 (C)		TDD	2.4/0.07	2.88	0.113
JP-CoMP 2 × 2 (C)			2.4/0.07	3.15	0.130
MU-MIMO 4 × 2 (C)			2.6/0.09	3.76	0.151
JP-CoMP 4 × 2 (C)			2.6/0.09	4.64	0.199
MU-MIMO 4 × 4 (C)			3.7/0.12	4.97	0.209

(Continued)

Table 11.22 (Continued)

Scheme and Antenna Configuration	Direction	Duplex Scheme	Rel-10 Requirements (Cell Spectral Efficiency/Cell-Edge Spectral Efficiency)	Cell Spectral Efficiency (bits/s/Hz/cell) $L = 3$	Cell-Edge Spectral Efficiency (bits/s/Hz) $L = 3$
CS/CB-CoMP 4 × 4 (C)			3.7/0.12	5.06	0.244
JP-CoMP 4 × 4 (C)			3.7/0.12	6.61	0.330
Rel-8 SIMO 1 × 2 (C)	Uplink	FDD	1.2/0.04	1.33	0.047
CoMP 1 × 2 (C)			1.2/0.04	1.40	0.051
SU-MIMO 2 × 4 (C)			2.0/0.07	2.27	0.091
Rel-8 SIMO 1 × 2 (C)		TDD	1.2/0.04	1.24	0.045
CoMP 1 × 2 (C)			1.2/0.04	1.51	0.051
SU-MIMO 2 × 4 (C)			2.0/0.07	2.15	0.090
MU-MIMO 2 × 4 (C)			2.0/0.07	2.59	0.079

Table 11.23 System-Level Simulation Parameters (Other Parameters Same as [4] Case 1 Scenario)

Parameter/Feature	Value/Configuration
Bandwidth	1.4 MHz
Frequency	2.1 GHz
Network layout	19-cell wrap-around (tri-sector with 3D antenna models)
Scheduler algorithm	Proportional fair
Channel model	WINNER +
Receiver type	Zero-forcing
Simulation length	5000 subframes
Number of UEs/Cell	10
Path loss model	$PL = 128.1 + 37.6 \log_{10} R$
Feedback delay	Modeled

reduce the simulation run time, a 1.4 MHz system bandwidth was assumed. Figures 11.14–11.19 show snapshots of the simulation results. Table 11.23 provides the assumptions that were made in addition to baseline configuration for 3GPP case 1 that is included in 3GPP TR 36.814 [4]. The UEs are randomly dropped in the cell, but all UEs are assumed to be in the outdoor area. MIESM link-to-system mapping scheme is used in the simulations.

Figure 11.14 shows the LTE-Advanced downlink throughput versus SNR, as well as downlink spectral efficiency CDF for SISO and closed-loop spatial multiplexing (CLSM) transmission mode 4 with various antenna configurations.

The CDF of wideband SINR (geometry) with macroscopic path loss with and without additional lognormal-distributed space-correlated shadow fading is illustrated in Figure 11.15. The downlink spectral efficiency (bits/s/Hz) for various MIMO configurations with lognormal-distributed space-correlated shadow fading effect is shown in Figure 11.16. This figure shows how spectral efficiency is distributed geographically across the cells and the network. In particular, the cell-edges and the effect of MIMO to improve cell-edge performance must be noted. Figure 11.17 illustrates the sector SINR calculated with distance-dependent macroscopic path loss and additional lognormal-distributed space-correlated shadow fading. In this case we assume a SISO configuration. Figure 11.18 depicts downlink spectral efficiency (bits/s/Hz) without the effect of shadow fading. The geographical distribution of sector SINR calculated with distance-dependent macroscale path loss is shown in Figure 11.19. Figure 11.19 further shows CQI mapping across the cell. As expected, the lower modulation order and coding rates are used near cell-edges, and as we move toward the eNB, higher CQI values are reported by the UEs. The results closely correlate with the expectations of the system behavior as well as those published in the literature under given assumptions.

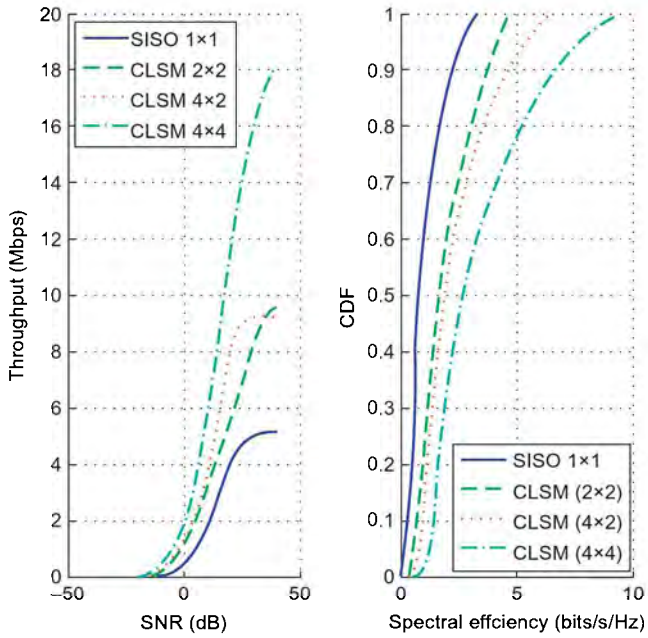


FIGURE 11.14

LTE-Advanced downlink throughput versus SNR and spectral efficiency CDF for various MIMO modes (1.4 MHz bandwidth) [45].

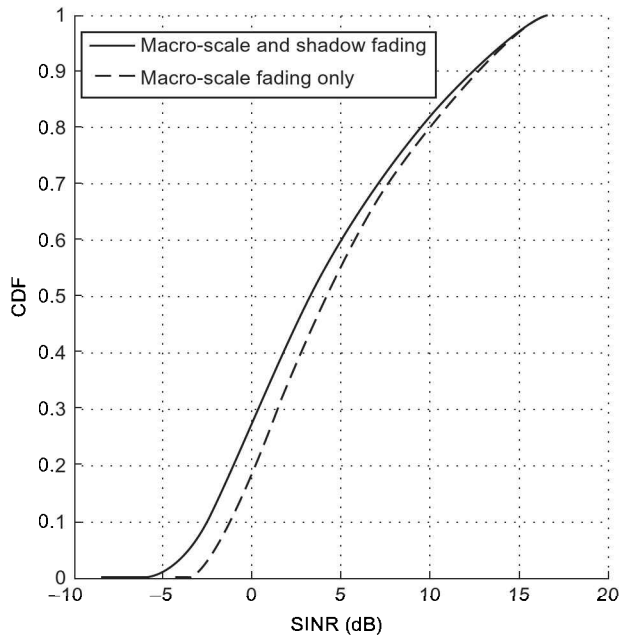


FIGURE 11.15

Distribution of downlink wideband SINR [45].

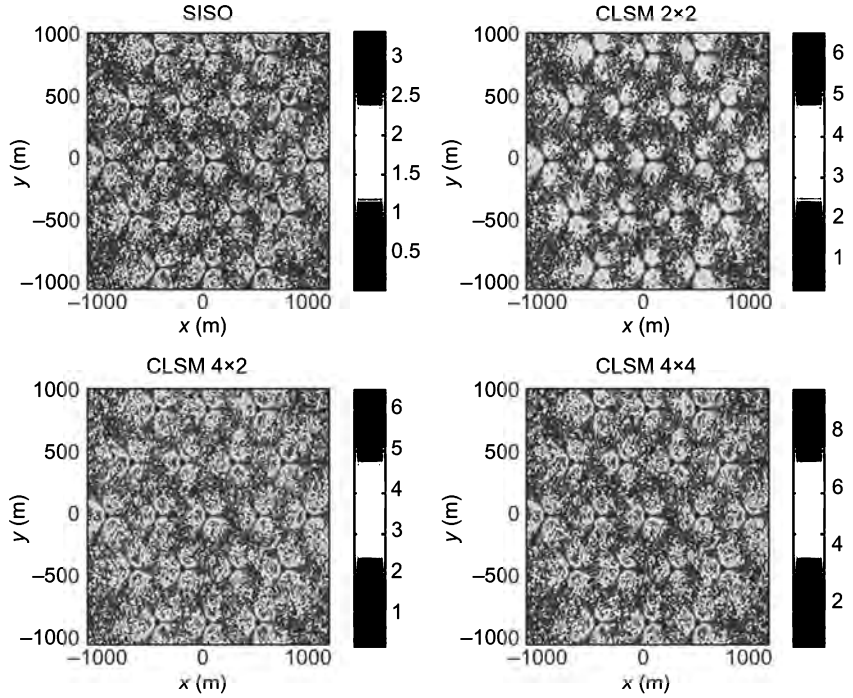


FIGURE 11.16

Spectral efficiency (bits/s/Hz) for various MIMO configurations (1.4 MHz bandwidth, with shadow fading) [45]

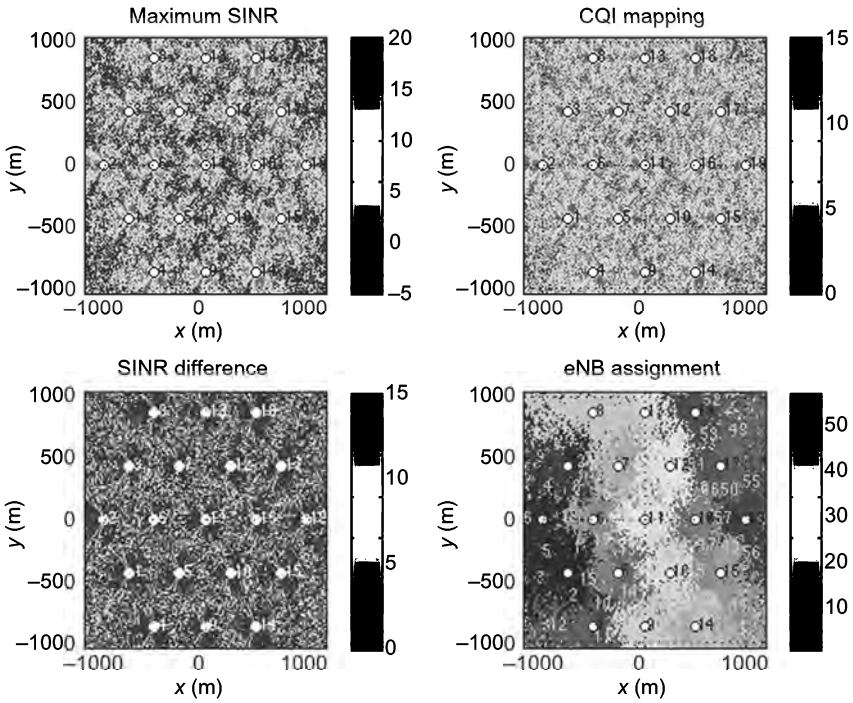


FIGURE 11.17

Sector SINR calculated with distance-dependent macroscopic path loss and additional lognormal-distributed space-correlated shadow fading (1.4 MHz bandwidth, SISO) [45]

Ex.1005.00976

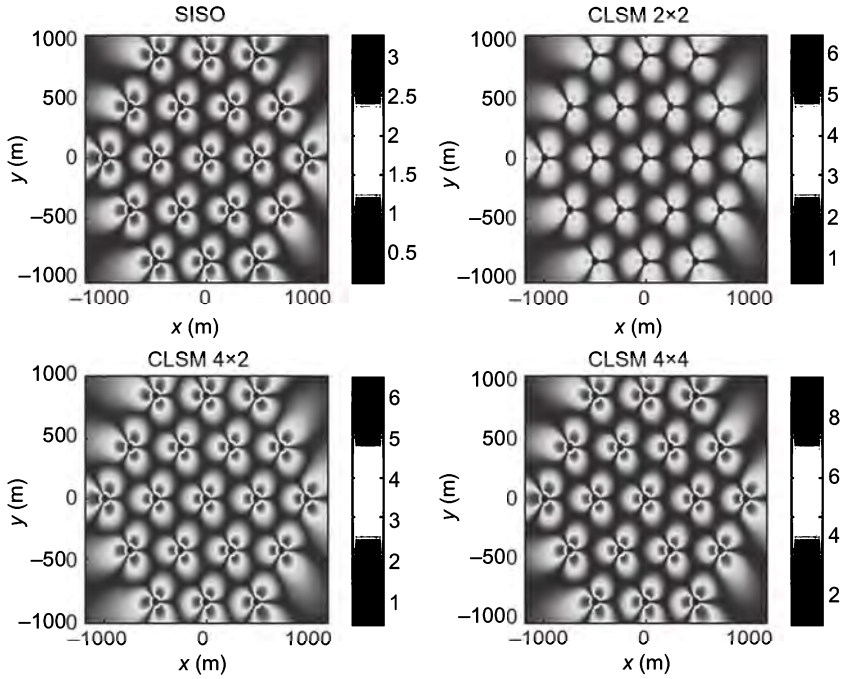


FIGURE 11.18

Spectral efficiency (bits/s/Hz) (1.4 MHz bandwidth and no shadow fading) [45]

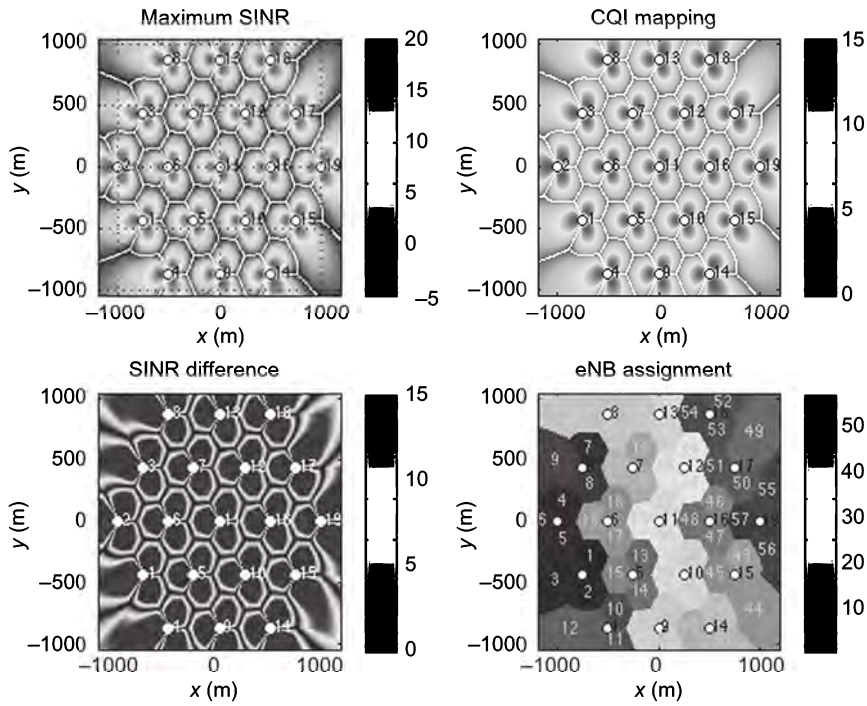


FIGURE 11.19

Sector SINR calculated with distance-dependent macro-scale path loss and CQI mapping (1.4 MHz bandwidth, SISO) [45]

Ex.1005.00977

References

3GPP Specifications

[1] 3GPP TR 25.996, Spatial Channel Model for Multiple Input Multiple Output (MIMO) Simulations (Release 11), September 2012.

[2] 3GPP TR 36.912, Feasibility Study for Further Advancements for E-UTRA (LTE-Advanced) (Release 11), September 2012.

[3] 3GPP TR 36.913, Requirements for further advancements for Evolved Universal Terrestrial Radio Access (E-UTRA) (LTE-Advanced) (Release 11), September 2012.

[4] 3GPP TR 36.814, Further Advancements for E-UTRA Physical Layer Aspects, March 2010.

[5] 3GPP TS 26.101, AMR Speech Codec Frame Structure (Release 11), September 2012.

[6] 3GPP RP-090738, TR 36.912 Annex A3: Self-Evaluation Results, September 2009.

[7] ETSI Technical Report 101 112 v3.2.0, Universal Mobile Telecommunications System (UMTS); Selection procedures for the choice of radio transmission technologies of the UMTS (UMTS 30.03 version 3.2.0), April 1998.

[8] 3GPP TS 36.211, Evolved Universal Terrestrial Radio Access (E-UTRA), Physical Channels and Modulation (Release 11), December 2012.

[9] 3GPP TS 36.212, Evolved Universal Terrestrial Radio Access (E-UTRA) Multiplexing and Channel Coding (Release 11), December 2012.

[10] 3GPP TS 36.331 Evolved Universal Terrestrial Radio Access (E-UTRA); Radio Resource Control (RRC); Protocol specification (Release 11), December 2012.

[11] 3GPP TR 36.819 Coordinated Multi-Point Operation for LTE Physical Layer Aspects (Release 11), December 2011.

ITU Specifications

[12] Report ITU-R M.2133, Requirements, evaluation criteria and submission templates for the development of IMT-Advanced, November 2008.

[13] Report ITU-R M.2134, Requirements related to technical performance for IMT-Advanced radio interface(s), November 2008.

[14] Report ITU-R M.2135-1, Guidelines for evaluation of radio interface technologies for IMT-Advanced, December 2009.

[15] Report ITU-R M.2012, Detailed specifications of the terrestrial radio interfaces of International Mobile Telecommunications Advanced (IMT-Advanced), January 2012.

[16] Recommendation ITU-R M.1225, Guidelines for evaluation of radio transmission technologies for IMT-2000, 1997.

[17] Recommendation ITU-T G.729: Coding of Speech at 8 kbit/s Using Conjugate-Structure Algebraic-Code-Excited Linear Prediction (CS-ACELP), January 2007.

Books

[18] L. Rade, Mathematics Handbook for Science and Engineering, Springer, Berlin Heidelberg, 2010.

[19] W.H. Tranter, et al., Principles of Communication Systems Simulation with Wireless Applications, Prentice Hall, 2004.

[20] J.D. Parsons, The Mobile Radio Propagation Channel, John Wiley and Sons, 2000.

[21] W.C. Jakes, Microwave Mobile Communications, John Wiley & Sons, New York, NY, 1974.

[22] M. Patzold, Mobile Fading Channels, John Wiley & Sons, 2002.

[23] A. Papoulis, Probability, Random Variables, and Stochastic Processes, fourth ed., McGraw Hill, 2002.

[24] A.T. Bharucha-Reid, Elements of the Theory of Markov Processes and Their Applications, McGraw-Hill, 1960.
[25] S. Sesia, I. Toufik, M. Baker, LTE, the UMTS Long Term Evolution: From Theory to Practice, second ed., John Willey & Sons, 2011.

Articles

[26] IEEE 802.16m-08/004r5, IEEE 802.16m Evaluation Methodology Document (EMD), March 2009.
[27] IETF RFC 3267, Real-Time Transport Protocol (RTP) Payload Format and File Storage Format for the Adaptive Multi-Rate (AMR) and Adaptive Multi-Rate Wideband (AMR-WB) Audio Codecs, J. Sjoberg, et al., June 2002.
[28] Rodriguez-Herrera, et al., Link-To-System mapping techniques using a spatial channel model, IEEE 62nd Vehicular Technology Conference 2005, vol. 3, 2005.
[29] 3GPP-3GPP2 Spatial Channel Ad-hoc Group, Spatial Channel Model Text Description, v7.0, August 2003.
[30] WINNER Project IST-4-027756, WINNER D1.1.2 v1.2, WINNER II Channel Models. <https://www.ist-winner.org>, September 2007.
[31] WINNER Project IST-2003-507581, WINNER D5.4 v. 1.4, Final Report on Link Level and System Level Channel Models. <https://www.ist-winner.org>, November 2005.
[32] WINNER Project, IST-2003-507581, WINNER D1.3 version 1.0, Final usage scenarios, June 2005.
[33] 3GPP2 TSG-C30-20061204-062A, cdma2000 Evaluation Methodology (v6), December 2006.
[34] S. Tsai, A. Soong, Effective-SNR Mapping for Modeling Frame Error Rates in Multiple-State Channels, 3GPP2-C30-20030429-010, April 2003.
[35] Digital mobile radio towards future generation systems, COST Action 231 Final Report, EUR 18957, 1999.
[36] Y. Oda, K. Tsunekawa, M. Hata, Advanced LoS path-loss model in microcellular mobile communications, IEEE Trans. Antennas Propag. 51 (2003).
[37] 3GPP R1-061001, Ericsson, LTE Channel Models and Link Simulations, March 2006.
[38] Source Code for a MATLAB/ANSI-C Implementation of the WINNER Phase I Channel Model. <https://www.ist-winner.org/phase_model.html>, August 2006.
[39] WINNER Project IST-WINNER II Deliverable D1.1.1 v1.0, WINNER II Interim Channel Models, December 2006.
[40] M. Steinbauer, A.F. Molisch, E. Bonek, The double-directional radio channel, IEEE Antennas Propag. Mag. (2001).
[41] G.J. Foschini, M.J. Gans, On limits of wireless communications in a fading environment when using multiple antennas, Wirel. Pers. Commun. 6 (1998).
[42] P. Almers, et al., Survey of channel and radio propagation models for wireless MIMO systems, EURASIP J. Wirel. Commun. Networking (2007).
[43] W. Dong, et al., Cluster Identification and Properties of Outdoor Wideband MIMO Channel, IEEE 66th Vehicular Technology Conference, VTC-2007, September 2007.
[44] R. Jain, D.M. Chiu, W. Hawe, A Quantitative Measure of Fairness and Discrimination for Resource Allocation in Shared Computer Systems, DEC Research Report TR-301, 1984.

[45] Technical University of Vienna LTE Simulators available at <http://www.nt.tuwien.ac.at/ltesimulator/>.
[46] J.C. Ikuno, M. Wrulich, M. Rupp, System level simulation of LTE networks, in: Proceedings of the 71st IEEE Vehicular Technology Conference, Taipei, Taiwan, May 2010.
[47] H. Claussen, Efficient modeling of channel maps with correlated shadow fading in mobile radio systems, September 2005.
[48] L. Hentila, et al., MATLAB implementation of the WINNER Phase II Channel Model ver1.1. <https://www.ist-winner.org/phase2model.html>, December 2007.
[49] L. Thiele, et al., Modeling of 3D Field Patterns of Down-tilted Antennas and Their Impact on Cellular Systems, in: International ITG Workshop on Smart Antennas, Berlin, Germany, February 2009.
[50] J. Olmos, et al., Link Abstraction Models Based on Mutual Information for LTE Downlink, Universitat Politècnica de Catalunya and Universidad Politécnica de Valencia, 2010.
[51] D. Martín-Sacristán, et al., LTE-Advanced System Level Simulation Platform for IMT-Advanced Evaluation, Universitat Politècnica de València, 2011.
[52] R. Jain, Channel models: a tutorial, WiMAX Forum AATG, February 2007.
[53] Confidence interval, Wikipedia, <http://en.wikipedia.org/wiki/Confidence_interval>.
[54] Markov Sequence, Wolfram MathWorld, <http://mathworld.wolfram.com/MarkovSequence.html>.
[55] H. Chernoff, A measure of asymptotic efficiency for tests of a hypothesis based on the sum of observations, Ann. Math. Stat. 23 (4) (1952).
[56] Monte Carlo method, Wikipedia, <http://en.wikipedia.org/wiki/Monte_Carlo_method>.
[57] Kronecker Product, Wolfram MathWorld, <http://mathworld.wolfram.com/KroneckerProduct.html>.
[58] Propagation Channel Models, Steepest Ascent Ltd, <http://www.steepestascent.com/content/mediaassets/html/LTE/Help/PropagationConditions.html>.

This page intentionally left blank

CHAPTER

Coordinated Multipoint Transmission and Reception (CoMP)

12

CHAPTER CONTENTS

12.1 Interference cancellation in cellular networks 952
12.2 Distributed antenna systems 955
12.3 Theory of CoMP operation 959
12.4 CoMP architectures 964
12.4.1 Air-interface and network support for CoMP schemes 968
12.4.2 Downlink CoMP 969
12.4.3 Uplink CoMP 971
12.4.4 CSI measurement and feedback in CoMP-enabled networks 974
12.5 Effects of X2 latency on CoMP performance 977
12.6 Performance of CoMP scenarios 978
References 981

The MIMO or network MIMO techniques are used for improving sector throughput and cell-edge throughput through multi-cell collaborative precoding, network coordinated beamforming, or inter-cell interference nulling. When a mobile station is at the cell-edge, it may be able to receive signals from multiple cell sites, and the mobile station's transmission may also be received at multiple cell sites. If the data transmission and signaling from multiple cell sites can be coordinated, the downlink performance can be significantly improved. This coordination can be similar to the interference avoidance techniques or the case where the same data is transmitted from multiple cell sites. In the uplink, since the signal can be received by multiple cell sites, the system can take advantage of coordinated multi-point reception to significantly improve the link performance. The coordinated multi-point (CoMP) transmission/reception specified in long-term evolution (LTE) Rel-11 is a method of MIMO transmission for interference reduction, which enables features such as network synchronization, cell- and user-specific reference signals, feedback of

LTE-Advanced.
© 2014 Elsevier Inc. All rights reserved.

Ex.1005.00982

multi-cell channel state information (CSI), and synchronous data transfer between the base stations that can be used for interference mitigation and to achieve macro-diversity gain [23–26].

The LTE Rel-11 specifications provide support for coordinated transmission in the downlink and coordinated reception in the uplink. The use cases include homogeneous configurations, where the points are different cells, as well as heterogeneous configurations, where a set of low-power nodes (e.g., remote radio heads (RRH) or pico-cells) are located in the geographical area served by a macro-cell. For coordinated transmission in the downlink, the signals transmitted from multiple transmission points are coordinated to improve the received strength of the desired signal at the UE or to reduce the co-channel interference. The main advantage of coordinated reception in the uplink is to ensure that the uplink signal from the UE is reliably received by the network while limiting uplink interference, taking into account the existence of multiple reception points. Note that the mechanisms discussed in this chapter apply to both FDD and TDD modes of operation [5].

In this chapter, we will discuss the theoretical and practical aspects of coordinated multipoint transmission/reception not only from the radio access network perspective, but also from the core network and backhaul point of view and will investigate whether some of the proposed schemes would realistically offer any gains when their backhaul implications and cost of implementation and operation are considered.

12.1 Interference cancellation in cellular networks

In the downlink of an LTE system, the UE often suffers from different types of interference. In the case of single-user MIMO (SU-MIMO), the signal received by the UE includes a linear combination of multiple streams, which causes inter-stream interference. On the other hand, in a multi-user MIMO (MU-MIMO) scenario, where a single cell communicates with many UEs simultaneously using the same time–frequency resources, the signal received by each UE suffers from interference caused by the signals intended for other UEs served by the same cell. This interference is known as inter-user interference. A UE at the cell-edge suffers from inter-cell interference, i.e., interference caused by the signals sent from a neighbor cell to its UEs. The neighbor cell might belong to the same site as the serving cell (intra-site) or to a different site (inter-site). Different interference cancellation schemes are applied at the receiver to mitigate the interference in the above cases. While the inter-stream interference cancellation can be performed at the UE without requiring any additional information, inter-user interference cancellation may require knowledge of the precoding matrices of the other UEs that one wishes to cancel. Moreover, the inter-cell interference cancellation needs an estimate of the channels seen between the neighbor interfering cells and the UE. The above interference models are illustrated in Figure 12.1 [26].

Ex.1005.00983

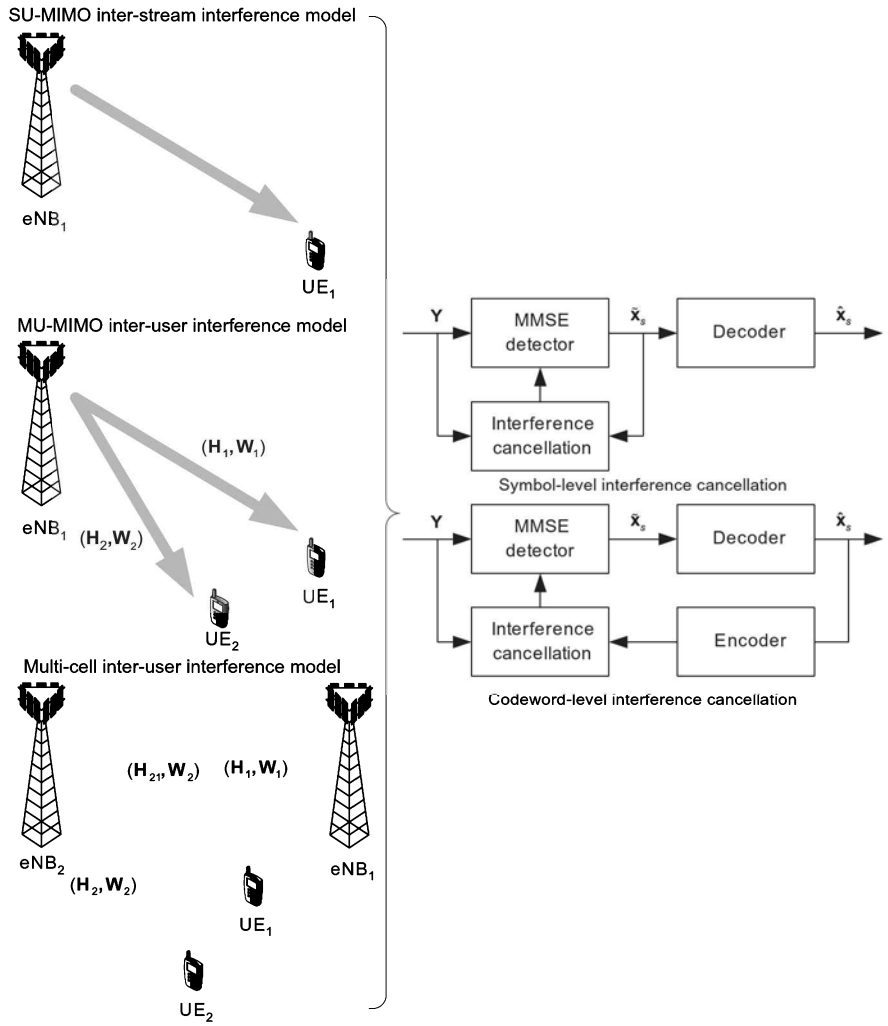


FIGURE 12.1

Illustration of interference models and cancelation at symbol and codeword level [26]. MMSE, minimum mean square error.

Let us consider a scenario where eNBs and UEs have multiple transmit/receive antennas (i.e., a MIMO channel). As shown in Figure 12.1 and in the case of a SU-MIMO inter-stream interference model, the signal received at the UE includes, in addition to noise, a linear combination of multiple streams. The beam is generated by using a non-identity precoding matrix. For simplicity, we assume that the channel is flat. In order to mitigate the inter-stream interference at the

UE, interference cancellation can be applied either at the modulated symbol level, where we cancel the estimated interfering stream before decoding, or at the codeword level where we cancel the interfering decoded codeword (see Figure 12.1).

Interference cancellation techniques have been widely studied in the literature [23–26]. While successive interference cancellation scheme processes each stream successively by canceling the previously decoded streams, parallel interference cancellation scheme processes all stream in parallel and cancel their interference after they have all been decoded independently. In order to avoid the propagation of interference cancellation error, each stream can be canceled only if it was correctly decoded by checking the corresponding decoded packet cyclic redundancy check (CRC). Successive interference cancellation can also be done iteratively, i.e., after the first iteration over all streams; we can further improve the quality of the decoded streams by canceling the residual errors estimated in the first iteration, and so on. There are methods proposed in the literature for reducing the complexity of iterative interference cancellation algorithms. In Figure 12.1, and in the case of the MU-MIMO inter-user interference model, the cell serves both UEs simultaneously using the same time–frequency resources. The first user UE_1 receives, in addition to its own data, interference due to data intended for the second user UE_2, i.e., inter-user interference. In order to cancel the inter-user interference, UE_1 needs to know the precoding matrix $\mathbf{W_2}$ that was used for UE_2. In general, $\mathbf{W_2}$ is not known by UE_1, and some additional signaling would be required in order to make $\mathbf{W_2}$ available at UE_1.

In Figure 12.1 and in the case of the multi-cell MU-MIMO interference model, UE_1 at the cell-edge is served by the eNB_1 through channel $\mathbf{H_1}$ and with the precoding matrix $\mathbf{W_1}$, and suffers from inter-cell interference, i.e., interference from the neighbor cell which serves another user UE_2 with the precoding matrix $\mathbf{W_2}$. In order to cancel the inter-cell interference, UE_1 needs an estimate of the channel $\mathbf{H}_{21}$ and the precoding matrix $\mathbf{W_2}$ intended for UE_2. The channel $\mathbf{H}_{21}$ can be estimated by UE_1 based on some reference signals sent from the neighbor cell. The precoding matrix $\mathbf{W_2}$ is in general not known by UE_1 and would require some additional signaling from eNB_2.

Let us consider the case of multi-cell inter-user interference shown in Figure 12.1. It can be shown that the signal to interference plus noise ratio (SINR) at UE_1 can be formulated as follows:

$$\mathrm{SINR}_1(\mathbf{W}_1, \mathbf{W}_2) = \frac{|\mathbf{H}_1\mathbf{W}_1|^2}{\sigma_n^2 + \sigma_I^2 + |\mathbf{H}_{21}\mathbf{W}_2|^2} \tag{12.1}$$

In Eq. (12.1), $\mathbf{W}_1$ and $\mathbf{W}_2$ represent the beamforming optimization matrices/vectors at the eNBs; $\mathbf{H}_1$ and $\mathbf{H}_{21}$ denote information that is not typically available at the CoMP scheduling unit, but measurable at the UEs; σ_n^2 denotes the receiver noise variance; and σ_I^2 indicates the interference from eNBs outside the coordinated set. Thus, the inter-cell interference propagated through channels $\mathbf{H}_{21}$ and $\mathbf{H}_{12}$ results in degradation of SINR measured at UE_1 and UE_2, respectively.

As mentioned above, the UE in the downlink of an LTE system can suffer from inter-stream, inter-user, and/or intra-site/inter-cell interference. While the UE is able to perform inter-stream interference cancellation without any additional information, it needs the precoding matrices of other UEs served by the same cell in an MU-MIMO system in order to cancel the interuser interference, and it additionally requires an estimate of the channels of the interfering neighboring cells in order to be able to cancel the inter-cell interference. An important use case for successive interference cancellation is MU-MIMO, but the principles can also be generalized to CoMP schemes. Multi-user MIMO is well known to improve the spectral efficiency by allowing a group of users to simultaneously share the same radio resources. In addition, MIMO provides antenna gain that improves the overall performance. The capacity region of the multi-user channel can be theoretically increased by MIMO through the so-called multiplexing gain. For the spatially separated (uncorrelated) users, the multiplexing gain can be achieved if CSI is available at the base station.

12.2 Distributed antenna systems

A distributed antenna system (DAS) is a network of spatially separated antennas connected to a common source via a transport medium that provides wireless service within a geographic area (cell) or a structure (indoor coverage). The basic notion of DAS was to split the transmit power among several antenna elements which are geographically separated, in order to provide coverage over the same area as a centralized antenna system, but with reduced total power and improved reliability. Thus, a set of centralized antennas radiating at high power are replaced by a group of low-power antenna elements to cover the same area. This concept was initially described in a paper by Saleh et al. [9]. Different variants of DAS have recently been deployed by selected network operators worldwide [10,16]. Examples include systems comprising RRH which consist of multiple outdoor units in which only the radio frequency (RF) front-end functionalities are implemented. The RRHs are connected to the baseband processing part of the base station through a bi-directional high-capacity/low-latency link. The DAS scheme can be implemented as a multi-airlink/multi-frequency/multi-wireless network, or a fiber-optic-based network. While the basic DAS concept is very similar to RRH, it can be differentiated with the latter features based on its greater flexibility and capacity that can be dynamically adapted to and optimized for varying traffic and user mobility conditions. The DAS enables independent operation of multiple frequency bands and multiple protocols across a single access network; consequently, multiple operator network sharing can be supported by a DAS [8,10–14,18]. Recent studies have shown that in addition to coverage improvements, a DAS can also provide other advantages such as reduced power and increased system capacity in a single-cell environment. Each distributed antenna module is connected to a home base station (or central unit) via dedicated wires,

fiber optics, or an exclusive RF link. Although the connections via the same RF link used in a cell are possible, the connections with the same RF link construct information-theoretic relay channels are categorized as another research area called cooperative communications. Since the distributed antenna modules and the home base station together construct a macroscopic multiple-input single-output (MISO) vector channel, the DAS can be also interpreted as a macroscopic multiple-antenna system [19].

The advantage of the DAS scheme is that less power is consumed in overcoming penetration and shadowing losses, since a line-of-sight channel is often present, leading to reduced fading depths and reduced delay spread. A DAS can be implemented using passive splitters and feeders, and active repeater amplifiers can be included to overcome the feeder loss. If a given area is covered by N distributed antenna elements rather than a single antenna, then the total radiated power is reduced by approximately a factor of $N^{1-n/2}$, and the power per antenna is reduced by a factor of $N^{n/2}$, where a path loss model with path loss exponent n[1] is assumed. As an alternative, the total area covered could be extended for a given limit of effective radiated power, which may be important to ensure compliance with regulatory limits. In other words, for a given target radiated power, an N-element antenna system will have increased coverage area over a single-antenna system by a factor of $N^{1-2/n}$. Given the same coverage area, the maximum path loss for an N-element distributed antenna system is reduced by a factor of $N^{n/2}$. The transmit power of user devices can then be reduced by a factor of $N^{n/2}$, resulting in a more energy-efficient uplink and lower battery consumption. The use of distributed antenna systems is expected to reduce inter-cell interference and to improve SINR especially for users near cell boundaries, which are often performance limiting users, compared to conventional cellular systems in an interference-limited multi-cell environment. As a result, distributed antenna systems achieve lower symbol error probability and higher capacity than conventional cellular systems. Recent studies suggest that distributed antenna architectures could be an effective solution for reducing inter-cell interference in an interference-limited cellular environment.

Let us look at a distributed antenna system from mathematical point of view. As shown in Figure 12.2, in a distributed antenna system the main baseband processing modules such as channel cards are centralized at a location (central processing unit), and are connected with distributed antenna modules. Each distributed antenna module is physically connected with a home base station via a dedicated link. The general architecture of a DAS in a multi-cell environment is illustrated in Figure 12.2, where a cell is covered by a small base station and six

[1]In the study of wireless communications, path loss can be represented by the path loss exponent, whose value is normally in the range of 2–4, where 2 is for propagation in free space and 4 is for a relatively lossy environment and for the case of full specular reflection from the earth's surface. In some environments, such as buildings, stadiums, and other indoor environments, the path loss exponent can reach values in the range of 4–6. On the other hand, a tunnel may act as a waveguide, resulting in a path loss exponent of less than 2.

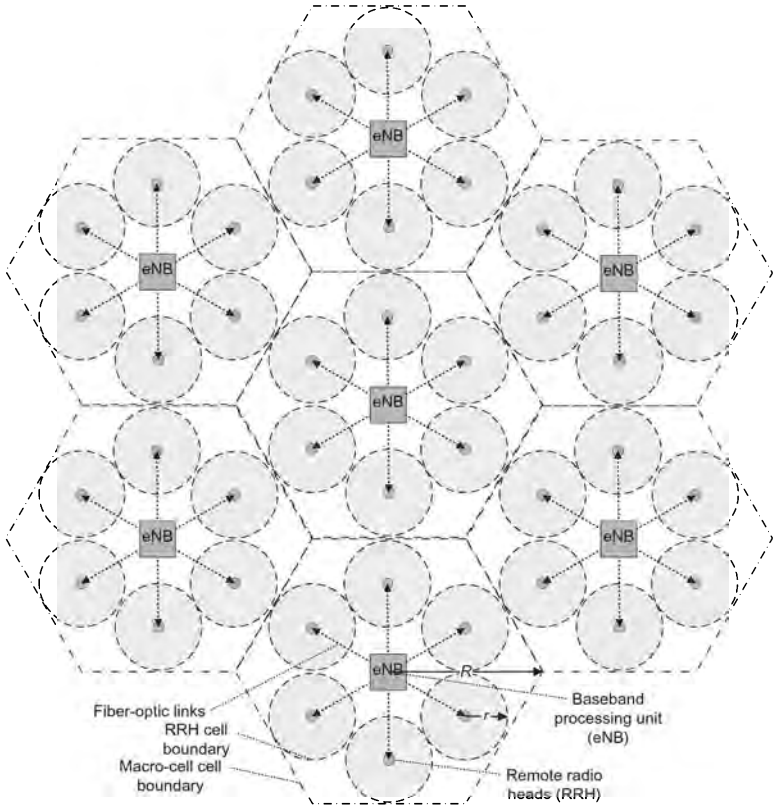


FIGURE 12.2

Example of the architecture of a distributed antenna system with one-tier interference model.

distributed antenna modules. In contrast, the same area is covered by only a single high-power base station in traditional cellular systems. The actual number of distributed antenna modules would be determined by coverage, user densities, and other deployment/economic/environmental factors. Let $P_i^{(j)}$ denote the total transmit power of the ith distributed antenna module of the jth cell, where the small base station of each cell and home cell are indexed by $i = 0$ and $j = 0$, respectively. Let us further assume that $\sum_{i=1}^{N_{\text{unit}}} P_i^{(j)} = P \; \forall j$, where P is the total transmit power of the conventional base station for a fair comparison. The radius of a cell is R, and the coverage radius of a distributed antenna module is r. We further assume a seven cell cellular structure with universal frequency reuse, where a given cell is surrounded by one continuous tier of six cells, as shown in Figure 12.2.

Let us assume (without loss of generality) that there are six RRHs in each cell, and further in each site, downlink signals are transmitted through all the

distributed antenna modules and the home base station. In this case, the multiple distributed antenna modules and the home base station together construct a macroscopic MISO vector channel given by [19]:

$$\mathbf{h} = \left(\sqrt{PL_0^{(0)}} h_0^{(0)} \quad \sqrt{\mathrm{PL}_1^{(0)}} h_1^{(0)} \quad \sqrt{\mathrm{PL}_2^{(0)}} h_2^{(0)} \quad \sqrt{\mathrm{PL}_3^{(0)}} h_3^{(0)} \right.$$
$$\left. \sqrt{\mathrm{PL}_4^{(0)}} h_4^{(0)} \quad \sqrt{\mathrm{PL}_5^{(0)}} h_5^{(0)} \quad \sqrt{\mathrm{PL}_6^{(0)}} h_6^{(0)} \right) \tag{12.2}$$

In Eq. (12.2), $h_i^{(j)}$ denotes short-term fading channel from the ith distributed antenna module in the jth cell which is an independent and identically distributed complex Gaussian random variable $h_i^{(j)} \sim \mathbb{C}(0,1)$. The fading channel is assumed to be static during orthogonal frequency division multiplexing (OFDM) symbol duration. The coefficient $\mathrm{PL}_i^{(j)}$ denotes path loss and shadow fading from the ith distributed antenna module in the jth cell. The transmitted signal vector is represented as $\mathbf{x} = (x_0^{(0)}, x_1^{(0)}, \ldots, x_6^{(0)})^{\mathrm{T}}$, where each entry $x_i^{(j)}$ represents the transmitted signal from the ith distributed antenna module in the jth cell with $\mathscr{E}\{|x_i^{(j)}|^2\} = P_i^{(j)}$. Under these conditions, the received signal at a mobile station in a given OFDM symbol duration is given by [19]:

$$y = \underbrace{\mathbf{hx}}_{\text{Desired signal}} + \underbrace{\sum_{j=1}^{6} \sum_{i=0}^{6} h_i^{(j)} \sqrt{\mathrm{PL}_i^{(j)}} x_i^{(j)}}_{\text{Inter-cell interference}} + \underbrace{n}_{\text{Receiver noise}} \tag{12.3}$$

where n is an additive white Gaussian noise with normal distribution $n \sim \mathcal{N}(0, \sigma_n^2)$. Since the number of interfering sources is sufficiently large and the interfering sources are independent of each other, the interference plus noise can be assumed to be a complex Gaussian random variable z with variance $\sigma_z^2 = \sum_{j=1}^{6} \sum_{i=0}^{6} \mathrm{PL}_i^{(j)} P_i^{(j)} + \sigma_n^2$ according to the central limit theorem[2], whereas the interference plus noise power of the conventional cellular system is given by $\sigma_c^2 = \sum_{j=1}^{6} \mathrm{PL}_0^{(j)} P_0^{(j)} + \sigma_n^2$. When only a single distributed antenna module or the

[2]In probability theory, the central limit theorem states that, given certain conditions, the mean of a sufficiently large number of independent random variables, each with finite mean and variance, will be approximately normally distributed. Let $X_1, X_2, \ldots, X_n$ be a set of n independent random variables and let each X_i have an arbitrary probability distribution $p(x_1, x_2, \ldots, x_N)$ with mean μ_i and a finite variance σ_i^2. Then, the normal form variable $X_{\text{normal}} = \left(\sum_{i=1}^{N} (x_i - \mu_i) \right) / \sqrt{\sum_{i=1}^{N} \sigma_i^2}$ has a limiting cumulative distribution function which approaches a normal distribution. Under additional conditions on the distribution of the addend, the probability density itself is also normal with mean $\mu = 0$ and variance $\sigma^2 = 1$. If conversion to normal form is not performed, then the random variable $X = \left(\sum_{i=1}^{N} x_i \right) / N$ is normally distributed with $\mu_X = \mu_x$ and $\sigma_X = \sigma_x / \sqrt{N}$ [28].

home base station is selected for transmission (based on the criterion of minimizing propagation path loss), the received signal is given by [19]:

$$y = \underbrace{h_m^{(0)}\sqrt{\mathrm{PL}_m^{(0)}}x_m^{(0)}}_{\text{Desired signal}} + \underbrace{\sum_{j=1}^{6} h_i^{(j)}\sqrt{PL_i^{(j)}}x_i^{(j)}}_{\text{Inter-cell interference}} + \underbrace{n}_{\text{Receiver noise}} \tag{12.4}$$

where $m = \arg\min_{k=0,1\ldots6}(\mathrm{PL}_0^{(j)}, \mathrm{PL}_1^{(j)}, \ldots, \mathrm{PL}_6^{(j)})$ and qj is randomly selected from the set $\{0, 1, \ldots, 6\}$. The interference plus noise can be shown to be a complex Gaussian random variable u with variance $\sigma_u^2 = \sum_{j=1}^{6} \mathrm{PL}_{qj}^{(j)} P_{qj}^{(j)} + \sigma_n^2$. Since other cells adopt the same transmission scheme as the home cell, only one of the interfering sources in the other cells can be randomly selected in a dynamic point switching scheme. If the CSI is known only at the receiver and the channel is ergodic, the ergodic capacity at a given location of the mobile station under study can be written as follows:

$$C_{\text{ergodic}} = \mathscr{E}_{\mathbf{h}}\left\{\log_2\left(1 + \frac{1}{\sigma_z^2}\mathbf{h}\Phi\mathbf{h}^H\right)\right\} \tag{12.5}$$

where Φ is the covariance matrix of the transmitted signal vector $\mathbf{x}$ given by $\Phi = \mathrm{diag}(P_0^{(0)}, P_1^{(0)}, \ldots, P_6^{(0)})$. When the channel is known in the transmitter side, the ergodic capacity at a given location of the mobile station is given by:

$$C_{\text{ergodic}} = \mathscr{E}_{\mathbf{h}}\left\{\max_{\varphi_{ii} \le P_i^{(0)} \forall i} \log_2\left(1 + \frac{1}{\sigma_z^2}\mathbf{h}\Phi\mathbf{h}^H\right)\right\} \tag{12.6}$$

where φ_{ii} is the ith diagonal element of matrix Φ. The maximum capacity is achieved by proper design of the transmit power spectrum matrix Φ under individual power constraints of the distributed antenna modules and the home base station. If power cooperation among the distributed antenna modules and the home base station is allowed, this problem reduces to a standard water-filling problem in a macroscopic MISO vector channel [19].

The above study suggests that the distributed antenna systems effectively reduce inter-cell interference and improve SINR especially for the cell-edge users, which are typically performance limiting users, compared to conventional cellular systems in an interference-limited multi-cell environment. As a result, distributed antenna systems achieve lower symbol error probability and higher capacity than conventional cellular systems; thus, distributed antenna architectures appear to be an effective solution for reducing inter-cell interference in an interference-limited cellular environment.

12.3 Theory of CoMP operation

Future cellular networks are required to provide high-data-rate services to a large number of users, which necessitates high spectral efficiency over the entire cell

coverage area. In order to address this problem, it is important to ensure robustness of the radio interface to interference, in particular inter-cell interference, which appears when the same radio resources are reused in different cells in an uncoordinated manner. The inter-cell interference particularly degrades the performance of users located in the cell-edge areas, which causes an inconsistent level of performance among cell-edge and inner-cell users. One possible solution to alleviate this performance discrepancy is to employ coordinated multi-point transmission and reception, which refers to a system where the transmission or reception at multiple, geographically separated antenna sites is dynamically coordinated in order to improve system performance. The coordination can be distributed either by means of direct communication between different sites, or by means of a central coordinating node [34–47].

The notion of clustering (grouping of the cooperating cells) is essential to coordinated beamforming and relaxed coherent joint processing. Indeed, the term CoMP suggests that a number of base stations share some knowledge about users. However, as the number of users and eNBs increases, the signaling overhead required for the inter-eNB information exchange and the amount of feedback needed from the users dramatically increase. Therefore, cooperation should be limited to a small number of cells/sites. To achieve this goal, the network is divided into clusters of cooperating cells. Cluster selection is important to the performance of cooperation strategies. Cluster formation may be static, if the clusters remain fixed in time, or dynamic (see Figures 12.7 and 12.8). Selection may be performed in a network-centric or in a user-centric manner. The network-centric clustering typically divides the network into a set of disjoint clusters of eNBs such that one eNB can belong only to one cluster. In contrast, in the user-centric clustering approach, one eNB may belong to more than one cluster, depending on the parameter under consideration. From the user point of view, this means that, in a given cell, each user may have a different set of cooperating eNBs. The concept of clustering is similar to cooperative sets and/or measurement sets, which will be defined later.

CoMP architectures may include centrally located or distributed processing among the collaborating nodes. The use of geographically distributed antennas in CoMP and the introduction of multiple transmission nodes is conceptually similar to the distributed antenna systems. In particular, in a CoMP scheme exploiting DAS principles, there are several possible transmission strategies including the power-weighted transmission scheme and the single transmit-selection scheme.

Assuming linear transceiver processing, a CoMP system with N antennas is ideally able to accommodate up to N streams without becoming interference limited. The inter-stream interference can be controlled or even completely eliminated by proper precoder selection. This is especially true in the coherent joint processing case, where user data is conveyed from multiple base station antenna nodes over a large virtual MIMO channel. The coherent multi-user multi-cell precoding techniques have strict requirements in terms of signaling and measurements. In addition to the complete channel knowledge of all jointly processed links, a stringent

synchronization across the transmitting nodes and centralized entities performing scheduling and computation of joint precoding weights is required in order to avoid carrier phase drifting at different transmit nodes. A large amount of data needs to be exchanged between the network nodes. Therefore, broadband links, such as optical fibers or dedicated radio links, are needed.

Another form of coordinated transmission is dynamic multi-cell scheduling and interference avoidance, where the network nodes coordinate their transmissions (precoder design, scheduling) in order to minimize the inter-cell interference. Carrier phase coherence between the transmit nodes is not required, since each data stream is transmitted from a single transmission point. As a result, the non-coherent coordinated multi-cell transmission approaches have somewhat looser requirements on the coordination and the backhaul, but could potentially need centralized resource management mechanisms.

In order to understand how the above coordinated transmission schemes are mathematically formulated, consider an example of a centralized non-codebook-based coordinated beamforming scenario with static cooperating clusters. Let us assume a general downlink system model for the network consisting of N_{cell} cells and N_{user} single-antenna UEs per cell. This scenario can be considered a traditional cellular network, in which only one transmitter per cell is used, or a CoMP network, in which more than one transmitter per cell is used. We refer to this model as a CoMP system made of N_{unit} single-antenna remote units per cell. In general, the downlink system model of a CoMP cellular network can be expressed as $\mathbf{y} = \mathbf{HWx} + \mathbf{n}$, where $\mathbf{H} \in \mathbb{C}^{N_{\text{user}} \times N_{\text{cell}} N_{\text{unit}}}$, and $\mathbf{W} \in \mathbb{C}^{N_{\text{cell}} N_{\text{unit}} \times N_{\text{user}}}$ are the CoMP processing matrices, which depend on the particular CoMP configuration, $\mathbf{x} = (x_1, x_2, \ldots, x_{N_{user}})^T \in \mathbb{C}^{N_{\text{user}} \times 1}$ is a complex vector that contains the transmitted signal, $\mathbf{y} = (y_1, y_2, \ldots, y_{N_{\text{user}}})^{\text{T}} \in \mathbb{C}^{N_{\text{user}} \times 1}$ is a complex vector containing N_{user} signals received by N_{user} UEs, and $\mathbf{n} \in \mathbb{C}^{N_{\text{user}} \times 1}$ is the noise vector. The ijth entry $\{h_{ij}^{(k)}\}$ of matrix $\mathbf{H}$ represents the complex-valued channel gain between the ith UE ($1 \le i \le N_{\text{user}}$) and the jth remote unit ($1 \le j \le N_{\text{unit}}$) belonging to the kth cell ($1 \le k \le N_{\text{cell}}$). The jith element $\{w_{ji}^{(k)}\}$ of the matrix $\mathbf{W}$ is the square root of the transmission power applied at the jth remote unit ($1 \le j \le N_{\text{unit}}$), transmitting toward the ith UE ($1 \le i \le N_{\text{user}}$), belonging to the kth cell ($1 \le k \le N_{\text{cell}}$). In this model, we assume a flat fading channel as typically observed at each subcarrier in an OFDM system. The above model can be extended to the case of remote units and mobile terminals equipped with multiple antennas. In the following, we assume that there are two cells in the network, and there are three remote units per cell, and further there are two users in each cell, thus $N_{\text{cell}} = 2$, $N_{\text{unit}} = 3$, and $N_{\text{user}} = 2$. Using the above hypotheses, one can rewrite the received signal equation as follows [24]:

$$\begin{pmatrix} y_1 \\ y_2 \end{pmatrix} = \begin{pmatrix} \mathbf{H}^{(1)} & \mathbf{H}^{(2)} \end{pmatrix} \begin{pmatrix} \mathbf{W}^{(1)} \\ \mathbf{W}^{(2)} \end{pmatrix} \begin{pmatrix} x_1 \\ x_2 \end{pmatrix} + \begin{pmatrix} n_1 \\ n_2 \end{pmatrix} \tag{12.7}$$

which can be further expanded as follows:

$$\begin{pmatrix} y_1 \\ y_2 \end{pmatrix} = \begin{pmatrix} h_{11}^{(1)} & h_{12}^{(1)} & h_{13}^{(1)} & h_{11}^{(2)} & h_{12}^{(2)} & h_{13}^{(2)} \\ h_{21}^{(1)} & h_{22}^{(1)} & h_{23}^{(1)} & h_{21}^{(2)} & h_{22}^{(2)} & h_{23}^{(2)} \end{pmatrix} \begin{pmatrix} w_{11}^{(1)} & w_{12}^{(1)} \\ w_{21}^{(1)} & w_{22}^{(1)} \\ w_{31}^{(1)} & w_{32}^{(1)} \\ w_{11}^{(2)} & w_{12}^{(2)} \\ w_{21}^{(2)} & w_{22}^{(2)} \\ w_{31}^{(2)} & w_{32}^{(2)} \end{pmatrix} \begin{pmatrix} x_1 \\ x_2 \end{pmatrix} + \begin{pmatrix} n_1 \\ n_2 \end{pmatrix} \tag{12.8}$$

where y_i is the signal received by the ith UE and x_j denotes the signal transmitted by the jth remote unit. The particular expressions of $\mathbf{W} \in \mathbb{C}^{N_{\text{cell}} N_{\text{unit}} \times N_{\text{user}}}$ for CoMP transmit-selection and power-weighted schemes when only one user per cell is considered are as follows:

$$\mathbf{W}_{\text{transmit-selection}} = \begin{pmatrix} 0 & 0 \\ w_{\text{ji}}^{(1)} & 0 \\ 0 & 0 \\ 0 & 0 \\ 0 & w_{\text{ji}}^{(2)} \\ 0 & 0 \end{pmatrix} \mathbf{W}_{\text{weighted-power}} = \begin{pmatrix} w_{11}^{(1)} & 0 \\ w_{21}^{(1)} & 0 \\ w_{31}^{(1)} & 0 \\ 0 & w_{12}^{(2)} \\ 0 & w_{22}^{(2)} \\ 0 & w_{32}^{(2)} \end{pmatrix} \tag{12.9}$$

In the above expressions, and for the CoMP transmit-selection scheme, the only non-zero term $w_{\text{ji}}^{(k)}$ for $k = 1, 2$ is selected by a certain criterion such as minimizing the path loss between any of the remote units transmitting toward the mobile user which is being served, i.e., $w_{\text{ji}}^{(k)} = \min_j \{PL(j, i)\}|_{k=1,2}$ for the ith mobile user. In the CoMP power-weighted scheme $\sum_{j=1}^{N_{\text{unit}}} w_{\text{ji}}^{(k)} = P_{\text{total}}$ for $k = 1, 2$ where P_{total} is the total transmit power of the conventional base station, for the ith mobile user.

Consider a coordination cluster with N_{TP} transmission points, each equipped with an antenna array comprising N_{TX} antenna elements, and N_{user} UEs equipped with N_{RX} receive antennas. Assuming an OFDM transmission, the baseband signal received by the ith UE at the kth subcarrier in the downlink is given by:

$$\mathbf{y}_i(k) = \mathbf{H}_i(k)\mathbf{x}(k) + \mathbf{n}_i(k) \tag{12.10}$$

where the $N_{\text{RX}} \times N_{\text{unit}} N_{\text{TX}}$ matrix $\mathbf{H}_i(k)$ is the composite channel between all transmission points and the ith UE; $\mathbf{n}_i(k)$ represents thermal noise vector including inter-cluster interference which is assumed to be white Gaussian distributed with

covariance matrix $\mathscr{E}\{\mathbf{n}_i(k)\mathbf{n}_i^H(k)\} = \sigma_i^2\mathbf{I}$; $\mathbf{x}$ is an $N_{\text{unit}}N_{\text{TX}} \times 1$ vector representing the sum signal transmitted from all transmission points, given by:

$$\mathbf{x}(k) = \sum_{i=1}^{N_{\text{user}}} \mathbf{x}_i(k) = \sum_{i=1}^{N_{\text{user}}} \sqrt{p_i}\mathbf{u}_i s_i(k) \tag{12.11}$$

where $s_i(k)$ is a modulation symbol drawn from a unit-variance symbol alphabet, which is transmitted to the ith UE using the transmit power p_i and beamforming vector $\mathbf{u}_i$, respectively. The beamforming vectors are normalized to have unit power $\mathscr{E}(\mathbf{u}_i^H\mathbf{u}_i) = 1$ for $i = 1, 2, \ldots, N_{\text{user}}$. The average SINR for the ith UE, assuming an MRC receiver type, is given by [24]:

$$\text{SINR}_i(\mathbf{U},\mathbf{p}) = \frac{\mathbf{p}_i\mathbf{u}_i^H\mathbf{R}_i\mathbf{u}_i}{\sum_{j\neq i}\mathbf{p}_j\mathbf{u}_j^H\mathbf{R}_i\mathbf{u}_j + \sigma_i^2} \tag{12.12}$$

where $\mathbf{U}$ is the transmit beamforming matrix given by $\mathbf{U} = (\mathbf{u}_1 \quad \mathbf{u}_2 \quad \ldots \quad \mathbf{u}_{N_{\text{user}}})$, $\mathbf{p}_i$ is the vector of transmit powers, and $\mathbf{R}_i$ is the transmit correlation matrix for the ith UE, given by $\mathbf{R}_i = \mathscr{E}\{\mathbf{H}_i^H(k)\mathbf{H}_i(k)\} = \text{diag}(R_{i1}, R_{i2}, \ldots, R_{iN_{\text{unit}}})$. Since the transmission points are separated by large distances, their antennas are mutually uncorrelated. The considered coordinated beamforming scheme is a modified form of the multiuser beamforming algorithm, in which the beamforming vectors and power allocations are obtained by maximizing the jointly achievable SINR margin as follows [24]:

$$C = \max_{\mathbf{U},\mathbf{p}} \min_{i\in\{1,2,\ldots,N_{\text{user}}\}} \frac{\text{SINR}_i(\mathbf{U},\mathbf{p}_i)}{\gamma_i} \tag{12.13}$$

The above optimization is performed under per-transmitter power constraint:

$$\sum_{i\in S_n} p_i \leq P_{\max} \quad n\in\{1, 2, \ldots, N_{\text{unit}}\} \tag{12.14}$$

where γ_i is the target SINR for the ith UE, S_n is the set of UEs connected to the nth transmission point, and $P_{\max}$ is the maximum transmission point transmit power. The beamforming vectors and downlink power allocations are found iteratively using the uplink–downlink duality theorem, which states that the downlink broadcast channel has a virtual dual uplink multiple access channel which has the same SINR achievable regions as the downlink, and the same beamforming vectors to achieve the SINRs in both links [24].

It can be expected that the most appropriate scenarios for coordinated beamforming have low angular spreads which are found in the urban, suburban, and rural environments with above-rooftop antenna deployment. Due to low feedback requirements, coordinated beamforming is especially of interest in the FDD mode. The joint processing might be difficult to realize in a practical system due to the stringent feedback requirements. It can also be expected that coordinated beamforming is robust to user mobility, hence making it an attractive alternative

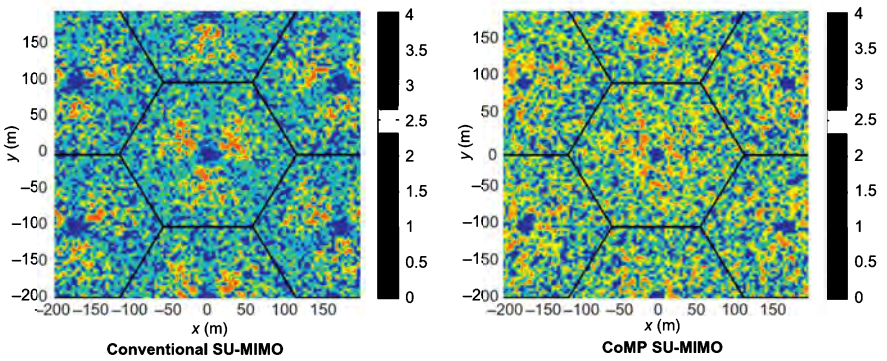


FIGURE 12.3

Performance of intra-eNB CoMP with SU-MIMO and implicit feedback relative to conventional SU-MIMO.

both in low and high mobility scenarios [24]. The performance (cell spectral efficiency) of an intra-eNB CoMP with SU-MIMO and implicit feedback relative to a conventional SU-MIMO scheme have been simulated and are shown in Figure 12.3. The improvement of cell spectral efficiency due to use of CoMP in different areas of the cell and in particular the cell-edge areas can be seen in Figure 12.3. The simulation assumptions are consistent with those recommended in 3GPP TR 36.814 [4].

12.4 CoMP architectures

In LTE Rel-8, MIMO transmission in each cell is controlled independent of that of the neighbor cells. Inter-cell interference coordination (ICIC) was supported by means of coordination message exchanges between base stations via a standardized inter-eNB interface known as X2 [6,7]. The goal of ICIC is to provide the scheduler at one cell with information about the current or prospective interference condition at its neighbors. However, in reality, the transfer latency of these coordination messages depends on the backhaul technology and is not negligible. While ICIC techniques are primarily designed for semi-static coordination, CoMP techniques target more dynamic coordination and may require much lower latency. The macro-cells constitute the basis of a mobile network's coverage; the deployment of low-power nodes (e.g., pico- or femto-cells or relay nodes) within the macro-cell is expected to be an effective solution in the future to address ever-increasing mobile traffic demands. Such networks, referred to as heterogeneous networks, are characterized by severe inter-cell interference between the macro and the low-power nodes due to their proximity and different transmit power classes. The inter-cell interference effect is even more detrimental when the effective cell size of the low-power node is expanded to balance the traffic

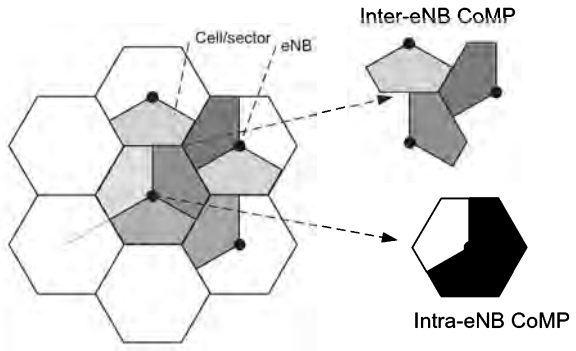


FIGURE 12.4

Illustration of inter-eNB and intra-eNB CoMP scenarios.

load between the macro-cell and the low-power node cell; thus, the UE may be associated with a cell that does not provide the strongest received signal power.

In general, and as shown in Figure 12.4, CoMP transmission/reception techniques can be classified into the following two major categories:

1. Inter-eNB CoMP, wherein coordination amongst eNBs is done via the X2 interface with typical feedback delay of 5–30 ms. This method requires standardization of the feedback channel with consideration for overhead and delay reduction.
2. Intra-eNB CoMP, wherein transmission points are usually connected via wideband/low-delay optical fibers with typical feedback delay of 5 ms and with minimal impact on the X2 interface.

LTE Rel-11 has focused on the intra-eNB CoMP scenarios in order to limit the scope of specification impacts on lower protocol layers.

One recent deployment trend that is foreseen to be widely applied to LTE networks consists of splitting the base station functionalities into a baseband unit, which performs in particular the scheduling and the baseband processing functions, and a number of RRHs responsible for all RF transmission/reception aspects. The baseband processing unit is typically located at the center of the cell and is connected via optical fiber to the RRHs. In addition to suppressing the feeder loss (since the power amplifier is immediately close to the antenna), this approach allows the baseband processing unit to manage different radio sites in a central manner. Furthermore, having geographically separated RRHs controlled from the same location enables either centralized baseband processing units jointly managing the operation of several radio sites, or the exchange of very low-latency coordination messages among individual baseband processing units. The RRH deployments facilitate the tight coordination between transmission/reception points that is required for some CoMP schemes. The applicability and benefits of CoMP techniques depend to a great extent on the backhaul characteristics (latency and capacity), which determine the type of CoMP processing and the corresponding

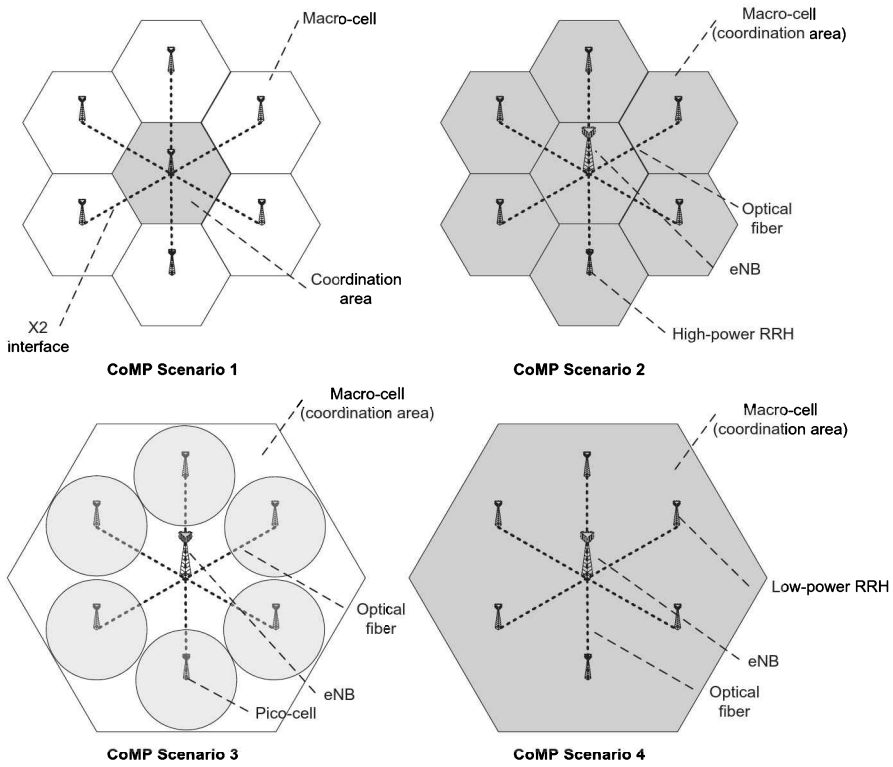


FIGURE 12.5

Illustration of CoMP scenarios [5].

performance. In order to account for the various possible network topologies and backhaul characteristics, the study of CoMP in 3GPP focused on the following scenarios (Figure 12.5) [5,27]:

- CoMP scenario 1 (homogeneous macro network with intra-site CoMP): Coordination among the cells (sectors) controlled by the same macro base station (where no backhaul connection is needed).
- CoMP scenario 2 (homogeneous macro network with inter-site CoMP): Coordination between cells belonging to different radio sites from a macro network.
- CoMP scenario 3 (heterogeneous network with low-power pico-cells within the macro-cell coverage area): Coordination between a macro-cell and low-power transmit/receive points within its coverage, each point controlling its own cell (with its own cell identity).
- CoMP scenario 4 (heterogeneous network with low-power RRH): Coordination between a macro-cell and low-power transmit/receive points

within its coverage, each point controlling its own cell, except that the low-power transmit/receive points constitute geographically distributed antennas of the macro-cell, and are thus all associated with the macro-cell identity.

CoMP scenario 1 is defined for homogeneous networks where the coordination area is restricted to the cells of a single site controlled by an eNB. Although the extent of coordination is limited to the cells of the same site, CoMP scenario 1 has the advantage of requiring no inter-eNB interface among different sites. Such an advantage would make CoMP scenario 1 attractive to the network operators.

CoMP scenario 2 is for homogeneous networks where the coordination area is expanded from the CoMP scenario 1 to include the cells of different sites. CoMP scenario 2 may be realized by having a single eNB control the RRHs at different sites, or by having multiple eNBs at different sites to coordinate with each other. CoMP scenario 2 is depicted in Figure 12.5 with high-power RRHs at different sites controlled by a single eNB. Depending on the number of cells involved and the latency of connections between the sites, which are both dependent on network implementation, different levels of performance gain over CoMP scenario 1 may be obtained.

CoMP scenario 3 relies on a heterogeneous network model where macro-cells with high transmission power and pico-cells with low transmission power are connected. In practice, this scenario may be realized by a single eNB controlling the high-power RRH of the macro-cell and the low-power RRHs of pico-cells within the macro-cell coverage area. Another possible network implementation is that the eNBs of the macro-cell and the pico-cells are different and coordinate with each other. Figure 12.5 illustrates CoMP scenario 3 with low-power RRHs at different sites controlled by a single eNB.

CoMP scenario 4 is defined for heterogeneous networks where low-power RRHs are distributed throughout the coverage area of a macro-cell. The difference between this scenario and the other intra-eNB scenarios is that all low-power RRHs in this case share the same physical cell identity with the macro-cell. Therefore, it can be construed that the low-power RRHs form a set of distributed antennas in the macro-cell area. Since the coordination is done among distributed antennas within the same cell, depending on the size of macro-cell, there may not be a need for conventional mobility support such as handover procedures among the RRHs. Furthermore, since each RRH is not an independent cell, a low-delay and high-capacity backhaul connection such as optical fiber can provide the radio connection between the macro-eNB and the RRHs. CoMP scenarios 3 and 4 are expected to find applications in metropolitan areas where network deployment is dense and RRHs with different transmission power levels can be deployed to improve control/data coverage and capacity [17].

A set of geographically collocated antennas that correspond to a particular sectorization scheme are traditionally configured as a cell. A UE attempts to connect to a single cell at any given time, if the measured received reference signal strength from that cell is higher relative to that from other cells. This cell then

becomes its serving cell. Given the new definition of CoMP scenarios as introduced earlier, the antennas configured as a cell may not be geographically collocated. The term transmission point can then be used to refer to a set of collocated antennas, and a cell can correspond to one or more such transmission points. Note that a single geographical site may contain multiple transmission points in the case of sectorization, with one transmission point corresponding to one sector. CoMP techniques can also be defined in a more straightforward manner as the coordination between transmission points.

A mobile station is said to be connected to a cooperating set/cluster if its serving cell belongs to the cluster. We assume no coordination between clusters, which also means that a cell belongs to one, and only one, cluster. The serving cell selection in LTE Rel-8 is based on the long-term average reference signal received power (RSRP) measurements. The cell with the strongest RSRP acts as the serving cell. The serving cell also defines the cluster to which the mobile is connected. Since each cell uniquely belongs to one cluster, the serving cluster is determined once the serving cell is selected. It is assumed that the measurement set of a UE is a subset of the cluster.

12.4.1 Air-interface and network support for CoMP schemes

In order to enable CoMP operation, the network architecture must be able to provide sufficient coordination and synchronization among different transmission points and/or cells/sites. If inter-eNB coordination is enabled, user data and/or CSI will be exchanged and shared between eNBs; thus, low-latency and high-capacity backhaul would be required to support inter-eNB CoMP deployment scenarios. The impacts on the radio interface mainly depend on type of CoMP scheme that is utilized, which may include, but is not limited to, the following [5]:

- CSI measurement and feedback mechanisms at the UE, which may include reporting dynamic channel conditions between transmission points in the CoMP measurement set and the UE. Depending on the duplex scheme, channel reciprocity may be exploited to facilitate channel estimation at the transmission points.
- Low-latency and configurable reporting mechanisms to facilitate the decision-making process concerning the set of participating transmission points.
- Static and dynamic coordination and tight synchronization are required prior to transmission of the signal over multiple transmission points.
- Reference signals with unique signatures are required to enable inter-cell/intra-cell interference and channel measurements. Depending on the CoMP scheme, the LTE Rel-10 CSI reference signal (CSI-RS) structures were found to be suitable to provide support for certain interference measurement and characterization [33].
- Improved control signaling design may be required to support signaling and feedback for certain CoMP algorithms. LTE Rel-11 provided the enhanced physical downlink control channel (ePDCCH) and other downlink control

signaling improvements, as well as transmission mode 10 to accommodate the CoMP design and operation.

Different impacts on the network architecture are foreseen depending on the CoMP scenario being deployed, including coordination among base stations, use of radio over fiber links to connect different transmission/reception points, or coordinated relaying, affecting both data-plane and control-plane protocols. The optical fiber links have a small impact on the current network architecture since the interface between base station control unit and the associated RRH can be either proprietary or based on an open standard interface such as the Common Public Radio Interface (CPRI)[3] standard which defines the interface between entities known as RECs and local or RRH referred to as radio equipment (RE) [29]. It is necessary to further study the transfer of data and control information over optical fiber interfaces. Cooperation among distributed base stations has a higher impact on the network. A central control/scheduling/processing unit may be necessary depending on the required coordination scheme.

Other important aspects to be considered when deploying CoMP in a network include centralized/decentralized management of UEs connected to multiple transmit/receive points. Most proposals addressing multi-antenna schemes often assume power constraints on the sum of power transmitted by different antennas. This assumption may not hold when each antenna in a multi-antenna base station is powered by its own power amplifier and is limited by the linearity of that amplifier, or when the system uses distributed antennas belonging to the same or coordinated base stations, and each one is subject to its own power limits and emission constraints [23].

12.4.2 Downlink CoMP

A set of geographically separated points directly and/or indirectly involved in downlink data transmission to a UE over a time–frequency resource is defined as a CoMP cooperating set. Note that this set may be transparent to the UE. The transmission points in a cooperating set are either directly participating in transmission of data in the time–frequency resource, or indirectly participating in transmission,

[3]The CPRI is an initiative to define a publicly available specification that standardizes the protocol interface between the radio equipment control (REC) and the radio equipment (RE) in wireless base stations. This allows interoperability of equipment from different vendors and preserves the software investment made by wireless service providers. Conventional base stations are located adjacent to the antenna in a small building at the base of the antenna tower. Finding suitable sites can be a challenge because of the footprint required for the building, the need for structural reinforcement of rooftops, and the availability of both primary and backup power sources. CPRI allows the use of a distributed architecture where base stations, containing the REC, are connected to remote radio heads via low-loss fiber links that carry the CPRI data. This architecture reduces costs for service providers because only the remote radio heads containing the REs need to be situated in environmentally challenging locations. The base stations can be centrally located in less challenging locations where footprint, climate, and availability of power are more easily managed [29].

which make them candidate points for data transmission that do not transmit data but contribute in making decisions on the user scheduling/beamforming in the time–frequency resource. The CoMP transmission points (TPs) are defined as a set of points transmitting data to a UE. It is understood that CoMP TPs are a subset of the CoMP cooperating set. In general, the downlink CoMP schemes may be classified into one of the following categories (see Figure 12.6) [5]:

- Joint processing (JP) where data for a UE is available at more than one transmission point in the CoMP cooperating set for a time–frequency resource. A subcategory of JP CoMP is the joint transmission (JT) in which data is simultaneously transmitted from multiple points (part of or an entire CoMP cooperating set) to a single UE or multiple UEs in a time–frequency resource. Alternatively, the data to a UE can be simultaneously transmitted from multiple points, e.g., to (coherently or noncoherently) improve the received signal quality and/or data throughput. Another subgroup of JP CoMP is known as dynamic point selection (DPS)/muting where data is transmitted from one point (within the CoMP cooperating set) in a time–frequency resource. The transmitting/muting point may change from one subframe to another, including varying over the resource block pairs within a subframe. The data is available simultaneously at multiple points. This includes dynamic cell selection (DCS). The DPS may be combined with JT, in which case, multiple points can be selected for data transmission in the time–frequency resource.
- Coordinated scheduling/beamforming (CS/CB) in which data for a UE is only available and is transmitted from one point in the CoMP cooperating set, i.e., downlink data is transmitted from that point for a time–frequency resource but user scheduling/beamforming decisions are made with coordination among points corresponding to the CoMP cooperating set. In this case, the transmission points are selected semi-statically. Semi-static point selection (SSPS) is a method where data is transmitted to a specific UE from one point at a time. The transmitting point may only change in a semi-static manner. Muting may be applied in a dynamic and semi-static manner to the above transmission schemes (Figure 12.6).

The CS/CB scheme reduces the interference level experienced by a UE terminal by appropriately selecting the beamforming weights of interfering points to steer the interference toward the null space of the interfered UE. The JT scheme allows one or more neighboring points to transmit the desired signal rather than interfering signals from the point of view of the selected UE. The transmission point selection scheme enables the UE to be dynamically scheduled via the most appropriate transmission point by exploiting changes in the channel slow/fast fading conditions. Hybrid methods may also be implemented in a network to cope with different types of interference. A combination of JP and CS/CB schemes is possible in the downlink. Data for a UE may be available only in a subset of points in the CoMP cooperating set for a particular time–frequency resource, but user scheduling/beamforming decisions are made with coordination among points

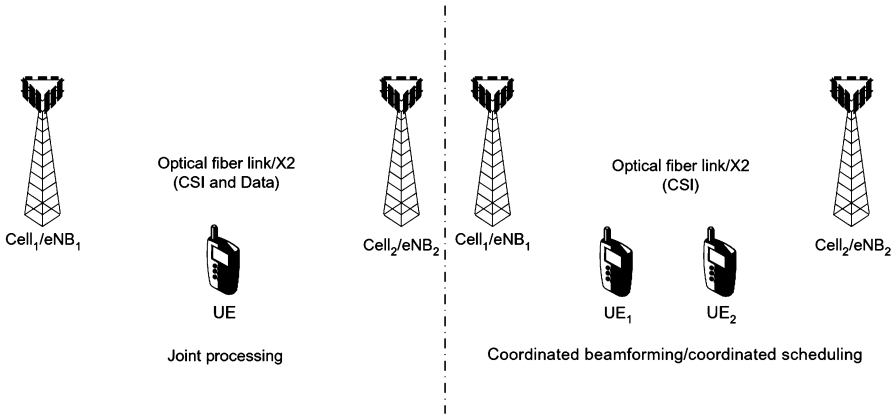


FIGURE 12.6

Illustration of downlink CB/CS and JT CoMP concepts.

corresponding to the CoMP cooperating set. For example, some points in the cooperating set may transmit data to the target UE according to a JP scheme, while other transmission points in the cooperating set may perform one form of CS/CB scheme. For the JT scheme, CoMP transmission points may include multiple points in the CoMP cooperating set at each subframe for a certain time–frequency resource, whereas in the case of CS/CB, DPS, SSPS, a single point in the CoMP cooperating set is the CoMP transmission point at each subframe for a certain time–frequency resource. For SSPS, this CoMP transmission point can change semi-statically within the CoMP cooperating set. Examples of static and dynamic formation of CoMP clusters (cooperating sets) are shown in Figures 12.7 and 12.8.

12.4.3 Uplink CoMP

The uplink CoMP schemes may be divided into one of the following categories:

- Joint reception (JR) in which physical uplink shared channel (PUSCH) transmitted by the UE is received jointly at multiple points which are part of or the entire CoMP cooperating set at a certain time, e.g., to improve the received signal quality.
- CS/CB where user scheduling and precoding decisions are made with coordination among points within the CoMP cooperating set. The user data is only intended for one recipient point in the set.

Similar to the downlink, the uplink CoMP cooperating set is a set of geographically separated points that may be designated for data reception from a UE. The uplink CoMP reception points are a set of points for receiving data from a UE. The CoMP reception points are a subset of the CoMP cooperating set in the uplink. For the JR scheme, CoMP reception points may include multiple points in

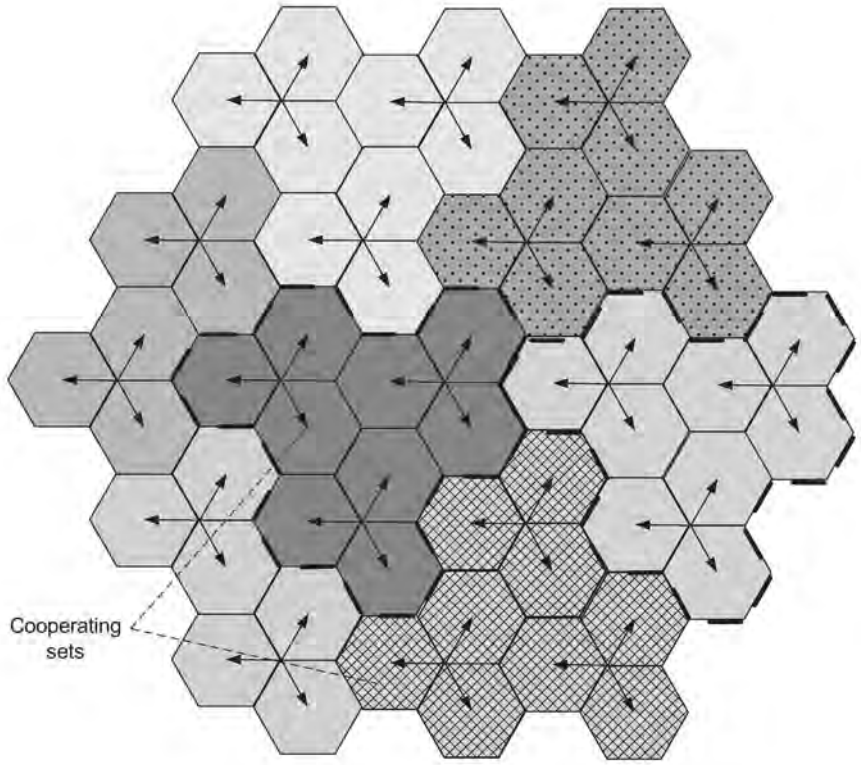


FIGURE 12.7

Illustration of static CoMP clusters (Scenario 2, 9 cells per cooperating set) [5].

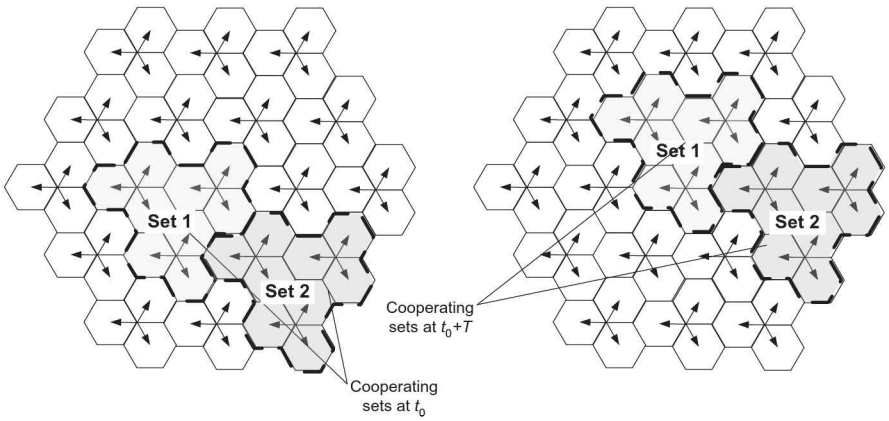


FIGURE 12.8

Dynamic clustering of CoMP (change of cooperating CoMP sets across time).

the CoMP cooperating set at each subframe for a certain time–frequency resource, whereas for uplink CS/CB, a single point in the CoMP cooperating set is the CoMP reception point at each subframe for a certain time–frequency resource [5].

In other words, uplink CoMP schemes can be divided into two major groups. The first group uses dynamic selection of the best reception point according to short-term channel quality. The second category uses joint reception, where several reception points act as a joint receiver with a larger number of antennas. Joint reception is more complex to implement, but it offers larger gains relative to DPS. One of the most important aspects of coordinated uplink reception is the decoupling of the points that transmit downlink control from those that receive uplink data. Important aspects of the implementation pertain to coordination and exchange of information among reception points in terms of selection of reception points, computation of the receive combiner, coordinated scheduling, and exchange of received signal samples (e.g., quantized received signals, locally combined signals, or log-likelihood ratios). These functions are typically centralized in the baseband processing unit connected to the coordinated eNBs via optical fiber links [17].

In uplink coordinated multi-point reception, the UE signals which were previously treated as interference at a reception points, other than the serving node, would become desired signals. Uplink reference signals that are used for channel estimation in the demodulation process of PUSCH are very sensitive to interference. In LTE Rel-8/9/10, the assignment of the pseudo-random base sequences for scrambling the reference signals of a UE was made by a single serving cell. It was possible to assign orthogonal sequences to the UE, whose reference signals were received by the same receiving point, via either different cyclic shifts of the same base sequence or orthogonal cover codes. At the same time, several interference randomization techniques improved the inter-cell interference generated by uncoordinated uplink scheduling assignments across multiple neighboring cells. These randomization techniques include sequence-group hopping, sequence hopping, and different cyclic shifts [1–3]. The opportunity offered by CoMP to receive the UE's signals at one cell when the UE's transmission is intended for another cell created new constraints for assigning orthogonal sequences to the users allocated in overlapping time–frequency resources [17].

LTE Rel-11 introduced new capabilities for configuring reference signal initialization parameters. In particular, the initialization of the pseudo-random sequences is no longer associated with the physical cell identity, but rather is explicitly signaled as a UE-specific virtual cell identity [1]. This enables the assignment of the same base sequence with different cyclic shifts to the UE which is connected to different cells, allowing virtual cells to be created within the coverage area of a macro-cell deployed with RRHs, as in CoMP scenario 4. Furthermore, it is possible to configure the initialization of the cyclic shift hopping in a dedicated manner for each UE, which enables grouping of UEs by orthogonal cover codes across different cells even when these UEs are assigned different base sequences [17].

12.4.4 CSI measurement and feedback in CoMP-enabled networks

A downlink CoMP measurement set is defined as a group of transmission points relative to which the UE measures and reports the CSI. The UE reports may select points for which actual feedback is transmitted. The measurement set typically encompasses cells for which the mobility-management-related measurements are conducted for the purpose of cell selection/reselection and handover. The proper operation of any CoMP scenario depends on the accuracy and timeliness of the CSI measurement and feedback in the network. Some CoMP schemes are more affected by CSI inaccuracy and feedback delays. LTE Rel-11 has specified a general control signaling framework that enables all CoMP schemes to properly operate by enhancing and extending the features that existed in the previous releases. The CoMP measurement set is alternatively defined as a set of CSI-RS resources on which the UE is required to measure and report the CSI that may include rank indicator, precoding matrix index, and channel quality indicator. There is typically a unique correspondence between a CSI-RS resource and a transmission point. As shown in Figure 12.9, the CoMP measurement set is a subset of the CoMP cluster/cooperating set ($S_{\text{measurement-set}} \subset S_{\text{cooperating-set}}$). The size of a CoMP measurement set that can be configured for a UE is limited to three CSI-RS resources in order to reduce the uplink signaling overhead. The UE at different locations may observe different sets of strong-signal transmission points; thus, the configuration of a CoMP measurement set is UE-specific. Due to UE mobility, CoMP measurement sets dynamically change and need to be reconfigured when necessary to ensure optimal CoMP performance. To assist the network in managing the CoMP measurement set of each UE, a CoMP resource management procedure based on CSI-RS measurement has been defined in LTE Rel-11. While the CoMP resource management concept can be applied to all CoMP scenarios, it is particularly useful for CoMP scenario 4 where the transmission points are not identifiable from their transmitted cell-specific reference signals, making it impossible to compare the received signal strengths based on cell-specific reference signals.

The CoMP resource management procedure requires the UE to perform CSI-RS-based received signal quality measurements on a set of CSI-RS resources that are candidates for inclusion in the CoMP measurement set. The set of CSI-RS resources explicitly configured by the network for CoMP resource management is called the CoMP resource management set. The latter set can be configured independently of the CoMP measurement set [17]. The measurement of CSI-RS received power is similar to that defined for RSRP measurement on cell-specific reference signals. Nevertheless, there are some differences between the two types of measurements. The UE is only required to conduct measurement on CSI-RS resources in the CoMP resource management set. Therefore, the UE does not autonomously detect CSI-RS resources, resulting in reduced UE operational complexity. The CoMP resource management measurement/reporting is event-driven and the triggers can be either absolute, i.e., a measurement report is triggered

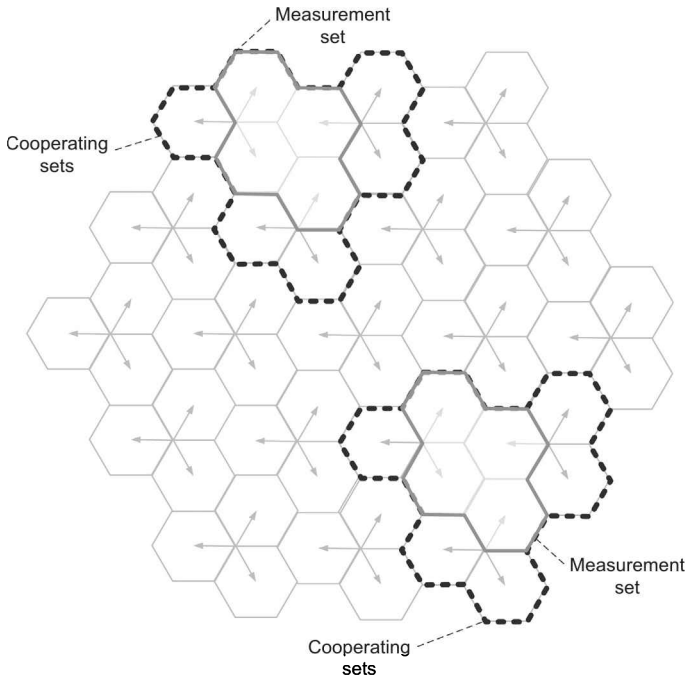


FIGURE 12.9

Example illustration of cooperating and measurement sets.

when the received signal power goes beyond an absolute threshold, or relative, i.e., the received signal power is compared to that of another CSI-RS resource.

To ensure the CSI-RS received power measurement is immune to interference and to ensure the accuracy of the measurement, the network can mute the transmissions on the resource elements from the neighboring TPs that correspond to the CSI-RS resource elements of the transmission point being measured. When performing CSI-RS received power measurements, the UE may assume that the timing of the received CSI-RS is the same as that derived from the primary and secondary synchronization signals of the serving cell. This allows the UE to use a single timing derived from the synchronization signals of the serving cell to receive CSI-RS that might be transmitted from a different TP. While this simplifies UE implementation, the impact on the accuracy of CSI-RS received power depends on the extent of the timing error. Studies suggest that there is no significant impact on CSI-RS measurement provided that a timing error is limited to ± 3 ms [17,21,27].

Since a UE needs to measure CSI-RS to generate CSI feedback and receive UE-specific reference signals to coherently demodulate PDSCH, it is imperative that the CSI-RS and DM-RS are transmitted such that the interference among the reference signals of multiple TPs is sufficiently randomized. LTE Rel-10

addresses this requirement by defining unique initialization seeds for generating the scrambling sequences of each transmission point/cell's reference signals based on the physical cell identity. This approach may not work for CoMP scenario 4 since multiple TPs share the same cell identity. In order to provide sufficient interference randomization, LTE Rel-11 replaced the use of the physical cell identifier for initialization of the scrambling sequences with a virtual cell identifier, which is signaled to the UE using higher layer signaling, allowing flexible deployment of transmission points in CoMP scenario 4, and providing sufficient interference randomization for DM-RS and CSI-RS. In the case of CSI-RS, the interference among CSI-RSs of different TPs is further reduced by allocating different time or frequency resources for CSI-RS transmissions. The use of a virtual cell identifier provides interference randomization when the same time and frequency resources are used across different cells for CSI-RS transmissions [1].

The feedback scheme for CoMP in LTE Rel-11 is defined per CSI-RS resource, where the UE reports the CSI individually for multiple CSI-RS resources. Note that each CSI-RS resource is transmitted from one transmission point. As a result, when the UE is configured with multiple CSI-RS resources and performs per CSI-RS resource feedback, it reports individual CSIs for each of the TPs transmitting the configured CSI-RS resources. There is at least one feedback process associated with each CSI-RS resource within the CoMP measurement set. Each feedback process provides the eNB with the measured CSI (measured on a particular CSI-RS resource). The CSI feedback can be configured to be periodically reported, or scheduled for aperiodic reporting. For CS/CB, separate CSI feedback for at least two TPs can be configured where one of the processes would be used for reporting the CSI for the serving TP, and the other(s) can be used for reporting the CSI associated with the interfering TP(s). Similarly, for a dynamic point switching scheme, multiple CSI feedback processes can be configured, allowing the network to dynamically switch the transmitting TPs. The above feedback mechanism can also support other CoMP schemes including non-coherent JT, where precoding is applied individually to the transmit antennas belonging to each TP, and coherent JT in a non-standardized form by aggregating multiple TPs under a single CSI-RS resource.

The reader's attention is drawn to the fact that there are two types of feedback in general to support CoMP operation, as follows:

1. Explicit feedback which is characterized by having a channel part and a noise-and-interference part. The channel part includes reports for each point in the UE's measurement set that is reported in a given subframe that contains one or several channel properties. The channel properties include instantaneous channel matrix either in the form of full matrix or main eigen component(s) of the channel matrix; and transmit channel covariance either in the form of full covariance matrix or main eigen component(s) of the channel covariance matrix. Inter-point channel properties may also be reported including a noise-and-interference part, total interference received power, total received signal covariance matrix, and covariance matrix of the noise and interference.

2. Implicit feedback is based on certain hypotheses at the UE, and the feedback is generated depending on the operation scheme, e.g., SU-MIMO/MU-MIMO, single cell/point or coordinated transmission, and single-point CS/CB or multi-point (JP) transmission. Under this category, other forms of feedback may be considered such as precoding matrix index (PMI) with fine quantization granularity, wideband/subband PMI, and channel quality indicator (CQI). Note that CQI only accounts for interference outside the CoMP measurement set or relative received power between CoMP transmission points.

LTE Rel-11 does not specify any standardized support for coherent JT. Another important feature that has been included in LTE Rel-11 to support CoMP is the interference measurement resource (IMR), which is a set of resource elements where a UE can be configured to measure interference. Prior to LTE Rel-11, interference measurement was mainly implementation-specific and based on cell-specific reference signals. Such interference measurement schemes may not be applicable to CoMP because in CoMP scenario 4, multiple TPs may share a common cell identity. In that case, TPs within a cell are not distinguishable since they are transmitting the same cell-specific reference signals. Moreover, the interference measured using cell-specific reference signals does not allow the network to adaptively control the interference measured by the UE. As an example, if the effect of a particular TP shutdown is desired, the network can configure two separate IMRs for two feedback processes. One of the IMRs would capture the interference with the TP turned off, while the other the IMR would capture the interference with the TP turned on. The configuration of the IMR is done on a per-UE basis via higher layer signaling. Depending on the measurement reports from the UE, the network can determine which transmission points should be added to, removed from, or replaced in the CoMP measurement set in order to select the set of transmission points with the strongest signal measured at the UE [3].

12.5 Effects of X2 latency on CoMP performance

The X2 latency is defined as the accumulation of the time needed to send a message across the X2 interface, as well as the required time to process the X2 message in the eNB [20,30]. The non-zero X2-latency affects HARQ ACK/NACK round trip time and the CSI feedback delay. The HARQ ACK/NACK round trip time is defined as the time interval between the first transmission of PDSCH using a HARQ process identifier and the earliest retransmission/fresh transmission using the same HARQ process identifier. The CSI feedback delay is the time interval between the CQI measurement period at the UE and the next downlink data transmission from the eNB that is based on the knowledge of this CQI. Since both CQI as well as HARQ information need to be transmitted from the serving cells to the master cell of a cluster across the X2 interface, the X2 delay impacts

both HARQ delay as well as CQI delay. The ACK/NACK delay determines the number of HARQ processes that are needed to guarantee continuous transmission (efficient channel utilization), if the mobile station is scheduled all the time. Therefore, the impact of long HARQ ACK/NACK delays is important for low to medium cell loads. In highly loaded cells, the number of required HARQ processes decreases, since each mobile station attains less access to the channel. This impact is therefore dependent on the cell load. Due to the increased CQI delay, the CQI contains less information about the channel at the time when it is accessed. This means that it becomes more difficult to adapt the MCS and other transmission parameters to the instantaneous channel conditions.

In order to investigate the effect of X2 latency on the inter-eNB JT CoMP operation, let us assume that a sufficient number of HARQ processes are available such that the impact of the X2 delay on the HARQ ACK/NACK delay can be neglected. This is ensured by setting the number of available HARQ processes to infinity. To investigate the impact of X2 latency on CQI delay, X2 delays of 0, 1, 3, 5, 10, 15, and 20 ms were simulated. Figure 12.10 shows the loss in average user throughput for various X2 delays relative to an ideal interface with zero delay. The losses are given for the 5th, 50th, and 95th percentile of the cumulative distribution function (CDF) of average user throughput without X2 delay. It can be seen that the losses become larger with increasing values of X2 delay. This indicates that inter-eNB JT CoMP is very sensitive to X2 delay.

12.6 Performance of CoMP scenarios

The performance of intra-eNB CoMP techniques has been extensively studied and evaluated in 3GPP and documented in Ref. [5] as part of the CoMP feasibility studies. The detailed simulation assumptions and simulation models used in this evaluation are described in 3GPP TR 36.814 and TR 36.819 [4,5]. The evaluations were conducted by various sources in the following deployment scenarios [31,32]:

1. Scenario 1: Homogeneous network with intra-site CoMP.
2. Scenario 2: Homogeneous network with high transmit-power RRHs.
3. Scenario 3: Heterogeneous network with low-power RRHs within the macro-cell coverage, where transmission/reception points are identified by different cell IDs.
4. Scenario 4: Heterogeneous network with low-power RRHs within the macro-cell coverage where the transmission/reception points created by the RRHs have the same cell IDs as the macro-cell.

Despite the fact that there was a detailed evaluation methodology that was used by all companies participating in the evaluations, there were discrepancies in the reported results among sources because they used different assumptions concerning (unspecified parameters) channel estimation error modeling, channel reciprocity modeling, the feedback/SRS mechanisms, scheduling algorithm, and the

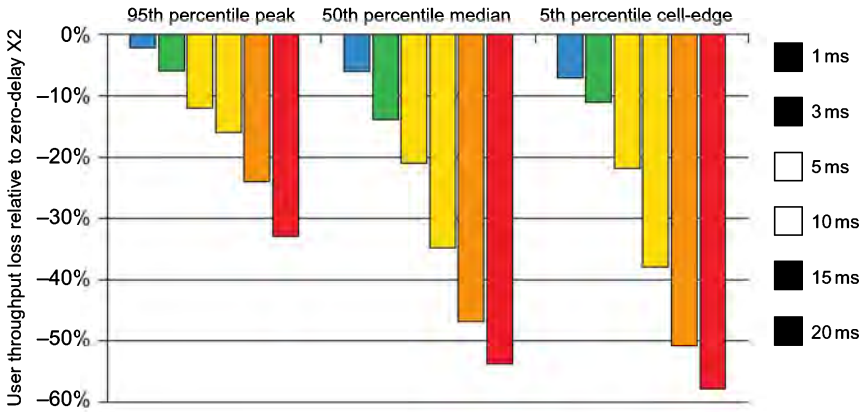


FIGURE 12.10

Impact of X2 latency on user throughput using inter-eNB JT CoMP scheme [15,22].

receiver architecture. In the full-buffer/non-full-buffer evaluations, cell average spectral efficiency in bits/s/Hz/cell and 5% user spectral efficiency in bits/s/Hz/user were evaluated and reported. The user spectral efficiency is defined as the amount of data (file size) per time needed to download data per occupied bandwidth. The time needed to download the data starts when the packet is received in the transmit buffer, and ends when the last bit of the packet is correctly delivered to the receiver. The serving cell spectral efficiency represents the total amount of data for all users during the entire observation time per the number of cells and per occupied bandwidth.

It was observed from the evaluation results for scenarios 1 and 2 that in the downlink, CoMP schemes offer performance gains in homogeneous networks. In the uplink, considerable gain is achievable with a CoMP JR scheme in scenarios 1 and 2. The results were obtained based on ideal and realistic assumptions. It was concluded from the evaluation results in scenarios 3 and 4 that CoMP can provide performance benefits in heterogeneous networks both with full-buffer and FTP traffic models. Based on the evaluation results on the impact of backhaul constraints (capacity/latency), it was concluded that the performance of CoMP schemes relying on spatial information exchange is sensitive to the delay between two transmission points; however, the level of sensitivity depends on the CoMP scheme.

The macro-cell area average spectral efficiency in Figure 12.11 is defined as the sum of cell throughputs in the macro-cell area, which also includes pico-cells/RRHs deployed in the macro-cell area. The results of evaluations show that performance gains can be achieved using CoMP compared to the traditional single-cell schemes in both homogeneous and heterogeneous networks. CoMP performance gains are noted for UEs severely affected by interference. These UEs are typically found at the cell-edges in homogeneous networks. In general, JT CoMP

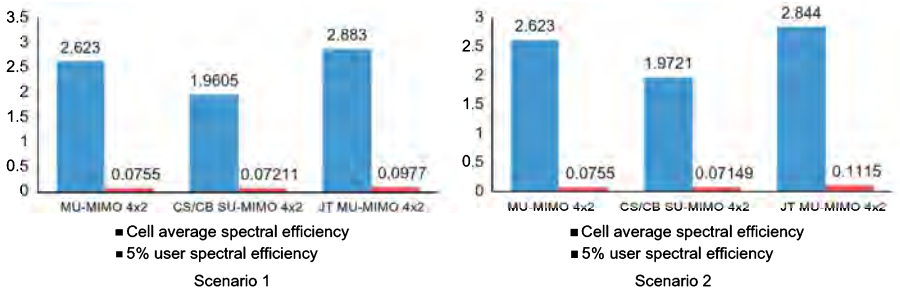


FIGURE 12.11

Comparison of the absolute performance downlink MU-MIMO, CS/CB SU-MIMO, and JT MU-MIMO (FDD, full-buffer, 3GPP spatial channel model, cross-polarized antennas) [4,5].

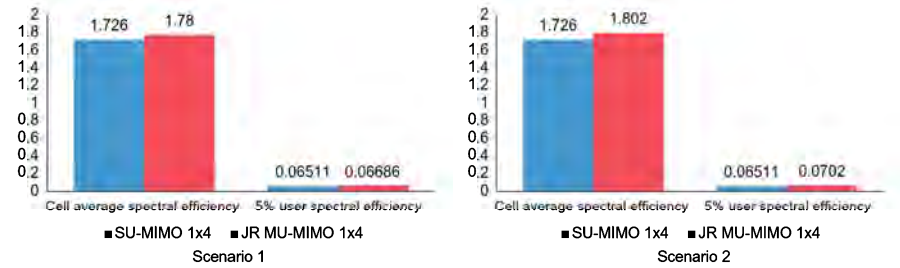


FIGURE 12.12

Comparison of the absolute performance uplink SU-MIMO and JR MU-MIMO (FDD, full-buffer, 3GPP spatial channel model, cross-polarized antennas) [4,5].

techniques provide larger performance gains relative to CS/CB CoMP schemes, but at the expense of larger backhaul overheads and more stringent requirements on backhaul capacity and latency (see Figure 12.11). These observations suggest that CoMP techniques are a promising trend for LTE-Advanced networks. CoMP will thereby contribute to providing the end users with a more consistent experience of mobile broadband across the network coverage areas (Figure 12.12).

The relative performance gains of CoMP scenarios 3 and 4 over HetNet with and without enhanced ICIC (eICIC) were evaluated and are shown in Figure 12.13.

The impact of lower capacity/higher latency links connecting the transmission points was also investigated. The evaluation results were obtained for CoMP in a homogeneous network [5]. Figure 12.14 shows the evaluation results for SU-MIMO CS/CB and MU-MIMO JT CoMP schemes with varying levels of backhaul delay. The CSI feedback delay is assumed to be 5 ms. The results suggest that the JT CoMP scheme demonstrates larger performance variation, and is more sensitive to backhaul delays compared to the CS/CB CoMP scheme.

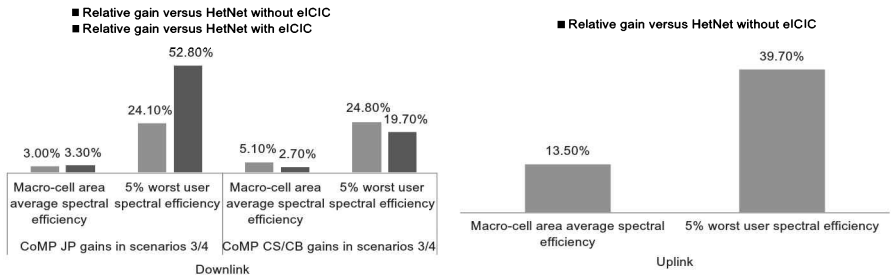


FIGURE 12.13

Relative performance gain of downlink/uplink CoMP in scenarios 3/4 (FDD, full-buffer, configuration 1) [4,5].

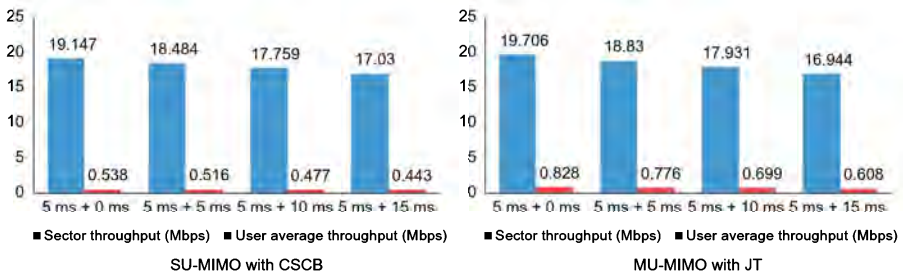


FIGURE 12.14

Effect of CSI feedback delay + backhaul delay on sector and user average throughput [4,5].

References

3GPP Specifications

[1] 3GPP TS 36.211, Evolved Universal Terrestrial Radio Access (E-UTRA); Physical Channels and Modulation (Release 11), December 2012.
[2] 3GPP TS 36.212, Evolved Universal Terrestrial Radio Access (E-UTRA); Multiplexing and Channel Coding (Release 11), December 2012.
[3] 3GPP TS 36.213, Evolved Universal Terrestrial Radio Access (E-UTRA); Physical Layer Procedures (Release 11), December 2012.
[4] 3GPP TR 36.814, Further Advancements for E-UTRA; Physical Layer Aspects (Release 9), March 2010.
[5] 3GPP TR 36.819, Coordinated Multi-point Operation for LTE Physical Layer Aspects (Release 11), December 2011.
[6] 3GPP TS 36.420, X2 General Aspects and Principles (Release 11), September 2012.
[7] 3GPP TS 36.423, X2 Application Protocol (X2AP) (Release 11), December 2012.

Books

[8] Y. Zhang, H. Hu, J. Luo, Distributed Antenna Systems: Open Architecture for Future Wireless Communications, Auerbach Publications, June 2007.

Articles

[9] A.M. Saleh, A.J. Rustako, R.S. Roman, Distributed antennas for indoor radio communications, IEEE Trans. Commun. 35 (December 1987).

[10] The distributed antenna systems forum. <http://thedasforum.org>.

[11] B. Chow, et al., Radio-over-fiber distributed antenna system for WiMAX bullet train field trial, IEEE Mobile WiMAX Symposium, California, USA, July 2009.

[12] Distributed antenna systems. <http://www.alino.com/Info/DistributedAntennaSystems/das.htm>.

[13] Jiwon Kang, Bin-Chul Ihm, Wookbong Lee, Distributed antenna system for future 802.16, LG Electronics, IEEE C802.16-10/0018, March 2010.

[14] Distributed antenna systems. <http://en.wikipedia.org/wiki/Distributed_Antenna_System>.

[15] S. Brueck, et al., Centralized scheduling for joint transmission coordinated multipoint in LTE-Advanced, International ITG Workshop on Smart Antennas (WSA 2010), 2010.

[16] O. Simeone, Distributed Antenna Systems: Open Architecture for Future Wireless Communications, New Jersey Institute of Technology, August 2006.

[17] J. Lee, et al., Coordinated multipoint transmission and reception in LTE-Advanced systems, IEEE Commun. Mag. (November 2012).

[18] S. Firouzabadi, A. Goldsmith, Downlink Performance and Capacity of Distributed Antenna Systems, Stanford University, September 2011.

[19] W. Choi, et al., Downlink performance and capacity of distributed antenna systems in a multi-cell environment, IEEE Trans. Wireless Commun. 6 (1) (January 2007).

[20] J. Robson, Guidelines for LTE backhaul traffic estimation, NGMN White Paper, NGMN Alliance, July 2011.

[21] R. Irmer, et al., Coordinated multipoint: concepts, performance, and field trial results, IEEE Commun. Mag. (February 2011).

[22] White Paper, Backhauling X2, Cambridge Broadband Networks Limited.

[23] P. Komulainen, M. Boldi, D1.4 initial report on advanced multiple antenna systems, wireless world initiative new radio—WINNER+. <http://projects.celtic-initiative.org/winner+/deliverables_winnerplus.html>, January 2009.

[24] S. Mayrargue, D1.8 intermediate report on CoMP (Coordinated Multi-Point) and relaying in the framework of CoMP, wireless world initiative new radio—WINNER+. <http://projects.celtic-initiative.org/winner+/deliverables_winnerplus.html>, January 2010.

[25] A. Osseiran, D2.2 enabling techniques for LTE-A and beyond, wireless world initiative new radio—WINNER+. <http://projects.celtic-initiative.org/winner+/deliverables_winnerplus.html>, July 2010.

[26] A. Tyrrell, H. Schöneich, Definitions and architecture requirements for supporting interference exploitation techniques, advanced radio interface technologies for 4G systems ARTIST4G. <https://ict-artist4g.eu/projet/deliverables>, August 2010.

[27] D. Lee, et al., Coordinated multipoint transmission and reception in lte-advanced: deployment scenarios and operational challenges, IEEE Commun. Mag. (February 2012).
[28] Wolfram MathWorld, Central limit theorem. <http://mathworld.wolfram.com/CentralLimitTheorem.html>.
[29] Common public radio interface (CPRI). <http://www.cpri.info/>.
[30] 3GPP R1-111174, Backhaul Modeling for CoMP, Orange, Telefónica, February 2011.
[31] 3GPP R1-111944, Phase 1 CoMP simulation evaluation results and analysis for full buffer, LG Electronics, May 2011.
[32] 3GPP R1-111944, Phase 1 CoMP results, Samsung, May 2011.
[33] Y.H. Nam, et al., Evolution of reference signals for LTE-advanced systems, IEEE Commun. Mag. 50 (2) (February 2012).
[34] S. Brueck, Backhaul Requirements for Centralized and Distributed Cooperation Techniques, ITG Heidelberg, July 2010. <http://www.ikr.uni-stuttgart.de/Content/itg/fg524/Meetings/2010-07-08-Heidelberg/index.html>.
[35] P. Marsch, S. Khattak, G. Fettweis, A framework for determining realistic capacity bounds for distributed antenna systems, Proceedings of the IEEE Information Theory Workshop, Chengdu, China, October 2006.
[36] K.M. Karakayli, G.J. Foschini, R.A. Valenzuela., Network coordination for spectrally efficient communications in cellular systems, IEEE Wireless Commun. 13 (4) (August 2006).
[37] P. Marsch, G. Fettweis, On multi-cell cooperative transmission in backhaul-constrained cellular systems, Ann. Télécomm. 63 (5–6) (May 2008).
[38] V. Jungnickel, et al., Interference aware scheduling in the multiuser MIMO-OFDM downlink, IEEE Commun. Mag. 47 (6) (June 2009).
[39] V. Jungnickel, et al., Field trials using coordinated multi-point transmission in the downlink, Third IEEE International Workshop on Wireless Distributed Networks, IEEE PIMRC, September 2010.
[40] P. Marsch, Coordinated Multi-Point Under a Constrained Backhaul and Imperfect Channel Knowledge, PhD thesis, Technische Universitat Dresden, March 2010.
[41] A. Müller, P. Frank, Cooperative interference prediction for enhanced link adaptation in the 3GPP LTE uplink, IEEE VTC, Spring 2010.
[42] A.Müller, P.Frank, Performance of the LTE uplink with intra-site joint detection and joint link adaptation, IEEE VTC, Spring 2010.
[43] M. Grieger, et al., Field trial results for a coordinated multi-point (CoMP) uplink in cellular systems, Proceedings of the ITG/IEEE Workshop on Smart Antennas, Bremen, Germany, February 2010.
[44] V. Kotzsch, G. Fettweis, Interference analysis in time and frequency asynchronous network MIMO OFDM systems, IEEE WCNC 2010, Sydney, Australia, April 2010.
[45] J. Giese, M.A. Awais, Performance upper bounds for coordinated beam selection in LTE-advanced, Proceedings of the ITG/IEEE Workshop on Smart Antennas, Bremen, Germany, February 2010.
[46] G. Fettweis et al., Field trial results for LTE-advanced concepts, Proceedings of the IEEE ICASSP, Dallas, TX, March 2010.
[47] L. Thiele, V. Jungnickel, T. Haustein, Interference management for future cellular OFDMA systems using coordinated multi-point transmission, IEICE Trans. Commun. (December 2010) Special issue on wireless distributed networks.

This page intentionally left blank

CHAPTER

Carrier Aggregation 13

CHAPTER CONTENTS

13.1 Principles of carrier aggregation 986
13.2 Deployment scenarios 990
13.3 Physical and MAC layer aspects of carrier aggregation 992
13.3.1 Physical layer aspects 992
13.3.2 MAC layer aspects 999
13.4 Protocol and signaling aspects of carrier aggregation 1002
13.5 Radio resource management aspects of carrier aggregation 1005
13.6 RF and implementation aspects of carrier aggregation 1006
13.6.1 Temporal/spectral masks and unwanted emissions 1008
13.6.2 Operating bands for carrier aggregation 1010
13.6.3 Transmitter characteristics for carrier aggregation 1016
13.6.4 Receiver characteristics for carrier aggregation 1022
References 1027

LTE Rel-8/9 specified system bandwidths of 1.4, 3, 5, 10, 15, and 20 MHz to meet different spectrum and deployment requirements. Support of wider bandwidths up to 100 MHz was one of the distinctive features of IMT-Advanced systems. The IMT-Advanced systems targeted peak data rates in excess of 1 Gbps for low mobility and 100 Mbps for high mobility scenarios [32,33]. In order to support wider transmission bandwidths, LTE Rel-10 introduced the carrier aggregation concept, where two or more component carriers with arbitrary bandwidths belonging to the same or different frequency bands could be aggregated. The support of system bandwidths up to 100 MHz would allow a substantial increase in link-level peak data rate, as well as in the system capacity and user throughput. Another advantage of carrier aggregation is to allow efficient use of fragmented spectrum in the form of a virtually wideband spectrum. The fragmented spectrum may belong to the same or different frequency bands and may be of different bandwidths. LTE Rel-11 further extended the advantages of carrier

LTE-Advanced.

© 2014 Elsevier Inc. All rights reserved.

Ex.1005.01016

aggregation by configuring extended carriers and carrier segments. Furthermore, carrier aggregation can be used to mitigate inter-cell interference in heterogeneous networks [30,31].

Using the carrier aggregation scheme, it would be possible to simultaneously schedule a user on multiple component carriers for downlink or uplink data transmission, resulting in some challenges in resource scheduling and load balancing across the network. In a non-contiguous inter-band carrier aggregation scenario, where the aggregated carriers belong to different frequency bands, the fading characteristics might be different between component carriers; as a result, the coverage may vary significantly from one carrier to another. At different locations in the cell, some users may only be scheduled on fewer carriers, while other users may have access to the entire carrier set, which may have a negative impact on sustained user throughput within the coverage area of an eNB.

To allow smooth network migration and upgrades to new releases, it was essential to ensure backward compatibility of LTE-Advanced with LTE Rel-8/9, as well as to support mixed operation of the legacy LTE systems and LTE Rel-10 on the same carrier in an operator's network. LTE Rel-10 carrier aggregation satisfied this requirement by configuring each component carrier in a backward compatible manner with LTE Rel-8/9, and by further supporting at least one of the bandwidths compatible with LTE Rel-8/9. The backward compatibility implies that the complete set of LTE Rel-8/9 downlink physical channels and signals are transmitted on each component carrier using LTE Rel-8/9 signaling procedures, including broadcast channel, synchronization signals, reference signals, and control channels. This would also allow reuse of the LTE Rel-8/9 RF designs and implementations at the eNB and the UE. Although we will primarily focus on carrier aggregation for FDD systems, carrier aggregation is fully supported in the TDD systems, as well.

In this chapter, we will take a pragmatic and systematic approach to describe carrier aggregation principles and its impact on different protocol layers. Various aspects of carrier aggregation including deployment scenarios, physical and MAC layer support, as well as higher-layer signaling and RF transceiver design challenges, will be discussed and examples will be provided.

13.1 Principles of carrier aggregation

In LTE-Advanced carrier aggregation terminology, a component carrier is often referred to as a serving cell, is assigned its own cell identifier, and is managed as a serving cell by the higher layers. Each individual RF carrier is known as a component carrier. A component carrier can be downlink and uplink or downlink only, but it cannot be an uplink-only RF carrier for obvious reasons. The number of downlink component carriers may be different than that of the

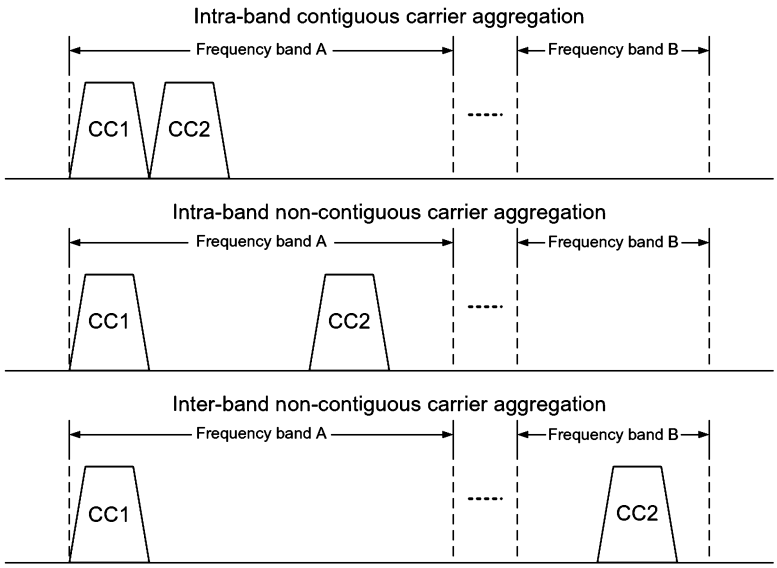


FIGURE 13.1

Carrier aggregation scenarios [16,18,20].

uplink. In general, a different number of component carriers can be aggregated for the downlink and uplink. The UE may support carrier aggregation only in the downlink or in both directions. Up to five component carriers, possibly each with different bandwidth can be aggregated, allowing transmission bandwidths of up to 100 MHz [12,14]. In FDD systems, a serving cell comprises a pair of different carrier frequencies for downlink and uplink transmissions, whereas for TDD, a serving cell is defined as a single-carrier frequency where downlink and uplink transmissions occur in different transmission time intervals. Given that component carriers do not have to be contiguous in frequency which enables utilization of fragmented spectrum, operators with a fragmented spectrum can provide high data-rate services based on the availability of a virtually wide bandwidth even though they do not own a single wideband spectrum allocation.

Each UE has a single serving cell that provides all necessary control information and functions, such as non-access stratum mobility information, security establishment, RRC connection establishment/reconfiguration, etc. This serving cell is referred to as the primary cell (PCell). Other auxiliary cells or component carriers are referred to as secondary cells (SCells).

As shown in Figure 13.1, there are three different carrier aggregation scenarios, as follows [11]:

1. Intra-band contiguous carrier aggregation: This type of carrier aggregation uses a single frequency band. It is the simplest form of carrier aggregation from an implementation point of view. In this scenario, the

carriers are contiguous and the frequency spacing between center frequencies of contiguously aggregated RF carriers is a multiple of 300 kHz in order to be compatible with the 100 kHz frequency raster of LTE Rel-8/9 and preserve orthogonality of the subcarriers with 15 kHz spacing.

2. Intra-band non-contiguous carrier aggregation: In this scenario, the aggregated carriers are not adjacent and the multi-carrier signal cannot be treated as a single signal; therefore, two transceivers may be required. This adds significant complexity particularly to the UE where form-factor, power consumption, and cost are the major concerns.
3. Inter-band non-contiguous: This type of carrier aggregation uses different frequency bands which might be appealing to network operators due to the possibility of using fragmented frequency bands. In this scenario, the UE may have to use multiple transceivers, having unavoidable impact on cost, performance, and power consumption. In addition, there are also further complexities resulting from the requirements to reduce intermodulation and cross-modulation impairments created by the transceivers. This type of carrier aggregation may improve mobility by exploiting radio propagation characteristics of different bands.

An enhanced carrier aggregation work item was approved for LTE Rel-11, where as part of that work item, new non-backward-compatible partially configured carrier types could be defined for LTE Rel-11 and beyond to address the ever-increasing demand for higher capacity and higher data rates in cellular networks [19]. The new carrier types are going to be useful in practical deployments where the size of the available frequency block does not match the provisioned bandwidths of 1.4, 3, 5, 10, 15, and 20 MHz in LTE Rel-8/9. If the size of the frequency block is smaller than 5 MHz (corresponding to 25 resource blocks), the number of resources on the carrier segment or extension carrier may not be adequate to efficiently transmit user data and synchronization signals, broadcast and control channels. Although it is desirable to reduce the overhead of the new carrier types (i.e., extension carrier and carrier segment), in practical deployment scenarios, if the frequency gap between the reference carrier and the extension/segment carrier is excessively large, the time and frequency synchronization and slot/subframe alignment of the carriers in a carrier set may not be maintained without including synchronization signals on the extension carrier/carrier segments.

Any fully configured backward compatible carrier in a carrier set may be extended by an extension carrier or appended by segment carriers. The design of the new carrier types has been required to support the operation in the following scenarios, but not necessarily equally optimized for both cases:

- Synchronized carriers: The base carrier and the new carrier types are synchronized in time and frequency to the extent that no separate synchronization is needed in the receiver.

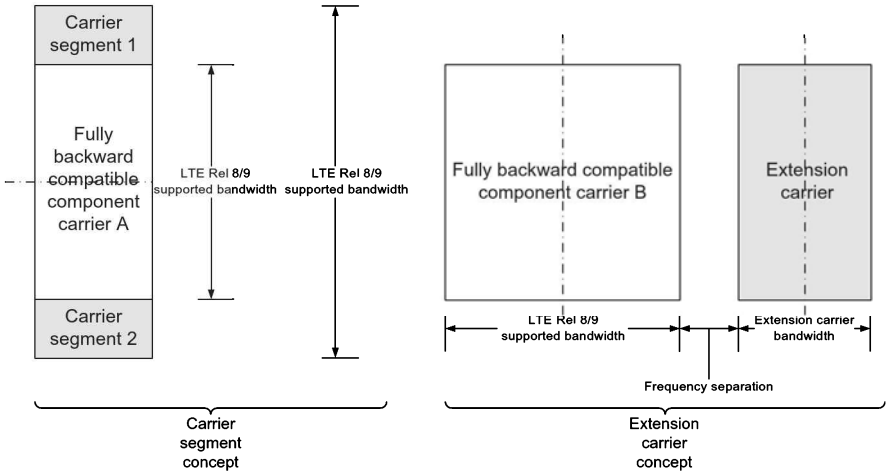


FIGURE 13.2

Illustration of the carrier segments and extension carriers [15].

- Unsynchronized carriers: The base carrier and the new carrier types are not synchronized with the same degree of accuracy as the synchronized carriers.

Note that synchronization is considered from the perspective of the UE receiver. Energy efficiency, flexible spectrum usage, heterogeneous network deployments, and machine type communications were identified as key objectives for the enhanced carrier aggregation project in 3GPP [19]. The considerations for the design of the additional carrier types that could assist in addressing the above goals mainly focused on operation with no cell-specific reference signals, enhanced control signaling with self-contained reference signals, and configurability of synchronization and other reference signal types when needed.

The new carrier types are defined as follows [15]:

- Carrier segment: The carrier segments are defined as the bandwidth extensions of an LTE Rel-8 compatible component carrier, provided that the total number of resource blocks is limited to 110. The combined RF carrier (i.e., LTE Rel-8 RF carrier + carrier segments as shown in Figure 13.2) utilizes the same backward compatible mechanisms of accessing the additional resources on the carrier segments as well as the base RF carrier. As an example, if two 2.5 MHz carrier segments are combined with a 5 MHz LTE Rel-8 RF carrier, the resulting 10 MHz RF carrier is going to be utilized as a 10 MHz LTE Rel-8 RF carrier. The use of carrier segments in the above manner would allow more efficient utilization of small fragments of spectrum without having to transmit additional overhead due to synchronization, broadcast, and control channels on the carrier

segments. The notion of carrier segment allows for aggregation of additional resource blocks to a component carrier, while still retaining the backward compatibility of the original carrier, Note that carrier segments are always adjacent and linked to one component carrier and cannot be used as stand-alone. They do not provide synchronization signals, system information, or paging, and therefore cannot be used for random access or camping. They support the same HARQ process and transmission mode as the component carrier to which they are linked.

- Extension carrier: The extension carrier is a carrier that cannot be operated as a single stand-alone RF carrier and must be part of a component carrier set where at least one of the carriers in the set is a stand-alone backward compatible component carrier. Depending on whether the extension carriers are adjacent or non-adjacent to a component carrier carrying synchronization signals, the extension carrier may or may not be required to carry synchronization signals. If the extension carrier does not carry the synchronization signals, then it must be located close to a component carrier with synchronization signals for reliable synchronization. No legacy control channel PDCCH, PHICH, PCFICH, and no cell-specific reference signals is another possible configuration for the extension carriers which allows reduced overhead and more efficient use of radio resources on that carrier. The extension carrier supports a separate HARQ process, PDCCH, and transmission mode, which is configured from its linked component carrier.

13.2 Deployment scenarios

Carrier aggregation enables various network deployments. In general, carrier aggregation is used to improve data rates for users within overlapped areas of the cells (cell boundaries). However, carrier aggregation can also be used to mitigate inter-cell interference in heterogeneous networks (see Chapter 14). The following network deployment scenarios were considered during the development of LTE-Advanced. Although exemplified with two component carriers at frequencies f_{c_1} and f_{c_2} as shown in Figure 13.3, the concept can be generalized to any number of component carriers [7,22,23,29]:

- Deployment Scenario 1: In this case, cells with carrier frequencies f_{c_1} and f_{c_2} are (geographically) collocated, and their coverage is overlaid with f_{c_1} and f_{c_2} in the same frequency band. They provide approximately the same coverage due to similar path loss characteristics within the same band. This carrier aggregation scenario achieves higher data rates throughout the cell where both layers provide sufficient coverage and mobility. An example scenario is the case where $f_{c_1} = 2000$ MHz and $f_{c_2} = 800$ MHz are of the same band where aggregation is possible between the overlaid cells.

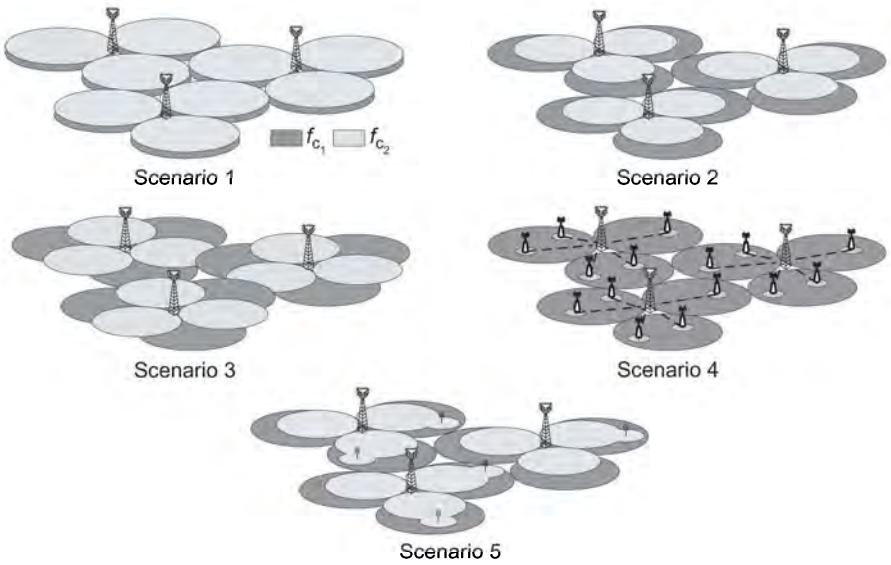


FIGURE 13.3

Carrier aggregation deployment scenarios [7].

- Deployment Scenario 2: In this case, the cells with carrier frequencies f_{c_1} and f_{c_2} are collocated and overlaid with f_{c_1} and f_{c_2} in different frequency bands. Different coverage is provided on different carriers due to the larger path loss in the higher frequency band. Mobility is typically supported on the carrier in the lower frequency band which further provides sufficient coverage. The carrier in the higher frequency band is used to improve data rates and throughput. The cells f_{c_1} and f_{c_2} are collocated and overlaid, but f_{c_2} has smaller coverage due to larger path loss. In other words, only f_{c_1} provides sufficient coverage and f_{c_2} is used to improve throughput. An example scenario would be the case where $f_{c_1} = \{800\ \text{MHz}, 2000\ \text{MHz}\}$ and $f_{c_2} = \{3500\ \text{MHz}\}$ where aggregation is possible between the overlaid cells.
- Deployment Scenario 3: In this case, the cells comprising carrier frequencies f_{c_1} and f_{c_2} are collocated with f_{c_1} and f_{c_2} in different frequency bands. The antennas for cells of f_{c_2} are directed to the cell boundaries of f_{c_1} to improve the cell-edge data rates and user throughput. Due to the larger path loss, coverage holes exist for cells in the higher frequency band on which mobility management is typically not performed. The carrier aggregation is supported in areas with overlapping coverage and the mobility is based on f_{c_1} coverage. An example would be the case where $f_{c_1} = \{800\ \text{MHz}, 2000\ \text{MHz}\}$ and $f_{c_2} = \{3500\ \text{MHz}\}$ in which aggregation is possible between the overlaid cells.

- Deployment Scenario 4: In this case the cells associated with carrier frequency f_{c_1} provide macro coverage and remote radio heads (RRHs) corresponding to carrier frequency f_{c_2} are used to improve throughput at hot spots. The mobility is performed based on the cell coverage of frequency f_{c_1}. In this deployment scenario, the carrier frequencies f_{c_1} and f_{c_2} are usually of different bands. The carrier aggregation is applicable to users within the coverage of RRHs and the underlying macro-cells. An example would be the case where $f_{c_1} = \{800$ MHz, 2000 MHz$\}$ corresponds to a larger cell and $f_{c_2} = \{3500$ MHz$\}$ corresponds to smaller cell, in which aggregation is possible between the overlaid cells.
- Deployment Scenario 5: This case is similar to the second scenario where frequency-selective repeaters or distributed antenna systems are additionally deployed to extend the coverage for one of the carrier frequencies. It is expected that f_{c_1} and f_{c_2} cells of the same eNB can be aggregated where coverage overlaps.

13.3 Physical and MAC layer aspects of carrier aggregation

In this section, we discuss the physical and MAC layer aspects of carrier aggregation, and we will particularly focus on the impacts of carrier aggregation on the system operation at the lower protocol layers. Note that scheduling and use of the RF carriers are related to physical and MAC layers, and to a great extent are transparent to the upper layers.

13.3.1 Physical layer aspects

The physical layer is in charge of processing and transmission of data and control signaling between the radio access network and the user device. The LTE-Advanced carrier aggregation feature enables concurrent data transmission on multiple component carriers (up to five), where the transmission schemes are largely inherited from LTE Rel-8/9 data transmission procedures per component carrier, including the multiple access scheme; modulation and coding; and multi-antenna processing. Some additional UE functionalities beyond those of LTE Rel-8/9 are supported in LTE Rel-10, including data transmissions over two clusters of contiguous bandwidth on the same carrier where the data is precoded by a single DFT unit (see Chapter 10 for a description of clustered SC-FDMA), simultaneous transmission of a control channel and a data channel in the PCell (see Chapter 10 for simultaneous PUCCH and PUSCH transmission), and data transmissions from multiple antennas with spatial multiplexing [3–6]. Nevertheless, improving the downlink and uplink control signaling to efficiently support data transmission was the main challenge in the design of LTE-Advanced carrier aggregation [29].

The PDCCH provides information on resource allocation; modulation and coding scheme HARQ; and other parameters for downlink and uplink data transmission on the physical downlink/uplink shared channel. It is possible to configure each component carrier to transmit the PDCCH for scheduling PDSCH/PUSCH on the same carrier frequency and associated linked uplink carrier, where the linkage of the downlink and uplink carriers is conveyed in SIB2 [10]. In addition, the PDCCH on a component carrier can be configured to schedule PDSCH and PUSCH transmissions on other component carriers through a cross-carrier scheduling feature. Cross-carrier scheduling was primarily developed to support heterogeneous networks comprising a combination of macro-eNBs and low-power nodes (e.g., pico-cell, femto-cell, and RRHs) where significant intercell interference may arise when those networks are deployed on the same carrier [30,31]. Since the PDCCH is transmitted across the entire bandwidth of the respective carrier, interference coordination methods based on fractional frequency reuse may not be adequate in reducing the inter-cell interference on the PDCCH. Carrier aggregation can address this issue by configuring the UE connected to different network nodes to receive the PDCCH on different carriers, thereby reducing or even eliminating inter-cell interference on the PDCCH. With cross-carrier scheduling, only one component carrier needs to be protected for the PDCCH transmission, which can be used to allocate resources on other component carriers.

Cross-carrier scheduling enables a PDCCH on a component carrier to be configured in order to schedule PDSCH and PUSCH transmissions on another component carrier using a 3-bit carrier indicator field (CIF) which is inserted at the beginning of the downlink control information (DCI) messages. The carrier aggregation can reduce or even eliminate inter-cell interference on the PDCCH using cross-carrier scheduling. Figure 13.4 shows a hypothetical heterogeneous network scenario where a component carrier at f_1 is used by the macro-cell at full power and by the pico-cells at reduced power; whereas component carrier f_2 is used by the macro-cell at reduced power and by the pico-cells at nominally low power. In this case, cross-carrier scheduling from component carrier f_2 allows inter-cell interference mitigation among the macro- and pico-cells.

Cross-carrier scheduling is also an effective mechanism to schedule data transmissions on carriers of small bandwidth from a carrier with a larger bandwidth, considering that the PDCCH reliability targets are more challenging to achieve on carriers with small bandwidth due to limited frequency diversity gain. The PDCCH search space consists of a set of PDCCH candidates over which the UE performs blind decoding operations to determine whether there is any PDCCH addressed to it in a subframe. A common PDCCH search space is monitored by all UEs only in their respective PCells for receiving system information, paging, power control, and random access-related control information. Each UE also monitors a UE-specific PDCCH search space primarily carrying scheduling grants for downlink and uplink data transmissions. The start of the UE-specific PDCCH search space is a function of the UE's radio network temporary identifier (RNTI).

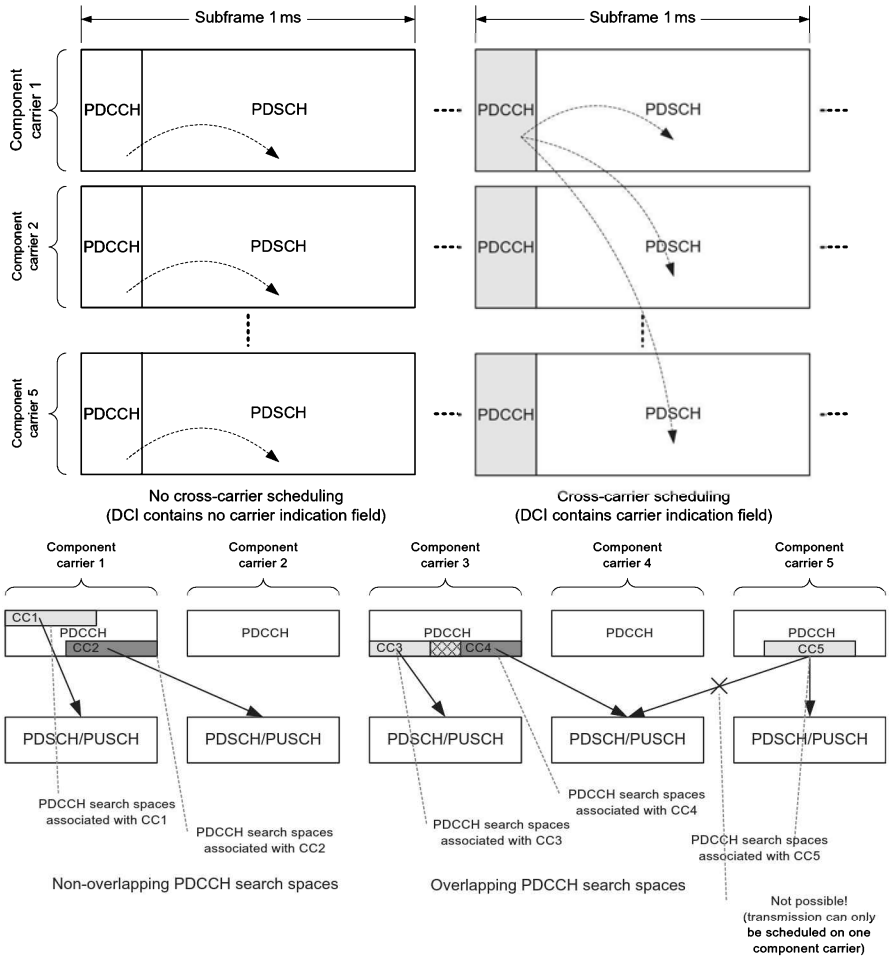


FIGURE 13.4

Illustration of the cross-carrier scheduling concept in carrier aggregation [13,14].

Since the same set of resources for PDCCH transmission is shared by all UEs, a PDCCH for a UE may not be transmitted due to partial overlapping with another PDCCH belonging to a different UE; this condition is referred to as PDCCH blocking. To maintain the PDCCH blocking probability at LTE Rel-8/9 level, an LTE Rel-10/11 UE monitors one UE-specific PDCCH search space for each activated component carrier. For a UE that is not configured with cross-carrier scheduling, the UE-specific PDCCH search space on each component carrier is the same as that in LTE Rel-8/9, whereas for a UE that is configured with cross-carrier scheduling, the UE-specific PDCCH search space is defined by a

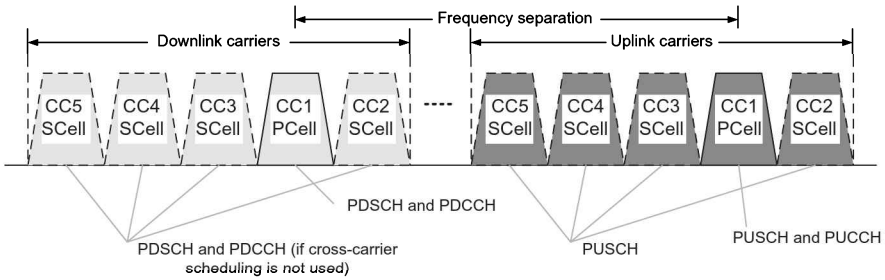


FIGURE 13.5

Symmetric carrier aggregation in the downlink and uplink (example) [16].

combination of the UE's RNTI and the serving cell index. The number of PDCCH blind decoding operations performed by a UE scales (approximately) linearly with the number of its activated component carriers [29]. If carrier aggregation is configured, the maximum number of blind decoding operations that a UE performs is 44 for the PCell plus 32 for each active downlink SCell. An additional 16 blind decodings are needed for each uplink component carrier that is configured for uplink MIMO operation. When cross-carrier scheduling is configured, CIF is only present in the PDCCH messages in the UE-specific search space and not in the common search space [13].

The PDSCH/PUSCH on a component carrier can only be scheduled from one component carrier. Therefore, for each PDSCH/PUSCH component carrier, there is an associated component carrier, configured via UE-specific RRC signaling, where the corresponding DCI can be transmitted. Figure 13.4 illustrates an example, where PDSCH/PUSCH transmissions on component carrier 1 are scheduled using PDCCHs transmitted on component carrier 1. In this case, since cross-carrier scheduling is not used, there is no carrier indicator in the corresponding DCI formats. The PDSCH/PUSCH transmissions on component carrier 2 are cross-carrier scheduled from PDCCHs transmitted on component carrier 1. Therefore, the DCI formats in the UE-specific search space for component carrier 2 include the CIF. Note that the transmissions on a component carrier can be scheduled by the PDCCHs on one component carrier; thus, component carrier 4 cannot be scheduled by PDCCHs on component carrier 5, given that there is a semi-static association between component carriers 3 and 4 for PDCCH transmission in this example [14].

As mentioned earlier, there is one UE-specific search space per aggregation level and component carrier used for PDSCH/PUSCH. This is illustrated in Figure 13.4, where PDSCH/PUSCH transmissions on component carrier 1 are scheduled using PDCCHs transmitted on component carrier 1. There is no CIF in the UE-specific search space for component carrier 1 since cross-carrier scheduling is not used. For component carrier 2, on the other hand, a carrier indicator field exists in the UE-specific search space, given that component carrier 2 is

cross-carrier scheduled from the PDCCHs transmitted on component carrier 1. Search spaces for different component carriers may overlap in some subframes. In Figure 13.4, this happens for the UE-specific search spaces for component carriers 3 and 4. The terminal can identify the two search spaces independently, assuming that a CIF is used for component carrier 4, but is not used for component carrier 3. If the UE-specific and common search spaces corresponding to different component carriers happen to overlap for some aggregation levels when cross-carrier scheduling is configured, the terminal only needs to monitor the common search space. The reason for this is to avoid ambiguities arising from this condition; if the component carriers have different bandwidths, a DCI format in the common search space may have the same payload size as another DCI format in the UE-specific search space corresponding to another component carrier [14].

The PCFICH is transmitted in each subframe and conveys a control format indicator (CFI) field, which indicates the number of OFDM symbols carrying control information in each subframe (up to three OFDM symbols per subframe). The UE derives the starting OFDM symbol used for the PDSCH transmission based on the decoded CFI value. For the PDSCH scheduled by PDCCH on the same component carrier, the UE is required to decode the PCFICH in order to determine the starting OFDM symbol used for the PDSCH. When cross-carrier scheduling is utilized, the starting OFDM symbol for the PDSCH transmission is configured by the network through higher layers, and the UE is not required to decode PCFICH on that component carrier.

The physical HARQ indicator channel carries HARQ feedback (ACK/NACK) information associated with a PUSCH transmission. The PHICH structure in LTE Rel-10/11 carrier aggregation is the same as that for LTE Rel-8/9. The PHICH corresponding to a PUSCH transmission is always transmitted on the component carrier where the PDCCH schedules the PUSCH transmission.

The uplink control information (UCI) includes HARQ feedback corresponding to one or more PDSCHs, channel state information, and scheduling request. Similar to LTE Rel-8/9, the UCI can be transmitted on the PUCCH, if there is no transmission on PUSCH in a subframe, or transmitted on PUSCH, if there is a scheduled transmission on PUSCH. LTE-Advanced further supports simultaneous PUCCH and PUSCH transmissions in a subframe (see Figure 13.6). This allows the eNB to flexibly control the performance of the PUCCH and PUSCH independently and to avoid the UCI overhead on PUSCH by utilizing existing PUCCH resources. The PUCCH can only be transmitted on the PCell, since it typically has more reliable link quality and coverage relative to the SCells (see Figure 13.5). When applicable, UCI is always transmitted on a single PUSCH.

HARQ feedback indicates whether a transport block is correctly received and decoded. LTE Rel-8/9 supports transmitting a maximum of two and four ACK/NACKs in an uplink subframe for FDD and TDD, respectively. Given independent HARQ processes per component carrier, the maximum number of HARQ feedback bits in a subframe in response to PDSCH transmissions can be 10 bits

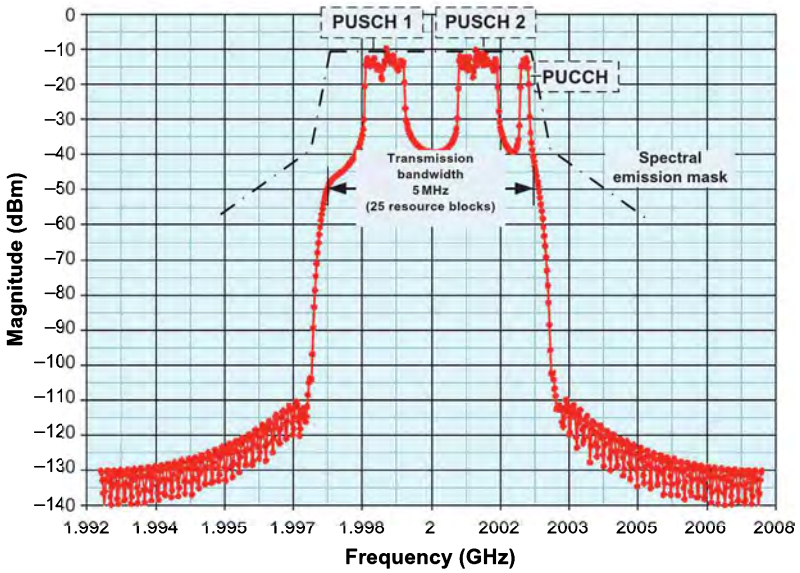


FIGURE 13.6

Snapshot of clustered SC-FDMA (simultaneous PUSCH and PUCCH transmission) in the uplink [17,18].

for FDD and up to 90 bits for TDD (assuming five component carriers with MIMO transmission modes per component carrier and TDD subframe configuration 5). Reliable transmission of large number of HARQ ACK/NACK bits in an uplink subframe requires a substantial amount of resources and sufficiently high signal to interference plus noise ratio. Therefore, HARQ feedback bundling/multiplexing schemes are designed for TDD systems to limit the maximum number of ACK/NACK bits in an uplink subframe to 20. Multiple HARQ feedback bits are bundled by a logical AND operation to produce one HARQ feedback bit per component carrier and per subframe for certain TDD subframe configurations. The PUCCH format 3 was introduced in LTE Rel-10 to support HARQ feedback for a UE configured with downlink carrier aggregation. The PUCCH format 3 uses a SC-FDMA waveform with five SC-FDMA symbols per slot carrying HARQ feedback information and one or two SC-FDMA symbols per slot (depending on the size of the cyclic prefix) for transmission of demodulation reference signals, to enable coherent demodulation of HARQ feedback (see Chapter 10 for more information on PUCCH format 3). An orthogonal cover code of length 5 is applied to the encoded HARQ feedback bits in the corresponding SC-FDMA symbols, allowing multiplexing of up to five UEs in one resource block. Assuming QPSK modulation, k HARQ feedback bits are encoded using the $(32, k)$ Reed–Muller code with circular rate matching into 48 encoded HARQ acknowledgment bits, which are transmitted in a subframe comprising two slots.

LTE-Advanced further supports the HARQ feedback multiplexing scheme for TDD, where two HARQ feedback bits are generated per component carrier, representing the number of consecutively correctly received PDSCHs on the component carrier. PUCCH format 1b can be used to carry four acknowledgments when channel selection is used, i.e., the PUCCH payload carries two acknowledgments and the selection of PUCCH resources carries the other two acknowledgments. The use of bundled acknowledgments in a single uplink subframe is not limited to the TDD duplex mode. The carrier aggregation in FDD with a different number of uplink and downlink component carriers encounters the same problem. In LTE Rel-10, there is only one PUCCH that is always transmitted on the primary component carrier. Hence, even in asymmetric carrier aggregation scenarios, the possibility to transmit more than two HARQ acknowledgment bits in the uplink must be supported. This is performed via resource selection or by using PUCCH format 3. The acknowledgments in response to PUSCH transmissions are transmitted using multiple PHICHs, where the PHICH is transmitted on the same downlink component carrier as the uplink scheduling grant which initiated the uplink transmission.

The channel-state information feedback enables the eNB to perform PDSCH scheduling including resource allocation, MCS selection, transmission rank adaptation, and the choice of precoding matrix. To accommodate different channel conditions and interference levels among different component carriers, CSI is fed back for each component carrier. Both periodic and aperiodic CSI feedbacks are supported in LTE Rel-10/11, where periodic CSI is transmitted on a set of semi-statically configured subframes, and aperiodic CSI is dynamically scheduled by the eNB via the PDCCH. Periodic CSI feedback is independently configured for each component carrier and transmitted on the PUCCH using PUCCH format 2. Since the payload size of PUCCH format 2 is limited, the periodic CSI for only one component carrier can be unconditionally transmitted in a subframe. A priority based on the periodic CSI reporting type determines the component carrier for which periodic CSI is reported in the event that periodic CSI feedback of multiple carriers collide in a subframe. If the collisions involve the same periodic CSI reporting type, the priority is according to ascending cell index. Aperiodic CSI feedback is transmitted on PUSCH and typically carries more CSI bits than periodic CSI feedback. LTE Rel-10/11 supports aperiodic CSI feedback for a single or multiple component carriers in a subframe so that the eNB can balance the CSI accuracy and feedback overhead [29].

Uplink power control is a mechanism to instruct the UEs to determine the PUSCH/PUCCH transmission power with the objective of ensuring that the target reception reliability of that channel is met. The uplink power control supported in LTE Rel-8/9/10 consists of an open-loop component adjusting for the path loss between the UE and its serving eNB, and of a closed-loop component based on transmission power control commands in the PDCCH. The uplink power control processes are independent among the respective activated cells and each process is the same as LTE Rel-8/9. The resulting transmission power for PUSCH or

PUCCH is referred to as nominal transmission power. The key differentiation with respect to the LTE Rel-8/9 uplink power control operation occurs when the sum of the nominal transmission powers from the UE exceeds the total maximum output power for which the UE is configured in a specific subframe. Depending on whether the UE is configured for simultaneous PUCCH and PUSCH transmissions, on the UCI types for transmission, and on the existence of any PUSCH transmission, the UE may transmit in a subframe one PUCCH, one PUSCH with UCI, one or more PUSCH transmissions without UCI, or any other combination. As control information is more important than data information and does not benefit from the use of HARQ, the UE transmission power is distributed by descending priority to the PUCCH, PUSCH with UCI, and PUSCH without UCI, where the nominal transmission power for a channel with higher priority is first guaranteed until the UE total maximum output power is reached. For one or more PUSCH transmissions without UCI, the UE scales each respective nominal PUSCH transmission power by the same factor, considering that the same quality of service for data transmission is required on all component carriers [29].

The eNB may not know the exact UE transmission power due to the possibility of missing power control commands, UE-specific implementation of maximum power reduction (MPR),[1] and additional maximum power reduction (A-MPR)[2] in order to meet regulatory requirements. To provide the eNB with more accurate information on the UEs transmission power, power headroom reporting was supported in LTE Rel-8/9. The UE may report type 1 and/or type 2 power headroom for an activated cell. The type 1 and type 2 power headroom reports indicate the amount of remaining the UEs transmission power beyond those already used for PUSCH, or PUSCH and PUCCH transmission in a subframe, respectively [29].

13.3.2 MAC layer aspects

From the MAC perspective, the carrier aggregation simply provides additional conduits, thus the MAC sublayer plays the role of a multiplexing entity for the aggregated component carriers. Figure 13.7 shows an overview of the downlink

[1]The purpose of MPR is to allow the UE, in some configurations, to lower its maximum output power in order to meet the general requirements on signal quality and out-of-band (OOB) emissions. Note that MPR is an allowance and the UE is not required to use it [13].

[2]The eNB may inform the UE of the possibility of further lowering its maximum power by signaling an additional MPR (A-MPR). The need for an A-MPR occurs with certain combinations of E-UTRA bands, channel bandwidths, and transmission bandwidths for which the UE must meet additional (more stringent) requirements for spectrum emission mask and spurious emissions. As with MPR, the A-MPR is an allowance, not a requirement, and it applies in addition to MPR. Regardless of whether the UE makes use of the allowed MPR and A-MPR, the additional requirements for spectrum emission mask and spurious emissions that are signaled by the network always apply. The reason for the complex set of conditions for the relaxation is the expected intermodulation products which may fall into adjacent bands which have different levels of sensitivity (e.g., public safety bands) [13].

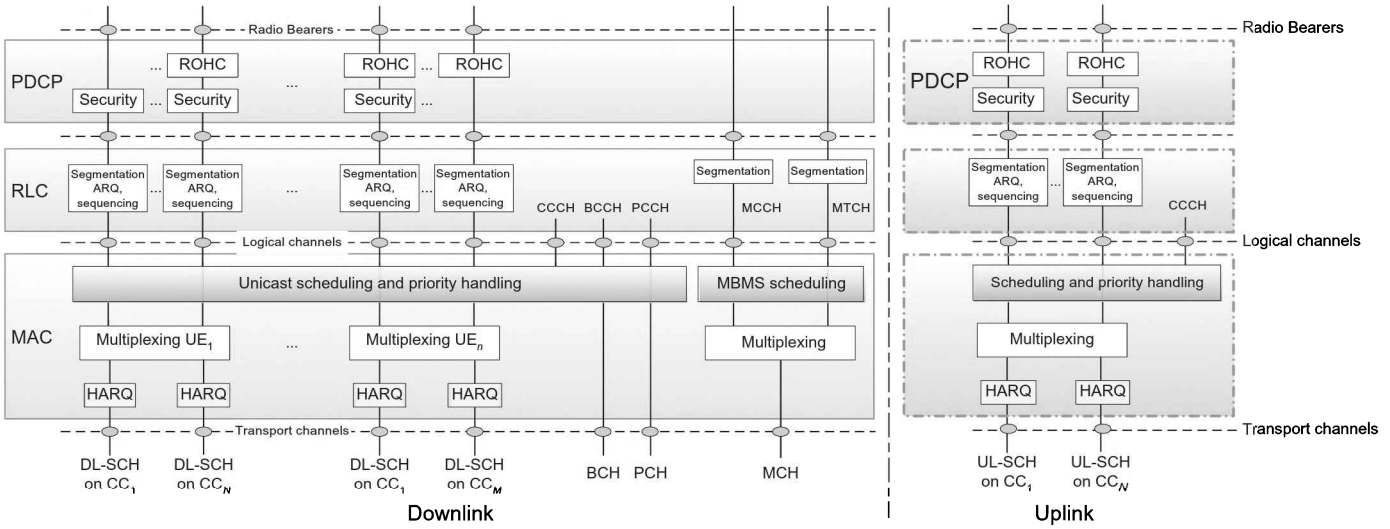


FIGURE 13.7

LTE-Advanced downlink/uplink layer 2 structure when carrier aggregation is configured [7].

user-plane protocol stack at the base station, as well as the corresponding mapping of the most essential radio resource management functionalities for carrier aggregation. Each user has at least one radio bearer which is referred to as the default radio bearer. The exact mapping of data to the default bearer is up to the operator policy and is configured via the traffic flow template. In addition to the default radio bearer, users may have additional bearers configured. There is one PDCP and RLC entity per radio bearer, including functionalities such as robust header compression, security, segmentation, and ARQ. As mentioned in the previous chapters, the interface between the RLC sublayer and MAC sublayer is referred to as the logical channel.

There is one MAC entity per user, which controls the multiplexing of data from all logical channels to the user, and further controls how this data is transmitted on the available component carriers. As illustrated in Figure 13.7, there is a separate HARQ entity per component carrier, which essentially means that if data transmission is on the ith component carrier, the HARQ retransmissions in case of erroneous reception must be performed on the ith component carrier. The interface between the MAC sublayer and the physical layer, which are referred to as transport channels, is also separate for each component carrier. The transport blocks sent on different component carriers can be transmitted with independent MCSs as well as different MIMO schemes. The latter allows data on one component carrier to be transmitted with open-loop transmit diversity (transmission mode 2), whereas data on another component carrier sent with dual-layer beamforming (transmission mode 8). There is independent link adaptation per component carrier in order to take advantage of more accurate link adaptation on different component carriers according to their respective propagation and radio channel conditions. Semi-persistent scheduling can only be configured for the PCell, and PDCCH allocations for the PCell can override the corresponding semi-persistent scheduling resource allocation.

The LTE Rel-8/9 control-plane protocol stack also applies to LTE-Advanced with multiple component carriers, meaning that there is one RRC per user, independent of the number of component carriers. Similarly, idle mode mobility procedures of LTE Rel-8/9 also apply in a network supporting carrier aggregation. It is also possible for a network to configure only a subset of component carriers for idle mode camping [26].

E-UTRA in general supports a synchronized uplink by means of un uplink timing advance (TA) adjustment procedure. The carrier aggregation in LTE Rel-10 only supports a single timing advance value which is applied to all component carriers. This means that the base station transceivers for different carriers should be at the same location to avoid different propagation delays. The use of RRHs, distributed antennas, and repeaters was limited. The signal should be received within the cyclic prefix length for a correct reception by a regular UE. The timing advance group (TAG) was introduced in LTE Rel-11 for supporting multiple timing advances typically encountered in inter-band carrier aggregation scenarios. A TAG includes one or more serving cells with the same uplink timing advance and

the same downlink timing reference cell. If a TAG contains the PCell, it is referred to as the primary timing advance group (pTAG). If a TAG contains only SCell(s), it is denoted as the secondary timing advance group (sTAG). There is one timing reference cell and one time alignment timer (TAT) per TAG, and each TAT may be configured with a different value. For pTAG, the PCell is used as the timing reference cell, whereas for sTAG, the UE may use any activated SCell from the same sTAG as the timing reference cell. From an RF requirement point of view, the number of component carriers is limited to two for LTE Rel-11; thus, if the sTAG is configured, there is only one SCell in the sTAG [7].

The initial uplink timing alignment of the sTAG is obtained by an eNB initiated random access procedure similar to the pTAG. The SCell in a sTAG can be configured with random access channel resources, and the eNB may instruct the UE to perform random access on the SCell. The Msg2 (or random access response) in response to the SCell preamble is transmitted on the PCell using an RA-RNTI that conforms to the LTE Rel-8 RACH procedure. The grant in Msg2 is valid for the SCell in which the preamble was transmitted. The UE stops transmission of the random access preamble on the SCell when reaching the maximum number of transmissions. However, the UE will not indicate a random access problem to upper layers, if the maximum number of preamble transmissions is reached for the random access procedure on the SCell. The UE tracks the downlink frame timing change of the SCell and adjusts the uplink transmission timing following the timing advance commands from the eNB [7].

13.4 Protocol and signaling aspects of carrier aggregation

In order to enable mobility when supporting carrier aggregation, a UE handles a component carrier in the same way as it would deal with another carrier frequency in LTE Rel-8/9. The UE performs various measurements as instructed by the eNB including intra- and inter-frequency measurements which are used for selecting LTE carriers, as well as inter-RAT measurements which are meant for non-LTE RAT selection. As of LTE Rel-10/11, the following event-triggered reporting criteria are defined [10]:

- Event A1: Serving cell becomes better than absolute threshold.
- Event A2: Serving cell becomes worse than absolute threshold.
- Event A3: Neighbor cell becomes better than an offset relative to the serving cell.
- Event A4: Neighbor cell becomes better than absolute threshold.
- Event A5: Serving cell becomes worse than one absolute threshold and neighbor cell becomes better than another absolute threshold.
- Event A6: Intra-frequency neighbor becomes better than an offset relative to an SCell (LTE Rel-10/11 only).

For inter-RAT mobility, the following criteria for measurement reporting are defined [10]:

- Event B1. Neighbor cell becomes better than absolute threshold.
- Event B2. Serving cell becomes worse than one absolute threshold and neighbor cell becomes better than another absolute threshold.

The new measurement event A6 was introduced for LTE-Advanced carrier aggregation to compare the neighbor cells' component carriers to the current SCell, thus allowing reconfiguration of SCells.

The discontinuous reception (DRX) mode was defined in LTE Rel-8/9. If one or more SCells are configured for a UE in addition to the PCell, the same DRX mode is applied to all serving cells. According to network configuration and ongoing HARQ processes, the UE determines the DRX activity cycle which is common to all serving cells. This means that the active times for PDCCH monitoring are identical across all downlink component carriers (see Figure 13.8).

The SCell activation/deactivation is an efficient mechanism to reduce the UE power consumption in LTE Rel-10/11 carrier aggregation in addition to DRX. On a deactivated SCell, the UE neither receives downlink signals nor transmits any uplink signal. The UE is also not required to perform measurements on a deactivated SCell. Deactivated SCells can be used as a path loss reference for measurements in uplink power control. It is assumed that these measurements would be less frequent while the SCell is deactivated in order to conserve the UE power. On the other hand, for an activated SCell, the UE performs normal activities for downlink reception and uplink transmission. Activation and deactivation of SCells is controlled by the eNB. As shown in Figure 13.8, the SCell activation/deactivation is performed when the eNB sends an activation/deactivation command in the form of a MAC control element. A timer may also be used for automatic deactivation, if no data or PDCCH messages are received on an SCell for a certain period of time. This is the only case in which deactivation can be executed autonomously by the UE. Serving cell activation/deactivation is performed independently for each SCell, allowing the UE to be activated only on a particular set of SCells. Activation/deactivation is not applicable to the PCell because it is required to always remain activated when the UE has an RRC connection to the network [29].

As already mentioned, if the UE is configured with one or more SCells, the network may activate and deactivate the configured SCells. The PCell is always activated. The network activates and deactivates the SCell(s) by sending an activation/deactivation MAC control element as described in Chapter 8. Furthermore, the UE maintains an *sCellDeactivationTimer* per configured SCell and deactivates the associated SCell upon its expiration. The same initial timer value is applied to each instance of the *sCellDeactivationTimer* and it is configured by RRC signaling. The configured SCells are initially deactivated upon addition and after a handover [9].

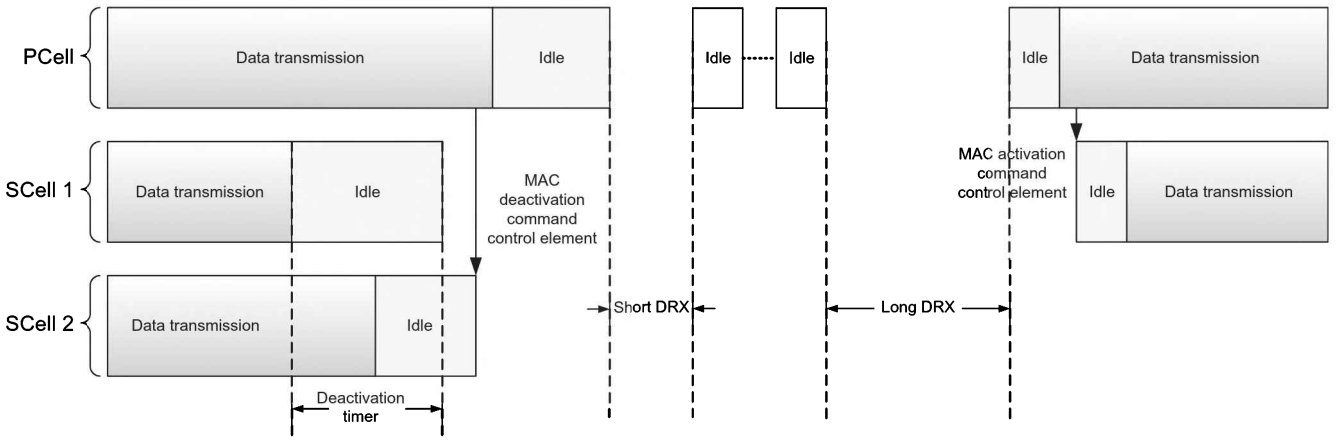


FIGURE 13.8

Illustration of SCell activation/deactivation procedure [20].

As mentioned earlier, the activation or deactivation of downlink component carriers are performed through a MAC control element. A command to activate a component carrier takes effect eight subframes after the receipt of the activation/deactivation command, i.e., if the MAC control element is received in subframe n, then the SCells are activated/deactivated starting from subframe $n + 8$. There is also a timer-based mechanism for deactivation such that a terminal may deactivate SCells after a configurable time with no activity. Note that the primary component carrier is always active. In the uplink, there is no explicit means of activation for uplink component carriers. However, whenever a downlink component carrier is activated or deactivated, the corresponding uplink component carrier is also activated or deactivated [14].

13.5 Radio resource management aspects of carrier aggregation

Cell management is the control procedure enabling the network to add, remove, or change SCells, or to switch the PCell of a UE. A UE in the RRC_IDLE state establishes RRC connection on a serving cell, which automatically becomes its PCell. Depending on the carrier where initial access is performed, different UEs in a network with carrier aggregation capability may have different PCells. With the RRC connection established on the PCell, the network can further configure one or more SCells for a carrier-aggregation-capable UE, considering the UEs capability [8] to meet the UE's data service requirements. The necessary information, including system information of an SCell is conveyed to the UE via dedicated RRC signaling. Addition, removal, or reconfiguration of SCells for a UE is performed via dedicated RRC signaling (see Figure 13.9). The network can further change the PCell of a UE to improve the link quality of the PCell on which critical control information is sent, or to provide load balancing among different SCells. The change of PCell in LTE Rel-10 carrier aggregation can only be performed via a handover procedure, and it does not necessarily require the UE to switch to single-carrier operation. Intra-LTE handover in LTE-Advanced allows the target PCell to configure one or more SCells for the UE to use immediately after handover [29].

The carrier aggregation additional SCells cannot be activated immediately at the time of RRC connection establishment, since there is no provision in the RRC connection setup procedure for SCells. SCells are added or removed from the set of serving cells through the RRC connection reconfiguration procedure. Note that, since intra-LTE handover is treated as an RRC connection reconfiguration, SCell handover is supported. The carrier aggregation-related information sent by the eNB pursuant to the RRC connection reconfiguration procedure can be summarized as follows [20]:

- Cross-carrier scheduling configuration: This indicates if scheduling for the referenced SCell is managed by that SCell or by another cell.

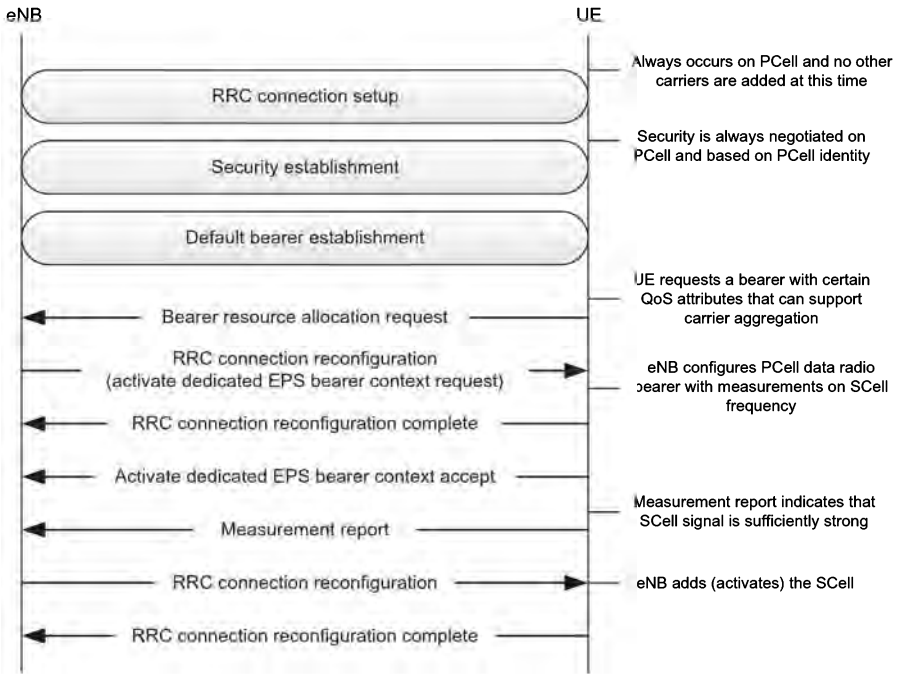


FIGURE 13.9

Summary of message exchange for addition of SCells [20].

- SCell PUSCH configuration: This indicates whether resource block group hopping is utilized on the SCell.
- SCell uplink power control configuration: This carries a number of primitives related to the SCell uplink transmit power command, including the path loss reference-linking parameter.
- SCell CQI reporting configuration: This carries a number of primitives related to CQI measurement reporting for SCells.

13.6 RF and implementation aspects of carrier aggregation

Although not considered a problem for the base station, carrier aggregation will undoubtedly pose major difficulties for the UE, which must handle multiple (simultaneously operating) transceivers. The addition of simultaneous non-contiguous transmitters creates a highly challenging radio environment in terms of spurious signal emissions and self-blocking. Carrier aggregation brings new technical challenges, especially for the LTE Rel-10/11 UE implementation. The complexity of the UE's RF front-end module can vary greatly, depending on which type(s) of carrier aggregation are supported, with contiguous carrier aggregation being the least

complex scenario. In LTE Rel-10 devices, contiguous carrier aggregation will not exceed two component carriers or 40 MHz maximum bandwidth. It may be possible to support this configuration with a single wideband transceiver in the UE. For non-contiguous component carrier allocations, the UE will have to use multiple transceivers or a single, extremely wide wideband transceiver. Using multiple transceivers may be more realistic in the sense that such configuration requires only the addition of parallel paths to process each frequency band, as in existing multiband devices. However, using multiple transceivers also increases the size, cost, and power consumption of the mobile device [12–14].

In a wideband transceiver, a single transceiver must process the multi-band non-contiguous carrier aggregation using wideband RF components. There are two main issues with this approach. First, as the bandwidth increases, the effective noise bandwidth increases, thus resulting in increased noise power. Second, with a wider bandwidth, more unwanted signals are likely to be received from other sources. Therefore, for non-contiguous carrier aggregation, most proposals today are leaning toward the use of multiple transceivers instead of a single wideband approach. In addition to increasing the RF front-end complexity, using simultaneous non-contiguous transmitters creates a highly challenging radio environment in terms of spurious signal management and self-blocking. Because these challenges particularly impact UE design, more work needs to be done before interband carrier aggregation can be successfully introduced in the uplink [14].

Simultaneous transmit or receive with mandatory MIMO support would aggravate the challenge of antenna design. The frequency bands designated for the deployment of LTE are mostly the existing IMT-2000 bands, or the bands where the legacy systems, including UMTS and GSM, were deployed. The frequency bands in some regions are defined in a technology-neutral manner, which means that coexistence among different technologies is a necessity. In general, the requirements for LTE operation in different frequency bands do not impose any specific requirements on the radio-interface design. However, there are implications for the RF requirements and the way they are defined in order to support coexistence between operators in the same geographical area, collocation of base station equipment of different operators, and coexistence with services in adjacent frequency bands and across country borders [14].

Operators may deploy LTE or other IMT-2000 technologies such as HSPA or EDGE in their respective bands. Such coexistence requirements to a large extent are developed within 3GPP, but there may also be regional requirements defined by regulatory bodies in some frequency bands. There are in many cases limitations to where base station equipment can be deployed. The base station sites are often shared between operators, or an operator will deploy multiple technologies in one site. This imposes additional requirements on base station transceivers. The use of the RF spectrum is regulated through international agreements governed by ITU-R. As a result, there are requirements for coordination among operators in different countries, and for coexistence with services in adjacent frequency bands. Coexistence between operators of TDD systems in the same band

is provided by inter-operator synchronization in order to avoid interference between downlink and uplink transmissions of different operators. Through the release-independent principle, it is possible to design terminals based on an early release of 3GPP specifications that support a frequency band added in a later release [14].

The requirements for carrier aggregation are defined for carrier aggregation configurations with associated bandwidth combination sets. For inter-band carrier aggregation, a *carrier aggregation configuration* is a combination of operating bands, each supporting a carrier aggregation bandwidth class. For intra-band contiguous carrier aggregation, a carrier aggregation configuration is a single operating band supporting a carrier aggregation bandwidth class. For each carrier aggregation configuration, requirements are specified for all bandwidth combinations contained in a *bandwidth combination set*, which is indicated per supported band combination in the UE radio access capability [8]. A UE can indicate support of several bandwidth combination sets per band combination [1].

13.6.1 Temporal/spectral masks and unwanted emissions

E-UTRA needs to ensure user orthogonality in the time-domain similar to UMTS systems. In UMTS, the requirements for user orthogonality were based on ON/OFF masks, which defined the allowable transmit power during the OFF and ON periods of transmission. In E-UTRA, similar requirements exist for the eNB for FDD and TDD operation modes. However, for the LTE UE, the requirements are considerably more complex than those for UMTS, due to the characteristics of the SC-FDMA scheme used for the uplink transmissions. Figure 13.10 shows the general ON/OFF mask in time which applies whenever the UE is required to switch on or off. Note that although the requirement is given in terms of a mask, it actually applies to the average power during the ON and OFF periods. In UMTS the transient period 20 μs is centered on the slot boundary, whereas in LTE, the transient period is in general shifted into the next subframe. Therefore, the first few SC-FDMA samples are more susceptible to corruption by insufficient transmit power or inter-UE interference, whereas the samples at the end of the subframe are protected. For PRACH, the transient periods are located outside the preamble in order to protect the entire random access preamble. The same principle applies to sounding reference signals to allow reliable uplink channel sounding without impairments arising from transient periods. This is also applicable to discontinuous transmission measurement gaps [1,13].

For TDD, where two sounding reference signals can be transmitted on adjacent symbols in the UpPTS field, the transient periods are located between the two sounding reference signals. The general temporal masks apply in the case of transitions into and out of the OFF power state. A general output power dynamic requirement also exists for continuous transmission at slot boundaries where frequency hopping occurs, and at subframe boundaries for either frequency hopping or power changes. In all these cases, the transient periods are symmetric around

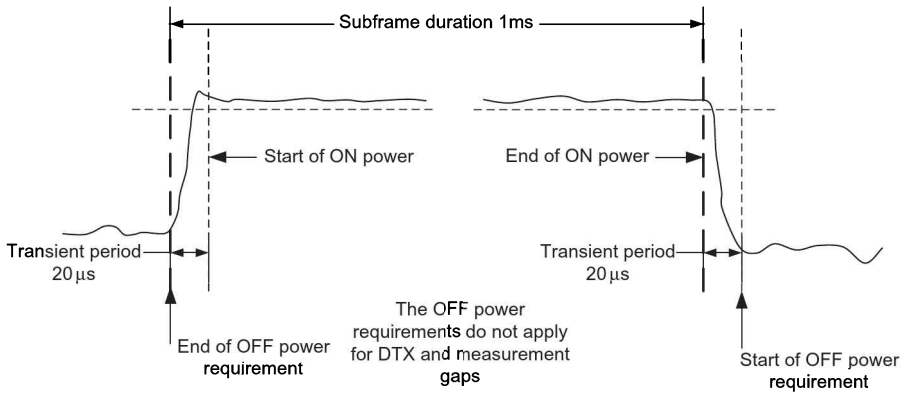


FIGURE 13.10

General ON/OFF temporal mask [1].

the slot or subframe boundaries. The transient power masks are applied in transition from the PUCCH/PUSCH to sounding reference signal with DTX after sounding reference signal, from the PUCCH/PUSCH to sounding reference signal to PUCCH/PUSCH, from DTX to sounding reference signal to PUSCH/PUCCH, or from PUCCH/PUSCH to DTX in a sounding reference signal symbol to PUCCH/PUSCH [1,13].

A radio transmitter is required not to transmit any signal outside its designated transmission band. However, in practice, all radio transmitters do transmit unwanted signals outside their designated transmission bands. The LTE specifications define two separate types of unwanted emissions: OOB emissions and spurious emissions. OOB emissions are unwanted emissions immediately outside the channel bandwidth resulting from the modulation process and non-linearity in the transmitter, but excluding spurious emissions. Spurious emissions are emissions which are caused by unwanted transmitter effects such as harmonics emission, parasitic emission, intermodulation products,[3] and frequency conversion products, but exclude OOB emissions. The OOB emissions requirement for the eNB transmitter is specified both in terms of adjacent channel leakage power ratio (ACLR) and operating band unwanted emissions. The operating band unwanted emissions define all unwanted emissions in the downlink operating band plus the frequency ranges 10 MHz above and 10 MHz below the band. Unwanted emissions outside of this frequency range are limited by a spurious emissions requirement. For an eNB supporting multi-carrier or intra-band contiguous carrier

[3]Intermodulation or intermodulation distortion (IMD) is the amplitude modulation of signals containing two or more different frequencies in a system with non-linearities. The intermodulation between each frequency component will form additional signals at frequencies that are not just at harmonic frequencies (integer multiples) of either, but also at the sum and difference frequencies of the original frequencies, and at multiples of those sum and difference frequencies.

aggregation, the unwanted emission requirements apply to channel bandwidths of the outermost carrier larger than or equal to 5 MHz. The occupied bandwidth is the width of a frequency band such that, below the lower and above the upper frequency limits, the mean powers emitted are each equal to a specified percentage $\beta/2$ of the total mean transmitted power. The value of $\beta/2$ is set to 0.5%. This requirement also applies during the transmitter ON period [1].

ACLR is the ratio of the filtered mean power centered on the assigned channel frequency to the filtered mean power centered on an adjacent channel frequency. The requirements apply outside of the edges of the RF bandwidth regardless of the type of transmitter considered, i.e., single carrier or multi-carrier. It applies to all transmission modes provisioned by the manufacturer's specification. In addition, for an eNB operating in non-contiguous spectrum, the ACLR applies to the first adjacent channel inside any sub-block gap with a sub-block gap size $W_{gap} \geq 15$ MHz. The ACLR requirement for the second adjacent channel applies inside any sub-block gap with a sub-block gap size $W_{gap} \geq 20$ MHz. This requirement is also applied during the transmitter ON period [1].

Since OOB emissions occur close to the desired signal transmission, increasing the power level of the desired signal will usually increase the level of the unwanted emissions. On the other hand, reducing the transmit power is usually an effective method for reducing the OOB emissions, thus providing one possible solution to network-signaled power-reduction requirements. The OOB emissions are an inevitable by-product of the modulation process, and are often caused by non-linearities in power amplifiers. In fixed-bandwidth radio systems, the OOB emission requirements were defined with respect to the center frequency of the transmission. Since E-UTRA supports variable bandwidth, it is more convenient to define OOB requirements with respect to the edge of the channel bandwidth rather than the center of the channel, as shown in Figure 13.11. In LTE, the OOB emissions are defined by means of spectrum emission masks and ACLR requirements.

The spectrum emission mask is a power attenuation function defined for out-of-channel emissions relative to the in-channel power spectrum. The spectrum emission mask of the UE applies to frequencies within Δf_{OOB} of the edge of the assigned LTE channel bandwidth, as shown in Figure 13.11. For intra-band contiguous carrier aggregation the spectrum emission mask of the UE applies to frequencies Δf_{OOB} starting from the $\pm$ edge of the aggregated channel bandwidth (see Figure 13.11). For intra-band contiguous carrier aggregation and bandwidth class C, the power of any UE emissions are required not to exceed the levels specified in Table 13.1 within the specified channel bandwidth [1].

13.6.2 Operating bands for carrier aggregation

E-UTRA was designed to operate in the frequency bands defined in [1,2]. The requirements were defined for 1.4, 3, 5, 10, 15, and 20 MHz bandwidths with a specific configuration in terms of number of physical resource blocks. Using carrier

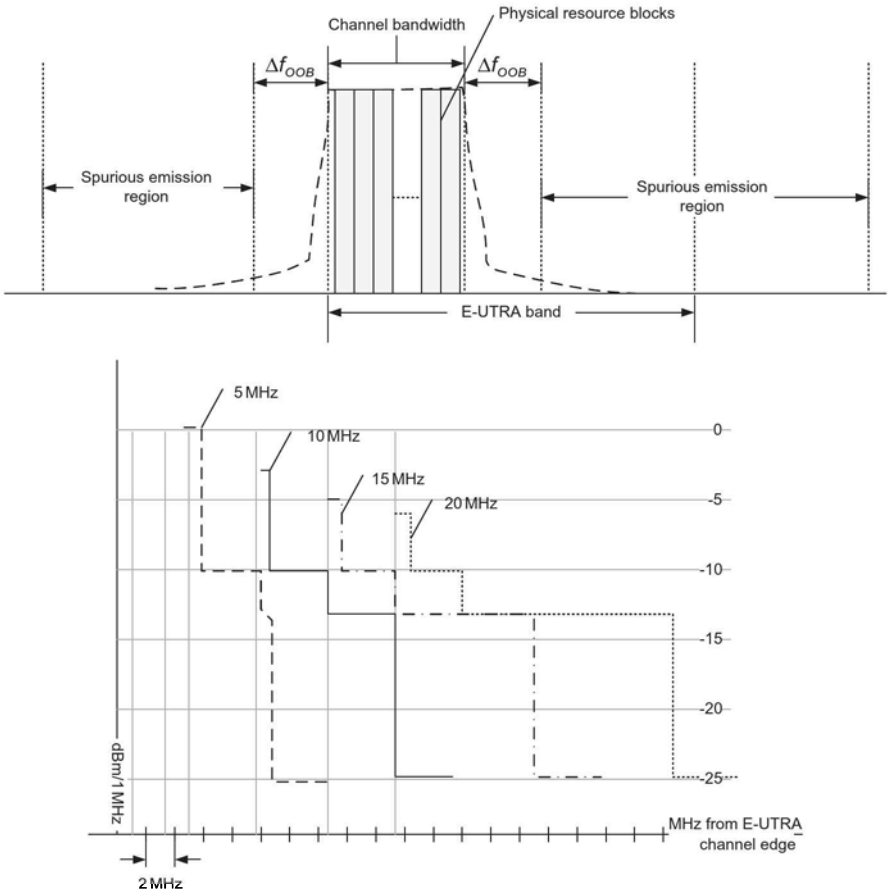


FIGURE 13.11

Transmitter RF spectrum and UE spectrum emission mask [1,13].

aggregation, a number of contiguous and/or non-contiguous frequency bands can be aggregated to create a virtually larger bandwidth. The channel raster is 100 kHz, which means the center frequency must be a multiple of 100 kHz [1]. To support transmission in paired and unpaired spectrums, two duplexing schemes are supported, i.e., FDD, allowing both full and half-duplex terminal operation, as well as TDD.

Figure 13.12 illustrates the relation between the channel bandwidth ($BW_{Channel}$) and the transmission bandwidth, i.e., the number of permissible physical resource blocks (N_{RB}). The channel edges are defined as the lowest and highest frequencies of the carrier separated by the channel bandwidth, i.e., $f_C \pm \frac{1}{2}BW_{Channel}$. In the case of carrier aggregation, the aggregated channel

Table 13.1 General E-UTRA Carrier Aggregation Spectrum Emission Mask for Bandwidth Class C [1]

	Spectrum Emission Limit (dBm/$BW_{channel-CA}$)				
Δf_{OOB}(MHz)	50 RB +100 RB (29.9 MHz)	75 RB + 75 RB (30 MHz)	75 RB + 100 RB (34.85 MHz)	100 RB + 100 RB (39.8 MHz)	Measurement Bandwidth (MHz)
±0–1	−22.5	−22.5	−23.5	−24	0.030
±1–5	−10	−10	−10	−10	1
±5–29.9	−13	−13	−13	−13	1
±29.9–30	−25	−13	−13	−13	1
±30–34.85	−25	−25	−13	−13	1
±34.85–34.9	−25	−25	−25	−13	1
±34.9–35		−25	−25	−13	1
±35–39.8			−25	−13	1
±39.8–39.85			−25	−25	1
±39.85–44.8				−25	1

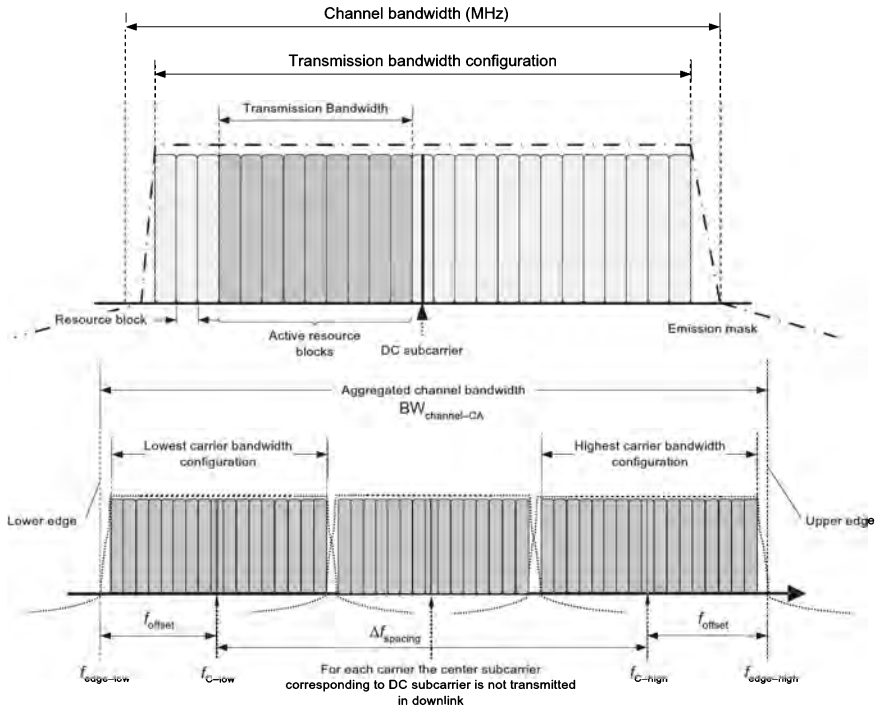


FIGURE 13.12

Relationship between channel bandwidth and transmission bandwidth in E-UTRA [2].

bandwidth $BW_{Channel\text{-}CA}$ is defined as $BW_{Channel\_CA} = f_{edge\text{-}high} - f_{edge\text{-}low}$ (see Figure 13.12). The lower band edge $f_{edge\text{-}low}$ and the upper band edge $f_{edge\text{-}high}$ of the aggregated channel bandwidth are used as the reference points in frequency for transmitter and receiver requirements, and are subsequently defined as follows: $f_{edge\text{-}low} = f_{C\text{-}low} - f_{offset\text{-}low}$ and $f_{edge\text{-}high} = f_{C\text{-}high} + f_{offset\text{-}high}$. The lower and upper frequency offsets depend on the transmission bandwidth configurations of the lowest and highest assigned edge component carriers, and are defined as $f_{offset\text{-}low} = 0.18N_{RB\text{-}low}/2 + BW_{Guard\text{-}band}$ and $f_{offset\text{-}high} = 0.18N_{RB\text{-}high}/2 + BW_{Guard\text{-}band}$ where $N_{RB\text{-}low}$ and $N_{RB\text{-}high}$ denote the transmission bandwidth configurations for the lowest and highest assigned component carrier, respectively, and $BW_{Guard\text{-}band}$ denotes the nominal guard band size. Note that the 0.18 multiplier in the equations is the bandwidth of a physical resource block in MHz. The aggregated transmission bandwidth is defined as the number of the aggregated resource blocks within the entire assigned aggregated channel bandwidth, and is defined per carrier aggregation band class.

As shown in Figure 13.12, the spacing between carriers depends on the deployment scenario and the size of the frequency block available to the network operator, as well as the channel bandwidth. The nominal channel spacing between

two adjacent E-UTRA carriers is defined as $\Delta f_{\text{spacing}} = (BW_{\text{Channel(1)}} + BW_{\text{Channel(2)}})/2$ where $BW_{\text{Channel(1)}}$ and $BW_{\text{Channel(2)}}$ parameters are the channel bandwidths of the two respective E-UTRA carriers. The channel spacing can be adjusted to optimize performance in a particular deployment scenario. For intra-band contiguous carrier aggregation bandwidth, the nominal channel spacing between two adjacent E-UTRA component carriers is specified as follows [1,2]:

$$\Delta f_{\text{spacing-CA}}(\text{MHz}) = 0.3 \left\lfloor \frac{BW_{\text{Channel(1)}} + BW_{\text{Channel(2)}} - 0.1\left|BW_{\text{Channel(1)}} - BW_{\text{Channel(2)}}\right|}{0.6} \right\rfloor$$

The channel spacing for intra-band contiguous carrier aggregation can be adjusted to any integer multiple of 300 kHz (less than the nominal channel spacing) to optimize performance in a particular deployment scenario. The E-UTRA channel raster (including the carrier aggregation scenarios) is 100 kHz for all bands, which means that the carrier center frequency must be an integer multiple of 100 kHz.

The carrier frequency in the downlink/uplink directions is designated by the E-UTRA absolute radio frequency channel number (EARFCN) in the range of 0–65,535. The relation between EARFCN and the downlink carrier frequency (in MHz) is given by $f_{\text{DL}} = f_{\text{DL-low}} + 0.1(N_{\text{DL}} - N_{\text{Offset-DL}})$, where $f_{\text{DL-low}}$, N_{DL}, and $N_{\text{Offset-DL}}$ parameters are given in [1,2]. Similarly, the relationship between EARFCN and the uplink carrier frequency (in MHz) for the uplink is defined as $f_{\text{UL}} = f_{\text{UL-low}} + 0.1(N_{\text{UL}} - N_{\text{Offset-UL}})$, where $f_{\text{UL-low}}, N_{\text{UL}}$, and $N_{\text{Offset-UL}}$ parameters are provided in [1,2]. Note that N_{DL} and N_{UL} in the latter equations are the downlink and uplink EARFCN, respectively. Figure 13.13 shows a snapshot of four adjacent 20 MHz component carriers chosen from the 3.5 GHz band that are aggregated with the adjacent center frequency spacing set to 20.1 MHz (a multiple of 300 kHz). This figure also shows the spectrum of two 20 MHz component carriers chosen from Band 7 in 2600 MHz that are aggregated with the center frequency spacing set to 20.1 MHz [18].

The channel numbers that designate carrier frequencies which are extremely close to the operating band edges are not used. This implies that the first 7, 15, 25, 50, 75, and 100 channel numbers at the lower operating band edge, and the last 6, 14, 24, 49, 74, and 99 channel numbers at the upper operating band edge are not utilized for channel bandwidths of 1.4, 3, 5, 10, 15, and 20 MHz, respectively.

A sub-block is defined as one contiguous allocated block of spectrum for transmission and reception by the same eNB. There may be multiple instances of sub-blocks within an RF bandwidth. Sub-block bandwidth is defined as the bandwidth of one sub-block. The frequency gap between two consecutive sub-blocks within an RF bandwidth is referred to as sub-block gap, where the RF requirements in the gap are based on coexistence for uncoordinated operation. The lower sub-block edge of the sub-block bandwidth $BW_{\text{Channel-block}}$ is defined as $f_{\text{edge\_block\_low}} = f_{C\_\text{block\_low}} - f_{\text{offset}}$. The upper sub-block edge of the sub-block

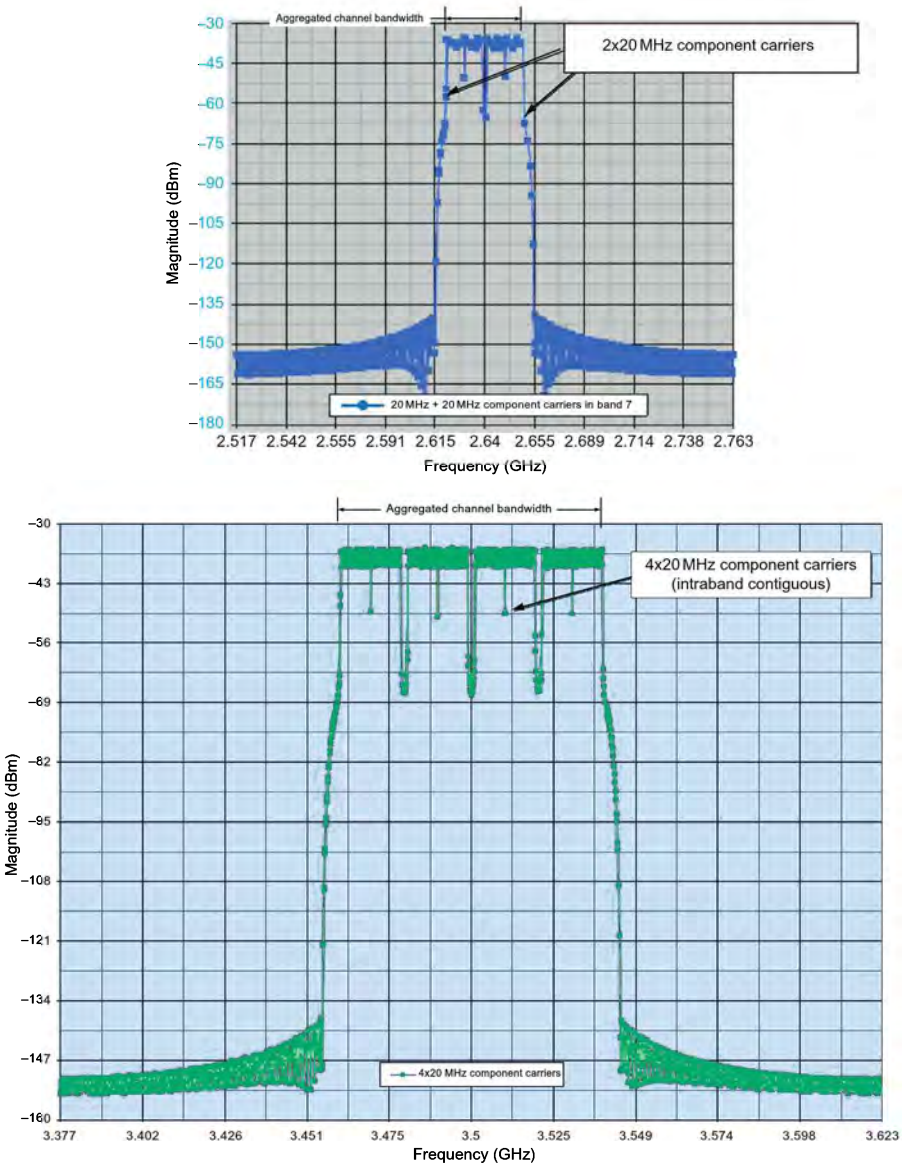


FIGURE 13.13

Snapshot of spectrum of two and four aggregated adjacent component carriers [17,18].

bandwidth is defined as $f_{\text{edge\_block\_high}} = f_{C\_\text{block\_high}} + f_{\text{offset}}$. The sub-block bandwidth $BW_{\text{Channel-block}}$ is alternatively defined as $BW_{\text{Channel\_block}} = f_{\text{edge\_block\_high}} - f_{\text{edge\_block\_low}}$ in MHz [2].

LTE Rel-10 specified the radio frequency aspects of inter-band carrier aggregation only for FDD, assuming aggregation of bands 1 and 5. However, network operators are interested in various band combinations, as shown in Table 13.2, depending on their available spectrum resources. Radio frequency properties of each band combination must be specified to comply with the regulations. In addition, inter-band carrier aggregation for TDD needs to be supported in future releases with the possibility of having different TDD uplink–downlink subframe configurations on different bands to coexist with the already deployed TDD systems in that band.

A carrier aggregation bandwidth class is defined by the aggregated transmission bandwidth configuration and the maximum number of component carriers supported by a UE. Table 13.3 shows supported bandwidth classes for LTE Rel-11 UE as defined in [1]. Figure 13.14 illustrates the standard notation used by the UE to indicate its support of carrier aggregation for a particular frequency band or band combination to the network. The example shows that in order to indicate support for intra-band, non-contiguous carrier aggregation in band 5 based on bandwidth class A, the notation would be CA_5A_5A. It informs the network that this device is able to receive (or transmit) two separate carriers in frequency band 5, each with a maximum bandwidth of 100 resource blocks, i.e., 20 MHz. Another example is CA_1C which indicates that the UE can operate with two contiguous component carriers with a maximum of 200 resource blocks which can be in the form of 15 + 15 or 20 + 20 MHz. Note that there might be different bandwidth combinations for each E-UTRA carrier aggregation configuration [1]. Table 13.4 summarizes some important parameters associated with UE categories as of LTE Rel-11.

13.6.3 Transmitter characteristics for carrier aggregation

The transmitter characteristics not only define RF requirements for the desired signal transmitted from the UE and the eNB, but also for the unavoidable unwanted emissions outside the transmission bandwidth. These requirements are fundamentally categorized as follows: (1) output power-level requirements set the limits for the maximum permissible transmitted power corresponding to dynamic variation of the power level during transmission; (2) transmitted signal quality requirements define the cleanliness of the transmitted signal and also the relationship between multiple transmitter branches; and (3) unwanted emissions requirements set the limits for all emissions outside of the transmitted carrier(s) operating band which are tightly coupled to regulatory requirements and coexistence with other systems. The following is a list of major UE and eNB transmitter attributes [14]:

- eNB: Output power level (maximum output power, output power dynamics, and on/off power for TDD), transmitted signal quality (frequency error, error vector magnitude (EVM), and time alignment between transmitter branches),

Table 13.2 Carrier Aggregation Bands and Band Aggregation as of LTE Rel-11 [1]

Band Combination	Carrier Aggregation Scenario	Uplink Frequency Range (MHz) $f_{UL\text{-}low} - f_{UL\text{-}high}$	Downlink Frequency Range (MHz) $f_{DL\text{-}low} - f_{DL\text{-}high}$	Duplex Mode
1	Intra-band contiguous	1920–1980	2110–2170	FDD
7		2500–2570	2620–2690	FDD
40		2300–2400	2300–2400	TDD
41		2496–2690	2496–2690	TDD
1 and 5	Inter-band	1920–1980 824–849	2110–2170 869–894	FDD
1 and 18		1920–1980 815–830	2110–2170 860–875	FDD
1 and 19		1920–1980 830–845	2110–2170 875–890	FDD
1 and 21		1920–1980 1447.9–1462.9	2110–2170 1495.9–1510.9	FDD
2 and 17		1850–1910 704–716	1930–1990 734–746	FDD
2 and 29		1850–1910 N/A (downlink only SCell)	1930–1990 717–728	FDD
3 and 5		1710–1785 824–849	1805–1880 869–894	FDD
3 and 7		1710–1785 2500–2570	1805–1880 2620–2690	FDD
3 and 8		1710–1785 880–915	1805–1880 925–960	FDD
3 and 20		1710–1785 832–862	1805–1880 791–821	FDD
4 and 5		1710–1755 824–849	2110–2155 869–894	FDD
4 and 7		1710–1755 2500–2570	2110–2155 2620–2690	FDD
4 and 12		1710–1755 699–716	2110–2155 729–746	FDD
4 and 13		1710–1755 777–787	2110–2155 746–756	FDD
4 and 17		1710–1755 704–716	2110–2155 734–746	FDD
4 and 29		1710–1755	2110–2155 717–728	FDD

(*Continued*)

Table 13.2 (Continued)

Band Combination	Carrier Aggregation Scenario	Uplink Frequency Range (MHz) $f_{UL\text{-}low} - f_{UL\text{-}high}$	Downlink Frequency Range (MHz) $f_{DL\text{-}low} - f_{DL\text{-}high}$	Duplex Mode
		N/A (downlink only SCell)		
5 and 12		824–849	869–894	FDD
		699–716	729–746	
5 and 17		824–849	869–894	FDD
		704–716	734–746	
7 and 20		2500–2570	2620–2690	FDD
		832–862	791–821	
8 and 20		880–915	925–960	FDD
		832–862	791–821	
11 and 18		1427.9–1447.9	1475.9–1495.9	FDD
		815–830	860–875	

unwanted emissions (operating band unwanted emissions, ACLR, spurious emissions, occupied bandwidth, and transmitter intermodulation).

- UE: Output power level (transmit power, output power dynamics, and power control), transmitted signal quality (frequency error and transmit modulation quality), unwanted emissions (spectrum emission mask, ACLR, spurious emissions, occupied bandwidth, and transmit intermodulation).

The ACLR is directly related to the operating point of the power amplifier. In general, leakage into adjacent channels increases abruptly as the power amplifier is driven into its non-linear operating region at the highest output power levels due to the intermodulation products. As a result, it is important that the peak output power of the UE does not drive the power amplifier too far into its non-linear region. On the other hand, most power amplifiers are designed to operate efficiently only in a small region at the top of the linear operating region. This corresponds to the rated output power of the power amplifier below which the efficiency drops abruptly. Since high efficiency is crucial to ensuring a long battery life for the UE, it is also desirable to maintain the power amplifier operating as close as possible to the top of the linear operating region. If the ACLR and spectrum mask requirements cannot be met, typically the UE output power must be reduced to bring the leakage to acceptable levels. This can be achieved without excessive loss of efficiency by reducing the peak output power of the power amplifier, a process known as derating. The amount of derating required is highly dependent on the peak to average power ratio (PAPR) and bandwidth of the transmitted signal. In general, for any given channel bandwidth and power amplifier, transmissions with a larger occupied bandwidth create more OOB emissions,

Table 13.3 Carrier Aggregation Bandwidth Classes and Corresponding Nominal Guard Bands [1]

Carrier Aggregation Bandwidth Class	Aggregated Transmission Bandwidth Configuration	Maximum Number of Component Carriers	Nominal Guard Band $BW_{\text{Guard Band}}$
A	$N_{\text{RB-Aggregated}} \leq 100$	1	$0.05BW_{\text{Channel-1}}$
B	$N_{\text{RB-Aggregated}} \leq 100$	2	–
C	$100 < N_{\text{RB-Aggregated}} \leq 200$	2	$0.05\max(BW_{\text{Channel-1}}, BW_{\text{Channel-2}})$
D	$200 < N_{\text{RB-Aggregated}} \leq 300$	–	–
E	$300 < N_{\text{RB-Aggregated}} \leq 400$	–	–
F	$400 < N_{\text{RB-Aggregated}} \leq 500$	–	–

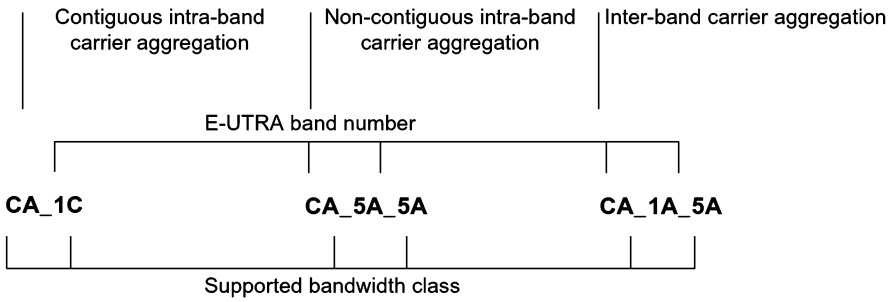


FIGURE 13.14

Standard notation for carrier aggregation support (type, frequency band, and bandwidth) [1,16].

resulting in larger adjacent channel leakage than transmissions with lower occupied bandwidth. The increase in OOB emissions from the larger occupied bandwidth of the LTE signal is mainly due to increased adjacent channel occupancy by third and fifth order intermodulation products (see Figure 13.15). For an LTE uplink transmitted signal, certain combinations of resource block allocations and modulation schemes create more OOB emissions than others [13].

For low-bandwidth applications such as VoIP, which typically use QPSK modulation, no power derating is required from the normal-rated maximum UE output power, ensuring broad coverage for such applications, since full output power of the power amplifier can be used to counter the path loss effect at the cell-edge. Moreover, the structure of the LTE uplink signal, with control information being usually positioned at the channel edge and high-bandwidth data transmissions toward the middle of the band, helps to improve OOB emissions and reduce ACLR. Taking the above considerations into account, the total power

able 13.4 UE Categories as of LTE Rel-11 [8]

E ategory	Peak Data Rate Downlink/ Uplink (Mbps)	Maximum Number of DL-SCH Transport Block Bits Received within a TTI	Maximum Number of Bits of a DL-SCH Transport Block Received within a TTI	Total Number of Soft Channel Bits in the Downlink	Maximum Number of Supported Layers for Spatial Multiplexing in the Downlink	Maximum Number of UL-SCH Transport Block Bits Transmitted within a TTI	Maximum Number of Bits of a UL-SCH Transport Block Transmitted within a TTI	Support for 64QAM in Uplink	Total Layer 2 Buffer Size (Bytes)	Maxi Numl Bits MCH Trans Block Rece withi TTI
ategory 1	10/5	10,296	10,296	250,368	1	5160	5160	No	150,000	10,29
ategory 2	50/25	51,024	51,024	1,237,248	2	25,456	25,456	No	700,000	51,02
ategory 3	100/50	102,048	75,376	1,237,248	2	51,024	51,024	No	1,400,000	75,37
ategory 4	150/50	150,752	75,376	1,827,072	2	51,024	51,024	No	1,900,000	75,37
ategory 5	300/75	299,552	149,776	3,667,200	4	75,376	75,376	Yes	3,500,000	75,37
ategory 6	300/50	301,504	149,776 (4 layers) 75,376 (2 layers)	3,654,144	2 or 4	51,024	51,024	No	3,300,000	(75,3
ategory 7	300/150	301,504	149,776 (4 layers) 75,376 (2 layers)	3,654,144	2 or 4	102,048	51,024	No	3,800,000	(75,3
ategory 8	1200/600	2,998,560	299,856	35,982,720	8	1,497,760	149,776	Yes	4,220,0000	(75,3

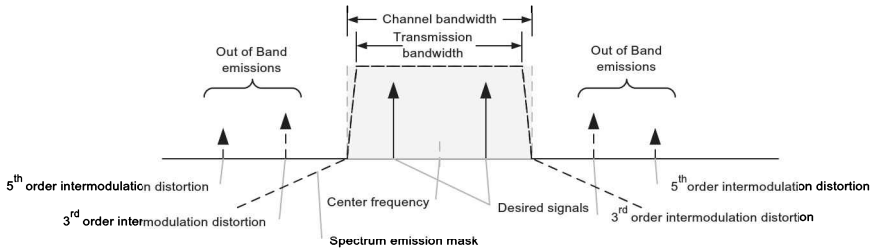


FIGURE 13.15

Illustration of the IMD components [20].

derating required to meet a target ACLR value can be decomposed into a term corresponding to the occupied bandwidth as a proportion of the channel bandwidth, and a term corresponding to the waveform of the transmitted signal. Small resource assignments at the edges of the band behave as tones and hence may produce highly concentrated IMD products [14]. Therefore, for simultaneous PUSCH and PUCCH transmission, the spectral emission mask is expected to be the limiting requirement, as it is for LTE Rel-8 with full resource allocation (see Figure 13.6).

As mentioned earlier, the ACLR metric defines the ratio of the power transmitted in the assigned channel bandwidth to the power of the unwanted emissions transmitted in an adjacent channel. There is a corresponding receiver requirement known as adjacent channel selectivity (ACS), which defines a receiver's ability to suppress a signal in an adjacent channel. Therefore, from the receiver's point of view, the unwanted emissions as a result of transmissions in the adjacent bands in the desired signal's receiver bandwidth are represented by ACLR, and the ability of the receiver to suppress the interfering signal in the adjacent channel is defined by ACS. The two parameters when combined define the total leakage between two transmissions on adjacent channels. That ratio is called the adjacent channel interference ratio (ACIR), and is defined as the ratio of the power transmitted on one channel to the total interference received by a receiver on the adjacent channel due to both transmitter RF filter imperfection (ACLR) and receiver RF filter imperfection (ACS) [14].

In LTE, the EVM is required to be less than 17.5% for QPSK, 12.5% for 16QAM and 8% for 64QAM (applicable to the downlink only). The EVM values are designed to correspond to no more than 5% loss in average and cell-edge throughputs in typical deployment scenarios. At the link level, EVM is equivalent to signal to noise ratio loss [13]. The occupied bandwidth is defined as the bandwidth containing 99% of the total integrated mean power of the transmitted spectrum on the assigned channel. The occupied bandwidth for all transmission bandwidth configurations (resource blocks) must be less than the channel bandwidth. For intra-band contiguous carrier aggregation the occupied bandwidth is a measure of the bandwidth containing 99% of the total integrated power of the

transmitted spectrum. The occupied bandwidth must be less than the aggregated channel bandwidth [1].

The output power dynamics are impacted by the UE transmitter architecture, which may be based on single or multiple power amplifiers. Figure 13.16 illustrates various options for UE transmitter architecture which can be used to support different carrier aggregation scenarios. As shown in Figure 13.16 for alternative 1, if two component carriers are contiguous, then a single IFFT module can be used to generate both OFDM signals. A single RF mixer can be used to convert the baseband signal frequency to RF frequency followed by a single power amplifier to amplify the power of the transmitted signal. If two component carriers are non-contiguous but within the same frequency band, then alternatives 2 or 3 shown in Figure 13.16 may be used as a general transmitter architecture. However, for non-contiguous component carriers in different frequency bands, separate IFFT modules, mixers, and power amplifiers would be required to process the OFDM signals, unless a multi-band power amplifier is utilized.

13.6.4 Receiver characteristics for carrier aggregation

Although the requirements for LTE receivers are similar to those defined for UMTS, they are defined differently due to the flexible bandwidth properties of LTE. The receiver RF requirements are primarily divided into three categories: (1) sensitivity and dynamic range requirements for receiving the desired signal; (2) receiver susceptibility to interfering signals defining receiver's vulnerability to different types of interfering signals at different frequency offsets; and (3) unwanted emission limits. The following is a list of attributes for the UE and eNB receivers [14]:

- eNB: Sensitivity and dynamic range (reference sensitivity, dynamic range, and in-channel selectivity), receiver susceptibility to interfering signals (OOB blocking, in-band blocking, narrowband blocking, ACS, and receiver intermodulation), and unwanted emissions from the receiver (receiver spurious emissions). The spurious emissions power is the power of emissions generated or amplified in a receiver that appear at the eNB receiver antenna connector. The requirements apply to all eNBs with separate receive and transmit antenna ports. The test for the FDD eNB must be performed when transmitter and receiver are on, with the transmit port properly terminated. For the TDD eNB with a common receive and transmit antenna port, the requirement applies during the transmitter OFF period. The blocking characteristic is a measure of the receiver's ability to receive a desired signal at its assigned channel in the presence of an unwanted interferer. Narrowband blocking is similar to ACS, but with interfering signals consisting of only one resource block.
- UE: Sensitivity and dynamic range (reference sensitivity power level and maximum input level), receiver susceptibility to interfering signals (OOB blocking,

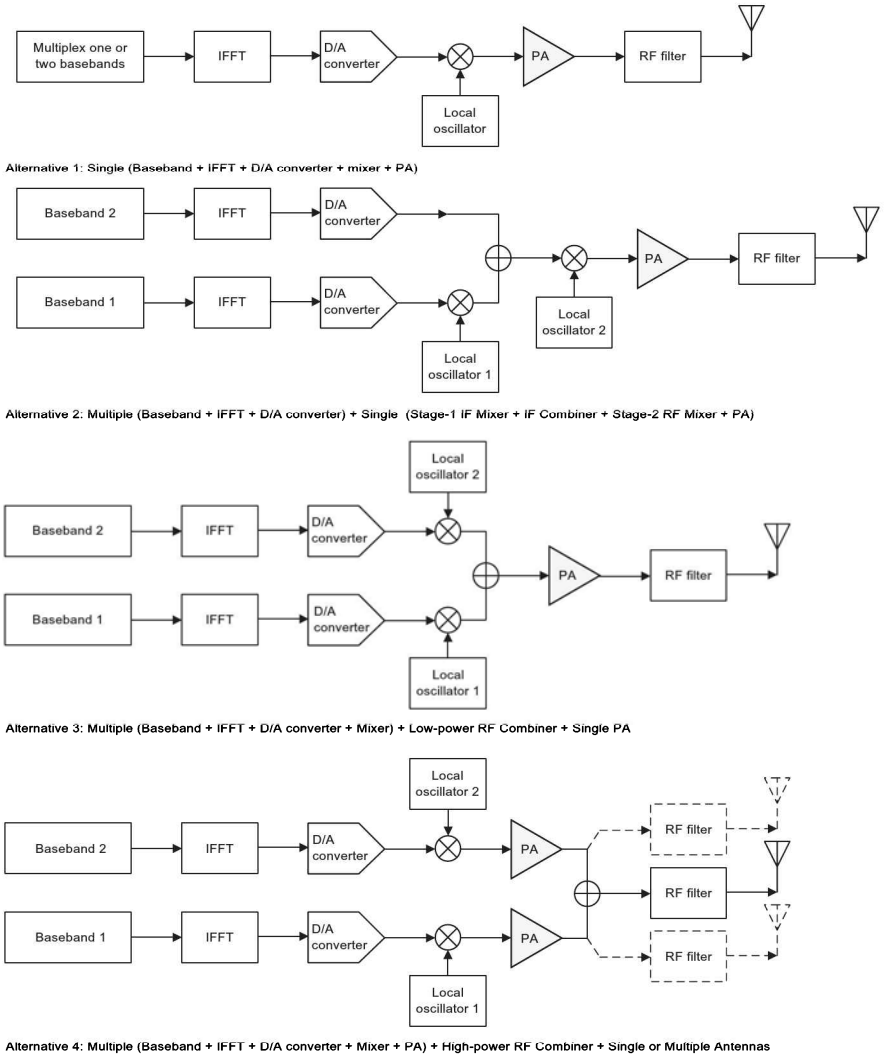


FIGURE 13.16

Example transmitter implementation for intra-band/inter-band carrier aggregation [11].

spurious response, in-band blocking, narrowband blocking, ACS, and intermodulation characteristics), and unwanted emissions from the receiver (receiver spurious emissions). Third and higher order mixing of the two interfering RF signals can produce an interfering signal in the band of the desired channel. Intermodulation response rejection is a measure of the capability of the receiver to receive a wanted signal on its assigned channel frequency in

the presence of two interfering signals (a continuous wave and E-UTRA signals).

The LTE RF receiver requirements were partly derived from UMTS. This was meant to ensure that the implementation of an LTE RF receiver is not going to be more complex than that of UMTS in order to reduce redesigning efforts. The main differences between the LTE and UMTS RF receiver requirements arise from the variable channel bandwidth and the different multiple access schemes. The receiver RF requirements are based on a number of specific assumptions for testing purposes including integrated antennas with 0 dBi gain; two antenna ports; test signals of equal power level applied to each antenna port; and use of a maximal ratio combining to combine the signals. It is assumed that the signals are received from independent AWGN channels, thus signal addition would provide 3 dB diversity gain.

LTE supports different MCSs; however, the RF receiver specifications are defined for only two MCSs, referred to as reference channels, which are at the extremes of the available range, in order to reduce the number of conformance tests which have to be performed. The low-SNR reference channel uses QPSK with a code rate of 1/3, while the high SNR reference channel uses 64QAM with a code rate of 3/4. For each of the reference channels, the SINR requirements, at which 95% throughput is achieved, are specified.

When the LTE receiver is tested in full-duplex FDD mode, the transmitter must also be operating so that signal leakage from the transmitter to the receiver due to insufficient isolation of the duplexer is taken into consideration. This condition does not apply to half-duplex FDD or TDD operation. In practice, the transmitted signal leakage interferes with the receiver not only because of the power of the fundamental components, but also because of the OOB phase noise of the transmitted signal when it falls into the receiver band. In LTE, the spurious emissions from the UE transmitter in its own receive band are required to be -47 dBm or less, measured in a 1 MHz bandwidth. This corresponds to -107 dBm/Hz. The maximum transmit power for an LTE mobile device is $+23$ dBm for power class 3, thus the spurious emissions requirement is -130 dBc/Hz. The LTE receiver sensitivity is measured with the transmitter operating at the full power for its class. In order to allow the transmitter to degrade the receiver sensitivity by no more than 0.5 dB, the transmitter noise needs to be 9 dB below the noise floor at the antenna connector. If we assume that the spurious emissions of the transmitter in the corresponding receiver band are just at the limit of the specifications, it can be shown that the duplexer isolation needs to be at least 78 dB for the LTE FDD mode. However, making duplexers smaller and cheaper is often achieved at the expense of compromised isolation, and typical duplexers might provide just $45-55$ dB isolation [14]. Therefore, the transmit signal could substantially desensitize the receiver. This is not acceptable, thus the LTE transmitter has to achieve spurious emissions about 20 dB lower than the transmitter requirements within the receiver band. The

transmit power at the input to the low-noise amplifier is equal to the transmit power at the antenna plus the duplexer attenuation from transmit port to antenna (about 2 dB) minus the duplexer transmit-to-receiver isolation ($\sim$50 dB). Therefore, at the maximum LTE UE output power of +23 dBm, the mean transmitter power leakage to the low-noise amplifier is −25 dBm [13].

This value is calculated based on the average transmit power, but the transmitted signal contains amplitude modulation, and therefore the peak signal will be higher. The transmitter leakage problem presents a particularly challenging requirement, if applied to RF bands with a small frequency separation. In FDD systems, when performing a selectivity or blocking test with a single interfering signal in one of the adjacent channels, the receiver is also exposed to its own transmitted signal as a second interferer, which, in the worst case scenario, can cause intermodulation, in which the interferers are mixed together to generate in-band IMD products.

The maximum input level is the maximum mean received signal strength, measured at each antenna port, at which there is sufficient SINR for a specified modulation scheme to meet a minimum throughput requirement. In LTE, the maximum input level is only specified for the high SINR reference channel, assuming that the high SINR reference channel is about 4 dB higher due to the PAPR of the signal. The downlink requirement is for a maximum average input level of −25 dBm at any channel bandwidth with full resource block allocation. In FDD systems, the requirement must be met when the transmitter is set at 4 dB below the maximum output power. If PAPR is measured on a bitwise basis and plotted as a complementary cumulative probability distribution, then for the LTE downlink it reaches a value of around 11 dB for QPSK and 11.5 dB for 64QAM, over a window of 106 bits. In OFDM, the PAPR is dominated by the multi-carrier nature of the signal, and therefore does not vary much with modulation [13].

The primary purpose of the reference sensitivity requirement is to verify the receiver noise figure, which is a measure of how much the receiver's RF signal chain degrades the SNR of the received signal. For this reason, a low-SNR transmission scheme using QPSK is chosen as a reference channel for the reference sensitivity test. The reference sensitivity is defined at a receiver input level where the throughput is 95% of the maximum throughput for the reference channel. For the base station, reference sensitivity could potentially be defined for a single resource block up to a group covering all resource blocks. Considering the complexity, a maximum granularity of 25 resource blocks has been chosen, which means that for channel bandwidths larger than 5 MHz, sensitivity is verified over multiple adjacent 5 MHz blocks, while it is only defined over the full channel for smaller channel bandwidths. For the UE, reference sensitivity is defined for the full channel bandwidth signals and with all resource blocks allocated to the desired signal. For channel bandwidths greater than 5 MHz in some operating bands, the nominal reference sensitivity needs to be met with a minimum number of allocated resource blocks [14]. In other words, the reference sensitivity level is the minimum mean received signal strength applied to both antenna ports (assuming two receive antennas) at which there is sufficient SINR for the specified modulation scheme to meet a

minimum throughput requirement of 95% of the maximum possible value. It is measured with the transmitter at full power. The reference sensitivity is a range of values that can be calculated as $P_{\text{Reference\_Sensitivity}} = 10\log(kT_0B) + NF + SINR + L_{\text{Implementation\_Margin}} - 3$ (dBm), where kT_0B is the thermal noise power in dBm, B is the noise equivalent bandwidth ($\sim$system bandwidth), NF is the maximum receiver noise figure, $SINR$ is the minimum SINR for the chosen MCS, $L_{\text{Implementation\_Margin}}$ is the implementation margin, and -3 represents the receive diversity gain [13]. Note that the noise floor for any receiver is defined as $Noise\_Floor = 10\log(kT_0B) + NF = -174 + NF + 10\log B$ (dBm), where $NF = SNR_{\text{in}} - SNR_{\text{out}}$ (in dB) is a measure of SINR degradation by the components in the RF signal path, including the RF filters and low-noise amplifier. The thermal noise power density $kT_0 = -174$ dBm/Hz is measured at typical room temperature of $290°K$. The LTE specifications require $NF \leq 9$ dB for the UE and $NF \leq 5$ dB for the eNB, nevertheless, commercial RF components and UE receivers can achieve lower than these limits [13].

The UE receiver dynamic range requirement is meant to ensure that the receiver can operate at received signal levels considerably higher than the reference sensitivity. The base station dynamic range testing assumes the presence of increased interference and corresponding higher signal levels, thereby testing the effects of different receiver impairments. In order to drive the receiver to the worst condition, a higher SNR transmission scheme using 16QAM is applied for the test. In order to further drive the receiver to processing higher signal levels, an interfering AWGN signal at 20 dB above the assumed noise floor is added to the received signal. The dynamic range requirement for the UE is specified as a maximum signal level at which the throughput requirement is met.

Blocking corresponds to the scenario when strong interfering signals received outside the operating band (OOB blocking) or inside the operating band (in-band blocking), but not adjacent to the desired signal. In-band blocking includes interferers in the first 20 MHz outside the band for the base station and the first 15 MHz for the UE. The scenarios are modeled with a continuous wave signal for the OOB case and an E-UTRA signal for the in-band case. There are additional base station's blocking requirements for the scenario when the base station is collocated with another base station in a different operating band. For the UE, a fixed number of exceptions are allowed from the OOB blocking requirement, for each assigned frequency channel and at the respective spurious response frequencies. At those frequencies, the UE must comply with the more relaxed spurious response requirement. Note that these effects and satisfaction of the requirements become more challenging when carrier aggregation is supported.

ACS is the case when there is a strong signal in the channel adjacent to the desired signal, and is closely related to the corresponding ACLR requirement. For the UE, the ACS is specified for two cases with a lower and a higher signal level. In-channel selectivity is the case when there are multiple received signals of different received power levels inside the channel bandwidth, where the performance of the weaker desired signal is verified in the presence of the stronger interfering

signal. In-channel selectivity is only specified for the base station. Narrowband blocking is an adjacent strong narrowband interferer, which in the requirement is modeled as a single resource block LTE signal for the base station and a continuous wave signal for the UE. Receiver intermodulation occurs when there are two interfering signals in the spectral proximity of the desired signal, where the interferers are one continuous wave and one LTE signal. The interferers are placed in frequency in such a way that the main intermodulation product falls within the desired signal's channel bandwidth. There is also a narrowband intermodulation requirement for the base station where the continuous wave signal is very close to the wanted signal, and the LTE interferer is a single resource block signal. For all requirements except in-channel selectivity, the wanted signal uses the same reference channel as in the corresponding reference sensitivity requirement. When the interference is added, the same 95% relative throughput is met as for the reference channel, but at a desensitized higher desired signal level [14].

References

3GPP Specifications[4]

[1] 3GPP TS 36.101, Evolved Universal Terrestrial Radio Access (E-UTRA); User Equipment (UE) Radio Transmission and Reception (Release 11), December 2012.
[2] 3GPP TS 36.104, Evolved Universal Terrestrial Radio Access (E-UTRA); Base Station (BS) Radio Transmission and Reception (Release 11), December 2012.
[3] 3GPP TS 36.211, Evolved Universal Terrestrial Radio Access (E-UTRA), Physical Channels and Modulation (Release 11), December 2012.
[4] 3GPP TS 36.212, Evolved Universal Terrestrial Radio Access (E-UTRA) Multiplexing and Channel Coding (Release 11), December 2012.
[5] 3GPP TS 36.213, Evolved Universal Terrestrial Radio Access (E-UTRA); Physical Layer Procedures (Release 11), December 2012.
[6] 3GPP TS 36.214, Evolved Universal Terrestrial Radio Access (E-UTRA); Physical Layer—Measurements (Release 11), December 2012.
[7] 3GPP TS 36.300, Evolved Universal Terrestrial Radio Access (E-UTRA) and Evolved Universal Terrestrial Radio Access Network (E-UTRAN) Overall Description, Stage 2 (Release 11), December 2012.
[8] 3GPP TS 36.306, Evolved Universal Terrestrial Radio Access (E-UTRA); User Equipment (UE) Radio Access Capabilities (Release 11), December 2012.
[9] 3GPP TS 36.321, Evolved Universal Terrestrial Radio Access (E-UTRA); Medium Access Control (MAC) Protocol Specification (Release 11), December 2012.
[10] 3GPP TS 36.331 Evolved Universal Terrestrial Radio Access (E-UTRA); Radio Resource Control (RRC); Protocol Specification (Release 11), December 2012.
[11] 3GPP TR 36.815, Further Advancements for E-UTRA; LTE-Advanced Feasibility Studies in RAN WG4 (Release 9), June 2010.

[4]3GPP specifications can be found at the following URL:http://www.3gpp.org/ftp/Specs/archive/

Books

[12] C. Johnson, *Long Term Evolutionin Bullets*, second ed., Create Space Independent Publishing Platform, July 2012.

[13] S. Sesia, I. Toufik, M. Baker, *LTE, the UMTSLong Term Evolution, From Theory to Practice*, second ed., John Wiley & Sons, August 2011.

[14] E. Dahlman, S. Parkvall, J. Skold, *4G, LTE/LTE-Advancedfor Mobile Broadband*, Academic Press, May 2011.

[15] X. Zhang, X. Zhou, *LTE-Advanced Air Interface Technology*, CRC Press, September 2012.

Articles

[16] A. Roessler, M. Kottkamp, M. Sandra, *Carrier Aggregation—(One) Key Enabler for LTE-Advanced*, Rohde & Schwarz, October 2012.

[17] J. Xu, *LTE-Advanced Signal Generation and Measurement Using SystemVue*, Agilent Technologies, December 2010.

[18] Application Note, Introducing LTE-Advanced, Agilent Technologies, March 2011.

[19] C. Hoymann, et al., A lean carrier for LTE, IEEE Commun. Mag. (February 2013).

[20] Application Note, Understanding Carrier Aggregation, Anritsu, February 2013.

[21] N. Miki, et al., Carrier aggregation for bandwidth extensions in LTE-advanced, NTT DoCoMo Tec. J. 12 (2) (September 2010).

[22] E. Seidel, LTE-A Carrier Aggregation Enhancements in Release 11, NOMOR Research GmbH, Munich, Germany, August, 2012.

[23] M. Iwamura, et al., Carrier aggregation framework in 3GPP LTE-advanced, IEEE Commun. Mag. (August 2010).

[24] C. M.Park, et al., System level performance evaluation of various carrier aggregation scenarios in LTE-advanced, 15th International Conference on Advanced Communications Technology (ICACT), January 2013.

[25] A. Li, et al., Search space design for cross-carrier scheduling in carrier aggregation of LTE-advanced system, Proceedings of 2011 IEEE ICC.

[26] M. Abduljawad, et al., Carrier aggregation in long term evolution-advanced, 2012 IEEE Control and System Graduate Research Colloquium (ICSGRC 2012).

[27] K.I. Pedersen, et al., Carrier aggregation for LTE-advanced: functionality and performance aspects, IEEE Commun. Mag. (June 2011).

[28] E. Seidel, 3GPP LTE—A Standardization in Release 12 and Beyond, NOMOR Research GmbH, Munich, Germany, January 2013.

[29] Z. Shen, et al., Overview of 3GPP LTE-advanced carrier aggregation for 4G wireless communications, IEEE Commun. Mag. (February 2012).

[30] A. Damnjanovic, et al., A survey on 3GPP heterogeneous networks, IEEE Wireless Commun. (June 2011).

[31] A. Ghosh, et al., Heterogeneous cellular networks: from theory to practice, IEEE Commun. Mag. (June 2012).

[32] Report ITU-R M.2133, Requirements, evaluation criteria and submission templates for the development of IMT-advanced, November 2008.

[33] Report ITU-R M.2134, Requirements related to technical performance for IMT-advanced radio interface(s), November 2008.

CHAPTER

14 Enhanced Inter-cell Interference Coordination and Multi-radio Coexistence

CHAPTER CONTENTS

14.1 Intra-cell/inter-cell interference mitigation methods 1030
14.2 Heterogeneous networks 1035
14.3 Enhanced inter-cell interference coordination (eICIC) 1040
14.3.1 CA-based eICIC schemes 1041
14.3.2 Non-CA-based eICIC 1044
14.3.3 Further enhanced ICIC 1048
14.4 Multi-radio coexistence and interference avoidance 1051
14.4.1 Collocated multi-radio coexistence issues 1052
14.4.2 In-device coexistence scenarios 1054
14.4.3 In-device coexistence interference avoidance 1056
References 1067

In this chapter, we discuss two important features that were included in the recent releases of LTE to address inter-cell interference problems in LTE systems and in-device inter-radio interference issues, where both problems adversely affect the system capacity, user throughput, and normal operation of the LTE system.

The proliferation of Internet-connected mobile devices will continue to drive growth in data traffic in an exponential order, forcing network operators to dramatically increase the capacity of their networks. The ever-increasing demand for mobile communication services has made it difficult for the conventional homogeneous networks to provide the required capacity and user throughput as they have approached their theoretical limits. One of the most promising and cost-effective solutions to improve the system capacity is to increase the node density, i.e., to deploy low-power nodes such as relay, pico-cell, femto-cell, and remote radio heads in homogeneous networks. The new network architecture is known as heterogeneous networks (HetNets). The deployment of low-power nodes can

LTE-Advanced.
© 2014 Elsevier Inc. All rights reserved.

Ex.1005.01060

provide a more flexible and more effective way to eliminate the coverage holes in macro-cells and improve the system capacity. Therefore, it is considered as a promising approach in the next generation wireless communication systems such as systems beyond IMT-Advanced [16,17]. One of the key issues in the new network architecture is the handover performance deterioration. In co-channel HetNets, the cell-edge UEs can experience more serious interference. The basic principle of inter-cell interference coordination (ICIC) is to avoid high-power transmission on time–frequency resources on which cell-edge users are scheduled in neighboring cells, users that would otherwise experience high interference and correspondingly low data rates. In the next sections, we study the causes and remedies of inter-cell interference in the HetNets [2].

We will then discuss signaling and procedures for in-device coexistence (IDC) and for interference avoidance. An increasing number of UEs are equipped with multiple radio transceivers for LTE, Wi-Fi, Bluetooth (BT), Global Navigation Satellite System (GNSS), and so on. The studies conducted for LTE Rel-11 IDC work item have shown that existing radio resource management mechanisms in some cases are not adequate to overcome the coexistence issues, and some enhanced signaling and other procedures are necessary to avoid or mitigate the collocated multi-radio interference in the identified usage scenarios. Therefore, a new IDC indication message has been defined in LTE Rel-11. This message enables the UE to alert the network to an interference issue, and provide information regarding the direction and nature of the interference, which may be identified in either the time- or frequency-domain. Upon receipt of the IDC message, the network will take appropriate steps to alleviate the problem by reallocating radio resources or configuring discontinuous reception mode parameters [1].

14.1 Intra-cell/inter-cell interference mitigation methods

The classic design principle of cellular communications systems is to divide a geographical area into non-overlapping cells, each served by a single base station. The intercell interference is a serious problem of such systems, in particular when frequency reuse one is utilized. One way to reduce the inter-cell interference within the system is to employ efficient interference averaging mechanisms that organize transmission such that the interference is evenly distributed among all users.

There are three major frequency reuse schemes in cellular systems for mitigating inter-cell interference: hard frequency reuse; fractional frequency reuse (FFR); and soft frequency reuse. A hard frequency reuse scheme splits the system bandwidth into a number of non-overlapping sub-bands according to a predetermined reuse factor, and lets neighboring cells transmit on different sub-bands (scenario A in Figure 14.1). As shown in Figure 14.2, an FFR scheme partitions the given bandwidth into an inner and an outer partition. It then allocates the inner part to the users closer to the base station with reduced power and applies a

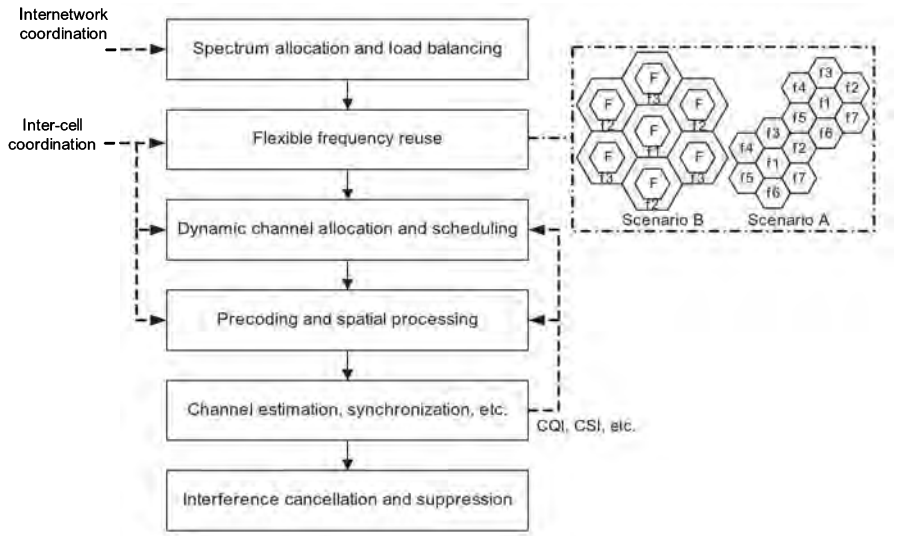


FIGURE 14.1

Co-channel interference mitigation schemes [12].

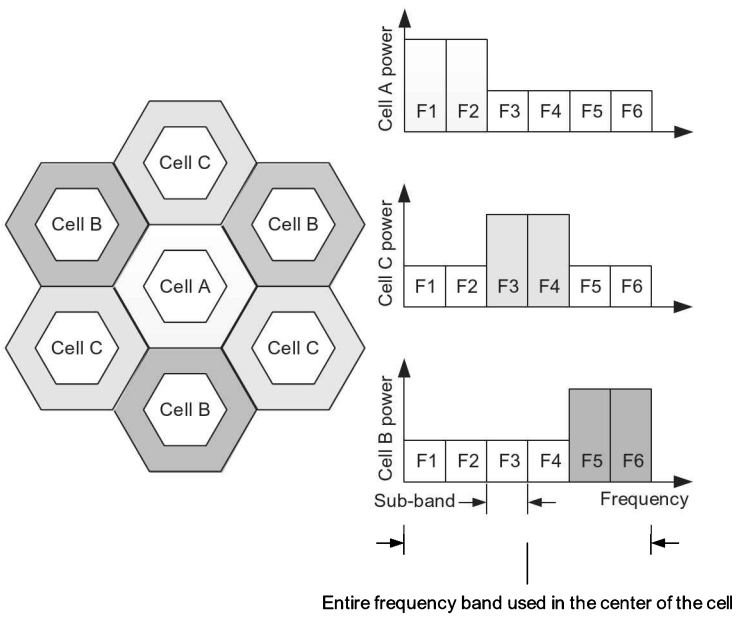


FIGURE 14.2

Illustration of fractional frequency reuse concept [17].

frequency reuse factor of 1, i.e., the inner part is completely reused by all base stations. For users closer to the cell-edge, a fraction of the outer part of the bandwidth is dedicated with a frequency reuse factor greater than 1 (see scenario B in Figure 14.1). With soft frequency reuse, the overall bandwidth is shared by all base stations, i.e., a reuse factor of 1 is applied, but for the transmission on each sub-band, the base stations are restricted to a certain power limit.

Depending on whether noise or inter-cell interference is the dominant effect, the cellular system is referred to as *noise-limited* or *interference-limited*. In an interference-limited system, the carrier to interference plus noise ratio (CINR) can approximately be replaced by the carrier to interference ratio (CIR), and the inter-cell interference plays an important role in terms of achievable system capacity and coverage. In a network deployment with a smaller frequency reuse factor, severe inter-cell interference may occur in the system. In fact, the closer the user is to the cell-edge, the more severe the inter-cell interference can be. Due to a large distance between the transmitter and the receiver, the desired signal power P_{C_j} is then relatively weak compared to the inter-cell interference signal strength. By increasing the frequency reuse factor, the inter-cell interference can be effectively limited, however, at the expense of sacrificing the available bandwidth for each cell and more complex network planning. In addition, in order to increase the data rate and spectral efficiency without requiring more spectrum resources in cellular networks, two traditional spatial reuse mechanisms, cell splitting and sectorization are often utilized. Several advanced antenna techniques such as MIMO and adaptive beamforming can also be used to enhance cellular system performance.

When properly selected transmission format and link adaptation are employed, the capacity of cellular systems depends essentially on the average quality of the received radio signals, which can be characterized by a CINR metric, defined as follows:

$$\text{CINR} = \frac{P_{C_j}}{P_N + \sum_{k \neq j} P_{I_k}}$$

where P_{C_j} is the received carrier signal power from the jth (serving) cell, P_{I_k} denotes the received co-channel interference signal from the kth cell (other than the serving cell), and P_N is the noise power. The received signal power P_{C_j} is determined by the distance between the transmitter and the receiver, the transmission power, and the associated path loss caused by the environment. The most dominant noise type is thermal noise originated from hardware components in the system. The background radiation originating from cosmic or terrestrial sources picked up by the receive antennas also adds to the overall noise in the receiver. As for the perceived interference, actually, the interference P_{I_k} includes not only co-channel interference, which is also known as inter-cell interference, but also intra-cell interference. Since inter-cell interference is the dominant component in an OFDMA system (due to orthogonality of the users in time and frequency) compared to the intra-cell interference, our focus in this section will therefore be only on the

inter-cell interference. The inter-cell interference depends on the number of co-channel cells, the distance between these cells, the transmission power, and the terrain characteristics, in which the first two factors depend on the choice of the frequency reuse factor.

The minimization of the inter-cell interference is desirable to fulfill the following objectives: (i) maximization of the overall network capacity; (ii) maximization of the cell-edge throughput; and (iii) enhancements in terms of both the overall network capacity and the cell-edge performance. Interference mitigation techniques can be generally classified into three major categories: interference cancellation, interference randomization, and interference coordination techniques.

Inter-cell interference cancellation techniques have been investigated and deployed with varying degrees of success in terrestrial mobile networks for more than 20 years. The basic principle of inter-cell interference cancellation techniques is to regenerate the interfering signals and subsequently subtract them from the desired signal. Various inter-cell interference cancellation techniques have been proposed in the literature, and they are mainly characterized as filter-based and multi-user detection (MUD) schemes [8–10]. Filter-based approaches try to mitigate intercell interference by means of linear filters and interference models. In contrast, MUD directly includes the interfering signals in the decoding process. This is done by jointly decoding the desired signal and the interfering signals, or by decoding and subtracting the interfering signals from the signal of interest. Inter-cell interference cancellation techniques can also be jointly used with multi-user MIMO techniques, if the UEs are equipped with multiple-receive antennas. From an implementation viewpoint, interference cancellation does not require any modification of the standards, making it an attractive technique. Although inter-cell interference cancellation promises significant gains and its algorithms are mature, it is considered mostly as a technique for the uplink due to processing complexity which scales exponentially with the number of active users. Furthermore, it requires exchange of information in real-time between the base stations about every few milliseconds to maximize the system gain. Moreover, inter-cell interference cancellation can potentially improve channel performance to that of AWGN if accurate channel estimation is available [8–10].

In contrast to inter-cell interference cancellation, which tries to eliminate the effect of interfering sources in the received signal, inter-cell interference randomization, which is also known as interference whitening or interference averaging, attempts to make the inter-cell interference appear as background noise, i.e., it averages the interference across the data symbols of a data block or the entire frequency band. The approaches include frequency hopping and interleave division multiple access. However, these methods randomize the interference into white Gaussian noise, which cannot reduce interference in nature. Therefore, these approaches can hardly achieve a substantial performance improvement [8–10].

ICIC techniques, also known as inter-cell interference avoidance, in OFDMA radio access systems have recently gained much attention from both the academia

and the standardization communities. In order to reduce inter-cell interference in cellular networks, the ICIC methods apply restrictions to resource management in a coordinated manner among neighboring cells. Resources for coordination can be space (with beamforming antennas), time, frequency, code resources, or transmit power. The restrictions can be in the form of time/frequency resource availability to the resource manager, and/or restrictions on the transmit power that can be applied to certain time–frequency resources. The impact on the system architecture as a result of support of ICIC schemes can be mainly divided into four major categories depending on the degree of distribution: global; distributed; decentralized; and local ICIC schemes.

Global ICIC schemes require an omniscient central entity with full system knowledge, which is capable of acquiring the global system state in zero time, and can distribute scheduling and other decisions instantly to all network nodes. Distributed ICIC schemes rely on one or more central components, which exchange information potentially with all nodes in the network. The central components thereby collect state information and distribute information relevant for coordination to the network nodes, e.g., coordinated multi-point transmission/reception. Decentralized ICIC schemes are distinguished from distributed schemes by having no central entity involved in the coordination process. The coordination is performed exclusively by communication and information exchange among the network nodes. Local ICIC schemes are based mainly on information that is available locally in each eNB. There is no coordination-related communication and information exchange among neighboring eNBs. The local information includes feedback received from the UEs about the strongest interferers. Information exchange among eNBs or with a central coordinator could result in higher performance gains at the expense of increased system complexity [8–10].

A global ICIC scheme is practically unfeasible, although it may potentially attain the highest performance improvements among all ICIC schemes. Local ICIC schemes require no separate network equipment and provide the most flexibility with respect to the network design, although using local ICIC schemes may not achieve the highest performance gain.

An interference mitigation scheme based on beamforming transmits a narrow beam toward the desired user instead of transmitting in the conventional omnidirectional or sectorized manner [12]. This scheme is capable of reducing the interference imposed on users of the system, particularly benefiting the cell-edge users. Therefore, the classic beamforming technique is sometimes also referred to as interference alignment. Beamforming techniques may be further classified into two types, namely, non-adaptive and adaptive beamforming, where both types require partial or full channel state information feedback. Adaptive beamforming techniques adapt the antenna complex-valued weights according to diverse optimization criteria by exploiting the channel knowledge. A particularly beneficial adaptive beamforming technique is the well-known eigen beamforming, where the antenna weights are chosen to be the eigenvector of the largest eigenvalue of the spatial MIMO channel covariance matrix. On the other hand, a beam-switching

technique uses the best-oriented beam among a number of preselected beams, where each array-weight vector is a function of the beam direction, as well as of the antenna element's position. In a typical 120° antenna pattern sector generated by a uniformly spaced linear array having four antenna elements, a total of eight beams may be created, where the adjacent beams are evenly spaced by an angle of 13° [12]. The index of the best beam vector resulting from the maximum mean channel gain measured at the receiver is signaled back to the transmitter, where the channel gain is averaged over a certain time period, a set of subcarriers, and over the spatial domain constituted by the receive antennas, depending on the accuracy of the CSI feedback as well as depending on the affordable feedback bit rate.

The combination of more advanced opportunistic transmission and beamforming techniques may attain further performance improvement in multi-user environments. The concept of beam hopping may be further utilized to intelligently avoid directional interference. Regardless of the use of the adaptive or non-adaptive variant, when transmitting directionally by exploiting the maximum equivalent channel gain, the received signal power and the SINR are enhanced, or alternatively, the transmitted power may be reduced despite maintaining a certain received SINR. As a result, the interference imposed on the adjacent cells is reduced, and the overall interference level in the entire system is reduced. In contrast to the directivity exploited by the above-mentioned beamforming techniques, the benefits of transmit diversity may be limited by transmitting the same signal from different antennas, provided that they experience independent fading. Since the transmit power required for maintaining a certain error probability may be reduced as a benefit of transmit diversity, the interference imposed becomes lower [10].

The concept of distributed antennas has been exploited to ensure that the antenna elements are sufficiently geographically dispersed and far apart to guarantee that the signals generated by each antenna are uncorrelated. The advantage of employing distributed antennas is the increased macro-diversity effect, which is particularly beneficial for the cell-edge users, which would otherwise suffer from severe co-channel interference. In contrast to the conventional single-cell transmission, where each user is served by its local base station only and suffers from co-channel interference caused by the adjacent cells, in the distributed antenna multi-cell transmission, each user is served by several coordinated base stations and each base station jointly processes multiple users' information, which is shared via the backhaul using a high-capacity low-latency optical fiber link. This leads to an equivalent distributed MU-MIMO system [10].

14.2 Heterogeneous networks

One of the most promising and cost-effective solutions to improve the system capacity is to deploy low-power nodes such as relays, pico-cells, femto-cells, and

remote radio heads overlaid by macro-cell networks. The new network architecture is known as heterogeneous networks (as shown in Figure 14.3) can provide a flexible and effective way to eliminate the coverage holes in macro-cells and improve the system capacity. One of the key issues in the new network architecture is the handover performance deterioration in co-channel HetNets, where the cell-edge UEs can experience more serious interference [2,13–15].

The output power of the low-power nodes varies depending on the type of deployment and usage scenario. If the low-power nodes are intended for outdoor deployments, their transmit power ranges from 250 mW to approximately 2 W. They do not require an air-conditioning unit for the power amplifier, and are much lower in cost than traditional macro base stations, where their transmit power typically varies between 5 and 40 W. Femto base stations are meant for indoor use, and their transmit power is typically 100 mW or less. Unlike pico base stations, femto base stations may be configured with a restricted association, allowing access only to its closed subscriber group (CSG) members, or alternatively they can be configured as an open subscriber group (OSG), allowing full or partial access to the public. A network that consists of a mix of macro-cells and low-power nodes, where some may be configured with restricted access and some may lack wired backhaul, is referred to as a HetNet [11,16].

Cellular systems have been traditionally deployed as homogeneous networks using a macro-node-centric planning process. A homogeneous cellular system is a network of base stations in a planned layout and a collection of user terminals, in which all the base stations have similar transmit power levels, antenna patterns, receiver noise floors, and similar backhaul connectivity to the packet data network. Furthermore, all base stations offer unrestricted access to user terminals in

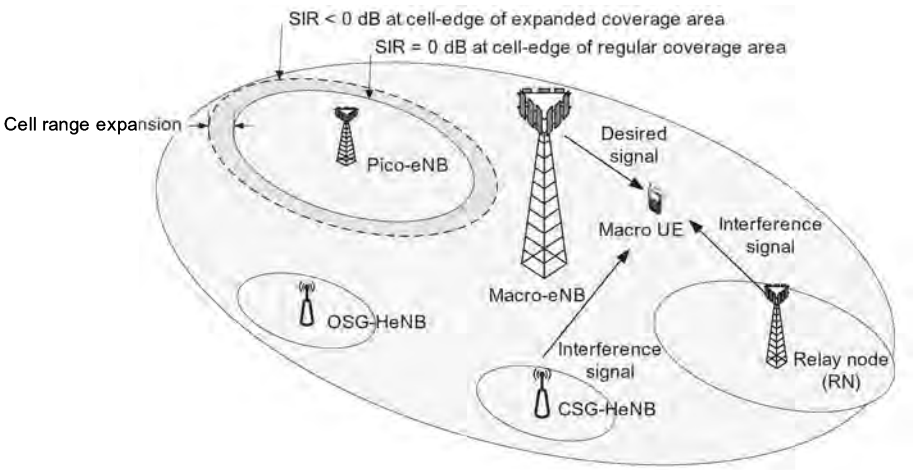


FIGURE 14.3

An example HetNet topology [22].

the network, and can serve approximately the same number of user terminals, all of which carry similar data flows with similar QoS requirements.

The locations of the macro base stations are carefully chosen through network planning, and the base station settings are properly configured to maximize the coverage and to control the interference between base stations. As the data traffic grows and the RF environment changes, the network relies on cell splitting or additional carriers to overcome capacity and link budget limitations in order to maintain uniform user experience. However, this deployment process is complex and iterative. Moreover, site acquisition for macro base stations with towers is becoming more difficult in a dense urban environment, thus a more flexible deployment model is needed for operators to improve broadband user experience in a ubiquitous and cost-effective way.

In a homogeneous network comprising macro-cells, each mobile terminal is served by the base stations with the strongest signal strength, while the unwanted signals received from other base stations are usually treated as interference. In a HetNet, such principles can lead to significantly suboptimal performance. In such systems, smarter resource coordination among base stations, better server selection strategies, and more advanced techniques for efficient interference management can provide substantial gains in throughput and user experience as compared to a conventional approach of deploying macro-cellular network infrastructure.

A pico base station is characterized by a substantially lower transmit power relative to a macro base station. The potentially large disparity between the transmit power levels of macro and pico base stations implies that in a mixed macro/pico deployment, the downlink coverage of a pico base station is much smaller than that of a macro base station. This is not the case for the uplink, where the strength of the signal received from a user terminal depends on the terminal transmit power, which is the same for uplink paths from the terminal to different base stations. Therefore, the uplink coverage of all the base stations is similar and the uplink handover boundaries are determined based on channel gains. This can potentially create a mismatch between downlink and uplink handover boundaries, and make the base station to device association or cell selection more difficult in HetNets, compared to homogenous networks, where downlink and uplink handover boundaries are closely matched (Figure 14.4).

If the cell selection is predominantly based on downlink signal strength, as in LTE Rel-8, the usefulness of pico base stations will be greatly diminished. In this scenario, the larger coverage of high-power base stations limits the benefits of cell splitting by attracting a large fraction of user terminals toward macro base stations based on signal strength without having enough macro base station resources to efficiently serve these user terminals, while lower power base stations may not be serving any user terminals. Therefore, from the point of view of network capacity, it is desirable to balance the load between macro and pico base stations by expanding the coverage of pico base stations and subsequently increasing cell splitting gains [11,16].

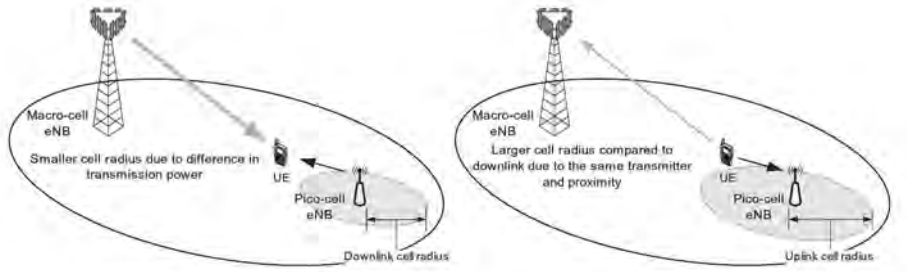


FIGURE 14.4

Illustration of uplink/downlink imbalance in HetNets [11].

Balanced load distribution between macro and pico base stations can be achieved if base station to device association is based on path loss (associating the base station with the minimum path loss rather than the base station with the maximum downlink signal strength), and a fixed partitioning of resources between the macro and pico base stations. As a result, more users are associated with the pico base stations, and the network is able to provide more equitable distribution of radio resources to each user. The effect is even more pronounced in hotspot layouts where users are clustered around pico base stations. Capacity gains can be achieved through sharing of the resources allocated for low-power base stations, while sufficient coverage is provided by high-power base stations on the resources that are allocated to them.

In a HetNet, in order for a user terminal to obtain service from a low-power base station in the presence of macro base stations with stronger downlink signal strength, the pico base station needs to perform interference coordination, for control and traffic channels, with the dominant macro interferers, and the user terminals need to support advanced receivers for interference cancellation. In the case of femto base stations, only the owner or subscribers of the femto base station may be allowed to access the femto base stations. For user terminals that are close to these femto base stations, but barred from accessing them, the interference caused by the femto base stations to the user terminals can be particularly severe, making it difficult to establish a reliable downlink communication to these user terminals. Therefore, as opposed to homogeneous networks, where resource sharing is a good transmission strategy, femto networks necessitate more coordination via resource partitioning across base stations to manage inter-cell interference.

The introduction of low-power nodes in a macro network creates imbalance between uplink and downlink coverage (see Figure 14.4). Due to the larger transmit power of the macro base station, the handover boundary is shifted closer to the low-power node, which can lead to severe uplink interference problems as the UEs served by macro base stations create strong interference to the low-power nodes. Given the relatively small footprint of low-power nodes, even in the case of the most optimized placement, low-power nodes may become underutilized due to geographic changes in data traffic. The performance of a mixed deployment of

macro-, pico-, and open femto-cells was evaluated in the literature [1,11,17,22], which showed that the limited coverage of low-power nodes is the main reason for limited performance gain in HetNets. Furthermore, some of the deployed femto-cells may have enforced restricted association, which effectively creates a coverage hole and aggravates the interference problem. In order to cope with the interference, it is necessary to introduce techniques that can adequately address these issues. Due to restricted association, a CSG femto-cell creates a downlink coverage hole at the vicinity of the femto-cell for non-member UEs. In order to reduce the effect of the coverage hole, a femto-cell could adapt the transmitted power intelligently such that interference is contained within the intended coverage area such as a residential site. Since the femto-cell coverage and femtocell interference to the macro-UE are directly proportional to the femto-to-macro signal strength ratio, a femto-cell could set the proper transmit power by estimating the additional interference that could be tolerated by a non-member UE near the femto-cell. As a result, the femto-cell maintains a similar coverage area regardless of its location within the overlaid macro-cell.

Pico-cells are eNBs with lower transmit power than traditional macro-cells. They are typically equipped with omnidirectional antennas and are deployed indoors or outdoors, often in a planned manner. Their transmit power ranges from 250 mW to approximately 2 W for outdoor deployments, while it is typically 100 mW or less for indoor deployments. Since pico-cells are regular eNBs from an architecture perspective, they can benefit from X2-based ICIC.

In light of the above challenges in the operation of HetNets, an ICIC scheme is critical to HetNet deployment. A basic ICIC technique involves resource coordination among interfering base stations, where an interfering base station avoids use of some resources in order to enable control and data transmissions to the victim user terminal. More generally, interfering base stations can coordinate their transmission power and/or spatial beams with each other in order to enable control and data transmissions to their corresponding user terminals.

The resource partitioning can be performed in time-domain, frequency-domain, or spatial-domain. Time-domain partitioning can better adapt to user distribution and network load variations, and is the most attractive method for spectrum-constrained environments. For example, a macro base station can choose to reserve some of the subframes in each radio frame for use by pico base stations, based on the number of user terminals served by pico and macro base stations, and/or based on the data rate requirements of the user terminals. Frequency-domain partitioning offers less granular resource allocation and flexibility, but is a viable method especially in an asynchronous network. Spatial-domain partitioning can be supported by a CoMP transmission/reception scheme, which was discussed in Chapter 12. For time-domain resource partitioning, a macro base station can use almost blank subframes (ABS) to reserve some subframes for pico nodes. The macro base station continues transmission of legacy common control channels during almost blank subframes to maintain backward compatibility with legacy user terminals. The user terminals can cancel interference on common

control channels within almost blank subframes caused either by higher power macro base stations or by nearby femto stations that they are prohibited to access. An interference cancellation receiver can handle colliding and non-colliding reference signal scenarios, and can eliminate the need for cell planning for heterogeneous deployment [22].

The studies in 3GPP concerning HetNet mobility improvement have continued in LTE Rel-11 [2]. The comprehensive simulations conducted in these studies concluded that handover performance of HetNets was not as good as homogeneous macro-cell deployments. Furthermore, it was shown that the UE speed has significant impact on the handover performance, and that careful DRX configurations are required to avoid negative impact on handover performance. The objective in LTE Rel-12 is thus to enhance handover performance in HetNet scenarios (e.g., minimization of handover failure rate, minimization of ping-pong effects, recovery from radio link failure), as well as supporting UE mobility and longer DRX cycles. The enhancement of mobility in small-cell scenarios with focus on inter-frequency schemes will also be part of the LTE Rel-12 development.

14.3 Enhanced inter-cell interference coordination (eICIC)

The basic principle of ICIC is to avoid high-power transmission on time–frequency resources on which cell-edge users are scheduled in neighboring cells, users that would otherwise experience high interference and correspondingly low data rates. In LTE Rel-8, ICIC is performed over the frequency-domain by transmission of messages across a standardized backhaul inter-eNB interface such as X2. Because the latency over X2 is typically in the order of a few milliseconds, it is expected that any updates or reconfiguration to the ICIC messages are relatively infrequent (in the order of seconds). The LTE Rel-8 frequency-domain ICIC in the downlink is based on event-triggered message exchange between eNBs approximately every 200 ms to allow adaptive FFR. Uplink ICIC is based on event-triggered *overload indicator* and *high interference indicator* messages exchanged between the eNBs approximately every 20 ms. In the context of ICIC, the following metrics are defined [11,7]:

- *High interference indicator (HII)*: The HII provides information about a set of resource blocks on which an eNB is going to schedule transmissions for cell-edge terminals, i.e., resource blocks on which a neighboring cell can expect higher inter-cell interference. Although it is not explicitly specified how an eNB should respond to an HII message (or any other ICIC-related X2 signaling) received from a neighboring eNB, a reasonable action for the receiving eNB would be to avoid scheduling its own cell-edge terminals on the same resource blocks, reducing the uplink interference to cell-edge transmissions in its own cell, as well as in the cell from which HII message was received. The HII is an indicator which is sent as a bitmap with one bit per resource

block/sub-band that the serving cell intends to use for scheduling cell-edge UEs, potentially causing high inter-cell interference to the neighboring cell. An eNB can send HII with different, neighbor-cell-specific contents to different neighbor cells.

- *Relative narrowband transmit power (RNTP)*: For the downlink, the relative narrowband transmit power is defined to support ICIC operation. The RNTP is similar to the HII in the sense that it provides information for each resource block whether the relative transmit power of that resource block exceeds a threshold level. Similar to the HII, a neighboring cell can use the information provided by the received RNTP when scheduling its own terminals, especially terminals in the cell-edge that are more likely to be interfered by the neighboring cell. The RNTP message is signaled using a bitmap wherein each RNTP bit value indicates whether the corresponding resource block pair is limited by a transmit power threshold. Upon receipt of the RNTP message, the recipient eNBs can take into account this information while making their scheduling decisions for subsequent subframes. One such example may be that the recipient eNB avoids scheduling UEs in resource blocks where the source eNB (e.g., macro-cell eNB) is transmitting above a certain power limit.
- *Overload indicator (OI)*: The overload indicator is an indicator exchanged over the X2 interface, reflecting the uplink interference plus noise level (low, medium, or high) of a resource block measured by an eNB. Although the reaction of the recipient eNB upon receipt of the OI is not standardized, a possible reaction to the OI by the recipient eNB would be to limit the maximum transmit power of a UE scheduled on resource blocks indicated by the OI to have high interference.

During LTE Rel-10 standardization, 3GPP developed two approaches to coordinate inter-layer interference, primarily targeting the aforementioned deployment scenarios. Both approaches rely on a semi-static resource partitioning across layers, but take two different approaches to ICIC of control and data channels. In one approach, interference avoidance is addressed by means of ICIC in the frequency-domain, relying on carrier aggregation (CA) as introduced in LTE Rel-10. In the other approach, interference avoidance is addressed by means of ICIC in the time-domain, relying on ABS. Both approaches target scenarios with low-power nodes, assuming time-synchronization with the macro-eNB.

14.3.1 CA-based eICIC schemes

In CA, a terminal may simultaneously receive/transmit data and control on multiple components carriers (CCs), where a component carrier is fully backward compatible with LTE Rel-8. A terminal supporting carrier aggregation can be configured by higher layer signaling to enable cross-carrier scheduling on certain component carriers. This implies that a terminal receiving a downlink assignment on one component carrier may receive associated data on another component carrier. One of

the main motivations for introducing cross-carrier scheduling was to enhance operations in HetNets in a multi-carrier deployment. The basic idea in CA-based ICIC is to create a protected component carrier for reliable reception of downlink physical signals, system information, and control channels at victim layers, but data can be received on any configured downlink component carrier via cross-carrier scheduling. This, in conjunction with RNTP at aggressor layers, forms the basis of CA-based eICIC. As shown in Figure 14.5, assume a macro–pico deployment scenario with two downlink component carriers, CC1 and CC2. In this particular scenario, a macro-cell creates a protected component carrier by reducing its transmit power on CC1 in order to enable larger picocell coverage on CC1. On CC2, the macro-cell transmits with its nominal output power, implying that the size of the pico-cell associated with CC2 will be reduced in comparison with the pico-cell coverage on CC1. The dashed areas in the figure represent cell range expansion zones, i.e., areas with reduced reception reliability of the downlink control channels, PDCCH, PHICH, and PCFICH [11,22].

As shown in Figure 14.5, it is obvious that without use of eICIC, a terminal configured with CC1 and CC2 can simultaneously receive from both carriers only in the following scenarios: (i) it operates within the coverage of the pico-cell associated with CC2 when connected to the pico-cell; (ii) it operates within the coverage of the macro-cell on CC1 when connected to the macro-cell. However, with cross-carrier scheduling a pico-cell-edge user can receive PDCCH on the protected CC1, whereas the associated PDSCH is received on CC2, on which the macro-cell will have reduced its transmit power on PDSCH in resource blocks known by the pico-cell via X2 signaling of RNTP. It is also shown that the operation of the CA-based eICIC, in which the macro-cell avoids transmissions or reduces its transmission power of PDSCH in resource blocks in the upper band of CC2, the users operating in the cell range expansion zones receive data via cross-carrier scheduling, whereas users closer to the eNB sites do not need to rely on data reception via cross-carrier scheduling. A UE typically associates with a base station that exhibits strong downlink SINR. If the macro-cell transmission interferes with that of a low-power node, the UE may not be able to select the low-power node. With cell range expansion, a UE can associate with a low-power node despite the fact that the downlink SINR may be much lower than 0 dB. Time-domain resource partitioning enables load balancing between high- and low-power nodes. Note that resource partitioning is dynamically adapted to network load. Capacity gains in HetNets are achieved by off-loading traffic from macro-cells to pico-cells, and the amount of off-loading is increased by cell range expansion. Cell range expansion virtually increases the footprint of the low-power node. The operating signal-to-interference ratio (SIR) in the expanded cell range may be less than 0 dB. The ABS facilitate serving UEs in the expanded cell range by the victim nodes. However, interference from cell-specific reference signals and other control signals within ABS limits the cell range expansion. LTE Rel-10 supports cell range expansion with SIR $= -6$ dB, which was further decreased to -9 dB in LTE Rel-11 [11,22].

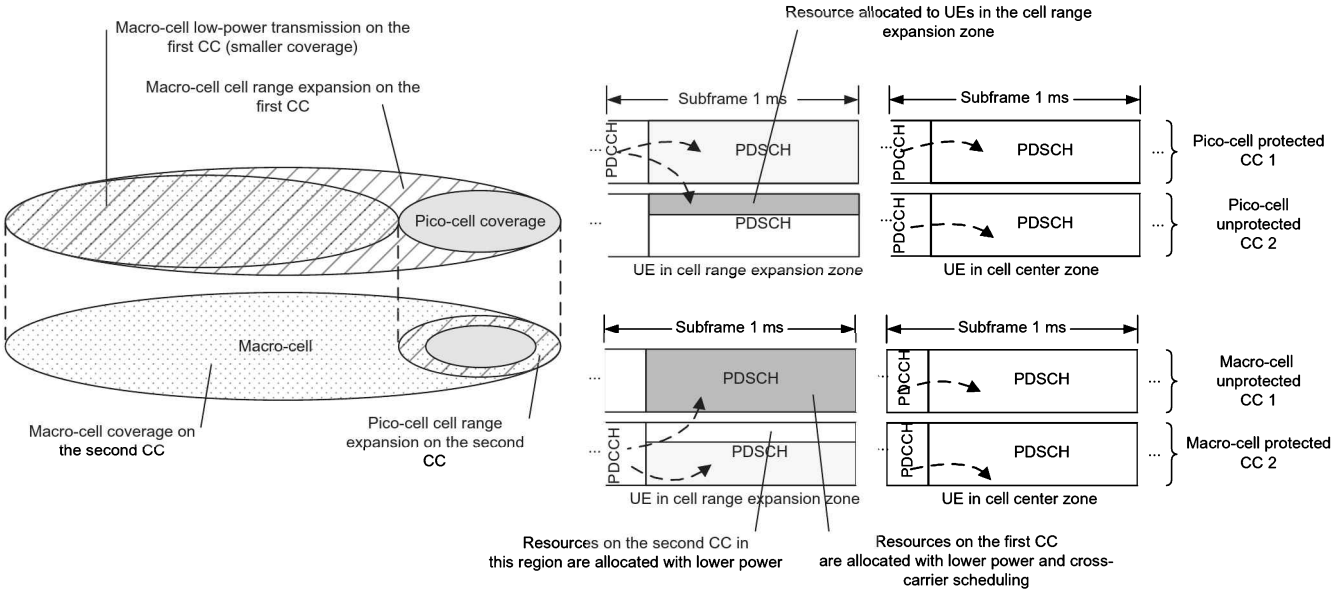


FIGURE 14.5

Illustration of the CA-based eICIC concept [11].

In CA-based eICIC, the primary cell associates with a protected component carrier. Pico-cell users would then have CC1 as their primary cell, whereas macro-cell users would have CC2 as their primary cell. The CRS transmission from an aggressor cell (necessary for backward compatibility with legacy LTE systems) will potentially create inter-cell interference toward victim users. Therefore, LTE Rel-10 introduced transmission mode 9 for which demodulation of PDSCH relies entirely on the UE-specific reference signals for data demodulation, and CSI reference signals for CSI measurement. Through RNTP signaling, DM-RS collisions across different cells can be avoided since DM-RS are only transmitted in resource blocks carrying PDSCH. Such UE-specific configuration is useful in HetNet scenarios where the CRS reception might be deteriorated. Furthermore, a terminal can be configured to conduct measurements corresponding to mobility and radio link monitoring on its primary cell only, i.e., the cell with the best CRS quality [5–7].

14.3.2 Non-CA-based eICIC

The underlying concept of time-domain eICIC is that an aggressor layer creates protected subframes for a victim layer by reducing its transmission activity in certain subframes. To do so, the aggressor eNB reduces its transmission power of some downlink signals, or alternatively mutes their transmission during a set of low-interference subframes designated as ABS whose occurrences are known in advance at the coordinated eNBs. The ABS patterns can be constructed by configuring MBSFN subframes and/or by not scheduling unicast traffic, or alternatively by reducing transmit power in certain subframes. During ABS, the aggressor eNB does not transmit PDSCH but may transmit CRS, critical control channels, and broadcast and paging information. If the victim cell schedules its UEs in subframes that overlap with aggressor cell ABS, the victim cell protects its UEs from strong inter-cell interference, thereby increasing the likelihood of successful PDCCH/PDSCH reception (Figure 14.6).

Backward compatibility is ensured by transmitting essential physical signals, system information, and paging in the same way as in LTE Rel-8. This implies that CRS transmission at the aggressor layers will create interference on either PDSCH signal or CRS signals at victim layers even during ABS, although the CRS interference on PDSCH can be reduced by configuring MBSFN subframes, since the CRS is not transmitted in the MBSFN region of MBSFN subframes. Furthermore, the primary and secondary synchronization signals, as well as system information, are transmitted in the zero and fifth subframes of a radio frame, and will thus be inter-layer interference sources that cannot be avoided by introducing ABS. In the case of a macro–femto deployment, CSG femto-cells represent the aggressor layer, whereas in the case of a macro–pico deployment, macro-cells represent the aggressor layer. With the time-domain ICIC, a macro-cell eNB may schedule users during protected subframes when they are in the proximity of CSG femto-cells, whereas a pico-cell eNB may schedule their cell-edge users only during protected subframes (Figure 14.7). The information

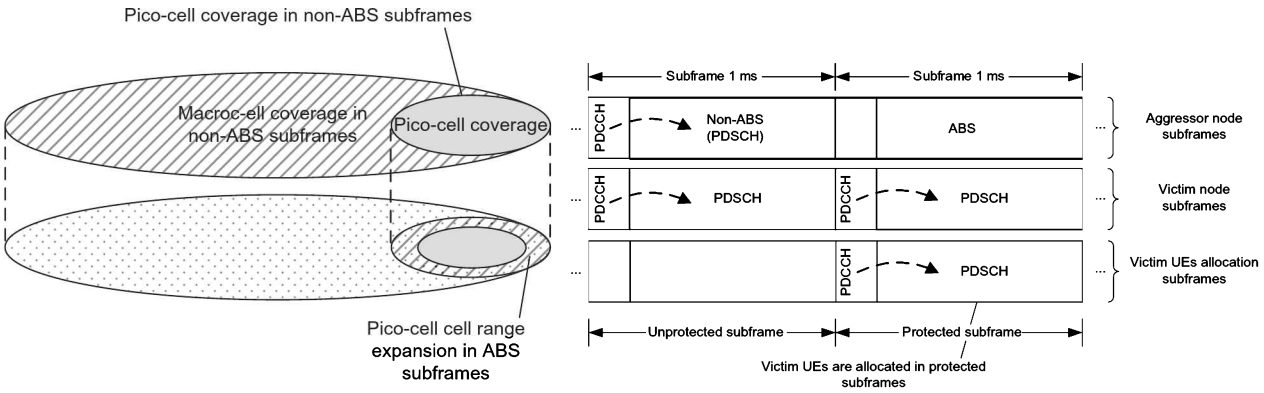


FIGURE 14.6

Illustration of the non-CA-based eICIC concept [11].

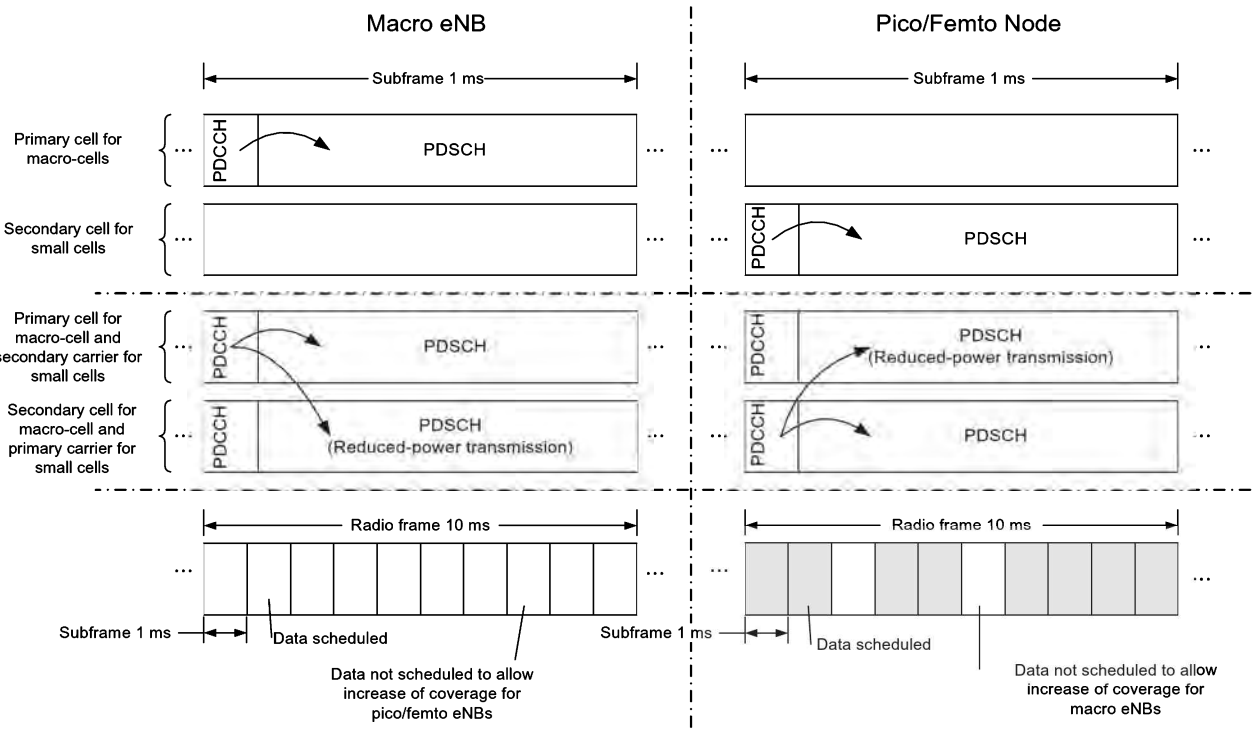


FIGURE 14.7

Illustration of CA-based and non-CA-based eICIC methods [16].

regarding the subframes on which coordinated low-interference transmission occurs is exchanged between coordinating eNBs via bitmap patterns. Upon receiving the bitmap pattern either via customized network operation administration and maintenance, or via the X2 interface, the recipient eNB can schedule data for its victim UEs on subframes that overlap with the aggressor ABS transmissions, as shown in Figure 14.7. In order to enable this, the time-domain eICIC requires time-synchronized eNB transmissions at least at the subframe boundaries. In an FDD system, for optimal operation with a synchronous uplink HARQ in a HetNet, a bitmap of length 40 bits (which is equivalent to a 40-ms periodicity) is used. Additional interference mitigation through subframe shifting is required to avoid cross-layer interference from broadcast channel and synchronization signals. It is also desirable to configure paging occasions, and scheduled system information, in non-ABS at the aggressor layer and in protected subframes at the victim layer [11].

In LTE Rel-8, a UE may average channel and interference estimates over multiple subframes to derive a CSI feedback. When time-domain eICIC is used, the interference level of these two types of subframes, i.e., protected and unprotected subframes, can be significantly different. In order to ensure that the UE does not average interference across the two different types of subframes, the eNB can configure two subframe subsets such that the UE only averages the channel and interference estimates over subframes within the subset, but not across the two subsets. The UE then reports the CSI measurements separately for the two subsets either periodically (with the respective configured reporting periods for each subset) or aperiodically (i.e., one of the CSI measurements from two subframe subsets is reported via PUSCH, when triggered by PDCCH) [11].

In the connected mode, where a UE's mobility is controlled by the network, the network may perform an inter-frequency or inter-RAT handover to a different carrier frequency when the network determines that a non-CSG UE (range-extended pico-cell UE) is in the proximity of a CSG femto-cell based on the UE's measurement reports. In the idle mode, where the mobility is controlled by the UE within the network, the UE autonomously performs an inter-frequency or inter-RAT cell reselection to a base station on a different carrier when the UE moves close to a dominant interferer. Thus, in both cases, an inter-frequency/inter-RAT handover can potentially create LTE coverage loss, possibly leading to LTE service discontinuity on a collocated carrier. To avoid occurrence of LTE coverage holes, LTE Rel-10 eICIC developed mobility support and radio link monitoring (RLM) [11].

In LTE, the UE performs RRM measurements to manage its network connection and to facilitate handover. In the connected mode, the UE reports RSRP and/or RSRQ of the serving and the neighboring cells to the serving eNB (see Chapter 9 for a description of RSRP and RSRQ). The network then performs a handover, transferring the UE to a neighbor cell when the serving cell's RSRP falls below the neighbor cell's RSRP plus an offset to ensure UE service continuity during mobility. In LTE Rel-10, a victim UE can be configured to perform

resource-specific RRM measurements only on protected subframes. The resource-specific RRM measurements can improve accuracy of RSRP/RSRQ reporting by eliminating persistent interference on the CRS. Note that the collision of CRSs transmitted from different cells can be avoided by properly assigning the physical cell identities.

Radio link monitoring is a measurement function for ensuring that UEs maintain time synchronization and can reliably receive their control information. In LTE, the UE continuously evaluates the quality of the serving eNB in the downlink, and ensures that it is time synchronized to the serving eNB. If downlink synchronization is lost, the UE must suspend its uplink transmissions and should try to recover its existing link or to find a new serving cell with which a reliable downlink channel can be established. The RLM functionality comprises out-of-sync and in-sync evaluation procedures where the UE monitors CRS quality of the serving cell in the presence of co-channel interference. If the UE's serving cell is not the strongest measured cell due to severe interference, the UE can potentially declare a radio link failure. In order to ensure predictable UE behavior, LTE Rel-10 provides a mechanism so that the serving eNB can configure resource-specific RLM measurements at the UE for recording its radio link quality as experienced by the UE in protected subframes. This ensures that the link quality is tied to that of the protected subframes, and the UEs can continue to maintain their connection in HetNet scenarios [11].

In summary, time-domain eICIC may be utilized for pico-cell users which are served in the edge of the serving pico-cell, e.g., for traffic off-loading from a macro-cell to a pico-cell, allowing such UEs to receive service from the pico-cell on the same frequency layer. The inter-cell interference in this case may be mitigated by the macro-cell(s) utilizing ABS to protect the corresponding pico-cell's subframes from interference. A UE served by a pico-cell uses the protected resources for cell measurements (RRM), RLM, and CSI measurements. For a UE served by a pico-cell, the RRM/RLM/CSI measurement resource restriction may allow more accurate measurement of the pico-cell under severe interference from the macro-cell(s). The pico-cell may selectively configure the RRM/RLM/CSI measurement resource restriction only for those UEs subject to strong inter-cell interference. Furthermore, for a UE served by a macro-cell, the network may configure a RRM measurement resource restriction for neighbor cells in order to facilitate mobility from the macro-cell to a pico-cell [3].

14.3.3 Further enhanced ICIC

Due to time limitations, some enhanced ICIC techniques were deprioritized in LTE Rel-10. Particularly, the impact of legacy transmissions on control and data channel demodulation when using ABS was left for consideration in LTE Rel-11, leading to a further enhanced ICIC (FeICIC) scheme development. The work on the FeICIC scheme attempted to identify the UE performance requirements, possible air-interface changes, and eNB signaling improvements. In order to significantly

improve detection of physical cell identity and system information in the presence of dominant interferers, the study focused on UE receiver implementation, UE performance requirements, and eNB signaling required for UE measurement/reporting, as well as network assisting information for CRS interference cancellation and usage of reduced-power ABS. In LTE Rel-11, the enhanced downlink physical control channel has been developed to allow improved control channel inter-cell interference mitigation.

Co-channel deployments are of interest due to cost-effectiveness and high spectral efficiency. The resource partitioning can effectively mitigate interference from the traffic channels. However, inter-cell interference originated from the synchronization and control channels as well as CRSs will persist, since transmission of these signals is necessary for legacy support. Subframe time shifting can be utilized in FDD systems to avoid collision of the control/synchronization channels between eNBs of different power classes that require partitioning, but it cannot be applied to TDD systems. There is no network solution for CRS interference mitigation for either FDD or TDD systems. Without additional interference mitigation of the aforementioned channels and CRS, only limited SIR bias values (approximately 6–10 dB) can be supported, which limits the potential for cell range expansion. It must be ensured that UEs are able to detect and acquire a weak cell and measure and report the measurements to the network, which is a prerequisite for handover and cell range expansion. The CRS interference mitigation has an important role in system performance. Strong CRS interference, even though present only in a relatively small fraction of resource elements, can significantly degrade turbo code performance and the overall SINR; therefore, the potential gains of cell range expansion can be severely reduced. Given that the aforementioned interference sources are all broadcast at full power targeting UEs at the cell-edge, it must be ensured that a robust UE-based interference cancellation solution is feasible, which decodes the strongest signal, performs channel gain estimation toward the interfering cell, cancels the interfering signal, and continues the procedure until the desired signals of the serving cell are acquired.

As mentioned earlier, adaptive inter-cell interference management in LTE Rel-10 is enabled by coordination of resources used for scheduling data traffic through the X2 interface. The granularity of the negotiated resource is a single subframe (Figure 14.8). The resource partitioning enables cell range expansion through use of a bias for cell range determination. In a typical case, cell range expansion is enabled to improve system capacity, and a cell bias is applied to low-power nodes. The bias value refers to a threshold that triggers handover between two cells [16]. A positive bias means that the UE will be handed over to a pico-cell as soon as the difference in the signal strength from the macro-cell and pico-cell falls below a threshold. The macro base station informs the pico base station which resources will be utilized for scheduling a macro-UE, and which subframes are assigned as ABS. Therefore, the low-power nodes are informed of the interference pattern from the high-power base station, and can

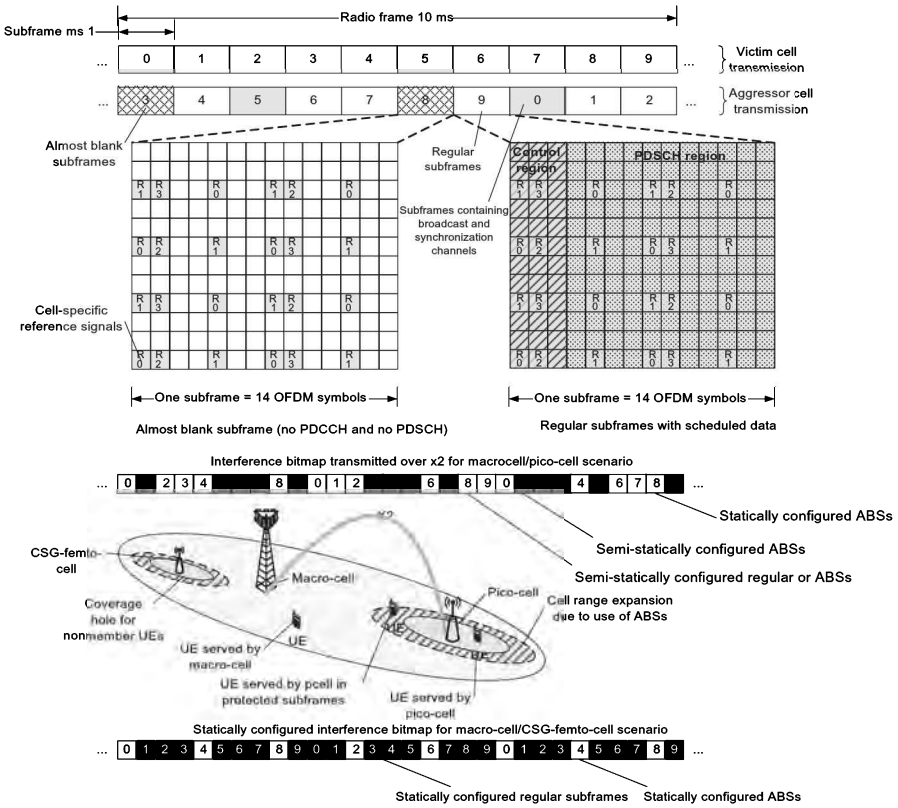


FIGURE 14.8

Illustration of the static/semi-static interference management eICIC schemes for FDD systems in macro-cell/pico-cell and macro-cell/CSG-femto-cell scenarios [16].

schedule the UE in the extended cell areas on subframes protected from high-power interference. Interference coordination is performed by means of a bitmap, where each bit in the bitmap is mapped to a single subframe (see Figure 14.8). The size of the bitmap is 40 bits, suggesting that the interference pattern repeats every 40 ms. Depending on the traffic volume, the pattern can change every 40 ms. The aggressor node effectively controls which resources can be used to serve the UE in the cell range expansion zones. An example of coordination between a macro-cell and pico-cell is shown in Figure 14.8. Note that the cell range expansion may be desirable for a macro base station as well. A typical use case for cell range expansion in the macro base station is to reduce the number of handovers. In a scenario with a large number of high-mobility users, the number of handovers in the network can become problematic, particularly in the deployment of pico base stations, the cells become small. The same resource partitioning

schemes can then be utilized to allow high-mobility macro-UEs to remain attached to a macro-cell while inside the coverage area of a pico-cell [16]. In this case, the pico base station needs to restrict scheduling data traffic on some resources. In a macro–femto scenario (see Figure 14.8), due to the lack of an X2 interface between the eNB and the HeNB, only a static network-configured solution is feasible when CSG-femto nodes are deployed on the same frequency as the macro-cell. Due to the static nature of the solution, the resource partitioning pattern cannot be adapted to the instantaneous characteristics of actual data traffic [16].

14.4 Multi-radio coexistence and interference avoidance

There has been a significant increase in the use of wireless devices equipped with a number of different radio technologies collocated on a single hardware platform in recent years, where each radio technology (depending on availability and coverage) can facilitate certain user applications/network services. A typical configuration of multi-radio mobile terminals consists of one or more wide-area RATs such as HSPA + , LTE, mobile WiMAX, cdma2000, and a number of short-range wireless technologies such as Bluetooth and Wi-Fi operating in the industrial, scientific, and medical (ISM) bands, as well as a GNSS or global positioning system (GPS) receiver for positioning. When these radios operate simultaneously in adjacent or overlapping RF spectrums, it results in interference from transmission of one radio to the reception of the other radios. This condition is referred to as in-device coexistence interference. IDC interference occurs when the frequency separation of less than 50 MHz is allotted between UMTS/LTE and the ISM-band radios (Table 14.1). With a frequency separation of less than 20 MHz, typically 50 dB of isolation is required to avoid IDC effects. The small form factor of mobile terminals usually provides only 10–30 dB isolation. As a result, an effective solution is required to mitigate the IDC interference without degrading the performance of the wireless access systems collocated on the user terminal [1,18].

Table 14.1 Experimental Results Concerning Minimum Frequency Gap Requirements [1]

		Minimum Frequency Gap Requirement (MHz)		
		Antenna Isolation		
Aggressor	**Victim**	**10 dB**	**15 dB**	**20 dB**
LTE Band 40	Wi-Fi	58	52	50
Wi-Fi	LTE Band 40	56	50	46
LTE Band 7	Wi-Fi	60	52	50

The commercial applications of GNSS receivers typically use the L1 band (1575.42 MHz) for location-based services. The uplink direction of LTE Band 13 (777–787 MHz) and Band 14 (788–798 MHz) can disrupt the operation of a GNSS receiver using the L1 band. This is because the second harmonic of Band 13 (i.e., 1554–1574 MHz) and the second harmonic of Band 14 (i.e., 1576–1596 MHz) are extremely close to the L1 band [1].

14.4.1 Collocated multi-radio coexistence issues

As shown in Figure 14.9, the lower portion of the ISM band is very close to LTE Band 40 (TDD). In the case of LTE-BT simultaneous operation, the LTE transmitter causes interference to the BT receiver, and the BT transmitter causes interference to the LTE receiver by desensitizing the receiver. Similar interference issues exist for LTE-Wi-Fi concurrent operation. It is also shown in Figure 14.9 that there is less than 20 MHz frequency separation between BT and LTE Band 7 (FDD uplink). Thus, the LTE transmitter causes interference to the BT receiver. There is no impact on the LTE receiver from the BT transmitter, because the

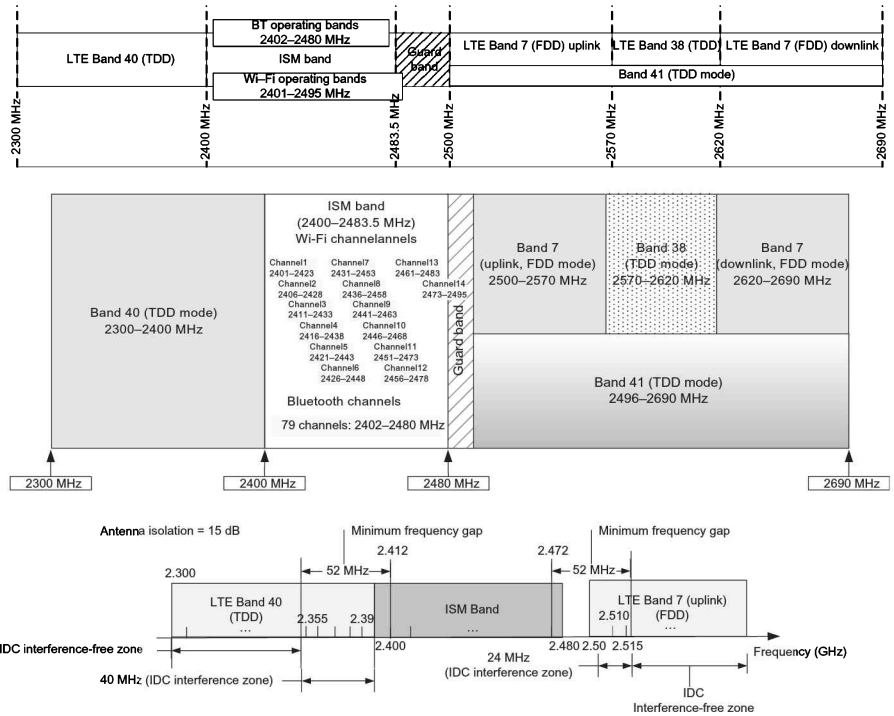


FIGURE 14.9

E-UTRA frequency bands around 2.4 GHz ISM band [1].

corresponding LTE Band 7 (FDD downlink) is far away from the ISM band. There is only 5 MHz separation between Wi-Fi and the LTE Band 7 uplink; however, since Wi-Fi operation is limited to channel 13 in most countries except Japan, there is often a frequency separation of 17 MHz. In the case of LTE-Wi-Fi coexistence, only the Wi-Fi receiver will be affected by the LTE uplink transmitter [1].

Interference between LTE Bands 7 and 40/41 with the 2.4 GHz ISM band is significant when operating in adjacent bands, where current RF filtering schemes are not adequate to mitigate the problem in a number of practical scenarios according to 3GPP RAN Working Group 4 studies [1]. The IDC interference level and its impact on the receiver performance depends on transmit power and receiver blocking characteristic of each radio, and physical characteristics of transceivers (e.g., filter frequency responses, antenna isolation). LTE Rel-8/9/10 already defined some mechanisms such as DRX mode and measurement gaps which would allow mitigation of some coexistence scenarios; however, these schemes are solely controlled by the eNB. The network-controlled UE assisted (i.e., providing triggers) and UE-based autonomous solutions were considered as part of the LTE Rel-11 IDC work item. The interference between LTE and the 2.4-GHz ISM band is significant when operating in adjacent bands, as shown in Figure 14.9. Those problems can be summarized as follows [1]:

- LTE Band 40 to ISM interference: LTE deployed in the upper 30 MHz of Band 40 can desensitize[1] the entire ISM band. LTE in any channel in Band 40 can desensitize the lower 20 MHz of the ISM band.
- ISM to LTE Band 40 interference: ISM in the lower 20 MHz can desensitize all channels in LTE Band 40. ISM in any part of its band can desensitize the upper 20 MHz of LTE Band 40.
- LTE Band 7 to ISM interference: LTE Band 7, in the uplink direction, deployed in 2510 MHz channel can desensitize the entire ISM band.
- With LTE deployed in Band 40, in some scenarios, and BT as a master can cause about 44% downlink error rates, and BT as a slave can cause about 55% downlink error rate.
- With LTE deployed in Band 7, the BT receiver error rate is 100% with high data rate applications on LTE.
- LTE Band 7/13/14 transmitter induces interference to GNSS receiver.

As shown in Figure 14.9, there are 14 channels in the ISM band designated for Wi-Fi operation. Each channel has 5 MHz separation from other channels,

[1]Desensitization is a common performance degradation indicator, where the desensitization is relative to an assumed reference sensitivity value. The desensitization is approximated as $10\log_{10}x$, where x is the ratio between the coexistence interference and the noise floor at the receiver sensitivity level. Using desensitization as the performance measure provides an indication of the degradation that can be expected when the victim system is in its most vulnerable state at the edge of its coverage, and thus may be descriptive of a worst case scenario. The error vector magnitude (EVM) measure can also indicate potential degradation in receiver performance because a signal with large EVM would likely be incorrectly decoded at the receiver.

with the exception of channel 14 where separation is 12 MHz. Channel 1 starts with 2401 MHz and channel 14 ends at 2495 MHz. Different countries have different policies for the number of allowed channels of Wi-Fi operation [21]. Since E-UTRA Band 7 is an FDD band, there is no impact on the LTE receiver from the Wi-Fi transmitter; however, the Wi-Fi receiver is interfered by the LTE uplink transmitter in this frequency band. Bluetooth operates in 79 channels, each having 1 MHz bandwidth in the ISM band. The first channel starts at 2402 MHz, and the last channel ends at 2480 MHz [20]. The LTE Band 40 and BT will adversely affect each other, and the transmission of LTE Band 7 in the uplink direction will affect BT reception, as well.

14.4.2 In-device coexistence scenarios

In order to find an efficient and effective solution for the IDC issues that were mentioned above, it is important to identify the use cases that are commonly encountered. This is due to the fact that different usage models result in different assumptions about the behavior of the LTE transceiver and other collocated radio technologies, which eventually impact solutions. The IDC scenarios of interest in this study are as follows [1]:

1. *LTE + BT earphone (VoIP service)*: In this scenario, LTE is used for VoIP, and the BT earphone is used to send or receive voice packets. The activities of LTE and BT transceivers are going to be very similar in this case because of the end-to-end latency requirement.
2. *LTE + BT earphone (multimedia service)*: In this scenario, multimedia content is downloaded via the LTE link, and audio is routed to a BT headset, where the activities of LTE and BT are correlated. The requirements for scheduling/unscheduled periods for a typical streaming application can be set based on the LTE and BT characteristics. Activity time for BT can vary dynamically with a streaming application. The BT audio stream typically uses the advanced audio data profile (A2DP) [20], in which transmission delays greater than 60 ms can cause audible playback artifacts; consequently, the scheduling period of LTE should not exceed this limit. The latency requirement is less stringent on the LTE side in this case, and depends on the QoS class of the content. The maximum unscheduled period for LTE can be as long as 150 ms. However, in order not to degrade the LTE performance, it is desirable to minimize the LTE unscheduled period, and the smallest unscheduled period is determined by the on-time needed by the BT transceiver to sustain the data rate, depending on the link condition. This number typically ranges from 15 to 60 ms. As a result, the LTE scheduling period should be less than 60 ms, and the unscheduled period should be between 15 and 60 ms [1].
3. *LTE + Wi-Fi portable router*: In this scenario, LTE is considered a backhaul link providing access to the Internet, and the connectivity is shared by other

local users using Wi-Fi. The Wi-Fi transceiver is operated as an access point and has full control over frequency channel and transmitting power. Given the ability of the Wi-Fi transceiver to select the frequency channel, it may be possible to avoid interference to/from Wi-Fi by moving the Wi-Fi signal away from the LTE band, as shown in Figure 14.10. In the downlink, the worst case latency will be for a packet arriving at the eNB at the beginning of the LTE unscheduled period; thus, the latency is the sum of the LTE unscheduled period (waiting time for LTE scheduling) and the LTE scheduling period (waiting time for Wi-Fi scheduling). In the uplink, the scheduling/unscheduled periods can be made as small as 1 ms to minimize latency, but this is not desirable due to the impact on retransmissions and other sensitive timings in LTE and Wi-Fi operation. In order to fulfill the latency requirements of

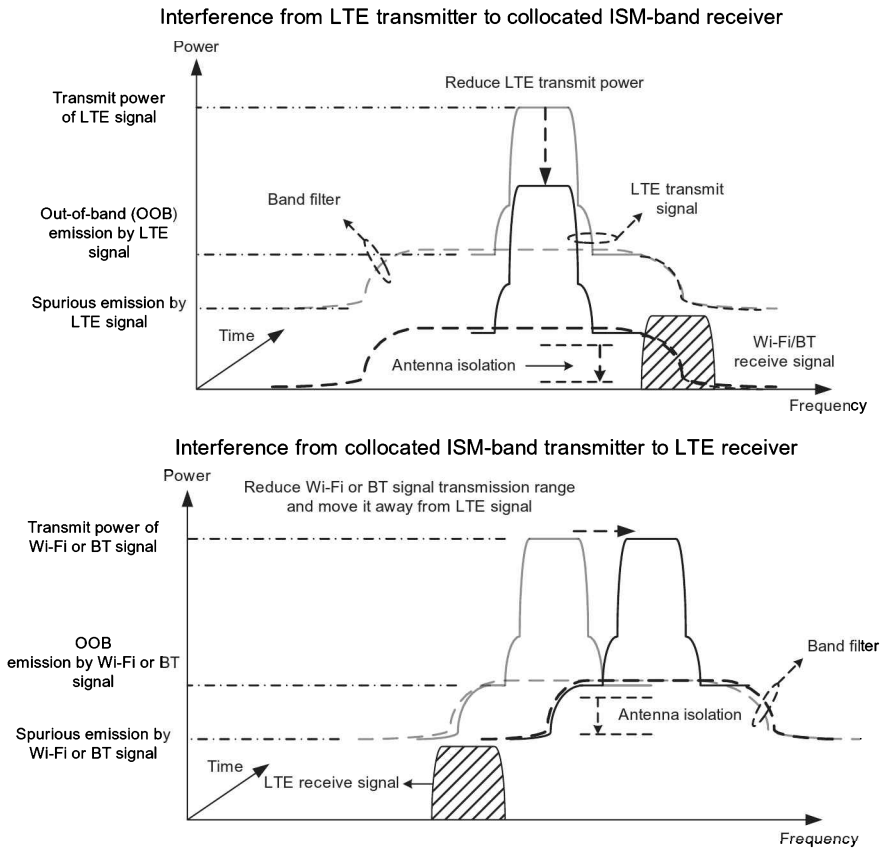


FIGURE 14.10

Illustration of IDC issues and some remedies [1].

common services under this scenario, the scheduling periods and unscheduled periods should be typically not more than 20–60 ms.

4. *LTE + Wi-Fi off-load*: In this scenario, an LTE UE can also connect to Wi-Fi to off-load traffic, and the Wi-Fi transceiver operates as a terminal in the infrastructure mode. It is difficult for the Wi-Fi transceiver to change the configured frequency channel in this case. In addition, the Wi-Fi radio is required to scan for the beacon signal transmitted from the Wi-Fi access point every 102.4 ms to maintain connection. The scheduling/unscheduled period requirements pertaining to this scenario differ from the previous scenario. One difference is about Wi-Fi beacon reception by the UE in Wi-Fi client mode, which implies alignment of the LTE unscheduled period with the Wi-Fi beacons. Furthermore, the scheduling period of LTE should less than 100 ms in order to facilitate beacon reception. In this case, the packets only go through one radio link (either Wi-Fi for off-load packets or LTE for normal packets), resulting in somewhat larger scheduling/unscheduled intervals that can meet the latency requirements. The ratio of the scheduling/unscheduled intervals should correspond to the traffic volume of the normal and offloaded traffic.
5. *LTE + GPS receiver*: In this scenario, the LTE UE is also equipped with a GPS receiver to support location-based services.

14.4.3 In-device coexistence and interference avoidance

The LTE network-controlled UE-assisted solutions which were studied during LTE Rel-10 can be categorized as follows [1]:

- Frequency division multiplexing (FDM) based solutions include moving the LTE signal away from the ISM band, or moving the ISM signal away from the LTE frequency band (see Figure 14.10).
- Time division multiplexing (TDM) based solutions include DRX mode, HARQ process reservation, and uplink scheduling restriction.
- Power control-based solutions include LTE power control or ISM-band radio power control (see Figure 14.10).
- UE autonomous solutions include time-domain remedies such as LTE denials for infrequent short-term events, LTE denials for ISM data packets, and ISM denials for LTE important signals reception.

The RF filtering in the transmit side reduces the out-of-band (OOB) spurious emissions of the aggressor leaking into the receive band of the victim. The receive filter reduces the blocking effect due to the transmissions in the band of the aggressor technology. When two radios operate in adjacent bands, there can be limited attenuation of each filter in the transition band that overlaps with the designated band of the other technology. This can lead to a large interference to the victim, due to spurious emissions and imperfect blocking performance. In some cases, such as LTE Band 40 and the ISM band starting at 2400 MHz, there is no guard

band between the frequencies of the two technologies. There are further challenges in RF design due to variations in filter response across manufacturing processes, as well as a wide temperature range over which the terminal must operate [18].

As shown in Figure 14.11, in a typical UE implementation, the baseband processing modules of UMTS/LTE and ISM-band radios are separated, whether within the same chip from the same vendor or different chips from the same or different manufacturers. In either case, the two chips may exchange handshake signals, referred to as inter-chip handshaking and signaling, to convey real-time status and control information including advanced notice of future activities. This advanced notification signal can be used as a trigger to notify the serving eNB of forthcoming IDC conditions. The eNB can suspend normal UE LTE operation during the ISM-band radio activities and resume normal operation once the IDC condition is resolved. The IDC coordination module (typically proprietary) resides in the UE, as shown in Figure 14.11, and is responsible for coordination and prioritization among different collocated radios, obtaining and interpreting the coordination information from different radios, and generating control commands to different radio modules including but limited to generation of the IDC trigger messages in the uplink (to be transmitted via LTE transceiver module), interpretation of the IDC acknowledgment messages, and so on.

The IDC solutions for interference avoidance are mainly considered for the UE in RRC connected mode. The idle mode operation itself is not considered a problem since the UE can just stop ISM-band radio transmissions at important LTE events such as paging. There are three interference avoidance approaches that can be taken to address the IDC issues: (1) uncoordinated, where different radio technologies within the same UE operate independently without any internal coordination; (2) UE only, where there is an internal coordination between different radio technologies within the UE, which means that the activities of one radio are known by other radios. However, in this case the network is not

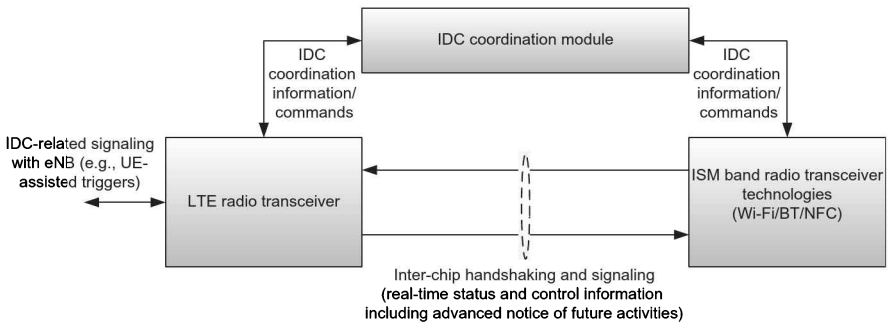


FIGURE 14.11

Example block diagram of the UE internal IDC signaling and coordination module.

aware of the coexistence issues experienced by the UE and is not involved in the coordination; and (3) network-coordinated with UE assistance, where different radio technologies within the UE are aware of possible coexistence problems and the UE can inform the network about such problems. The latter method is illustrated in Figure 14.11, and has become the basis for the solutions that have been developed in LTE Rel-11 for collocated multi-radio coexistence problems.

Based on the above assumption that different collocated radio modules can handshake and exchange (advance) information/notification about their current or upcoming activities, we now study the solutions that were developed in 3GPP to mitigate collocated multi-radio coexistence issues. It must be noted that other standardization organizations such as Wi-Fi Alliance [21] and Bluetooth Special Interest Group [20] have also taken steps on their side to find solutions that can alleviate or ideally resolve the in-device coexistence and interference problems. For example, BT devices may by default configure themselves as masters; thus, in-device BT may only behave as a BT slave under certain scenarios. On the 3GPP side, the standard solution in LTE Rel-11 enables the UE, with the assistance from the serving eNB, to resolve the IDC interference issues in situations where the actions taken by BT/Wi-Fi radios are not sufficient to solve the problem [18].

Based on RF analysis results, one straightforward solution to effectively mitigate or reduce the IDC interference is to let radio transceivers work in different frequency bands with sufficient frequency separation. The basic concept of an FDM-based solution is to move the victim (or aggressor) signal farther away from the aggressor (or victim) signal and increase the frequency separation for better filtering performance. An LTE FDM-based solution is to move the LTE signal farther away from the ISM band by performing inter-frequency handover within LTE according to the existing procedure specified in [3,4]. On the contrary, in the ISM FDM-based solution, the ISM radio signal is moved away from the LTE frequency band in the frequency-domain by switching the Wi-Fi channel in the portable router scenario, or by making use of the BT adaptive frequency hopping (AFH) feature to select a set of BT channels away from the LTE operating band (see Figure 14.9). The LTE FDM-based solution is applicable to all usage models as long as an alternative LTE frequency channel is available. In some deployments, using the FDM-based solution to resolve IDC interference problems may not be possible or desirable. As an example, the LTE FDM-based solution may not be applicable when all available LTE bands are impacted by ISM radio activities, the UE is in an area with only one LTE frequency band, or the UE does not have good channel quality in the alternative bands. It is also possible that the operator has alternative frequency bands, but those bands are congested due to a large number of active UEs. To ensure efficient network operation, it can be beneficial to balance load between RF bands and retain the UE in the current frequency, even if the LTE receiver is disturbed by the ISM signals. In that case, time multiplexing of LTE and ISM-band radios is more desirable [18].

In LTE TDM-based solutions, the basic idea is to time-multiplex the transmission or reception of different radios by either adapting the LTE transmission/reception timing to that of ISM-band radios, or vice versa. In LTE, DRX was adopted as a TDM-based solution for IDC interference avoidance. In the DRX mode, the UE is allowed to switch its LTE receiver off and stop monitoring the PDCCH. Since uplink transmissions are scheduled on the PDCCH, the gaps in PDCCH reception imply that uplink transmissions cannot be scheduled when the UE is in DRX mode. As a result, the time is divided into scheduled and unscheduled periods from the LTE device perspective. Unscheduled time can be used for ISM-band communication. To facilitate the DRX solution for coexistence of LTE and other radios, the UE should provide assisting information to the eNB.

The UE provides the eNB with a desired TDM pattern. For example, the parameters related to the TDM pattern can consist of periodicity of the TDM pattern and scheduling period (or unscheduled period), as shown in Figure 14.12. It is up to the eNB to decide and signal a suitable DRX configuration to the UE based on a UE suggested TDM pattern and other criteria. The scheduling period corresponds to the active time of DRX operation, while unscheduled period corresponds to the inactive time. The eNB would attempt to guarantee the unscheduled period using appropriate downlink/uplink scheduling, sounding reference signal transmission configuration, DRX command MAC control element usage, and so on. During the inactive time, the UE is allowed to delay the initiation of dedicated

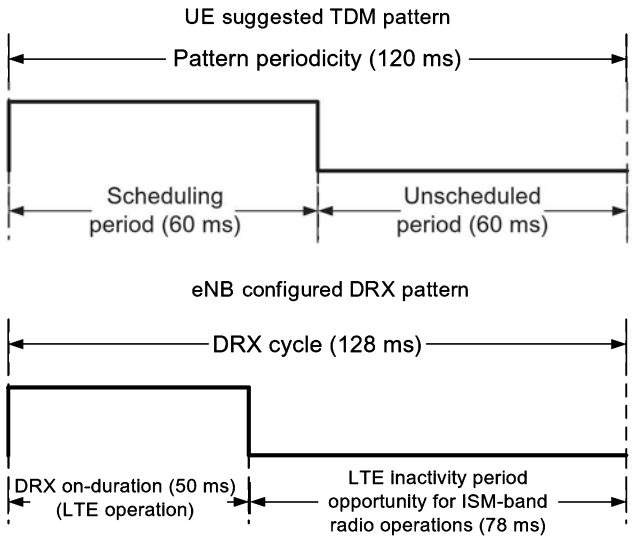


FIGURE 14.12

Example UE suggested TDM pattern and eNB configured DRX pattern [1].

scheduling request and/or random access procedure. Figure 14.12 illustrates an example where the eNB signals a DRX configuration based on a UE suggested pattern [1].

In the LTE + Wi-Fi off-load usage model introduced earlier, long scheduling and unscheduled periods are desired to enable completion of pending data transmissions. However, long periods would increase the latency of packet transmission. In addition, since in this scenario Wi-Fi acts as a terminal, it should be able to receive a beacon signal transmitted once every 102.4 ms. As a result, a suitable TDM pattern suggested by the UE should be 128 ms, where LTE occupies the first 60 ms. However, due to a limited number of DRX patterns in LTE, the eNB may configure the UE with a long DRX cycle of 128 ms and "on duration" of 40 ms. It should be noted that because of pending HARQ retransmissions in the LTE side, transition from scheduling time to unscheduled time is not unexpected. Therefore, LTE transmissions may stop before expiration of the on duration timer.

In an LTE + BT voice scenario, scheduling and unscheduled periods for each radio alternate much faster than in the Wi-Fi coexistence scenario. In enhanced synchronous connection oriented (eSCO) mode in BT [20], the transmission interval is 3.75 ms having six transmit/receive slots; thus, in order to maintain the minimum QoS requirements for voice conversation, the network should ensure at least a pair of correct BT transmit/receive instances in each BT interval of 3.75 ms. The remainder of the time can be allocated to LTE radio activities. The UE indicates to the network the desired subframes reservation bitmap (10 bits, one for each subframe). For short-term subframe reservation patterns, it is desirable that the pattern is consistent with uplink/downlink HARQ timing so that none of the HARQ processes is interrupted. Based on the assisting information, the network configures suitable DRX parameters.

In certain cases where the IDC interference condition cannot be predicted in advance, it is impossible to perform inter-frequency handover, or to provide unscheduled periods via DRX configuration. For example, one such condition may be the case where an unpredicted BT connection setup occurs and the DRX cannot be configured early enough to accommodate this critical communication. In another scenario, some critical signaling may occur irregularly where the UE can neither perform handover to an alternative band or be configured with a specific DRX configuration. Therefore, there are conditions where FDM-based or TDM-based schemes may not be applicable, and the UE has to deny LTE uplink transmissions autonomously to protect important signaling on other radios. However, the denial rate should be very low so that it does not significantly impact LTE operation. In addition to the TDM-based solution performed under the control of an LTE network, the UE may also use time-multiplex solutions through internal coordination. For example, the UE may terminate Wi-Fi or BT transmission when the LTE is receiving critical downlink signals. This would be useful to prevent disruption in the LTE signaling procedure as a result of unpredictable IDC interference from the ISM-band radios. Consequently, the

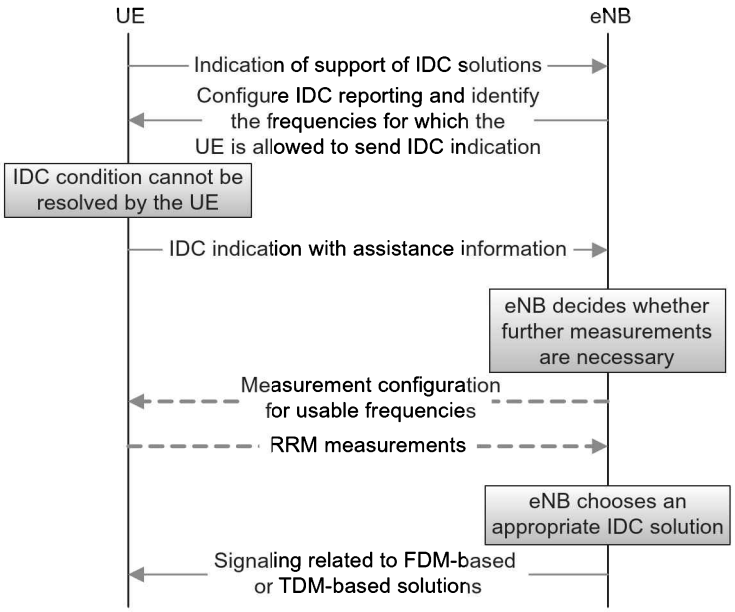


FIGURE 14.13

Signaling procedure for network-coordinated UE-assisted IDC resolution [18].

UE must carefully assess the IDC conditions before deciding on the best mitigation strategy in order not to compromise the performance and normal operation of the collocated radios.

Figure 14.13 illustrates the signaling procedure in network-coordinated UE-assisted IDC interference mitigation solution. When a UE experiences an IDC condition that cannot be locally resolved and network assistance is required, the UE sends an IDC indication via dedicated RRC signaling to report the problem [3]. The detail of the IDC indication trigger is left to UE implementation. The UE may rely on the existing LTE measurements and/or UE internal coordination. The IDC indication should be triggered based on ongoing IDC interference on the serving or non-serving frequencies, instead of assumptions or predictions of potential interference. A UE that supports IDC functionality indicates this capability to the network, and the network can then configure the UE through dedicated signaling whether the UE is allowed to send an IDC indication. The UE may only send an IDC indication for E-UTRA uplink/downlink RF carriers for which a measurement object is configured [4].

The term "ongoing IDC interference" should be treated as a general guideline by the UE. For the serving frequency, the ongoing interference may be related to the interference caused by an aggressor radio to a victim radio during either active data exchange or upcoming data activity which is expected in

a few hundred milliseconds. For a non-serving frequency, the ongoing interference may be an anticipation of the LTE radio becoming an aggressor or a victim, if it makes handover to a non-serving frequency. Similarly, concerning activation of secondary cells in the case of carrier aggregation, the ongoing interference may be an anticipation of the LTE radio becoming an aggressor or a victim. Ongoing interference may affect several subframes/slots. When the eNB is notified of an IDC condition through an IDC indication from the UE, the eNB can choose to apply an FDM-based or a TDM-based solution. To assist the eNB in selecting an appropriate solution, all necessary/available assisting information for both methods is sent together as part of IDC indication message to the eNB. The IDC assisting information contains the list of E-UTRA carriers suffering from ongoing interference, the direction of the interference and depending on the scenario; it may also contain preferred time-multiplex patterns or parameters to enable appropriate DRX configuration for the UE on the serving E-UTRA carrier. The IDC indication is also used to update the IDC assistance information, including the cases when the UE no longer encounters the IDC condition. In the case of inter-eNB handover, the IDC assisting information is transferred from the source eNB to the target eNB. The UE should only indicate that the IDC condition is over when it is not experiencing an IDC condition any more. The UE should not resend the same IDC indication message to the network, but it may resend the same IDC indication after handover. The IDC condition can be divided into three phases: (i) the UE detects the start of IDC condition but does not initiate the transmission of the IDC indication to the eNB; (ii) the UE has initiated the transmission of the IDC indication to the eNB and no solution is configured by the eNB to resolve the IDC issue; (iii) the eNB has provided the UE with a solution that resolves the IDC issue (Table 14.2) [3].

In addition, once configured by the network, the UE can autonomously deny LTE uplink transmission in all phases to protect ISM-band transmission in special circumstances, if other solutions cannot be used. On the other hand, it is assumed that the UE also autonomously denies ISM-band transmission to ensure LTE connectivity to the eNB in order to perform LTE procedures, e.g., RRC connection reconfiguration and paging. The network may configure a long-term denial rate by dedicated RRC signaling to limit the amount of LTE uplink autonomous denials. Otherwise, the UE must not perform any LTE uplink autonomous denials [3].

In summary, the IDC interference level and its impact on the receiver performance depends on transmit power and receiver blocking characteristic of each radio and physical characteristics of transceivers (e.g., filter responses, antenna isolation). The following conclusions were drawn from the analyses performed in 3GPP related to this work item:

- For most cases, we observe that frequency-domain solutions, i.e., moving to other frequencies, and RF filtering can sufficiently suppress the coexistence interference.

Table 14.2 RRM, RLM, CSI Measurements in Different Phases of IDC Interference [3]

Phases of IDC Interference	RRM Measurements	RLM Measurements	CSI Measurements
Phase 1	It is up to the UE implementation and RRM measurement requirements	It is up to the UE implementation and RLM measurement requirements	It is up to the UE implementation and CSI measurement requirements
Phase 2 (If the UE determines that the network does not provide a solution that resolves its IDC problem, it performs measurements)	The UE is required to ensure that the measurements are free of IDC interference	The UE is required to ensure that the measurements are free of IDC interference effects. The UE should maintain LTE connectivity in this phase, meaning that RLM measurements are not impacted by IDC interference. If no solution is provided within a time, which is up to UE implementation, the UE may declare RLF or it may continue to deny the ISM transmission	–
Phase 3 (If the IDC indication message reports the IDC condition on a neighbor frequency, the UE performs RRM measurements for that frequency)	The UE is required to ensure that the measurements are free of IDC interference	The UE is required to ensure that the measurements are free of IDC interference effects	–

Table 14.3 LTE Blocking Levels for Bluetooth and Wi-Fi Receivers for Different LTE Transmit Powers and Operating Bands [1]

LTE Transmit Power (dBm)	Blocking with FBAR Filter (dBm)				
	2300–2370 MHz	2360–2380 MHz	2380–2400 MHz	2500–2520 MHz	2520–2570 MHz
23	−34	−28	7	−37	−40
21	−36	−30	5	−39	−42
19	−38	−32	3	−41	−44
17	−40	−34	1	−43	−46
15	−42	−36	−1	−45	−48
13	−44	−38	−3	−47	−50
11	−46	−40	−5	−49	−52
9	−48	−42	−7	−51	−54
7	−50	−44	−9	−53	−56
5	−52	−46	−11	−55	−58
3	−54	−48	−13	−57	−60
1	−56	−50	−15	−59	−62
−1	−58	−52	−17	−61	−64
−3	−60	−54	−19	−63	−66
−5	−62	−56	−21	−65	−68
−7	−64	−58	−23	−67	−70
−9	−66	−60	−25	−69	−72

- For the uppermost region of LTE Band 40 (2380–2400 MHz), LTE transmitting with the maximum power of 23 dBm can block the Wi-Fi or BT signal in the entire ISM band, thus limiting the maximum LTE transmit power below 23 dBm, moving LTE signal away from ISM, or TDM-based solution needs to be considered (Table 14.3).
- For 2300–2380 MHz in LTE Band 40, Wi-Fi or BT desense due to the LTE interference may be acceptable except for the lower 20 MHz of the ISM band, since the performance of the state-of-the-art film bulk acoustic resonator (FBAR) filtering[2],

[2]FBAR filters are a form of bulk acoustic wave (BAW) filter that have superior performance with steeper rejection curves compared to surface acoustic wave (SAW) filters. The FBAR filters also feature 0.3–0.5 dB less insertion loss, resulting in up to 50 mA less current consumption, thereby improving battery life and talk time of the mobile devices. A thin-film bulk acoustic resonator is a device consisting of a piezoelectric material contained between two electrodes and acoustically isolated from the surrounding medium. The FBAR devices using piezoelectric films with thicknesses ranging from several micrometers down to tenths of micrometers resonate in the frequency range of approximately 100 MHz to 10 GHz. Aluminum nitride and zinc oxide are two common piezoelectric materials used in FBARs [19].

device OOB/spurious emissions, sensitivity, and blocking of implementations are typically better than specification limits. Additionally, limiting the number of data/control bearing resource blocks and assigning resources away from the ISM band, which directly impact the OOB emissions, can help reduce desensitization to the lower 20 MHz of the ISM band.

Table 14.3 shows LTE blocking for Wi-Fi and BT receivers for different LTE transmit powers and operating bands in E-UTRA Band 40 and Band 7. As shown in Table 14.3, a cell-edge UE with maximum transmitting power of 23 dBm in the uppermost 20 MHz segment of Band 40 can result in a maximum of 7 dBm OOB blocking interference[3] in the Wi-Fi/BT receiver. The LTE transmit power level needs to be limited for the simultaneous operation with ISM-band reception, if the LTE transceiver is operated in the upper 20 MHz of Band 40. The maximum allowed LTE transmit power for coexistence varies depending on the blocking characteristics of the Wi-Fi/BT receivers [1].

The RF analyses conducted in 3GPP related to the IDC interference between ISM-band and LTE technologies, and the conclusions that were made and documented as a result of those analyses were mainly based on four information sources. The analyses and measurements presented in 3GPP TR 36.816 [1] indicate that for some IDC scenarios, significant degradation on both LTE and ISM-band radios can occur despite the use of state-of-the-art RF filtering technology. The precise quantitative results differed from one source to another due to different assumptions in the analyses or the measurement approaches. Nonetheless, the conclusions were consistent in that at least a significant fraction of spectrum is highly desensitized when the other technology is transmitting. The assumptions used by those sources in the simulation or measurements presented to 3GPP are summarized in Table 14.4.

[3]Radio receiver blocking or receiver desensitization is an important parameter for any radio receiver. A good radio receiver blocking or desensitization performance is particularly important in the scenarios where a number of radios of various forms are used in close proximity to each other. With wireless communications being used for everything from Wi-Fi to cellular communications and Bluetooth, as well as many more traditional applications, there are many instances where two radios operate very close to each other, and the receiver blocking performance will be very critical. Blocking rejection is the ability of a receiver to tolerate an OOB signal and avoid blocking. A good automatic gain control design is part of achieving good blocking rejection. When a very strong OOB signal appears at the input of a receiver, it is often found that the sensitivity is reduced. The effect arises because the front-end amplifiers are saturated as a result of the strong OOB signal. This often occurs when a receiver and transmitter are operated from the same site and the transmitter signal is exceedingly strong. When this occurs, it has the effect of suppressing all the other signals trying to pass through the amplifier, giving the effect of a reduction in gain. Blocking is generally specified as the level of the unwanted signal at a given offset, which will give a 3-dB reduction in gain. Depending on the type of receiver, the values for blocking will vary considerably. As a reference point, a good radio receiver should be able to withstand blocking signals of about 10 dBm before this effect becomes noticeable.

Table 14.4 Assumptions for the RF Analyses in 3GPP IDC Studies [1]

Parameter	Analysis 1	Analysis 2	Analysis 3	Analysis 4
LTE frequency band	40 and 7	40 and 7	40	40 and 7
ISM radio	BT, Wi-Fi	Wi-Fi	Wi-Fi	BT, Wi-Fi
Interference directions considered for B and 40	LTE to BT/ Wi-Fi; BT/Wi-Fi to LTE	LTE to Wi-Fi; Wi-Fi to LTE	LTE to Wi-Fi	LTE to BT/ Wi-Fi; BT/Wi-Fi to LTE
Interference mechanisms	Spurious emission and blocking	Spurious emission and blocking	Spurious emission	Spurious emission and blocking
RF filtering method	FBAR	No filters external to test setup	Commercially available filter (typical/minimum)	FBAR
Antenna isolation (dB)	12	15, 20, 25	12	12
LTE transmitter power (dBm)	23	23	N/A	0, 15, 23
Wi-Fi transmitter power (dBm)	20	20	20	20, 14.5
BT transmitter power (dBm)	10	N/A	N/A	4, 0
LTE RSSI as victim (dBm)	−94	−70	−94	−94 (Band 40) −92 (Band 7)
Wi-Fi RSSI (dBm)	−79	−50	N/A	−89, −76
BT RSSI (dBm)	−90	N/A	N/A	−70
LTE bandwidth (MHz)	20	25–100 resource blocks (over 20)	20	20
Wi-Fi bandwidth (MHz)	22	22	22	22
BT bandwidth (MHz)	1	N/A	N/A	1
Performance measure	Desensitization (dB)	EVM	Desensitization (dB)	Desensitization (dB)

References

3GPP Specifications[4]

[1] 3GPP TR 36.816, Evolved Universal Terrestrial Radio Access (E-UTRA), Study on Signaling and Procedure for Interference Avoidance for In-Device Coexistence (Release 11), December 2011.

[2] 3GPP TR 36.839, Evolved Universal Terrestrial Radio Access (E-UTRA), Mobility Enhancements in Heterogeneous Networks (Release 11), December 2012.

[3] 3GPP TS 36.331, Evolved Universal Terrestrial Radio Access (E-UTRA), Radio Resource Control (RRC), Protocol specification (Release 11), December 2012.

[4] 3GPP TS 36.300, Evolved Universal Terrestrial Radio Access (E-UTRA) and Evolved Universal Terrestrial Radio Access Network (E-UTRAN) Overall description, Stage 2 (Release 11), December 2012.

Books

[5] C. Johnson, Long Term Evolution in Bullets, second ed., Create Space Independent Publishing Platform, July 2012.

[6] S. Sesia, I. Toufik, M. Baker, LTE, the UMTS Long Term Evolution, From Theory to Practice, second ed., John Wiley & Sons, August 2011.

[7] E. Dahlman, S. Parkvall, J. Skold, 4G, LTE/LTE-Advanced for Mobile Broadband, Academic Press, May 2011.

Articles

[8] IST-4-027756 WINNER II, D4.7.1 Interference averaging concepts, June 2007.

[9] IST-4-027756 WINNER II, D4.7.2 Interference avoidance concepts, June 2007.

[10] IST-4-027756 WINNER II, D4.7.3 Smart antenna based interference mitigation, June 2007.

[11] L. Lindbom et al., Enhanced Inter-cell Interference Coordination for Heterogeneous Networks in LTE-Advanced: A Survey, Cornell University Library (eprint), December 2011.

[12] R. Zhang, L. Hanzo, Co-channel interference mitigation:active and passive techniques, IEEE Vehicular Technology Magazine, December 2010.

[13] S. Xu1, J. Han, T. Chen, Enhanced inter-cell interference coordination in heterogeneous networks for LTE-Advanced, IEEE 75th Vehicular Technology Conference, May 2012.

[14] R. Ghaffar, R. Knopp, Fractional frequency reuse and interference suppression for OFDMA networks, Proceedings of the Eighth International Symposium on Modeling and Optimization in Mobile, Ad Hoc and Wireless Networks (WiOPT), June 2010.

[15] Y. Peng, W. Yang, Y. Zhang, Y. Zhu, Mobility performance enhancements for LTE-Advanced heterogeneous networks, IEEE 23rd International Symposium on Personal, Indoor and Mobile Radio Communications (PIMRC), 2012.

[16] A. Damnjanovic, et al., A survey on 3GPP heterogeneous networks, IEEE Wireless Communications, June 2011.

[17] A. Ghosh, et al., Heterogeneous cellular networks: from theory to practice, IEEE Communications Magazine, June 2012.

[4] 3GPP specifications can be found at the following URL: http://www.3gpp.org/ftp/Specs/archive/.

[18] Z. Hu, et al., Interference avoidance for in-device coexistence in 3GPP LTE-Advanced: challenges and solutions, IEEE Communications Magazine, November 2012.
[19] Thin-film bulk acoustic resonator, Wikipedia. <http://en.wikipedia.org/wiki/Thin_film_bulk_acoustic_resonator>.
[20] Bluetooth Core Specifications, Bluetooth Special Interest Group. <https://www.bluetooth.org/Technical/Specifications/adopted.htm>.
[21] Wi-Fi Alliance Published Specifications. <https://www.wi-fi.org/knowledge-center/published-specifications>.
[22] Stefan Brück, 3G/4G mobile communications systems, Qualcomm Technologies Inc. <http://www.ant.uni-bremen.de/en/courses/mcs/>.

CHAPTER

Positioning and Multimedia Broadcast/Multicast Services 15

CHAPTER CONTENTS

15.1 Positioning and location-based services 1071
15.1.1 E-UTRA positioning network architecture 1074
15.1.2 Network-based and UE-based positioning methods 1078
15.1.3 Positioning methods in LTE/LTE-Advanced 1080
15.1.3.1 Principles of GPS 1081
15.1.3.2 A-GNSS positioning 1085
15.1.3.3 Observed time difference of arrival positioning 1086
15.1.3.4 E-CID-based positioning 1088
15.1.3.5 UTDOA positioning 1089
15.2 Evolved multimedia broadcast/multicast service 1090
15.2.1 E-MBMS network architecture 1091
15.2.2 Basic definitions 1094
15.2.3 E-MBMS user-plane and control-plane protocols 1094
15.2.4 Physical and MAC layer aspects of E-MBMS 1095
15.2.5 E-MBMS single frequency network transmission 1098
15.2.6 Mobility support in E-MBMS 1102
15.2.7 E-MBMS counting 1103
References 1104

In this chapter, we take a top-down systems approach to describe two important service enablers of LTE/LTE-Advanced that both started in LTE Rel-9 and have been enhanced in the later releases. The UE positioning and location-based services, as well as the evolved multimedia broadcast/multicast services (E-MBMS), are considered the key enablers of various services in modern cellular systems. There are numerous applications that rely on these functionalities to provide the

© 2014 Elsevier Inc. All rights reserved.

Ex.1005.01100

users with the best quality of experience and ease of access to location-optimized and customized content.

This chapter begins with the description of the positioning standard for LTE/LTE-Advanced systems. We review the positioning requirements, positioning architectures, and signaling. The coordinate systems and the transformations used in positioning systems are described in detail. There are many different use cases for positioning information. The positioning functions may be used internally by the EPS, value-added network services, the UE itself, or through the network by a third party. While the location-based services may be used for emergency services (which may be mandated), the feature has not been exclusively developed for emergencies.

We will then describe the E-MBMS feature in LTE/LTE-Advanced. The E-MBMS bearer service is the service provided by the packet-switched domain to E-MBMS user services in order to deliver IP multicast[1] datagrams to multiple receivers using minimal network and radio resources. An E-MBMS user service is a service provided to the end user by means of the MBMS bearer service, and possibly other EPS bearers. The E-MBMS is a point-to-multipoint service in which data is transmitted from a single source entity to multiple recipients. Transmitting the same data to multiple recipients allows the sharing of network resources. The E-MBMS for EPS bearer service supports broadcast mode over E-UTRAN and UTRAN. The E-MBMS is realized by the addition of a number of new features and new functional entities to the 3GPP network architecture.

An E-MBMS counting function was introduced that allows counting the number of connected mode users that are either receiving or are interested in receiving particular MBMS services. In LTE Rel-11, E-UTRAN MBMS is enhanced to ensure service continuity when multi-carrier functionality is deployed in an MBMS service area. The MBMS services may be deployed on different frequencies over different geographic areas. LTE Rel-11 enhancements allow the network to inform MBMS-capable devices of information related to MBMS deployment, such as carrier frequencies and service area identities (SAIs). In LTE Rel-11, an MBMS-capable device can inform the network of its interest in MBMS services by indicating the carrier frequencies associated with the MBMS services of interest. The MBMS interest indication by the device also allows the device to indicate the priority between MBMS service and unicast service. The network uses the MBMS interest indication provided by the device for mobility management decisions so that the device is always able to use its receiver at the appropriate carrier frequency to ensure continuity of MBMS services. In idle mode, an MBMS-capable device can prioritize a particular carrier frequency during cell reselections depending on the availability of the MBMS service of interest on that carrier frequency. To ensure

[1]IP multicast is a method of transmitting IP datagrams to a group of interested receivers in a single transmission. It is often employed for streaming media applications on the Internet and private networks. The method is the IP-specific version of the general concept of multicast networking. It uses especially reserved multicast address blocks in IPv4 and IPv6. In IPv6, IP multicast addressing replaces broadcast addressing as implemented in IPv4. IP multicast is described in IETF RFC 1112 [20].

MBMS service continuity in connected mode, the MBMS interest indications received from the device are signaled to the target cell as part of handover preparation procedure [4].

15.1 Positioning and location-based services

Positioning defines the process of determining the position and/or velocity of a device using radio signals. Location-based services are considered a significant feature of the modern cellular networks which allow the users to locate themselves and each other, as well as enable the mobile applications to offer services and information customized to the current users' locations. In addition to the commercial usage, there are also public safety applications for positioning. As an example, an emergency call made from a mobile device can be tracked and sufficiently accurate location of the caller can be determined, even though the caller may not know where he/she is. Many government regulatory organizations around the world have made support of accurate positioning functionality mandatory for all mobile devices. In the United States, it is mandatory for network operators to support FCC's Enhanced 911[2], making the location of a cell phone available to emergency call dispatchers. With this mandate, the FCC has defined accuracy requirements for different position estimation methods. Cellular network operators are responsible for positioning wireless terminals with an accuracy of 50 and 150 m in 67% and 95% of all positioning attempts, respectively. These figures are valid for UE-based positioning methods, i.e., where the positioning method involves functionality located in the UE such as global positioning system (GPS) receiver hardware. The requirements for network-based methods, without such UE functionality, are 100 m (67%) and 300 m (90%) [17]. These are stringent accuracy requirements that need to be fulfilled and guaranteed no matter what position estimation technology is used, or in which environment the position

[2]The FCC's wireless Enhanced 911 (E911) requirements seek to improve the effectiveness and reliability of wireless 911 services by providing the dispatchers with additional information on wireless 911 calls. The FCC's wireless E911 rules apply to all wireless licensees, broadband personal communications service (PCS) licensees, and certain specialized mobile radio (SMR) licensees. The FCC has divided its wireless E911 program into two phases: Phase I and Phase II. Under Phase I, the FCC requires carriers, within 6 months of a valid request by a local public safety answering point (PSAP) to provide the PSAP with the telephone number of the originator of a wireless 911 call and the location of the cell site or base station transmitting the call. Under Phase II, the FCC requires wireless carriers, within 6 months of a valid request by a PSAP to begin providing information that is more precise, specifically, the latitude and longitude of the caller. This information must meet FCC accuracy standards, generally within 50–300 m, depending on the type of technology used. The deployment of E911 requires the development of new technologies and upgrades to local 911 PSAPs, as well as coordination among public safety agencies, wireless carriers, technology vendors, equipment manufacturers, and local wireline carriers [17].

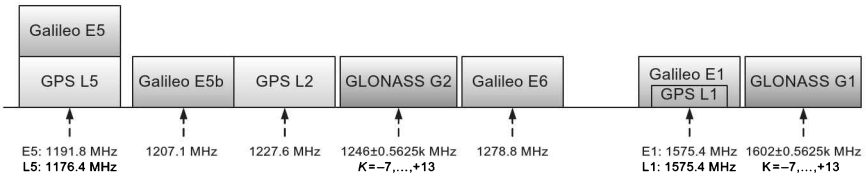


FIGURE 15.1

Frequency bands used by prominent positioning methods [15].

is estimated (i.e., indoor or outdoor). Determining a user's device position is traditionally based on satellite-based position estimation using Global Navigation Satellite Systems (GNSS) such as GPS. Figure 15.1 provides the frequency bands of the prominent global positioning systems.

The majority of modern mobile devices have an integrated GNSS receiver. To properly estimate the position, the receiver needs to have an unobstructed line of sight to at least four satellites, and this is one of the main drawbacks of GNSS-based methods. In indoor environments, line of sight reception of the low-power radio signals transmitted from the medium-earth-orbit satellites is not guaranteed, if not impossible. To overcome this limitation, especially in an environment with poor signal conditions, Assisted-GNSS (A-GNSS) methods have been developed, e.g., Assisted-GPS. In A-GPS, a cellular network uses network resources to provide assistance data that helps the device to locate and utilize the available GPS satellites faster. A-GNSS reduces start-up and acquisition times, increases sensitivity, and reduces the UE's power consumption. While there is often an acceptable coverage by a cellular network to determine the A-GPS information, this does not help if the satellites cannot be detected due to extremely weak reception of GPS signals inside a building. In that case, position estimation using radio signals is more feasible. In GSM, position estimation based on radio signals has been around for many years. As mobile broadband technology advances and the demand for more accurate positioning and location-based services increases, more sophisticated and accurate positioning methods have been developed. In this section, we will only focus on the positioning methods developed for E-UTRA.

The positioning methods supported in LTE mainly rely on the high-level network architecture as shown in Figure 15.2. The positioning network architecture has been defined in such a way that it is generally independent from the underlying network. There are three main entities in this architecture, location service (LCS) client, LCS server, and LCS target. An LCS client is the entity requesting the service and in the majority of the cases is located in the LCS target. This service obtains the location information by sending a request to the server. The location server is a physical or logical entity that collects measurements and other location information from the device and base station, and assists the device with measurement and estimation of its position. The server processes the request from the client and provides the client with the requested information [15,18].

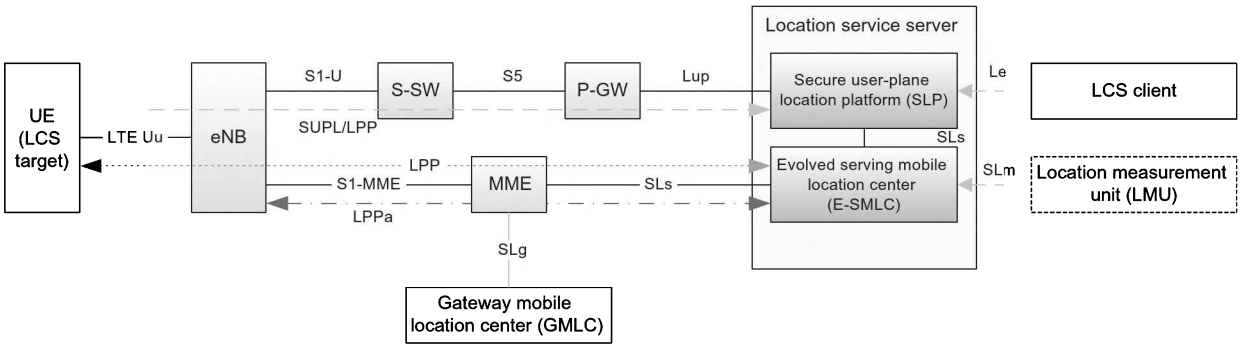


FIGURE 15.2

E-UTRA location service architecture [7,15].

15.1.1 E-UTRA positioning network architecture

Some location-based services are targeted at individual users, while others are focused on aggregated user behavior that will be of value to enterprises and application and content providers. In general, the services can be grouped into the following categories [12]:

- Regulatory-based applications such as emergency call services.
- Consumer applications, such as social networking, service finder, and navigation services.
- Business applications such as fleet management or social networking tailored to business needs.
- Third-party applications that enable merchants or application and content providers to target specific end users for their advertising or services.
- Network operator applications that help detect internal problems, or optimize networks and business capabilities.

Given that location-based services have generally diverse requirements, the communication service providers must carefully identify and prioritize a particular service's requirements before choosing methods of gathering and delivering location information. The following list summarizes some of the most important general requirements [12]:

- Providing the required degree of location accuracy.
- Promptness of response to a location request.
- Scalability to support a large number of user locations.
- Support for real-time, periodic, or event-triggered location updates.
- Ease of implementation.
- Battery consumption for mobile devices.
- Impact on network resources.
- Differentiation of the network provider service from application and content providers offerings.

The EPS provides several methods for delivering location information when it is determined. Each method has certain capabilities, strengths, and constraints, which necessitate satisfaction of the unique requirements of each specific service.

The user-plane method requires minimal interaction with the underlying wireless access technologies; thus, this method can be used ubiquitously across LTE and the legacy networks. It is also scalable, which makes it well suited to support commercial location-based services with less complexity, cost, and impact on the network than the control-plane solution. This solution relies on user-plane data bearers to transfer location-assistance and positioning-related messages between the secure user-plane location[3] (SUPL)-enabled terminal (SET) and the SUPL location platform

[3]SUPL is an IP-based protocol for assisted-GPS in order to receive positioning information of GPS satellites faster via IP connections instead of slow GPS satellite links.

(SLP). An SUPL client is required on the user device. Lack of direct connection to the access network is a disadvantage for supporting positioning methods, which require assistance data from the network. In addition, because this solution can only enable single-user location requests, it is not suitable for applications that need periodic reporting on all user locations within a cell or zone. Depending on the location technology used, the user-plane solution can support a high level of accuracy to meet the needs of the majority of location-based services targeted at the individual user, such as turn-by-turn navigation and fleet management.

In the control-plane method, which was specified in LTE Rel-9, positioning data is transferred over the control-plane, between the UE, the eNB, and the positioning elements, i.e., evolved serving mobile location center/gateway mobile location center (GMLC). This method provides convenient access to assistance data from the network, and enables more reliable service performance than the user-plane solution. Since the control-plane method does not require a client on the UE, it can be used to support emergency services on LTE networks for limited service devices. On the other hand, this solution has less scalability than the user-plane, only supports single-user location requests, and is more difficult to interwork with legacy networks.

The 3GPP legacy technologies (GSM and UMTS) have supported LCSs network architecture for the purpose of positioning mobile devices since 3GPP Rel-4. With the introduction of EPS in 3GPP Rel-8, control-plane location-service architecture for the EPS was introduced in 3GPP Rel-9. Figure 15.2 illustrates the control-plane location service architecture for the EPS, which introduced new interfaces SLg and SLs, and allowed the EPS control-plane element mobility management entity to interconnect with the location service core network elements, making location services using the positioning functionality provided by the E-UTRAN possible.

The location service architecture follows a client/server model with the GMLC acting as the location server providing location information to location service clients. The GMLC sends location requests to the evolved serving mobile location center (E-SMLC) through the MME to retrieve this location information. The E-SMLC is responsible for interaction with the UE through E-UTRAN to obtain the UE position estimate or to obtain position measurements that help the E-SMLC to estimate the UE position. Note that the GMLC interaction over the interfaces connected to it other than SLg was already available before 3GPP Rel-9 for GSM and UMTS access.

The location service clients can be part of the core network or external to the core network, and can also reside in the UE or be attached to the UE. Depending on the location of the location service client, the location request initiated by the location service client may be a mobile-originated, mobile-terminated, or network-induced location request. Emergency location service is possible even if the UE does not have a valid service subscription due to regulatory mandates. Support of location service-related functionality in the E-UTRAN, MME, and UE are optional. The location service is applicable to any target UE, no matter

whether the UE supports location service. The following is a description of various LCS architectural elements and interfaces shown in Figure 15.2 [18]:

- *Gateway mobile location center*: This entity receives and processes location requests from location service clients; obtains routing information from the home subscriber server; performs registration authorization; communicates information needed for authorization, location service requests, and location information with other GMLC; checks the target UE privacy profile settings; and depending on roaming support, it may assume the role of requesting GMLC, visited GMLC, or home GMLC.
- *Evolved serving mobile location center*: This entity manages the overall coordination and scheduling of resources required for the location determination of a UE that is attached to E-UTRAN. It calculates the final location and estimates velocity, as well as the location accuracy. It interacts with the UE to exchange location information applicable to the UE-assisted and the UE-based positioning methods. It interacts with the E-UTRAN to exchange location information applicable to the network-assisted and the network-based positioning methods.
- *Mobility management entity*: This entity is responsible for UE subscription authorization. It coordinates location services and positioning requests. It handles charging and billing, and performs E-SMLC selection (e.g., based on network topology to balance the load on E-SMLC, location service client type, and requested QoS). It is further responsible for authorization and operation of the location service.
- *Home subscriber server*: This entity is used for storage of location services subscription data and routing information.
- *Location measurement unit*: The location measurement unit (LMU) conducts measurements and communicates the measurements to an E-SMLC. All positioning measurements obtained by an LMU are supplied to the E-SMLC that made the request. A UE positioning request may involve measurements by multiple LMUs. The SLm interface between the E-SMLC and the LMU is used for uplink positioning. It is used to transport SLm-application protocol (AP) messages over the E-SMLC-LMU interface. Both stand-alone LMU and LMU integrated into an eNB are supported in LTE Rel-11.

Two protocols are used for the overall information exchange concerning location services: (i) LTE positioning protocol (LPP); and (ii) LTE positioning protocol annex (LPPa). The latter protocol is used for communication between the location server and the eNB. The base station (when using the observed time difference of arrival (OTDOA) method) is in charge of properly configuring the radio signals that are used by the terminal for positioning measurements, i.e., positioning reference signals (PRSs). It further provides information to the E-SMLC; it enables the device to conduct inter-frequency measurements, if required; and based on the E-SMLC request, it conducts measurements and sends the results to the server. The LPP can be used in the user-plane and control-plane methods. The LPP is a

point-to-point protocol that allows multiple connections to different devices. The exchanged LPP messages and information can be divided into four categories:

1. UE positioning capability information transfer to the E-SMLC.
2. Positioning assistance data delivery from the E-SMLC to the device.
3. Location information transfer.
4. Session management.

The SLm-AP (application protocol), terminated between the E-SMLC and the LMU, is used to support the following functions: (i) delivery of target UE configuration data from the E-SMLC to the LMU; and (ii) request of positioning measurements from the LMU and delivery of positioning measurements to the E-SMLC. The SLm-AP is directly used between the E-SMLC and the LMU.

The MME receives a request for location service associated with a particular target UE from another entity (e.g., GMLC, eNB, or UE), or the MME by itself decides to initiate some location service on behalf of a particular target UE (e.g., for an IP multimedia subsystem (IMS) emergency call from the UE). The MME then sends a location service request to the E-SMLC. The E-SMLC processes the location service request, which may include transferring assistance data to the target UE to help UE-based and/or UE-assisted positioning. The E-SMLC then returns the result of the location service to the MME, e.g., a position estimate for the UE and/or an indication of any assistance data transferred to the UE. In the case of a location service requested by an entity other than the MME (e.g., UE, eNB, or E-SMLC), the MME returns the location service result to this entity.

The UE positioning is an access network function (e.g., GERAN, UTRAN, and E-UTRAN). An access network may support one or more UE positioning method, which may be the same or different from another access network. In E-UTRAN, the following UE positioning methods are supported: Cell ID (CID)-based; enhanced Cell ID (E-CID)-based; downlink OTDOA; and network-assisted GNSS positioning methods. Determining the position of a UE involves two main steps: (i) radio signal measurements; and (ii) position and optionally velocity estimation based on the measurements. The signal measurements may be conducted by the UE or the E-UTRAN. Both TDD and FDD radio interfaces will be supported in E-UTRAN positioning methods. The basic signals measured for terrestrial position methods are typically the E-UTRA radio transmissions. Other transmissions such as general radio navigation signals, including those from global navigation satellites systems, can also be measured. The position estimation may be performed in the UE or in the E-SMLC. In UE-assisted positioning, the UE performs the downlink radio measurements and the E-SMLC estimates the UE position, while in UE-based positioning, the UE performs both downlink radio signal measurements and position estimation. The UE may require some assistance from the network in the form of assistance data in order to perform the downlink measurements, and these are provided by the network either autonomously or upon UE request. The E-UTRAN positioning capabilities are intended to be forward compatible to other access types and

other positioning methods, in an effort to reduce the amount of additional positioning support needed in the future [7].

15.1.2 Network-based and UE-based positioning methods

A network service provider needs to select an appropriate method for determining the location of a user device, based on the service requirements that have been identified. There are three primary network-enabled modes of operation for determining a user's location. In the UE-based mode, the user device obtains location measurements with assistance from the network and calculates the user's position. In the device-assisted mode, the user device provides positioning measurements, which the network uses to calculate the user's location. In the network-based mode, the network calculates the user's position without involving the device. The following location technologies support one or more of the above modes.

The differentiation between supported positioning methods is based on two facts. First, what the "measurement entity" is, which could only be the device or the base station. Second, what the "position estimation entity" is. The terms "-based" and "-assisted" refer to the node that is responsible for performing the positioning calculation (which may also provide measurements), and a node that provides measurements (but does not perform the positioning calculation), respectively. Thus, an operation in which measurements are provided by the UE to the E-SMLC to be used in the calculation of a position estimation is described as "UE-assisted" (and alternatively "E-SMLC-based"), whereas one in which the UE calculates its own position is described as "UE-based." With that knowledge, the positioning methods supported in LTE can be further categorized. Table 15.1 provides an overview of supported positioning methods in LTE.

In Table 15.1, A-GPS refers to the case where the network assists GPS-enabled mobile devices to improve the performance of their GPS receivers by providing assistance information such as reference time, visible satellite list, reference position, and satellite ephemeris. In general, A-GPS provides the highest accuracy of any network-enabled technique. However, it is not reliable in indoor or in dense urban or high-rise building environments, in which case A-GPS can be supplemented with other techniques such as downlink OTDOA or E-CID. In CID-based methods, a user device is located within the coverage area of its serving eNB, typically to the specific cell/sector within the eNB. Although this method is the least accurate one, it is the easiest to implement, and highly scalable. In E-CID-based methods, the position of the UE is determined to a finer level compared to the CID-based method, using additional radio signal measurements. This method has low accuracy (50–1000 m) depending on the size of the cell, but it is easier to implement than other methods, and is generally available across diverse vendor products and networks. Downlink OTDOA uses the measured timing of downlink signals received from multiple eNBs to locate the user device in relation to neighboring eNBs. In dense urban and indoor environments, OTDOA can be used to supplement A-GPS, provided that the user device can

Table 15.1 E-UTRA UE Positioning Methods [7]

3GPP Release	Method	UE-based	UE-Assisted (E-SMLC-Based)	LMU-Assisted/ E-SMLC-Based	eNB-Assisted	Secure User-Plane Location
9	A-GNSS	Yes Measurement: UE Estimation: UE	Yes Measurement: UE Estimation: LCS server	No	No	Yes (UE-based and UE-assisted)
9	Downlink OTDOA	No	Yes Measurement: UE Estimation: LCS server	No	No	Yes (UE-assisted)
9	Enhanced Cell-ID	No	Yes Measurement: UE Estimation: LCS server	No	Yes Measurement: eNB Estimation: LCS server	Yes (UE-assisted)
11	Uplink TDOA	No	No	Yes	No	No

detect PRSs transmitted from three or more eNBs. The uplink time difference of arrival (UTDOA) has been specified as part of LTE Rel-11, and has minimal impact on air-interface resources. This uplink positioning method makes use of the measured timing at multiple LMUs of uplink signals transmitted from the UE. The LMU measures the timing of the received signals using assistance data received from the positioning server, and the resulting measurements are used to estimate the location of the UE.

15.1.3 Positioning methods in LTE/LTE-Advanced

The positioning feature provides a means to determine the geographic location and/or velocity of the UE based on measuring radio signals. The position information may be requested by and reported to a client (e.g., an application) associated with the UE, or by a client within or attached to the core network. The position information is reported in standard formats such as those for cell-based or geographical coordinates, together with the estimated errors (uncertainty) in the position and velocity estimation as well as the positioning scheme(s) used to obtain the position estimate.

The uncertainty of the position measurement is dependent on network implementation and is controlled by the network operator. The uncertainty may vary between networks, as well as from one area within a network to another. The uncertainty may be hundreds of meters in some areas and only a few meters in others. In the event that a particular position measurement is provided through a UE-assisted process, the uncertainty may also depend on the capabilities of the UE. The uncertainty of the position information is dependent on the method used, the position of the UE within the coverage area, and the activity of the UE. Several design options of the E-UTRAN system (e.g., size of cell, adaptive antenna technique, path loss estimation, timing accuracy, and eNB surveys) allow the network operator to choose a suitable and cost-effective UE positioning method. The following assumptions are made for the operation of UE positioning in E-UTRAN [7]:

- The positioning method is equally applicable to TDD and FDD systems.
- The provision of the UE positioning function in EPS is optional through support of the specified methods in the eNB and the E-SMLC.
- UE positioning is applicable to any target UE, no matter if the UE supports location service, but with restrictions on the use of certain positioning methods depending on UE capability [6].
- The positioning information may be used for internal system operations to improve system performance.
- The location service architecture and functions include the option to accommodate several techniques of measurement and processing to ensure adaptability to the future technologies and service requirements.
- The LMU aspects are implementation-specific.

The following sections describe the specific positioning methods that are specified in E-UTRAN specifications as of LTE Rel-11.

15.1.3.1 Principles of GPS

The GPS is a space-based satellite navigation system that provides location and time information in all weather conditions, anywhere on or near the earth where there is an unobstructed line of sight to four or more GPS satellites. The system provides critical capabilities to military, civil, and commercial users around the world. It is maintained by the United States government, and is freely accessible to anyone with a GPS receiver.

A GPS receiver calculates its position by precisely timing the signals sent by GPS satellites in medium earth orbits. Each satellite continuously transmits messages that include the time at which the message was transmitted, and the satellite position at the time of message transmission. The receiver uses the messages it receives to determine the transit time of each message and computes the distance to each satellite. Each of these distances and satellites' locations define a sphere. The receiver is on the surface of each of these spheres when the distances and the satellites' locations are correctly calculated. These distances and satellites' locations are used to compute the location of the receiver using the navigation equations. This location is then displayed, perhaps with a moving map display or latitude and longitude; elevation information may be included. Many GPS units show derived information such as direction and speed, calculated from position changes.

In typical GPS operation, four or more satellites must be visible to obtain an accurate result. Four sphere surfaces typically do not intersect; thus, we can confidently conclude that when we solve the navigation equations to find an intersection, this solution gives us the position of the receiver along with accurate time, thereby eliminating the need for a very large, expensive, and power-consuming clock. The very accurately computed time is mainly used only for display and is not utilized in many GPS applications, which use only the location. However, a number of applications for GPS do use this highly accurate timing.

The receiver uses the messages received from satellites to determine the satellites' positions and the transmission times. Let (x_i, y_i, z_i, t_i) denote the coordinates of the ith satellite position and the transmission time, where the subscript $i = 1, 2, 3, \ldots, N$ is the satellite number, assuming $N \geq 4$. When the transmission time of message reception is indicated by the local clock t_r, the true reception time is going to be $t_r + t_{bias}$, where t_{bias} denotes the receiver's clock bias. The message transit time is $t_r + t_{bias} - t_i$. Assuming the message is traveling at the speed of light, the distance traveled is calculated as $(t_r + t_{bias} - t_i)c$. Having the knowledge of the distance between the receiver and the satellite, and the satellite's position, implies that the receiver is on the surface of a sphere centered at the satellite's position with radius equal to this distance. Thus, the receiver is at or near the intersection of the surfaces of the spheres if it receives signals from more than one satellite. In the

ideal case with no errors, the receiver is at the intersection of the surfaces of the spheres [13].

The clock error or bias t_{bias} is the amount that the receiver's clock is off. The receiver has four unknowns, the three coordinates of the GPS receiver position, and the clock bias (x,y,z,t_{bias}). The equations of the sphere surfaces are given by $(x-x_i)^2 + (y-y_i)^2 + (z-z_i)^2 = (t_r + t_{\text{bias}} - t_i)^2 c^2 \quad i = 1,2,3,\ldots,N$. These equations can be solved by algebraic or numerical methods.

Each GPS satellite continuously broadcasts a navigation message on the L1 C/A and L2 P/Y frequencies (see Figure 15.1) at a rate of 50 bps. Each message takes 750 s to be completely received. The message structure has a basic format of a 1500-bit long frame comprising five subframes, each subframe having 300 bits (6 s) long. Subframes 4 and 5 are sub-commutated 25 times each, so that a complete data message requires the transmission of 25 full frames. Each subframe consists of 10 words, each 30 bits long. Thus, with 300 bits in a subframe, times 5 subframes in a frame, times 25 frames in a message, each message is 37,500 bits long. At a transmission rate of 50 bps, it would take 750 s to transmit the entire almanac message. Each 30-s frame begins precisely on the minute or half-minute as indicated by the atomic clock on each satellite [13].

The first subframe of each frame encodes the week number and the time within the week, as well as the data about the condition of the satellite. The second and the third subframes contain the ephemeris or the precise orbit for the satellite. The fourth and fifth subframes contain the almanac, which contains coarse orbit and status information for up to 32 satellites in the constellation, as well as data related to error correction. Thus, in order to obtain an accurate satellite location from the transmitted message, the receiver must demodulate the message from each satellite it includes in its solution for 18–30 s. In order to collect the transmitted almanacs, the receiver must demodulate the message for 732–750 s [13].

All satellites broadcast at the same frequencies. Signals are encoded using code division multiple access (CDMA) codes, allowing messages from individual satellites to be distinguished from each other based on unique encodings for each satellite that the receiver must be aware of. Two distinct types of CDMA encodings are used: the coarse/acquisition code, which is accessible by the general public; and the precise code, which is encrypted so that only the US military can access it. The ephemeris is updated every 2 hours and is generally valid for 4 hours, with provisions for updates every 6 hours or longer in non-nominal conditions. The almanac is updated typically every 24 hours. Figure 15.3 illustrates the overall structure of the GPS frame.

It would take 12.5 min to download the entire almanac, and it would take even longer if the signal quality becomes poor and the receiver fails to correctly decode any portions of this data. To determine the location of the GPS satellites, two types of data are required by the GPS receiver: the almanac and the ephemeris. This data is continuously transmitted by the GPS satellites, and the GPS receiver collects and stores this data. The almanac data is data that describes the

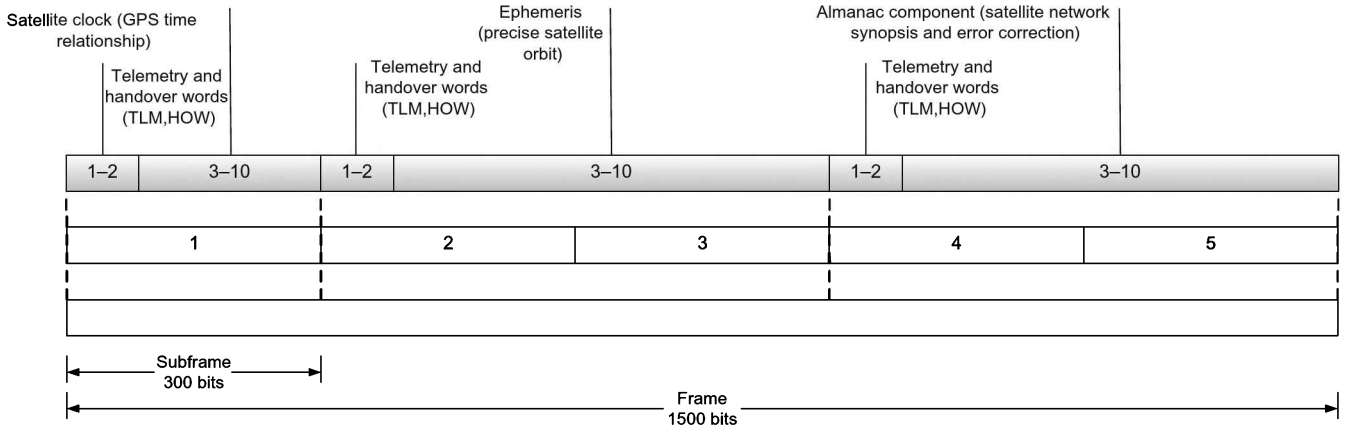


FIGURE 15.3

Overall structure of the GPS frame [16].

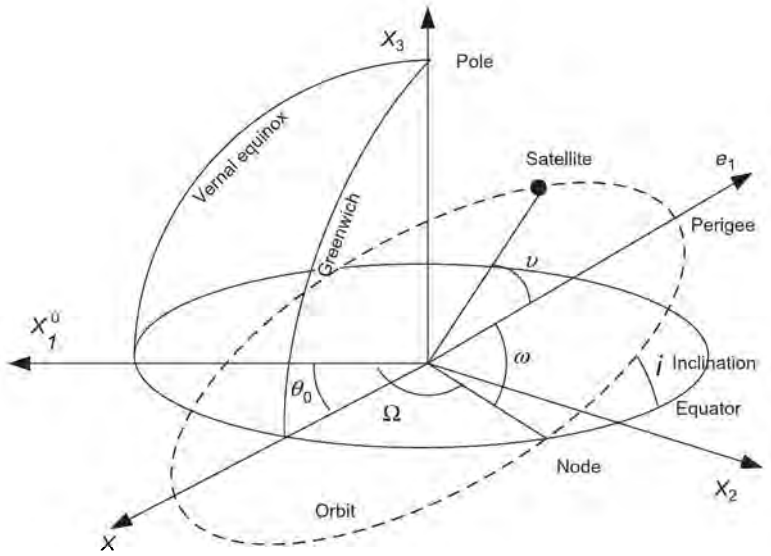


FIGURE 15.4

Illustration of almanac parameters [16].

orbital information of the satellites. Each satellite will broadcast almanac data for all satellites. The GPS receiver uses this data to determine which satellites are going to be visible in the sky. It can then determine which satellites should be tracked. With the almanac data, the receiver can focus on those satellites it can see, and exclude those that are over the horizon or out of view. Figure 15.4 illustrates the GPS almanac parameters.

The almanac parameters consist of size and shape of orbit (represented by semi-major axis a and eccentricity e), orientation of the orbital plane in the inertial system (represented by right ascension of ascending node Ω, argument of perigee ω, and inclination i), and position of the satellite in the orbital plane (represented by epoch of perigee T_0).

Ephemeris data provides the GPS receiver with the position of each GPS satellite at any time throughout the day (Figure 15.5). Each satellite will broadcast its own ephemeris data showing the orbital information for that satellite only. Given that the ephemeris data provides very precise orbital and clock correction data necessary for accurate positioning, its validity is much shorter. It is broadcast in three 6-s blocks and repeated every 30 s. The validity of data is implementation-specific and is usually up to 4 hours. The ephemeris data includes the following list [13,16]:

- $\sqrt{a}$ square root of the semi-major axis.
- e eccentricity.
- i_0 inclination angle at the reference time.

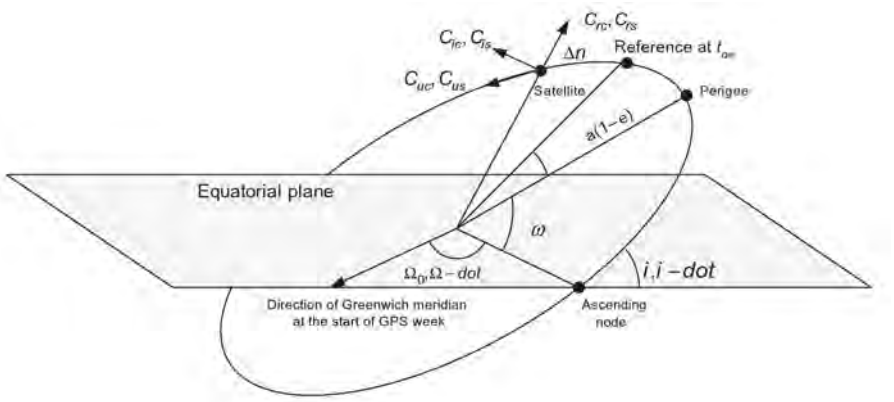


FIGURE 15.5

Illustration of ephemeris information [16].

- Ω_0 longitude of the ascending node at the beginning of the GPS week.
- ω argument of perigee.
- M_0 mean anomaly at the reference time.
- Δn correction to the mean motion computed using $\sqrt{a}$.
- $i{-}dot$ the rate of change of inclination with time.
- $\Omega{-}dot$ the rate of change of the right ascension of the ascending node with time.
- C_{uc}, C_{us} amplitude of the correction terms for the computed argument of latitude.
- C_{rc}, C_{rs} amplitude of the correction terms for the computed orbit radius.
- C_{ic}, C_{is} amplitude of the correction terms for the computed inclination angle.
- t_{oe} ephemeris reference time.

15.1.3.2 A-GNSS positioning

GNSS refers to satellite navigation systems that provide autonomous geospatial positioning with global or regional coverage. Different GNSS methods can be used separately or in combination to determine the location of a UE. In the E-UTRAN, the GNSS is designed to work with assistance data provided by the network. A-GNSS uses signals broadcast by satellites to determine the positions of UEs equipped with GNSS receivers.

Two types of assistance data are provided to improve the positioning speed and accuracy which include data assisting the measurements (e.g., reference time, visible satellite list, satellite signal Doppler, code phase Doppler, and code phase search windows), and data assisting position calculation (e.g., reference time, reference position, satellite ephemeris, and clock corrections). A-GNSS provides improved accuracy relative to the stand-alone GNSS, and it can further reduce the UE GNSS start-up and acquisition times, it can increase the UE GNSS sensitivity, and it can allow the UE to consume less power with the GNSS-capable receiver

put in idle mode when it is not needed. The A-GNSS methods can be operated in UE-assisted mode, where the UE performs GNSS measurements and sends them to the E-SMLC to calculate its position, or the UE-based mode, where the UE performs GNSS measurements and calculates its own location.

15.1.3.3 Observed time difference of arrival positioning

The OTDOA positioning method is based on measuring the time difference of arrival (TDOA) on special reference signals, embedded into the overall downlink signal, received from different eNBs. Each TDOA measurement describes a hyperbola, where the two focal points (F_1,F_2) are at the two measured eNBs. The measurement needs to be conducted at least for three pairs of base stations. The position of the device is the intersection of the three hyperbolas for the three measured base stations (A-B, A-C, and B-C), as shown in Figure 15.6.

The measurement conducted between a pair of eNBs is defined as the reference signal time difference (RSTD). The measurement is defined as the relative timing difference between a subframe received from the *j*th (neighboring) cell and the corresponding subframe from the *i*th (serving) cell. These measurements are conducted on the PRSs and the results are reported back to the location server, where the calculation of the position takes place. PRSs were introduced in

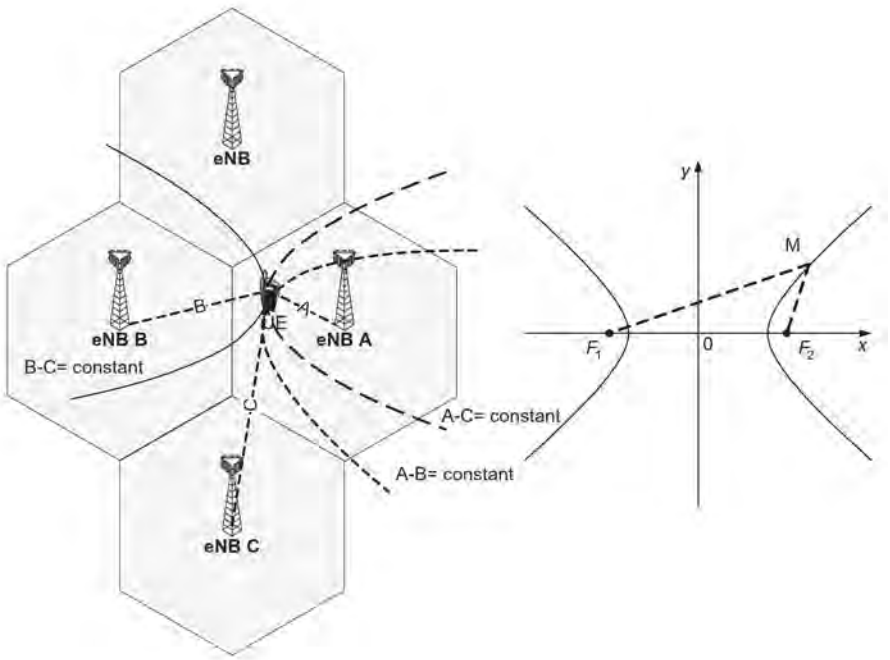


FIGURE 15.6

Illustration of downlink OTDOA positioning method [15].

LTE Rel-9 associated with antenna port 6, since the performance of cell-specific reference signals was not deemed sufficient for positioning. The reason is that the required high probability of detection could not be guaranteed. A neighbor cell with its synchronization signals (primary/secondary synchronization signals) and reference signals is seen as detectable, when the post-processing SINR is at least −6 dB. The results of the simulations performed during standardization of LTE Rel-9 suggested that this could be only guaranteed for 70% of all cases for the third best-detected cell, means second best neighboring cell. This is not enough, and further it assumed an interference-free environment, which cannot be ensured in a realistic scenario. However, PRSs still have some similarities with cell-specific reference signals as defined in LTE Rel-8. It is a pseudo-random QPSK sequence that is mapped in diagonal patterns with shifts in frequency and time to avoid collision with cell-specific reference signals and the control channels. The structure of the PRSs is described in Chapter 9. The PRSs can be muted on certain occasions to further reduce inter-cell interference. Therefore, PRS configuration and PRS muting is provided via the LPP protocol from the location server [15].

At least three timing measurements from geographically dispersed base stations with a good geometry are needed to solve for two coordinates of the UE, where the good geometry means that no two branches of the distinct hyperbolas intersect twice so that a unique solution can be found. In practice, a larger number of measurements, typically at least six to seven, are desirable. The position calculation is based on the multilateration approach by which an intersection of hyperbolas is found, where a hyperbola for a pair of cells corresponds to a set of points with the same RSTD for the two cells. The OTDOA positioning method is illustrated in Figure 15.6, where a UE is receiving downlink signals from the eNBs A, B, and C, and performing RSTD measurements τ_{AB}, τ_{AC}, and τ_{BC} which form three intersecting hyperbolic strips, the widths of which correspond to the RSTD measurement uncertainties. The distance equivalents of the RSTD measurements are d_{AB}, d_{AC}, and d_{BC}, respectively. Assuming the UE is located at (x,y) in a Cartesian coordinate system, and eNBs are located at $(x_A, y_A), (x_B, y_B)$, and (x_c, y_c), respectively, the system of equations to be solved in the least squares sense to find two-dimensional coordinates (x,y) is as follows:

$$\begin{aligned}
\sqrt{(x-x_A)^2-(y-y_A)^2}-\sqrt{(x-x_B)^2-(y-y_B)^2} &= d_{AB}-\Delta d_{AB}\\
\sqrt{(x-x_A)^2-(y-y_A)^2}-\sqrt{(x-x_C)^2-(y-y_C)^2} &= d_{AC}-\Delta d_{AC}\\
\sqrt{(x-x_B)^2-(y-y_B)^2}-\sqrt{(x-x_C)^2-(y-y_C)^2} &= d_{BC}-\Delta d_{BC}
\end{aligned}$$

Accurate knowledge of the transmitter locations and timing offsets is needed to solve the above equations for the UE's coordinates. Determining transmitter timing is nontrivial at the required accuracy level. The advantage of OTDOA is that synchronization between the eNBs and the UE is not required, unlike when the time of arrival measurement is used. Although RSTD measurements can be

performed on a number of downlink signals, e.g., cell-specific reference signals or synchronization signals, it has been recognized that the existing signals suffer from poor reception, which is critical for OTDOA when multiple remote neighbor cells have to be detected. Therefore, to ensure the possibility of positioning measurements of a proper quality, and for a sufficient number of distinct locations, PRS having transmission patterns with an effective reuse of six has been introduced in LTE Rel-9. The interference to PRS can be further minimized, allowing simultaneous PRS transmissions for groups of cells with either orthogonal PRS patterns or low inter-cell interference. In OTDOA, the UE receiver has to deal with PRS from neighbor cells much weaker than those received from the serving cell. Furthermore, without the approximate knowledge of when the measured signals are expected to arrive in time and what is the exact PRS pattern, the UE would need to search the signals blindly, which would impact the time and accuracy of the measurements. To facilitate UE measurements, the network transmits assistance data to the UE, including a neighbor cell list with CIDs, the number of antenna ports, the number of consecutive downlink subframes per positioning occasion, PRS transmission bandwidth, expected RSTD, and the estimated uncertainty [11]. It should be noted that the detection of at least three eNBs is an absolute minimum. In practice, additional measurements are often necessary to be able to suppress outliers in the measurements. Such outliers may arise due to non-line-of-sight propagation. Thus, the detection capability of a TDOA method can often be the limiting factor, which makes it important to understand how the detection performance is computed.

15.1.3.4 E-CID-based positioning

The downlink OTDOA is the method of choice for dense urban and indoor environments where the A-GNSS method may not be able to provide reliable availability and satisfactory performance. Another method of positioning in LTE is the E-CID based on the cell of origin concept. With cell of origin, the position of the device is estimated using the knowledge of the geographical coordinates of its serving base station. The knowledge of the serving cell can be obtained after performing a tracking area update, or through paging. The position accuracy in this case is linked to the cell size, as the location server is only aware that the device is served by this base station. This method would of course not be able to fulfill the accuracy requirements mandated by the FCC [17]. Therefore, the E-CID method was defined in LTE, mainly for devices with no integrated GNSS receiver. In addition to the use of geographical coordinates of the serving base station, the position of the device is estimated more accurately by performing measurements on radio signals.

The E-CID method can take three approaches, based on different types of measurements: (i) E-CID with estimation of the distance from one base station; (ii) E-CID with measurement of the distance from three base stations; and (iii) E-CID by measuring the angle of arrival (AoA) from at least two base stations. In the first two cases, the possible measurement can be reference signal received

power (RSRP), a standard quality measurement for LTE Rel-8 terminals, TDOA, and the measurement of the timing advance or round-trip time.

In the first case, the position accuracy would be just a circle. The second and third methods can provide position accuracy of a point, when measuring more radio sources. In the first and second cases, the measurements are conducted by the UE; thus, they are considered UE-assisted. In the third case, the measurements are performed by the base station; thus, it is eNB-assisted. Ever since LTE Rel-9 was introduced, the timing advance measurement has been enhanced; as a result, there are now two types of measurements: Type 1 and Type 2. The Type 2 measurement relies on the timing advance estimated from receiving a PRACH preamble during the random access procedure. Type 1 is defined as the sum of the receive–transmit timing difference at the eNB (positive or negative value), and the receive–transmit timing difference at the terminal, which is always a positive value. The base station first measures its own timing difference and instructs the device to adjust its uplink timing using a timing advance MAC command (see Chapter 8). The UE measures and reports the receive–transmit timing difference, as well. Both timing differences allow the calculation of the timing advance Type 1, corresponding to the round-trip time. The round-trip time is reported to the location server, where the distance to the base station is calculated using $d = cT_{\mathrm{RTT}}/2$.

The round-trip time and timing advance can be used for distance estimation; nevertheless, they do not provide any information on direction. This can only be obtained through an AoA measurement. The AoA is defined as the estimated angle of a UE with respect to a reference direction which is geographical north, positive in a counterclockwise direction, as seen from an eNB. The base station can usually estimate this angle on any uplink signal; however, typically, sounding reference signals (SRSs) are used for this purpose. The antenna array configuration has an impact on AoA measurements, the larger the array size, the higher the accuracy. With a linear array of equally spaced antenna elements, the received signal at any adjacent element is phase-rotated by a fixed angle whose value is a function of the AoA as well as the antenna element spacing and carrier frequency [15].

15.1.3.5 UTDOA positioning

In the uplink positioning methods, the UE's position is estimated based on timing measurements of uplink radio signals conducted at different LMUs, along with the knowledge of the geographical coordinates of the LMUs. The time required for a signal transmitted by a UE to reach an LMU is proportional to the length of the transmission path between the UE and the LMU. A set of LMUs are designated to sample the UE's signal at the same time [7].

In order to obtain uplink measurements, the LMUs need to know the characteristics of the SRSs transmitted by the UE for the time period required to conduct the uplink measurement. These characteristics should be static over the periodic transmission of SRS during the uplink measurements. Therefore, the E-SMLC will inform the serving eNB to configure the UE to transmit SRSs for the purpose

of uplink positioning. It is up to the eNB to make the final decision on resources to be assigned, and to communicate this configuration information back to the E-SMLC so that E-SMLC can configure the LMUs. The eNB may decide (e.g., in case no resources are available) to configure no resources for the UE, and to report the empty resource configuration to the E-SMLC [7].

The conceptual difference between the UTDOA and OTDOA positioning methods is that the latter requires multiple transmit points, while the former utilizes multiple receive points at different locations, although the position calculation principle is the same. In order to perform UTDOA timing measurements on user data, one reference receiver decodes the UE signals and forwards the sequence to cooperating receivers. This procedure is relatively complex and requires a significant amount of signaling. Therefore, SRSs have been selected for UTDOA measurements. For UTDOA positioning, periodically transmitted SRSs are scheduled in a non-dynamic manner to allow a sufficiently long time for the measurements. This reduces the need for signaling of the full scheduling information to communicate the SRS configuration parameters. The SRS occupies the last SC-FDMA symbol in an uplink subframe. The bandwidth and the periodicity of SRS transmission can be configured to meet the positioning requirements. The SRS-based measurements for positioning may be performed and processed directly at a base station, or the operation may be performed by specific measurement units that may share the antennas with the base stations. The main disadvantage of the UTDOA method relative to OTDOA is a potential reception problem due to the power control of the UE transmissions. The UEs close to their serving base station transmit at a lower power level to avoid unnecessary interference to other UEs; this is known as the near–far problem. The consequence is that such signals may not be strong enough to reach the required uplink signal strength for UTDOA measurements at neighbor cells.

15.2 Evolved multimedia broadcast/multicast service

As we discussed earlier, the E-MBMS bearer service is the service provided by the packet-switched domain to E-MBMS user services in order to deliver IP multicast datagrams to multiple receivers by minimal use of network and radio resources. An E-MBMS user service is a service provided to the end user by means of the E-MBMS bearer service, and possibly other EPS bearers. The E-MBMS is a point-to-multipoint service in which data is transmitted from a single source entity to multiple recipients over a large geographical area. Transmitting the same content to multiple recipients allows the sharing of network resources. The E-MBMS for EPS bearer service supports broadcast mode over E-UTRAN and UTRAN. The E-MBMS is realized by the addition of a number of new features and functional entities to the LTE network architecture. In the next sections, we describe the E-MBMS network architecture, user-plane and

control-plane protocols, and interfaces, as well as E-UTRAN functions and protocols that support MBMS services in LTE/LTE-Advanced systems.

15.2.1 E-MBMS network architecture

MBMS is a bearer service for simultaneous transmission of content over a large number of synchronized cells to all (or a group of) UEs subscribed to the service over a common bearer. In that case, the resulting signal will appear to the UE as one transmission over a time-disperse radio channel. This is concept is known as multimedia broadcast multicast service single frequency network (MBSFN). A group of cells that transmit the same content to multiple users forms an MBSFN area. Multiple cells can belong to a single MBSFN area, and each cell can be part of up to eight MBSFN areas. There can be up to 256 different MBSFN areas defined in a network, each one with a unique identity. Once defined, MBSFN areas will not change dynamically. It is not required that a terminal simultaneously receive content from multiple MBSFN areas. In other words, an MBSFN area is a geographical area comprising one or several cells that transmit the same content. For example, in Figure 15.7, which illustrates a hypothetical MBSFN network, cells 2 and 3 belong to both MBSFN areas 1 and 2. The MBSFN areas are static and do not vary over time. The usage of MBSFN transmission requires not only time synchronization among the cells participating in an MBSFN area, but also usage of the same set of radio resources in each of the cells for a particular service. This coordination is the responsibility of the multi-cell/multicast coordination entity (MCE), which is a logical node in the radio access network that controls resource allocation and transmission parameters across the cells in the MBSFN area [10].

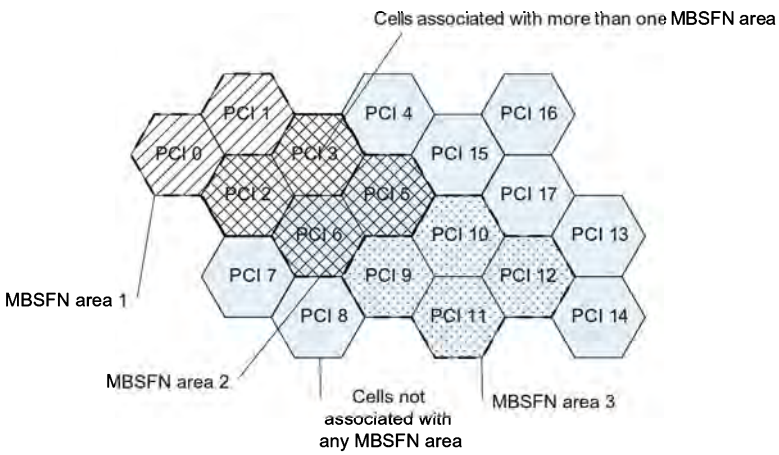


FIGURE 15.7

Illustration of MBSFN areas.

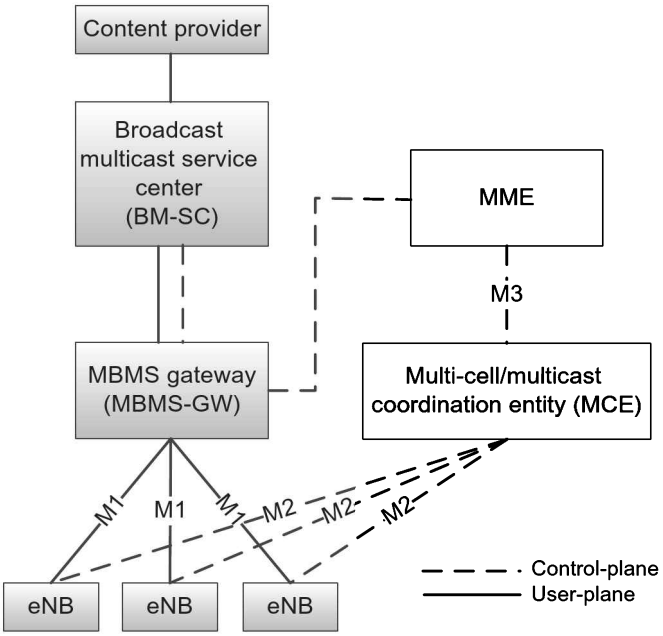


FIGURE 15.8

E-MBMS network architecture [5].

Figure 15.8 illustrates the E-MBMS network architecture. As shown in the figure, the MCE can control multiple eNBs, each controlling one or more cells. The broadcast multicast service center (BM-SC), located in the core network, is responsible for authorization and authentication of content providers, charging, and overall configuration of the data flow through the core network. The MBMS gateway (MBMS-GW) is a logical node handling multicast of IP packets from the BM-SC to all eNBs involved in transmission in an MBSFN area. It also manages session control signaling via the MME. From the BM-SC, the MBMS data is forwarded using IP-based multicast, a method of sending IP packets to multiple receiving network nodes in a single transmission, via the MBMS-GW to the cells. The MBMS is not only efficient from a radio-interface point of view, but it also saves resources in the transport network by avoiding unicast transmission of the same packet to multiple nodes unless necessary. This can lead to significant savings in the transport network.

More specifically, an MBMS-enabled network consists of the following entities and interfaces [5]:

- *Multi-cell/multicast coordination entity*: The MCE is a logical entity whose functions are admission control and allocation of the radio resources used by all eNBs in the MBSFN area for multi-cell MBMS transmissions. The MCE decides whether to establish radio bearer(s) for the new MBMS service(s), if

the radio resources are not sufficient for the corresponding MBMS service(s), or may allocate radio resources from other radio bearer(s) of ongoing MBMS service(s) according to allocation and retention priority (ARP). In addition to allocation of the time/frequency radio resources, the MCE controls the radio configuration, e.g., modulation and coding scheme, counting and acquisition of counting results for MBMS service(s), resumption of MBMS session(s) within MBSFN area(s) based on the ARP and/or the counting results for the corresponding MBMS service(s), suspension of MBMS session(s) within MBSFN area(s) based on the ARP and/or on the counting results for the corresponding MBMS service(s). In the case of distributed MCE architecture, the MCE manages the above functions for a single eNB of an MBSFN area.

- *E-MBMS gateway*: The MBMS-GW is a logical entity that is located between the BM-SC and eNBs whose functions include sending/broadcasting of MBMS packets to each eNB participating in the service. The MBMS-GW uses IP multicast as the method of forwarding MBMS user data to the eNBs. The MBMS-GW performs MBMS session control signaling (i.e., session start/update/stop) toward the E-UTRAN via MME.
- *MCE−MME interface:* The application part of the MCE−MME (M3) control-plane interface allows MBMS session control signaling on E-UTRAN radio access bearer (E-RAB) level (i.e., does not convey radio configuration data). The procedures include MBMS session start and stop. The stream control transmission protocol (SCTP)[4] is used as the signaling transport method.
- *MCE−eNB interface*: The application part of the MCE−eNB (M2) control-plane interface conveys radio configuration data for the eNBs configured with multi-cell transmission mode and session control signaling. The SCTP protocol is used as signaling transport.
- *MBMS−GW−eNB interface*: The user-plane interface MBMS-GW-eNB (M1) carries IP packets between the two network entities and uses IP multicast for point-to-multipoint delivery of user packets.

There are two MBMS architectures defined in 3GPP. In the "distributed MCE architecture," the MCE is part of the eNB and the M2 interface is maintained between the MCE and the corresponding eNB, whereas in the "centralized MCE architecture" (shown in Figure 15.8), the MCE is a logical entity and can be deployed as a stand-alone physical entity or collocated in another physical entity

[4]SCTP is a transport layer protocol, performing a similar role as the commonly used protocols transmission control protocol (TCP) and user datagram protocol (UDP). It provides some of the service features of both protocols, i.e., it is message-oriented like UDP and ensures reliable and in-sequence transport of messages with congestion control like TCP. The protocol is defined by IETF RFC 4960 [19]. The SCTP protocol may be characterized as message-oriented, i.e., it transports a sequence of messages comprising a group of bytes, rather than transporting an unbroken stream of bytes as does TCP. As in UDP, a sender sends a message in SCTP in one operation, and that exact message is passed to the receiving application process in one operation. In contrast, TCP is a stream-oriented protocol, transporting streams of bytes reliably and in order.

such as eNB. In both cases, the M2 interface is maintained between the MCE and all eNB(s) belonging to the corresponding MBSFN area [5].

15.2.2 Basic definitions

In the context of MBMS, the following definitions are used [5]:

- *MBSFN synchronization area* is defined as an area of the network where all eNBs can be synchronized and perform MBSFN transmissions. MBSFN synchronization areas are capable of supporting one or more MBSFN areas. On a given frequency layer, an eNB can only belong to one MBSFN synchronization area. MBSFN synchronization areas are independent from the definition of MBMS service areas.
- *MBSFN transmission or a transmission in MBSFN mode* is a simulcast transmission technique realized by transmission of identical waveforms at the same time from multiple cells (macro diversity). An MBSFN transmission from multiple cells within the MBSFN area is considered like a single transmission from a UE point of view.
- *MBSFN area* is defined as a geographical area consisting of a group of cells within an MBSFN synchronization area of a network, which are coordinated to perform an MBSFN transmission. Except for the reserved cells, all cells within an MBSFN area contribute to the MBSFN transmission and advertise its availability. The UE may only need to consider a subset of nodes in the MBSFN areas that are configured to broadcast the desired service.
- *MBSFN area reserved cell* is a cell within an MBSFN area which does not contribute to the MBSFN transmission. The cell may be allowed to transmit for other services, but at restricted power on the resources allocated for the MBSFN transmission.
- Each *Synchronization sequence* (SYNC) protocol data unit contains a time stamp which indicates the start time of the synchronization sequence. For an MBMS service, each synchronization sequence has the same duration which is configured in the BM-SC and the MCE.
- The *synchronization period* provides the time reference for the indication of the start time of each synchronization sequence. The time stamp which is provided in each SYNC PDU is a relative value which refers to the start time of the synchronization period. The duration of the synchronization period is configurable.

15.2.3 E-MBMS user-plane and control-plane protocols

The overall user-plane protocol termination of content synchronization is shown in Figure 15.9. This structure is based on the functional allocation for unicast, and the SYNC protocol is defined additionally on the transport network layer to

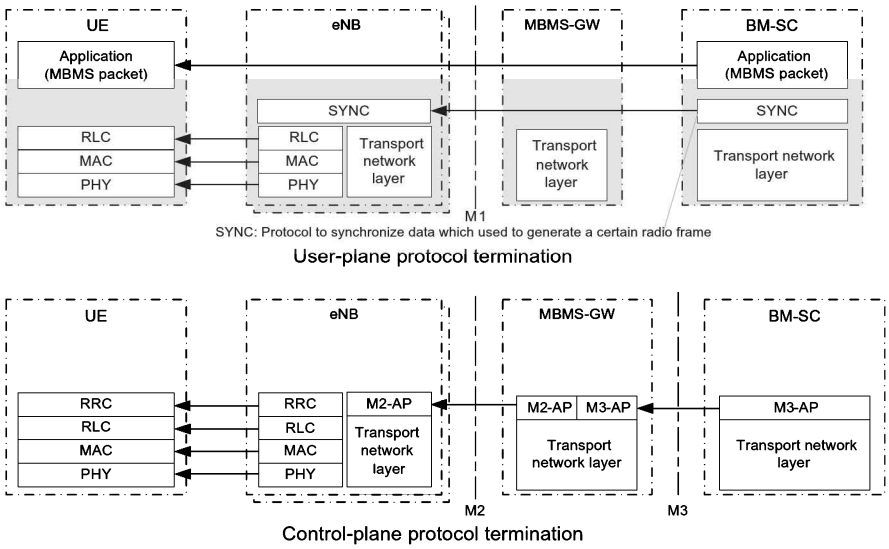


FIGURE 15.9

E-MBMS user-plane and control-plane protocol structure [5].

support the content synchronization mechanism. The SYNC is a protocol for transporting additional information that enables eNBs to identify the timing for radio frame transmission and detect packet loss. Each MBMS service uses its own SYNC entity. The SYNC protocol is applicable to downlink and is terminated in the BM-SC. The multicast control logical channel is terminated in the eNB on the network side. The control-plane protocol structure and termination is further shown in Figure 15.9.

15.2.4 Physical and MAC layer aspects of E-MBMS

The MBSFN transmission is made possible through use of a new transport channel known as a multicast channel (MCH). As shown in Figure 15.10, two types of MBMS-related logical channels are multiplexed to MCH, i.e., the multicast traffic channel (MTCH) and multicast control channel (MCCH). The MTCH is a logical channel that is used to carry MBMS data corresponding to a certain MBMS service. If the number of services provided in an MBSFN area is large, multiple MTCHs can be configured. For MBSFN transmission, no acknowledgments are transmitted by the terminals, no RLC retransmissions can be used, and consequently, the RLC unacknowledged mode is utilized. The MCCH is a logical channel that is used to transport control information necessary for reception of a certain MBMS service, including the subframe allocation and MCS for each MCH. There is one MCCH per MBSFN area. Similar to MTCH, the RLC sublayer uses unacknowledged mode [2].

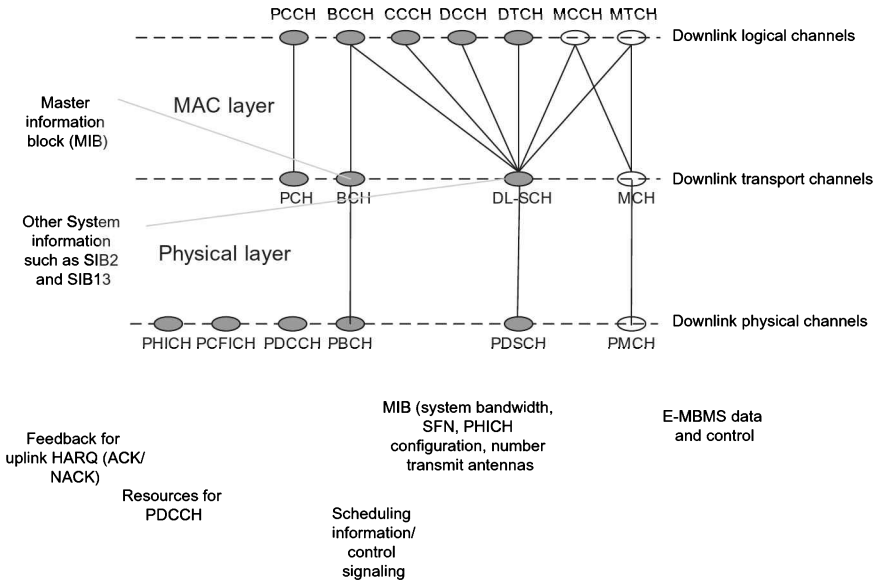


FIGURE 15.10

Logical, transport, and physical channel mapping to support E-MBMS [3,5].

Multiple MTCHs and one MCCH can be multiplexed in the MAC sublayer to form an MCH transport channel. The MAC header contains information about MTCH/MCCH multiplexing, such that the terminal can demultiplex the information upon reception. The MCH is transmitted using MBSFN in one MBSFN area. The transport channel processing for MCH is similar to the downlink shared channel with some exceptions. In the case of MBSFN transmission, the same data is transmitted with the same transport format using the same physical resource from multiple cells typically belonging to different eNBs. Thus, the MCH transport format and resource allocation cannot be dynamically adjusted by the eNB. As described above, the transport format is instead determined by the MCE and signaled to the terminals as part of the information sent on MCCH. As the MCH transmission is simultaneously targeting multiple terminals, and therefore no feedback is used, HARQ is not used for MCH transmission. As already mentioned, multi-antenna transmission (transmit diversity and spatial multiplexing) does not apply to MCH transmission. The physical multicast channel (PMCH) scrambling is unique in each MBSFN area, i.e., identical for all cells participating in MBSFN transmission. The MCH is mapped to PMCH and transmitted in MBSFN subframes (see Chapter 9 for a description of MBSFN subframes). An MBSFN subframe consists of two parts: a control region, used for transmission of non-MBSFN unicast control signaling; and an MBSFN region, used for transmission of MCH. Unicast control signaling may be needed in an MBSFN

subframe, e.g., to schedule uplink transmissions in the next subframe or for MBMS-related signaling [10].

In the case of MBSFN transmission, the cyclic prefix should not only cover the main part of the actual channel time dispersion, but also the timing difference between the transmissions received from the cells involved in the MBSFN transmission. Therefore, MBSFN transmissions, which can take place in the MBSFN regions only, use an extended cyclic prefix. As there are different cyclic prefix lengths and subcarrier spacing defined for LTE, there are different modes for MBMS that take advantage of these configurations. In a mixed mode of MBMS and unicast transmission, the subcarrier spacing is 15 kHz, and resources (subframes) are shared between MBMS data and unicast traffic/control signaling. In a dedicated MBMS mode or single-cell scenario, the RF carrier is only used for MBMS transmission. In this case, a different subcarrier spacing of 7.5 kHz can be used, offering a larger cyclic prefix of 33.3 μs which leads to a further improved broadcast over large cells (that exhibit larger delay spreads).

If a normal cyclic prefix is used for normal subframes, and also in the control region of MBSFN subframes, there will be a small gap between the two parts of an MBSFN subframe. The reason is to keep the start time of the MBSFN region fixed, irrespective of the cyclic prefix length used for the control region. The MCH is transmitted by means of MBSFN from a group of cells that are part of the corresponding MBSFN area. Thus, from the UE's perspective, the radio channel through which the MBMS content has been propagated is the aggregation of the channels of each cell within the MBSFN area. In order to estimate the channel for coherent demodulation of MCH, the UE cannot rely on the cell-specific reference signals transmitted from each cell; rather, in order to coherently demodulate MCH, dedicated MBSFN reference signals are inserted within the MBSFN part of the MBSFN subframe (see Chapter 9 for a description of MBSFN reference signals). These reference signals are transmitted by means of MBSFN over a set of cells that form the MBSFN area, i.e., they are transmitted in the same time–frequency resources and with the same reference signal values from each cell. As a result, the channel estimation based on these reference symbols correctly reflects the overall aggregated channel corresponding to MCH transmission of all cells that are part of the MBSFN area. The MBSFN transmission in conjunction with specific MBSFN reference signals can be seen as transmission using antenna port 4.

The MBSFN-enabled UE can assume that all MBSFN transmissions within a given subframe correspond to the same MBSFN area. Therefore, the UE may choose to interpolate over all MBSFN reference signals within a given MBSFN subframe when estimating the aggregated MBSFN channel. In contrast, MCH transmissions in different subframes may correspond to different MBSFN areas. The frequency-domain density of MBSFN reference signals is much higher than the corresponding density of cell-specific reference signals, given that the aggregated channel of all cells involved in the MBSFN transmission (due to large coverage area) is equivalent to a highly time-dispersive

or highly frequency-selective channel. There is only a single MBSFN reference signal in MBSFN subframes. Thus, multi-antenna transmission such as transmit diversity and spatial multiplexing is not supported for MCH transmission. The main argument for not supporting any standardized transmit diversity scheme for MCH transmission is that the high frequency selectivity of the aggregated MBSFN channel in itself provides substantial frequency diversity [10].

15.2.5 E-MBMS single frequency network transmission

Multiple MBMS services can be mapped to the same MCH transport channel. One MCH contains data belonging to only one MBSFN area. An MBSFN area contains one or more MCHs. All MCHs have the same coverage area. For MCCH and MTCH, the UE does not perform RLC reestablishment upon cell change between the cells belonging to the same MBSFN area. Within the MBSFN subframes, all MCHs within the same MBSFN area occupy a pattern of subframes, not necessarily adjacent in time, which is common for all of these MCHs and which is referred to as a common subframe allocation (CSA) pattern. As shown in Figure 15.11, the CSA pattern is periodically repeated with the CSA period. The MCH subframe allocation (MSA) for every MCH carrying MTCH is defined by the CSA pattern, the CSA period, and the MSA-end, which are all signaled on MCCH. The MSA-end indicates the last subframe of the MCH within the CSA period. Subsequently, the MCHs are time multiplexed within the CSA period, which ultimately defines the interleaving between the MCHs. It is further possible for MCHs not to use all MBSFN resources signaled as part of the Rel-8 MBSFN signaling. Furthermore, such MBSFN resources can be shared for more than one purpose (e.g., MBMS, positioning). During one MCH scheduling period (MSP), which is configurable per MCH, the eNB multiplexes different MTCHs and (optionally) MCCH for transmission on MCH. The MCH scheduling information (MSI) is provided per MCH to indicate which subframes are used by each MTCH during the MSP [5].

In the example provided in Figure 15.11, the scheduling period for the first MCH is 16 frames, corresponding to one CSA period, and the scheduling information for this MCH is therefore transmitted once every16 frames. The scheduling period for the second MCH is 32 frames, corresponding to two CSA periods, and the scheduling information is transmitted once every 32 frames. The MSPs can range from 80 ms to 10.24 s.

The MCCH information is transmitted periodically with a fixed repetition period, and changes to the MCCH information can only occur at specific times. Whenever MCCH information is changed, which can only be done at the beginning of a new modification period, as shown in Figure 15.12, the network notifies the UEs about the upcoming MCCH information change in the preceding MCCH modification period. The notification mechanism uses the PDCCH for this purpose. An 8-bit bitmap, where each bit represents a certain MBSFN area, is

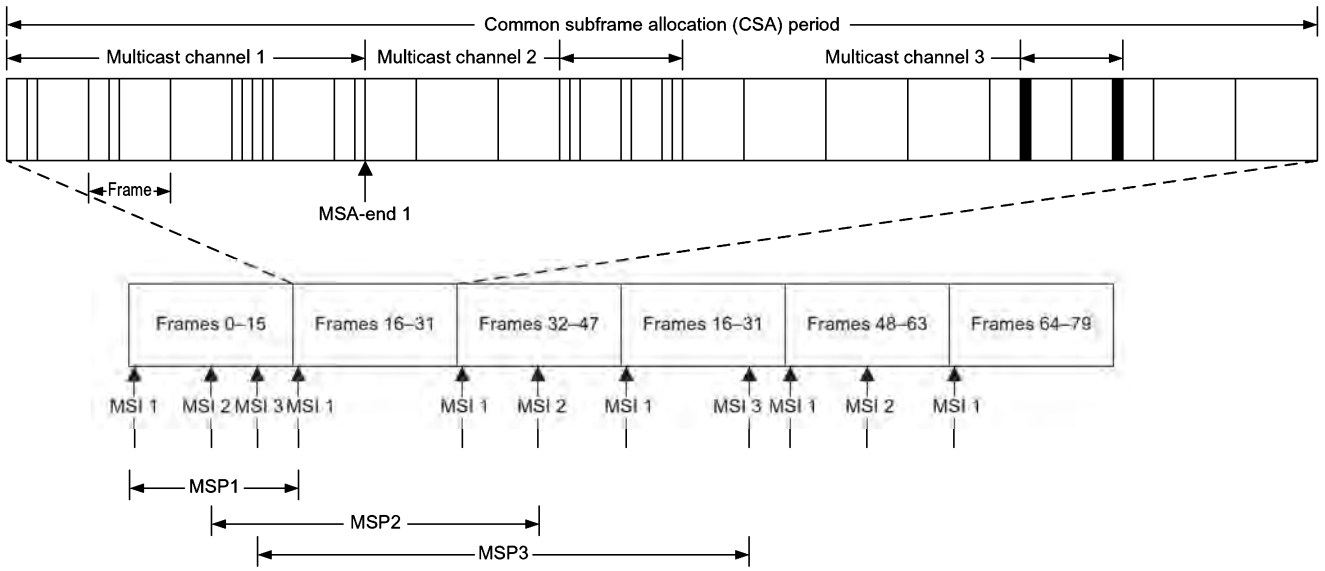


FIGURE 15.11

Example scheduling of MBMS content [10].

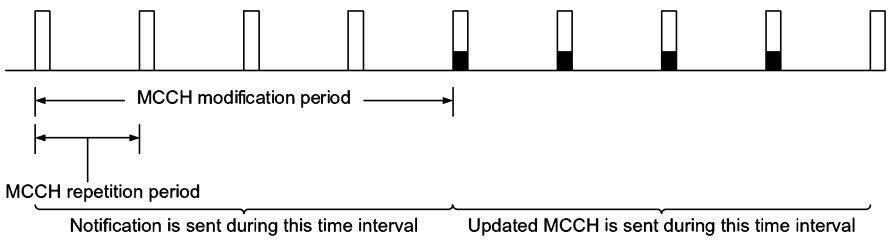


FIGURE 15.12

Example MCCH transmission schedule [1].

transmitted in the PDCCH in an MBSFN subframe using DCI format 1C and the M-RNTI (see Chapter 8 for a description of multicast RNTI). The notification bitmap is only transmitted when there are changes in the services, as well as to indicate a counting request in an MBSFN area. The purpose of notification indicators and modification periods is to maximize the amount of time the UE may sleep to reduce power consumption. In the absence of any changes to MCCH information, a terminal not subscribed to E-MBMS may enter the DRX mode, and only wake up when the notification indicator is transmitted. The periodic transmission of MCCH is useful in order to support mobility, because a terminal entering a new MBSFN area or a terminal that has missed the first MCCH transmission does not have to wait until the start of a new modification period to receive MCCH information [10].

System information block type 2 (SIB2) carries all relevant information about common and shared channels in LTE. LTE Rel-9 has extended the scope of this information to include MBMS-specific information. The new information element *MBSFN-SubframeConfig* defines which radio frames contain subframes that can be used for MBMS (see the example in Figure 15.13). The MBSFN subframes can be used by all MBSFN areas. The E-MBMS information in SIB2 includes the radio frame allocation period and a radio frame allocation offset, as well as the subframe allocation mode, which can be one or four consecutive radio frames containing MBSFN subframes. A maximum of six subframes in each radio frame can be used for MBMS transmission. This is due to the fact that zero and fifth subframes carry synchronization signals and broadcast channel, and subframes 0, 4, 5, and 9 can be used for paging depending on the paging cycle. A bitmap is used to indicate which of the six possible subframes are used for MBMS transmission.

System information block type 13 (SIB13) provides MBSFN identity (MBSFN ID), non-MBSFN region length (one or two OFDM symbols), and MCCH configuration. The MCCH configuration provides information on the repetition period for MCCH, the MCCH offset as well as the actual subframe where MCCH is transmitted, and the MCS used for MCCH. It is important to note that for MCCH, only four MCSs are allowed: MCS indices 2, 7 (both QPSK); 13 (16QAM); and 19 (64QAM). The MCCH always defines one MBSFN area and carries a single

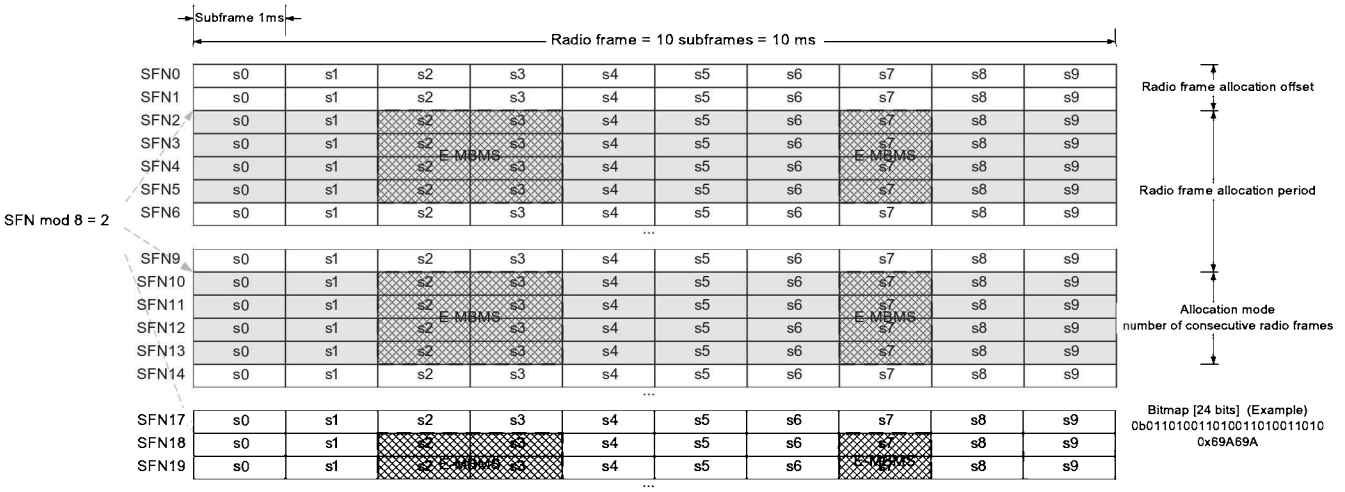


FIGURE 15.13

Example interpretation of E-MBMS information in SIB2 [15].

message, i.e., *MBSFNAreaConfiguration*. This information element provides all required information for scheduling MBMS services, including all PMCH belonging to that particular MBSFN area and the configuration parameters for the sessions that are carried by the corresponding PMCH. There are up to 15 PMCH, where each one has up to 29 MTCHs. For each PMCH, there is information about which MBSFN subframe carries that PMCH (start, end), as well as the MCS that has been utilized.

In general, the control information for the UEs supporting E-MBMS is separated as much as possible from unicast control information. Most of the E-MBMS control information is provided on MCCH. The E-UTRA employs one MCCH logical channel per MBSFN area. In the case where the network configures multiple MBSFN areas, the UE acquires the MBMS control information from the MCCHs that are configured to identify whether the services which the UE is interested to receive are ongoing. The behavior of the UE when it is unable to simultaneously receive MBMS and unicast services depends on the UE implementation. As of LTE Rel-11, an E-MBMS-capable UE is only required to support reception of a single MBMS service at a time, and reception of more than one MBMS service is implementation specific. The MCCH carries the *MBSFN Area Configuration* message, which indicates the ongoing E-MBMS sessions as well as the corresponding radio resource configuration. The MCCH may also carry the *MBMS Counting Request* message, when E-UTRAN needs to count the number of UEs in the RRC_CONNECTED state that are receiving or are interested in receiving specific MBMS services. A limited amount of E-MBMS control information is provided on the broadcast control channel. This is primarily the information needed to acquire the MCCH(s), and is carried via SIB13. An MBSFN area is identified by the *mbsfn-AreaId* in SIB13. During mobility, the UE assumes that the MBSFN area is continuous when the source cell and the target cell broadcast the same value in the *mbsfn-AreaId* [1].

15.2.6 Mobility support in E-MBMS

The E-MBMS mobility is based on the same procedures that are specified for unicast services. There are no additional mechanisms to instruct the E-MBMS-capable UEs to select a carrier frequency providing E-MBMS. Furthermore, there are no provisions to reduce the service interruption time when moving from one MBSFN area to another. Nevertheless, the E-UTRAN can assign the highest cell reselection priority to the carrier frequency that provides E-MBMS to facilitate the transfer of ongoing MBMS service during E-MBMS-subscribed UE mobility. The E-MBMS mobility procedures would allow the UE to start or continue receiving MBMS service(s) via MBSFN when moving across cell(s). The E-UTRAN procedures provide support for service continuity with respect to mobility within the same MBSFN area. Within the same geographic area, MBMS services can be provided on more than one frequency, and the frequencies used to provide MBMS services may change from one geographic area to another within

a PLMN. The E-MBMS-subscribed UEs can be either in the RRC_IDLE state performing cell reselection, or in the RRC_CONNECTED state obtaining target cell MTCH information from the target cell MCCH. To avoid the need for acquiring the E-MBMS related system information and MCCH of neighbor frequencies, the UE is provided with assistance information on the frequency of MBMS services via MBSFN as follows [1,5]:

- *User service description*: The application layer provides temporary mobile group identities (TMGIs) for each service, the session start and end time, the frequencies, and the MBMS SAIs belonging to the MBMS service area.
- *System information*: MBMS and non-MBMS cells use *System Information Block Type 15* to provide the MBMS SAIs of the current frequency, and of each neighbor frequency. The E-MBMS SAIs of the neighboring cells may be provided via X2 signaling.

15.2.7 E-MBMS counting

The MBMS counting in LTE is used to determine if there is a sufficient number of UEs interested in receiving a service to enable the operator to decide whether it would be efficient to deliver the service via MBSFN. It allows the operator to choose between enabling or disabling MBSFN transmission for the service. The MBMS counting applies only to the UEs in the connected mode. Enabling and disabling MBSFN transmission is realized by the MBMS service suspension and resumption function. The counting scheme can be applied to a service already provided by MBSFN in an MBSFN area (an ongoing service), or a service that has not been provided via MBSFN in an MBSFN area (service not started yet), which may be a service provided via unicast bearers [5].

The counting procedure is initiated by the network. Initiation of the counting procedure results in a request to each eNB within the MBSFN area to send a counting request (extended MCCH message), which contains a list of TMGIs, which uniquely identifies an MBMS bearer service. A single globally unique TMGI is allocated by the BM-SC per MBMS bearer service requiring UE feedback. The connected mode UEs which are receiving or are interested in the services will respond with a *Counting Response* message, which includes short MBMS service identities (unique within the MBSFN service area), and may optionally include the information to identify the MBSFN area. The network has the means to disable UE counting per service, and the UE is able to report on multiple MBMS services via a single *Counting Response* message. It is not necessary to retransmit the *Counting Response* message when the UE moves within the same MBSFN area. The network obtains one response from the UE related to one *Counting Request* message, which is broadcast for one modification period. The UE cannot automatically indicate to a network a change of interest in MBMS service(s). The network counts the UE's interest per service [5].

References

3GPP Specifications[5]

[1] 3GPP TS 36.331, Evolved Universal Terrestrial Radio Access (E-UTRA), Radio Resource Control (RRC), Protocol Specification (Release 11), December 2012.

[2] 3GPP TS 36.322, Evolved Universal Terrestrial Radio Access (E-UTRA), Radio Link Control (RLC), Protocol Specification (Release 11), December 2012.

[3] 3GPP TS 36.321, Evolved Universal Terrestrial Radio Access (E-UTRA), Medium Access Control (MAC), Protocol Specification (Release 11), December 2012.

[4] 3GPP TS 36.304, Evolved Universal Terrestrial Radio Access (E-UTRA), UE Procedures in Idle Mode (Release 11), December 2012.

[5] 3GPP TS 36.300, Evolved Universal Terrestrial Radio Access (E-UTRA) and Evolved Universal Terrestrial Radio Access Network (E-UTRAN) Overall Description, Stage 2 (Release 11), December 2012.

[6] 3GPP TS 36.306, Evolved Universal Terrestrial Radio Access (E-UTRA), User Equipment (UE) Radio Access Capabilities (Release 11), December 2012.

[7] 3GPP TS 36.305, Evolved Universal Terrestrial Radio Access Network (E-UTRAN), Stage 2 Functional Specification of User Equipment (UE) Positioning in E-UTRAN (Release 11), December 2012.

Books

[8] C. Johnson, Long Term Evolution in Bullets, second ed., Create Space Independent Publishing Platform, July 2012.

[9] S. Sesia, I. Toufik, M. Baker, LTE, the UMTS Long Term Evolution, From Theory to Practice, second ed., John Wiley & Sons, August 2011.

[10] E. Dahlman, S. Parkvall, J. Skold, 4G, LTE/LTE-Advanced for Mobile Broadband, Academic Press, May 2011.

[11] R. Zekavat, R.M. Buehrer, Handbook of Position Location: Theory, Practice, and Advances, Wiley-IEEE Press, November 2011.

Articles

[12] S. Cherian, A. Rudrapatna, A primer on location technologies in LTE networks, Alcatel-Lucent, July 2012. <http://www2.alcatel-lucent.com/techzine/a-primer-on-location-technologies-in-lte-networks>.

[13] Global Positioning System, Wikipedia <http://en.wikipedia.org/wiki/Global_Positioning_System>.

[14] MSF Services Working Group, MSF Whitepaper on Location Services in LTE Networks, Multi Service Forum, April 2010 <http://www.msforum.org/>.

[15] M. Kottkamp, et al., LTE Release 9 Technology Introduction White paper, Rohde & Schwarz, December 2011.

[16] LTE System Description. <http://www.sharetechnote.com/>.

[17] Federal Communications Commission (FCC), Wireless E911 location accuracy requirements, June 2011. <http://www.fcc.gov>.

[5]3GPP Specifications can be found at the following URL: http://www.3gpp.org/ftp/Specs/archive/

[18] 4G Americas White Paper, 4G Mobile Broadband Evolution: Release 10, Release 11 and Beyond, October 2012. <http://www.4gamericas.org/>.

[19] R. Stewart, Stream control transmission protocol, IETF RFC 4960, September 2007. <http://www.rfc-editor.org/rfc/rfc4960.txt>.

[20] S. Deering, Host extensions for IP multicasting, IETF RFC 1112, August 1989. <http://www.ietf.org/rfc/rfc1112.txt>.

This page intentionally left blank

Index

Note: Page numbers followed by "*f*", and "*t*" refers to figures and tables respectively.

A

Access point name (APN), 183
Access point name-aggregate maximum bit rate (APN-AMBR), 46
Access stratum (AS), 154
Acknowledged mode (AM), 289, 311–312
Adaptive beamforming technique, 1034–1035
Adaptive modulation and coding (AMC), 691–692
Adaptive multi-rate (AMR), 92
Additional maximum power reduction (A-MPR), 999
Adjacent channel interference ratio (ACIR), 1021
Adjacent channel leakage power ratio (ACLR), 774–776, 1009–1010
Adjacent channel selectivity (ACS), 1021
Aggregated channel bandwidth, 1015*f*
Allocation and retention priority (ARP), 193, 244–245
Almost blank subframes (ABS), 1039–1040
AMR-wideband (AMR-WB), 92
APN. *see* Access point name (APN)
APN aggregate maximum bit rate (APN-AMBR), 193
AS. *see* Access stratum (AS)
Assisted-GNSS (A-GNSS) methods, 1072
Authentication and key agreement (AKA), 74–75
Authentication center (AuC), 35, 126
Authorization, authentication and accounting (AAA) server, 42–43

B

Backoff indicator (BI), 394
Band aggregation, 1017*t*
Bandwidth parts, 794*t*
Beamforming, 642
  differential feedback, 635*f*
  techniques, 1034–1035
Bearers, 35–36, 37*f*
  EPS, 35–36
  radio, 144*f*
Block diagonalization (BD), 650–651
Broadcast channel (BCH), 143, 445
Broadcast control channel (BCCH), 142, 1102
Broadcast multicast service center (BM-SC), 1092
Buffer status report (BSR), 372
  MAC control element, 853

C

Call session control function (CSCF), 80–82
Capacity region, 647*f*
Carrier aggregation (CA), 990–992, 1006–1007
  bands, 1017*t*
  bandwidth, 1016
    classes, 1019*t*
  cross-carrier scheduling, 994*f*
  deployment scenarios, 990–992, 991*f*
  physical layer aspects, 992–999
  principles, 986–990
  protocol/signaling aspects, 1002–1005
  radio resource management aspects, 1005–1006
  receiver characteristics, 1022–1027
  RF/implementation aspects, 1006–1027
  scenarios, 986, 987*f*
  transmitter characteristics, 1016–1022
Carrier frequency offset (CFO), 420–421, 861
Carrier indicator field (CIF), 993
Carrier segments, 989*f*
Carrier to interference plus noise ratio (CINR), 1032
Carrier to interference ratio (CIR), 1032
Cell ID (CID)-based methods, 1077–1080
Cell identity, 597
Cell radio network temporary identifier (C-RNTI), 155, 232, 353, 759
Cell selection procedures, 165–166, 1037
Cell-specific reference signal (CRS), 467, 480, 759, 916, 1042
  generation, 494*f*
  mapping
Cell spectral efficiency, 10, 888–889, 916–922
Cell-splitting gain, 20
Channel bandwidth, 414, 439–440, 1011–1013
Channel coding, 522, 546, 772
  convolutional coding, 521–527
  turbo coding, 527–533
Channel estimation, 486, 916–922
Channel quality indicator (CQI), 977
Channel raster, 1010–1011

Ex.1005.01138

Channel-state information (CSI), 478–479
estimation, 753
feedback, 664–665, 975–976, 998, 1034–1035
interference measurement (IM) resource, 682
measurements, 1063*t*
reference signals, 502–511
reporting modes, 854*f*
RS configuration, 505–507
RS density, 508–509
RS patterns, 505
Circuit-switched fallback (CSFB), 94–100, 217–218
Client-based IP mobility, 113
Closed-loop antenna selection, 839
Closed-loop power control, 697
Closed-loop spatial multiplexing (CLSM), 841
Closed subscriber group (CSG), 250, 1036
Clustered SC-FDMA, 997*f*
Code block concatenation, 811*f*
Code block segmentation, 805–807, 806*f*
Collaborative MIMO (Co-MIMO), 652–653
Commercial mobile alert service (CMAS), 172
Common control channel (CCCH), 143
Common public radio interface (CPRI), 63–64, 969
Common search space, 592–593
Control channel elements (CCEs), 568–569, 784
Control format indicator (CFI), 553–554, 996
Control-plane latency, 10–11
Convolutional code, 521–522
Convolutional turbo code (CTC), 519–521
Cooperating/measurement sets, 975*f*
Cooperative MIMO. *see* Virtual MU-MIMO
Coordinated multipoint (CoMP)
architectures, 960, 964–977
dynamic clustering, 972*f*
network, 961–962
operation theory, 959–964, 976–977
reception, 951–952
scenarios, 966–967
techniques, 964–965
downlink, 969–971
inter-eNB, 965
intra-eNB, 965
uplink, 971–973
transmission points (TPs), 969–970, 1034
C-RNTI (Cell-radio network temporary identifier), 52*t*, 60–61
Cross-carrier scheduling, 993–995
CSG ID (Closed subscriber group ID), 52*t*
CSG identity (CSG ID), 61
CSIT feedback, 655–656
Cubic metric (CM), 734*t*
Cyclic delay diversity (CDD), 551
Cyclic prefix (CP), 419–420
detection algorithm, 477*f*
sizes, 446*f*

D

Data call establishment procedures, 194–198
mobile-originated data call, call flow, 195*f*
mobile-terminated data call, call flow, 197*f*
UE-originated data call procedure, 194–196
UE-terminated data call procedure, 196–198
Data radio bearer (DRB), 92–93
Dedicated control channel (DCCH), 143, 293
Dedicated EPS bearer, 35–36
Dedicated traffic channel (DTCH), 143
Default EPS bearer, 35–36
Delay diversity, 621–622
Demodulation reference signal (DM-RS), 478–479, 739–741, 1044
group hopping pattern, 759
relative position, 782*f*
structure
Device-to-device (D2D) communication, 22–23
Dirty paper coding (DPC), 639
Discontinuous reception (DRX), 168, 1003
cycle, 277
mode, 1098–1100
retransmission timer, 368
Discontinuous transmission (DTX)
capability, 922–923
measurement gap, 1008
pattern, 232
Discrete Fourier transform (DFT)
spread OFDM (DFT-S OFDM), 724–726
Distributed antenna system (DAS), 955–959
Donor cell's eNB (DeNB), 61, 64–66, 144–145, 147–148
Doppler effects, 401
Doppler power spectrum, 408–409, 431–433
Doppler spread, 408–409
Downlink assignment index (DAI), 750–751
Downlink carrier aggregation, 784–785
Downlink CB/CS, 971*f*
Downlink CoMP schemes
categories, 969–970
coordinated scheduling/beamforming (CS/CB), 970
joint processing (JP), 970
Downlink control information (DCI), 457, 1098–1100
Downlink MIMO, 842

Downlink MU-MIMO, 980*f*
CS/CB SU-MIMO, 980*f*
JR MU-MIMO, 980*f*
Downlink OTDOA, 1088
Downlink physical channel processing, 546–608
physical broadcast channel, 556–560
physical control format indicator channel, 553–556
physical downlink control channel, 568–596
DCI formats, 574–576
enhanced PDCCH, 597–603
PDCCH physical layer processing, 568–574
UE-specific search spaces/blind decoding, 576–596
physical downlink shared channel, 604–608
physical hybrid-ARQ indicator channel, 560–567
Downlink pilot time slot (DwPTS), 447–448
Downlink power control, 698
Downlink shared channel (DL-SCH), 143
Downlink TFT (DL-TFT), 36–38
Downlink transport channels, 143
Dual stack mobile IP (DSMIP), 110–111
Duplex modes, 440–445
Dynamic host configuration protocol (DHCP), 46
Dynamic overhead, 890*f*
Dynamic resource allocation, 76

E

ECGI (E-UTRAN cell global identifier), 52*t*
ECI (E-UTRAN cell identifier), 52*t*
Effective SINR mapping (EESM), 898
E-MBMS Gateway (MBMS-GW), 70
EMM-DEREGISTERED state, 167–168
EMM-REGISTERED state, 168
Energy efficiency, 989
Energy per resource element (EPRE), 698
Enhanced cell ID (E-CID) method, 1077–1078, 1088
Enhanced control channel elements (eCCEs), 513
Enhanced ICIC (eICIC) techniques, 689, 980, 1048–1049
Enhanced physical downlink control channel (ePDCCH), 599, 968–969
DM-RSs, 479
structure, 512*f*
Enhanced serving mobile location center (E-SMLC), 71, 73
ePDCCH formats, 600*t*
EPS. *see* Evolved packet system (EPS)
EPS connection management (ECM), 48, 166–167, 234–235
EPS mobility management (EMM), 74, 166–168, 234–235
E-RAB ID (E-UTRAN radio access bearer identifier), 52*t*
eREG, structure/formation, 601*f*
Error vector magnitude (EVM), 428–429, 1016–1018
E-UTRA. *see* Evolved universal terrestrial radio access (E-UTRA)
E-UTRA absolute radio frequency channel number (EARFCN), 415, 1014
E-UTRAN cell global identifier (ECGI), 61
E-UTRAN radio access bearer (E-RAB), 136–138
EVA/ETA multipath power delay profiles, 915*t*
Event-triggered periodic reporting, 260–261
Evolved multimedia broadcast/multicast service (E-MBMS), 70, 1069, 1090–1103
architecture, 67–71
basic definitions, 1094
counting, 1103
gateway, 1093
logical, transport, and physical channel mapping, 1096*f*
MCE-eNB interface, 1093
MCE-MME interface, 1093
mobility support, 1102–1103
multi-cell/multicast coordination entity, 1092–1093
physical and MAC layer aspects, 1095–1098
single frequency network transmission, 1098–1102
Evolved node B (eNB), 38, 137–138, 290–291, 879–880, 986
Evolved packet core (EPC), 30, 42–50
Evolved packet system (EPS), 30, 121, 154, 307, 1070
bearer, 191
bearer ID, 52*t*
bearer service architecture, 35–36, 241*f*
reference model, 124–135
Evolved Serving Mobile Location Center (E-SMLC), 73, 1076
Evolved universal terrestrial radio access (E-UTRA), 30, 142–143, 914, 1001–1002, 1053–1054, 1072
Evolved universal terrestrial radio access network (E-UTRAN), 30, 33, 38, 98, 135–138, 149, 290–291, 1070
Extended pedestrian A (EPA) model, 915
Extended typical urban (ETU) model, 915

Extensible markup language (XML), 82
Extension carrier, 990

F

Fairness measures, 886–887
Femto-cells, 148–149
Film bulk acoustic resonator (FBAR) filtering, 1064–1065
Fractional frequency reuse (FFR), 1030–1032
Frame structure, 445–453
  MBSFN, 452–453
  type 1, 446–447
  type 2, 447–452, 448*f*
Frequency division duplex (FDD), 357–358, 411–414, 952
Frequency-selective CQI reporting, 855–857
Frequency-switched transmit diversity (FSTD), 666–667
Full-buffer user traffic model, 893
Further enhanced ICIC (FeICIC) scheme, 1048–1049

G

Gateway GPRS support nodes (GGSN), 129
Gateway mobile location center (GMLC), 71–72, 1075–1076
Generic linear combining receiver, 628*f*
Generic multi-user MIMO transmission model, 647*f*
Global eNB ID (Global eNB identifier), 52*t*
Globally unique temporary identifier (GUTI), 266–270
Global navigation satellite system (GNSS), 1030, 1071–1072
  measurements, 1085–1086
  receivers, commercial applications, 1052
Global positioning system (GPS), 1051
Gold code, 802
Gold pseudo-random sequence, 494–496
GPRS tunneling protocol (GTP), 127–129
  GTP-U, 129
  tunnel endpoint identifiers (TEIDs), 146
Gram-Schmidt orthogonalization procedure, 661
Grassmannian manifold, 634–635
Gray-coded constellations, 533–534
Guaranteed bit rate (GBR), 36–38, 191–193
Guard period (GP), 442
Guard time (GT), 822–823
GUMMEI (Globally unique MME identity), 52*t*, 61
GUTI (Globally unique temporary UE identity), 52*t*

H

Half-duplex FDD (H-FDD), 442
Handover interruption time, 11
Hard/soft decoding, 524*f*
Heterogeneous networks (HetNet), 689
HetNets, 1029–1030, 1038, 1041–1042
  capacity gains, 1042
HetNet scenarios, 1044
HetNet topology, 1036*f*
Home eNB gateway (HeNB GW), 62, 149
Home eNBs (HeNBs), 61
  nodes, support for, 148–151
Home location register (HLR), 35
Home subscriber server (HSS), 35, 126, 183, 271–273
Homogeneous network, 1037
Householder transformation, 636
Hybrid automatic repeat request (HARQ), 140–142, 312, 734–735, 877–879, 1044–1047, 1096–1097

I

IMEI (International mobile equipment identity), 52*t*
IMS centralized services (ICSs), 85
IMS communication service identifier (ICSI), 91–92
IMSI (International mobile subscriber identity), 52*t*
IMT-Advanced, 916
IMT-2000 systems, 2
In-device coexistence (IDC), 1030
Industrial, scientific, and medical (ISM) bands, 1051
Integrated services data digital network (ISDN), 43
Integrity protection, 295*f*
Inter-band noncontiguous, 988
Inter-cell interference cancellation techniques, 1033
Inter-cell interference coordination, 76, 964–965, 1029–1030, 1033–1034, 1039
Interference measurement resource (IMR), 977
Interference rejection combining (IRC) receiver, 628
Inter-frequency neighbor cell measurements, 250–251, 258
Interleaved FDMA (IFDMA), 727–728
Inter-LTE mobility, 259
Internet key exchange (IKE), 78–79
Internet protocol (IP), 154
  addresses, 232
  connectivity, 180–181

flow mobility, 107–110
network layer, 401–402
Inter-radio access technology (inter-RAT)
handover procedures, 255–256
measurements, 1002–1003
mobility procedures, 216–221, 216*f*, 229, 256*f*, 259
RRM, 77
Interrogating-CSCF (I-CSCF), 81
Inter-symbol interference (ISI), 723–724
Intra-band contiguous carrier aggregation, 987–988
Intra-band non-contiguous carrier aggregation, 988
Intra-cell/inter-cell interference mitigation methods, 1030–1035
Intra-eNB CoMP techniques, 978
Intra-frequency neighbor cell measurements, 258
Intra-LTE/inter-RAT cell reselection procedure, 280–281
Intra-MME/S-GW handover procedures, 254*f*
IP connectivity access network (IP-CAN), 192
IP multimedia subsystem (IMS), 36–38
IP security protocol (IPsec), 78–79

J

Joint reception (JR), 971
Joint transmission (JT) CoMP concepts

K

Kronecker product, 913–914

L

Large-delay cyclic delay diversity, 673*t*
Layer mapping
for 2 and 4 layer transmit diversity, 549*f*
for spatial multiplexing with 2, 3, and 4 layers, 550*f*
Linear minimum mean-square error (LMMSE) receiver, 849
Linear/non-linear precoding concept, 657*f*
Link adaptation, 537–539, 690–712
Link budget, 882–883
Link-level channel models, 904–915
Link-to-system mapping, 893–901, 899*f*
Local IP access (LIPA), 30–31, 101–105
Localized/distributed allocation schemes, 462*f*
Local mobility anchor (LMA), 35
Location-based services, 1071–1090
Location measurement unit (LMU), 73, 1076
Location service (LCS), 71
Logical channel group (LCG), 374
Logical channel ID (LCID), 348
Logical channels, 138, 349–350
Logical to transport channel mapping, 145*f*
Log-likelihood ratio (LLR), 530–531
Lorentz distribution, 435–436
LTE positioning protocol (LPP), 1076–1077
LTE positioning protocol annex (LPPa), 1076–1077
LTE RRC_CONNECTED state, radio bearers, 236*f*

M

Machine-to-machine (M2M) applications, 22
Machine type communication (MTC), 22
Macroscopic fading, 404–405
Master information block (MIB), 157–158, 262–263, 445, 557*t*
Maximal ratio combining (MRC), 627, 729–730
Maximum bit rate (MBR), 192–193
Maximum likelihood detection (MLD) receivers, 846
Maximum-likelihood (ML) detector/decoder, 522, 527–528
Maximum power reduction (MPR), 999
Max-Log-MAP decoding algorithm, 531
MCC (Mobile country code), 52*t*
MCH subframe allocation (MSA), 1098
Mean mutual information per bit (MMIB), 901
Medium access control (MAC), 344, 722–723
Message authentication code for integrity (MAC-I), 294
MMEC (MME code), 52*t*
MMEGI (MME group identifier), 52*t*
MMEI (MME identifier), 52*t*
MNC (Mobile network code), 52*t*
Mobile access gateway (MAG), 47
Mobile IP, 111–114
client-based IP mobility, 113
network-based IP mobility, 113–114
Mobile switching center (MSC), 43, 98
Mobile-terminated data call
call flow, 195*f*
Mobility classes, 11
Mobility management entity (MME), 32, 74–75, 98, 125, 138, 1076
Mobility procedures, 198–221
Modem, transmitter/receiver chain, 861
Modulation and coding scheme (MCS), 344, 668–669, 722–723, 880, 993
Monte Carlo method, 902–903
Moore-Penrose inverse, 625–626
MSIN (Mobile subscriber identification number), 52*t*

M-TMSI (MME mobile subscriber identity), 52*t*
Multi-antenna techniques, 609–610
Multi-antenna transmission, principles, 608–661
Multi-antenna transmission schemes, 483–485
Multi-antenna transmit-diversity techniques, 844–846
Multicast channel (MCH), 143, 1095
Multicast control channel (MCCH), 143, 1095
Multicast traffic channels (MTCHs), 143, 350–351
Multi-cell/multicast coordination entity (MCE), 68–70, 1091–1093
Multimedia broadcast multicast service (MBMS), 227–229, 350–351
Multimedia broadcast multicast service single frequency network (MBSFN), 1044, 1091
Multiple access channel (MAC), 641
Multiple access schemes, 439*f*
Multiple-input and multiple-output (MIMO), 157, 861–864, 1032
  advantages, 661–662
  channels, 905–906, 952
  codebooks, 638
  detectors, soft-output, 864–865
  general principle of, 610*f*
  receivers, 610–611
Multiple-input single-output (MISO), 611–612
Multiplexing/de-multiplexing entity, 345–347
Multi-radio mobile terminals, 1051
Multiuser detection (MUD), 1033
Multi-user MIMO channel, 650
Multi-user MIMO techniques, 24–25, 502–503, 955
  BC model, 646*f*
Mutual information effective signal to interference and noise ratio mapping (MIESM), 880

N

Narrowband blocking, 1026–1027
Network architecture, 29
  E-MBMS architecture, 67–71
  EPC architecture, 42–50
  E-UTRAN architecture, 57–67
Network-based IP mobility, 113–114
Network-based positioning methods, 1078–1080
Network-coordinated UE-assisted IDC resolution signaling procedure, 1061*f*
Network virtualization. *see* software-defined networking (SDN)
New data indicator (NDI), 774
Non-access stratum (NAS), 34–35, 154
Non-CA-based eICIC methods, 1046*f*
Non-codebook-based transmission, 676–677
Non-contention-based random access procedure, 185–186

O

Observed time difference of arrival (OTDOA) method, 1086–1087
Open base station architecture initiative (OBSAI), 63–64
Open-loop power control, 697
Open-loop spatial multiplexing, 662–663, 672
Open systems interconnection (OSI), 122
Originating identification presentation (OIP), 82
Orthogonal cover code (OCC), 500, 757–758
Orthogonal frequency division multiple access (OFDMA), 437
Orthogonal frequency division multiplexing (OFDM), 2–3, 30
Out-of-band (OOB), 1056–1057
  blocking, 1026
  emissions, 739–740
Overload indicator, 1041

P

Packet data convergence protocol (PDCP), 127–128, 344, 999–1001
Packet data network gateway, 46
Packet delay budget (PDB), 193–194
Packet delay, DRX effect, 371
Packet loss rate (PLR), 193–194
Packet scheduling (PS), 76
Paging channel (PCH), 143
Paging control channel (PCCH), 142, 607
Paging frame (PF), 266–270
Paging occasion (PO), 266–270
Paging-RNTI (P-RNTI), 591
Parallel concatenated convolutional codes (PCCCs), 519–521
PDN (Packet data network) connectivity, 180–181
PDN ID (Packet data network identity), 52*t*
Peak spectral efficiency, 10, 20
Peak to average power ratio (PAPR), 1018–1019
Per-antenna rate control (PARC), 624–625
Performance metrics
  cell-edge user spectral efficiency, 888–889
  cell spectral efficiency, 888–889
  definition of, 882–889
  effective IoT, 887–888
  geometry, 887
  Jain fairness index, 886–887

link budget, 882–883
outage throughput, 885
packet delay, 885–886
sector throughput, 883–884
spectral efficiency, 886
user throughput, 883–884
wideband SINR distribution, 887
P-GW ID (PDN GW identity), 35, 52*t*, 126
Physical broadcast channel (PBCH), 157–158, 453–454
Physical control format indicator channel (PCFICH), 454
Physical downlink control channel (PDCCH), 454, 1098–1100
Physical downlink shared channel (PDSCH), 353, 454, 993
Physical hybrid-ARQ indicator channel (PHICH), 454
Physical hybrid automatic repeat request (HARQ) indicator channel (PHICH), 159
Physical multicast channel (PMCH), 454, 1096–1097
Physical random access channel (PRACH), 155, 390, 430, 705, 740–741, 925, 1089
Physical resource blocks (PRBs), 382, 411–414, 743
Physical uplink control channel (PUCCH), 430, 734, 739–740, 992
Physical uplink shared channel (PUSCH), 357, 430, 734, 738–739, 1047
Pico-cells, 148–149, 1039
Pilot-based channel estimation, 480–481
PLMN. *see* Public land mobile network (PLMN)
PLMN ID (Public land mobile network identifier), 52*t*
Policy and charging enforcement function (PCEF), 48–49
Policy and charging rules function (PCRF), 32–33, 126
Policy control enforcement function (PCEF), 36–38, 245–246
Positioning, definitions, 1071–1072
Positioning network architecture, 71–74
Positioning reference signal (PRS), 480, 1076–1077
Position measurement, uncertainty, 1080–1081
Power amplifier (PA), 1018–1019
Power control, 690–712
basic concepts, 691–698
downlink power allocation, 698–700
headroom, 706–707
link adaptation, 707–712
PRACH, 705–706
PUCCH, 703–704
PUSCH power control, 700–702
SRS, 704–705
Power headroom reports (PHRs), 706
Precoding matrix index (PMI), 977
feedback, 791*t*
sub-band, 665–666
UE-selected sub-band, 666
wideband, 665
Proportional fair (PF) scheduling algorithm, 386–387
Protocol data unit (PDU), 122–123, 722–723, 932–933
Proxy binding update (PBU), 113
Proxy-CSCF (P-CSCF), 81
Proxy MIPv6 (PMIPv6), 109–110
Proxy mobile IP (PMIP), 47
P-RS structure, in time/frequency domain, 517*f*
Public land mobile network (PLMN), 34–35, 154–155, 230–231, 1102–1103
Public switched telephone network (PSTN), 43

Q

QoS class identifier (QCI), 35–36, 244
QPSK modulation, 427*f*, 556, 571, 787–789
Quadratic permutation polynomial (QPP), 537–539
Quadrature amplitude modulation (QAM)
Quality of experience (QoE), 77–78
Quality of service (QoS)
Quasi-collocated antenna ports, 682

R

Radio access network (RAN), 11–13, 14*t*, 952
Radio admission control (RAC), 75–76
Radio bearer control (RBC), 76
Radio link control (RLC), 36–38, 179–180, 311–312, 1095
Radio link control acknowledged mode (RLC-AM) mode, 232–233
Radio link monitoring (RLM) measurements, 1063*t*
Radio network controllers (RNCs), 31
Radio network layer, 136–137
Radio network temporary identifier (RNTI), 499
Radio resource control (RRC), 127–128, 138–140, 155, 227–229, 987, 1057–1058
Radio resource management (RRM), 30–31, 75–77
measurements, 1063*t*

Radio resource management (RRM) (*Continued*)
mechanisms, 1030
RLM/CSI measurement, resource restriction, 1048
RAKE receiver, 729–730
Random access channel (RACH), 144, 232–233
Random access preamble identifier (RAPID), 394
Random-access preamble sequences, 833
Random access response, 185–186, 348–349
Rate matching process, 541*f*
Rayleigh distribution, 427
Rayleigh fading channel, 621
Received bit mutual information rate (RBIR) link-to-system mapping, 901
Received signal strength indicator (RSSI), 246, 496
Receiver antenna array, angle of arrival (AoA), 409
Receiver blocking, 440–441
Reed-Muller code, 785–786
Reference signal received power (RSRP), 231–232, 247, 496–497, 968, 1088–1089
Reference signal received quality (RSRQ), 247, 496–497
Reference signals, 518
Reference signal time difference (RSTD), 1086–1087
Relay nodes (RNs), 130–131
Remote radio heads (RRHs), 30–31, 512
Resource allocation, 698–700
type 0, 464*f*
type 1, 466*f*
type 2, 468*f*
Resource block group (RBG), 454–456, 748
Resource element groups (REGs), 467
Resource element mapping, 554*f*, 772
Resource indication value (RIV), 465–467, 747
Resource partitioning, 1039–1040
Rician channels, 614–616
Rician factor, 405
Roaming architecture and interworking with other networks, 50–56
Robust header compression (ROHC), 299–303
RRC_CONNECTED state, 257–258, 389–390

S

SAE temporary mobile subscriber identity (S-TMSI), 138
Satellite navigation systems, 1085
sCellDeactivationTimer, 378, 1003
SCells
activation/deactivation procedure, 1003
channel quality indicator (CQI), 1006
message exchange for addition, 1006*f*
PUSCH configuration, 1006
uplink power control configuration, 1006
S1 control-plane protocol stack, 129–131, 146
Sector SINR, 946*f*
Security Mode Command message, 163
Selected IP traffic offload (SIPTO), 105–107
Semi-static point selection (SSPS), 970
Sequence-group hopping, 758–759
Service access point (SAP), 289–290, 312
Service data flows (SDFs), 35–36, 191
Service data unit (SDU), 122–123, 232–233, 311–312
Serving-CSCF (S-CSCF), 82
Serving gateway (S-GW), 35, 47, 125–126
Serving GPRS support nodes (SGSN), 129, 220
Session description protocol (SDP), 82
Shannon capacity, 619
Shannon limit, 527–528
Short message service (SMS), 32
Signaling radio bearers (SRBs), 61, 383–384
Simultaneous voice and LTE (SVLTE), 90–91
Single-carrier frequency division multiple access (SC-FDMA), 723, 992
clustered SC-FDMA, 734–736
Single-input multiple-output (SIMO), 611–612
Single-input single-output (SISO), 609, 899–900
Single/multiple timing advance concepts, 689*f*
Single radio voice call continuity (SRVCC), 84–90
Single-user multiple-input multiple-output (SU-MIMO) system, 2–3, 637, 952
Singular value decomposition (SVD) concept, 640*f*
Singular value decomposition (SVD) precoding, 639
SLm-application protocol (AP) messages, 1076
Small cells, 148–149
Software-defined networking (SDN), 25–26, 25*f*
Sounding reference signal (SRS), 430, 742, 1089
resources, 373
transmission configuration, 1059–1060
Space-division multiple access (SDMA), 651
Spaced-time correlation function, 408–409
Space-frequency block code (SFBC), 485
Space-time block code (STBC), 623
Spatial channel model (SCM), 905–906
Spatial orthogonal resource transmit diversity (SORTD), 800–801
concept, illustration of, 801*f*
Spatial tapped-delay-line reduced-complexity model, 907–908

Spectral efficiency, 946*f*
Sphere decoding (SD), 630–631
Static/dynamic overhead, calculation, 889–891
Static/semi-static interference management eICIC schemes, 1050*f*
S-TMSI (SAE temporary mobile subscriber identity), 52*t*
Stream control transmission protocol (SCTP), 59–60, 128, 130–131, 133–134, 1093
Sub-band frequency hopping, 744
Sub-band PMI, 665*f*
Sub-block interleavers, 541–542
Sub-carrier spacing, 434
Sub-channelization, 437
Subscriber identity module (SIM) access, 305–307
Subscriber profile ID (SPID), 77
Successive interference cancelation (SIC), 624–625
Successive MMSE (SMMSE), 651
SUPL-enabled terminal (SET), 1074–1075
SUPL location platform (SLP), 1074–1075
Symmetric carrier aggregation, in downlink/uplink, 995*f*
Synchronization signals, 471
  algorithm for coherent detection, 476*f*
  generation and mapping, 475*f*
  primary/secondary, 514–515
System architecture evolution temporary mobile subscriber identity (S-TMSI), 163, 238
System frame number (SFN), 159, 354, 445
System information (SI)
System information blocks (SIBs), 157–158, 262–263, 556–557
System information RNTI (SI-RNTI), 263–264
System information transmission timing, 164*f*
System-level channel models, 904–915
System-level simulations, 877

T

TAC (Tracking area code), 52*t*
TAI (Tracking area identity), 52*t*
Tail-biting convolutional coding, 525
TAI list (Tracking area identity list), 52*t*
TAU procedure, 172–174
TEID (Tunnel endpoint identifier), 52*t*
Time alignment timer (TAT), 1001–1002
Time difference of arrival (TDOA) method, 1086–1088
Time division duplex (TDD), 357–358, 411–414, 1077–1078
Time-varying spatial channel model, 908
  correlation-based, 908
  ray-based, 908
Timing advance group (TAG), 373–374, 686–690, 1001–1002
TIN (Temporary identity used in next update), 52*t*
Tomlinson-Harashima precoding (THP) algorithm, 651
Tracking area code (TAC), 154–155
Tracking area identities (TAIs), 159, 238
Tracking areas (TAs), 231
Traffic channels, 138, 142–143
Traffic flow templates (TFTs), 36–38, 192, 242
Traffic models, 891–893
Transmission bandwidth, 414
Transmission control protocol (TCP), 36–38, 383–384
Transmission control protocol/IP (TCP/IP), 293
Transmission time interval (TTI), 344
  bundling, 746
  duration, 925
Transmit power control (TPC), 801–802
Transparent mode (TM), 311–312
Transport control protocol (TCP), 82
Transport network layer, 136–137
Turbo decoding, 531

U

UE aggregate maximum bit rate (UE-AMBR)
UE-specific/common search space, 594*f*
UE-specific demodulation reference signals (DM-RS), 932–933
Unacknowledged mode (UM), 311–312
Un interface, 144–145
Universal integrated circuit card (UICC), 91
Universal mobile telecommunications system (UMTS), 2–3, 32–33, 38–39, 124–125, 155, 1007, 1051
Universal subscriber identity module (USIM), 231
Unsynchronized carriers, 989
Uplink
  cell-specific hopping/mirroring, 746
  control information (UCI), 996
  DM-RS generation
  frame structure, 736–737
    physical signals/channels, location of, 740*f*
  peak spectral efficiency, 925
  physical resource structure, 743*f*
  pilot time slot (UpPTS) field, 1008–1009
  positioning methods, 1089
  power control, 998–999
  resource allocation, 747*f*
    type 1, 751*f*

Uplink (*Continued*)
type 0, illustration of, 749*f*
shared channel (UL-SCH), 143–144, 802
SINR, statistical distribution of, 924*f*
spatial multiplexing, codeword-to-layer mapping for, 818*t*
virtual and physical antennas, 839*t*
Uplink/downlink radio frames, relative timing, 686*f*
Uplink TFT (UL-TFT), 36–38
Uplink time difference of arrival (UTDOA) method, 1078–1080, 1090
Uplink timing advance (TA) adjustment procedure, 1001–1002
Uplink transport channels, 143–144
Used in universal mobile telecommunications system (UMTS), 723

V

Virtual MIMO technique
collaborative spatial multiplexing, 652
Virtual MU-MIMO, 840–841
Virtual resource block (VRB), 454–456, 743–744
Viterbi decoder, 525–527, 624
Voice over Internet protocol (VoIP), 121–122, 178, 296, 369–370, 384–385, 891
Voice over LTE (VoLTE), 80, 90–94

W

Walsh sequences, 798–799
Wideband feedback, 858–859

X

X2-based handover procedure, 254–255
X2 control-plane protocol stack, 147
X2 interface, 60
X2 user-plane protocol stack, 132–134, 133*f*
XML configuration access protocol (XCAP), 82

Z

Zadoff-Chu sequences, 473–474, 739–740, 754, 758–759, 821, 829
Zero correlation zones (ZCZ) configuration, 831
Zero-forcing (ZF), 624